27 March 2008 | www.nature.com/nature | $10

THE INTERNATIONAL WEEKLY JOURNAL OF SCIENCE

nature

THE FIRST EUROPEAN?

The jaw that puts humans in Spain a million-plus years ago

CARBON NANOTUBES
Electron spin–orbit coupling

OBESITY
The genetic network of a disease

VISION
Retina cells are looking up

NATUREJOBS
Vaccine design

$10.00US $12.99CAN
13
0 71486 03070 6

nature 452, 387-502 27 March 2008

www.nature.com/nature

no.7186

npg

Presenting!

Prestige Antibodies™

SIGMA Life Science

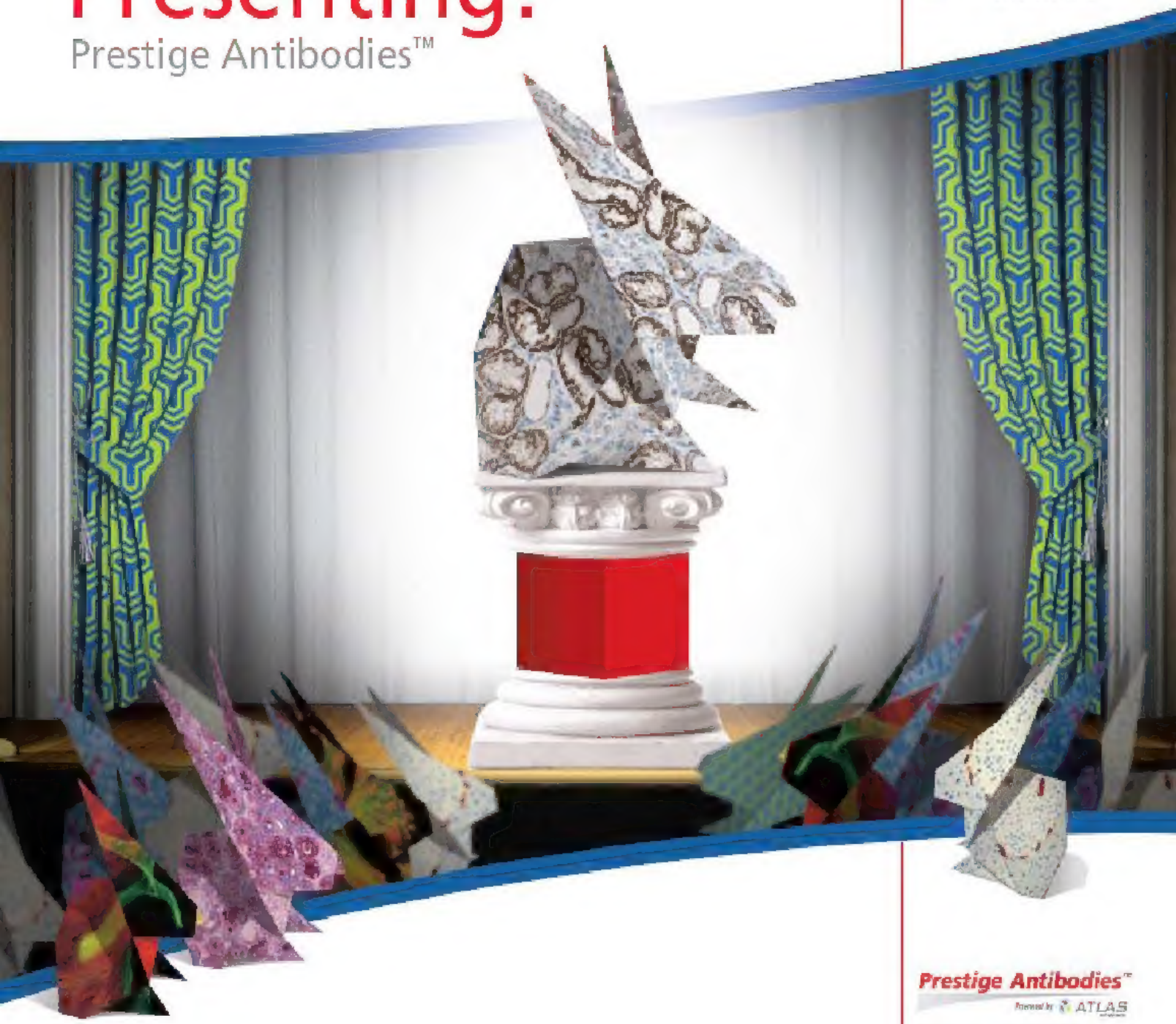

Antibodies that work, right out of the box!

The most highly characterized antibodies in the industry — **1,800 NEW** Prestige Antibodies™, Powered by Atlas Antibodies.

- Designed & validated by the Human Proteome Resource (HPR)
- Standardized in universal protocols
- Over 500 immunohistochemical images for every antibody
- Publicly available data on the web

Look even closer. Go to ***sigma.com/prestige*** for more information.

Our Innovation, Your Research — Shaping the Future of Life Science

Prestige Antibodies™
Powered by ATLAS

Anti-BID Cat No. HPA000722 on A-431 cells shown in green, nucleus in blue, microtubules in red and endoplasmic reticulum (ER) in yellow.

Just one of the over 500 IF, IHC and WB images available

LOST:

Ability to detect proteins with chemiluminescence after 4 hours

FOUND:

Detect proteins with the brightest, longest-lasting western blot detection chemistry!

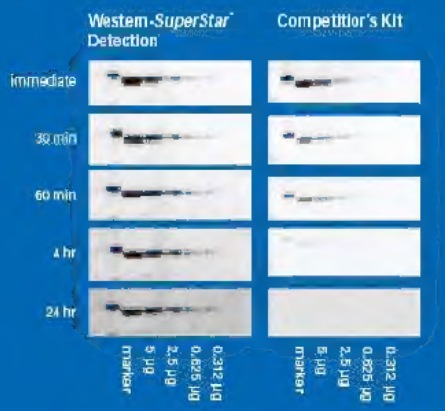

Tropix® Western-*SuperStar*™ Immunodetection System is the most complete chemiluminescence-based western blotting kit on the market, and offers five- to ten-fold higher intensity than competitors' products.

- You choose when you want to expose your blot after adding the substrate (immediately or up to 4.5 days)
- You choose the membrane (PVDF, nitrocellulose or nylon)
- You choose the imaging method (CCD imager or x-ray film)
- You choose whether you want to strip and reprobe (up to 3 times)

FIND your protein with Western-*SuperStar*™ Immunodetection System!

Go to **www.appliedbiosystems.com/westernsuperstar** to download the product bulletin and place your order.

Applied Biosystems

You think Taq is hot? This is pure

Phire™

Phire™ Hot Start DNA Polymerase – speed and specificity for PCR

Finnzymes' novel PCR enzyme outperforms every *Taq*-based hot start polymerase on the market. Phire DNA Polymerase is an ideal solution for routine and high throughput PCR applications.

Short protocols: Amplify 3 times faster than with hot start *Taq*
Specific products: Unique hot start technology with zero-time reactivation
High yields: Efficient PCR results in more product

For more information visit **www.finnzymes.com**
To receive a sample please contact your local distributor.

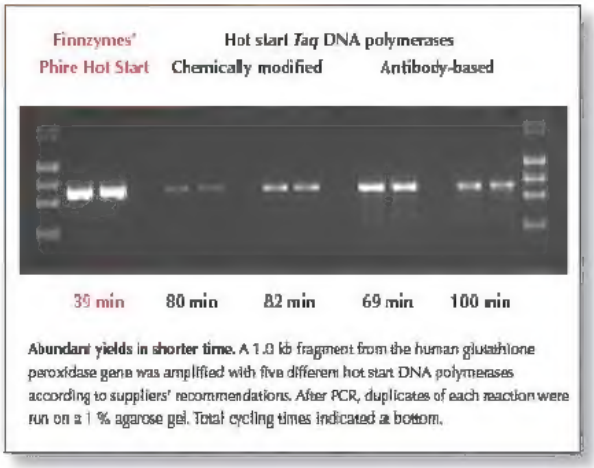

Abundant yields in shorter time. A 1.0 kb fragment from the human glutathione peroxidase gene was amplified with five different hot start DNA polymerases according to suppliers' recommendations. After PCR, duplicates of each reaction were run on a 1 % agarose gel. Total cycling times indicated at bottom.

NEW ENGLAND BioLabs Inc.
the leader in enzyme technology

Distributed in the US and Canada by New England Biolabs.
Other countries visit www.finnzymes.com.

FINNZYMES
TOOLS FOR MOLECULAR BIOLOGY

The power of small x8

1µl analysis — increased throughput

The NanoDrop® ND-8000 8-Sample Spectrophotometer

1µl samples. No cuvettes. No dilutions.

Revolutionary technology. **8 readings in under 30 seconds.** The NEW NanoDrop® ND-8000 8-Sample Spectrophotometer is powerful — eight 1 µl samples at once.

Full spectrum UV/Vis analysis of 1 µl samples for quantitation, purity assessments and more: nucleic acids, microarrays, proteins and general spectrophotometry.

Measurement is quick and easy — pipette up to eight samples and measure. Each sample is read using two path lengths to achieve an extensive dynamic range (e.g., 2-3700 ng/µl dsDNA), virtually eliminating the need for dilutions. Then just a quick wipe clean and you're ready for your next samples. What could be easier — or more powerful?

And for the power of small in single-sample absorbance or fluorescent measurements, check out the NanoDrop® ND-1000 Spectrophotometer or the NanoDrop® ND-3300 Fluorospectrometer (ultra low fluorescent detection limit of sample mass — e.g., 2 pg dsDNA).

Ready to experience the power of small x8? **Test a NanoDrop® ND-8000 8-Sample Spectrophotometer in your own lab.**

FREE one-week evaluation **www.nanodrop.com**
302.479.7707

Now Part of Thermo Fisher Scientific

NanoDrop

Nature Publishing Group
The Macmillan Building,
4 Crinan St, London N1 9XW, UK
e-mail: nature@nature.com

NATURE'S MISSION, 1869:
'The objective which it is proposed to attain by this periodical may be broadly stated as follows. It is intended, first, to place before the general public the grand results of scientific work and scientific discovery; and to urge the claims of science to move to a more general recognition in education and in daily life…Secondly, to aid scientific men [sic] themselves, by giving early information of all advances made in any branch of natural knowledge throughout the world, and by affording them an opportunity of discussing the various scientific questions which arise from time to time.'

Nature's mission statement was updated in 2000:
www.nature.com/nature/about
Submissions and Guide to Authors:
www.nature.com/nature/authors

Author and referee policies and services:
www.nature.com/authors

Nature® (ISSN 0028-0836) is published by Nature Publishing Group, a division of Macmillan Publishers Ltd (The Macmillan Building, 4 Crinan Street, London N1 9XW). Registered as a newspaper at the British Post Office.
North and South American orders to Nature, Subscription Dept, 342 Broadway PMB 301, New York NY 10013-3910, USA.
Other orders to Nature, Brunel Road, Basingstoke, Hants RG21 2XS, UK.

Identification code for Nature: 0028-0836/03
CPC PUB AGREEMENT #40032744.
In the US Nature (ISSN 0028-0836) is published weekly on Thursday, except the last week in December by Nature Publishing Group, 75 Varick St, 9th Fl, New York NY 10013-1917, USA. US Periodicals postage paid at New York NY, and additional mailing post offices.
US POSTMASTER: send address changes to Nature, Subscription Dept, 342 Broadway PMB 301, New York NY 10013-3910, USA.
Published in Japan by NPG Nature Asia-Pacific, Chiyoda Building, 2-37 Ichigayatamachi, Shinjuku-ku, Tokyo 162-0843, Japan.

nature publishing group

nature

EDITORIALS

RESEARCH HIGHLIGHTS

NEWS

NEWS FEATURES

CORRESPONDENCE

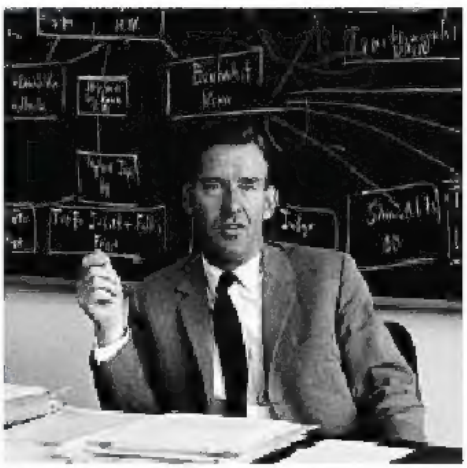

FRAUCH

History man: a personal view of Germany in Europe, p. **411**.

B.KAYES/M.FILLER

Will we ever match plants at photosynthesis? Page **400**.

BOOKS & ARTS

NEWS & VIEWS

NATUREJOBS

FUTURES

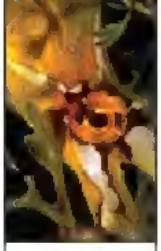

Innovative Discovery Tools for Signal Transduction Research

PathScan® Sandwich ELISA Kits

...from Cell Signaling Technology

PathScan® Cell Growth Multi-Target Sandwich ELISA Kit #7239

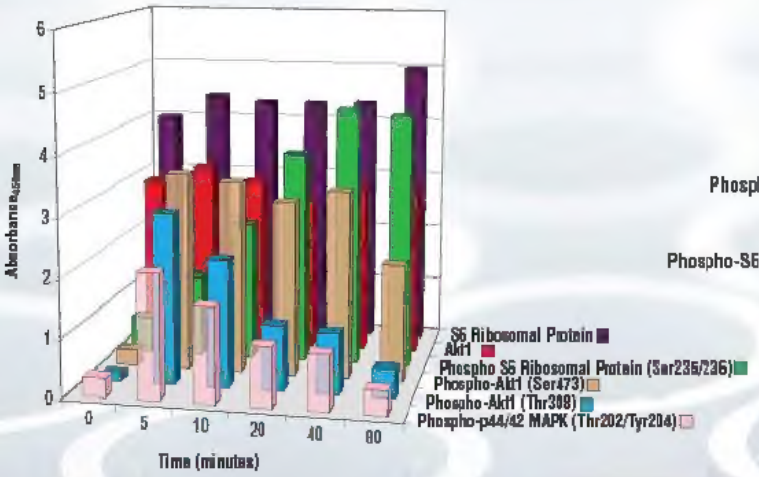

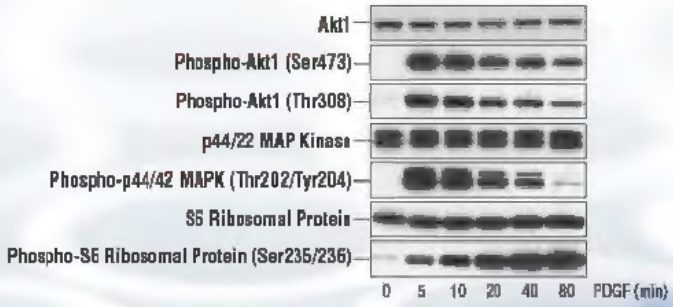

Treatment of NIH/3T3 cells with PDGF induces phosphorylation of Akt1 at Thr308 and Ser473, S6 Ribosomal Protein at Ser235/236 and p44/42 MAPK at Thr202/Tyr204 as detected by the PathScan® Cell Growth Multi-Target Sandwich ELISA Kit #7239.

Cell Signaling Technology (CST) has applied its antibody expertise to identify antibody pairs with optimal activity in sandwich ELISAs. These assays enable the detection of low amounts of target protein from cell lysates.

:: In-house development, production and validation ensures the highest kit quality

:: Technical support provided by the same scientists that develop and produce the kits

:: Matched modification state and total ELISA kits available

:: Custom 96- and 384-well formatting available upon request

:: Select antibody pairs available separately

:: New multitarget kits available for parallel analysis of several signaling molecules

New PathScan® Multi Target ELISA Kits Available

PathScan® Inflammation Multi-Target Sandwich ELISA Kit #7276	new
PathScan® Cell Growth Multi-Target Sandwich ELISA Kit #7239	new
PathScan® MAP Kinase Multi-Target Sandwich ELISA Kit #7274	new
PathScan® Signaling Nodes Multi-Target Sandwich ELISA Kit #7272	new

Over 80 PathScan® Sandwich ELISA Kits available, including...

Target		PathScan® Sandwich ELISA Kits	PathScan® ELISA Antibody Pair
Phospho-4E-BP1 (Thr37/Thr46)		#7216	
Total 4E-BP1 Sandwich ELISA Kit	new	#7179	
Phospho-Akt (Thr308)		#7252	#7144
Phospho-Akt1 (Ser473)		#7160	#7143
Akt1		#7170	#7142
β-Catenin		#7308	
Phospho-EGF Receptor (Tyr1068)		#7240	
Acetylated Histone H3		#7232	#7209
Phospho-Histone H3 (Ser10)		#7155	#7207
Phospho-IκB-α (Ser32)		#7355	
Phospho-IRS-1 (panTyr)	new	#7133	#7347
Phospho-IRS-1 (Ser302)		#7283	#7284
Phospho-c-Kit (Tyr719)	new	#7296	#7299
Phospho-MEK1 (Ser217/221)		#7175	#7211
MEK1		#7165	#7215
Phospho-p38α MAPK (Thr180/Tyr182)		#7140	#7221
Phospho-p44/42 MAPK (Thr202/Tyr204)	new	#7177	#7246
Phospho-S6 Ribosomal Protein (Ser235/236)		#7205	#7201
S6 Ribosomal Protein		#7225	#7203
Phospho-Stat3 (Tyr705)		#7300	#7146
Phospho-TrkA (Tyr490)		#7210	

For a complete product listing visit...

www.cellsignal.com

Cell Signaling TECHNOLOGY®

Orders (toll-free) 1-877-616-CELL (2355) orders@cellsignal.com Fax ordering 1-978-867-2488 Technical support (toll-free) 1-877-678-TECH (8324) support@cellsignal.com Inquiries info@cellsignal.com

Postcards from the Moon, Futures, p. 502.

JACEY

ARTICLES

LETTERS

NATURE ONLINE

ADVANCE ONLINE PUBLICATION

PUBLISHED ON 23 MARCH 2008

The genome of the model beetle and pest *Tribolium castaneum*
Tribolium Genome Sequencing Consortium
doi:10.1038/nature06784

REST maintains self-renewal and pluripotency of embryonic stem cells
S K Singh, M N Kagalwala, J Parker-Thornburg, H Adams & S Majumder
doi:10.1038/nature06863

Control of T_{reg} and T_H17 cell differentiation by the aryl hydrocarbon receptor
F J Quintana, A S Basso, A H Iglesias, T Korn, M F Farez, E Bettelli, M Caccamo, M Oukka & H L Weiner
doi:10.1038/nature06880

The aryl hydrocarbon receptor links T_H17-cell-mediated autoimmunity to environmental toxins
M Veldhoen, K Hirota, A M Westendorf, J Buer, L Dumoutier, J-C Renauld & B Stockinger
doi:10.1038/nature06881

PUBLISHED ON 26 MARCH 2008

Sequence- and target-independent angiogenesis suppression by siRNA via TLR3
M E Kleinman, K Yamada, A Takeda, V Chandrasekaran, M Nozaki, J Z Baffi, R J C Albuquerque, S Yamasaki, M Itaya, Y Pan, B Appukuttan, D Gibbs, Z Yang, K Karikó, B K Ambati, T A Wilgus, L A DiPietro, E Sakurai, K Zhang, J R Smith, E W Taylor & J Ambati
doi:10.1038/nature06765

LNA-mediated microRNA silencing in non-human primates
J Elmén, M Lindow, S Schütz, M Lawrence, A Petri, S Obad, M Lindholm, M Hedtjärn, H F Hansen, U Berger, S Gullans, P Kearney, P Sarnow, E M Straarup & S Kauppinen
doi:10.1038/nature06783

Retinotopic order in the absence of axon competition
N J Gosse, L M Nevin & H Baier
doi:10.1038/nature06816

TGF-β-induced Foxp3 inhibits T_H17 cell differentiation by antagonizing RORγt function
L Zhou, J E Lopes, M M W Chong, I I Ivanov, R Min, G D Victora, Y Shen, J Du, Y P Rubtsov, A Y Rudensky, S F Ziegler & D R Littman
doi:10.1038/nature06878

PODCAST LATEST

Each week the Nature podcast mines the current issue and the week's new online offerings for the background on the hottest stories.
www.nature.com/podcast

For the podcast archive (in mp3 format) and English transcripts of previous episodes, visit:
http://tinyurl.com/k62cvt

nature geoscience

First issues now published

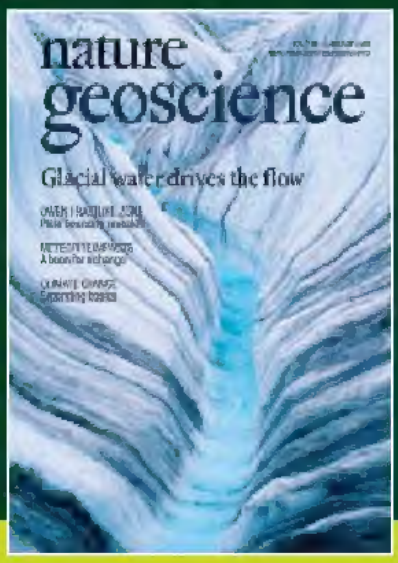

With *Nature Geoscience* now published and online, visit **www.nature.com/naturegeoscience** to browse the contents list and abstracts published to date. These first issues reflect the journal's broad scope, publishing science spanning the Earth's core, oceans, glaciers, the atmosphere and the planets, using chemistry, physics and biology, and field work as well as modelling. A snapshot of this content published to date includes:

Progress article: Widening of the tropical belt in a changing climate, *Dian J. Seidel, Qiang Fu, William J. Randel & Thomas J. Reichler*

Progress article: Biophysical controls on organic carbon fluxes in fluvial networks, *Tom J. Battin, Louis A. Kaplan, Stuart Findlay, Charles S. Hopkinson, Eugenia Marti, Aaron I. Packman, J. Denis Newbold & Francesc Sabater*

Review article: Core–mantle boundary heat flow, *Thorne Lay, John Hernlund & Bruce A. Buffett*

Review article: The methane cycle on Titan, *Jonathan I. Lunine & Sushil K. Atreya*

Letter: Persistent earthquake clusters and gaps from slip on irregular faults, *Tom Parsons*

Letter: Decreased abundance of crustose coralline algae due to ocean acidification, *Ilsa B. Kuffner, Andreas J. Andersson, Paul L. Jokiel, Ku'ulei S. Rodgers & Fred T. Mackenzi*

Letter: Atmospheric carbon dioxide linked with Mesozoic and early Cenozoic climate change, *Benjamin J. Fletcher, Stuart J. Brentnall, Clive W. Anderson, Robert A. Berner & David J. Beerling*

Letter: A recent volcanic eruption beneath the West Antarctic ice sheet, *Hugh F. J. Corr & David G. Vaughan*

Enjoy the 'backstory', a new section specific to *Nature Geoscience*. In the form of a question-and-answer piece geoscientists tell the story of their research before it was written up neatly in a paper. In the first issue's 'backstories' read about the commute to work by helicopter in the high Arctic; about a black bear climbing easily up an Alaskan glacier moraine that was such a struggle to the scientist and the experience of the team who crossed the equator on the day of the autumn equinox.

Visit www.nature.com/naturegeoscience to find out more, including options to register for the monthly content e-alert, subscription information and submission guidelines.

THIS ISSUE

STEM CELL FEVER A report last December that mice with a human sickle-cell anaemia disease trait had been successfully treated with skin cells reprogrammed to become pluripotent — capable of generating many cell types — raised the media profile of iPSCs (induced pluripotent stem cells) from high to frenzied. They have been hailed as a breakthrough in stem cell therapy, even as sufficient grounds for stopping work on therapeutic cloning and embryonic stem cell research. Not surprisingly, there has been exaggeration and misunderstanding in much of the speculation as to what can be achieved with iPSCs. David Cyranoski takes a considered view of the iPSC scene, and attempts to separate fact from fiction. [News Feature p. 406]

OPEN SECRET This week's 'Hidden Treasure', the Herbarium Centrale Italicum, now part of the botanical collection of University of Florence, was founded in 1842. That's long before the unification of Italy — in fact the herbarium was one of the early fruits of the unification

SBAMB./MDSN FLORENCE

Shelf life. from Florence's historic herbarium.

movement. One of the great collections, with important material from Italy's former colonies in Africa, the collection is still open, in the sense that new material is still being added. And it is open to visitors by appointment. [Books & Arts, p. 414]

RADICLE SOLUTIONS The Svalbard Global Seed Vault, built underground near the village of Longyearbyen on the island of Spitsbergen in Norway, is now open and gathering seeds. With its temperature guaranteed for the foreseeable future by its Arctic surroundings, it is the ultimate back-up to the 1,400 national and regional seed banks worldwide. But more needs to be done to safeguard food diversity. Some experts are advocating a pro-active programme of genetic manipulation to breed and grow crops that can resist drought and other impending dangers. Michael Hopkin reports. [News Feature p. 404]

EIA/JORDI MESTRE

One of the most debated topics in stone-age archaeology is the date of the earliest human occupation of Europe. This has been frustratingly hard to establish, because the ages of the oldest-known occupation sites are hard to pin down with precision, and the sites contain stone tools rather than human remains. Now there is something more solid to go on, with the discovery of a human lower jaw associated with stone tools and animal bones from the Sima del Elefante cave deposit at the famous complex of fossil-human-bearing sites at Atapuerca in northern Spain. The finds have been dated to between 1.1 and 1.2 million years old using a variety of dating techniques. Of course it's impossible to know if these hominins were the *first* Europeans, but this site is certainly the oldest and most accurately dated record of human occupation in western Europe. The cover shows the key find, mandible fragment ATE9-1, now in the Centro Nacional de Investigación sobre la Evolución Humana, in Burgos. [Letter p. 465, www.nature.com/podcast]

Specialization in the retina

The function of any neural circuit, such as the retina in the eye, is directly related to its connectivity, as determined by the functions of different classes of neuron and their choice of partners. Those attributes are governed by the genetic make up and molecular interactions of each neuron, but it has been difficult to demonstrate a continuous link from the genetic level to that of cellular structure and circuit function. In Jung Kim *et al.* have developed a novel multidisciplinary approach to the problem and apply it to retinal ganglion cells. They have discovered a new type of retinal neuron, identified by a genetic marker, with a unique cell shape, and a unique function. All cells of this type 'point' in a single direction. Remarkably, these cells respond best to objects moving in the direction predicted biophysically by their structure: upwards. The finding raises an intriguing question: why has the mouse invested so heavily in sensitivity to upward motion? [Letter p. 478; www.nature.com/podcast]]

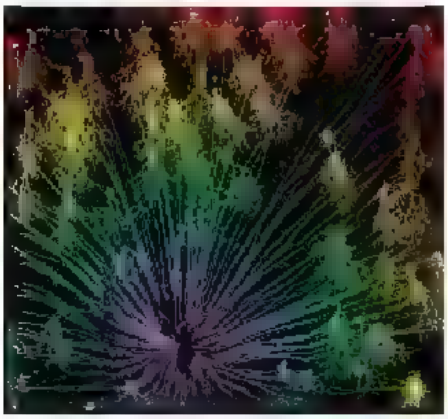

The only way is up, a whole-retina display of 'up' neurons.

Spinning into control

Carbon-based materials are seen as promising candidates for applications such as spintronics and as spin qubits, as their electron spins are thought to be exceptionally stable. In particular, it was assumed that the effect of electron spin coupling to its orbital motion — a source for spin decoherence — is negligible. Kuemmeth *et al.* have now disproved this assumption. Based on a detailed set of electronic transport measurements on high-quality, clean, single-walled carbon nanotubes, they observe direct signatures of electron spin–orbit coupling. The findings may lead to new design principles for the realization of qubits in nanotubes. And the observed spin–orbit coupling may prove to be a valuable tool as a mechanism for all electrical control of spins in carbon nanotubes. [Letter p. 448; News & Views p. 419]

Obesity gets complicated

Complex human diseases result from the interplay of many genetic and environmental factors. To build up a picture of the factors contributing to one such disease, obesity, gene expression was evaluated as a quantitative trait in blood and adipose tissue samples from hundreds of Icelandic subjects aged 18 to 85. The results reveal a tendency to certain characteristic patterns of gene activation in the fatty tissues — though to a much lesser extent in the blood — of people with a higher body mass index. A transcriptional network constructed from the adipose tissue data has significant overlap with a network based on mouse adipose tissue data. [Article p. 423] Exper-

Microsoft®
HealthVault™
Be Well Fund

It's time to bring healthcare into the Internet Age.

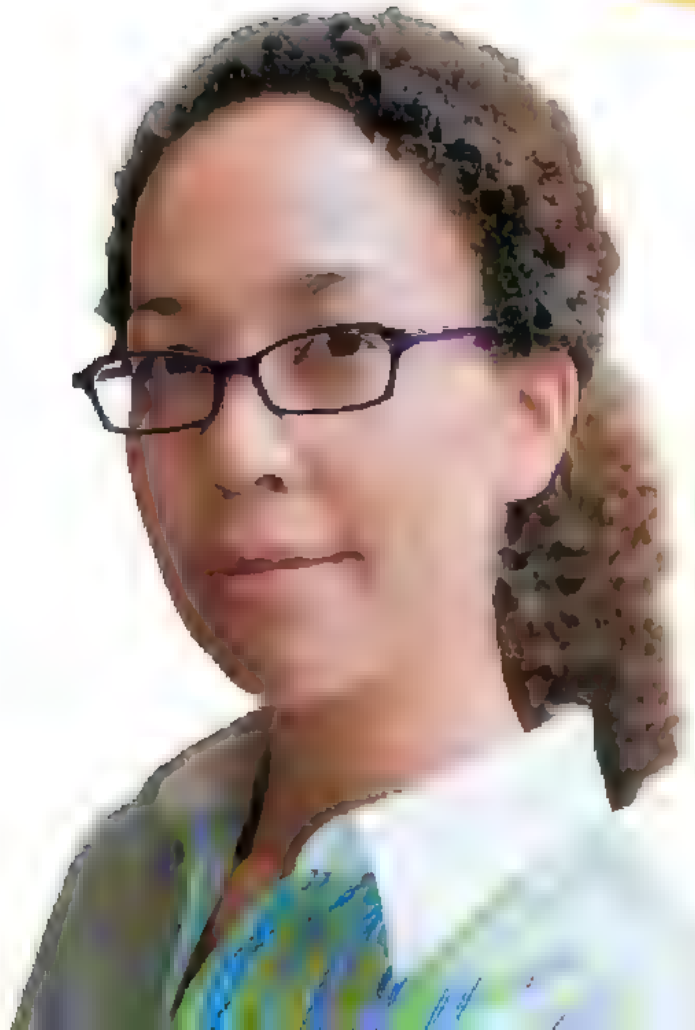

Let's do it *together*.

Microsoft is calling on research and academic health institutions to join us in the search for new, innovative health applications that accelerate connections between consumers and physicians and the information they need to make informed and personalized decisions.

Working together, we can empower physicians and patients with the solutions they need to make a difference.

Building on the Microsoft® HealthVault™ consumer health platform, you have the potential to enable fundamentally new and innovative scenarios.

Submit your ideas to the HealthVault Be Well Fund and join our goal of identifying and developing new, yet-to-be-imagined Web applications that will help people live longer, healthier lives.

For more information on how your institution can submit a proposal to the HealthVault Be Well Fund, visit **www.healthvault.com/fund**

Microsoft

imental support for the idea that complex diseases are emergent properties of molecular networks influenced by genes and environment comes from a study in mice. Mice were examined for disturbances in genetic expression networks that correlate with metabolic traits associated with obesity, diabetes and atherosclerosis. Three genes — *Lpl*, *Lactb* and *Ppm1l* — were identified as previously unknown obesity genes. This 'molecular network' approach raises the prospect that therapies might be directed at whole 'disease networks', rather than at one or two specific genes. [Article p. 429; Author page]

Stem cells got rhythm

Haematopoietic stem cells (HSCs) circulate in the blood, where they can home to sites throughout the body. The release of these cells into the blood stream has now been found to be regulated by circadian rhythms. In mice, HSCs undergo pronounced fluctuations corresponding to circadian oscillations induced by continuous light or by a 12-hour time-shift or 'jet lag'. Timing of the expression of the chemokine CXCL12 in the stem cell niche was also in step with the oscillations in response to adrenergic signals delivered locally by nerves in the bone marrow. The rhythmic release of stem cells into the blood during the animal's resting period suggests a possible role in regeneration. [Article p. 442; News & Views p. 416]

More Mannich reactions

Traditionally, catalysts for organic chemical reactions have been either enzymes or metal complexes. But small organic molecules, known as organocatalysts, have recently burst on to the scene. Organocatalysts are effective in promoting in a wide range of useful transformations, including a carbon–carbon bond forming process known as the Mannich reaction. But frustratingly, these reactions have always failed when the simplest possible substrate, acetaldehyde, was used. Yang *et al.* have now filled this gap in the organocatalysis spectrum by establishing effective catalytic conditions for Mannich reactions with acetaldehyde. This greatly expands the chemical 'toolkit' of organic chemists, and will be especially useful for making chiral, biologically active compounds. [Letter p. 453; Author page]

Oxygen steps in the ocean

The oxygenation of the Earth's atmosphere is thought to have occurred in two steps near the beginning and the end of the Proterozoic eon, around 2,500 to 550 million years ago. The oxidation state of the ocean between these two steps and the timing of deep ocean oxygenation, however, remain poorly known. Scott *et al.* now use molybdenum and total organic carbon data from black shales to track the redox state of the ocean at this time. Molybdenum is an essential participant in nutrient cycling, and its availability is highly sensitive to Earth's redox state. The results provide a new narrative for the historical texture of Earth's oxygenation, and will be of relevance for the study of the events that presaged the appearance of animals on Earth. [Letter p. 456]

Complexity no handicap

As more genetic sequence data are generated, evolutionary biology questions about inheritance and phenotypes can be subjected to sophisticated analyses. Wagner *et al.* address a fundamental problem in evolutionary biology, the relationship between organismal complexity and the ability to evolve, by measuring the effects of pleiotropy, or multiple effects from one genetic mutation, on the skeletal characteristics of mice. Data on 102 quantitative trait loci affecting 70 skeletal traits across the mouse genome suggest that there is no 'cost of complexity' for higher organisms, because most mutations affect few traits and the size of the effects does not increase with complexity. [Letter p. 470]

Scent's different directions

Despite dramatic behavioural differences between the sexes, surprisingly few anatomic features have been observed that differentiate the male and female brain in any species. Work in the *Drosophila* fruit fly has now uncovered a striking difference in male and female responses to the insect pheromone cVA (*cis*-vaccenyl acetate). Males release the pheromone, which is detected by both sexes via apparently identical neural circuits in their antennae. The scent induces females to become receptive to males, but in rival males it inhibits courtship behaviour. The single neuron tracing technique developed to make this discovery should be applicable to study the nervous systems of other genetically tractable species, such as the mouse. [Letter p. 473]

A stomatal ion channel

The stomata on the undersides of leaves control the exchange of carbon dioxide and water between plants and the atmosphere. Stomatal pore aperture is regulated by transport of ions and metabolites across guard-cell membranes. Perhaps surprisingly, until now no plant plasma membrane anion channel subunits have been cloned — and the homologues of animal anion channels have been shown not to encode functional ion channels in plants. Now two groups working independently have identified a protein that is an essential component for S-type anion channel function and is required for stomatal closure in response to a variety of physiological and stress stimuli. Termed SLAC1, it is a distant homologue of fungal and bacterial dicarboxylate/malic acid transport proteins. [Letters pp. 483, 487]

Purify!

SIGMA Life Science

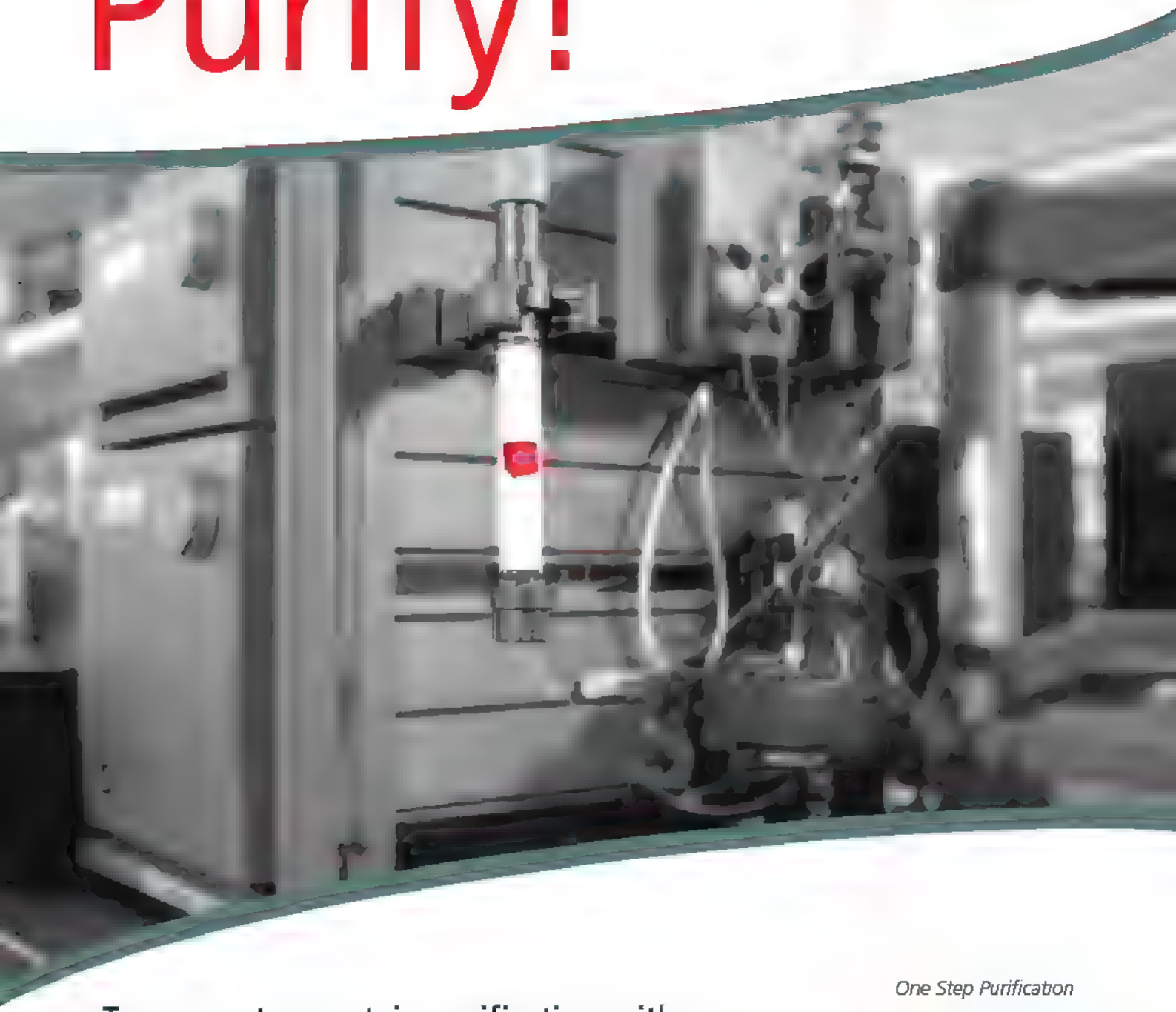

True one-step protein purification with Sigma's HIS-Select® Technology

Sigma's HIS-Select Affinity Gels utilize a proprietary nickel chelate linkage for highly selective histidine-tagged protein purification

- High binding capacity
- Target protein enrichment from a single pass
- Reduced non-specific binding for higher purity

To learn more, visit ***sigma-aldrich.com/his_select***

One Step Purification

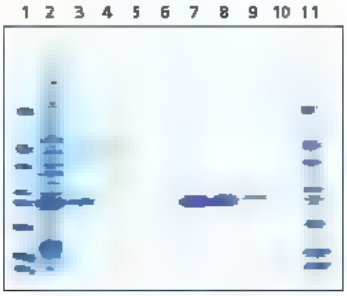

1 Low Range Sigma Marker (M 3913)
2 Whole Cell Extract in Sample Buffer
3 Whole Cell Extract with Cellytic™ B
4 Flow Through
6 Wash 2
7 Elute 1
8 Elute 2
9 Elute 3
10 Elute 4
11 Low Molecular Weight Sigma

Our Innovation, Your Research — Shaping the Future of Life Science

Abstractions

LAST AUTHOR

Susceptibility to many common conditions and diseases, from obesity to cancer, involves the combined effects of many genes and of the many environmental factors that influence how these genes function. On pages 423 and 429, Eric Schadt of Rosetta Inpharmatics in Seattle, Washington, and his colleagues detail an approach to identifying such 'gene networks' — an advance that could potentially lead to diagnostic markers and therapeutic targets for common diseases.

When did you realize a gene-network approach was needed?

During my graduate training in mathematics and molecular biology, I realized that many changes — and not just at the DNA level — lead to disease. When I started this work in 2000, very few people thought this way. Luckily, our collaborators at the Icelandic pharmaceutical company deCODE Genetics and at the University of California, Los Angeles, immediately joined our push towards a more holistic, gene-network approach.

Is the traditional, reductionist appoach of searching for 'the disease gene' pointless?

Absolutely not. Genome-wide association studies comparing individuals' genomes identify the dominant genetic variations that lead to disease — if not 'the disease gene'. We've developed statistical methods to determine connections among genes on the basis of their activities in different tissues. We then combine these findings from humans with mouse models of disease to assess how perturbations to gene-expression networks could cause disease traits.

What computational power is involved in this approach?

We needed high-performance computing equivalent to 7,000 central processing units. Without that scale of computational horsepower, we couldn't have done this work.

Is Merck, Rosetta's parent company, adopting this approach?

Yes. Once you know how a whole network of genes is perturbed, you can better assess the best points for therapeutic intervention.

Are clinicians collecting the samples necessary for these types of studies?

Not as quickly as we'd like, but once clinicians see the point they will do it. To uncover the relevant gene networks, we need complementary sets of disease and normal tissues. For example, one clinician is collecting matched liver, stomach and fat tissues from his gastric bypass surgeries. These samples will help us to determine why the severity of diabetes is often greatly reduced following surgery. ■

MAKING THE PAPER

Benjamin List

N. STARN CK

Getting acetaldehyde to behave as a substrate for organic synthesis.

Organic chemists had all but given up on acetaldehyde when it came to certain types of reactions because this deceptively simple molecule has a tendency to go through many side reactions. Benjamin List's group at the Max Planck Institute for Coal Research in Mülheim an der Ruhr, Germany, have managed to tame the highly reactive molecule and use it in the Mannich reaction (a process for forming carbon–carbon bonds), opening the door to a broad range of applications in drug design.

Many small biological molecules come in two mirror-image forms, or enantiomers, that can have dramatically different biological effects. Chemical reactions that produce one enantiomer only were thought to be catalysed by either enzymes or heavy metals. But simple organic molecules such as amino acids recently burst on the scene as a third class of inexpensive catalysts for reactions with enantiomer selectivity, which are required for drug synthesis.

In 2000, List used the amino acid proline to catalyse a Mannich reaction — which combines a carbonyl, an aldehyde, and an amine compound to produce β-amino carbonyl compounds, and is used widely in the synthesis of biologically active molecules, including medicinal drugs. The new proline-catalysed Mannich reaction yielded high amounts of only one enantiomer.

But the simplest of all substrates, acetaldehyde, still wouldn't work. Acetaldehyde has many desirable qualities for chemistry: it's a small, plentiful and inexpensive molecule. But it also likes to react with itself. "The general feeling was that it would not work because it was considered a really troublesome reagent," says List.

His view changed in 2006, when his group discovered that the substrate *N*-tert-butoxycarbonyl (*N*-Boc)-imine gave very high amounts of essentially a single enantiomer in proline-catalyzed Mannich reactions. "Because these reactions were so extremely efficient, we decided to give acetaldehyde another try," says List.

The first time List's group tried combining acetaldehyde with *N*-Boc-imines in a proline-catalysed Mannich reaction they obtained only about 1% of product. "The yields were tiny, but the product was formed as essentially a single enantiomer, so in a sense this was encouraging," he explains.

Over the next few months, colleagues tried to improve the yield without much success. Then, during a Monday morning jog, inspiration struck and List realized how to tackle the problem. Back in the lab he put together a four person team that sketched out the different conditions to test and what kind of products they should synthesize to demonstrate the reaction's applications. Four weeks later they had accomplished their goal (see page 453). They had optimized the reaction and were able to synthesize a newly approved anti-AIDS drug and several other biologically active substances.

List says pharmaceutical companies have already expressed an interest in this work and a number of researchers, including himself, are trying to use acetaldehyde in other types of chemical reactions. "The biggest challenge was not really a technical or chemical one but rather having to give up the notion that it was impossible to use acetaldehyde in these types of reactions," he says. "It was not easy to convince ourselves that this would work, given the initial ridiculous yields." ■

FROM THE BLOGOSPHERE

There is never a dull moment on 'In the Field', *Nature* reporters' blog for scientific conferences and events. Rachel Courtland recently blogged from the American Physical Society conference in New Orleans (http://tinyurl.com/37jjuy) on a Town Hall talk on ultra-high pressures: "The basic idea? Squeeze hard on any element, ratchet up the temperature, and you end up with some unexpected new phases. At high enough pressures and temperatures, ordinary, transparent water becomes opaque. Push even further, and it becomes transparent. Dive down into Jupiter's atmosphere, and the pressures quickly become so high that even hydrogen becomes metallic."

Simultaneously, Eric Hand was rocking at the lunar and planetary science conference in Houston (http://tinyurl.com/3axrrc). Read about the graduate student who was shot at Northern Illinois University, but still turned in his conference poster on time, and enjoy a valedictory account of NASA administrator Mike Griffin's lecture and the characteristically blunt question and answer session that followed it. ■

Visit Nautilus for regular news relevant to *Nature* authors ▸ http://blogs.nature.com/nautilus and see Peer-to-Peer for news for peer reviewers and about peer review ▸ http://blogs.nature.com/peer-to-peer.

nature

Vol 452 | Issue no. 7186 | 27 March 2008 **www.nature.com/nature**

EDITORIAL

LONDON nature@nature.com
The Macmillan Building, 4 Crinan Street, London N1 9XW
Tel: +44 (0)20 7833 4000 Fax: +44 (0)20 7843 4596/7
EDITOR-IN-CHIEF: Philip Campbell
PUBLISHING EXECUTIVE EDITOR: Maxine Clarke
EDITORIALS: Philip Campbell, M Mitchell Waldrop
NEWS/FEATURES/ONLINE NEWS: Oliver Morton, Geoff Brumfiel, Daniel Cressey, Michael Hopkin, Nicola Jones, Anna Petherick, Katharine Sanderson, Sarah Tomlin, Gaia Vince
BOOKS & ARTS/CORRESPONDENCE & ESSAYS/COMMENTARIES: Sara Abdulla, Joanne Baker, Lucy Odling-Smee, Sarah Tomlin
NATURE PODCAST: Sara Abdulla, Adam Rutherford, Kerri Smith, Charlotte Stoddart
NEWS AND VIEWS: Tim Lincoln, Andrew Mitchinson, Sadaf Shadan, Richard Webb
PHYSICAL, CHEMICAL AND EARTH SCIENCES: Karl Ziemelis, Rosamund Daw, Joshua Finkelstein, Magdalena Helmer, Juliane Mössinger, Karen Southwell, John VanDecar, Liesbeth Venema
BIOLOGICAL SCIENCES: Ritu Dhand, Lesley Anson, Tanguy Chouard, Henry Gee, Marie-Thérèse Heemels, Rory Howlett, Claudia Lupp, Barbara Marte, Deepa Nath, Ursula Weiss **INSIGHTS/REVIEWS/PROGRESS:** Lesley Anson
SUBEDITORS: Colin Sullivan, Sarah Archibald, Anne Blewett, Catherine Cassidy, Davina Dadley-Moore, Isobel Flanagan, Paul Fletcher, Jenny Gillion, Dinah Loon, David Price, Nicola Robinson, Chris Simms, Anna York
EDITORIAL PRODUCTION: James McQuat, Alison Hopkins, Marta Rusin, Charles Wenz, Lauren Wethmar
MANUFACTURING PRODUCTION: Jenny Henderson, Stewart Fraser, Susan Gray, Jocelyn Hilton, Yvonne Strong
ART AND DESIGN: Martin Harrison, Wesley Fernandes, Madeline Hutchinson, Barbara Izdebska, Paul Jackman, Fern McNulty, Nik Spencer
ADMINISTRATION: Karen Jones, Helen Anthony, Jayne Henderson, Diane Kempinski, Aimee Knight, Alison McGill, Jenny Meyer, Nichola O'Brien, Naomi Thornhill, Holly Welham
PRESS OFFICE: Ruth Francis, Katherine Anderson, Jen Middleton, Rachel Twinn

WASHINGTON DC nature@naturedc.com
968 National Press Building, 529 14th St NW, Washington DC 20045-1938
Tel: +1 202 737 2355 Fax: +1 202 628 1609
EDITORIAL: Eric Hand, Gene Russo, Leslie Sage, Jeff Tollefson, M Mitchell Waldrop, Alexandra Witze **ADMINISTRATION:** Katie McGoldrick, Kenneth Simpson

NEW YORK nature@natureny.com
75 Varick St, 9th Floor, New York, NY 10013-1917
Tel: +1 212 726 9200 Fax: +1 212 696 9006
EXECUTIVE EDITOR: Linda Miller
EDITORIAL: I-han Chou, Chris Gunter, Kalyani Narasimhan, Helen Pearson

BOSTON nature@boston.nature.com
25 First Street, Suite 104, Cambridge, MA 02141
Tel: +1 617 475 9275 Fax: +1 617 494 4960
EDITORIAL: Angela Eggleston, Joshua Finkelstein, Heidi Ledford **ADMINISTRATION:** Eric Schwartz

SAN FRANCISCO nature@naturesf.com
225 Bush Street, Suite 1453, San Francisco, CA 94104
Tel: +1 415 403 9027 Fax: +1 415 781 3805
EDITORIAL: Erika Check Hayden, Natalie DeWitt, Alex Ecclestone
ADMINISTRATION: Jessica Kolman

SAN DIEGO r.dalton@naturesf.com
3525 Del Mar Heights Road, PMB No. 462, San Diego, CA 92130
Tel: +1 858 755 6670 Fax: +1 858 755 8779
EDITORIAL: Rex Dalton

MUNICH a.abbott@nature.com
Josephspitalstrasse 15, D-80331 München
Tel: +49 89 549057-13 Fax: +49 89 549057-20
EDITORIAL: Alison Abbott, Quirin Schiermeier

PARIS d.butler@nature.com
2 rue Moreau Vincent, 37270 Veretz Tel: +33 2 47 35 72 15
EDITORIAL: Declan Butler

TOKYO editnature@natureasia.com
Chiyoda Building 5-6th Floor, 2-37 Ichigaya Tamachi, Shinjuku-ku, Tokyo 162-0843
Tel: +81 3 3267 8751 Fax: +81 3 3267 8754
EDITORIAL: David Cyranoski, Mika Nakano, Akemi Tanaka

CONTRIBUTING CORRESPONDENTS
AUSTRALASIA: Carina Dennis Tel: +61 2 9404 8255
INDIA: K. S. Jayaraman Tel: +91 80 26966579
ISRAEL: Haim Watzman Tel: +972 2 6714077
SOUTH AFRICA: Michael Cherry Tel: +27 21 886 4194
WASHINGTON DC: Meredith Wadman Tel: +1 202 626 2514
MISSOURI: Emma Marris Tel: +1 573 256 0611

NATURE ONLINE

www.nature.com/nature
CHIEF TECHNOLOGY OFFICER: Howard Ratner **PUBLISHING DIRECTOR, NATURE.COM:** Timo Hannay
WEB PRODUCTION/DESIGN: Jeremy Macdonald, Glennis McGregor, Alexander Thurrell
WEB PRODUCTION TECHNOLOGIES: Paul Donohoe **APPLICATION DEVELOPMENT:** Peter Hausel

PUBLISHING

LONDON feedback@nature.com
The Macmillan Building, 4 Crinan Street, London N1 9XW
Tel: +44 (0)20 7833 4000 Fax: +44 (0)20 7843 4596/7
MANAGING DIRECTOR: Steven Inchcoombe
PUBLISHER: Steven Inchcoombe
ASSISTANT PUBLISHER: Samia Mantoura
PUBLISHING ASSISTANT: Claudia Banks

TOKYO feedback@natureasia.com
Chiyoda Building 5-6th Floor, 2-37 Ichigaya Tamachi, Shinjuku-ku, Tokyo, 162-0843
Tel +81 3 3267 8751 Fax +81 3 3267 8754
PUBLISHING DIRECTOR — ASIA-PACIFIC: David Swinbanks
ASSOCIATE DIRECTOR — ASIA-PACIFIC: Antoine E Bocquet

DISPLAY ADVERTISING

MANAGEMENT: John Michael

NORTH AMERICA display@natureny.com
NEW ENGLAND: Sheila Reardon Tel +1 617 494 4900 Fax +1 617 494 4960
NEW YORK/MID-ATLANTIC/SOUTHEAST: Jim Breault Tel: +1 212 726 9334 Fax +1 212 696 9481
MIDWEST: Mike Rossi Tel: +1 212 726 9255 Fax: +1 212 696 9481
WEST COAST SOUTH: George Lui Tel: +1 415 781 3804 Fax: +1 415 781 3805
WEST COAST NORTH: Bruce Shaver Tel: +1 415 781 6422 Fax +1 415 781 3805

EUROPE/REST OF WORLD display@nature.com
GERMANY/SWITZERLAND/AUSTRIA/OTHER EUROPE: Sabine Hugi-Fürst
Tel +41 52 761 3386 Fax. +41 52 761 3419
UK/IRELAND/FRANCE/BELGIUM: Jeremy Batts
Tel +44 (0)20 7843 4959 Fax: +44 (0)20 7843 4749
SCANDINAVIA/THE NETHERLANDS/ITALY/SPAIN/PORTUGAL/ISRAEL/ICELAND Graham Combe
Tel. +44 (0)20 7843 4914 Fax. +44 (0)20 7843 4749

ASIA-PACIFIC display@natureasia.com
JAPAN: Kate Yoneyama, Ken Mikami
Tel. +81 3 3267 8765 Fax. +81 3 3267 8746
GREATER CHINA/SINGAPORE: Gloria To
Tel: +852 2811 7191 Fax: +852 2811 0743

SPONSORSHIP

EUROPE/NORTH AMERICA e.green@nature.com
NATURE BUSINESS DEVELOPMENT EXECUTIVE: Emma Green
Tel +44 (0)20 7833 4000 Fax +44 (0)20 7843 4749

NATUREJOBS

naturejobs@nature.com

Please refer to panel at the start of the *NatureJobs* section at the back of the issue.

MARKETING & SUBSCRIPTIONS

USA/CANADA/LATIN AMERICA subscriptions@natureny.com
Nature Publishing Group, 75 Varick St, 9th Floor, New York, NY 10013-1917
Tel. (USA/Canada) +1 866 363 7860; (outside USA/Canada) +1 212 726 9365
MARKETING: Sara Girard **FULFILMENT:** Karen Marshall

JAPAN/CHINA/KOREA subscriptions@natureasia.com
Chiyoda Building 5-6th Floor, 2-37 Ichigaya Tamachi, Shinjuku-ku, Tokyo, 162-0843
Tel: +81 3 3267 8751 Fax: +81 3 3267 8746
MARKETING/PRODUCTION: Keiko Ikeda, Takeshi Murakami

EUROPE/REST OF WORLD subscriptions@nature.com
Nature Publishing Group, Subscriptions, Brunel Road, Basingstoke, Hants RG21 6XS, UK
Tel: +44 (0)1256 329242 Fax +44 (0)1256 812358
MARKETING: Katy Dunningham, Elena Woodstock

INDIA npgindia@nature.com
Nature Publishing Group, 3A, 4th Floor, DLF Corporate Park, Gurgaon 122002
Tel. +91 124 2881053/54 Fax +91 124 2881052
HEAD OF BUSINESS DEVELOPMENT, INDIA: Jaishree Srinivasan **MARKETING:** Harpal Singh Gill

Annual subscriptions (including post and packing)

INSTITUTIONAL/CORPORATE RATE:	$2,730
PERSONAL RATE:	$199
STUDENT RATE:	$99
POSTDOC RATE:	$119

Printed in USA. Individual rates available only to subscribers paying by personal check or credit card. Orders for student/postdoc subscriptions must be accompanied by a copy of student ID. Rates apply to USA, Canada, Mexico/Central & South America
Add 7% GST tax in Canada (Canadian GST number 140911595).
BACK ISSUES: US$ 20.00

SITE LICENSES, FULFILMENT & CUSTOMER SERVICES

feedback@nature.com
SITE LICENSES: npg.nature.com/libraries
OPERATIONS DIRECTOR: John Carroll
FULFILMENT: Dominic Pettit **CUSTOMER SERVICE:** Gerald Coppin

SMALL DOTS, FINE PATTERNING

Hamamatsu Photonics Micro-Droplet technology brings a new era of microfabrication.

DNA microarray applications have expanded rapidly with increasing capacity, accomplished through smaller spot size Hamamatsu Photonics has now made it possible to cut the spot size of current arrays to a mere 1μm in diameter

This is just one application of the Hamamatsu Photonics micro-droplet technology, a method that uses electrostatic force to guide samples with tremendous accuracy onto substrates. An electric pulse creates the charge that transports the samples, and the "on-demand" sample size is readily adjusted by vary ng the length of the pulse Samples can be 10 femtoliters or smaller in volume

Unlike conventional spotting technologies, like the ink jet printer, Hamamatsu Photonics micro-droplet technology can even handle viscous samples such as glycerin and UV cured resins. The resins can be patterned in lines less than 5μm in width. The micro-droplet technology thus has a wide range of applications in microfabrication: printing gold nanosuspensions that can be used for fabricating circuits, spotting the ink on unpainted pixels of the red-green-blue filters used in flat panel displays, or the creation or repair of photomasks used in fabricating semiconductors.

Hamamatsu Photonics researchers came across the idea of the micro-droplet technology when working on the optical properties of single molecules—another example of Hamamatsu Photonics "following the light" to far reaching technological applications.

Basic principle of the Micro-Droplet technology

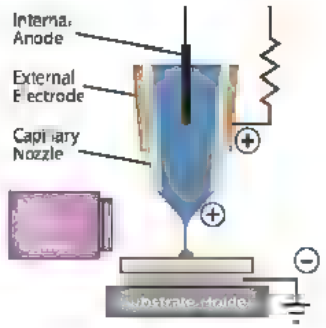

Hamamatsu Photonics' expertise with light has revealed an elegant solution to a complex problem.

HAMAMATSU

Photon is Our Business

For more information, visit our site at: http://jp.hamamatsu.com/en/rd/publication

HAMAMATSU PHOTONICS K. K.
325-6, Sunayama-cho, Naka-ku, Hamamatsu City, 430-8587 Japan Telephone: (81)53-452-2141, Fax: (81)53-456-7889 URL http://www.hamamatsu.com

ELECTROCOMPETENT STRAINS
NOW AVAILABLE

NEW ENGLAND BIOLABS

Competent Cells from New England Biolabs

NEW STRAINS, NEW FORMATS, NEW CHOICES

At NEB, we make transformation as simple as selecting the best strain for your experiment. Our expanded line of competent cells includes a variety of strains for cloning and expression, as well as strains with unique properties (see chart). For added convenience, we offer a choice of efficiencies, formats and customized packaging. Choose the superior performance and quality of competent cells from New England Biolabs.

Advantages:

- Extremely high transformation efficiencies
- Phage T1 resistance (*fhuA2*) preserves clone integrity
- Choice of protocols: high efficiency or 5 minute transformation
- Nonspecific endonuclease activity eliminated, resulting in highest quality plasmid preparations
- Express difficult or toxic proteins with T7 Express strains containing $lacI^q$ and/or a novel lysY variant
- Obtain colonies faster than any other commercial strain with NEB Turbo
- SOC Outgrowth Media and pUC19 Control Plasmid included
- Free of animal products

[illegible]	Strain	[illegible]
Obtain colonies faster than any other commercial strain (6.5 hours)	NEB Turbo Competent *E. coli*	C2984H/I
Versatile cloning strain	NEB 5-alpha Competent *E. coli*	C2987H/I
Cloning of toxic genes	NEB 5-alpha $F'I^q$ Competent *E. coli*	C2992H/I
Cloning of large plasmids and BACs	NEB 10-beta Competent *E. coli*	C3019H/I
Growth of unmethylated plasmids	ER2925 Competent *E. coli*	C2925H/I

Expression strain characteristics	Strain	NEB
Most popular non-T7 protein expression strain	BL21 Competent *E. coli*	C2523H/I
Added control of IPTG induced expression with non-T7 plasmids	BL21-Gold Competent *E. coli*	C3037H/I
Most popular T7 protein expression strain	T7 Express Competent *E. coli*	C2566H/I
Reduced basal expression	T7 Express $lysY/I^q$ Competent *E. coli*	C3016H/I
Tight control of protein expression by inhibition of T7 RNA Polymerase	T7 Express $lysY/I^q$ Competent *E. coli*	C3010H/I
Highest level of protein expression control	T7 Express $lysY/I^q$ Competent *E. coli*	C3013H/I
For crystallography experiments/SeMet labeling	T7 Express $lysY/I^q$ Competent *E. coli*	C3022H/I

† *Available as subcloning efficiency* * *Available as electrocompetent cells*

For more information and our international distribution network, please visit www.neb.com
For a copy of our new **Competent Cell Brochure**, please visit: **www.neb.com/literaturerequest**

New England Biolabs Inc. 240 County Road, Ipswich, MA 01938 USA 1-800-NEB-LABS Tel. (978) 927-5054 Fax (978) 921-1350 info@neb.com
Canada Tel. (800) 387-1095 info@ca.neb.com • **China** Tel. 010-62378266 beijing@neb-china.com • **Germany** Tel. 0800/246 5227 info@de.neb.com
Japan Tel. +81 (0)3 5669 6191 info@neb-japan.com • **UK** Tel. (0800) 318486 info@uk.neb.com

NEW ENGLAND BioLabs® Inc.
the leader in enzyme technology

nature

www.nature.com/nature Vol 452 | Issue no. 7186 27 March 2008

1917–2008: A Space Optimist

Arthur C. Clarke's technological prescience deserves to be honoured; his endless optimism needs to be cherished.

It took an unusual mind for a Londoner living in 1944 to see the V2 rockets bombarding the city as a cause for hope. But the intellectual milieu of the time, enriched as it was by the cosmic visions of the likes of Desmond Bernal, J. B. S. Haldane and Olaf Stapledon, produced a few such optimists. Freeman Dyson, a brilliant young mathematician then working on the more traditional bombardments crossing the North Sea in the other direction, saw his hope in the opportunity costs: enemy resources spent on inefficient rockets could not be spent on more effective fighter aircraft. Arthur C. Clarke, then a young radar engineer and soon to be a budding science-fiction author, saw his hope in the fact that, en route from mainland Europe to England, the rockets were passing through outer space, and the technology required for travel to other planets was thus at hand. Legend has it that when Clarke and his friends from the British Interplanetary Society heard a V2 while drinking in a pub, they stood and cheered the space age that was about to begin.

Such optimism comes from an ability to look beyond the obvious, an ability that served Clarke, who died on 19 March, as both a writer and a prognosticator. Clarke, who founded his writing in rigorous science, foresaw not just the technology of the geostationary communications satellite, but also the effect that such distance-denying technologies would have in drawing the world together. As he said with typical optimism to the dignitaries signing the agreements in 1964 that created the Intelsat system: "You have just signed the first draft of the Articles of Federation of the United States of Earth." But he did not just see upsides: in 1960, he published in *Playboy* a wry little piece on decadence and satellite-delivered porn called "I Remember Babylon".

Wryness was a frequent tool. But Clarke's aim in his writing was mostly to inspire wonder, specifically the wonder of transcendence — the wonder in gazing into a featureless artefact and reporting back, stunned, "My God, it's full of stars!". In that moment from *2001: A Space Odyssey*, as in many other instances, Clarke showed his readers the wonder of the scientific threshold about to be crossed, the cosmos about to be joined. Yet he did so with a humanity that insisted that his readers were not insignificant in the face of such immensity — or rather, that their insignificance did not diminish them, perched as they were for ever on the shores of what was to come.

The book's technological vision of lunar cities and men bound for Jupiter, magnificently realized in film by Stanley Kubrick, was flanked by just such shores — the dawn of human consciousness in the ape-man Moonwatcher, the space-age Odysseus's return through the pit of stars to a home about to be utterly changed. Moonwatcher or moon-walker, Clarke was saying, we are always on the brink of the beginning, always in some way pre-historical. Seeing the whole dazzling day to come in the first thin cord of the Sun was his great delight.

In the 1970s, Dyson, by then a luminary of mathematical physics, explored the possibilities of life running off into the furthest reaches of the future. It was an idea to stir Clarke's soul. As he wrote in response:

> "[Not for] billions of years, will the real history of the universe begin.
>
> It will be a history illuminated only by the reds and infrareds of dully glowing stars that would be almost invisible to our eyes; yet the sombre hues of that all-but-eternal universe may be full of color and beauty to whatever strange beings have adapted to it. They will know that before them lie ... years to be counted literally in trillions.
>
> They will have time enough, in those endless aeons, to attempt all things, and to gather all knowledge. They will be like gods, because no gods imagined by our minds have ever possessed the powers they will command. But for all that, they may envy us, basking in the bright after glow of Creation, for we knew the universe when it was young."

It is a rare gift — although one potentially shared by any scientist — to find satisfied joy in being poised before the transcendent, filled with hope by the wonders that the intellect, rather than blind faith, promises to those who explore it. Clarke devoted himself to passing on that gift, and we should cherish it. ■

Critical journalism

Science coverage is on the wane when public scrutiny of science is more important than ever.

Watch five hours of US cable news, and on average you will see around 35 minutes on election campaigns, another 36 minutes on US foreign policy, and 26 minutes on crime — but only about one minute on science and technology, slightly more on the environment, and only a little over 3 minutes on medicine and health care. This is not just an issue with cable: science fares little better in other forms of television, radio, or print news, according to the Pew Research Center's *The State of the News Media 2008* report, released on 17 March.

It would be a mistake to get too alarmed about this analysis. Science news in the United States has indeed been squeezed to around 2% of the total since the events of 11 September 2001. But it was never that high, hovering around 4–5% from the mid-1970s until 2001. And the drop does not reflect a falling public interest in science, as much as the media's increased emphasis on foreign policy, war and the homeland: the diversity of US news coverage has decreased across the board since 9/11.

The Pew Center's numbers offer another reason not to be gloomy:

the Internet is overtaking television as the public's main source of science news. This means that a larger global audience can now access, on demand, a great diversity of science coverage from media outlets around the world. Moreover, the public are no longer just passive consumers of information. The Internet is now the first place people go to look for more information on a scientific topic, such as stem cells or climate change. Thanks to the Internet, in short, one could argue that the overall state of science communication is better now than at any time in the past.

Yet there is no reason to be complacent. As the media industry moves online, some shakeout is inevitable. Straight news is becoming a commodity, which will be dominated by fewer players. Independent science desks and media can have a future in this environment, but only if they move up the food chain and provide proactive, deeper, must-read analyses instead of me-too articles reacting to the latest press releases.

In that context, perhaps the most worrisome finding in the Pew report is that this type of resource-intensive science coverage is precisely the most threatened: as the newspaper industry responds to falling circulation with sweeping cuts, science desks are among the first to suffer.

Media executives should pause to rethink these cuts to science desks and coverage on two counts. One is that this choice is often influenced by the widespread notion that science is of comparatively little interest to readers. According to Pew Center data, however, around two-thirds of all those who search online for news are after science and health news — second only to the weather — with technology coming third, ahead of politics and business. That trend is confirmed in reports published this past December by the European Commission.

Another, and more important, reason to sustain high-quality science journalism is that, in this context as much as any other, the media have a responsibility (with rewards in audience response) to fulfil their watchdog role. Many contemporary societal issues are both science-related and complex. Science reporters are essential for keeping tabs on government at every level, ensuring that decision-makers listen to the best experts and scientific evidence available. They should also be in the front line of countering the misrepresentation of science, whether by anti-science groups, multinational corporations, or politicians — or indeed, by scientists and their institutions hyping their own work to gain fame and funding. ■

A reprogramming rush

Stem-cell research is in danger of falling foul of haste.

In the most recent of his series of stunning articles on induced pluripotent stem (iPS) cells (T. Aoi *et al. Science* doi:10.1126/science.1154884; 2008), Shinya Yamanaka made a couple of small mistakes. Happily, he has since given plausible explanations for the mistakes, and has effectively argued that they do not affect the article's central conclusions — thus heading off worries (and one unsubstantiated accusation) that the errors signalled deeper problems with the article.

Still, the incident illustrates why there is cause for concern as scientists hop on the iPS bandwagon (see page 406). The very existence of such carelessness by the leading light of iPS cell research, a scientist known for his thorough, careful work, shows how much the race mentality has taken over the field. The paper was published online a mere five and a half weeks after it was submitted. Other key articles in the field show similar signs of being rushed for publication. One biotech company recently announced its iPS cell results without even bothering to publish (see *Nature* 452, 132; 2008). And authors have been pushing journal editors to speed up peer review — under the threat of taking the paper elsewhere — which puts even more pressure on the small circle of reviewers sufficiently versed in iPS cell science.

Competition is good. Indeed, it is a major reason why iPS cell research has flourished since 2006, when Yamanaka first showed that a handful of genes can reprogram a cell to a pluripotent state. Nonetheless, the fast-moving fields of science are showing some unpleasant tendencies. Researchers are cutting corners and making mistakes. They are making over-hyped promises that will probably be broken. And they are neglecting other valuable fields of research. All this has already been seen in iPS cell research.

Hype may also carry researchers away from their mission and raise the spectre of fraud. Indeed, as Alan Trounson, head of the California Institute of Regenerative Medicine in San Francisco recently told *Nature Reports Stem Cells*, "excessive" media attention on iPS cell research could "separate science from reality" in the same way it did during the therapeutic-cloning scandal surrounding South Korea's Woo Suk Hwang. "Cool heads and a close connection with the lab should prevail in order to ensure science progresses truly by reliable evidence," he says.

The errors in Yamanaka's article are unfortunate — not least because they play into the hands of those who want to tarnish the science or the scientists. The criticism of Yamanaka's article came from an anonymous source who seemed bent on a personal attack. From the address "Reprogrammer Yamanaka" on 29 February, the e-mailer sent an account of Yamanaka's mistakes to journal editors, science journalists and scientists, scolding Yamanaka for his "embarrassing inconsistencies" and calling on him "to either retract their paper or provide meticulous and thorough new analysis".

Yes, this attack was overly dramatic. And yes, Yamanaka owned up to his mistakes with commendable speed and honesty. But even so, this incident should be a wake-up call.

Post-Hwang, scientists and journals undertook much soul-searching about what went wrong. Some came to the bad-apple theory — that Hwang was just an anomaly. Most, rightly, saw it as a deeper problem that could affect any field of science. In the aftermath, many researchers vowed to redouble their efforts to guard against honest mistakes (usually attributed, as Hwang did at first, to the rush to submit articles), as well as against the whole spectrum of selective presentation of data, manipulation of images and outright fraud. iPS cell research may be the first substantial test of these efforts. ■

TaKaRa

PCR PRODUCTS

Switch to Superior High Fidelity PCR

PrimeSTAR®

Top Five Reasons to Switch to PrimeSTAR®:

- **Higher Accuracy:** A strong exonuclease activity results in an extremely low error rate, with only 15 errors per 480,000 bp on a GC-rich template.
- **Higher Efficiency:** Higher than *Taq* Polymerase.
- **Robust Amplifications:** A single PCR cycling protocol can be used to amplify products of varying sizes.
- **Greater Specificity:** The antibody mediated Hot Start formulation prevents false initiation events during reaction assembly.
- **Excellent with GC-Rich Targets:** Robust performance with GC-rich templates using the GC buffer formulation.

Amplification Efficiency of a 2 kb Human Genomic DNA Fragment (DCLRE1A). Excellent sensitivity and yield are observed when amplifying with PrimeSTAR®. Quantities: Lane1: 0 ng (dH_2O), Lane 2: 100 pg, Lane 3: 1 ng, Lane 4: 10 ng, Lane 5: 100 ng.

TaKaRa

See our website Today!

www.takara-bio.com

Japan:
Takara Bio Inc.
+81 77 543 7247
www.takara-bio.com

USA:
Takara Bio USA
888-251-6618
www.takarabiousa.com

Europe:
Takara Bio Europe S.A.S.
+33 1 3904 6880
www.takara-bio.eu

China:
Takara Biotechnology (Dalian) Co., Ltd.
+86 411 8764 1681
www.takara.com.cn

Korea:
Takara Korea Biomedical Inc.
+82 2 2081 2525
www.takara.co.kr

RESEARCH HIGHLIGHTS

PARTICLE PHYSICS

Nearly caught in a trap

Phys. Rev. Lett. **100**, 113001 (2008)

Why is the Universe mostly matter, when the Big Bang should have produced equal amounts of matter and antimatter? Researchers from the Antihydrogen Trap collaboration at CERN, near Geneva, have nudged along the search for an answer.

Gerald Gabrielse of Harvard University and his team hope to measure subtle differences in the properties of antihydrogen and hydrogen that might explain antimatter's demise. But antihydrogen annihilates on the walls of a confining apparatus too quickly for it to be probed in detail.

So the team prolonged the interaction of antiprotons and positrons using a form of magnetic confinement called an Ioffe trap. However, full proof that antihydrogen is trapped inside its new container still awaits.

SEDIMENTOLOGY

Natural beauty

Nature Phys. doi:10.1038/nphys911 (2008)

The beauty of limestone landscapes such as those loved by the poet W. H. Auden comes from sculptural erosion. That of landscapes of travertine, another form of calcium carbonate (pictured below), is built through patterns of deposition. A new way of modelling this growth has been developed by John Veysey and Nigel Goldenfeld of the University of Illinois at Urbana-Champaign.

The authors simulated the environment as a lattice of rule-obeying cells, an approach that yielded similar results to data they collected from two years of time-lapse photography of travertine pools and terraces forming in hot springs.

The method ignores the microscopic specifics of deposition and thus might prove applicable to other environments.

K. RHENDA/NATURE-SPRINGER.COM

R. CALDWELL

A secret visual world

Curr. Biol. **18**, 1–6 (2008)

The mantis shrimp *Odontodactylus* (pictured) has a secret and unique way of looking at the world that it may use for sexual signalling. Whereas humans can see only the colour and intensity of light, some invertebrates can see linearly polarized light. This gives them cues to navigate and helps them communicate surreptitiously.

Justin Marshall of the University of Queensland in Brisbane, Australia, and his colleagues now report that species of *Odontodactylus* can discern circularly polarized light, the first organism shown to do this. The mantis shrimps even have specialized cells in their eyes that distinguish between right- and left-handed circularly polarized light.

GENETICS

Self-sterile squirts

Science doi:10.1126/science.1152488 (2008)

Avoidance of self-fertilization in the hermaphrodite sea squirt *Ciona intestinalis* intrigued the genetic pioneer Thomas Hunt Morgan. His breeding experiments have now been replicated by Yoshito Harada of Nagoya University in Toba, Japan, and colleagues, who have identified two cooperatively acting pairs of genes controlling self-sterility, each pair containing a 'male' and a 'female' gene.

The male determinant is thought to encode a receptor in sperm that recognizes the 'self' product of the female gene, which is part of the matrix surrounding the egg. Sperm thus fail to attach to the matrix of an egg from the same individual.

CELL IMAGING

Sweet glow of success

Angew. Chem. Int. Edn **46**, 2394–2397 (2008)

Seeing where particular fat and sugar molecules congregate inside live cells has been made easier by chemists at the University of California, Berkeley, who have found a way to fluorescently label these biomolecules without causing other constituents of the cell to glow.

Producing pictures of particular proteins and nucleic acids inside living cells is fairly routine, but achieving good pictures of fats and sugars has proved more difficult, the background fluorescence tends to be too strong.

Matthew Hangauer and Carolyn Bertozzi designed a reagent with an ester bond that keeps its fluorescence quenched. When the reagent meets its target a chemical reaction breaks the bond, causing the labelled compound to glow.

PHYSICS

Universal freeze

Phys. Rev. Lett. **100**, 093003 (2008)

An instrument called a reverse coilgun may soon bring atoms to a full stop. Using a series of independently controlled coils, physicists have successfully slowed a beam of paramagnetic neon atoms from 447 to 56 metres per second.

The approach, devised by Mark Raizen at the University of Texas in Austin and his

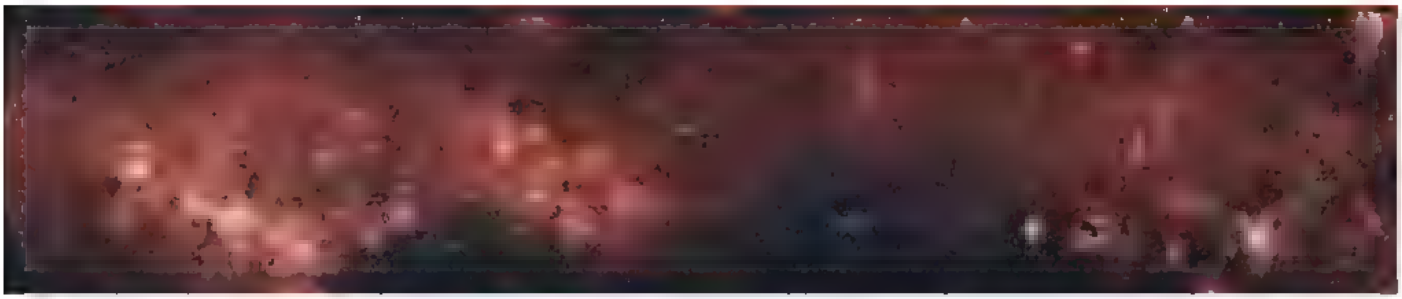

NASA/JPL-CALTECH/UNIV WISCONSIN

colleagues, might eventually be able to halt any atom that has an unpaired electron. Slowed atoms could then be held in a magnetic trap.

Containing and cooling atoms in this way could lead to the study of a process such as β-decay in tritium, which has never been trapped before.

COSMOLOGY

Separated by birth

Astron. J. **135**, 1106–1116 (2008)

The Small Magellanic Cloud is 2 billion or 3 billion years younger than the Milky Way and other nearby galaxies, a finding that suggests the galaxies of the early Universe did not form all at once, as had been previously thought.

The Small Magellanic Cloud is a dwarf galaxy about 200,000 light years from the Milky Way (pictured above). Katharina Glatt from the University of Basel, Switzerland, and her colleagues determined the age of its oldest star cluster using images taken by the Hubble Space Telescope.

Although other, older star clusters in the dwarf galaxy might have existed but not survived, the authors conclude it is more likely that star formation in the Small Magellanic Cloud began much later than imagined.

ZOOLOGY

Croc 'n' roll

J. Exp. Biol. doi:10.1242/jeb.015339 (2008)

Alligators use muscles normally employed in breathing to shunt their lungs around like a buoyancy aid, enabling them to perform death rolls and dives.

Todd Uriona and C. G. Farmer at the University of Utah in Salt Lake City discovered the secret of these manoeuvres by implanting electrodes in young alligators' diaphragm, pelvic, abdominal and rib muscles. These recorded how the creatures worked those muscles to shift the lungs towards the tail during a dive — and then back towards the head to resurface. The same muscles move the lungs sideways when the alligator wants to roll.

PALAEOCHRONOLOGY

Righting the rings

Nature Geosci. doi:10.1038/ngeo128 (2008)

Palaeoclimate researchers can now use tree-ring records to make more precisely dated measurements further back than 12,400 years, the original maximum. Raimund Muscheler of Lund University in Sweden and his team used comparisons with isotopic data from ice cores to ascertain the true age of more ancient tree-ring chronologies that until now had 'floated' in time.

The abundances of both carbon-14 and beryllium-10 vary with solar activity. The researchers used this correlation to link the floating tree-ring records, which contain carbon-14, to a period chronicled in ice cores from Greenland, which are dated by their beryllium-10 content.

ECOLOGY

Better than bleaching

Proc. R. Soc. Lond. B doi:10.1098/rspb.2008.0069 (2008)

A shift in the composition of their symbiotic algae can enable corals to acclimatize after periods of higher water temperatures leave them 'bleached'.

Ray Berkelmans of the Australian Institute for Marine Sciences in Townsville, Queensland, and his colleagues monitored the types of zooxanthellae inside the coral *Acropora millepora* on the Great Barrier Reef before and after natural bleaching. They report a dramatic reshuffling of the symbiotic community within the surviving coral. of the colonies with predominantly heat-sensitive algae before bleaching, 71% had predominantly heat-resilient varieties a few months later.

JOURNAL CLUB

Moty Heiblum
Weizmann Institute of Science, Rehovot, Israel

A physicist applauds evidence for the quantum spin Hall effect.

I have been fascinated by the ballistic (collisionless) motion of charge carriers in solids since the start of my career. In practice this motion is often impeded by unavoidable impurities in the solid. But when it works, the charge carriers maintain their quantum properties while dissipating a minimum amount of energy.

Applying a strong magnetic field perpendicular to a two-dimensional conducting layer can accomplish the feat. Then, the quantum Hall effect kicks in, forcing the charges to the edges of the sample where they skip along in so-called 'chiral edge channels'. Backward scattering is virtually eliminated because that would require the charges to find a way to the opposite edge, where charges move in the opposite direction.

Recently, Laurens Molenkamp of the University of Würzburg in Germany and his colleagues took a step towards verifying the quantum spin Hall effect (M. König *et al.* *Science* 318, 766–770; 2007). This is where chiral edge channels form spontaneously in semiconductor insulators with peculiar electronic structures — namely, where the valence band is energetically higher than the conduction band because of the strong spin-orbit interaction between electron spins and electron velocities. This means that spin-up electrons are carried only by edge channels moving in one direction and spin-down electrons are carried by edge channels moving in the opposite direction.

Molenkamp's team used a thin layer of mercury telluride sandwiched between two layers of mercury cadmium telluride. Because measuring spin current is difficult, they recorded the conductance of this middle layer to verify the ballistic transport that characterizes edge-channel transport. It was quantized, as predicted.

With further verification, the finding could lead to low-power devices based on the transport of spins rather than charges. Thus a quirk in the scientific field I have always loved might find a practical application.

Discuss this paper at **http://blogs.nature.com/nature/journalclub**

NEWS

£130-million cut to grants hits UK physical scientists

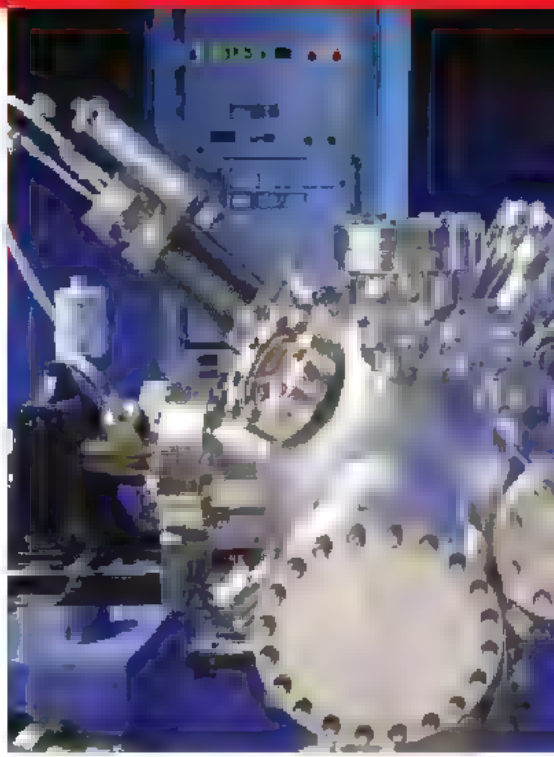

UK physicists, still reeling from massive funding cuts announced earlier this year, have learnt of worse to come. Roughly £130 million (US$260 million) is being slashed from research grants awarded by the Engineering and Physical Sciences Research Council (EPSRC), it announced on 17 March.

The EPSRC scale-back, which will mean grant cuts of up to 15% for investigator led research areas and job losses, comes just months after the UK Science and Technology Facilities Council announced funding cuts of around £80 million and a 25% reduction in grant money (see *Nature* 451, 386; 2008).

"This could be as big a problem as the £80 million cuts in the Science and Technology Facilities Council," says Philip Moriarty, a nanotechnologist at the University of Nottingham.

The EPSRC says its 'responsive-mode' grants will be affected by the cuts. These are grants for which proposals can be submitted on any topic related to engineering or physical sciences. The council says much of this money will instead be channelled into funding research in specific government-defined areas. But, overall, the amount of research funded by the council will drop by between 3% and 5%, it says.

Physicists, chemists, engineers and other researchers whose work does not fit into the six government-defined themes of nanoscience, health, IT, security environmental change and energy will have to fight hard for the remaining responsive-mode money. Even before these cuts, fewer than one-third of research-grant proposals submitted to the EPSRC were successful last year.

"The 12% to 15% cut to investigator-driven research, coupled with the EPSRC's knowledge-transfer strategy, means that truly innovative science is less likely to result from EPSRC funding," says Moriarty. "Work on fundamental quantum mechanics, of the type that won Tony Leggett the Nobel Prize in Physics in 2003, would struggle for funding in the current EPSRC system."

Peter Main, director of science and education at the UK Institute of Physics, says there is real concern about a shift from curiosity-driven research to applied programmes. "The real danger is that if you're not careful you end up funding lower-quality research simply because it is related to a particular topic," he says.

The EPSRC was given a budget increase of 18.6% by the government last year, but the extra money has been eaten up by inflation and its commitment to paying the full costs of research, which include maintaining equipment and building infrastructure. Rather than

String theorists hope to classify the cosmos

Physicists' search for a theory of everything is entering territory more familiar to biologists: taxonomy. A small team of theorists is meeting in Tucson, Arizona, in April to discuss how to classify the billions upon billions of different possible universes created by string theory, which describes fundamental particles and forces as vibrating strings.

"String theory is notorious for having a lot of solutions," says Keith Dienes, a physicist at the University of Arizona in Tucson. "We are having this big kick-off meeting to try and organize ourselves," he says. The String Vacuum Project aims to begin placing the various solutions into broad categories. If it works, then theorists may finally begin honing down the version of the theory that best fits with the cosmos.

But that's a pretty big if. There's no guarantee that the different possibilities will be easy to classify, or that the solution matching our Universe will be easy to find, according to Nathan Seiberg, a string theorist at the Institute for Advanced Study in Princeton, New Jersey. "I wouldn't hold my breath," he says, "but it is possible."

String theory is beloved by theorists because it is one of the few paradigms that promises to merge quantum mechanics, which explains the behaviour of particles on a subatomic level, with general relativity, which describes how gravity shapes large entities such as galaxies. To do so, the theory uses 10 or 11 dimensions of space-time. To make the theory resemble the physical world, theorists get rid of the extra dimensions by folding them up.

Like a sheet of paper, there are a nearly infinite number of ways to fold the extra dimensions, and each leads to a different 'vacuum' or fundamental state of the Universe. Some vacua have four forces, like ours, whereas others might have six or eight or ten. The strengths of those forces, the masses and number of fundamental particles, and even the number of dimension in a given cosmos, can all vary according to how the extra dimensions are folded.

The number of possibilities has been steadily rising in recent years and current sits at nearly 10^{500}, although there could be still more.

In the 1980s and 1990s, theorists had hoped that there might be a vacuum 'selection process' — a natural extension of string theory that would select a single vacuum resembling our Universe. But

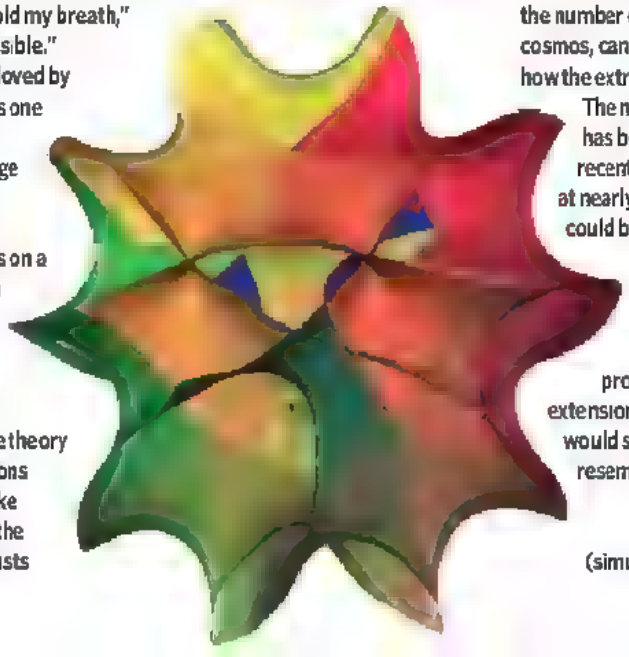

A cosmos folded up (simulation — not actual size).

A. J. HANSON, ND ANA JNIv

J. K NG-HOI MES/SPL

Investigator-led research will be hardest hit.

reducing all its funding by 3–5%, the EPSRC has decided to continue to fund the same number of PhD students and to prioritize support for the six themes.

It is not clear how much of the £130 million will be put into research grants in the themed areas and how much is covering inflation and the move to paying full costs.

"If what is happening is that the responsive mode is taking a bigger hit than [government themed research], the scientific community will not be happy with that," says Peter Cotgreave, director of public affairs at the Royal Society. "People find it very uncomfortable when the decision about what to fund is made before they apply."

Not everyone thinks the shift is necessarily bad. While saying there needs to be more clarity over the decision, Richard Pike, chief executive of the Royal Society of Chemistry, says that "more focus is a good thing".

And Sue Ion, vice-president of the Royal Academy of Engineering and a member of the EPSRC council, points out the proportion of funding given through the responsive-mode channel has traditionally been high at the EPSRC. "More attention needs to be given to the directed, theme-based topics," Ion says. "They [researchers] need to look for opportunities rather than go 'woe, woe and thrice woe.'"

In 2006/2007, the EPSRC funded 36% of all UK engineering and physical-sciences researchers, including 4,347 postgraduate and postdoctoral research assistants.

Unlike the Science and Technology Council cuts, there will be no high profile projects cancelled, but fewer grants may mean fewer jobs in the long run. "It will mean 3% to 5% fewer grants, and the average grant employs a postdoc," says Cotgreave. ■

Daniel Cressey

more recently, some theorists have begun to believe that there indeed may be as many as 10^{500} universes out there. They argue that we just happen to live in our cosmos because it can support life as we know it (see *Nature* 439, 10–12; 2006).

To date, nobody's bothered to look at how many different kinds of vacua there may be, or whether they fit into any sort of systematic categories, according to Dienes. That will be the goal of the new String Vacuum Project. Like biologists, physicists on the project will try to classify the 10^{500} solutions into different taxonomic ranks, such as kingdoms and phyla.

Among the project's main goals is to make string theory more predictive, says Gordon Kane of the University of Michigan in Ann Arbor. A major criticism of the theory is that it fails to provide experimental tests that would support or falsify it. If the vacuum project succeeds, then physicists would be able to find the class of vacua that fit with our own Universe. They can use those solutions to make predictions about what might show up in experiments such as the Large Hadron Collider — a massive proton-smasher being built at CERN, the European particle-physics lab outside Geneva in Switzerland. Kane says that, if the project works, he believes that evidence supporting string theory could emerge "within a few weeks" of the accelerator's start-up.

But others are less optimistic about the vacuum project's chances of success. There's no guarantee that the 10^{500} possibilities predicted by the theory will be easily categorized, and it's likely they won't be, says Seiberg. "It's a very complicated system," he says. Searching for the few solutions that match our own Universe will be worse than looking for a needle in a haystack, he adds. Still, he believes the project may yield interesting findings.

Others are more sceptical. Sifting through a near-infinite number of vacua provides no deeper understanding of the theory, according to mathematician Peter Woit of Columbia University in New York City, who is frequently critical of string theory. The fact that physicists are interested in a statistical approach is a sign of desperation, he argues. "It would be better to say, 'okay, [string theory] doesn't work.'"

Dienes accepts these criticisms, and concedes that the plan is "absolutely controversial". Nevertheless, he believes it is the best way forward. "The plethora of vacua is an urgent issue," he says. "I want to understand our space of possibilities." ■

Geoff Brumfiel

ON THE RECORD

"I've got a student working on an application where you enter a city and it will tell you what grades and types of marijuana are available."

Clemson University economist Todd Kendall discusses the rising trend of websites that act as consumer guides to illicit activities

SCORECARD

WiFi
According to Google, the unused 'white space' between the frequencies used by US television stations could be co-opted to give wireless broadband to everyone in the country.

Internet users
An editorial in the *American Journal of Psychiatry* has called for Internet addiction to be added to the official inventory of mental illnesses.

ROBOT NEWS

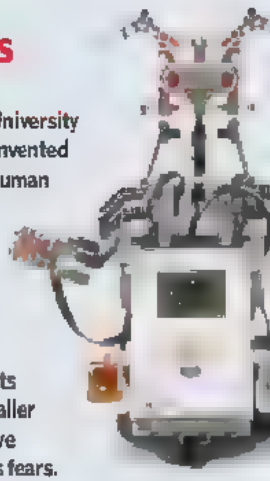

T TEN VELDEN/UNIV. AMSTERDAM

Brave little toaster
Roboteers from the University of Amsterdam have invented a robot that mimics human phobias — and the steps needed to overcome them. The 'Phobot' retreats when it first meets a larger robot, but then gradually gets comfortable with smaller ones until it feels brave enough to conquer its fears.

NUMBER CRUNCH

40% is the proportion of scientists and technologists in the European Union (EU) aged between 45 and 64.

27% is the proportion of people in this age bracket in the EU population as a whole. The scientific workforce is ageing faster than other sectors.

47% of senior scientists are female, which indicates that science has greater gender equality than many other professions.

Sources: Wired, BBC, Am. J. Psychiatry, Associated Press, Eurostat

SIDELINES

SPECIAL REPORT

Bagged and boxed: it's a frog's life

As many amphibians face the very real threat of being completely wiped out by disease, climate change and pollution, **Emma Marris** looks at a controversial approach to save some of them in glass boxes.

With bright orange freckles and tiny proportions, the Carrikeri harlequin frog population spotted earlier this month delighted its discoverers with more than its good looks. The creatures (*Atelopus carrikeri*), found in the remote mountainous Paramo region of Columbia, had not been seen in 14 years and were feared extinct. Their rediscovery — and that of another species of the same critically endangered genus in 2006 — brings rare cheer to amphibian biologists.

These are desperate times for frogs, toads, salamanders and caecilians, whose sensitivity to climate disturbance means they provide an early window into the way that other biodiversity could be affected. The numbers are shocking: it is estimated that half of the world's 6,000-odd species of amphibians are now threatened by disease, pollution, habitat destruction, the consumer trade or climate change; about one-third of all amphibians are at risk of extinction (1,896 species).

Among the more than 100 species of amphibian thought by some experts to have become extinct since 1980 are Australia's southern gastric-brooding frogs (*Rheobatrachus silus*), which carried their young in their stomachs, and the golden toad of Costa Rica (*Bufo periglenes*). Only 34 species are officially declared extinct, as it is very difficult to prove that there are no individuals left. One of biggest threats these animals face is a species of chytrid fungus called *Batrachochytrium dendrobatidis*, which is thought to have originated in South Africa. The infection is often fatal to whole populations and has spread across the globe with devastating consequences (see 'Fatal fungus').

Faced with the incredible scale of the problem, biologists have embarked on an experiment of last resort. Rather than letting the animals become extinct, a number of conservationists have started gathering up frogs believed to be doomed — in some areas collecting every last individual of a species — in an effort to enable some to persist in captivity. Some believe it would be worth causing the extinction of a species in the wild if it prevents the species from disappearing altogether.

"It is absolutely our obligation," says Jeffrey Bonner, president of the Saint Louis Zoo in Missouri. He chairs an enterprise called Amphibian Ark, under the aegis of the global conservation body, the IUCN, which is raising money for captive breeding. Its goal is to transfer 500 members of 500 species into protective custody within five years.

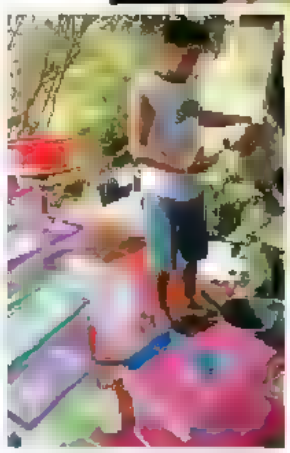

Bagged for life: workers at Panama's frog hotel hope to conserve the creatures. One researcher describes the animals in the facility as "kind of ghosts".

B. KONSTANT/HOUSTON ZOO

It is a melancholy task; there is something pathetic about species that exist only in glass boxes. And it is not without controversy. Although no one is calling for captive breeding to be abandoned, some amphibian specialists feel that it has been oversold as a solution. "Let's assume for the moment that the spiralling decay, including global warming, continues unabated," says Alan Pounds, an ecologist at the Monteverde Cloud Forest Preserve in Costa Rica. "I would say that under such circumstances captive breeding programmes can save amphibian diversity in about the same sense that a museum of Incan art can save Incan culture."

> "There is a wave of death moving through Central America."

Still, biologists feel they have to do something — and fast. "These creatures have no chance," says Joseph Mendelson, a curator of herpetology at Zoo Atlanta, talking about frogs threatened with the chytrid fungus. "If you can't protect them and there are only a few left, they've got to come in." Mendelson was one of a team of conservationists who made emergency collections of frogs in 2005 in El Valle, Panama, an area that researchers predicted would soon be hit with the fungus. The 35 species collected were sent to a zoo and botanical garden in Atlanta with the permission and support of the Panamanian authorities. By January 2006, the fungus had arrived in El Valle.

Another conservation team, supported by Houston Zoo in Texas, collected frogs in the same region for a planned captive-breeding centre at a local Panamanian zoo, called the El Valle Amphibian Rescue Center. But construction delays and the arrival of the fungus sooner than predicted meant that several hundred frogs spent a year in a couple of rooms at the Hotel Campestre in El Valle during 2006. The hotel guests included the Panamanian golden frog (*Atelopus zeteki*), a national symbol of luck, which was last seen in the wild in June 2006. Some species began to breed well, including the kohl-eyed lemur leaf frog (*Phyllomedusa lemur*) and the marsupial frog *Gastrotheca cornuta*, which carries its eggs on its back until they hatch. In all, 600 individuals of 40 species were collected over the course

of the past two years, says Paul Crump, a herpetologist at Houston Zoo.

The future is hazy for these 'saved' amphibians. At the moment, the El Valle Amphibian Center employs four full-time staff to keep the animals alive and is funded by three zoos. But what if funding runs out? Even if the project continues, no one has any idea when or under what circumstances these creatures could return to the wild. And the same is true of any of the captive-breeding programmes around the world. "Any commitment to long-term captive maintenance of a species is effectively an infinite commitment of time and resources. The idea that we have any hope of doing that for more than a tiny handful of particularly charismatic species is clearly wrong," says Ross Alford, a herpetologist at James Cook University in Townsville, Australia.

One concern is that captive breeding will have an effect on the amphibians' genomes. They may become genetically adapted to domesticated life, rendering them less able to live in the wild. A recent study showed a measurable decline in fitness in hatchery raised steelhead trout (*Oncorhynchus* spp.) after just one generation[1]. "Nobody knows how general this effect will be," says Hitoshi Araki, an ecologist at Eawag, the Swiss Federal Institute of Aquatic Science and Technology in Kästanienbaum, who carried out the study on hatchery fish. "We could see something similar in frogs."

Amphibian Ark partner projects are taking steps to avoid one cause of reduced fitness: inbreeding. "We are aiming to maintain 90% of the genetic diversity of the group over 100 years," says programme director Kevin Zippel.

Hotel residents: the Panamanian golden frog (*Atelopus zeteki*), now extinct in the wild, and *Dendrobates auratus*, below.

M. JACOB/ST LOU S ZOO

A problem of equal complexity is what will happen to an amphibian's native ecosystem in the amphibian's absence. It may be that the things it ate will immediately increase in number and the animals that fed on it will become fewer. Such adjustments may lead to other changes in an unpredictable cascade through the ecosystem. Depending on how long the amphibian is gone, its ecological niche might not be there when it returns. And, adds Pounds, climate change is reshuffling which species are found where, especially on mountains. "That's another reason why amphibians that are reintroduced decades down the road may encounter an alien world," he says.

There is reason for hope, though. In 1998 after a chytrid infestation, the last spotted tree frog (*Litoria spenceri*) in the Australian state of New South Wales — a male — was brought into captivity at the Amphibian Research Centre near Melbourne. There the optimistically named Dirk Diggler was mated with captured females from an endangered population in a neighbouring state. Happily, Dirk proved quite the stud and the centre has released many hundreds of his progeny back into his ancestral creek. Follow-up surveys of the tagged captive-reared frogs found 150 of them doing well in the past year.

The reality is that successes like this and the unexpected rediscovery of the harlequin frogs are rare glimmers in the otherwise bleak future facing amphibians. Without urgent interventions to address pressures such as climate change and habitat destruction, the only frogs left may be ones in glass boxes. ■

Additional reporting by *Nature* staff.

1. Araki, H. *et al. Science* **318**, 100–103 (2007)
2. http://www.cdc.gov/ncidod/EID/vol10no12/03-0804.htm
3. Youngs, S. *et al. Int. Zoo Yearbook* **41**, 85–95 (2007).
4. Pounds, J. A. *et al. Nature* **439**, 161–167 (2006)
5. Alford, R. A. *et al. Nature* **447**, E3–E4 (2007)

B. KONSTANT/HOUSTON ZOO

Fatal fungus

Commerical trading of the African clawed frog (*Xenopus laevis*) probably spread the chytrid fungus *Batrachochytrium dendrobatidis* that is destroying amphibian populations. From 1934 until the 1950s, this frog was used as a living pregnancy test — the urine of pregnant women stimulates the production of the frog's eggs — and it remains popular in labs[2].

More than 100 species worldwide have been infected by the chytrid fungus. Its spores infect the outer layer of the amphibian's skin and kill the frog through an unknown mechanism, perhaps by secreting toxins or by disturbing the moisture balance in frogs[3].

Scientists disagree about how predictable the fungal spread is. "Chytrid is going to cover the planet," says Jeffrey Bonner, chair of conservation group Amphibian Ark and president of Saint Louis Zoo in Missouri. It is particularly lethal at certain altitudes and temperatures. "In those places, it is going to kill 85% of the population, and the rest are walking dead because they can't find each other to mate."

But others including Alan Pounds, an ecologist at the Monteverde Cloud Forest Preserve in Costa Rica, find the 'lone-killer model' of the fungus to be an oversimplification. Pounds believes that the mortality of infected frogs is linked to climate change and local factors[4]. But Kevin Zippel, programme director at Amphibian Ark, disputes Pounds' theory. "If it were climate change then why is there a wave of deaths gradually moving through Central America at 26 kilometres a year?" he asks.

Ross Alford, a herpetologist at James Cook University in Townsville, Australia, says that in his country "the evidence for the 'wave-like' nature of outbreaks is extremely equivocal." He has found cases where the fungus infected the population but did not kill any frogs for a year[5]. The fungus can be killed through sun exposure, Alford says. But a cloudy spell of three to four weeks could be long enough to prevent the frogs' normal sunbasking, he says, allowing chytrid populations to build to lethal levels.

There is at least one species of frog that chytrid infection does not kill: African clawed frogs. In other species, a few individuals have lived to croak another day. Studying these exceptions might eventually lead to a cure. And even if the mechanism of resistance is never found out, the individuals that survive could start a breeding pool of chytrid-resistant frogs. **E.M.**

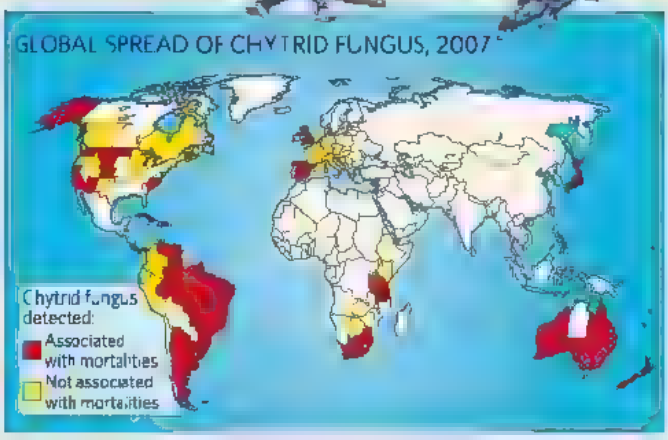

SOURCE: D. OLSEN & K. RONNENBERG/USDA FOREST SERVICE

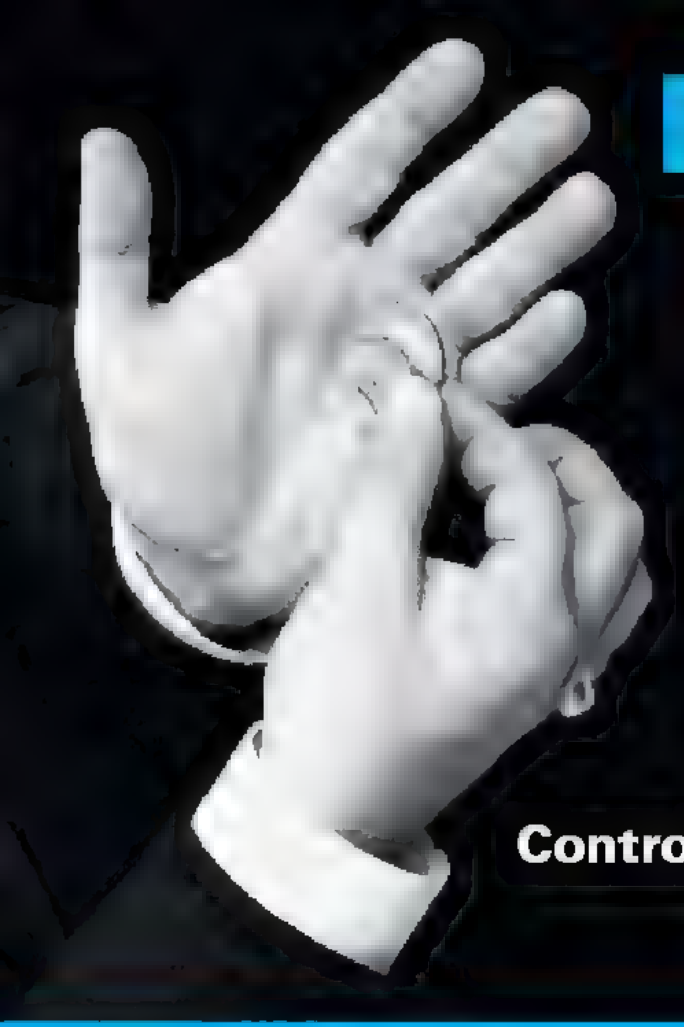

Now You See It... Now You Don't!

Control your protein level like magic!

ProteoTuner™ Systems

Analyze the function of your specific protein,

Visit our website tod
www.clontech.com/magic
and plan for tomorrow!

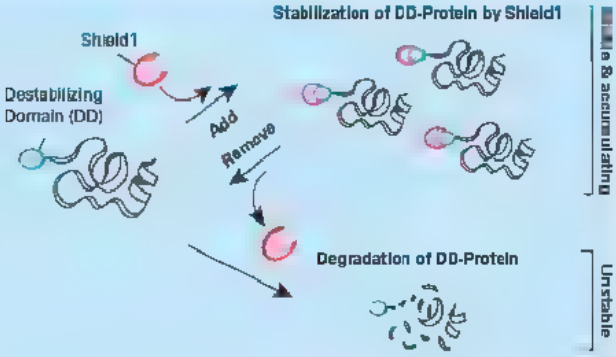

Clone your protein of interest into the DD-containing ProteoTuner vector. Rapidly and reversibly modulate protein levels by adding or removing the Shield1 small molecule.

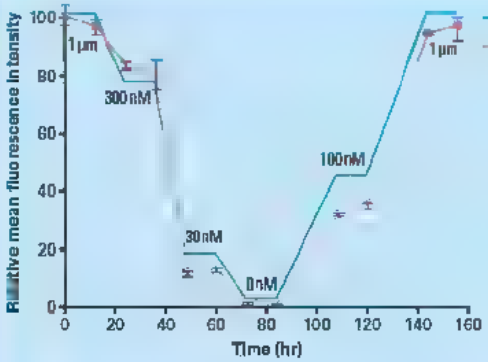

Fusion of the DD to the N-terminus of YFP results in predictable and reversible regulation of intracellular protein levels by Shield1. Reprinted with author's permission from Banaszynski *et al.* (2006) Cell 126(5):995–1004.

Clontech Laboratories, Inc.
A Takara Bio Company

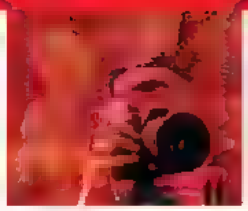

EVENTS BLOG
Get the inside story from science conferences this week
http://blogs.nature.com/news

Laptops track Earth's shakes, rattles and rolls

PALO ALTO, CALIFORNIA

A seismologist at Stanford University in California has developed a computer program for tracking earthquakes in real time. It uses thousands of volunteers' computers and may someday be fast enough to issue warnings just before an earthquake strikes.

Quake-Catcher Network, as it's called, uses the accelerometers built into many new computers, which sense when a computer is dropped so that the hard drive can be shut down. But seismologist Jesse Lawrence found that the sensors could also pick up on more subtle movement. Thus was born the latest iteration in distributed computing, which turns the unused computing power of thousands of home computers into a giant supercomputer.

The most popular distributed computing program, SETI@home, searches for signals from extraterrestrial intelligence. Quake-Catcher looks instead at the inner workings of earthquakes. Little is known about how seismic waves travel and refract deep in Earth's crust, and modelling this movement accurately takes enormous computing power, which can be generated by combining many different users on the network.

"Our approach is just to have massive numbers."

But another of Quake-Catcher's jobs is to wait for an earthquake to happen. When a computer signed up to the program senses shaking, it calculates the intensity and pings the information back to the servers at Stanford in less than a second. If enough computers detect ground shaking in the same area, the system could send out a warning to users who haven't felt it yet that an earthquake is on its way, Lawrence says.

If it works, it will be the cheapest seismic network on the planet and could operate in any country. It wouldn't be as sensitive as traditional networks of seismometers, but Lawrence says that's not the point. "If you have only two sensors in an area, you have to have a perfect system. If you have 15 sensors in a system it [can] be less perfect. One hundred, one thousand, ten thousand — your need for the system to be perfect becomes much smaller," he says. "That's really our approach — just to have massive numbers."

To accurately target an earthquake of magnitude 5 or greater, Lawrence estimates that he would need at least 15 users in a 900 square-kilometre area near the epicentre. (SETI@home currently has more than 340,000 computers worldwide.)

The program also has a large educational component, in which students can drop heavy objects on the floor at varying distances from the computer to design and monitor their own earthquakes. Lawrence hopes that this function — with a US$30 plug-in accelerometer for computers that don't have one built in — will make it attractive to schools, increasing the network.

Currently, his team is in the final stages of testing the program and expects to offer it to the public this summer. ■

Erik Vance

Veto blocks Kansas coal plants — for now

The governor of Kansas, Kathleen Sebelius, vetoed legislation last week that would have allowed two new coal-fired power plants, citing concerns about global warming.

The bill was a response to an earlier block by the state secretary of health and environment, Roderick Bremby. In October, he rejected an air-quality permit sought by Sunflower Electric Power Corporation for the pair of 700-megawatt plants, the first time a power plant has been blocked strictly to protect the climate (see *Nature* 449, 953; 2007).

Backers of the bill do not have enough votes to override the veto, but the legislative battle is expected to continue. Sunflower has filed lawsuits challenging the state's decision.

Sebelius says she would be willing to sign legislation authorizing one power plant, as long as it is capable of capturing carbon emissions for future storage. It should also address renewable energy and energy efficiency, she says.

Science debate looking less likely in Philadelphia

D MCNEW/GETTY IMAGES

Organizers of a potential science debate between leading US presidential candidates have not given up on hopes for it to take place in Philadelphia on 18 April — even though Barack Obama and Hillary Clinton (pictured) have agreed to participate in another, non-science debate in the city two days earlier.

With the Democratic primary race so tight, the stakes are high for the 22 April Pennsylvania primary. Obama has also agreed to a debate in North Carolina on 19 April, before the 6 May primary there.

Organizer Shawn Otto says that supporters still hope to hold a science debate to raise the profile of science and technology issues in the campaign. They hope to hold the debate in Philadelphia's Franklin Institute.

Valuable bacterial archive destroyed

Researchers are demanding an investigation into the destruction of a large collection of bacterial samples, some irreplaceable, from a lab at the Pittsburgh Veterans Affairs Medical Center in Pennsylvania. The archive, of nearly 10,000 samples of infectious bacteria, was the result of more than 20 years' work and included some very rare strains.

The samples were destroyed after the medical centre closed down its special pathogens laboratory, headed by Vincent Yu, in July 2006. Yu and his colleagues were planning to move the samples elsewhere, but did not get the chance.

David Snydman of the Tufts–New England Medical Center in Boston and 242 other researchers have signed a petition, published in the April issue of *Clinical Infectious Diseases*, asking an independent review committee to investigate what led to the repository's destruction.

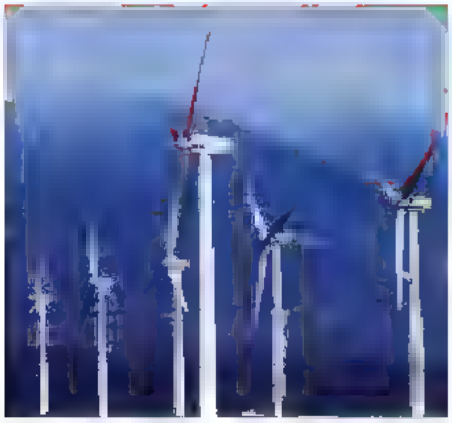

CHINA NEWS/PHOTOQUEST/REUTERS

China aims to expand the number of wind turbines.

China declares ambitious alternative-energy plans

Renewable energy will contribute 10% of China's energy consumption by 2010, forecasts the country's latest 5-year plan. This ambitious target, equivalent to the energy produced from burning 300 million tonnes of coal, was announced by the country's National Development and Reform Commission last week.

The scheme will promote the development and commercialization of biofuels, wind power, solar energy, hydropower and natural gas. Economic incentives, such as funding and tax relief, will be offered to companies, and taxation, concessions and price regulation will be used to provide guarantees for the market.

China hopes that the policies will help it to meet its targets of reducing the amount spent on energy per unit of gross domestic product by 20% and of major pollutant discharge by 10% from 2005 levels between 2006 and 2010. At the end of the first year, the country was already behind its target.

Separately, energy officials announced that they would scale up construction of nuclear power plants to get at least 5% of the country's energy needs from nuclear sources by 2020. Overall, nuclear power and renewable energy are set to contribute at least half of China's energy mix by 2050.

Faculty protest at sale of Canadian observatory

The University of Toronto's David Dunlap Observatory, which houses a 1.88-metre reflecting telescope in the town of Richmond Hill, Ontario, may see last light as soon as 30 June. The university is negotiating the sale of the observatory and 77 hectares of surrounding land, estimated to be worth Can$100 million (US$98 million).

Proceeds of the sale will fund a new astronomy and astrophysics institute. But Tom Bolton, one of two members of the university's faculty who still use the telescope regularly, argues that it should be kept for educational purposes at least.

Joint drug venture to end after 30 years

Drug firms Takeda of Osaka, Japan, and Abbott Laboratories of Chicago, Illinois, are splitting up a joint venture begun in 1977.

Takeda, which may pay Abbott US$1.5 billion for the split, is expected to retain the heartburn drug Prevacid (lansoprazole), with Abbott taking the cancer drug Lupron (leuprolide). Both drugs had been produced through the joint venture TAP Pharmaceutical Products, based in Lake Forest, Illinois. Together, the two drugs accounted for around $3 billion in sales last year.

Outstanding mentors in Germany

This week sees the launch of the 2008 *Nature* Awards for Mentorship in Science. This year the competition will be held in Germany. Readers wishing to nominate outstanding mentors working in Germany should go to: www.nature.com/nature/mentoringawards/germany. The deadline for nominations is 4 July. The winners, who each receive a cash prize of €10,000 (US$15,450), will be announced in October.

NATURE | Vol 452 | 27 March 2008

Fuel from the Sun: these silicon nanorods are designed to capture energy from sunlight to split water.

The photon trap

Chemists have long wanted to recreate photosynthesis in the lab — and to improve on its efficiency at converting sunlight into fuel. **Katharine Sanderson** reports on their latest efforts.

Solar cells can take sunlight and produce a current, giving instant power. But as soon as the Sun goes down, the lights go dim. If you could turn sunlight into fuel — to use for transportation or simply to store for later — you'd be on to a good thing.

Nature can already do this thanks to photosynthesis. Green plants take water, sunlight and carbon dioxide to make sugars and starches. This provides all the fuel they need, and most of the fuel we need too, in the form of food or oil.

The problem is that plants aren't very efficient at fuel making — only about 3% of the Sun's energy ends up as a useable fuel. And the fuel that works for plants doesn't necessarily work for us — the sugars and starches have to be further processed if our needs are more sophisticated than simply eating or burning.

But where plants excel is in getting electrons out of water to produce a fuel. A photovoltaic system, or solar cell, is simply a means of shifting electrons from one place to another. To make a fuel, the electrons are siphoned off, and stored in chemical bonds.

Plants get their electron supply from water. Chemists worldwide are trying to design synthetic systems that do the same. And the design they have to beat, or at least mimic, not only works at room temperature, it does so without the need for expensive metal catalysts. Making something cheap and similar to the machinery used by plants, the photosystem II protein complex (PSII), remains a fundamental challenge.

Some US chemists taking on the challenge are part of a collaborative effort called Powering the Planet, backed by the National Science Foundation. Three basic chemistry problems, each tackled by a different research team, form the crux of the project. One is to design an affordable material to collect energy from the Sun and convert it into current (led by Nate Lewis at the California Institute of Technology, or Caltech). Another is to perfect a catalyst at one end of the material to split water and produce oxygen (led by Dan Nocera at the Massachusetts Institute of Technology). And, the third is to design another catalyst at the other end to produce hydrogen, to be used as a fuel (led by Harry Gray, also at Caltech).

"We've made dramatic advances," says Gray, who can be seen as the father of the project, having supervised both Nocera and Lewis as students in the 1980s. "We're not close to assembling the full device yet."

To start the fuel-making process, sunlight hits a photo-active material. In plants this is chlorophyll, but in the lab it can be a silicon semiconductor, which has its electrons whacked out of position by the incoming photons. The dislodged electrons start to flow in one direction, creating a current. Left behind are positive charges, known as holes, and they drift in the opposite direction. This is a basic solar cell, which requires silicon of high purity, otherwise material defects cause the electrons and holes to recombine, reducing its performance.

B. KAYES, M. FILLER

Plant power

In the Powering the Planet design[1], catalysts at either end of the semiconductor are used to drag the electrons and holes out of the system, preventing them from recombining with each other (see graphic). And water is added to provide the raw material for making the fuel.

One catalyst uses the holes in the semiconductor to drag further electrons from water. This process splits water, releasing oxygen and positively charged hydrogen ions (protons). These protons flow to the other catalyst, which combines them with the electrons in the semiconductor ultimately to make hydrogen molecules.

As well as providing hydrogen fuel for combustion, both the hydrogen and oxygen gases can be fed into a fuel cell — a means of reacting hydrogen with oxygen to produce water and electricity for powering an electric vehicle.

There are other ways to split water artificially. In 1975, Nobel prizewinning physicist Jack Kilby invented an electrolysis system that

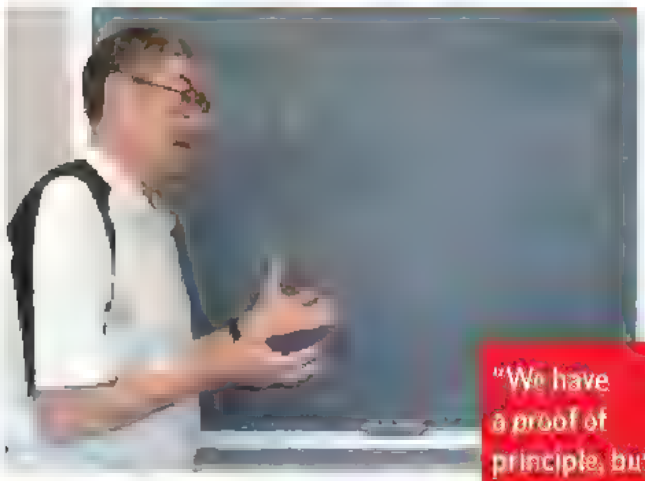

Harry Gray uses sunlight to make hydrogen fuel.

used power from a solar cell to drive electric current through a water-based solution (an electrolyte). This process produced protons and hydroxide ions, which reacted at the electrodes to make hydrogen and oxygen.

Aside from Kilby's simple system, more complex electrolysis cells have been built that use a photoactive semiconductor coated on one side with a platinum catalyst as one of the electrodes. When immersed in water, the semiconductor can both harvest light and generate the electrons and holes needed to split water into protons and oxygen. Hydrogen is released directly from the surface of the semiconductor, and oxygen is produced at a second platinum electrode.

This cell was built in 1998 by John Turner from the National Renewable Energy Laboratory in Golden, Colorado. His device converted water to hydrogen with 12.4% efficiency, four times as good as photosynthesis. But Turner had to use expensive materials such as platinum, the system had a lifetime of just 20 hours, and the hydrogen produced cost US$13 per kilogram[2]. "We can do better," says Turner.

The problem with all electrolysis systems is that the electrode materials degrade rapidly in solution, and need to be replaced, increasing costs and decreasing efficiency. The main difference between Turner's cell and future technologies will be the materials used, with the precious-metal catalyst and expensive single-crystal silicon superseded by cheaper materials. "If we're going to solve this problem we can't use materials that are toxic or expensive," says Gray. "This rules out most standard catalysts."

Nate Lewis is leading Powering the Planet's light harvesting effort. His team is refining a silicon material that he describes as "cheap and scaleable". Instead of expensive single-crystal silicon, Lewis's photoelectric material is a carpet of nanoscale silicon rods, all pointing upwards. He's done this work with Harry Atwater, director of the Caltech Center for Sustainable Energy Research.

The rods are each single crystals, but the method used to grow them is much simpler than the precision wafer-processing technology needed for conventional solar cells. Atwater claims that this makes the rod silicon only as expensive as the silicon feedstock, at between $40 and $70 per kilogram.

> "We have a proof of principle, but we have a long way to go."
> — Harry Gray

The nanorods are also amazingly defect-free. "Once a nanowire begins to grow a little taller than it is wide, it expels defects," says Atwater. This means that the only place where the holes and electrons could recombine is at the tip of each tiny rod.

In the device imagined by the Powering the Planet team, Lewis and Atwater's silicon-rod carpet will be held inside a plastic membrane. The catalysts are coated on opposite sides of the membrane to prevent the oxygen and hydrogen reuniting, potentially explosively.

Catalysing success

Harry Gray is making good progress at the hydrogen-producing end of the system. His catalyst is a cobalt molecule. "It works really well, with quite reasonable efficiency," he says. This rather depends on your expectations. In catalysis, turnover rates are used to measure how many substrate molecules are converted to a product each second. Hydrogenase enzymes, which power the same reaction in plants, have turnovers of about 6,000 per second[2], but Gray's catalyst is still a factor of a thousand less efficient than the hydrogenase enzyme, he says. "We have a proof of principle, but we have a long way to go," says Gray.

Dan Nocera, at the Massachusetts Institute of Technology, Cambridge, is developing the oxygen-producing catalyst, which is proving to be the hardest part of the challenge. Nocera's team began by looking at expensive metals that are related to cheaper metals: a trick often used by chemists. Choose a target metal that could be potentially used, then look at its position in the periodic table and move down a row to a heavier, more expensive metal, where processes happen more slowly, and are more easily studied. Nocera has been using ruthenium, directly below iron. He hopes to transfer what he has learned to iron, copper or nickel, and is confident that this leap will happen soon, making a working system possible within five years, he says.

James Durrant, a chemist at Imperial College London, is also investigating water-splitting materials. He is well aware of the chemistry problems faced by Nocera in his quest for a cheaper catalyst. "Oxidizing water is vicious chemistry," he says. The catalytic reactions involve molecules undergoing multi-electron processes, which are poorly understood. "As bad as it is to transfer one electron, the molecule is even more reluctant to give up the second electron," explains Atwater.

This is because adding solar energy to water, and tying it up in molecules with higher energy bonds (oxygen and hydrogen) is what's known as a thermodynamically uphill process. And most of that uphill struggle happens at the oxygen-producing site. Making a single molecule of oxygen involves splitting two water molecules, and the whole process involves four electrons and four protons. "That's a lot of electrons and protons," says Nocera. For this reason, Nocera says he doesn't want to simply copy photosynthesis. "It took two billion years of evolution," he says. "I don't think I can do it in 20."

Other chemists are still trying to beat nature at its own game. A dozen European research partners, coordinated by Stenbjörn Styring

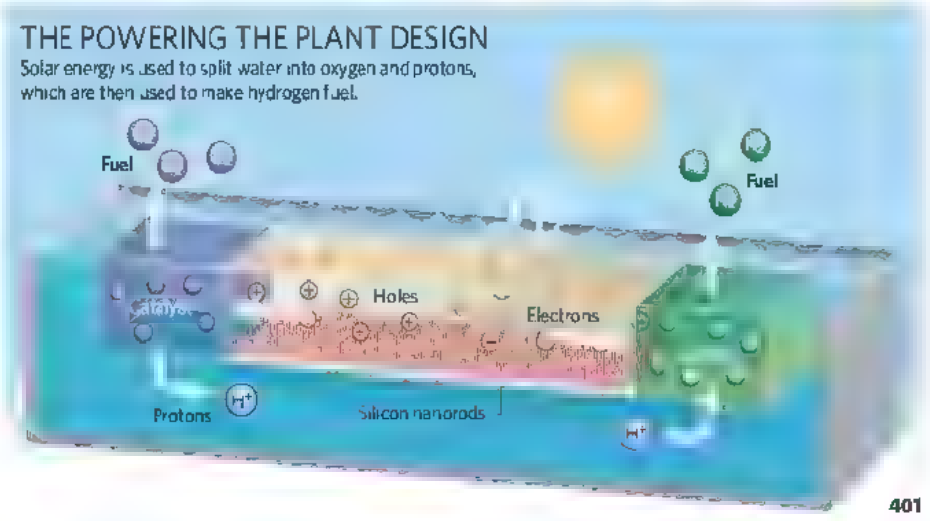

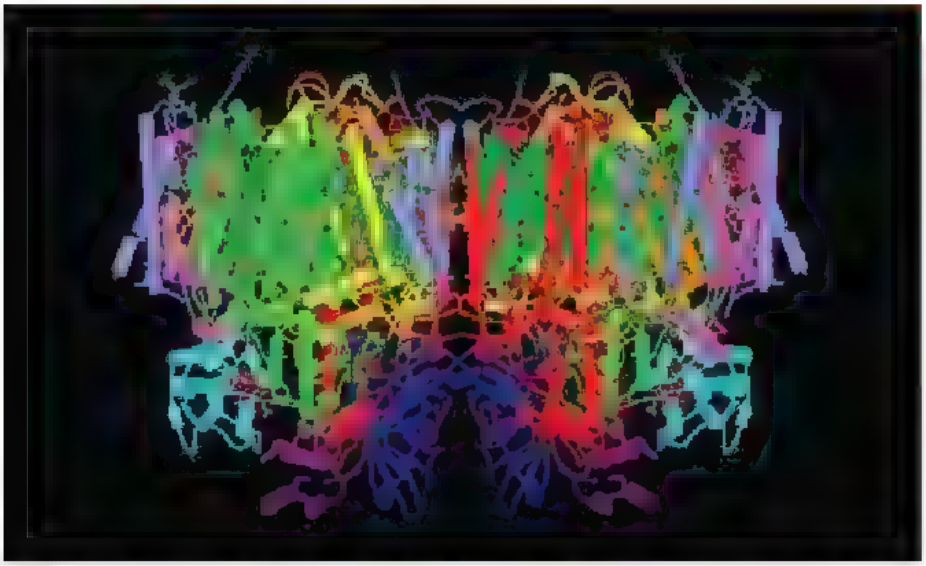

Chemists want to replicate photosystem II (modelled above), used by plants to convert light into fuel.

from Uppsala University, Sweden, form the Solar-H network, funded by the European Union. They are looking closely at natural photosynthesis for inspiration.

To harvest energy from sunlight, the Solar-H team uses a ruthenium-centred molecule that helpfully absorbs light at a similar wavelength to chlorophyll. For the hardest part of the problem — the oxygen catalyst — the Solar-H team turns to the heart of PSII, which contains a molecule with four manganese atoms known as the oxygen-evolving complex.

Styring has been working on this problem for 15 years, and he has shown that it isn't necessary to fully replicate the oxygen-evolving complex. Instead, he thinks that just two manganese atoms are sufficient. Styring says he has recently had a breakthrough: a molecule that can split water into oxygen and protons, although the system is powered electrochemically, not by light.

Even after this prolonged effort, Styring expects criticism when he publishes the work, partly because the oxygen-evolving molecule isn't fully catalytic — the molecule is changed by the reaction and so probably cannot be reused. "People will be very sceptical, and so are we," he says. "This is a very difficult field."

He will have a hard time convincing researchers such as Durrant. "The only molecular system known to perform thermodynamically efficient water oxidation is PSII," says Durrant. "We're a long way from having a molecular system that works as well," he says.

Other chemists say that simply mimicking photosynthesis is too short sighted. "Photosynthesis is basically a failure for energy conversion," says Tom Mallouk at Pennsylvania State University. To beat the world's energy problems, scientists have to be more ambitious than the 3% efficiency achieved by plants. "If that's all we want, the thing to do is grow corn," says Mallouk. He thinks the goal should be at least 10%, preferably 20% power conversion efficiency, using materials that do not cost much more per unit area than house paint, he says.

The Powering the Planet team is optimistic it can beat photosynthesis, even if it doesn't beat Turner's efficiency record. And they are determined to beat Turner on cost. "In the end, we want to be at 5–10% solar-to-fuels efficiency," says Lewis. "We know the materials that work. It's just a question of making it work faster, better, cheaper."

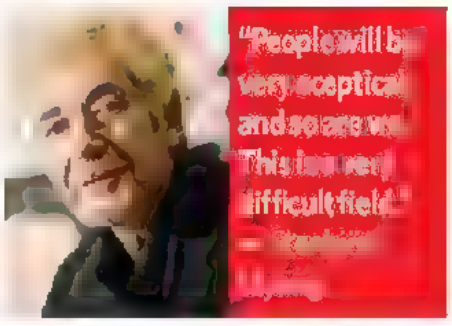

Another materials approach to water splitting is being taken by Kazunari Domen at the University of Tokyo. In future, says Domen, if human beings use solar energy on a huge scale, we need to use technology that captures solar energy over much larger areas. To achieve this, he uses a photocatalyst particle that generates hydrogen and oxygen simultaneously on its own surface. The material is a solid solution, a mixture of metal oxides impregnated with nanoparticles of another mixed oxide. Domen is still developing these materials, which as yet don't work for all wavelengths of light.

Domen admits there is still lots of basic research to be done. Indeed, all of the groups defend their work as basic chemistry first — and applied research second. "We're doing fundamental chemistry, unashamedly," says Lewis. "There's lots of basic stuff to do to solve this."

To get a fully practical system may take years, although Atwater thinks that the silicon-rod carpets are already ripe for commercialization as light-capturing solar panels. A few small companies are investigating water-splitting, including Nanoptek, a start-up firm in Maynard, Massachusetts, which is building on the original Kilby approach by developing photoelectrodes that will harvest photons over a wider energy range.

Fueling the future

G24 Innovations (G24i) in Cardiff, Wales, is developing small-scale electricity generating systems based on organic dyes — again mimicking nature's use of chlorophyll in photosynthesis — for personal electronics, mobile phones and laptops, with the goal of bringing these mass communication devices to remote parts of the world. The company's first products — solar-powered chargers — rolled off the production line in February.

The approach is based on technology pioneered by Michael Grätzel at the Swiss Federal Institute of Technology in Lausanne. In his photoelectrochemical cells, the amount of silicon needed is greatly reduced, because the expensive semiconductor is used purely to ferry electrons and holes around, and sunlight is captured by an organic dye. But G24i's products only generate electricity, rather than convert sunlight to fuel.

There are different opinions in the field about when a commercial fuel-generating device will become reality. Where Atwater sees immediate commercial opportunities for his part of the project, Durrant can't see there being anything practical working for at least ten years. Gray thinks the problem requires at least another three or four years' work, and can see good motivation for pushing ahead. "This is a big deal in terms of competitiveness and innovation," says Gray. "When solar energy comes in big time this is a trillion-dollar business."

Turner wants to see a longer-term approach to pay for this kind of research. For the past 30 years, he says, funding has been "spotty and not focused". This is a mistake, he thinks, if the future energy needs of the world are to be met. "Sunlight is truly our largest energy resource by far — it outshines everything else." ■

Katharine Sanderson is a reporter for *Nature* based in London.

1. Lewis, N. S. & Nocera, D. G. *PNAS* **103**, 15729–15735 (2006)
2. Khaselev, O. & Turner, J. *Science* **280**, 425–427 (1998)

Unlock the Power of Gene Expression Analysis with the Right Combination

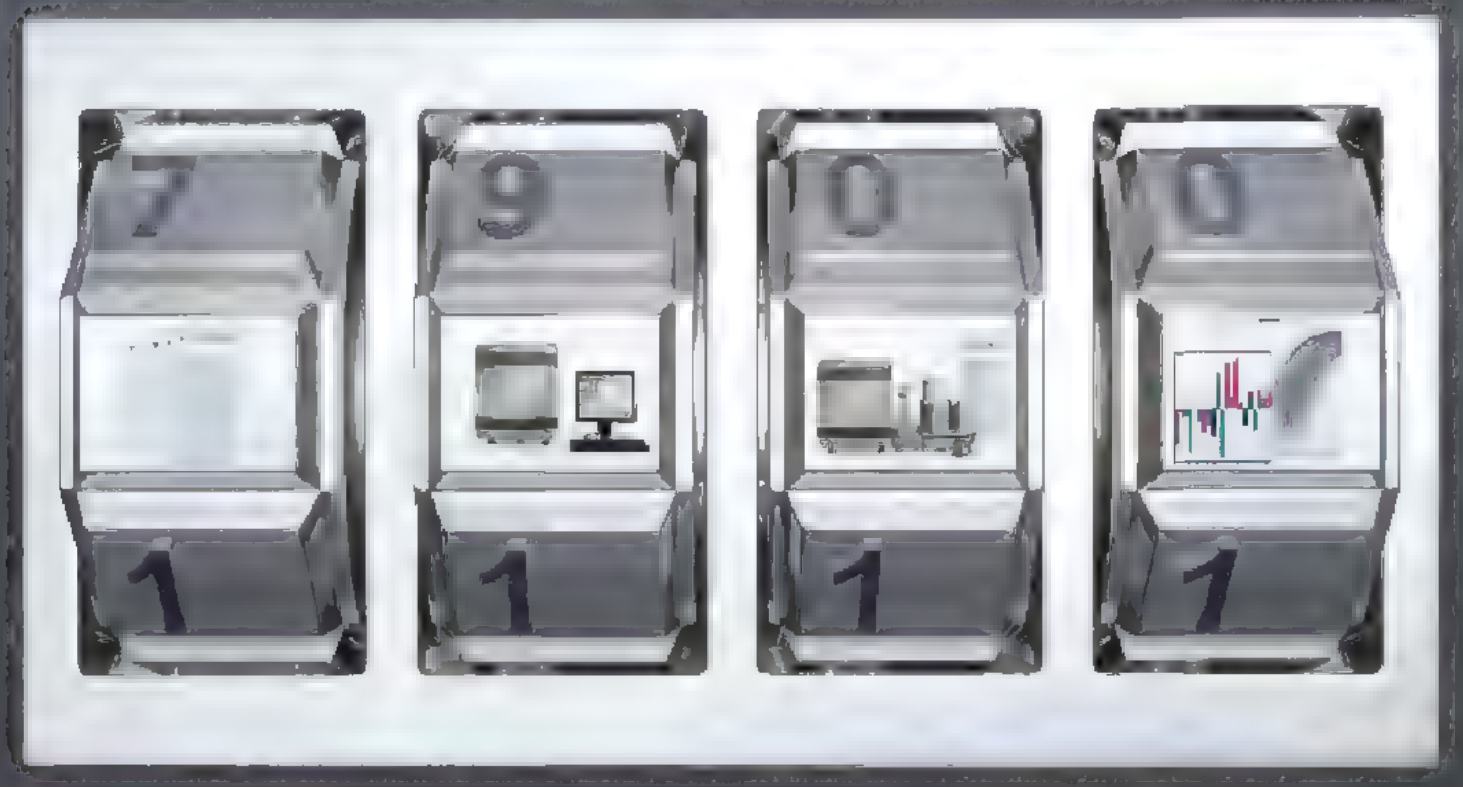

TaqMan® Arrays and the 7900HT Fast Real-Time PCR System: The Superior, Single-Solution for High-Throughput Gene Expression Analysis

Achieve optimal performance and flexibility in high-throughput gene expression analysis when you combine TaqMan® Arrays with the 7900HT Fast Real-Time PCR System. Choose from pre-designed TaqMan® Gene Signature Arrays, configurable TaqMan® Gene Sets, or TaqMan® Custom Arrays. Each format offers the accuracy, reproducibility, and specificity you expect from an industry leader. Experience high-throughput and performance synergy in a winning combination.

TaqMan® Arrays:

- Convenient for disease target classes and pathways
- Proven quality, speed, and ease-of-use
- Pre-loaded with TaqMan® Gene Expression Assays
- Increased sensitivity and precision
- Ideal for small and archival tissue samples
- Low sample consumption
- 384-well loading without liquid-handling robotics

7900HT Fast Real-Time PCR System

- Proven gold standard, industry-leading performance
- Interchangeable block formats offer easy application adaptability and flexibility
- Seamless integration with TaqMan Arrays
- Automation Accessory provides hands-free plate-loading and unloading for 24-hour operation
- Powerful software tools enable high quality data analysis

Access more information at www.7900HT.com

Applied Biosystems

For Research Use Only. Not for use in diagnostic procedures.

Practice of the patented 5' Nuclease Process requires a license from Applied Biosystems. The purchase of the TaqMan® Array includes an immunity from suit under patents specified in the product insert to use only the amount purchased for the purchaser's own internal research when used with the separate purchase of an Authorized 5' Nuclease Core Kit. No other patent rights are conveyed expressly, by implication, or by estoppel. For further information on purchasing licenses contact the Director of Licensing, Applied Biosystems, 850 Lincoln Centre Drive, Foster City, California 94404, USA. The TaqMan® Array is covered by U.S. Patents Nos. 6,514,750; 6,942,837; 7,211,443; and 7,235,406. Microfluidic Card developed in collaboration with 3M Company. The Applied Biosystems 7900HT Fast Real-Time PCR System is a real-time thermal cycler covered by one or more of US Patents Nos. 6,814,934; 5,038,852; 5,333,675; 5,656,493; 5,475,610; 5,602,756; 6,703,236; 6,814,437; 7,008,789; 5,563,58[illegible]; 6,965,105 and 6,7[illegible]9,949 and corresponding claims in their non-US counterparts, owned by Applera Corporation. No right is conveyed expressly, by implication or by estoppel under any other patent claim, such as claims to apparatus, reagents, kits, or methods such as 5' nuclease methods. Further information on purchasing licenses may be obtained by contacting the Director of Licensing, Applied Biosystems, 850 Lincoln Centre Drive, Foster City, California 94404, USA.

NATURE | Vol 452 | 27 March 2008

FROZEN FUTURES

Fittingly, the end-of-the-world vault lies at the end of the world. The plane to Svalbard gets you to within about 1,000 kilometres of the North Pole — further north than any other commercial flight. Today, the beautiful if desolate island of Spitsbergen in the Svalbard archipelago is home to a tight-knit population of just 2,000 miners, hoteliers and Arctic researchers. In a few years time, it will also be home to seeds from some 1.5 million varieties of crop.

On 26 February, a small group of officials, politicians, scientists and journalists carried the first deliveries of seeds down an icy tunnel dug deep into the frozen flank of an Arctic mountain and into the Svalbard Global Seed Vault. When the collection is completed over the next four or five years, the vault will have amassed seeds from virtually all the recognized varieties of 150 crop species routinely grown and eaten by humans — including the 100,000 varieties of rice, the world's top staple and the crop that accounts for more than 20% of all calories eaten worldwide.

> "If we had built this vault ten years ago, we would have used it ten times already."
> — Cary Fowler

Conserving crop biodiversity is an urgent undertaking. The Intergovernmental Panel on Climate Change (IPCC) predicts that 25–30% of plant species will be extinct or endangered in the next century. "We're losing crop diversity every day, going out with a whimper, not a bang," says Cary Fowler, executive director of the Global Crop Diversity Trust, which will curate the vault's collection. "In a real sense, Doomsday is every day."

Built by the Norwegian government at a cost of 45 million kroner (US$8.8 million), the vault was built in Svalbard partly because its storage rooms, deep under the permafrost and chilled to the optimum seed-storing temperature of −18 °C, will remain insulated even in the unpredictable centuries to come.

The seeds it will store are copies of those already held by the roughly 1,400 existing national and regional seed banks worldwide. It's nicknamed the Doomsday vault because of its intended role in bailing out these banks in the event of mishaps — anything from power cuts, to flooding, to war. "If we had built this vault ten years ago, we would have used it at least ten times already, for the loss of the gene [seed] banks in Iraq and Afghanistan, for example," Fowler says. It's an extra insurance policy.

But no matter how well intentioned and executed, Svalbard cannot single-handedly save the world's threatened biological resources, edible or otherwise. A seed vault won't help to conserve the threatened livestock breeds that billions of people depend on for both dietary and financial sustenance, or indeed the complex ecosystems that exist alongside both crops and livestock and in many cases allow them to thrive. Conserving these, and hence securing humanity's food supply, will require schemes even more impressive than an Arctic dugout. Nevertheless, the global approach behind the Doomsday vault may offer inspiration to those aiming to conserve these other resources.

The Svalbard effort already shares its ethos with another scheme, called the Millennium Seed Bank Project, run by Britain's Kew Gardens. Based in the temperate garden of an English stately home, this bank is somewhat less theatrical than a frozen mountain bunker. But Britain's freezer is the only other to be storing seeds from all over the world, and aims to safeguard more than 24,000 wild plant species, including some crops. Together with Svalbard, the banks will still preserve only a fraction of the world's plant species.

Cold comfort

Keeping spares of the animal kingdom poses even more of a challenge. "It's a lot easier to put 1,000 radish seeds in cold storage than frozen animal material," says Don Bixby, a cryopreservation technician and former executive director of the American Livestock Breeds Conservancy (ALBC), a North Carolina-based non-profit organization. Yet the problem of dwindling diversity is just as great, if not greater, in the world's livestock as it is in its crops. Last year, a survey by the United Nations Food and Agriculture Organization revealed that 16% of the world's 7,600 recorded indigenous breeds of cattle, pigs, sheep and poultry are at risk of disappearing — 11% have already gone extinct.

This has mostly resulted from the rise of high yield breeds such as the familiar black-and-white Holstein–Friesian dairy cow, now found in 120 countries. International breeding companies have promoted these breeds, and

Rice crop from Bali, Indonesia (above) will be among 1.5 million varieties sent to Svalbard.

MIKA/ALAMY

CIMMYT

farmers, keen to increase their output, have willingly adopted them. All of the estimated one billion Holstein–Friesians in the world were ultimately sired by the same few dozen bulls, who have been bred for daughters with high milk yields and whose sperm is collected, frozen and sold worldwide. "We're dealing with an effective population of 30–35 animals globally," says Bixby. This is a "very worrying number", because the homogeneous animals are not adapted to local drought conditions or to resist disease.

Can endangered livestock breeds be given their own version of the Svalbard seed vault? It's a tricky proposition. Unlike seeds, which are generally capable of germinating after being frozen, delicate sperm, eggs and embryos are far more susceptible to damage by freezing — and methods for doing so have to be refined for every species' unique physiology. Cattle sperm is one success story "Fifty-year-old semen still produces calves," Bixby says, but, "for many species we're not able to put away material that can be reconstructed into live animals."

If there is hope of developing an animal counterpart to Svalbard, it may lie in the network of regional tissue banks being developed by the US Department of Agriculture. It has given itself a mandate to collect reproductive material from every livestock breed found in the country, with an emphasis on conserving genes that will be useful for maintaining future food production. This could go a long way towards saving the world's resources, because the United States' history of importing and breeding animals with valuable traits — which these days would be decried as biopiracy — means that many foreign breeds are represented there. But the US tissue banks are not designed to be a global repository for animal diversity, and there is no talk of starting such a store elsewhere.

Cryobanks cannot, however, be the whole story, and parallels can be drawn with wildlife conservation, where breeding from cryopreserved material is still seen as a last resort. The argument here, in essence, is that there is little point in resurrecting frozen seeds or embryos if their natural environment has vanished too. "Wildlife conservation realized 15 or 20 years ago that it's not good enough to just save a seal, or a quail — we have to save the ecosystems where they live, and in many cases that's also true for livestock and food plants," Bixby says.

"It's not good enough to just save a quail … we have to save the ecosystem."
— Susan Bixby

But agricultural systems are often excluded from conservation efforts because they are, by their nature, artificial. Some credit the organic farming movement with helping to preserve indigenous crops and livestock and their surrounding ecosystem.

The Svalbard seed vault is generating almost universal good will, but even its supporters acknowledge that it's not enough to bank existing biodiversity for use after Doomsday. They also advocate efforts to withstand impending disaster — by creating breeds that can resist whatever endangers them.

Gordon Conway, chief scientific adviser to the UK government's Department for International Development (DFID), argues that biotechnology techniques will prove instrumental in preserving biological diversity. They allow, he says, genes that confer drought resistance or other valued traits to be moved from one variety to another more quickly than conventional selective breeding. Conway cites the example of a new, devastating variant of wheat rust fungus, called Ug99, which is spreading through East Africa towards the Indian subcontinent. Earlier this month, the UN reported that it has already been detected in Iran

Efforts are underway to cross disease-susceptible strains with natural varieties carrying a gene resistant to Ug99. "We have to get that gene into Asian variants, and we have to do it quickly," Conway says. In this sense, he argues, environmentalists need to embrace techniques such as genetic modification that are sometimes viewed with suspicion.

The Svalbard vault's creators have not so far suggested using its seeds as a gene bank that can be mined in the future. But the bunker is "not the only element in the master plan", says Fowler. Besides overseeing the vault, the Global Crop Diversity Trust has amassed a war chest of more than $260 million, much of which will be spent on projects to breed hardier crops, and strengthen national and regional seed banks. Donors include the Bill & Melinda Gates Foundation, DFID, agribiotech giants such as DuPont and, most recently, the Norwegian government. The trust's work will add to the existing efforts of international philanthropists such as the Rockefeller Foundation to boost the effectiveness of plant breeding, not to mention the profit driven activities of multinational crop firms.

Farms thus represent the real battleground where the fight to save food diversity will be won: it is there that the many varieties of food species grow today — and it is there, ideally, that they will be preserved intact. For those at the Svalbard vault's bitterly cold opening ceremony, it's hard to imagine its icy caches ever being thawed. And that, really, would be the best case scenario — after all, no one wants to have to cash in their insurance policy. ■

Michael Hopkin is a senior reporter for *Nature* in London.

NATURE|Vol 452|27 March 2008

5 things to know before jumping on the iPS bandwagon

Induced pluripotent stem cells look just like embryonic stem cells, but are easier to create and free of the heavy ethics baggage. **David Cyranoski** separates fact from fiction in a burgeoning field.

Excited by their potential for biomedical research and therapy and lured by the ease with which they can be created, many researchers are looking into induced pluripotent stem (iPS) cells. Created from adult cells by a simple genetic trick, iPS cells seem to have regained an embryonic 'stemness' that might allow them to become any type of cell in the body. The concept is so appealing that some scientists and policy-makers even argue that related approaches such as therapeutic cloning and embryonic stem-cell research, which require the destruction of embryos, should be halted. But for biologists, iPS cells still present a black box. As resources pour in and patients' expectations rise, some scientists wonder whether the cells are being overhyped. Here, *Nature* looks at the status of the five most pertinent issues on people's minds.

1 Anyone can do it

When Shinya Yamanaka and his postdoctoral student Kazutoshi Takahashi from Kyoto University in Japan discovered that four genes could reprogram adult mouse cells, they kept it secret for nearly six months. They stopped having weekly laboratory meetings, and Takahashi fibbed to colleagues about the status of his work. All because the process is so simple. "If someone found out, they could have caught up in a flash," he says.

Familiar genes — *Oct3/4*, *Sox2*, *c-Myc* and *Klf4*, in Yamanaka's original recipe — do the trick[1]. The genes are cloned into viral vectors, and simply adding the vectors to a culture of skin cells under the right conditions results in reprogrammed cells.

But as simple as this procedure might seem, iPS cells are not easy to make. Kathrin Plath at the University of California, Los Angeles, estimates that each of the reprogramming genes (she used six) has only a 15% chance of making it into a given cell. Even if they all make it, the cell has only a 5% chance of being fully reprogrammed. The low efficiency presents a riddle for scientists, but with millions of cells available in a biopsy sample, it is not a roadblock. The trickiest part, says Konrad Hochedlinger from the Harvard Stem Cell Institute in Cambridge, Massachusetts, is finding the few cells that have been reprogrammed and culturing them. But the new iPS cells are picky: they require just the right culture conditions — much the same as those needed for embryonic stem cells — to stop them differentiating into more specialized cell types. "Expertise in human embryonic stem-cell culture is absolutely critical," says Hochedlinger.

"Expertise in human embryonic stem-cell culture is absolutely critical."

Nevertheless, this type of expertise is becoming more common. Within a year, Yamanaka's results had been repeated and improved in mice by his own and two other groups. And since Yamanaka[2] and James Thomson[3] from the University of Wisconsin in Madison first produced human iPS cells independently of each other in November 2007, several other groups have now achieved that feat. The stakes are high; the technique is easy to learn; and researchers are flocking to the field, says Thomson. "The whole world is doing it now."

Status: Fact (mostly)

2 Everyone can have their own custom-tailored cells

'Therapeutic cloning' — cloning human embryos to generate stem cells that can be used to replace tissue that has been lost or damaged without the fear of rejection by the host's body — has floundered since it was first proposed

ILLUSTRATIONS BY C. ALEN-FLETCHER

in the late 1990s, mainly because of the unexpectedly difficult challenge of acquiring the human eggs necessary for the procedure. iPS cells are moving full-steam ahead towards the same goal, patient-specific stem cells.

But don't expect to have custom-made cells any time soon. Some of the viral vectors used to transfer the genes into cells, as well as some of the genes themselves,

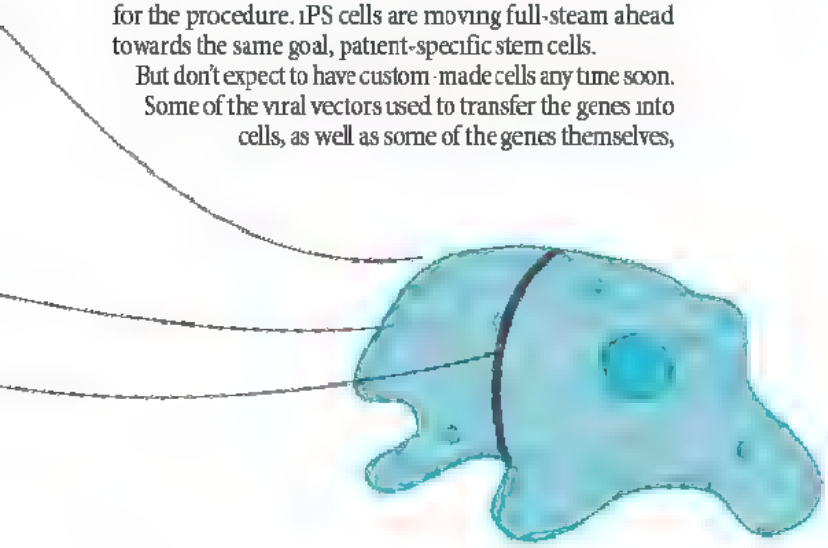

may cause cancer. Scientists expect that the heated race to find alternative systems, such as proteins or drugs that simulate the crucial genes, or safer ways to deliver the genes, will produce results soon — perhaps in the next two years.

Nevertheless, says Hans Keirstead of the University of California, Irvine, the "greatest challenge still exists: the generation of high-purity, clinically relevant cell populations". It takes a couple of months to establish a cell line, several more to expand it, more still to differentiate the iPS colonies into the cell types required, a few more to expand those, and then a good half year of testing to ensure that the cells do not form tumours. The cells also have to be processed in facilities that adhere to 'good manufacturing practice', which adds greatly to the cost.

> "Grafting even a very small number of undifferentiated stem cells carries a risk of tumorigenesis."
> — Arnold Kriegstein

To use custom-made cells "would take a ridiculous amount of money", says Yonehiro Kanemura, a neurosurgeon at Osaka National Hospital in Japan. It would be several times more, he estimates, than the current, rare, patient-specific skin grafts, which cost as much as US$100,000. The roughly two-year process is also too slow to treat disorders such as spinal-cord injury, which require prompt treatment if the damage is to be minimized.

Kanemura's solution is 'ready-made' iPS cells. This April, working with Yamanaka and Hideyuki Okano of Keio University in Tokyo, he will start establishing a national library of therapy-ready cell lines from donated placental and cord blood tissue. At first he plans to use viral vectors, switching to virus-free lines as these become available. Over the next five years, he aims to generate 200 iPS cell lines and 200 neuronal cell lines derived from those cells.

These cell lines will not be patient specific, but Kyoto University's Norio Nakatsuji estimates that 50 well-chosen lines could provide close immunological matches for 90% of the Japanese population. People who need the treatment urgently could use the best immunological match, whereas those with chronic disorders might decide to fork out the money for a line specific to them, says Kanemura. Rich people might want to bank their own iPS cells for a rainy day — a desire that some companies will no doubt try to capitalize on.

Status: Fiction (unless you're rich)

3 The cures are on their way

iPS cells will probably provide models for disease first, cures later. Researchers could soon culture a 'disease in a dish' of, say, motor neurons from a patient with amyotrophic lateral sclerosis, heart muscle cells from a person with heart disease, or retinal cells from a patient with macular degeneration. Those lines could be screened and observed as they develop, and biotech companies could test preventative or therapeutic drugs on them.

The University of California, Los Angeles, and the Harvard Stem Cell Institute, among others, are discussing plans to start iPS cell banks for this purpose. Hochedlinger says that the stem-cell institute is considering "the major diseases — neurodegenerative, metabolic, cardiovascular, diabetes".

Reaching the clinic will depend, like modelling, on how faithfully iPS cells differentiate into the affected cell type as well as on the development of safe and effective ways to deliver them into the body. The foundations are already being laid.

Rudolf Jaenisch, from the Massachusetts Institute of Technology in Cambridge, for example, used blood progenitor cells created from mouse iPS cells to treat a mouse with a humanized version of sickle-cell anaemia[4]. He says that blood disorders, in which clinicians have considerable experience in transplanting cells, might see early application of iPS cells. Kyoto University's Jun Takahashi, who studied neuronal precursor cells derived from embryonic stem cells in monkey models of Parkinson's disease[5], is now pursuing clinical treatment with neuronal precursor cells derived from both embryonic stem cells and iPS cells. He hopes that the cells will be in clinical trials within five years.

Whether cultures of differentiated cells for therapeutic use still retain undifferentiated embryonic stem cells or iPS cells is a point of grave concern. "Grafting even a very small number of undifferentiated stem cells, perhaps as few as one pluripotent cell, carries a risk of tumorigenesis," says Arnold Kriegstein of the University of California, San Francisco. Everyone will be watching closely a clinical trial planned for the middle of this year — the first trial of embryonic-stem-cell-based treatment — in which the pharmaceutical firm Geron of Menlo Park, California, will be implanting oligodendrocytes derived from embryonic stem cells in patients with spinal-cord injuries. "Application of iPS cells largely depends on how that trial goes," says Okano.

Unpublished work by Okano, based on iPS-cell treatment of spinal-cord injury in mice, could accelerate application. He claims that he has a method to weed out the potentially dangerous cells before they are transplanted into the mice.

Status: Too soon to tell

4 Embryonic stem cells are the same as iPS cells

"There are no major differences, yet," says Plath, based on a rigorous characterization of morphology, chromosome profile and gene expression of human iPS cells[6].

But everyone is hedging their bets as dozens of scientists start to examine the key question: whether iPS cells will differentiate as stably and diversely as embryonic stem cells. For the time being, iPS pioneers are looking at subtler hints, such as protein markers that characterize the two types of cells. But

NATURE | Vol 452 | 27 March 2008

Hochedlinger says that "markers don't mean anything". Some tumour cell lines express protein markers of pluripotency but don't make anything other than tumour cells, for example.

And reports of the iPS cells' properties have been conflicting. Thomson, for instance, found that iPS cells not only expressed similar genes to embryonic stem cells, they also expressed them more consistently[7]. This means that their differentiation might be more predictable than that of embryonic stem cells. However, Robert Lanza of Advanced Cell Technology, a biotech firm in Los Angeles, California, says that iPS cells are much more variable. "Embryonic stem cells all do more or less the same tricks. But some iPS cells express just a few markers of pluripotency, some express all," he says. "The resulting cell types will presumably differ as well."

Even if iPS cell lines seem to differentiate into the cell of choice, some variation between lines is unavoidable. Each line will require rigorous testing, says Keirstead, who is involved in the Geron trial. "A different line may have a different tumorigenic potential, differentiation potential, migratory potential, and react with the host in a unique way. It represents a different product, so must be fully tested as such." For the same reason, Plath recommends doing any tests or drug screens with multiple lines.

Despite some scepticism about iPS cells, many key researchers embrace them as a preferred alternative to embryonic stem cells. "Only time will tell, but I know where I'm going," says Thomson, who was the first to establish human embryonic stem-cell lines in 1998. If things go as he predicts, it could be the end of an era. "If you can't tell the difference between iPS cells and embryonic stem cells, the embryonic stem cells will turn out to be a historical anomaly," he says.

Status: Fact (so far, anyway)

> "If you can't tell the difference between iPS cells and embryonic stem cells, the embryonic stem cells will turn out to be a historical anomaly."
> — James Thomson

5 iPS cells have no ethical issues

Days after Yamanaka and Thomson announced the creation of human iPS cells, President George Bush hailed the research as a sign of "scientific advancement within ethical boundaries" — a feat for which he gives himself partial credit.

A week later, though, Yamanaka told *Nature*: "We are presenting new ethical issues, maybe worse ones, because many people can do this — and without telling anybody." Yamanaka was concerned that someone might use iPS cells to derive gametes — human reproductive cells. Eggs and sperm could both be derived from iPS cells from a man, for example, and then be used in an *in vitro* fertilization procedure. The result would not be an identical clone because genes reassort during formation of the gamete. But it would be "strange and potentially dangerous", says Yamanaka.

Gametes from iPS cells could meet demands for infertility treatments. And producing eggs from male iPS cells would allow a gay couple to produce offspring between them. (Lesbian couples would be out of luck, as Y-chromosome genes are needed to produce sperm.)

Such fertility treatments would be plagued by safety issues, but judging from experiments with embryonic stem cells, they won't happen soon. Morphologically similar versions of both eggs and sperm have been derived from embryonic stem cells, but only one group has reported that embryonic-stem-cell-derived gametes — mouse sperm in this case — led to live births when combined with normal eggs, and the results have yet to be repeated[8].

iPS cell adventurers might also try to create a live, cloned human. Jaenisch managed to clone mice, by transferring iPS cells into a specially developed embryo made by fusing the cells of a two-cell embryo. By putting these embryos into surrogate mothers, Jaenisch produced several fetuses that were genetically identical to the iPS cell source. (There were no live births, but Jaenisch says that is only a matter of trying.)

Repeating the experiment in humans would, according to Jaenisch, "be possible in principle". He adds, however, that because "more than 100" embryos are probably needed to make it work, it would be unrealistic and a ridiculous thing to do. But as fertilized embryos are easier to get than the fresh eggs used in cloning, some maverick might give it a try. iPS cells generated from a person could also be inserted into a fertilized embryo to make a chimaeric baby.

These reproductive strategies would probably fail, at least with the current state of the technology. But given the rapid rate of innovation and the wide range of iPS cell capabilities, dangerous experiments will be more difficult to monitor. "Before, you had a specific community to focus in on — the practitioners of assisted reproduction. [With iPS cells] it will be difficult, especially in a place such as the United States, where there is so much dependence on self-regulation," says Paul De Sousa of the Scottish Centre for Regenerative Medicine in Edinburgh.

Yamanaka's concern about the ethics drove him to lobby the government for regulation. On 21 February, Japan's science ministry sent all universities and research agencies a notification specifically forbidding "the implantation of embryos made with iPS cells into human or animal wombs, the production of an individual in any other way from iPS cells, the introduction of iPS cells into an embryo or fetus, and the production of germ cells from iPS cells".

Status: Fiction (depends on what you want to do)

Yamanaka says that society, not scientists, must quickly deal with the challenges that iPS cells present. "I am proud of this technology, but I feel a great responsibility," he says. ■

David Cyranoski is *Nature*'s Asia-Pacific correspondent.

1 Takahashi, K. & Yamanaka, S. *Cell* **126**, 663–676 (2006)
2. Yu, J. *et al. Science* **318**, 1917–1920 (2007)
3 Takahashi, K. *et al. Cell* **131**, 861–872 (2007)
4 Hanna, J. *et al. Science* **318**, 1920–1923 (2007)
5. Takagi, Y. *et al. J. Clin. Invest.* **115**, 102–109 (2005)
6. Lowry, W. E. *et al. Proc. Natl Acad. Sci. USA* **105**, 2883–2888 (2008)
7. Yu, J. *et al. Science* **318**, 1917–1920 (2007)
8 Nayernia, K. *et al. Dev. Cell* **11**, 125–132 (2006)

See Editorial, page 388.

Canadian government is committed to science

SIR — In your Editorial 'Science in retreat' (*Nature* **451**, 866; 2008), you criticize the Canadian Conservative government's record on science issues. This criticism is unwarranted.

First, our government is committed to attracting and retaining talent, supporting world-leading research and ensuring that, through commercialization, the research discoveries of Canada's best and brightest are transformed into practical applications. When prime minister Stephen Harper unveiled the national strategy Mobilizing Science and Technology to Canada's Advantage in May 2007, he charted out the government's much-needed change of direction on science and technology policy, heralded by the creation of the 18-member Science, Technology and Innovation Council to advise government and benchmark Canada's performance against international standards of excellence.

Second, the Editorial neglected to mention important investments made by the government in research. For example, the Canadian Institutes for Health Research spends more than $700 million a year, supporting the work of more than 11,000 researchers and trainees in universities, teaching hospitals and research institutes across Canada.

Third, the government has reversed years of cuts to federal fisheries science. The department's science budget has been permanently increased, including an additional $39 million over two years. We are modernizing our research facilities and have started to renew the coastguard fleet so that scientists have reliable platforms for their experiments. More researchers have been hired to work on Arctic science, and we have committed personnel, equipment and financial resources to the International Polar Year — the largest-ever international research programme into the Earth's polar regions. Our $150-million investment in this initiative will enable our scientists to work with colleagues from 60 other nations to study climate change and the health and well-being of northern communities.

Your comments about this government's attitude towards climate change are misleading. Both the prime minister and the minister of the environment have frequently made it clear that the government considers climate change to be one of the greatest threats facing the world today and that it accepts the Intergovernmental Panel on Climate Change reports on the topic.

Finally, accusations that Environment Canada's scientists are being "muzzled" are false. The government's new media policy is in line with that of many other government departments, echoing the 2002 Government Communications Policy. Since this new policy has been in place, Environment Canada's scientists have done dozens of interviews in a variety of areas.

As for Canadian scientists who contributed to the Nobel Prize-winning IPCC group, the government has formally recognized them with a motion in the House of Commons in honour of their work, which was passed unanimously by all parties.

A factual assessment of our government's record demonstrates a clear commitment to enhancing Canada's reputation as a world leader in science and technology.

Jim Prentice
Office of the Minister of Industry
House of Commons, Ottawa,
Ontario K1A 0A6, Canada

Call for a centralized grant proposal repository

SIR — Writing grant proposals is difficult enough, keeping track of different deadlines makes for an endless cycle of procrastination and frantic preparation. The added stack of bureaucratic forms, with arcane variations from agency to agency, can tip one over the edge as a deadline nears.

Is it almost too obvious to wish for a centralized proposal repository? Investigators could submit proposals at any time, in a common format that highlights the science rather than obliterating it with red tape. Funding agencies could search the repository for proposals matching their interests. A minimum of bureaucratic information would be required up front. Budget details could be worked out between funding agencies and investigators as necessary.

Ideally, all proposals would be publicly accessible. However, most of the scientific community has not yet accepted the inevitable dawn of truly open science. Submissions to the repository could therefore be made accessible only to funding agencies that agree to keep proposals private (unless a submitting investigator indicates a willingness to share his or her proposal publicly).

A repository would make life easier for scientists by eliminating the hassle of searching for suitable grant mechanisms and the stress of meeting various deadlines. It would make life easier for funding agencies by expanding the pool of applications from which to choose. Of course, the best proposals could attract offers from multiple agencies. Rather than forcing investigators to choose non-overlapping sources of funding for each project, why not use the repository to mediate shared funding agreements that could benefit everyone involved? In effect, it would serve as the mediator between grant-seekers and grant-providers.

In a world where eBay, Facebook and Google powerfully demonstrate the communal nature of the Web, it is a pity that scientists and funding agencies don't have a similarly modern forum for matching their interests and offers.

Noam Y. Harel
Yale University Department of Neurology,
PO Box 208018, 333 Cedar Street, New Haven,
Connecticut 06520 USA

Readers are welcome to comment at Nautilus, our blog for authors: http://tinyurl.com/2zdar9.

Unfair statistics take the bloom off St Louis

SIR — I take issue with a statistic quoted from *Congressional Quarterly*'s 2007 publication 'City Crime Rankings' in your Naturejobs Regions feature 'Almost in bloom' (*Nature* **452**, 122–124, 2008).

This statistic does a disservice to St Louis in ranking it as the second most dangerous city in the United States. *Congressional Quarterly*'s comparisons are unreliable because they are based on the FBI's Uniform Crime Reports rankings, which are affected not only by the size of a city's population but also by that of the surrounding suburbs.

As the crime rate equals the number of police-recorded crimes divided by the city's residential population, cities with a small population relative to the surrounding suburbs will have inflated crime rates. The city of St Louis has about 10% of the metropolitan-area population (about 90% of the population lives in the suburbs), whereas the city of Memphis, for example, houses more than 50% of the relevant metropolitan-area population. Because assaults on suburbanites that happen in the city are included in the numerator but the victim is not included in the denominator, the crime rate of St Louis is inflated relative to that of Memphis.

If crime-rate comparisons are limited to metropolitan areas, the rankings can change dramatically — the position of St Louis moves to 120th (see R. Rosenfeld and J. Lauritsen *Contexts* **7**, 66–67; 2008). Understanding the actual situation is important because, as noted in your feature, the way is then open for St Louis to become "a hip, feisty biotech hub".

Scott Jacques
Department of Criminology and Criminal Justice,
University of Missouri–St Louis, St Louis,
Missouri 63121, USA

Contributions may be submitted to correspondence@nature.com. Please see the Guide to Authors at http://tinyurl.com/373jsv.

nature podcast

Sponsored by

BIO-RAD

www.nature.com/nature/podcast

Subscribe via iTunes http://tinyurl.com/2rszua

BOOKS & ARTS

View from the top

From prisoner-of-war to head of Europe's space agency, astrophysicist Reimar Lüst reflects on his career.

Der Wissenschaftsmacher
Reimar Lüst in dialogue with Paul Nolte
C. H. Beck. 2008. 300 pp. €24.90
(in German)

Stefan Klein

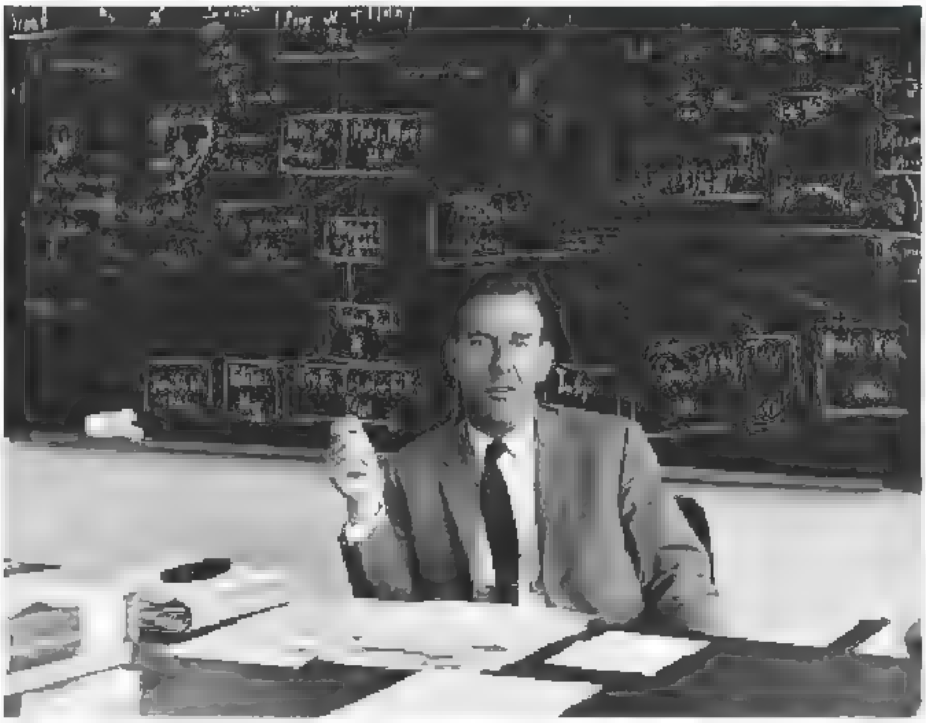
FRAUCH

Reimar Lüst, who turns 85 this week, realized that German research and politics needed each other.

Reimar Lüst was born into a pious household in the west German town of Barmen on 25 March 1923. His rebirth, as he calls it, came 20 years later in the icy-cold waters of the Bay of Biscay in the North Atlantic. A British depth charge had destroyed the U-boat on which he was serving as a submarine officer of the German Nazi navy. Eleven men drowned. Lüst was rescued by a British vessel and was sent to a prisoner-of-war camp where, for relaxation, he solved calculus problems on toilet paper. Thus began his career, first as a leading astrophysicist and space scientist, and then as an influential science manager and policy-maker.

In *Der Wissenschaftsmacher* (*The Science Maker*), Lüst's personal reminiscences are recorded as a series of discussions with the Berlin historian Paul Nolte. They cast a unique light on contemporary German history — and the integration of Europe — as the astrophysicist reaches his eighty fifth birthday.

Lüst had volunteered for the navy in the Second World War hoping to escape the regimented life imposed by the paramilitary Hitler Youth organization. Yet, at the time, he was also convinced that Germany needed an authoritarian regime. The Weimar Republic, the attempt to install a democracy in Germany after the First World War, had proved to be a dismal failure. He objected to the Nazis mainly because he could not bear the egos of party functionaries. Naively, Lüst believed that the Führer would not have accepted the excesses of his followers had he known about them.

> "Lüst seems to be curiously ambivalent about the tension between science and politics, the running theme of his career."

Lüst could not — and did not want to — see what was going on around him during the war. When he was stationed in Amsterdam in 1942, he enjoyed a performance of the St Matthew Passion in the city's Concertgebouw while the German occupation regime was preparing for the deportation of the Jews. Lüst remembers that spring only as the "nicest time" he spent in the navy. Seldom has the state of mind of a highly intelligent young man of good family during the Third Reich been described so candidly.

His awakening finally came in one of the US prisoner-of-war camps where he was interned. Inmates were required to look at photographs that were taken during the liberation of the Bergen-Belsen concentration camp by the British army, who found tens of thousands of starving, sick and dead prisoners. Only then did he realize that "criminals had sent us to war". The camp also offered him a chance to study. Behind the barbed wire, imprisoned German officers ran a nearly complete university. Lüst says he "never heard better lectures".

Returning to a destroyed Germany in 1946, Lüst raced through graduate and post-graduate degrees, obtaining his doctorate at the Max Planck Institute for Physics in Göttingen, which was then headed by Werner Heisenberg. His supervisor was the physicist and philosopher Carl Friedrich von Weizsäcker, brother of the future German president Richard. Lüst worked in theoretical plasma physics and astrophysics for the next 10 years. Four of these he spent in the United States, where "life seemed to be a lot easier". The California Institute of Technology, where he did his last stint, still seems to him today to be the "ideal university". 'Learn from America' became a recurring theme throughout his life, as it did for the young Federal Republic of Germany.

At first, Lüst had little inclination to get involved in politics. He even avoided the student advisory council, saying that the Hitler Youth and the war had satisfied his political appetite. His position changed after 1960 when space science became, as Nolte puts it, the "focus of euphoria about the future". Lüst grasped that space research and politics needed each other. He became a member of the space-research planning committee in Konrad Adenauer's government and, in 1962, became the science director of the newly founded European Space Research Organization.

Over the following four decades, he occupied numerous high offices in a nation that first had to wrestle with the concept of its own democracy, then with recognizing its finite resources, and then belatedly had to find a place for itself amid the sharpened international competition. He was, among other things, chairman of the German Science Council, president of the Max Planck Society and founding director of the private International

University Bremen. "For the family there were the summer holidays," he says.

At the European level he rose to be general director of the European Space Agency, just as big science was establishing itself. It became increasingly difficult to defend basic research against demands for immediate economic, military or societal returns. In Europe, in particular, a consensus needed to be found among the various nations because space research and other expensive projects exceeded the resources of even the large countries. Lüst remains convinced that Europe must develop its own technologies, saying, "You should give up the idea of ever being able to cooperate with the Americans in technological projects."

The final conversation in the book concerns science ethics. Here, Lüst seems to be curiously ambivalent about the tension between science and politics, the running theme of his career. He refers to the moral responsibility of politicians to listen to the opinion of scientists before making a decision, yet criticizes the same politicians for hiding their indecisiveness behind scientific expertise.

Nolte is a perceptive and well-prepared interviewer. His role in the discussions is to link Lüst's reminiscences to their historical context, and he succeeds well in doing so. But the concept of the book is, at times, also its weakness. Nolte's title, *The Science Maker*, confines his questioning to Lüst's active professional roles rather than simply inviting the researcher to act as an educated witness to his times. This memoir fills a long standing hole, placing the voice of a scientist among the many historical accounts of the twentieth century written by novelists and social scientists. More than that, it is an appeal from an exceptional scientist to his colleagues to accept responsibility in society. ■

Stefan Klein is a science writer based in Berlin. His latest book is *Time: A User's Guide* (US title *The Secret Pulse of Time*).

EXHIBITION

Industrial paint's artistic legacy

Now at MoMA: Duchamp's *Tu m'* comments on the death of painting with the arrival of industrial paint.

YALE JUV ART GAL. ERY/ART RESOURCE, NEW YORK/SCALA, FLORENCE

Christopher Turner

Since Isaac Newton, colour has often been equated with visual music. *Color Chart: Reinventing Color, 1950 to Today*, showing at New York's Museum of Modern Art (MoMA), takes a different view. It celebrates the influence of industrial, mass-produced and standardized hues on the art of the past 60 years. Astonishingly, it is the first exhibition devoted exclusively to colour in the museum's 79-year history.

Newton unified the art and science of colour by dividing the spectrum into seven colours — rather than eight — to make an analogy between the chromatic and musical scales. In his *Opticks* treatise of 1704, Newton pictured the primary colours and their complements as a circular diagram. Artists relied on this 'colour wheel' for the next two centuries to create visual harmonies in their paintings. In the synaesthetic abstractions of Vasily Kandinsky or the subtle vibrations of Josef Albers' geometric canvases, colours were given spiritual or affective attributes that built on Newton's scheme.

MoMA's exhibition takes its cue instead from a 1918 surrealist work by Marcel Duchamp enigmatically titled *Tu m'* (*You* (fill-in-the-blank) *Me*). The three-metre-wide canvas was the artist's last painting; disillusioned with conventional art, he intended it as a comment on the end of painting itself. Juxtaposed with the ghostly grey shadows of Duchamp's famous 'ready-mades' — the urinal, the bicycle wheel and the bottle rack, which he exhibited to demonstrate that art could be found in utilitarian objects — is a cascade of lozenges of different colours that resemble samples from a commercial colour chart. In interpreting this canvas, the MoMA curators have made a case for industrial paint as a ready-made item in itself, and explore the revolutionary impact of Duchamp's legacy in the use of colour by contemporary artists.

Ready-mixed industrial paints became widely available for household use in the 1880s, and were advertised with colour charts that altered Newton's circle by displaying hues in random rather than scientific order. In the 1950s, the more robust acrylic paint was invented. A fast-drying polymer, acrylic did not lend itself to the painterly mixing and layering of colours that oils allow. Consequently, the work of many of the 44 selected artists on show feature large monochromes or flat applications of colour. The artist's palette was jettisoned and colours applied directly to the canvas so as to, in Frank Stella's words, "keep the paint as good as it is in the can". Working in this way, as Andy Warhol affirmed, was essentially 'painting-by-numbers'.

In 1954, Yves Klein created a spoof brochure, designed to mimic a paint catalogue, to 'advertise' a series of non-existent canvases. This sample book was filled with large colour swatches with grandiose titles such as *A Londres* or *A Paris* (the latter is painted using the brilliant azure that Klein later patented as International Klein Blue). Twelve years later, Gerhard Richter enlarged the little sample cards that are available in hardware stores into panels forming a painting of 2.5-metre-high columns of vivid colour that is more than nine metres long.

Other works, including a series of collages by Ellsworth Kelly composed of squares of gum-backed paper and a spot painting by Damien Hirst, see colour applied in random, jarring combinations to queasy effect. Perhaps these works show us a portrait of our time. Kandinsky wrote that he saw the art of the past as if it were an orderly message from a vanished age. After experimenting with his own colour theory, and rejecting Newton's visual harmonies, he concluded that modernity was characterized instead by disorder: "Clashing discords, loss of equilibrium … opposites and contradictions — this is our harmony." ■

Christopher Turner is a writer based in New York.

***Color Chart: Reinventing Color, 1950 to Today* runs at the Museum of Modern Art, New York, until 12 May.**

EXHIBITION

How faces share feelings

Jascha Hoffman

Forty years ago, psychologist Paul Ekman took his camera to the island of New Guinea to photograph the faces of the South Fore people. He wanted to prove that the expressions on their faces did not mirror social convention but were universal displays of human emotion. A set of these photographs, which launched Ekman's long career deciphering the secrets of the human face, is now on display in the new *Mind* exhibition at San Francisco's Exploratorium.

In the 1960s, many anthropologists thought that a smile could convey joy in one culture and disgust in another. Ekman had a hunch that this relativistic thinking was wrong. Almost a century before, Charles Darwin had conducted his own international survey of facial expressions in the belief that they were universal. Inspired by this approach, Ekman secured military funding for a series of experiments that showed that people from Japan and Chile, among others, could read expressions on North American faces. When the American anthropologist Margaret Mead protested that exposure to magazines and films might have obscured the differences between cultures, Ekman set out to test the most isolated humans he could find. "I needed to study people who had never had contact with the outside world," he explained. "I wanted to settle it decisively."

When he arrived in New Guinea, there were some misunderstandings. Ekman's attempt, recorded on film, to inspire fear by lunging at a South Fore boy with a rubber knife caused nothing but laughter. After this experiment failed he had to hand out cigarettes and soap to get people to take part in further ones. Yet when participants were asked to point to a pictured face that matched the emotion evoked by a particular story — anger, disgust, fear, joy, sadness or surprise — they made the same associations as people living elsewhere. There was one exception. The South Fore people did not distinguish between fear and surprise. Ekman now speculates that they may have had trouble telling these two emotions apart because, as he says: "In that culture, anything totally unexpected is going to be threatening."

"There was one exception. The South Fore people did not distinguish between fear and surprise."

Since his South Fore study, Ekman has found only one more emotion with a universal expression: contempt. Some other emotions, such as guilt, shame and interest, have not been added to the list of universals because they are expressed in different ways even in the same culture. One might expect some expressions to be learned by mimicry, but Ekman cites evidence to the contrary: psychologist David Matsumoto found that blind judo wrestlers show the thrill of victory and conceal the agony of defeat in precisely the same ways that sighted athletes do. "It's not something we have to learn by observing others," Ekman says. "It's got to be stored in the brain. Nobody knows where."

P. EKMAN/M. MCGOWAN

Facial expressions do not always mirror social conventions.

Ekman went on to devise a system to classify facial expressions using the movements of 43 muscles in the face. He discovered that hidden emotions, such as those caused by lying, can be revealed by fleeting 'micro-expressions'. His system is now used by computer animators to create realistic facial animations and by police officers interviewing suspects. Ekman is also working with the US Department of Homeland Security to train airport staff to identify potential hijackers by searching for suppressed fear and disgust in passengers' faces.

One item in the exhibition stands out. A tiny video screen shows Ekman's 1967 footage of a group of boys playing outside the window of his hut in New Guinea. After disappearing from view, a young boy suddenly sticks his head back into the frame and pulls faces at the camera. The scene is so familiar, yet, after one has paid such close attention to facial detail, it seems utterly foreign. It is a reminder of how flexible our faces are, and of how much we can convey when we know someone is watching. ■

Jascha Hoffman is a writer based in New York City.

The Search for Universals in Human Emotion: Photographs from the New Guinea Expedition **runs until 11 May at The Exploratorium, San Francisco, California.**

EXHIBITION

An eye for detail

Jenny Meyer

Maria Sibylla Merian is one of the most significant seventeenth-century artists of natural history. Her carefully observed records of plants, insects and animals are on display at the Rembrandt House Museum in Amsterdam until May, moving to the Getty Center in Los Angeles, California, in June.

Showing her as both scientist and artist, the exhibition *Maria Sibylla Merian & Daughters: Women of Art and Science* offers glimpses of Merian's methods, and includes mounted insects in varying states of metamorphosis. The collection is interspersed with paintings and prints by other artists who influenced her, including her stepfather and teacher, Jakob Marrel.

Merian led an unconventional life. Aged 38 and already the author of two books on caterpillars and a three-volume set on flowers, she left her husband and entered a religious commune with her two daughters. Five years later, she and her daughters moved to Amsterdam and established a business selling artists' materials alongside preserved insects and animals.

In 1699, Merian travelled to Suriname (then a Dutch colony) in South America with her youngest daughter, Dorothy, and stayed there for two years to observe and record life in the tropical rainforest. Ill health forced Merian to return to Amsterdam where she published her findings in the *Metamorphosis Insectorum Surinamensis*, a breathtaking work. Merian's watercolours from the British Royal Collection (pictured) are also on public display for the first time, and still retain their original brilliant colours. ■

ROYAL COLLECTION, HM QUEEN ELIZABETH

Maria Sibylla Merian & Daughters: Women of Art and Science **is at the Rembrandt House Museum, Amsterdam, until 18 May and then at the J. Paul Getty Center, Los Angeles, from 10 June to 31 August.**

Hidden treasures: Florence's botanical collection

Italy's first centralized museum of plants was one of the early flowerings of the unification movement. **Alison Abbott** reports on an important scientific legacy.

During the nineteenth-century movement for the unification of Italy known as the *risorgimento*, governors of the fractious independent states on the Italian peninsula were wary of gatherings of intellectuals — they tended to talk unification politics, and to be patriots. It is a measure of the open-mindedness of the liberal Leopold II, Grand Duke of Tuscany, that in 1841 he allowed the Third Congress of Italian Scientists to be held in his capital, Florence, despite that incendiary label 'Italian'.

Better still, Leopold rushed the completion of a special room in which to host the congress: the Tribune of Galileo in the city's Imperial and Royal Museum of Physics and Natural History, which Leopold's ancestor had created a century earlier in a medieval palace on the outskirts of town. The Tribune, with its marble busts, frescos and mosaics, doubled as a shrine to Galileo, whom risorgimentists had adopted as a symbol of united Italy.

It was at the Third Congress of Italian Scientists that the idea of a centralized herbarium in the Italian-speaking countries was proposed by Filippo Parlatore. This lively Sicilian had recently abandoned a medical career in favour of botany, his true passion, and he left his native Palermo in 1840 to tour the botanic centres of Europe. From Paris, he sent the congress a missive deploring the state of the small collections he had visited in Italy and arguing for the foundation of a single herbarium to develop the new disciplines of taxonomy and phytogeography, the geographical distribution of plant species.

His proposal struck a chord with the congress attendees. More importantly, it won the approval of the Grand Duke, who would be paying for it. Leopold subsequently invited Parlatore to be the first director of the *Herbarium Centrale Italicum* in the Imperial and Royal Museum. Today, the herbarium is among the most scientifically valuable historical plant collections.

Parlatore took office in 1842, and Italy's most important botanists began to send him their collections of dried plants pressed between sheets of paper. His acquisitions were crowned in 1850 by a bequest from his friend, the famous English botanist Philip Barker Webb. Webb left his entire collection of around 500,000 specimens as well as his extensive library to the herbarium. He had collected widely in Europe, Morocco and Brazil, and wrote one of the most important texts on the natural history of the Canary Islands.

Parlatore organized exotic collecting expeditions for the herbarium; these continued into the twentieth century, with many specimens being added from Italy's East African colonies. Botanists from all over Europe regularly visited the resulting collection.

Parlatore also curated an extraordinary collection of wax plants and fruits, including some models of plant anatomy and pathology. The collection showed visitors all parts of a plant, at all times of year. The wax models were made by the same artists who produced the more widely known human anatomy ones.

These artists worked under the guidance of expert botanists, such as Giovanni Battista Amici (1786–1863), a polymath whose interest in optics led him from telescopes and astronomy to microscopes and plant anatomy. The pots in which the wax plants stand, and the ceramic shells displaying their wax seeds, were made at the Doccia porcelain factory near Florence, supplier of fine figurines and tableware to the rich and royal.

Visitors can now see more than 500 of these bright and beautiful wax specimens, which at first glance are indistinguishable from the real thing. They can also enjoy a collection of around 60 botanical portraits — oil paintings that were commissioned by Florence's powerful Medici family, in part to show off their valuable exotic plants all year round.

After Italy's unification in 1861, botanical research came to be dominated by the microscopy techniques that Amici helped to develop. Taxonomy fell out of fashion and the herbarium and its curious wax models were mostly relegated to teaching tools. The collection was moved to the nascent university in the centre of town, where it is still housed. To this day, many of the holdings have not yet been examined by scholars. In the 1930s, Galileo's instruments and other memorabilia — including his mummified finger — were transferred from the Tribune of Galileo to Florence's new Institute and Museum of the History of Science. But the Tribune itself and the entire Imperial and Royal Museum of Physics and Natural History more than reward a visit. Through their political ideals, the risorgimentists facilitated a wonderful scientific legacy. ■

Alison Abbott is *Nature*'s Senior European Correspondent.

© BAMB., MUSEO DI STORIA NAT.LE, FLORENCE

Intricate wax models (above and left) of plants at Florence's Museum of Natural History look just like the real thing.

The botany section of the Museum of Natural History can be visited by appointment at 4 Via la Pira, 50121 Florence, Italy.

Immunology & Cell Biology

Special feature

The Power of One Idea: The Golden Anniversary of Burnet's Clonal Selection Theory

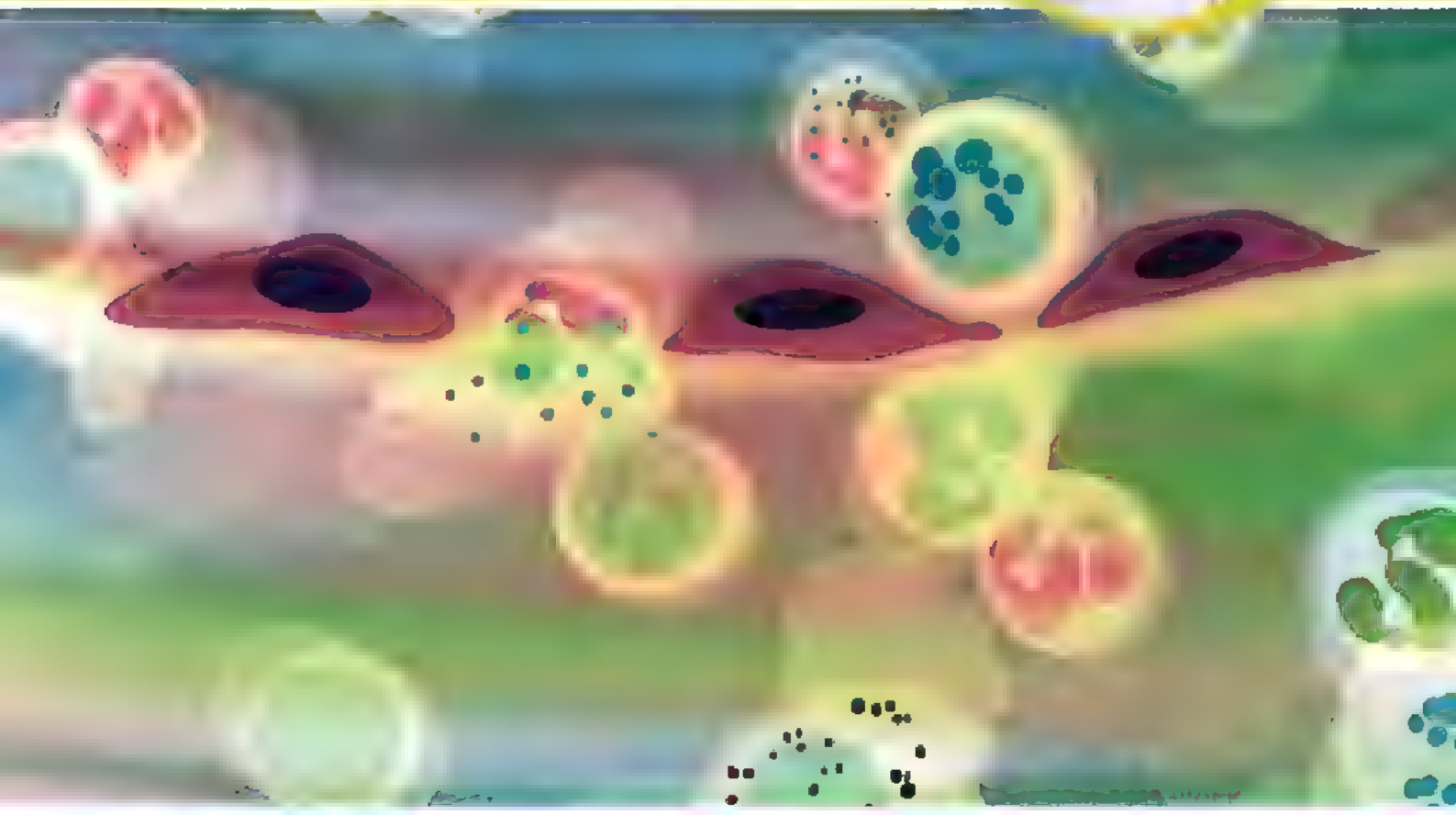

Two part special feature

www.nature.com/icb

npg

Fewer steps deliver faster, better data

New Luminometer Provides Bioluminescence and Multiplexing Capabilities

The Promega GloMax®-Multi Detection System gives you bioluminescent, colorimetric and fluorescent solutions for quantifying your most challenging and complex cell signaling experiments. It's an integrated system of hardware, software, reagents and service that is perfect for reporter gene assays, cell viability and drug discovery. Now you can get faster, better data in a lot fewer steps.

See for yourself. Arrange for a GloMax-Multi demonstration and we'll give you a FREE T-shirt*. To learn more visit: www.promega.com/3glomax

Promega

*While supplies last. Demo instrument subject to availability.

NEWS & VIEWS

CATALYSIS

Triumph of a chemical underdog

Gorka Peris and Scott J. Miller

In the fable of the tortoise and the hare, the reptilian slowcoach beats its fleet-footed rival in a race. A zinc catalyst recreates this story by giving a less reactive chemical group a turn of speed over a rival group.

Ranking the inherent reactivity of chemical groups was crucial for propelling organic chemistry into the realms of rational science. This groundwork was achieved over the course of many decades, and a basic knowledge of which groups react faster than others is still essential today. But can the reactivity of chemical groups be tinkered with, so that, in a molecule containing several groups, the less-active ones react before the more reactive? Reporting in the *Journal of the American Chemical Society*, Ohshima *et al.*[1] report a remarkable catalyst that can reorder the reactivity of two common chemical groups — a revelation that is certain to inspire chemists everywhere.

Catalysts come in many forms (enzymes, metal complexes, polymers, small organic molecules and so on), each with an armoury of features that chemists exploit in different situations. The most powerful catalysts enable otherwise inert groups to take part in all sorts of useful reactions. But one of the toughest challenges for a catalyst is to distinguish between many reactive sites within a single, complex molecule, especially when the same chemical group occurs several times. Furthermore, in organic synthesis, it isn't always desirable to work with the most reactive chemical groups first, so catalysts that allow reactions to occur selectively at less reactive sites are highly desirable.

Enzymes are the acknowledged masters at reversing the reactivity of chemical groups in molecules[2], but non-enzymatic catalysts may on occasion compete for the accolade. For example, transition-metal complexes have been discovered that reverse the order in which carbon–carbon double bonds (C–C) tend to react in oxidation reactions of geraniol[3], a molecule commonly used in studies of chemical synthesis and biosynthesis. In some reactions, antibodies can be generated that control the conformation of a substrate in a transition state, redirecting the course of the reaction so that the less reactive of two otherwise similar bonds is broken[4]. In our own laboratory[5], we have found that small, peptide-based catalysts can reorder the reactivity of several hydroxyl (OH) groups within the antibiotic erythromycin A.

But changing the order in which two different chemical groups react is another matter entirely, especially if one of those groups ordinarily reacts much faster than the other. A good example from classical chemistry uses copper catalysts to make organomagnesium reagents react at C–C bonds, rather than at adjacent, more polarized carbonyl (C–O) bonds[6] that would normally react first.

Perhaps more dramatic is reversing the order of reactivity of hydroxyl groups and amino groups (nitrogen-containing groups found in organic bases known as amines). These two chemical groups are nucleophilic — they attack other molecules, called electrophiles, that contain areas of positive charge. But amino groups are generally far more nucleophilic than hydroxyls, so that when an amine and an alcohol (a compound that contains a hydroxyl group) are mixed together with a limited amount of a common electrophile, the electrophile reacts almost exclusively with the amine[7]. Similarly, for compounds that contain both an amino group and a hydroxyl group, an electrophile will typically react at the amine part of the molecule. Reaction at the hydroxyl is often not possible unless the amino group is first modified in a separate step using a 'protecting group' to make it less reactive.

But Ohshima *et al.*[1] have successfully reversed the reactivity of hydroxyl and amino groups by using a zinc catalyst (Fig. 1). When they mixed equal molar quantities of an amine and an alcohol together with an electrophile, in the presence of the catalyst, the alcohol reacted far more rapidly to form an ester product (instead of the amine reacting to form an amide). Likewise, when the authors mixed a compound containing both amino and hydroxyl groups with the same electrophile and catalyst, the hydroxyl group reacted much faster to produce an ester (Fig. 1b). The reactions are remarkable not only for their selectivity, but also for their speed and high yields: uncatalysed versions of these reactions are staggeringly slow under similar conditions.

The net result of these reactions is known as an 'ester interchange', because the electrophile, like the product, contains an ester group (an oxygen adjacent to a C–O bond). Catalytic ester-interchange reactions have been described before[8], as have the analogous

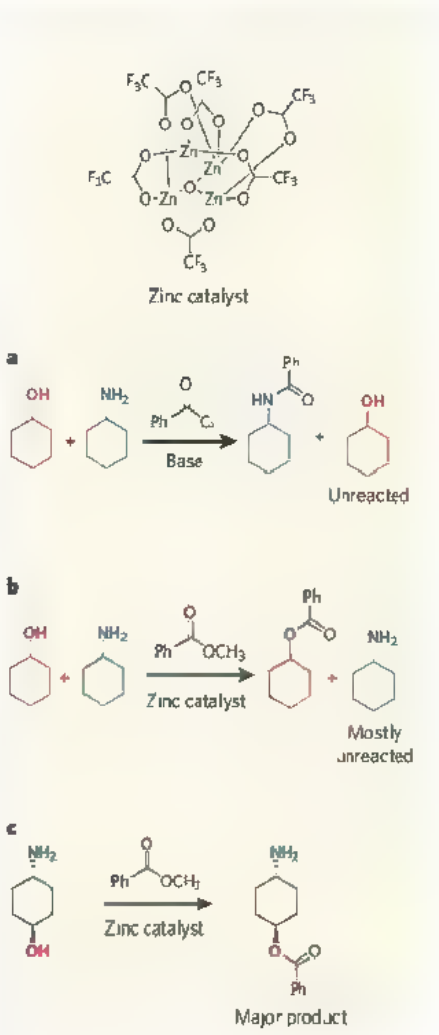

Figure 1 | Selective reactions with a zinc catalyst. Ohshima *et al.*[1] have made a zinc catalyst that reverses the intrinsic reactivity of alcohols (which contain OH groups) and amines (which often contain NH_2 groups). Zn is zinc, F is fluorine. **a**, When a 1:1 mixture of an alcohol (red) and an amine (blue) is reacted with an 'electrophile' (such as benzoyl chloride) in the presence of a base, only the amine will react. **b**, In the presence of Ohshima and colleagues' catalyst, the alcohol reacts preferentially. Here, the electrophile is methyl benzoate, a less reactive analogue of benzoyl chloride. **c**, When a molecule containing both an OH group and an NH_2 group reacts with methyl benzoate in the presence of the catalyst, the OH group reacts preferentially.

— and chemically more demanding — catalytic amide-interchange reactions[9]. But Ohshima and colleagues' reaction[1] is truly striking because it overrides the order of reactivity that would be expected in the absence of catalysts.

It has long been known that catalysts not only speed up chemical transformations, but can also make reactions occur in ways that would otherwise be impossible. Similarly, the ability to manipulate reactions to obtain just one product when many others are likely to form is a long-standing goal of synthetic chemists. Ohshima and colleagues' work[1] thus represents a real advance in nucleophilic reactions. But it also reminds chemists to challenge their assumptions about the relative reactivity of the chemical groups in organic molecules. Such assumptions may be the biggest barrier to the discovery of exciting new reactions. ■

Gorka Peris and Scott J. Miller are in the Department of Chemistry, Yale University, 225 Prospect Street, New Haven, Connecticut 06520-8107, USA.
e-mail: scott.miller@yale.edu

1. Ohshima, T., Iwasaki, T., Maegawa, Y., Yoshiyama, A. & Mashima, K. *J. Am. Chem. Soc.* **130**, 2944–2945 (2008)
2. Gardossi, L., Bianchi, D. & Klibanov, A. M. *J. Am. Chem. Soc.* **113**, 6328–6329 (1991)
3. Sharpless, K. B. & Michaelson, R. C. *J. Am. Chem. Soc.* **95**, 6136–6137 (1973)
4. Janda, K. D. *et al. Science* **259**, 490–493 (1993)
5. Lewis, C. A. & Miller, S. J. *Angew. Chem. Int. Edn* **45**, 5616–5619 (2006)
6. Kharasch, M. S. & Tawney, P. O. *J. Am. Chem. Soc.* **63**, 2308–2316 (1941)
7. Sontag, N. O. *Chem. Rev.* **52**, 237–416 (1952)
8. Stanton, M. G. & Gagne, M. R. *J. Am. Chem. Soc.* **119**, 5075–5076 (1997)
9. Hoerter, J. M. *et al. J. Am. Chem. Soc.* **128**, 5177–5183 (2006)

CIRCADIAN RHYTHMS

Stem cells traffic in time

David T. Scadden

Circadian activity in the brain regulates the movement of blood stem cells into and out of the bone marrow. Perhaps this process is testing the suitability of these cell 'tenants' for their new home — the remodelling bone.

All tissue-specific stem cells move around during embryonic development. But mammalian haematopoietic stem cells (HSCs), which are precursors to all blood cell types, continue to migrate via the bloodstream throughout adulthood. Many of the molecules that locally mediate HSC movement between the bone marrow and the bloodstream have been identified, perhaps the most prominent example being CXCL12. This protein is essential for the movement of HSCs to the bone marrow during development and their retention there in adulthood. By contrast, the mechanisms underlying the trafficking of stem cells in adulthood, and their physiological significance, have remained relatively obscure. On page 442 of this issue, Frenette and colleagues (Méndez-Ferrer *et al.*)[1] show that HSC circulation and CXCL12 expression are coupled to the homeostatic oscillatory processes that regulate broad aspects of an organism's function — circadian rhythms.

Virtually all life forms, from unicellular organisms to humans, experience cyclic increases and decreases in the levels of cellular molecules as a consequence of self-inhibitory regulatory networks. So, were it not for the hierarchical organization of pacemaker regulation, the complexity of the switches involved and the networks of interacting regulators would together result in the molecular equivalent of a cacophony. The more advanced pacemakers are often influenced by external cues, such as the light–dark cycle, resulting in circadian (daily) and circannual (yearly) physiological rhythms.

In mammals, certain circadian events are intrinsic to a specific tissue or cell type, but they are largely subservient to the master pacemaker in the central nervous system, the suprachiasmatic nucleus located in the hypothalamus. The phased activity of this brain structure in response to the light–dark cycle leads to a profound array of fluctuations, including changes in metabolic rate, cognitive function and immune-system reactivity. The effect of the suprachiasmatic nucleus is largely mediated by noradrenaline, an adrenergic neurotransmitter that is secreted by the sympathetic nervous system. Méndez-Ferrer and colleagues' work[1] directly links circadian control of the sympathetic nervous system to HSC function.

The stem-cell repertoire of adult tissues generally consists of a small number of self-replenishing cells that turn over very slowly — for primate HSCs, turnover occurs over months to years[2]. In culture, these cells are relatively unaffected by immune mediators such as inflammatory cytokines. But when in their niche (microenvironment) in the body, they respond to stressors that may be occurring at the organismal level, for example infection or cancer chemotherapy. How signals at the organismal level are integrated into activity in the stem-cell niche remains an underexplored area of research. The Frenette laboratory[3] is a leader in this area, having been the first to show[3] that, by means of their niche, HSCs respond to the ultimate integrating system in the body, the nervous system, or, specifically, to the adrenergic signals originating from it.

The authors now show that, during a day, CXCL12 levels in the bone marrow oscillate with periods of light and dark in counterpoint to the concentration of HSCs in the blood, during times when it is light — the rest period for mice — HSC levels are about 2.5-fold higher than those during times of darkness, and this is mirrored in the opposite direction for CXCL12 levels in the bone marrow. These cycling events do not seem to be mediated by the clock genes within either HSCs or the bone-marrow stromal support cells; rather, the authors find that oscillations in both circulating HSC levels and CXCL12 expression are regulated by adrenergic stimulation.

The function of adrenergic signals from the suprachiasmatic nucleus varies depending on the receptor subtype to which they bind on their target cells. Méndez-Ferrer *et al.* find that, in the bone marrow, noradrenaline activates β_3-adrenergic receptors. As bone-forming cells called osteoblasts have β_2, but not β_3, receptors,

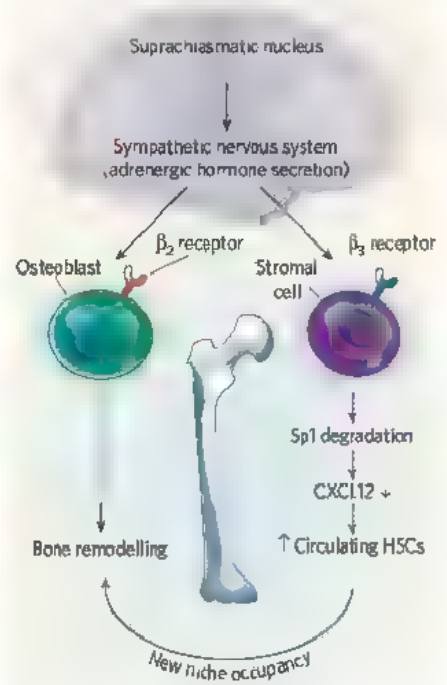

Figure 1 | Pacemaker activity and cooperativity between bone and bone-marrow cells. Circadian activity is regulated by a central neural pacemaker, the suprachiasmatic nucleus, which activates distant sites by stimulating the secretion of adrenergic hormones by the sympathetic nervous system. These hormones are known to bind to β_2-adrenergic receptors on osteoblasts, activating a signalling cascade that alters cell proliferation (not shown) and ends in bone remodelling. Méndez-Ferrer *et al.*[1] find that adrenergic hormones also activate β_3 receptors on the surface of bone-marrow stromal cells. This results in the degradation of the Sp1 transcription factor and decreased levels of the anchoring protein CXCL12. The result is that haematopoietic stem cells (HSCs) are free to leave the bone marrow and transiently enter the bloodstream. The movement of HSCs into and out of non-osteoblast stromal niches is probably synchronized with circadian growth and remodelling of their 'home' osteoblast-generated bones.

this suggests that a different CXCL12-producing cell regulates the mobilization of HSCs. It has been shown[4] that HSCs in the bone marrow are affected by a type of CXCL12-producing reticular cell (a cell that contributes to the stroma), although the specific nature of these cells is unclear.

The authors find that, downstream of the β_3 receptor, the stability of the gene transcription factor Sp-1 is reduced by the removal of a phosphate group. Such dephosphorylation might contribute to the decreased expression of the *Cxcl12* gene. With reduced CXCL12 to anchor HSCs to the bone marrow, these cells would be able to transiently enter the circulation.

The task ahead is to discern the physiological significance of the cyclic changes in stem-cell circulation. On noting circadian variation in a stem-cell circulation, the authors of a previous study[5] proposed that it could be used to harvest stem cells for transplantation. This clinical application would certainly be good. But from an evolutionary perspective, the advantage for the organism of circadian variation in the circulating levels of HSCs, or indeed HSC circulation at all, is unclear.

A clue to why HSC circulation is advantageous might lie in its circadian nature. Perhaps bone and bone marrow function as an integrated system. Bone formation occurs in a diurnal manner in rodents, with the greatest remodelling occurring during periods of light[6]. Many hormones affecting skeletal mass, including parathyroid hormone and leptin, undergo circadian cycling[7]. Also, clock genes, such as *Per1*, *Per2* and *Cry*, in osteoblasts inhibit bone formation and, in their absence, leptin-driven adrenergic stimulation has a proliferative effect on osteoblasts[8]. Circadian bone-modifying events might occur in synchrony with adrenergic stimulation of the β_3 receptors on stromal cells, causing Sp1 degradation, decreased CXCL12 production and increased HSCs in the blood (Fig. 1).

Because modifications to bone would also be expected to modify both bone marrow and the niches it provides for blood-cell production, it could be that it is the remodelling of their 'home' that sends HSC residents packing. If remodelling or making new bone creates bone-marrow niches, filling them with stem cells rather than with 'foreign' cell types such as more mature or even mutant cells may be advantageous. In invertebrate animal models, foreign cells occupying niches can undergo dedifferentiation and other events inducing cell division[9,10]. This might be problematic considering the risk of malignancy in longer-lived organisms.

During embryonic development, blood-cell production in the bone marrow requires circulating HSCs to migrate to and engraft in the niche[11]. Perhaps the same is true for the constantly remodelling adult bone and bone-marrow niches, in that they require a circulating cell to undergo migration and engraftment as a selection process for the fittest stem cells. Circadian oscillations in stem-cell location might contribute to synchronized generation of niches and their rapid occupancy by the best-suited stem cells. Perhaps a good breakup can ultimately ensure 'domestic tranquillity'. ■

David T. Scadden is at the Center for Regenerative Medicine, Massachusetts General Hospital, Harvard Stem Cell Institute, Boston, Massachusetts 02114, USA.
e-mail: dscadden@mgh.harvard.edu

1. Mendez-Ferrer, S., Lucas, D., Battista, M. & Frenette, P. S. *Nature* **452**, 442–447 (2008)
2. Shepherd, B. E. *et al. Exp. Hematol.* **32**, 1040–1050 (2004)
3. Katayama, Y. *et al. Cell* **124**, 407–421 (2006)
4. Sugiyama, T. *et al. Immunity* **25**, 977–988 (2006)
5. D'Hondt, L. *et al. J. Cell. Physiol.* **200**, 63–70 (2004)
6. Simmons, D. J. & Nichols, G. Jr *Am. J. Physiol.* **210**, 411–418 (1966)
7. Fraser, W. D., Ahmad, A. M. & Vora, J. P. *Curr. Opin. Nephrol. Hypertension* **13**, 437–444 (2004)
8. F., L. *et al. Cell* **122**, 803–815 (2005)
9. Ka., T. & Spradling, A. *Proc. Natl Acad. Sci. USA* **100**, 4633–4638 (2003)
10. Ka., T. & Spradling, A. *Nature* **428**, 564–569 (2004)
11. Laird, D. J. *et al. Cell* **132**, 612–630 (2008)

ASTRONOMY

Starbursts near and far

Yu Gao

Observations of intensely bright star-forming galaxies both close by and in the far Universe seem to emphasize their similarities. But look a little closer, and telling differences emerge.

In a recent issue of the *Astrophysical Journal*, two papers[1,2] present the latest measurements of 'starburst' galaxies — galaxies whose extreme brightness is thought to indicate short, intense bursts of star formation. This latest work is a fine example of the instruments and methods that are providing ever deeper insight into these spectacular objects. But equally, it exposes gaps in our knowledge that cannot be filled by using current instrumentation, and that must wait for the next generation of more powerful telescopes.

The first of the papers, by Mangum *et al.*[1], provides perhaps the most accurate measurements so far of the density of star-forming molecular gas in nearby starburst galaxies. The authors used the National Radio Astronomy Observatory's 100-metre-aperture Green

50 YEARS AGO

Handbuch der Physik
Herausgegeben von S. Flügge.
Band 14: Kältephysik I. Band 15: Kältephysik II. — To find, in an encyclopædia of physics running to fifty volumes, that two should be devoted specifically to low-temperature physics raises the question whether nowadays it is a sufficiently distinct branch to justify separate treatment ... Indeed, so much labour has gone into these exhaustive compilations of facts that it may seem ungrateful to complain that the total effect is one of deplorable dullness. Yet there is indeed only one article, that by J. Bardeen on the theory of superconductivity, which can be said to be exciting; and this is distinguished from the rest chiefly because the author is not content to act as an impassive recorder of what is known, but is eager to explore those regions where the meaning of the observations is obscure.
From *Nature* 29 March 1958.

100 YEARS AGO

An interesting lecture was given by Sir William Preece at the Institution of Electrical Engineers on March 12 on his recent visit to America, and the various improvements in constructional and engineering works since his previous visits were dealt with. The sky-scraper buildings appear to afford a considerable day load, in that they employ numerous lifts which are constantly in use ... On the telephone question, America seems to have gone ahead of us on this side. In most of the hotels telephones are installed in every bedroom, so that business may be transacted with any part of the country. This applies also to the restaurants, where telephones may be plugged on to your table if desired. The Telephone Tariff question has also been thoroughly considered in America, and the message rate has been adopted in preference to the simple annual rental.
From *Nature* 26 March 1908.

50 & 100 YEARS AGO

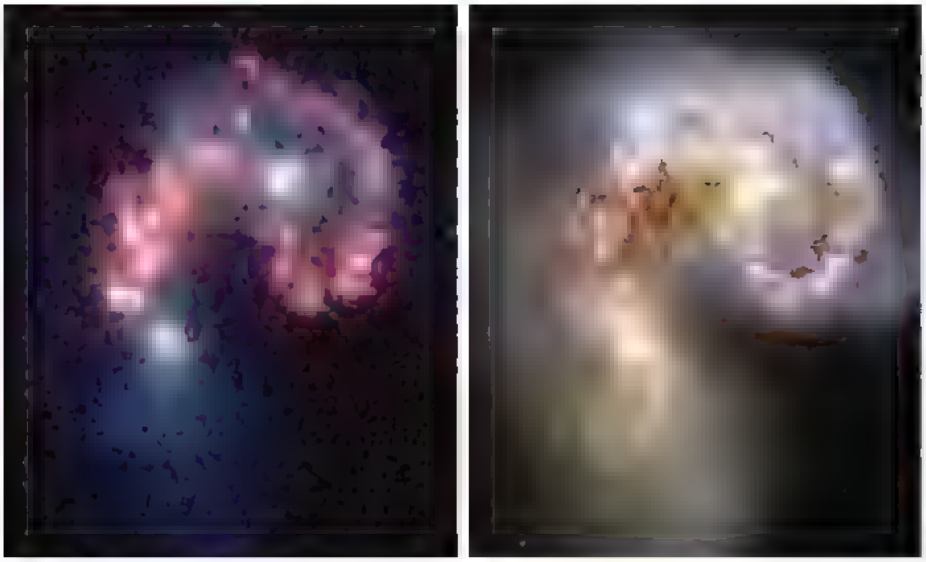

Figure 1 | Buried in dust. These two images of the spectacular merger of the nearby Antennae galaxies — on the left from NASA's Spitzer Space Telescope, on the right from the Hubble Space Telescope — show the train wreck of two gas-rich spirals. The proximity of the galaxies allows detailed imaging of newborn star clusters and the infrared hotspots that mark starburst sites. The dusty regions between the two galaxies, heavily obscured in the Hubble optical image, are in fact the dominant sites of active star formation as traced by the Spitzer Infrared Array Camera at an infrared wavelength of 8 micrometre emission (red). Indeed, the brightest infrared hotspot (centre left of the Spitzer image) is almost entirely unseen. Extreme starbursts near and far are more than several tens of times brighter than the Antennae galaxies, and the most intense examples are usually hidden in dust, making comparisons between observations at different redshifts particularly tricky.

Bank Telescope in West Virginia to investigate 19 close galaxies that emit strongly in the infrared. They surveyed radio waves emitted by the galaxies at centimetre wavelengths corresponding to two '*K*-doublet' transitions of the organic molecule formaldehyde (H_2CO) — a reliable density and temperature probe in the star-forming molecular clouds in our own Galaxy.

The weakness of these transitions, coupled with the presence of intermingling emission and absorption features in the spectrum, makes such measurements complicated, even for nearby galaxies. The authors could detect one transition from most of the galaxies, but both transitions (allowing precise measurement of spatial densities) from only five. The findings confirm what had been observed with other dense-gas tracers such as hydrogen cyanide (HCN)[3]: that galaxies with higher star-formation rates tend to have higher gas density. This correlation supports the idea that vigorous starbursts are driven by the amount of dense molecular gas available to form stars[4].

In the second paper, Hathi *et al.*[2] extend observations of starburst intensities to much more distant galaxies, at redshifts of up to 6. Redshift describes the fact that the Universe is expanding, and that light from a distant cosmic source will therefore be stretched to longer (redder) wavelengths as it travels towards us. Redshift is thus a measure both of 'lookback time' — light with a redshift of 6, for example, is light emitted when the Universe was about a tenth of its current age — and also, because light travels at a finite speed through the cosmos, of a source's distance from us. Accordingly, Mangum and colleagues' sample of nearby galaxies has a redshift of almost zero.

Newborn stars emit light mostly at ultraviolet wavelengths. This light heats the surrounding interstellar dust, which then radiates at infrared wavelengths. Because of the redshift effect, Hathi *et al.*[2] used two cameras aboard the Hubble Space Telescope that were sensitive at optical and near-infrared wavelengths, respectively, to observe the original ultraviolet light from two galaxy samples lying at redshifts of 3–4 and 5–6. The authors deduce a constant maximum star-formation intensity for both samples, one that is broadly in agreement with earlier observations of starbursts at lower redshifts.

Before we hasten to draw physical conclusions from these similarities, we must bear in mind that we might not be comparing like with like. The most powerful local starbursts, ultraluminous infrared galaxies or ULIRGs, typically have extreme starburst regions smaller than 1,000 light years across. The mass of gas in those regions is the equivalent of a billion solar masses, and their luminosity can be greater than that of a couple of hundred billion Suns[5] — several times more than is emitted by an entire typical spiral galaxy such as our Milky Way.

But ultraviolet imaging of the central regions of nearby ULIRGs indicates that ultraviolet emissions make up at most only around 7% of total emissions[6], and that a thousand light years or more separate peaks of ultraviolet and infrared emission. The implication is that Hathi and colleagues' intensity measurements represent just residual light leaking from stars in dust-enshrouded star-forming regions, and miss the dominant infrared radiation re-radiated by the dust. That supposition is supported by recent surveys of the deep Universe, such as COSMOS[7], GOODS[8] and SWIRE[9], which are finding more and more high-redshift dust-obscured galaxies with large infrared-to-ultraviolet luminosity ratios that had been missed in traditional optical surveys.

That would seem to lead to one of two conclusions. First, that Hathi and colleagues' high-redshift galaxies are powered by even brighter extreme starbursts, largely hidden in dust, than those found in the local Universe — with concomitantly much higher densities of molecular gas than could possibly be extrapolated from Mangum and colleagues' H_2CO results. Recent efforts to detect HCN at high redshifts have offered some evidence for a higher ratio of star-formation rate to dense gas at early cosmic times[10–12]. An alternative explanation for the anomaly is that the earlier starbursts might simply be very much larger in extent, with intensities comparable to those of the nearby starburst galaxies.

If the earlier starbursts are indeed in general much more intense, we might suppose that they have a different physical origin. The extreme starburst activity of nearby ULIRGs is thought to have been triggered by the strong interaction or merger of gas-rich spiral galaxies (Fig. 1). A possibility for the high-redshift starbursts is that a fraction of the luminosity is caused by at least one dust-obscured 'active galactic nucleus' (AGN) — a black hole at the centre of the merging galaxies. If that is so, are there any evolutionary connections between extreme starbursts, the build-up of massive AGNs, and how galaxies assemble? A link between the mass of the black hole at the centre and the mass of the central bulge of the host galaxy certainly exists[13,14]. Extreme starbursts close to the galaxy centre might well help to speed up the assembly of mass around the bulge through rapid, runaway star formation, which in turn would feed the growth of the central black hole, causing stronger AGN activity.

Combining optical and infrared observations is one way to improve our estimation of the all-important star-formation rate in starburst galaxies[15]. But ultimately, observations of distant starbursts at longer far-infrared and submillimetre wavelengths will be the key to better quantifying their true star-formation rate and intensity. We might not know the full answer until the resolving power and sensitivity of next generation facilities such as the international Atacama Large Millimeter/submillimeter Array (ALMA)[16] and NASA's James Webb Space Telescope (JWST)[17] come to fruition in the next few years. ALMA will be able to reveal the obscured starburst intensity maps, as well as the distribution of dense molecular gas and its kinematics, at high redshifts. The capability of the JWST in the mid-infrared will directly expose hidden starbursts buried in their surrounding dust.

We will have to wait a little longer before we have the means to apply Mangum and

colleagues' finely tuned H_2CO densitometer[1] to Hathi and colleagues' high-redshift galaxy sample[2]. But even that capability might come with the Square Kilometre Array[18], an international radio telescope currently at the planning stage. ■

Yu Gao is at Purple Mountain Observatory, Chinese Academy of Sciences, Nanjing, Jiangsu 210008, China
e-mail: yugao@pmo.ac.cn

1. Mangum, J. G., Darling, J., Menten, K. M. & Henkel, C. *Astrophys. J.* **673**, 832–846 (2008)
2. Hathi, N. P., Malhotra, S. & Rhoads, J. E. *Astrophys. J.* **673**, 686–693 (2008)
3. Gao, Y. & Solomon, P. M. *Astrophys. J. Suppl. Ser.* **152**, 63–80 (2004)
4. Gao, Y. & Solomon, P. M. *Astrophys. J.* **606**, 271–290 (2004)
5. Downes, D. & Solomon, P. M. *Astrophys. J.* **507**, 615–654 (1998)
6. Goldader, J. D. *et al. Astrophys. J.* **568**, 651–678 (2002)
7. http://cosmos.astro.caltech.edu
8. www.stsci.edu/science/goods
9. http://swire.pac.caltech.edu
10. Solomon, P. M., Vanden Bout, P., Carilli, C. L. & Guelin, M. *Nature* **426**, 636–638 (2003)
11. Gao, Y., Carilli, C. L., Solomon, P. M. & Vanden Bout, P. *Astrophys. J.* **660**, L93–L96 (2007)
12. Riechers, D. A., Walter, F., Carilli, C. L. & Bertoldi, F. *Astrophys. J.* **671**, L13–L16 (2007)
13. Ferrarese, L. & Merritt, D. *Astrophys. J.* **539**, L9–L12 (2000)
14. Gebhardt, K. *et al. Astrophys. J.* **539**, L13–L16 (2000)
15. Cauzetti, D. *et al. Astrophys. J.* **666**, 870–895 (2007)
16. www.alma.nrao.edu
17. www.jwst.nasa.gov
18. www.skatelescope.org

NANOELECTRONICS

Spin surprise in carbon

Arne Brataas

Spintronics is an emerging branch of electronics that exploits electrons' spin, rather than charge. In carbon nanotubes, the coupling of this spin with electron motion could offer a desirable way to control quantum information.

Electrons have an electrical charge and a spin — an intrinsic angular momentum as if the electron were spinning around its own axis. The spin adopts one of two states, the manipulation and detection of which forms the basis of a branch of electronics known as spintronics. If the spin interacts with electron motion, it can cause the spin to change state, leading to loss of information in a spintronics device. In carbon, these spin–orbit interactions were thought to be weak, making the material ideal for sending spin information over long distances. In this issue, McEuen and colleagues (page 448) show that in carbon nanotubes, spin and orbital motion are more strongly coupled than previously thought. Far from being a bad thing, this opens up new possibilities for manipulating electron spin.

The spin state of electrons can be used as a binary variable in much the same way that oppositely charged particles (electrons and positively charged 'holes') are used in semiconductor devices. This has opened up new fields of science and technology and has already led to commercial devices, such as read heads for computer hard disks. These devices rely on a spin-dependent principle known as giant magnetoresistance, the discovery of which won the 2007 Nobel Prize in Physics for Albert Fert and Peter Grünberg[2].

Carbon nanotubes have great appeal as possible components of spintronics devices. These carbon structures consist of sheets of carbon atoms rolled up into a cylinder, and this topology separates electron movement into two orbitals of equal energy: one that circles the tube in a clockwise direction, and one that circles anticlockwise. This simple orbital arrangement could make it easier to manipulate electrons and offers another binary variable that might be useful for carrying information. Furthermore, spintronic signals in carbon are expected to be stable because the small size of the nucleus reduces electronic spin–orbit interactions, and because carbon nuclei have no nuclear spin to cause the signal to decay.

McEuen and colleagues[1] now demonstrate that in carbon nanotubes the interaction between an electron's spin and its orbital motion is strong. This is no mean feat, because the effects of the spin–orbit interaction first have to be isolated from those of other interactions. In particular, electron–electron interactions in carbon nanotubes have a marked effect on electron properties. The authors addressed this problem by constructing a nanotube quantum dot — a nanotube that contains just one, or a few, charge carriers (electrons or holes) constrained in all three spatial dimensions.

The authors used a method known as a Coulomb blockade to confine the charge carriers. This involves applying a 'gate' voltage part of the way along the nanotube, inducing a background potential that dictates the number of electrons or holes in the dot. They also applied a 'source-drain' voltage across contacts placed at either end of the nanotube. By measuring the current through the nanotube, the authors were able to determine a quantity known as differential conductance (a measure of the rate of change of current as a function of the source-drain voltage). When they plotted the differential conductance against the gate and source-drain voltage, they observed peaks that correspond to the energy required to add or subtract a confined electron (or hole). This allowed them to calculate the corresponding energy levels for these charge carriers.

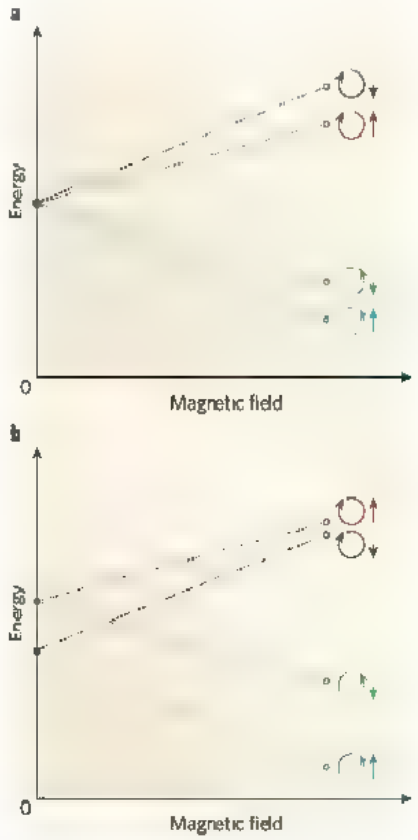

Figure 1 | Spin–orbit coupling of electrons in carbon nanotubes. Electrons in carbon nanotubes exist in quantized energy levels. **a**, The ground state was believed to consist of four states of equal energy, representing different combinations of orbital states (clockwise and anticlockwise motion, indicated by circular arrows) and spin states (spin up and spin down, indicated by straight arrows). When a magnetic field is applied parallel to the nanotube, the energies of the four states can be differentiated. **b**, McEuen and colleagues[1] show that, in the absence of a magnetic field, the four states do not have equal energies, but form two distinct pairs. This suggests that the spin and orbital movement of electrons in carbon nanotubes are strongly coupled. This may provide a means of controlling spin in nanotubes electrically, which would be useful for nano-electronics applications.

In the absence of spin–orbit interactions, the electronic ground states of carbon nanotubes were thought to be four-fold degenerate — that is, at each energy level there are four states (Fig. 1). Two of these are spin states (spin up and spin down) and two are orbital states (clockwise and anticlockwise). The existence of these states can be revealed by applying a magnetic field parallel to the tube's axis. The magnetic field couples independently to the spin and orbital moments, changing the energies of the states so that they are no longer equivalent.

McEuen and colleagues' results shatter the dogma of the degeneracy of carbon nanotubes.

When they applied a magnetic field to their nanotube quantum dot, they observed the four expected states. But, surprisingly, in the absence of a magnetic field, the four states had different energies. This is most probably the result of strong spin–orbit interactions, confounding the notion that such interactions are weak in carbon. Previous studies had missed this effect, possibly because the nanotubes used in those experiments had defects that confused the data.

This study[1] is the first experimental proof of spin–orbit coupling in carbon nanotubes. But recent theoretical studies[3–6] had predicted such interactions in curved carbon structures (such as nanotubes). These theories also suggested that spin–orbit interactions in nanotubes cause electrons and holes to behave differently in their ground states. For electrons, the magnetic moment associated with spin was expected to align in the same direction as that associated with orbital movement, but for holes the moments were expected to align in opposite directions. McEuen and colleagues[1] confirmed this to be the case by studying the changes in energy of the ground states of electrons and holes in a magnetic field; their observations matched the theoretical predictions.

The authors' results raise many interesting questions. For example, the sign and size of the observed spin–orbit interactions broadly agree with theoretical calculations, but the size of the interaction is different for electrons and holes; current theories can't explain this.

The observation of spin–orbit interactions in carbon nanotubes could also help to explain spin behaviour in another form of carbon — single sheets of graphite (known as graphene). In graphene, electron spin states can be retained for a long time, yet spin-polarized electrons don't move much further than they do in conventional metals[7]. This could be because of enhanced spin–orbit coupling resulting from corrugation in the graphite sheet.

If spin–orbit interactions lead to the decay of spin signals, you might expect McEuen and colleagues' results[1] to rule out carbon nanotubes as a medium for spintronics devices. But the interaction isn't strong enough to cause insurmountable problems. In fact, this effect could be exploited to allow electron spin to be manipulated by electrical means alone, a long-sought capability that would open the door to many more spintronics applications. ■

Arne Brataas is in the Department of Physics, Norwegian University of Science and Technology, NO-7491 Trondheim, Norway
e-mail: arne.brataas@ntnu.no

1. Kuemmeth, F., Ilani, S., Ralph, D. C. & McEuen, P. L. *Nature* **452**, 448–452 (2008)
2. http://nobelprize.org/index.html
3. Ando, T. J. *Phys. Soc. Jpn* **69**, 1757–1763 (2000)
4. De Martino, A., Egger, R., Hallberg, H. & Balseiro, C. A. *Phys. Rev. Lett.* **88**, 206402 (2002)
5. Huertas-Hernando, D., Guinea, F. & Brataas, A. *Phys. Rev. B* **74**, 155426 (2006)
6. Bulaev, D. V., Trauzettel, B. & Loss, D. preprint at http://arxiv.org/abs/0712.3767 (2007)
7. Tombros, N., Jozsa, C., Popinciuc, M., Jonkman, H. J. & van Wees, B. J. *Nature* **448**, 571–574 (2007).

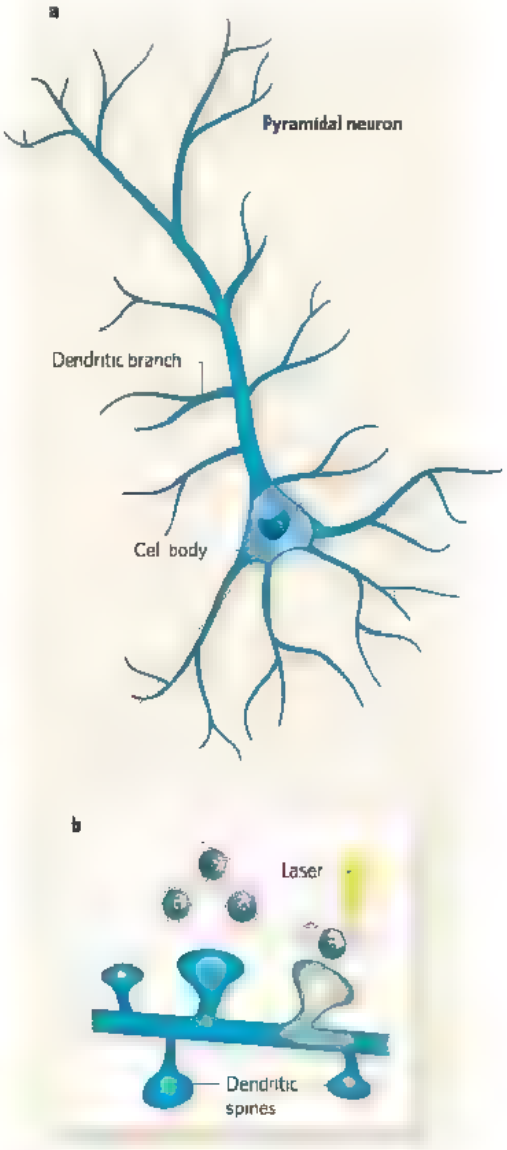

Figure 1 | A closer look at plasticity. To investigate the neural basis of plasticity at a fine scale, Losonczy *et al.*[2] activated individual dendritic branches. **a**, A typical pyramidal neuron consists of a large cell body and many dendritic branches receiving thousands of excitatory synapses, most of which are on dendritic spines. **b**, Losonczy *et al.* mimicked precisely patterned synaptic activation using laser stimulation of dendritic spines. Caged glutamate (G) is released from the cage by the laser, allowing glutamate to act locally on the dendritic spine. The laser is moved rapidly from one spine to the next to precisely mimic patterned synaptic activation. The authors found that activation of multiple spines led to a spike in the dendritic branch, and spread of the spike to the cell body could be enhanced by repeated activation under appropriate conditions.

NEUROSCIENCE

Strength in numbers

Nelson Spruston

To store information, the brain modulates synapses, which mediate communication between neurons. A closer look hints that subcellular changes in response to groups of synapses facilitate this process.

Ever since the Spanish neuroscientist Ramón y Cajal put forward his 'neuron theory'[1], synapses have been the focus of research aiming to explain learning in terms of brain plasticity, or the functional reorganization of neural pathways in response to new experiences. But synapses, which mostly spread out along highly branched neuronal processes called dendrites, are relatively tiny and have been difficult to stimulate with any precision. Using a sophisticated new method that allows precise stimulation of activity patterns generated at specific locations in a single neuron, Losonczy and colleagues[2] (page 436 of this issue) show that when clusters of synapses on a dendritic branch are stimulated simultaneously, under conditions thought to mirror brain states during learning, repeated activation leads to gradual changes in the response of the branch.

The technique used involves releasing caged molecules of the neurotransmitter glutamate at precise locations along a dendritic branch by photo-activation with a long-wavelength, pulsed laser, thus mimicking the precisely patterned input that the dendrite would naturally receive from its presynaptic partners. The free glutamate molecules can locally activate a small spot on the neuron — in this case, a dendritic spine, which is a specialized structure bearing a single excitatory synapse — with high spatial and temporal precision (of the order of 1 micrometre and 1 millisecond)[3] (Fig. 1). By rapidly scanning the laser from one spot to the next, adjacent spines can be activated almost synchronously.

In a previous study[4], the same team showed that, when stimulating several spines almost simultaneously, the responses add together until a threshold is reached. Beyond this threshold, activation of additional spines results in a proportionally much larger response, believed to be due to the generation of an action potential — or spike — in the dendrite. A spike consists of a fast component, mediated by voltage-gated sodium channels, and a slower component mediated by voltage-gated calcium channels and by receptors that

ANALYTICAL CHEMISTRY

Do-it-yourself microfluidics

Derek Bruzewicz and his colleagues have found a new application for the desktop plotter. They have used it to create an impressively simple microfluidics device that can be produced without a clean room or photolithographic equipment.

According to Bruzewicz and colleagues, second-hand desktop plotters can be had for as little as $50. Other simple components of their device are paper and the commonly used organic polymer poly(dimethylsiloxane), or PDMS, which is cheap, can be diluted in hexane solvent and is flexible when cured. The team's study is described in *Analytical Chemistry* (D. A. Bruzewicz *et al. Anal. Chem.* 10.1021/ac702605a, 2008).

The system works like this. By replica moulding, the pens of the plotter are replaced with PDMS versions that can deliver various types of 'ink'. The purpose of the ink, when cured, is to create channels in a filter-paper substrate, and after experimenting with the possibilities Bruzewicz *et al.* found that a syrupy mixture of 3:1 PDMS:hexane did just fine. Having chosen the appropriate paper, the trick then is to use the plotter to draw channel shapes, with the PDMS syrup penetrating the full depth of the paper to create water-tight chambers in various patterns.

One form the device takes is what the authors call a "dip star". Filter paper is patterned with eight PDMS channels radiating out from the centre; in principle, each of these channels can be loaded with a different chemical indicator. The flexibility of the channels means that the paper can be folded, with the centre becoming one corner that can be dipped into the fluid to be assayed. The channels are at least 1 millimetre wide. In keeping with the guiding principle of the system, the readout equipment is similarly widely available: the human eye.

The authors have tested different types of the device with well-tried colorimetric assays for identifying excess protein and glucose in urine, and found they performed well, with no cross-contamination between channels.

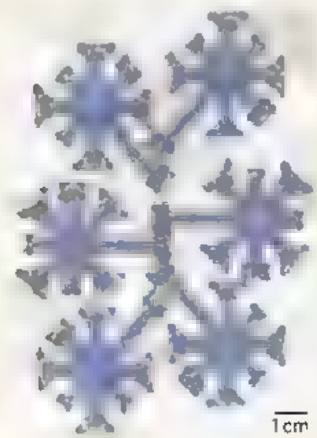

Another pattern, shown here, is a variant on the dip star. It shows that channels can be printed over a large area of paper, and can be designed for loading by multipipette rather than dipping.

Tim Lincoln

are activated by glutamate and are named after their chemical agonist NMDA. These findings are consistent with the emerging concept that voltage-gated ion channels, as well as voltage-sensitive NMDA receptors, are crucial to the integrative function of dendrites[5]. In addition, they suggest that each dendritic branch could generate a unitary (all-or-none) output in the form of a localized dendritic spike; this conclusion has fuelled emerging theories that treat dendritic branches as the functional units of neurons[6,7].

In their latest work[2], Losonczy *et al.* ask how dendritic spikes could be shaped by experience, in the form of repeated stimulation under conditions that are known to facilitate functional plasticity. They studied pyramidal neurons, which are the principal type of neuron in the brain's cortex, the region that contributes to higher cognitive functions.

They find that, when groups of spines are repeatedly activated so that they produce a spike in a dendritic branch, an increase in the size of the spike (from about 1 millivolt before to roughly 5 millivolts after repeated stimulation) is observed at the cell body. They call this change in response 'branch-spike plasticity'. Furthermore, they find that, even before repeated activation, some branches show a weak response and others a stronger one; this observation is consistent with the view that such branch-spike plasticity occurs spontaneously *in vivo*, and may therefore genuinely reflect a natural process, not just an experimental phenomenon.

Because of the structural properties of branching dendrites, and the types of ion channel in their membranes, spikes do not propagate well in dendrites[8]. The amplitude of the spike reaching the cell body depends on these same factors. But Losonczy and colleagues find that branch-spike plasticity results in a several-fold increase in voltage at the cell body, compared with the voltage normally produced by a single branch. This increase, which results from enhanced propagation of the spike along the dendritic branch, seems to be due to a downregulation of the Kv4.2 voltage-gated potassium channels, which otherwise limit the excitability of the branch.

Are these observations surprising? Although the synapse has been considered to be the main functional unit of plasticity in neurons mediating learning, forms of plasticity involving voltage-gated ion channels have been described before, and it has been suggested that different types of plasticity cooperate to form the set of neuronal changes that collectively underlie learning[9]. But the argument against plasticity of voltage-gated ion channels as a mechanism for learning is that it is less specific than synaptic plasticity, and thus could potentially shift the minimal unit of plasticity from the synapse to the whole neuron. This problem is mitigated by the finding[10] that these channels could mediate plasticity in restricted portions of the dendritic tree.

Losonczy and colleagues' finding[2] — that such localized plasticity might even be restricted to individual dendritic branches — supports the notion that regulation of voltage-gated channels can cause changes that are specific to small groups of synapses rather than to the whole neuron or large parts of it. Together with the recently described spread of communicative signals among adjacent spines on a single dendritic branch[11], the emphasis seems to be shifting from individual spines to groups of spines and dendritic branches as the functional units of plasticity underlying information storage and memory formation. By restricting changes to a limited number of spatially localized and temporally coactivated synapses, experience may be able to 'tune' neurons to respond to several different spatio-temporal patterns of synaptic input.

As is always the case, several questions remain. First, Kv4.2 potassium channels are probably not the only player in this story. The authors observe considerable variability in the size of dendritic spikes, as measured in the cell body, even in animals lacking Kv4.2, which indicates that other channels also regulate the excitability of dendritic branches. Second, for practical reasons, the authors restricted their study to dendritic branches quite close to the cell body. Does branch spike plasticity also occur in more distant branches? Does the influence of a branch on the cell body depend on the distance between them?

The broader functional relevance of branch spike plasticity must also be explored. Does branch-spike plasticity occur in other types of neuron? Is it something that happens in intact animals, and, if so, is it required for learning? Answering these questions will be challenging, but will be essential for a better understanding of the neural basis of learning and memory. ■

Nelson Spruston is in the Department of Neurobiology and Physiology, Northwestern University, 2205 Tech Drive, Evanston, Illinois 60208, USA.
e-mail: spruston@northwestern.edu

1. Ramón y Cajal, S. *Neuron Theory or Reticular Theory?* (Consejo Superior de Investigaciones Cientificas, Madrid, 1954)
2. Losonczy, A., Makara, J. K. & Magee, J. C. *Nature* **452**, 436–441 (2008)
3. Matsuzaki, M. *et al. Nature Neurosci.* **4**, 1086–1092 (2001)
4. Losonczy, A. & Magee, J. C. *Neuron* **50**, 291–307 (2006)
5. Häusser, M., Spruston, N. & Stuart, G. J. *Science* **290**, 739–744 (2000)
6. Poirazi, P., Brannon, T. & Mel, B. W. *Neuron* **37**, 989–999 (2003)
7. Poirazi, P. & Mel, B. W. *Neuron* **29**, 779–796 (2001)
8. Spruston, N. *Nature Rev. Neurosci.* **9**, 206–221 (2008)
9. Zhang, W. & Linden, D. J. *Nature Rev. Neurosci.* **4**, 885–900 (2003)
10. Frick, A., Magee, J. & Johnston, D. *Nature Neurosci.* **7**, 126–135 (2004)
11. Harvey, C. D. & Svoboda, K. *Nature* **450**, 1195–200 (2007)

OBITUARY

Joshua Lederberg (1925–2008)

Decisive discoveries in bacterial genetics.

I think it was 1941 when I first met Josh Lederberg. The location was the American Institute Science Laboratory in New York city, in the shadow of the Empire State Building. These labs were established to enable high-school students to conduct after-school research, and were an inspiring place for the science nerds of the time. Lederberg and I had much in common. We were born in the same year, spent much of our youthful spare time in branches of the New York Public Library, and were prompted to enter medical research by reading Paul de Kruif's *Microbe Hunters*.

Even then, his talent and energy marked him out. Lederberg, who died on 2 February 2008, became a brilliant biologist and an exceptional leader whose influence extended to space science and computing.

He was educated at Stuyvesant High School, an élite institution that produced four Nobel laureates in science, and then Columbia University. But before completing his medical education at Columbia he migrated to Yale University to do research. Inspired by Oswald Avery's discovery that DNA, not protein, is the genetic material in *Pneumococcus*, he embarked on testing the widely held hypothesis that bacteria simply divide into two offspring from a single genome. Lederberg, however, showed that sexual reproduction occurs in *Escherichia coli*, so revealing both an unexpected feature of microbial reproduction and providing an essential tool for genetic research and biotechnology.

More was to come following the award of his PhD in 1947 and a move in that same year to the University of Wisconsin, Madison. Together with colleagues, including Esther Zimmer (to whom he was then married) and Norton Zinder, he discovered that viruses that infect bacteria can transfer genetic information between their hosts. This mechanism — transduction — was an unexpected way of altering the host's genetic make-up, and later assumed special significance with the recognition that viral sequences can be inserted in the human genome and can presumably be inherited. The discovery of transduction opened a vast area for research on the role of viruses in evolution and disease, and — even more intriguing — into the non-pathological characteristics of microorganisms.

Another surprise was the finding that small, ring shaped pieces of DNA, termed plasmids, reside in microbial cells and are distinct from chromosomal DNA, being capable of autonomous replication. Plasmids can be introduced into other cells to produce vast amounts of useful proteins such as human insulin and the hepatitis B virus vaccine. Lederberg's work was seminal in initiating a new approach to biology based on the genome and its interactions with the environment. This was recognized by the award of the Nobel prize in 1958, at the age of 33, which he shared with George Beadle and Edward Tatum.

By then he was already widening his horizons, stimulated in particular by the launch of Sputnik on 4 October 1957. He was excited by the prospect of space exploration, but was also concerned about possible biological cross-contamination between Earth and other planetary bodies. In December 1957 he wrote to the US National Academy of Sciences (NAS) to warn of this danger. The eventual consequence was that objects and crews returning from Moon missions were subject to decontamination and quarantine.

Lederberg was appointed as a founder member of the NAS Space Science Board in 1958, and continued to stimulate both professional and public interest in biological space research (particularly in his "Science and Man" columns in *The Washington Post*). He coined the word 'exobiology', which signalled the arrival of the discipline dedicated to the search for extraterrestrial life. This term was criticized as inappropriate, because there was no life known beyond Earth, and as designating a discipline without a subject. Its descendant discipline is 'astrobiology', a term often used interchangeably with exobiology. Astrobiology involves study of the origins of life on Earth, and testing the hypothesis that life exists elsewhere, maintaining Lederberg's vision of biology as an essential component of space research.

His connection with space science became especially close when he was involved in planning, along with colleagues, experiments to be carried by the Viking landers to seek evidence of microbial life on Mars. The experiments consisted of the collection and spectrometric analysis of soil samples, and the landers commenced operations in 1976. The results were inconclusive, but they marked the beginning of a search that continues in the astrobiology programmes in the United States and elsewhere.

Stimulated by his space research, Lederberg became a pioneer in the use of computers for biology and medical science. The DENDRAL program aided the determination of chemical structures from the spectrometric data collected on the Viking mission. Later, it was used to characterize structures of other compounds and was eventually applied to the organization and analysis of large biomedical data sets. This in turn led to medical 'expert systems', including INTERNIST, an expert system for clinical diagnosis and treatment.

As if all of this were not enough, Lederberg took on senior management responsibilities at Stanford University, to which he moved in 1959, and other institutions, culminating in his appointment in 1978 as president of the Rockefeller University in New York. He served on various prominent committees and agencies, and was an adviser to many US presidential administrations. He was concerned about the hazards of biological warfare and was a consultant to the US Arms Control and Disarmament Agency, and served on the Defense Science Board, which advises the Department of Defense. He was also a member of the science advisory board of the NASA Astrobiology Institute, an intellectual offspring of his early interests in space biology. In 2006 he was awarded the US Presidential Medal of Freedom.

As a researcher, Lederberg emphasized the importance of honesty and clarity in reporting scientific results. He recognized that science is a powerful problem-solving tool but that it has its limitations for individuals and society. His father was a rabbi and may have wanted his son to follow in his footsteps, which perhaps prompted Josh's awareness that acquiring knowledge is a blessing, yet comes laden with obligations.

Scientists are not usually thought of as heroes. I write as an old friend and colleague, but to my mind Joshua Lederberg was just such a man. Through his far-ranging interests and achievements, often accomplished against entrenched opinions, he has left an enduring imprint on science.

Baruch S. Blumberg
Baruch S. Blumberg is at the Fox Chase Cancer Center, Philadelphia, Pennsylvania 19111-2497, USA.
e-mail: baruch.blumberg@fccc.edu

ARTICLES

Genetics of gene expression and its effect on disease

Valur Emilsson[1,2], Gudmar Thorleifsson[1], Bin Zhang[2], Amy S. Leonardson[2], Florian Zink[1], Jun Zhu[2], Sonia Carlson[2], Agnar Helgason[1], G. Bragi Walters[1], Steinunn Gunnarsdottir[1], Magali Mouy[1], Valgerdur Steinthorsdottir[1], Gudrun H. Eiriksdottir[1], Gyda Bjornsdottir[1], Inga Reynisdottir[1], Daniel Gudbjartsson[1], Anna Helgadottir[1], Aslaug Jonasdottir[1], Adalbjorg Jonasdottir[1], Unnur Styrkarsdottir[1], Solveig Gretarsdottir[1], Kristinn P. Magnusson[1], Hreinn Stefansson[1], Ragnheidur Fossdal[1], Kristleifur Kristjansson[1], Hjortur G. Gislason[3], Tryggvi Stefansson[3], Bjorn G. Leifsson[3], Unnur Thorsteinsdottir[1], John R. Lamb[2], Jeffrey R. Gulcher[1], Marc L. Reitman[4], Augustine Kong[1], Eric E. Schadt[2]* & Kari Stefansson[1]*

Common human diseases result from the interplay of many genes and environmental factors. Therefore, a more integrative biology approach is needed to unravel the complexity and causes of such diseases. To elucidate the complexity of common human diseases such as obesity, we have analysed the expression of 23,720 transcripts in large population-based blood and adipose tissue cohorts comprehensively assessed for various phenotypes, including traits related to clinical obesity. In contrast to the blood expression profiles, we observed a marked correlation between gene expression in adipose tissue and obesity-related traits. Genome-wide linkage and association mapping revealed a highly significant genetic component to gene expression traits, including a strong genetic effect of proximal (*cis*) signals, with 50% of the *cis* signals overlapping between the two tissues profiled. Here we demonstrate an extensive transcriptional network constructed from the human adipose data that exhibits significant overlap with similar network modules constructed from mouse adipose data. A core network module in humans and mice was identified that is enriched for genes involved in the inflammatory and immune response and has been found to be causally associated to obesity-related traits.

The comprehensive assessment of molecular quantities in biological samples using high-throughput technologies has already led to the identification of disease subtypes[1,2], novel genes and gene structures[3,4], and biomarkers for disease[5], as well as the elucidation of transcriptional networks associated with disease traits[6–8]. The analysis of genotypes and gene expression data in animal models and human cell lines has proven useful for identifying genetic determinants of expression traits[1,9–13] and for mapping genes in regions linked to complex traits[6,10,11,14]. In general, such studies provide the means to examine the overall genetic complexity of gene expression traits, including a characterization of the relative effect of *cis* versus *trans* control[15,16].

Associating patterns of gene expression with DNA and complex trait variation is necessarily limited to those changes that are reflected in the transcriptional network. Although a number of studies have highlighted the importance of post-transcriptional alterations in gene activity that induce changes in biological processes[17], variation in protein structure and state may be reflected in the transcriptional network because such variation often induces a change in transcript stability, rates of transcription, transport of RNA from the nucleus, alternative splicing events, and other processes that affect expression levels[1]. Importantly, given the context specificity of many critical biological processes[18] and the fact that most common diseases are thought to be the outcome of a complex interaction between many genetic loci and the environment, it follows that there are obvious advantages to studying the genetics of gene expression in cells that represent the *in vivo* state.

Towards this end, we collected blood and subcutaneous adipose tissues in a population-based sampling of hundreds of Icelandic subjects ranging in age from 18 to 85 years old. These cohorts are referred to as the Icelandic Family Blood (IFB) cohort ($N = 1{,}002$) and the Icelandic Family Adipose (IFA) cohort ($N = 673$) (see Supplementary Table 1 for cohort description). A number of clinical traits including differential blood cell count as well as biometric traits such as body mass index (BMI), percentage body fat (PBF, measured by bioimpedance) and waist-to-hip ratio (WHR) were collected for all subjects of the IFB and the IFA cohorts (Supplementary Table 1). The relatively large sample size used in this study design provided the means to assess the relationship between sequence variants and gene expression with more statistical power than previous studies[12,13,16].

Gene–clinical trait correlations

Expression profiles produced for this study contained measurements of relative abundances of 23,720 transcripts, representing 84% of the 24,060 protein-coding genes annotated in the Ensembl database (v.33)[19]. Given that probes overlapping single nucleotide polymorphisms (SNPs) may give rise to artificial signals, we sequenced a number of probes implicated as strong expression quantitative trait loci (eQTL) in 470 subjects from the IFB (see Supplementary Results and Supplementary Table 2). In short, we found that probes overlapping SNPs is not a concern in the present study.

The distribution of biometric traits such as BMI in our cohorts is not unlike the distribution that one would encounter in the general Western population, with BMI ranging from 16 to 70 and a median of

[1]deCODE genetics, 101 Reykjavik, Iceland. [2]Rosetta Inpharmatics, LLC, 401 Terry Ave N, Seattle, Washington 98109, USA. [3]Department of Surgery, National University Hospital, 101 Reykjavik, Iceland. [4]Merck Research Laboratories, Rahway, New Jersey 07065, USA
*These authors contributed equally to this work

28.8 (Supplementary Fig. 2a). Given the known associations of biometric traits with age and sex, and the fact that gene expression traits in blood have been found to be correlated with these covariates as well as with white blood cell counts[20], we adjusted for these covariates using multiple linear regression (Methods) in all analyses of correlation between gene expression and clinical traits, as well as in the analyses of the genetic component of gene expression (see below). In blood, fixing the false discovery rate (FDR)[21] at 5%, we found 2,172 (9.2%) gene expression traits to be correlated with BMI, 1,098 (4.6%) with PBF, and 711 (3.0%) with WHR in the IFB cohort (Supplementary Table 3). In adipose tissue, at a 5% FDR, the expression levels of 17,080 (72.0%) genes were correlated with BMI, 16,977 (71.6%) with PBF, and 14,901 (62.8%) with WHR (Supplementary Table 3). Thus, there is at least an order of magnitude more expression traits that are significantly correlated with these biometric traits in adipose tissue than in blood. Furthermore, 2,784 of the gene expression traits in adipose tissue explained more than 10% of the BMI variation in the IFA ($R^2 \geq 0.1$, $P \leq 10^{-15}$; see Supplementary Fig. 2b), whereas none of the expression traits in blood achieved this level of correlation. To ensure equivalent statistical power for making these detections between the tissues, we compared these associations in the 553 subjects represented in both the IFB and IFA cohorts. Using these paired samples, we found an even more marked difference between the two tissues (Supplementary Table 3). For example, there was a notable 34.6-fold enrichment of expression traits correlated with BMI in adipose tissue compared with blood using the 553 subjects (FDR ≤ 0.01), whereas this enrichment was 13.9-fold in the full data sets.

Overall, our results suggest that a substantial fraction of the transcriptional network in adipose tissue, together with infiltrated macrophages[22–24], is associated with the obesity of subjects. There are several reasons why this strong relationship between gene expression levels in adipose tissue and obesity should not come as a surprise. First, obesity is a disorder of excessive body fat. Second, the physiology and morphology of the adipocyte is known to be drastically altered in obese subjects[25]. Third, the number of macrophages is markedly increased in the adipose tissue of obese subjects, and they have been shown to have an important role in obesity and related metabolic disorders[22–24].

Heritability of gene expression traits

The subjects in the IFB and IFA cohorts were clustered into multigenerational families (for details, see Methods). In the case of the IFB cohort, it was possible to cluster 938 out of the 1,002 subjects into 209 families, whereas for the IFA cohort, 570 out of the 673 subjects clustered into 124 families. Using this family structure, we estimated the heritability of each of the 23,720 gene expression traits, both with and without adjusting for sex, age, cell count (IFB only) and BMI (IFA only). The number of traits with statistically significant heritability is summarized in Table 1. With no adjustment, the number of significantly heritable traits at a 5% FDR was 13,910 in IFB and 16,825 in IFA, or 58.6% and 70.9% of all assessed transcripts, respectively. For those significantly heritable expression traits in the IFA and IFB cohorts, the genetic variance component on average explained nearly 30% of the variation observed (Supplementary Fig. 2c). After adjustment, the number of heritable traits fell by as much as 26% (Table 1). When combined with the high heritability estimated for the expression traits, these results indicate that a significant proportion of the heritability mediated by BMI or differential cell count is also reflected by a large number of gene expression traits. The heritability values (percentage) of all expression traits for the different types of adjustments and in both cohorts are listed in Supplementary Tables 4 and 5.

Detection of *cis* and *trans* eQTL

All subjects in the two tissue cohorts were genotyped using a framework set of 1,732 microsatellites and were used for genome-wide linkage analysis. Because one of the main aims of this analysis was to detect eQTL signals that are proximal to the physical locations of genes corresponding to the expression traits (referred to here as *cis*-acting eQTL signals), this analysis was restricted to the 20,877 expression traits that had well-defined map positions (NCBI Build 34). For comparison, the eQTL analysis was performed both with and without adjusting the trait values for sex, age, differential cell-count (IFB only) and BMI (IFA only).

We defined a *cis*-acting eQTL signal for a given expression trait as the logarithm of the odds (eLOD) score at the nearest microsatellite to the location of the corresponding probe. The number of traits with significant *cis* eQTL is summarized in Table 1. For instance, at a 5% FDR and without any adjustment, we observed significant *cis* eQTL for 1,970 (9.4%) traits in blood and 1,215 (5 8%) traits in the adipose tissues. After adjusting for sex, age and blood cell counts in IFB, the number of *cis* eQTL signals increased to 2,529. In adipose tissue, this number was 1,307 after adjusting for age and sex and was 1,489 after also adjusting for BMI (Table 1). Out of the 1,489 significant *cis*-acting eQTL in adipose tissue, 762 (51.2%) were also observed in blood. Furthermore, expression traits with high heritability in both blood and adipose tissue showed greater reproducibility between the tissues (Fig. 1a). Here, 70% of all expression traits within the upper 25th percentile for heritability in blood that had a significant *cis*-acting eQTL in adipose tissue, also had a significant *cis* eQTL in blood (Fig. 1a). In fact, the proportion of significant *cis* eQTL signals in both tissues was notably higher for traits with greater levels of differential expression or heritability (Fig. 1b). The *cis*-acting eQTL LOD scores for each of the expression traits in the different cohorts are listed in Supplementary Tables 4 and 5.

Our finding of a strong genetic effect associated with *cis* signals in these tissues is consistent with results from previous studies[1,11–13]. The results on the detection of eQTL signals that were distal to the physical locations of the genes corresponding to the expression traits (referred to here as *trans*-acting linkage signals) are shown in the Supplementary Results and in Supplementary Table 6. We note that

Table 1 | Heritability, *cis* eQTL and *cis* eSNP detection

		IFB*		IFA†		
Variable	FDR or η‡	No adjustment	Age, sex and cell-count adjusted	No adjustment	Age and sex adjusted	Age, sex and BMI adjusted
Heritability	0.05	13,910	10,364	16,825	16,714	15,727
	0.01	10,829	8,047	12,309	12,392	11,251
	η	0.68	0.55	0.78	0.77	0.75
cis eQTL	0.05	1,970	2,529	1,215	1,307	1,489
	0.01	1,256	1,567	737	773	820
	η	0.40	0.44	0.33	0.32	0.37
cis eSNPs	0.05	2,417	2,714	3,048	3,149	3,364
	0.01	1,827	2,026	2,271	2,323	2,506
	η	0.33	0.32	0.37	0.35	0.36

The number of *cis* eQTL and *cis* eSNPs were as determined for a unique set of gene expression traits, for example the single most significant *cis* eSNP for any given trait
* Multiple regression analysis in blood, adjusting for sex and age as (age × sex) or for age, sex and differential cell-count as (age + neutrophil + monocyte + lymphocyte) × sex
† Multiple regression analysis in adipose, adjusting for sex and age as (age × sex) or for age, sex and BMI as (age + log(BMI)) × sex.
‡ The proportion of significant tests, η, was estimated as $\eta = 1 - \pi_0$ (see Methods for details).

the number of traits with significant *trans* eQTL in blood and adipose tissue are 50 times fewer than the number of expression traits with significant *cis* eQTL, consistent with what has been found in other studies[1,9,12,14]. Finally, although others have reported hotspots of localized linkage activity in a number of species[1,6,9–11,13,14], we failed to detect such activity beyond what was expected by chance (Supplementary Results).

Identification of *cis* and *trans* eSNPs

For the identification of sequence variants that have *cis* and *trans* regulatory effects on expression traits, we selected a subset of 150 unrelated (excluding all first-degree relatives) subjects who donated both blood and adipose tissue, and performed a whole-genome genotyping of these samples employing 317,503 SNPs using the Illumina platform[26]. The strongest *cis* effect for a given expression trait was then mapped by testing all SNPs located within a 2 megabase (Mb) window centred at the location of the probe corresponding to the expression trait, again restricting the analysis to the 20,877 genes with well defined positions in the genome. For each expression trait, because multiple correlated SNPs were tested for *cis* association, simulation was used to adjust the *P* value of the most significant expression (e)SNPs (see Methods). The effect of testing multiple expression traits was, as before, taken into account by means of the FDR approach[21]. The number of significant *cis*-acting eSNPs is summarized in Table 1. Assuming an FDR of 5%, we detected *cis* eSNPs for 2,417 (11.5%) expression traits in blood and 3,048 (14.6%) traits in adipose without any adjustment (Table 1). After adjusting for sex, age and cell count in blood, the number of *cis* eSNPs increased to 2,714 (Table 1). After adjusting for sex, age and BMI in the adipose tissue, the number of *cis* eSNPs increased to 3,364 (Table 1). Thus, we detected 650 more gene expression traits with significant *cis* eSNPs in the adipose tissue than in blood. This difference may reflect a more homogenous cell population in adipose tissue compared to blood, granting greater power to detect the *cis* effect in adipose. Furthermore, the number of significant *cis* eSNPs observed in both blood and adipose tissue increased as the heritability increased (Fig. 2a). For example, at an FDR of 1%, at least 50% of all SNPs that were *cis*-acting in blood and within the upper 25th percentile for heritability or differential expression were also *cis*-acting in adipose tissue (Fig. 2a).

Figure 2b summarizes the number of significant *cis* associations plotted as a function of heritability and differential expression. As observed in our analysis of *cis*-acting eQTL signals, the number of significant *cis* eSNPs increases with greater heritability scores or greater differential expression (Fig. 2b). A direct comparison of the results obtained from the genome-wide linkage and association analyses of *cis*-acting signals revealed a marked agreement between these two approaches (Supplementary Results and Supplementary Fig. 3). The significance of the *trans* association effect was assessed using the FDR approach[21], and the number of significant *trans* eSNPs summarized in Supplementary Table 6, again showing significantly fewer effects in *trans* than in *cis*, as described and discussed in Supplementary Results.

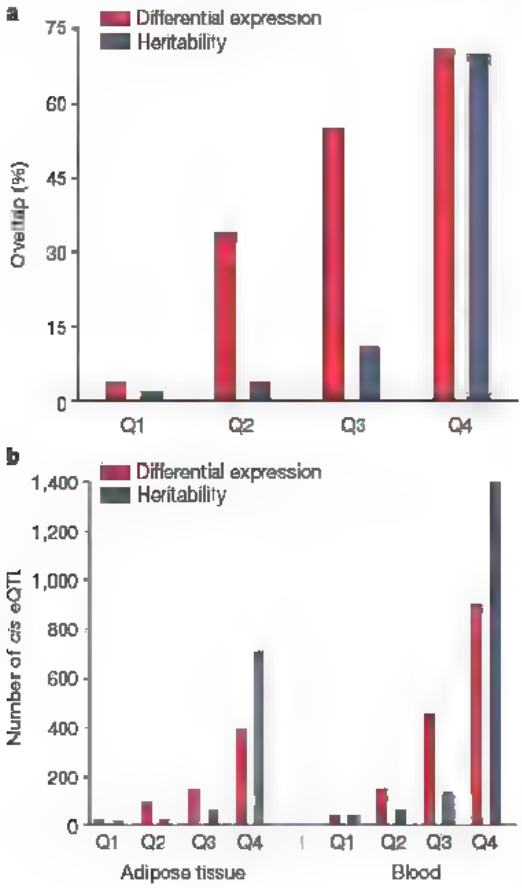

Figure 1 | eQTL mapping in human blood and adipose tissue. Individuals from large multi-generational families were genotyped for 1,732 microsatellites, and linkage analysis was performed on 20,877 standardized gene expression traits (see Methods for detail). Expression traits, ranked according to their differential expression or heritability strength, were binned into quartiles (Q1 → Q4), each comprised of 5,939 genes. **a**, Shown is the fraction of traits that have varying levels of differential expression and heritability with significant *cis*-acting eQTL in adipose that reproduced in blood at 1% FDR. **b**, Shown is the number of significant *cis* eQTL in both tissues, as a function of differential expression and heritability at 1% FDR.

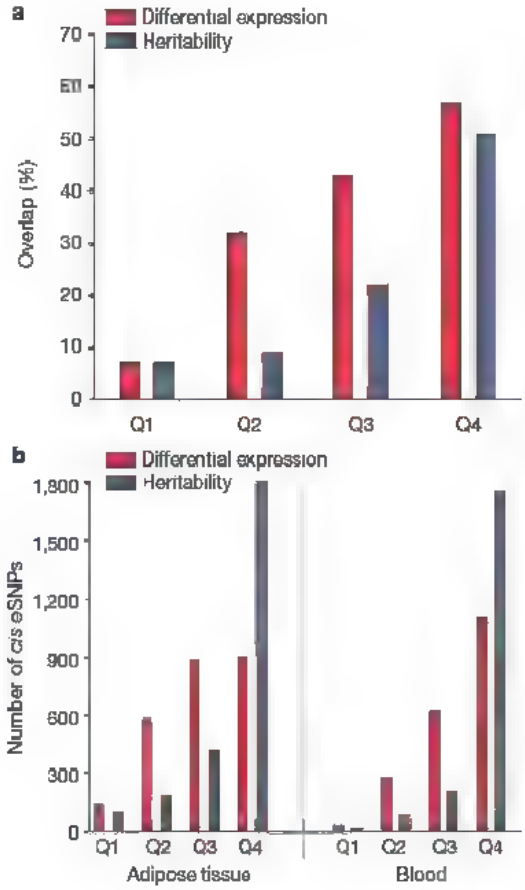

Figure 2 | Genome-wide association screens for eSNPs. A subset of 150 unrelated subjects who donated both blood and adipose tissue were genotyped at 317,503 tag SNPs (ILMN). The *cis* eSNP effects were assessed using linear regression on 20,877 standardized gene expression traits (see Methods for details). As described in Fig. 1, all traits were binned into quartiles at varying strengths of differential expression or heritability. **a**, Shown is the fraction of traits at varying degrees of differential expression or heritability with significant *cis* eSNPs in adipose tissue that reproduced in blood at 1% FDR. **b**, Shown is the number of significant *cis* associations in both tissues plotted as a function of heritability and differential expression.

Characterizing the transcriptional network

The analysis of gene expression traits in a large sample of individuals allows for a direct and unbiased assessment of the connectivity structure of transcriptional networks[27]. This further provides a basis for the identification of key functional modules within such networks that contribute to disease risk[28]. We have previously described the characterization of transcriptional networks based on brain, adipose and liver tissues in a cross between two inbred strains of mice (referred to here as the B × H cross)[29–31]. Building on this approach, we constructed extensive, sex-specific, gene co-expression networks based on the human adipose tissue data to identify modules strongly associated with obesity and, more generally, comparing the structure of this human network to that constructed in the mouse B × H cross using similar tissues. The adipose co-expression network was constructed by considering all pair-wise correlations among the most differentially expressed genes detected in this tissue (Methods). The resulting gene–gene correlation matrix was then transformed into an adjacency matrix in which the connectivity of a given gene was defined as the sum of its connection strengths with all other genes in the network[27]. The gene–gene interconnectivity represented in this matrix (referred to here as the connectivity map) was then characterized using a topological overlap measure[28]. The identification of functional modules of highly co-regulated genes in the resulting network was carried out using a dynamic programming procedure to search the network for sets of maximally interconnected genes[29].

Figure 3a depicts the connectivity map for the male human adipose tissue as a heat map of the topological overlap matrix. In this type of map, the rows and the columns represent genes in a symmetric fashion, and the colour intensity represents the interaction strength between genes. This connectivity map highlights that genes in the adipose transcriptional network fall into distinct network modules, where genes within a given module are more highly interconnected with each other (blocks along the diagonal of the matrix) than with genes in other modules, as has been described previously for mice[30]. A comparison of the connectivity structure between the male and female human adipose networks reveals a number of network modules that are well conserved between gender, both in terms of gene identities and the connectivity strength (hub status or centrality; see Supplementary Figs 6 and 7). However, there are also network modules that are strictly gender specific (Supplementary Fig. 6).

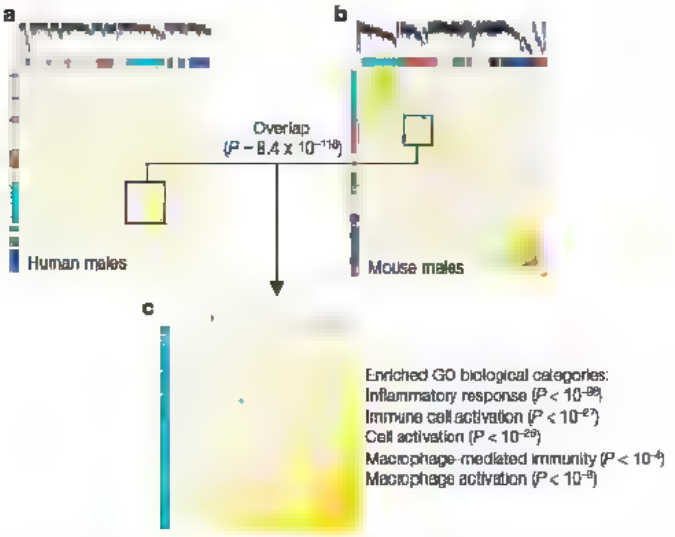

Figure 3 | The human and mouse gene transcriptional networks. **a**, Clustering of the connectivity matrix for the top 25% most differentially expressed genes in the male human adipose data. In the heat map, rows and columns represent genes in a symmetric fashion. The colour intensity signifies the connection strength between two genes, with red colour representing the strongest connection and white representing no connection. The colour bars along the *x*- and *y*-axes delineate the highly interconnected gene modules. **b**, Same as **a**, but for the male mouse B × H adipose data. **c**, The turquoise module in the male human network (**a**) is significantly overlapping the male mouse brown module (**b**), as well as the turquoise module in human females. The GO list in **c** shows the enrichment of inflammatory pathways in the conserved module.

An explicit comparison of the human and mouse adipose gene co-expression networks revealed a single core module in humans that was highly conserved in mice (Fig. 3a–c). The mouse module corresponding to this human module (Fig. 3b) is very significantly enriched for genes with eQTL that co-localize with obesity-associated-trait QTLs as well as for genes shown to be in a causal relationship with obesity-associated traits[31]. This mouse module significantly overlapped the human network module (Fig. 3a), with 196 out of the 673 (~29%) genes in the mouse module overlapping the set of 886 genes in the corresponding human module (only 8 were expected to overlap by chance; Fisher's Exact Test, $P = 8.4 \times 10^{-118}$). In addition, the Gene Ontology (GO) Biological Process categories that were enriched in this conserved network module were virtually identical in mouse and human (Supplementary Table 7). This conserved module was also strongly indicative of macrophage function for a number of reasons. First, GO Biological Process categories enriched in this module relate to inflammatory response and macrophage activation pathways. Second, well known macrophage-specific cell-surface markers such as *EMR1* and *CD68* are represented in the mouse and human modules. Third, using a recently constructed mouse body gene expression atlas comprised of more than 60 tissues and cell lines[31], this conserved module had an over-representation of genes enriched for expression in bone-marrow-derived macrophages (Fisher's Exact Test, $P < 1 \times 10^{-21}$), spleen, thymus and lymphoid tissue (Fisher's Exact Test, $P < 1 \times 10^{-20}$). These findings are consistent with results from recent studies showing that the adipose tissue secretes factors that regulate a wide variety of physiological states, including energy homeostasis and the immune response[25]. Given all of these significant enrichments and the association of this module to macrophage function and metabolic traits, we refer to it as the macrophage-enriched metabolic network (MEMN).

Because the mouse MEMN described above had previously been shown to be significantly enriched for genes associated with obesity[31], we investigated whether a similar association to obesity could be detected for the corresponding human module. Our results show that the expression of 868 (or 98%) of the 886 genes in the human MEMN module were significantly correlated with BMI in adipose tissue at an FDR of 1%, indicating that the human MEMN module may have a key role in obesity. Although the connection between inflammation and metabolic disorders such as obesity and diabetes has been reported previously[25], these data suggest that there may be many immune pathways or entire networks functioning in the adipose tissue. In fact, a number of genes previously identified and validated as being in a causal relationship with obesity-associated phenotypes are represented in this module, and perturbing many of these genes perturbs the entire module (see Supplementary Results for additional information).

If the MEMN module has a role in human obesity, then variations in DNA that result in expression changes in genes in the MEMN module should, in the obese, be enriched for variations that are associated with obesity. Therefore, we combined genotype and gene expression data to identify the SNP in the vicinity of each gene in the human MEMN module (Fig. 3a) that was most strongly associated with the corresponding gene expression trait. We then tested these variants jointly for association to BMI and PBF—the biometric traits most widely used to assess human obesity. Of the 886 expression traits represented in this module, 785 had a well defined genomic position and were used in this analysis. A selection of 768 *cis* eSNPs for the blood and adipose tissue data were successfully genotyped in a cohort of 8,685 individuals measured for BMI and 1,939 for PBF (Table 2). We used multiple linear regression analysis to test the association of the sex- and age-adjusted trait values to genotype counts for all the *cis* eSNPs jointly (see Methods for details).

Table 2 | Association of eSNPs to obesity traits

Cohort	Trait	All *P* (*N*)	All *P* adjusted*	Male *P* (*N*)	Male *P* adjusted*	Female *P* (*N*)	Female *P* adjusted*
Human MEMN							
IFA	BMI	3.8×10^{-6} (8,685)	0.0051	0.033 (3,606)	0.24	0.0022 (5,079)	0.049
	PBF	0.0011 (1,939)	0.047	0.20 (906)	0.47	0.12 (1,035)	0.27
IFB	BMI	5.3×10^{-7} (8,685)	0.0022	0.00041 (3,606)	0.015	0.016 (5,079)	0.16
	PBF	0.063 (1,939)	0.46	0.64 (906)	0.87	0.39 (1,035)	0.61
Combined MEMN							
IFA	BMI	0.14 (8,685)	0.41	0.22 (3,606)	0.39	0.27 (5,079)	0.47
	PBF	0.010 (1,939)	0.055	0.23 (904)	0.49	0.011 (1,035)	0.021
IFB	BMI	0.0014 (8,685)	0.018	0.028 (3,606)	0.075	0.028 (5,079)	0.081
	PBF	0.23 (1,939)	0.51	0.46 (904)	0.73	0.45 (1,035)	0.56

785 out of the 886 expression traits in the human turquoise module (see Fig. 3) mapped to a unique position and had a corresponding *cis* eSNP, this corresponds to 768 unique *cis* eSNPs that were used in the analysis. Missing genotypes were substituted with the mean genotype frequency. 128 out of the 146 expression traits in the combined human and mouse MEMN module had a unique map position and a *cis* eSNP; this corresponds to 123 unique *cis* eSNPs that were used in the analysis.
* The adjusted *P* value was based on up to 20,000 sets of simulated genotypes (see Methods).

Furthermore, we constructed 20,000 sets of simulated genotypes for all the variants conditioned on the familial relatedness of the individuals from the Icelandic genealogy database to compare the observed association with that expected to occur by chance, and used these to generate the adjusted *P* values represented in Table 2. In the larger data set with BMI measurements, we find that the *cis* eSNPs selected for genes in the human MEMN module showed some evidence for association to BMI, with *P* values of 3.8×10^{-6} (adjusted $P = 0.005$) and 5.3×10^{-7} (adjusted $P = 0.002$) for the *cis* eSNPs in adipose tissue and blood, respectively (see Table 2). Although these analyses were crude for individual *cis* eSNPs and the corresponding genes, these results suggest that the human MEMN module is enriched for sequence variants that confer risk of obesity in humans, and that genetic perturbations affecting gene expression traits may more generally perturb networks that in turn lead to increased susceptibility to disease. These data combined offer a glimpse of the complicated network of interactions that could drive at least a portion of obesity in humans, and demonstrate that at least a part of obesity is a property of the macrophage gene network.

Discussion

Previous studies of the genetics of gene expression in humans have been restricted to lymphoblastoid cell lines with no clinical phenotypes[12,13,16]. Before our study, the validation of this type of data in primary human tissues from subjects scored for clinical traits was lacking. Our analysis of genetic variation and gene expression in population-based sampling of blood and subcutaneous adipose tissue from a large number of extended families begins to fill this gap. We showed that more than 50% of all gene expression traits in adipose tissue are strongly correlated with clinical traits related to obesity, compared to less than 10% in blood. Furthermore, through segregation analysis and genome-wide linkage and association studies, we demonstrated an extensive genetic component underlying gene expression traits in blood and adipose tissue. This was evidenced by detection of heritability as a highly significant contributor to variation in gene expression and by the identification of a large number of significant linkage and association signals for the expression traits in the two tissues, with approximately 50% overlap of genetic signals between the two tissues. Consistent with previous reports, the signals detected using both linkage and association analysis was strongly biased towards *cis*- rather than *trans*-acting genetic signals.

We also constructed an extensive co-expression network on the basis of the human adipose tissue data with the aim of identifying key functional modules within this network that associated with obesity. A core gene expression module, the MEMN module, was identified in humans that has significant overlap with a previously described mouse network module. The gene sets in the core human and mouse modules were highly enriched for genes involved in inflammatory response and macrophage activation pathways. Furthermore, the mouse MEMN module has previously been shown to be enriched for genes that contribute to the risk of obesity, diabetes and atherosclerosis-associated traits. By using the strongest *cis*-acting SNPs for each of the gene expression traits from the human MEMN module and testing them jointly as a group, we observed a significant enrichment of genetic associations to clinical traits related to human obesity in this module. The identification of SNPs that are associated with variation in gene expression provides a level of functional support for such SNPs that makes them ideal candidates to identify genetic determinants of complex traits including diseases and drug response. Clearly this approach warrants serious consideration given the potential to affect our understanding of human health.

METHODS SUMMARY

Subjects used in the present study were of Caucasian descent. They were recruited as dense three-generation pedigrees, and comprehensively scored for multiple phenotypes including biometric traits related to obesity. Peripheral blood ($N = 1,002$) and subcutaneous fat ($N = 673$) were collected, and DNA and RNA extracted. The RNA samples (a total of 1,765 samples), including reference pools, were hybridized to a single custom-made human array containing 23,720 unique oligonucleotide probes. We estimated the differential expression, heritability, *cis* and *trans* eQTL, and association signals for each gene expression trait in each tissue. For the genetics of gene expression analysis, all subjects in these cohorts were genotyped at 1,732 microsatellites. A subset of 150 unrelated subjects, donating both blood and adipose tissue, was genotyped at 317,000 SNPs. Multiple testing for significance was taken into account through the use of an FDR procedure. The expression and clinical data were adjusted for standard covariates including age and sex for all analyses. The gene–gene co-expression network was constructed from the human adipose tissue expression data and compared to a similarly constructed adipose tissue network from an experimental mouse cross. Finally, expression variation markers (eSNPs) mapping to a core network module identified in human adipose tissue and found to be conserved in mice and previously shown to be enriched for genes in a causal relationship with obesity were tested jointly for association to obesity-related traits in humans using multiple regression analysis.

Full Methods and any associated references are available in the online version of the paper at www.nature.com/nature.

Received 23 July 2007; accepted 28 January 2008.
Published online 16 March 2008.

1. Schadt, E. E. *et al.* Genetics of gene expression surveyed in maize, mouse and man. *Nature* 422, 297–302 (2003)
2. Golub, T. R. *et al.* Molecular classification of cancer: class discovery and class prediction by gene expression monitoring. *Science* 286, 531–537 (1999)
3. Johnson, J. M. *et al.* Genome-wide survey of human alternative pre-mRNA splicing with exon junction microarrays. *Science* 302, 2141–2144 (2003)
4. Shoemaker, D. D. *et al.* Experimental annotation of the human genome using microarray technology. *Nature* 409, 922–927 (2001)
5. Welsh, J. B. *et al.* Analysis of gene expression profiles in normal and neoplastic ovarian tissue samples identifies candidate molecular markers of epithelial ovarian cancer. *Proc. Natl Acad. Sci. USA* 98, 1176–1181 (2001)
6. Schadt, E. E. *et al.* An integrative genomics approach to infer causal associations between gene expression and disease. *Nature Genet.* 37, 710–717 (2005)
7. Schadt, E. E., Sachs, A. & Friend, S. Embracing complexity, inching closer to reality. *Sci. STKE* 2005, pe40 (2005)

8 Zhu, J. *et al.* An integrative genomics approach to the reconstruction of gene networks in segregating populations. *Cytogenet. Genome Res.* 105, 363–374 (2004).
9 Brem, R. B., Yvert, G., Clinton, R. & Kruglyak, L. Genetic dissection of transcriptional regulation in budding yeast. *Science* 296, 752–755 (2002).
10. Bystrykh, L. *et al.* Uncovering regulatory pathways that affect hematopoietic stem cell function using 'genetical genomics'. *Nature Genet.* 37, 225–232 (2005).
11 Chesler, E. J. *et al.* Complex trait analysis of gene expression uncovers polygenic and pleiotropic networks that modulate nervous system function. *Nature Genet.* 37, 233–242 (2005).
12 Monks, S. A. *et al.* Genetic inheritance of gene expression in human cell lines. *Am. J. Hum. Genet.* 75, 1094–1105 (2004).
13. Morley, M. *et al.* Genetic analysis of genome-wide variation in human gene expression. *Nature* 430, 743–747 (2004).
14. Mehrabian, M. *et al.* Integrating genotypic and expression data in a segregating mouse population to identify 5-lipoxygenase as a susceptibility gene for obesity and bone traits. *Nature Genet.* 37, 1224–1233 (2005).
15. Brem, R. B., Storey, J. D., Whittle, J. & Kruglyak, L. Genetic interactions between polymorphisms that affect gene expression in yeast. *Nature* 436, 701–703 (2005).
16. Cheung, V. G. *et al.* Mapping determinants of human gene expression by regional and genome-wide association. *Nature* 437, 1365–1369 (2005).
17 Ranganathan, P. *et al.* Expression profiling of genes regulated by TGF-β: differential regulation in normal and tumour cells. *BMC Genom.* 8, 98, doi:10.1186/1471-2164-8-98 (2007).
18. Brem, R. B. & Kruglyak, L. The landscape of genetic complexity across 5,700 gene expression traits in yeast. *Proc. Natl Acad. Sci. USA* 102, 1572–1577 (2005).
19 Hubbard, T. *et al.* Ensembl 2005. *Nucleic Acids Res.* 33, D447–D453 (2005).
20 Whitney, A. R. *et al.* Individuality and variation in gene expression patterns in human blood. *Proc. Natl Acad. Sci. USA* 100, 1896–1901 (2003).
21. Storey, J. D. & Tibshirani, R. Statistical methods for identifying differentially expressed genes in DNA microarrays. *Methods Mol. Biol.* 224, 149–157 (2003).
22 Di Gregorio, G. B. *et al.* Expression of CD68 and macrophage chemoattractant protein-1 genes in human adipose and muscle tissues: association with cytokine expression, insulin resistance, and reduction by pioglitazone. *Diabetes* 54, 2305–2313 (2005).
23. Lumeng, C. N., Bodzin, J. L. & Saltiel, A. R. Obesity induces a phenotypic switch in adipose tissue macrophage polarization. *J. Clin. Invest.* 117, 175–184 (2007).
24 Neels, J. G. & Olefsky, J. M. Inflamed fat: what starts the fire? *J. Clin. Invest.* 116, 33–35 (2006).
25. Wellen, K. E. & Hotamisligil, G. S. Obesity-induced inflammatory changes in adipose tissue. *J. Clin. Invest.* 112, 1785–1788 (2003).
26. Steemers, F. J. & Gunderson, K. L. Illumina, Inc. *Pharmacogenomics* 6, 777–782 (2005).
27 Zhang, B. & Horvath, S. A general framework for weighted gene co-expression network analysis. *Stat. Appl. Genet. Mol. Biol.* 4, Article17 (2005).
28. Ravasz, E., Somera, A. L., Mongru, D. A., Oltvai, Z. N. & Barabasi, A. L. Hierarchical organization of modularity in metabolic networks. *Science* 297, 1551–1555 (2002).
29. Ghazalpour, A. *et al.* Integrating genetic and network analysis to characterize genes related to mouse weight. *PLoS Genet.* 2, e130 (2006).
30 Lum, P. Y. *et al.* Elucidating the murine brain transcriptional network in a segregating mouse population to identify core functional modules for obesity and diabetes. *J. Neurochem.* 97 (suppl. 1), 50–62 (2006).
31. Chen, Y. *et al.* Variations in DNA elucidate molecular networks that cause disease. *Nature* doi:10.1038/nature06757 (this issue).

Supplementary Information is linked to the online version of the paper at www.nature.com/nature.

Acknowledgements The authors acknowledge the participating families and the staff at the Clinical Research Centre for their cooperation. Genotyping service was provided at the deCode Genetics genotyping facilities.

Author Contributions V.E., E.E.S., K.S. and G.T. wrote the paper. G.T., E.E.S., A.K., D.G. and F.Z. performed statistical analysis. Tissue sampling and/or molecular profiling was carried out by H.G.G., T.S., B.G.L., G.H.E., S.C., M.M., Aslaug Jonasdottir, Adalbjorg Jonasdottir, G.B. and K.K. V.E., J.Z., U.T., A.S.L., A.H., B.Z., G.B.W., S. Gunnarsdottir, S. Gretarsdottir, K.P.M., V.S., I.R., A.H., U.S., H.S., R.F., J.R.G., K.S., M.L.R. and J.R.L. performed the genetic analysis and/or data-mining. K.S. and E.E.S. contributed equally to this work.

Author Information All the gene expression data generated for this study have been deposited into the GEO database under accession numbers GSE7965 and GPL3991. The authors declare competing financial interests: details accompany the full-text HTML version of the paper at www.nature.com/nature. Reprints and permissions information is available at www.nature.com/reprints. Correspondence and requests for materials should be addressed to K.S. (karl.stefansson@decode.is) or E.E.S. (eric_schadt@merck.com).

ARTICLES

Variations in DNA elucidate molecular networks that cause disease

Yanqing Chen[1]*, Jun Zhu[1]*, Pek Yee Lum[1], Xia Yang[1], Shirly Pinto[2], Douglas J. MacNeil[2], Chunsheng Zhang[1], John Lamb[1], Stephen Edwards[1], Solveig K. Sieberts[1], Amy Leonardson[1], Lawrence W. Castellini[3], Susanna Wang[3], Marie-France Champy[6], Bin Zhang[1], Valur Emilsson[1], Sudheer Doss[3], Anatole Ghazalpour[3], Steve Horvath[4], Thomas A. Drake[5], Aldons J. Lusis[3,4] & Eric E. Schadt[1]

Identifying variations in DNA that increase susceptibility to disease is one of the primary aims of genetic studies using a forward genetics approach. However, identification of disease-susceptibility genes by means of such studies provides limited functional information on how genes lead to disease. In fact, in most cases there is an absence of functional information altogether, preventing a definitive identification of the susceptibility gene or genes. Here we develop an alternative to the classic forward genetics approach for dissecting complex disease traits where, instead of identifying susceptibility genes directly affected by variations in DNA, we identify gene networks that are perturbed by susceptibility loci and that in turn lead to disease. Application of this method to liver and adipose gene expression data generated from a segregating mouse population results in the identification of a macrophage-enriched network supported as having a causal relationship with disease traits associated with metabolic syndrome. Three genes in this network, lipoprotein lipase (*Lpl*), lactamase β (*Lactb*) and protein phosphatase 1-like (*Ppm1l*), are validated as previously unknown obesity genes, strengthening the association between this network and metabolic disease traits. Our analysis provides direct experimental support that complex traits such as obesity are emergent properties of molecular networks that are modulated by complex genetic loci and environmental factors.

A challenge in the post-genome era is deciphering the biological function of individual genes and gene networks that drive disease. Given the availability of low-cost, high-throughput technologies for genotyping hundreds of thousands of DNA markers, successes are being realized in identifying associations between DNA variants and diseases such as age-related macular degeneration[1–3], diabetes[4] and obesity[5]. Although these and coming discoveries from a slew of genome-wide association studies currently under way provide a peek into pathways that underlie disease, they are usually devoid of context, so elucidating the functional role of such genes in disease can linger for years, as has been the case for ApoE, an Alzheimer's-susceptibility gene identified 15 years ago[6]. Even when an association to disease has been localized to a given region representing a single gene, in the absence of experimental support the gene cannot be definitively claimed to be the susceptibility gene. This problem is exacerbated in experimental crosses derived from inbred mouse strains, for which in addition to the problem of inferring the function of positionally cloned genes from the genetic data alone, the extent of linkage disequilibrium operating in such populations makes positional cloning a difficult and time-consuming process.

An alternative to the forward genetics approach is the construction of molecular networks that define the molecular states of a system that underlie disease, where such networks are constructed from molecular phenotype data scored in populations that manifest disease. The information that defines how variations in DNA lead to variations in complex traits flows through molecular networks. Characterizing molecular networks that underlie complex traits such as disease can provide a more comprehensive view, which in turn can lead to the direct identification of genes underlying disease processes and the functional roles of these genes with respect to disease. Recent studies characterizing gene networks have demonstrated how genetic loci associated with expression traits can be combined with clinical data to infer causal associations between expression and disease traits[7–12]. By leveraging DNA variations as a systematic source of perturbations on molecular networks and clinical traits, biological processes can be studied at the systems level, in addition to studying gene function at the level of individual pathways[13,14].

Here we report the development of an approach to uncover the components of co-expression networks that respond to variations in DNA associated with obesity-, diabetes- and atherosclerosis-related traits. In contrast to a forward genetics approach, we leverage quantitative trait loci (QTL) associated with disease to identify components of the co-expression network that are perturbed by the QTL and that in turn cause variations in disease traits. After constructing co-expression networks from liver and adipose tissues collected from a segregating mouse population, we identify sub-networks that are significantly associated with a complex of linked genetic loci related to obesity-, diabetes- and atherosclerosis-associated traits. A macrophage-enriched metabolic sub-network was found to be significantly enriched for expression traits supported as having a causal relationship with these metabolic traits. The connection to obesity and other metabolic syndrome traits is confirmed by validating three genes in this sub-network, *Lpl*, *Lactb* and *Ppm1l*, as previously unknown obesity genes.

[1]Rosetta Inpharmatics, LLC, Merck & Co., Inc., 401 Terry Avenue North, Seattle, Washington 98109, USA [2]Department of Metabolic Disorders, Merck & Co., Inc., 126 East Lincoln Avenue, Rahway, New Jersey 07065, USA [3]Department of Microbiology, Molecular Genetics, and Immunology [4]Department of Human Genetics, and [5]Department of Pathology and Laboratory Medicine, UCLA, 650 Young Drive South, Los Angeles, California 90095, USA [6]Institut de Genetique et de Biologie Moleculaire et Cellulaire, CNRS/INSERM/ULP 67404 Illkirch, France.
*These authors contributed equally to this work

A complex linkage to metabolic traits

A number of QTL mapping studies in experimental mouse cross populations have identified the distal half of chromosome 1 as a major contributor to metabolic traits such as weight, fat mass, and plasma glucose and cholesterol levels[15–18]. Much effort has been expended to map the quantitative trait genes (QTGs) underlying this locus, and these efforts have met with some success. For example, apolipoprotein A-II (*Apoa2*) and tumour necrosis factor superfamily, member 4 (*Tnfsf4*) have been mapped as QTGs for the cholesterol, fat mass, weight, insulin and atherosclerosis QTL mapped to the distal half of chromosome 1 (refs 19–23). However, it remains to be shown whether other genes in this chromosome 1 region contribute to these linkages beyond *Apoa2* and *Tnfsf4*. Furthermore, how the chromosome 1 QTL affect molecular networks in different tissues that in turn lead to pleiotropic effects on metabolic traits has not been characterized. An alternative to mapping QTGs for QTL is to incorporate molecular network data into these analyses to identify those network components that are perturbed by the QTL and that in turn lead to variations in disease traits. After characterizing the complexity of the chromosome 1 genomic region associated with metabolic traits, we implement a procedure to identify components of molecular networks that respond to genetic perturbations and in turn induce changes in metabolic traits. This procedure includes reconstructing co-expression networks and identifying highly interconnected functional sub-networks constituting these networks supported as having a causal relationship with disease traits.

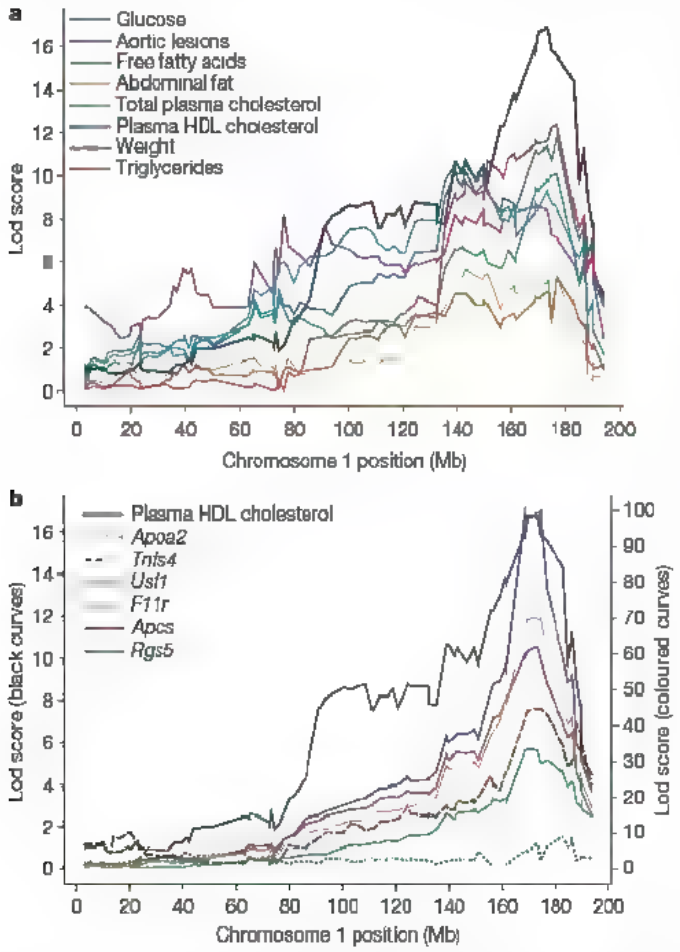

Figure 1 | The distal half of chromosome 1 strongly influences metabolic and gene expression traits. a, Lod score curves for metabolic traits scored in the B × H cross demonstrate that they are all driven by one or more QTL on chromosome 1. **b**, Lod score curves for expression traits corresponding to genes mapped as QTGs for the metabolic traits in **a** (*Apoa2* and *Tnfs4*) or to genes within ten-million base pairs of *Apoa2* that give rise to strong, putative *cis* eQTL and that are significantly correlated with at least one of the metabolic traits depicted in **a**

In a previously described cross between C57BL6/J (B6) and C3H/HeJ (C3H) on an *Apoe*$^{-/-}$ background (referred to here as the B × H cross)[17], the importance of distal chromosome 1 as a key driver of metabolic traits became apparent because every metabolic trait scored in the B × H cross links to this region of the chromosome (Fig. 1a). *Tnfsf4* and *Apoa2* are located within 10 megabases (Mb) of one another and are proximal to the peak log likelihood ratio (lod) score curves for the metabolic traits on chromosome 1. These two genes were positionally cloned from the B × H background and validated using transgenic and knockout animals as having a causal relationship with plasma cholesterol and high-density lipoprotein (HDL) levels, fat mass, weight, insulin levels and atherosclerotic lesion size[19,21,22]. *Apoa2* was specifically identified as having a mutation in C3H relative to B6 that affected *Apoa2* translational efficiency, leading to lower liver transcript and protein levels in C3H relative to B6 (refs 22 and 24). Liver gene expression traits scored in the B × H cross provide a unique opportunity to confirm *Apoa2* as a QTG and to assess its total contribution to the metabolic traits. Because the expression of *Apoa2* and its association to the chromosome 1 linkage region and metabolic traits can be considered simultaneously on the mixed genetic background in which the disease trait QTL were originally mapped, the gene can be validated in the exact context in which it was identified.

Apoa2 liver gene expression in the B × H cross gave rise to a significant expression QTL (Fig. 2a) that was proximal to the *Apoa2* structural gene, confirming that *Apoa2* expression is significantly perturbed between B6 and C3H mice as previously reported[22]. However, of the eight metabolic traits tested (Fig. 1a), *Apoa2* liver expression levels were only modestly correlated with glucose levels (expected P value = 0.014), and not at all correlated with obesity traits (Supplementary Fig. 1a). Interestingly, *Apoa2* gene expression was strongly supported as being independent of each of the metabolic traits with respect to the chromosome 1 locus (see Fig. 2a, b for weight). Results for *Apoa2* liver protein expression in the B × H cross were consistent with these gene expression results (Supplementary Results). Although the lack of association between *Apoa2* expression and the metabolic traits cannot exclude *Apoa2* as at least one of many genes underlying the chromosome 1 metabolic trait QTL, it is consistent with genes other than *Apoa2* having a more dominant role in this linkage region. *Tnfsf4* was similarly examined in the B × H cross but was not found to be associated with any of the metabolic traits linked to chromosome 1 in the B × H cross (Supplementary Results). However, because heart and aorta were demonstrated as the relevant tissues for *Tnfsf4* activity associated with metabolic traits[21], our failure to detect an association in this instance may be because we have not profiled the relevant tissue.

Whereas the expression data in this specific B × H cross did not support *Apoa2* and *Tnfsf4* as having a causal relationship with the metabolic traits, we identified 112 liver expression traits corresponding to genes located in the chromosome 1 linkage region (from 90 Mb to the end of the chromosome) that gave rise to expression QTL (eQTL) in this region supporting the metabolic trait QTL (Supplementary Table 1). Although none of these genes completely explains the linkage of the clinical traits to chromosome 1, the expression levels of 54 of these genes are statistically supported as at least partially explaining variation in the metabolic traits in a causal way[11] (Supplementary Table 1), suggesting that there may be many genes in this region that support the metabolic trait QTL. Figure 1b highlights strong liver *cis* eQTL for 4 of these 54 genes that are physically located within 10 Mb of *Apoa2* as well as the peak lod scores for each of the metabolic traits. Upstream transcription factor 1 (*Usf1*) was identified as a susceptibility gene for familial combined hyperlipidemia (FCH)[25]; F11 receptor (*F11r*) is supported as being a susceptibility gene for FCH and other inflammatory processes[26,27]; serum amyloid P component (*Apcs*) is implicated in atherosclerotic lesion formation[28]; and regulator of G-protein signalling 5 (*Rgs5*), a gene involved in vessel development and physiology, can distinguish the

fibrous cap from other atherosclerotic plaque components[29] and has recently been associated with hypertension in humans[30]. Of these four expression traits, *Rgs5* is the most strongly associated with the metabolic traits linked to the chromosome 1 genomic region (see Fig. 2 and Supplementary Fig. 1c for weight). Therefore, unlike *Apoa2* and *Tnfsf4*, these expression traits are significantly correlated with the metabolic traits, are strongly linked to the chromosome 1 locus, are physically located near the chromosome 1 linkage peaks, and are strongly supported as having a causal relationship with the metabolic traits.

The extensive linkage disequilibrium operating in the B × H cross, the number of possible QTGs in this region, the small-to-modest effects of each QTG and potential interactions among the QTGs make dissecting the individual contributions of the QTGs in the chromosome 1 region nearly impossible from the cross data alone. However, using gene expression data scored in the B × H cross, expression traits that capture the multiple genetic perturbations in this region and that in turn lead to variations in the metabolic traits[11,31] can be more readily identified. As an example, Fig. 2a highlights transcript abundances for an uncharacterized gene (GenBank accession number, BB433460) that is positioned in an intron of intraflagellar transport 88 homologue (*Ift88*). The liver expression of this gene is highly correlated with metabolic traits such as obesity (Supplementary Fig. 1d), is significantly linked across the entire distal half of chromosome 1 (lod score > 8 across most of the distal half of chromosome 1) and is supported as having a large contribution to the weight trait (Fig. 2a, b). Although BB433460 physically resides on chromosome 14, it captures more of the genetic variation driving the metabolic traits at the chromosome 1 locus than any of the genes physically located in this region, suggesting that networks of expression traits may be perturbed *in trans* by this complex of closely linked QTL and, as a result, lead to variation in the metabolic traits.

Network changes induce phenotypic change

Liver and adipose co-expression networks were reconstructed from the B × H data to identify components of these networks that, like BB433460, mediate the transfer of information from QTL in the chromosome 1 region to the metabolic traits. Supplementary Fig. 3a depicts the most highly connected expression traits in this network as an ordered connectivity matrix. The pattern of distinct clusters or sub-networks that emerge among the highly connected nodes in liver and adipose (Supplementary Fig. 3) are notable and support a hierarchical structure in these networks (Supplementary Fig. 4). The different sub-networks highlighted are seen to be enriched for a number of biological processes (Supplementary Table 2), including insulin signalling (sub-network 1), inflammation (sub-network 5), muscle-related processes (sub-network 7) and cell cycle (sub-network 9). These sub-networks represent key functional units that make up the co-expression network and that underlie processes specific to the different cell types that constitute each tissue. For example, in the female liver co-expression network, sub-network 5 is enriched for genes involved in inflammatory processes, potentially reflecting activity in Kupffer cells. Sub-network 7 is enriched for muscle-related genes such as actin and myosin, potentially reflecting hepatic stellate cell activity, where these cells are known to control microvascular tone and, when activated, can turn into myofibroblasts and express smooth muscle actin filaments and desmin.

The sub-networks represent different sets of overlapping pathways and are readily seen to be enriched for genes that are perturbed by specific genetic loci. For example, 85% of the genes in liver sub-network 1 give rise to eQTL on chromosome 1 (Supplementary Fig. 5). To establish whether a given sub-network was supported as having a causal relationship with the metabolic traits linked to chromosome 1, we used a statistical procedure to test whether the gene expression traits in each sub-network supported a causal, reactive or independent relationship with each of the metabolic traits with

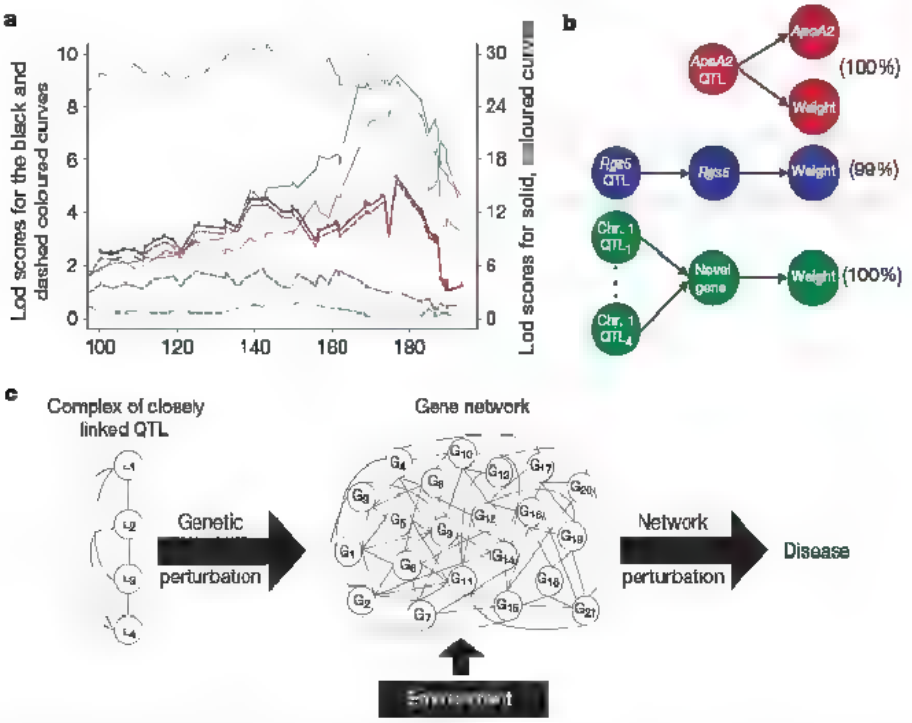

Figure 2 | Genetic loci perturb molecular phenotypes that in turn lead to variations in disease-associated traits. a, Lod score plots for weight (solid black line), *Apoa2* liver expression (solid red), *Rgs5* liver expression (solid blue) and BB433460 liver expression (solid green) traits in the B × H cross. The dashed curves represent the lod score curves for weight conditional on the *Apoa2* (dashed red), *Rgs5* (dashed blue) and BB433460 (dashed green) liver gene expression traits. Conditioning on *Apoa2* expression does not significantly reduce the weight lod score (independent relationship), whereas conditioning on *Rgs5* or BB433460 does (causal relationship). **b**, Relationships supported between the expression and weight traits described in **a**: *Apoa2* (top), *Rgs5* (middle) and *BB433460* (bottom) are predicted to be related to weight in an independent (*Apoa2*) and causal (*Rgs5* and *BB433460*) way. Percentages represent the number of times the model shown was inferred out of 1,000 random samples drawn from the B × H cross. **c**, Generalization of the relationship discovered between BB433460 and weight, in which genetic loci (L_i) and environment perturb molecular networks of genes (G_j) that in turn leads to disease.

respect to the genetic loci driving metabolic traits scored in the B × H cross: abdominal fat mass, weight, plasma insulin levels, free fatty acids, total plasma cholesterol levels and aortic lesion sizes. We identified a sub-network as having a causal relationship with a given metabolic trait if it was significantly enriched ($P < 0.01$) for expression traits that have been supported as having a causal association with that trait. For liver, only five sub-networks were identified as being enriched for at least one of the metabolic traits (Supplementary Fig. 3c). Two of the sub-networks were weakly enriched for insulin, fat mass, weight or cholesterol candidate causal genes (sub-networks 6 and 14), whereas sub-networks 2 and 9 were strongly enriched for only cholesterol and weight candidate causal genes, respectively. However, one of the sub-networks (sub-network 5) was very significantly enriched for expression traits supported as having a causal relationship with every metabolic trait tested, directly implicating this sub-network as a key mediator of the genetic loci driving variation in the metabolic traits scored in the B × H cross (Supplementary Fig. 3c). This sub-network was also the most highly conserved between the sexes and tissues in the B × H cross. In fact, 90% of the genes in female liver sub-network 5 overlapped a corresponding male sub-network ($P < 10^{-305}$ by the Fisher Exact Test), and 50% of these genes overlapped a corresponding adipose sub-network ($P \sim 6.47 \times 10^{-147}$ by the Fisher Exact Test). Furthermore, the adipose sub-network corresponding to liver sub-network 5 was the only adipose sub-network found to be significantly enriched for expression traits supported as having a causal relationship with all of the metabolic traits tested (Supplementary Fig. 3d).

A macrophage sub-network causes disease

To explore the strong pleiotropic effects of sub-network 5 on the metabolic traits in the B × H cross, we formed a supermodule by combining this sub-network with the corresponding sub-network identified in the adipose co-expression network (Supplementary Table 3). Compared to the individual sub-networks, this supermodule systematically increased the fold-change enrichments and corresponding significance scores for expression traits supported as having a causal relationship with the metabolic traits (Table 1). In fact, the percentage of expression traits in this supermodule supported as having a causal relationship with aortic lesions, weight or fat mass, plasma insulin or glucose levels, total cholesterol and HDL cholesterol were 75%, 50%, 45%, 50% and 47%, respectively (Supplementary Table 4). The probability that these overlaps occurred by chance are small. For example, the probability that 50% of the 762 expression traits supported as having a causal relationship with obesity fall in this single supermodule (out of the 23,574 transcripts represented on the array) is 2.30×10^{-262}. We also searched this supermodule comprised of 1,406 transcribed sequences against a body atlas of gene expression representing 60 distinct mouse tissues. For each tissue in the atlas, gene sets were formed on the basis of tissue-specific expression (Supplementary Methods) and these sets were intersected with the supermodule. Bone-marrow-derived macrophages and spleen were the two most enriched tissues (Table 1 and Supplementary Table 4), not liver and adipose as one might expect given the module origins. These enrichments, combined with the significant enrichment of genes in inflammatory pathways, suggest that this module reflects the significant macrophage populations resident in liver and adipose tissues. This macrophage connection is further supported by a number of known macrophage markers represented in this supermodule, including *Cd14*, *Cd68* and *Emr1* (refs 32–34). Given the apparent macrophage-derived origins of this supermodule and its association with the metabolic traits in the B × H cross, we refer to it here as the macrophage-enriched metabolic network (MEMN) (Fig. 3a).

The MEMN is comprised of a number of expression traits corresponding to genes that we recently identified and validated as having a causal relationship with obesity traits, including *Zfp90* (ref. 11), *Tgfbr2* (ref. 11), *C3ar1* (ref. 11) and *Alox5ap* (arachidonate 5-lipoxygenase-activating protein)[31]. Because this network comprises a highly interconnected set of expression traits supported as having a causal relationship with the different metabolic traits, we hypothesized that perturbing single genes in the MEMN that had been previously validated as having a causal relationship with these traits would significantly perturb the entire MEMN. To test this, we constructed single gene perturbation signatures for two of the genes, *Zfp90* and *Alox5*, recently validated as having a causal relationship with obesity-associated traits[11,31]. In addition, we constructed a single gene perturbation signature for *Pparg*, a gene that also resides in the MEMN and that has previously been validated as having a causal relationship with obesity and diabetes traits[35]. In all cases, the perturbation signatures (Supplementary Table 4) were significantly enriched for expression traits in the MEMN (Table 1). For example, the *Zfp90* transgenic signature comprised approximately 3,000 expression traits; 468 of these overlapped the MEMN, whereas only 179 would have been expected by chance—a greater than 2.5-fold enrichment (Fisher Exact P value $= 4.83 \times 10^{-94}$). Furthermore, genes validated as having a causal relationship with obesity were observed in these different perturbation signatures. For example, *Pparg* falls in the *Zfp90* signature, whereas *Tgfbr2* and *C3ar1* fall in the *Pparg* and *Alox5* signatures, respectively. More generally, all signatures are enriched for expression traits supported as having a causal relationship with the metabolic traits. Therefore, expression traits supported as having a causal relationship with the metabolic traits

Table 1 | Gene sets significantly over-represented in the MEMN

Gene set type	Gene set description	Gene set count*	Overlap (fold enrichment)†	Enrichment nominal P value (corrected P value)‡
GO biological process categories	Immune response	1,503	246 (2.6)	4.26×10^{-43} (1.94×10^{-39})
	Defence response	1,565	251 (2.4)	1.97×10^{-42} (8.98×10^{-39})
	Inflammatory response	584	110 (2.8)	4.66×10^{-24} (2.12×10^{-20})
Tissue-specific expression	Bone-marrow-derived macrophage specific expression	289	65 (3.3)	1.10×10^{-18} (1.04×10^{-16})
	Spleen-specific expression	186	47 (3.8)	7.56×10^{-15} (5.81×10^{-14})
Environmental perturbations	Diet-induced obesity versus wild-type signature	1,108	415 (6.2)	5.17×10^{-232}
Causal gene sets	Genes supported as causal for atherosclerotic lesions	159	119 (12.4)	3.22×10^{-111}
	Genes supported as causal for obesity traits	762	375 (8.2)	2.30×10^{-262}
	Genes supported as causal for diabetes	589	272 (7.7)	4.76×10^{-176}
	Genes supported as causal for total cholesterol levels	245	131 (8.9)	1.01×10^{-93}
	Genes supported as causal for HDL levels	77	36 (7.8)	7.98×10^{-24}
Single gene perturbation experiments	*Zfp90* transgenic signature	3,006	468 (2.6)	4.83×10^{-94}
	5-LO knockout signature	5,264	605 (1.9)	5.95×10^{-70}
	Rosiglitazone signature	837	118 (2.3)	3.03×10^{-18}

* The number of sequences in the MEMN used to compare to these gene sets is 1,406.
† The overlap count is computed by counting the number of genes in the intersection between the indicated gene set and the MEMN. The fold enrichment is computed as the observed overlap count divided by the expected overlap count, estimated by multiplying the MEMN transcript count (1,406) by the fraction 'gene set count divided by total gene count (23,574)'.
‡ Nominal P values represent the significance of the Fisher Exact Test statistic under the null hypothesis that the frequency of the indicated gene set is the same between a reference set of all transcripts represented on the array and the set of genes comprising the MEMN. The corrected P values represent the Bonferroni-corrected P values (nominal P value multiplied by the number of gene sets searched).

falling in the MEMN and moving this network when perturbed provide direct support that the metabolic traits are an emergent property of this network, with hundreds of expression traits supported as having a causal relationship with the metabolic traits.

Lpl and *Lactb* validated as obesity genes

In the MEMN, there were 375 expression traits supported as having a causal relationship with the obesity traits linked to the chromosome 1 locus. Although many of the genes corresponding to the expression traits in this network have been validated as having a causal relationship with metabolic traits (*Pparg*, *Alox5*, *Tgfbr2*, *C3ar1* and *Zfp90*, to name just a few), many others have not. We used replication over multiple studies as a way to prioritize genes for validation. Genes supported in multiple independent experiments as having a causal relationship with disease are more likely to be truly causal. Therefore, we intersected the MEMN with a set of genes we previously predicted to have a causal relationship with obesity in a completely independent experiment[11]. Three of the ten genes predicted in an independent F_2 intercross population[11] were represented in the MEMN: *Zfp90*, *Lpl* and *Lactb*. *Zfp90* has already been validated as having a causal relationship with obesity, so we proceeded to validate the other two 'replicated' genes.

Lpl has previously been supported as a susceptibility gene for atherosclerosis- and diabetes-associated traits[36]. However, an association between *Lpl* and obesity has not been established. To our knowledge, *Lactb* has not ever been associated with any of the B × H metabolic traits. Given the prediction that *Lpl* and *Lactb* have a causal relationship with obesity, we recorded weight, fat mass and lean mass for $Lpl^{+/-}$, *Lactb* transgenic mice and wild-type littermate controls every 2 weeks starting at 11 weeks of age using quantitative NMR. As predicted, the growth curves for the $Lpl^{+/-}$ and *Lactb* transgenic animals were significantly different from those of controls (Fig. 3b, c), with the fat-mass-to-lean-mass (FMLM) ratio difference generally increasing over time. At the final quantitative NMR measurement, the FMLM ratios in the $Lpl^{+/-}$ and *Lactb* transgenic mice were increased by 22% and 20%, respectively, over the wild-type controls ($P = 1.09 \times 10^{-5}$ and $P = 4.48 \times 10^{-5}$, respectively).

Lpl is the principal enzyme responsible for the hydrolysis of circulating triglycerides and is active in differentiated macrophages[37], consistent with its presence in the MEMN. Although *Lpl* has not previously been functionally validated as a susceptibility gene for obesity, several studies have established an inverse relationship between *Lpl* activity and obesity-related traits, including a negative correlation observed between *Lpl* activity and percentage body fat in humans[38]. *Lactb* is a serine protease with high similarity to the bacterial lactamase gene, but very little is known about its function in eukaryotes[39,40]. Lactamase metabolizes peptidoglycan in the bacterial cell wall but neither the substrate nor the function of *Lactb* in eukaryotes is known[41]. *Lactb* has been detected in the mitochondria as part of the mitochondrial ribosomal complex[42–44]. Interestingly, a strain of rat that exhibits late-onset obesity was found to contain a mutation in the S26 subunit of the mitochondrial ribosome, at least partially explaining the obesity phenotype[45].

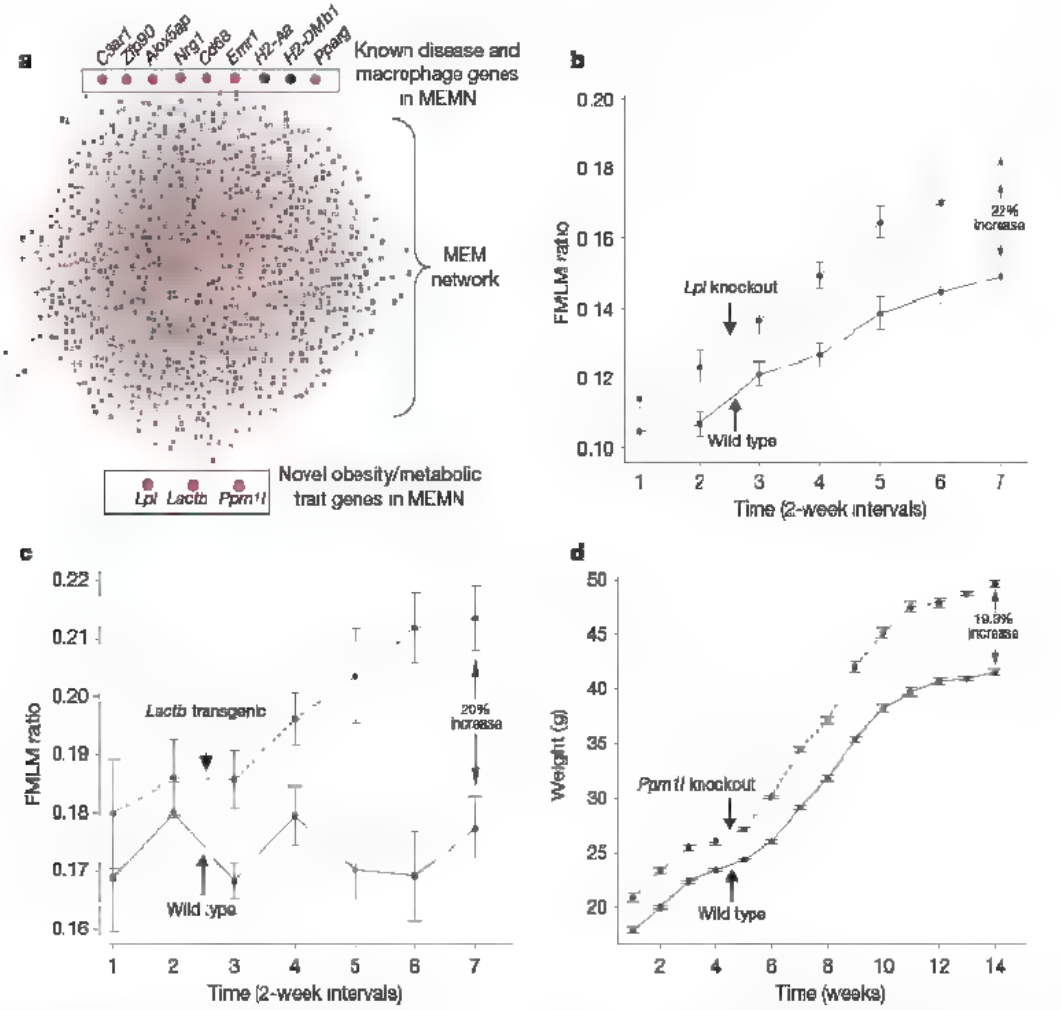

Figure 3 | Genes in the MEM network validated as having a causal relationship with obesity traits. **a**, The MEMN is enriched for genes supported as having a causal relationship with disease traits in the B × H cross (red nodes). The black nodes represent genes in the MEMN not supported as causal for disease traits in the B × H cross. **b**, FMLM ratio curves for *Lpl* knockout ($n = 25$) and wild-type control ($n = 23$) mice ($P = 1.09 \times 10^{-5}$ that the difference at the last time point is significant) **c**, FMLM ratio curves for the *Lactb* transgenic ($n = 36$) and wild-type control ($n = 27$) mice ($P = 4.48 \times 10^{-5}$ that the difference at the last time point is significant) **d**, Weight curves for the $Ppm1l^{-/-}$ ($n = 18$) and wild-type control ($n = 18$) mice ($P = 1.93 \times 10^{-11}$ that the difference at the last time point is significant). Error bars in **b**–**d** represent ±1s.d. of the indicated measures based on replicates and signal-to-noise ratios derived from the model applied to the weight and fat mass differences.

Table 2 | Comparison of metabolic traits between *Ppm1l*$^{-/-}$ and *Ppm1l*$^{+/+}$ mice

		Ppm1l$^{-/-}$		*Ppm1l*$^{+/+}$			
Trait	Age of mice (weeks)	Mean trait value	Sample size	Mean trait value	Sample Size	Percentage change	Difference *P* value*
Weight (g)	21	49.69	17	41.65	18	19.3	1.93×10^{-11}
Total fat mass (g)	9	3.54	17	2.54	18	39.4	0.0037
Total fat mass (g)	20	22.10	17	15.06	18	46.7	0.00030
Baseline glucose (mg ml^{-1})	21	1.55	17	1.39	18	11.5	0.0075
OGTT area under curve (male mice only) (min (mg ml^{-1}))	21	186	8	279	9	−33 3	0.0069
OGTT insulin at 30 min (μg/l)	21	5.17	17	2.44	18	111.9	0.017
Free fatty acids (mequiv l^{-1})	29	0.4116	14†	0.5457	17†	−24.6	0.00050
Non-invasive blood pressure (mm Hg)	25	90.13	17	86.07	18	4,7	0.027

* All *P* values reported, except weight and OGTT AUC, represent the significance of the *t* statistic under the null hypothesis that the difference in mean, sex-adjusted trait values between the *Ppm1l* knockout and *Ppm1l* wild-type groups is equal to 0. For OGTT AUC, this same null hypothesis was tested but for males only. See Supplementary Methods for calculation of the *P* value for weight. † By the 29 week time point, 3 male knockout mice and 1 male wild-type mouse had died.

Ppm1l has a causal relationship with metabolic syndrome

Given the causal association between the MEMN and many metabolic traits, we rank-ordered genes on the basis of the number of metabolic traits for which they were supported having a causal relationship with (Supplementary Table 5) as an alternative to replication as a way to prioritize genes for validation. Four genes ranked at the top of the list: *Fgd6*, *Mmp27*, *BC032204* and *Ppm1l*. However, not only is *Ppm1l* a classically 'druggable' gene, but a knockout mouse for this gene was available from Deltagen, so we selected this gene for validation. *Ppm1l* is a newly discovered protein phosphatase, the function of which is not well characterized.

Weight, fat mass, insulin and glucose levels, blood pressure and other biochemical measures in blood were recorded in *Ppm1l*$^{-/-}$ and wild-type littermate controls. The growth curves for the knockout mice were significantly different from those of wild-type controls (Fig. 3d); at the final weight measurement, the knockout mice weighed 19.3% more than wild-type mice (Table 2). *Ppm1l*$^{-/-}$ mice also exhibited increased fat mass compared to wild-type controls, with an overall 46.7% increase in fat mass at 20 weeks of age (Table 2). At 21 weeks of age, an oral glucose tolerance test (OGTT) was performed on all mice. Baseline plasma glucose levels were observed to be 11.5% higher in *Ppm1l*$^{-/-}$ mice relative to wild-type mice. Male knockout mice demonstrated an improved glucose tolerance, with a 33.3% decrease in the area under the curve (AUC) relative to male wild-type mice (Table 2). In contrast, although glucose levels for females at the 60, 90 and 180 min time points were significantly increased (*P* value = 0.0077, 0.050 and 0.0043, respectively), the difference in AUC was not statistically significant (*P* value = 0.11). At the 30-min OGTT time point, insulin levels in male and female *Ppm1l*$^{-/-}$ mice were more than 100% increased compared to those of controls (Table 2). Blood was also collected in all mice at 29 weeks of age, and total cholesterol, triglycerides and free fatty acids were recorded. A significant decrease in free fatty acids was recorded in *Ppm1l*$^{-/-}$ mice relative to controls (Table 2), but no other major changes were observed for the other parameters (data not shown). Finally, given that the MEMN is supported as having a causal relationship with a number of traits associated with metabolic syndrome, and given the presence of genes such as ACE in this network, non-invasive blood pressure was monitored in all mice at 25 weeks of age. Overall, the blood pressure in *Ppm1l*$^{-/-}$ mice was significantly increased compared to that of controls (Table 2).

Discussion

By integrating co-expression networks and genotypic data from an F_2 intercross population, we identified a liver and adipose macrophage-enriched sub-network that was associated with disease traits comprising the metabolic syndrome and enriched for expression traits supported as having a causal relationship with these traits. Unlike classic genetics approaches that aim to identify genes underlying genetic loci associated with disease, the approach developed here seeks to identify whole gene networks that respond *in trans* to genetic loci driving disease, and that in turn lead to variations in the disease traits. Our results demonstrate that there may in fact be thousands of genes capable of increasing susceptibility to metabolic disease traits such as obesity, diabetes and atherosclerosis. Because the causal predictions made in this study rely on conditional dependency arguments that are statistical in nature, experimental validation is critical. Towards that end, *Lpl* and *Lactb* were identified and validated *in vivo* as previously unknown obesity genes, whereas *Ppm1l* was identified and validated as a gene capable of modulating multiple obesity, diabetes and hypertension traits.

Network-based approaches for elucidating the complexity of disease traits cast a broad net for genes that drive disease relative to classic genetic linkage or association studies that limit the search to genes that harbour DNA variations that associate with disease in the population under study. As a result, predictive networks provide the potential to identify hundreds of genes that drive disease and that could serve as points for therapeutic intervention. Our results support the idea that common forms of disease may be emergent properties of networks, where the networks associated with disease are highly interconnected, with many genes in the network potentially having a causal relationship with disease if perturbed strongly enough. With large-scale molecular profiling, genotypic and clinical data collected from large-scale populations, studying how a network of gene interactions affects disease will come to complement more strongly the classic focus of how a single protein or RNA affects disease. The integration of genetic, molecular profiling and clinical data has the potential to paint a more detailed picture of the particular network states that drive disease, and this in turn has the potential to lead to more progressive treatments of disease that may ultimately involve the targeting of whole networks as opposed to current therapeutic strategies focused on targeting one or two genes[46].

METHODS SUMMARY

Liver and adipose tissue were extracted from 334 F_2 animals in the B × H cross and profiled on an Agilent custom murine gene expression microarray[17]. All F_2 animals were genotyped at more than 1,300 single nucleotide polymorphism markers and clinically characterized with respect to obesity-, diabetes- and atherosclerosis-related traits[17]. The gene expression and genotype data were combined to construct co-expression networks comprised of the most highly connected nodes from each tissue and sex using previously described methods[47]. Highly interconnected sub-networks were then detected from each co-expression network using an iterative search algorithm[47,48]. QTL were detected for each of the expression and metabolic traits using a forward stepwise regression procedure[17,49]. QTL with pleiotropic effects on expression and metabolic traits were identified using a multivariate likelihood test[11,50]. The B × H QTL, expression and metabolic trait data were then integrated to assess whether each expression trait in each tissue was supported as having a causal relationship with each of the metabolic traits, with respect to QTL detected with pleiotropic effects on the expression and metabolic traits[3]. To identify sub-networks as having a causal relationship with the metabolic traits, each sub-network was tested for enrichment of expression traits supported as having a causal association with the metabolic traits using the Fisher Exact Test. Genes comprising the sub-network supported as having a causal relationship with all metabolic traits scored in the B × H cross were selected for validation on the basis of one of two criteria: the gene was supported as having a causal relationship with the metabolic traits in an

independent, previously published study, or the gene was supported as having a causal relationship with the most metabolic traits scored in the B × H cross. The three genes chosen for validation using these criteria were validated by constructing gene-knockout mouse strains (*Lpl* and *Pmp11*) or transgenic mouse strains overexpressing the gene of interest (*Lactb*). Full Methods are provided in the Supplementary Information.

Received 5 October 2007; accepted 28 January 2008.
Published online 16 March 2008.

1. Edwards, A. O. *et al.* Complement factor H polymorphism and age-related macular degeneration. *Science* 308, 421–424 (2005).
2. Haines, J. L. *et al.* Complement factor H variant increases the risk of age-related macular degeneration. *Science* 308, 419–421 (2005).
3. Klein, R. J. *et al.* Complement factor H polymorphism in age-related macular degeneration. *Science* 308, 385–389 (2005).
4. Sladek, R. *et al.* A genome-wide association study identifies novel risk loci for type 2 diabetes. *Nature* 445, 881–885 (2007).
5. Frayling, T. M. *et al.* A common variant in the FTO gene is associated with body mass index and predisposes to childhood and adult obesity. *Science* 316, 889–894 (2007).
6. Strittmatter, W. J. *et al.* Apolipoprotein E: high-avidity binding to β-amyloid and increased frequency of type 4 allele in late-onset familial Alzheimer disease. *Proc. Natl Acad. Sci. USA* 90, 1977–1981 (1993).
7. Brem, R. B., Yvert, G., Clinton, R. & Kruglyak, L. Genetic dissection of transcriptional regulation in budding yeast. *Science* 296, 752–755 (2002).
8. Bystrykh, L. *et al.* Uncovering regulatory pathways that affect hematopoietic stem cell function using 'genetical genomics'. *Nature Genet.* 37, 225–232 (2005).
9. Chesler, E. J. *et al.* Complex trait analysis of gene expression uncovers polygenic and pleiotropic networks that modulate nervous system function. *Nature Genet.* 37, 233–242 (2005).
10. Monks, S. A. *et al.* Genetic inheritance of gene expression in human cell lines. *Am. J. Hum. Genet.* 75, 1094–1105 (2004).
11. Schadt, E. E. *et al.* An integrative genomics approach to infer causal associations between gene expression and disease. *Nature Genet.* 37, 710–717 (2005).
12. Schadt, E. E. *et al.* Genetics of gene expression surveyed in maize, mouse and man. *Nature* 422, 297–302 (2003).
13. Hartwell, L. H., Hopfield, J. J., Leibler, S. & Murray, A. W. From molecular to modular cell biology. *Nature* 402, C47–C52 (1999).
14. Schadt, E. E., Sachs, A. & Friend, S. Embracing complexity, inching closer to reality. *Sci. STKE* 2005, pe40 (2005).
15. Paigen, B., Albee, D., Holmes, P. A. & Mitchell, D. Genetic analysis of murine strains C57BL/6J and C3H/He to confirm the map position of *Ath-1*, a gene determining atherosclerosis susceptibility. *Biochem. Genet.* 25, 501–511 (1987).
16. Yang, X. *et al.* Tissue-specific expression and regulation of sexually dimorphic genes in mice. *Genome Res.* 16, 995–1004 (2006).
17. Wang, S. *et al.* Genetic and genomic analysis of a fat mass trait with complex inheritance reveals marked sex specificity. *PLoS Genet.* 2, e15 (2006).
18. Paigen, B. *et al. Ath-1*, a gene determining atherosclerosis susceptibility and high density lipoprotein levels in mice. *Proc. Natl Acad. Sci. USA* 84, 3763–3767 (1987).
19. Castellani, L. W., Goto, A. M. & Lusis, A. J. Studies with apolipoprotein A-II transgenic mice indicate a role for HDLs in adiposity and insulin resistance. *Diabetes* 50, 643–651 (2001).
20. Wang, X., Korstanje, R., Higgins, D. & Paigen, B. Haplotype analysis in multiple crosses to identify a QTL gene. *Genome Res.* 14, 1767–1772 (2004).
21. Wang, X. *et al.* Positional identification of *TNFSF4*, encoding OX40 ligand, as a gene that influences atherosclerosis susceptibility. *Nature Genet.* 37, 365–372 (2005).
22. Warden, C. H., Hedrick, C. C., Qiao, J. H., Castellani, L. W. & Lusis, A. J. Atherosclerosis in transgenic mice overexpressing apolipoprotein A-II. *Science* 261, 469–472 (1993).
23. Welch, C. L. *et al.* Novel QTLs for HDL levels identified in mice by controlling for *Apoa2* allelic effects, confirmation of a chromosome 6 locus in a congenic strain. *Physiol. Genomics* 17, 48–59 (2004).
24. Doolittle, M. H., LeBoeuf, R. C., Warden, C. H., Bee, L. M. & Lusis, A. J. A polymorphism affecting apolipoprotein A-II translational efficiency determines high density lipoprotein size and composition. *J. Biol. Chem.* 265, 16380–16388 (1990).
25. Pajukanta, P. *et al.* Familial combined hyperlipidemia is associated with upstream transcription factor 1 (*USF1*). *Nature Genet.* 36, 371–376 (2004).
26. Babinska, A. *et al.* F11-receptor (F11R/JAM) mediates platelet adhesion to endothelial cells: role in inflammatory thrombosis. *Thromb. Haemost.* 88, 843–850 (2002).
27. Huertas-Vazquez, A. *et al.* Familial combined hyperlipidemia in Mexicans: association with upstream transcription factor 1 and linkage on chromosome 16q24.1. *Arterioscler. Thromb. Vasc. Biol.* 25, 1985–1991 (2005).
28. Ezzahiri, R. *et al. Chlamydia pneumoniae* infections augment atherosclerotic lesion formation: a role for serum amyloid P. *APMIS* 114, 117–126 (2006).
29. Adams, L. D., Geary, R. L., Li, J., Rossini, A. & Schwartz, S. M. Expression profiling identifies smooth muscle cell diversity within human intima and plaque fibrous cap: loss of RGS5 distinguishes the cap. *Arterioscler. Thromb. Vasc. Biol.* 26, 319–325 (2006).
30. Chang, Y. P. *et al.* Multiple genes for essential-hypertension susceptibility on chromosome 1q. *Am. J. Hum. Genet.* 80, 253–264 (2007).
31. Mehrabian, M. *et al.* Integrating genotypic and expression data in a segregating mouse population to identify 5-lipoxygenase as a susceptibility gene for obesity and bone traits. *Nature Genet.* 37, 1224–1233 (2005).
32. Austyn, J. M. & Gordon, S. F4/80, a monoclonal antibody directed specifically against the mouse macrophage. *Eur. J. Immunol.* 11, 805–815 (1981).
33. Ramprasad, M. P., Terpstra, V., Kondratenko, N., Quehenberger, O. & Steinberg, D. Cell surface expression of mouse macrosialin and human CD68 and their role as macrophage receptors for oxidized low density lipoprotein. *Proc. Natl Acad. Sci. USA* 93, 14833–14838 (1996).
34. Wright, S. D., Ramos, R. A., Tobias, P. S., Ulevitch, R. J. & Mathison, J. C. CD14, a receptor for complexes of lipopolysaccharide (LPS) and LPS binding protein. *Science* 249, 1431–1433 (1990).
35. Kubota, N. *et al.* PPARγ mediates high-fat diet-induced adipocyte hypertrophy and insulin resistance. *Mol. Cell* 4, 597–609 (1999).
36. Hu, Y., Liu, W., Huang, R. & Zhang, X. A systematic review and meta-analysis of the relationship between lipoprotein lipase Asn291Ser variant and diseases. *J. Lipid Res.* 47, 1908–1914 (2006).
37. Preiss-Landl, K., Zimmermann, R., Hammerle, G. & Zechner, R. Lipoprotein lipase: the regulation of tissue specific expression and its role in lipid and energy metabolism. *Curr. Opin. Lipidol.* 13, 471–481 (2002).
38. Yost, T. J., Jensen, D. R. & Eckel, R. H. Tissue-specific lipoprotein lipase: relationships to body composition and body fat distribution in normal weight humans. *Obes. Res.* 1, 1–4 (1993).
39. Liobikas, J. *et al.* Expression and purification of the mitochondrial serine protease LACTB as an N-terminal GST fusion protein in *Escherichia coli*. *Protein Expr. Purif.* 45, 335–342 (2006).
40. Smith, T. S. *et al.* Identification, genomic organization, and mRNA expression of LACTB, encoding a serine β-lactamase-like protein with an amino-terminal transmembrane domain. *Genomics* 78, 12–14 (2001).
41. Jacobs, C. Life in the balance: cell walls and antibiotic resistance. *Science* 278, 1731–1732 (1997).
42. Gaucher, S. P. *et al.* Expanded coverage of the human heart mitochondrial proteome using multidimensional liquid chromatography coupled with tandem mass spectrometry. *J. Proteome Res.* 3, 495–505 (2004).
43. Mootha, V. K. *et al.* Integrated analysis of protein composition, tissue diversity and gene regulation in mouse mitochondria. *Cell* 115, 629–640 (2003).
44. Taylor, S. W. *et al.* Characterization of the human heart mitochondrial proteome. *Nature Biotechnol.* 21, 281–286 (2003).
45. Bains, R. K. *et al.* Visceral obesity without insulin resistance in late-onset obesity rats. *Endocrinology* 145, 2666–2679 (2004).
46. Schadt, E. E. & Lum, P. Y. Reverse engineering gene networks to identify key drivers of complex disease phenotypes. *J. Lipid Res.* 47, 2601–2013 (2006).
47. Lum, P. Y. *et al.* Elucidating the murine brain transcriptional network in a segregating mouse population to identify core functional modules for obesity and diabetes. *J. Neurochem.* 97 (suppl. 1), 50–62 (2006).
48. Ravasz, E., Somera, A. L., Mongru, D. A., Oltvai, Z. N. & Barabasi, A. L. Hierarchical organization of modularity in metabolic networks. *Science* 297, 1551–1555 (2002).
49. Haley, C. S. & Knott, S. A. A simple regression method for mapping quantitative trait loci in line crosses using flanking markers. *Heredity* 69, 315–324 (1992).
50. Jiang, C. & Zeng, Z. B. Multiple trait analysis of genetic mapping for quantitative trait loci. *Genetics* 140, 1111–1127 (1995).

Supplementary Information is linked to the online version of the paper at www.nature.com/nature.

Acknowledgements This work was supported in part by grants from the NIH/NIDDK and NHLBI to A.J.L. and T.A.D.

Author Contributions S.P., D.J.M. and M.-F.C. constructed and characterized the *Ppm1l* knockout mouse. X.Y., L.W.C., S.W., S.D., A.G., T.A.D. and A.J.L. constructed and characterized the B × H cross, the *Lpl* knockout mouse and the *Lactb* transgenic mouse. S.H., A.G., S.D. and B.Z. assisted in the co-expression network analyses. S.E. and A.J.L. performed bioinformatic analyses. All authors discussed the results and commented on the manuscript. S.K.S. and C.Z. aided in the data analysis. P.Y.L. and J.L. aided in the study design and interpretation of the experimental results. Y.C., J.Z. and E.E.S. designed the study, developed methods, analysed the data and wrote the paper.

Author Information The liver and adipose microarray data for the B × H cross have been deposited into the GEO database under accession numbers GSE2814 and GSE3086, respectively. Expression data associated with the diet-induced obesity, *Zfp90* transgenic, *Alox5*$^{-/-}$ and rosiglitazone-treated animals have been uploaded to the GEO database under accession numbers GSE7028, GSE7029, GSE7026 and GSE7027, respectively. The authors declare competing financial interests: details accompany the full-text HTML version of the paper at www.nature.com/nature. Reprints and permissions information is available at www.nature.com/reprints. Correspondence and requests for materials should be addressed to E.E.S. (eric_schadt@merck.com).

ARTICLES

Compartmentalized dendritic plasticity and input feature storage in neurons

Attila Losonczy[1]*, Judit K. Makara[1]* & Jeffrey C. Magee[1]

Although information storage in the central nervous system is thought to be primarily mediated by various forms of synaptic plasticity, other mechanisms, such as modifications in membrane excitability, are available. Local dendritic spikes are nonlinear voltage events that are initiated within dendritic branches by spatially clustered and temporally synchronous synaptic input. That local spikes selectively respond only to appropriately correlated input allows them to function as input feature detectors and potentially as powerful information storage mechanisms. However, it is currently unknown whether any effective form of local dendritic spike plasticity exists. Here we show that the coupling between local dendritic spikes and the soma of rat hippocampal CA1 pyramidal neurons can be modified in a branch-specific manner through an *N*-methyl-D-aspartate receptor (NMDAR)-dependent regulation of dendritic Kv4.2 potassium channels. These data suggest that compartmentalized changes in branch excitability could store multiple complex features of synaptic input, such as their spatio-temporal correlation. We propose that this 'branch strength potentiation' represents a previously unknown form of information storage that is distinct from that produced by changes in synaptic efficacy both at the mechanistic level and in the type of information stored.

A distinctive morphological feature of neurons is the large number of dendritic branches that compartmentalize their primary input regions. Generally, these branches contain voltage-dependent ion channels, the activation of which produce local membrane potential nonlinearities (Na^+, Ca^{2+} or NMDA spikes) that markedly shape incoming synaptic input and action potential output[1–9]. These channels are modifiable by physiologically relevant stimuli and by behaviour[10,11]. Recent reports suggest that channel modifications can take place within restricted dendritic regions, raising the possibility of a compartmentalized regulation of local dendritic nonlinearities[12–14]. Such plasticity might function as a powerful mechanism for storing particular input features encoded in highly correlated patterns.

Variable spike strength and propagation

We used multi-site two-photon glutamate uncaging to deliver spatially clustered and temporally synchronous input patterns required to evoke local dendritic spikes in basal and radial oblique dendrites of rat hippocampal CA1 pyramidal neurons (Fig. 1a, b)[4]. These dendritic spikes produce a nonlinear depolarization at the soma consisting of a fast Na^+-channel-dependent component and a slow NMDA-receptor component (Fig. 1a, b)[4]. We observed that the strength of the Na^+ spike (amplitude and rate of rise (dV/dt)) within a branch was relatively invariant between trials and independent of input configuration or strength (Supplementary Fig. 2a, b)[4]. There was, however, a remarkable variation of spike strength between branches (Fig. 1a, b). We proposed that differences in the propagation of dendritic spikes within branches might underlie this variability. Therefore, we examined the within-branch propagation by measuring Ca^{2+} transients associated with dendritic spikes at various distances from the input location (Fig. 1c–e). In most cases, spike-associated Ca^{2+} signals propagating towards the soma decreased markedly within 20–40 μm of the input site (fluorescence change ($\Delta F/F$), from $109 \pm 5\%$ to $24 \pm 2\%$, $n = 65$ of 76 dendrites, Fig. 1c, e), whereas those propagating towards the sealed end attenuated much less over a similar distance ($\Delta F/F$, from $111 \pm 11\%$ to $100 \pm 8\%$, $n = 21$; Fig. 1e and Supplementary Fig. 3a). Notably, dendritic spikes propagated towards the soma much more robustly in a minority of branches ($\Delta F/F$, $104 \pm 12\%$ to $92 \pm 6\%$, $n = 11$; Fig. 1d, e). In these dendrites, spike-associated Ca^{2+} signals did not attenuate over the ~60 μm of forward propagation measured. As expected, the amplitude and dV/dt of the fast spike component was directly proportional to propagation strength (strong, 5.06 ± 0.36 mV, 5.43 ± 0.78 V s^{-1}, $n = 11$; weak, 1.15 ± 0.06 mV, 0.45 ± 0.05 V s^{-1}, $n = 65$, $P < 0.001$; Fig. 1f and Supplementary Fig. 3b), whereas there was no difference in local spike threshold measured at the soma (strong, 3.34 ± 0.35 mV, $n = 7$; weak, 3.34 ± 0.24 mV, $n = 34$, $P = 0.551$) or in slow component amplitudes at threshold level (Supplementary Fig. 3c). These data indicate that variability in branch spike forward propagation produces heterogeneity in the coupling between various dendrites and the soma/axonal output region[15].

To determine whether there were indeed two distinct populations of branch strengths, we focused on the spike dV/dt as a measure of propagation strength[4,6] using data from a larger population that included branches without simultaneous Ca^{2+} recordings ($n = 479$). Data were better fit by a double gaussian function with peaks that were an order of magnitude apart (Fig. 1g, first peak, 0.37 ± 0.001 V s^{-1}; second peak, 3.49 ± 0.11 V s^{-1}) than by a single gaussian function ($P < 0.001$, Shapiro–Wilk test). Thus, there are two distinct populations of dendrites with most (78%) exerting weak coupling strength (weak dendrites) and a minority (22%) with a ten-fold stronger coupling (strong dendrites).

Action potential output depends on spike strength

The amplitudes of weak dendritic spikes are quite small at the soma (spike amplitude, 1.52 ± 0.05 mV; peak amplitude near threshold, 4.38 ± 0.20 mV, $n = 188$) with maximum depolarization at the slow NMDAR-dependent peak, even when two separate weak dendrites are simultaneously activated (Supplementary Fig. 3d, e). Because of this, weak dendritic spikes produce imprecisely timed action potential

[1]Howard Hughes Medical Institute, Janelia Farm Research Campus, 19700 Helix Dr Ashburn, Virginia 20147, USA.
*These authors contributed equally to this work

output with variable latency (latency and jitter, 11.64 ± 1.28 ms and 3.51 ± 0.85 ms, respectively, $n = 24$, Fig. 1h). In contrast, the fast spike component of strong branches is usually large enough to evoke action potential output (spike, 4.95 ± 0.26 mV; peak, 7.81 ± 0.56 mV, $n = 35$). The action potentials initiated by strong dendritic spikes required much fewer inputs (~55% of weak dendrite inputs, Supplementary Fig. 3f) and showed a latency and jitter an order of magnitude lower than that observed for weak dendritic spikes (latency, 1.94 ± 0.19 ms; jitter, 0.13 ± 0.04 ms, $n = 13$; Fig. 1h). Thus, local spikes from strongly coupled dendrites are capable of evoking an invariant, precise action potential output for a much reduced input level.

Dendritic morphology and spike strength

We next examined whether the pattern of weak and strong spikes varied with distance of the branch from the soma. Using the above bimodal distribution and the dV/dt versus $\Delta F/F$ data (Fig. 1f) to establish a criterion, we separated dendritic spikes into a strong group ($dV/dt > 2\ V\ s^{-1}$) and a weak group ($dV/dt < 2\ V\ s^{-1}$). Although both weak and strong branches could be observed among basal and radial oblique dendrites originating within ~80 µm of the soma, the proportion of strong spikes decreased for radial oblique dendrites bifurcating from the apical trunk >40 µm from the soma (Fig. 1i). A similar pattern was observed during dendritic recordings. Because of this relationship, the remainder of our analysis was limited to this perisomatic region (basal or radial oblique bifurcating from the trunk within ~40 µm from the soma). The infrequent observation of strong Na^+ spikes in distal oblique compartments does not, however, mean that branch strength is invariant in this region, as distal branch strength may be expressed through a different nonlinear mechanism than the Na^+ spike. We next plotted spike dV/dt versus distance of input location along dendrites for this proximal population (Supplementary Fig. 4a). Data points for weak branches varied as a function of distance ($\lambda = 69$ µm), whereas spikes from strong branches did not.

Saltatory-like spike propagation

Proximal dendrites are rarely single branches (~11% here), rather they divide further, forming complex dendritic families that consist of a primary branch, terminal dendrites and occasionally intermediate segment(s). By systematically testing the proximal dendritic families (Fig. 2a and Supplementary Fig. 4b), we discovered that branch coupling strength was hierarchically structured such that the majority of primary branches were strong (75%, 88 out of 117 branches), whereas much fewer terminal branches showed strong spikes (18%, 35 out of 194). To quantify this hierarchical relationship, we calculated the within-family spike ratio, defined as dV/dt of the higher order daughter (D) branch divided by dV/dt of the lower order parent (P) branch (Fig. 2b and Supplementary Fig. 4c). The distribution of spike ratio in families with strong parent branches demonstrated that by 15–40 µm distal to the branch point, daughter branches were already either extremely weak (spike ratio, 0.18 ± 0.01, $n = 90$) or slightly stronger than the parent branch to which they were connected (spike ratio, 1.17 ± 0.05, $n = 30$, $P < 0.001$) (Fig. 2b and Supplementary Fig. 4c, d). Consistent with this, two nearly coincident but separable spike dV/dt components were usually found in the total fast spike of strong daughter branches (dV/dt_Σ), with one small component corresponding to the daughter branch itself (dV/dt_D) and a second dV/dt component approximately the same size as the strong parent branch spike (dV/dt_P; Fig. 2c). In several cases, two daughter branches bifurcating from a common parent branch showed highly divergent spike ratios,

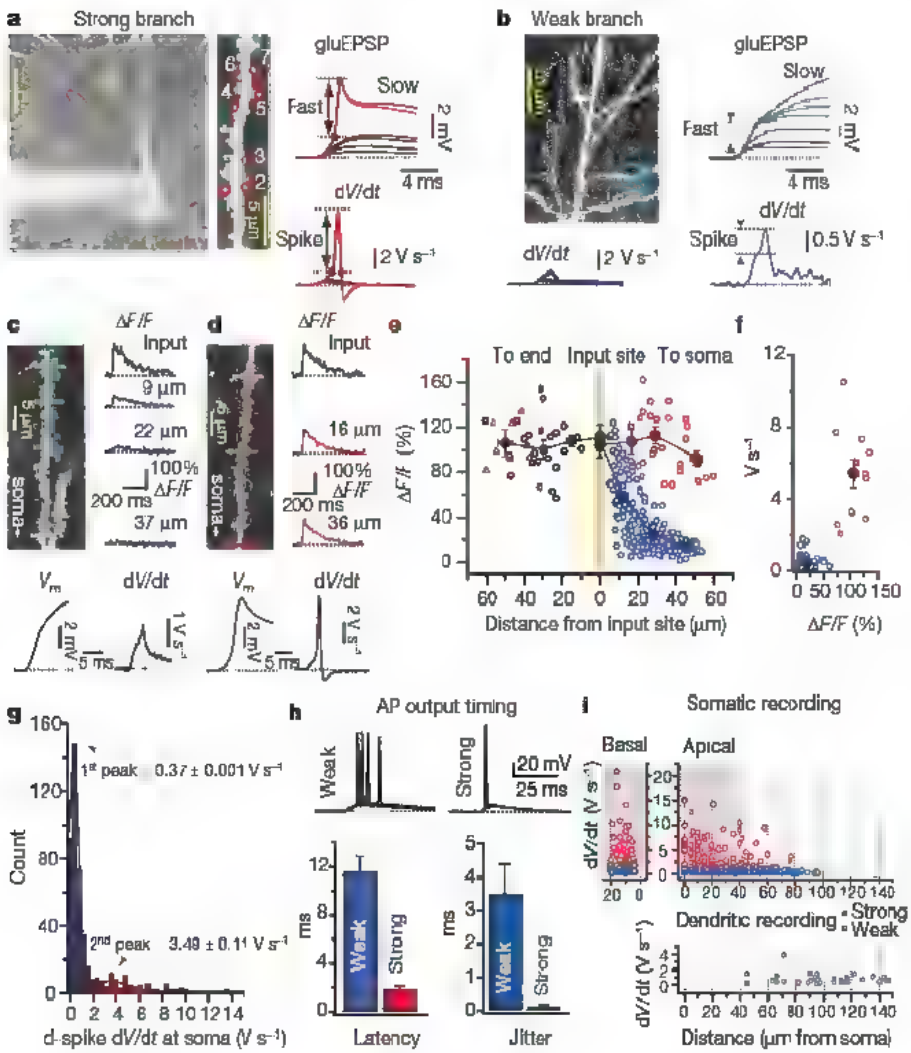

Figure 1 Two populations of dendritic spike strengths. **a**, Left, image stack. The input region is expanded with numbered uncaging locations indicated. Right: membrane potential (V_m, top) and dV/dt (bottom) traces of a strong dendritic spike. Black traces, subthreshold gluEPSPs; red traces, dendritic spike. **b**, Weak branch. **c**, **d**, Spike-associated Ca^{2+} signals in weakly (**c**) and strongly (**d**) forward propagating dendrites. Distances from input site (dots and orange line) are indicated. **e**, Forward propagating Ca^{2+} signals versus distance from input site in weak (blue dots) and strong (red dots) dendrites and for spikes propagating towards the sealed end in weak (black) and strong (red triangles) branches. **f**, Spike dV/dt versus spike Ca^{2+} signals (at 20–40 µm proximal to input). **g**, Distribution of spike dV/dt fit by a double gaussian function (d-spike, dendritic spike). **h**, Action potential (AP) output evoked by weak (upper left) or strong (upper right) dendritic spikes (four trials each). Action potential latency (lower left) and jitter (lower right) for weak and strong branches is shown. **i**, Spike dV/dt versus dendrite distance from soma in somatic and dendritic recordings.

with one being strong and the other weak (Fig. 2d, e and Supplementary Fig. 4e). In these cases, the dV/dt_D component from the strongly coupled daughter branch was nearly twice that of the weakly coupled sister branch (strong, $0.89 \pm 0.08\,V\,s^{-1}$; weak, $0.51 \pm 0.05\,V\,s^{-1}$, $n = 9$, $P < 0.001$; Fig. 2f). Ca^{2+} imaging confirmed that only strong daughter branches fired local spikes capable of propagating through the branch point into the strong proximal compartment (Fig. 2d, e, g). The strength of the daughter branch spike was independent of any particular synaptic property of the initiating input (Supplementary Fig. 2b, c). Thus, local spikes within daughter branches act as variable, all-or-none triggers of stronger parent branches, with only a minority of daughter branches possessing adequate excitability to support effective propagation. These data indicate that basal and proximal radial oblique dendrites form a distinct, extensively branching perisomatic integration zone with a large number of terminal compartments (~70% of total)[16] whose internal properties can be independently regulated to shape the impact of their synaptic input (which originates primarily from subregions CA3a and b)[17,18].

Branch strength potentiation

The variable pattern of branch coupling strengths observed within dendritic arborizations might reflect a natural regulatory process governing the excitability of local branches. If this is the case, we should be able to alter experimentally the coupling strength of selective branches. We tested this hypothesis on weak daughter branches (15–40 μm from branch point; dV/dt_D, $0.72 \pm 0.05\,V\,s^{-1}$, $n = 36$) that originated from strong parent dendrites (dV/dt_P, $5.31 \pm 0.59\,V\,s^{-1}$, $n = 36$). We first tested whether input patterns designed to mimic those found during exploratory sharp waves (SPWs)[19] could induce a change in local spike propagation. More than 40 min of repeated local spike initiation by itself caused only a minor change in the strength of the weak daughter branch (dV/dt_D, to $111 \pm 3\%$, $P < 0.01$, $n = 7$; Fig. 3A, D, E) and did not result in recruitment of the strong branch spike. However, when we combined the same repeated local spike initiation with a transient application of the cholinergic agonist carbachol (CCh, 5 μM, 20 min), to mimic the neuromodulatory state of exploratory behaviour[20], the stimulus induced a robust, slowly developing enhancement of weak branch spike strength that continued even after CCh washout (dV/dt_D in CCh, to $158 \pm 9\%$ of control, $P < 0.001$, $n = 13$; Fig. 3B, D, E). In most cases the daughter spikes became effective enough to evoke the strong parent branch spike, leading to a large step increase in dV/dt and in spike ratio (9 out of 13 experiments, dV/dt_Σ, to $548 \pm 129\%$; spike ratio, from 0.27 ± 0.05 to 1.09 ± 0.07; Fig. 3B, F–H). Dendritic spike amplitude was also significantly enhanced (to $245 \pm 35\%$, $n = 13$, $P < 0.01$). We also used a more general associative theta (θ)-pairing protocol that involved local branch spike initiation paired with two or three back-propagating action potentials (Fig. 3C). This induction protocol also successfully enhanced weak branch spike strength (dV/dt_D, to $188 \pm 13\%$, $n = 16$, $P < 0.001$; Fig. 3C–E), often to a level where it recruited the parent branch spike (11 out of 16 experiments, dV/dt_Σ, to $1{,}198 \pm 294\%$; spike ratio, from 0.16 ± 0.03 to 1.09 ± 0.06, $n = 11$; amplitude, to $409 \pm 72\%$, $n = 16$; Fig. 3C, F–H). We named this form of dendritic plasticity 'branch strength potentiation' (BSP).

BSP was found to be branch specific, as both induction protocols enhanced only those weak branches where local spikes were repeatedly initiated, while leaving other unstimulated branches unaffected (dV/dt_D in CCh: stimulated, to $148 \pm 13\%$, $n = 5$, $P < 0.05$; unstimulated, to $103 \pm 13\%$, $n = 5$, $P = 0.649$; dV/dt_D after pairing: stimulated, to $173 \pm 12\%$, $n = 4$, $P < 0.01$; unstimulated, to $99 \pm 5\%$, $n = 7$, $P = 0.839$; Fig. 4a–c), including the strong parent branches to which they were connected (dV/dt_P in CCh, to $116 \pm 39\%$, $n = 4$, $P = 0.446$; θ-pairing, to $111 \pm 11\%$, $n = 4$, $P = 0.546$). Also, both local spikes and back-propagating action potentials were required

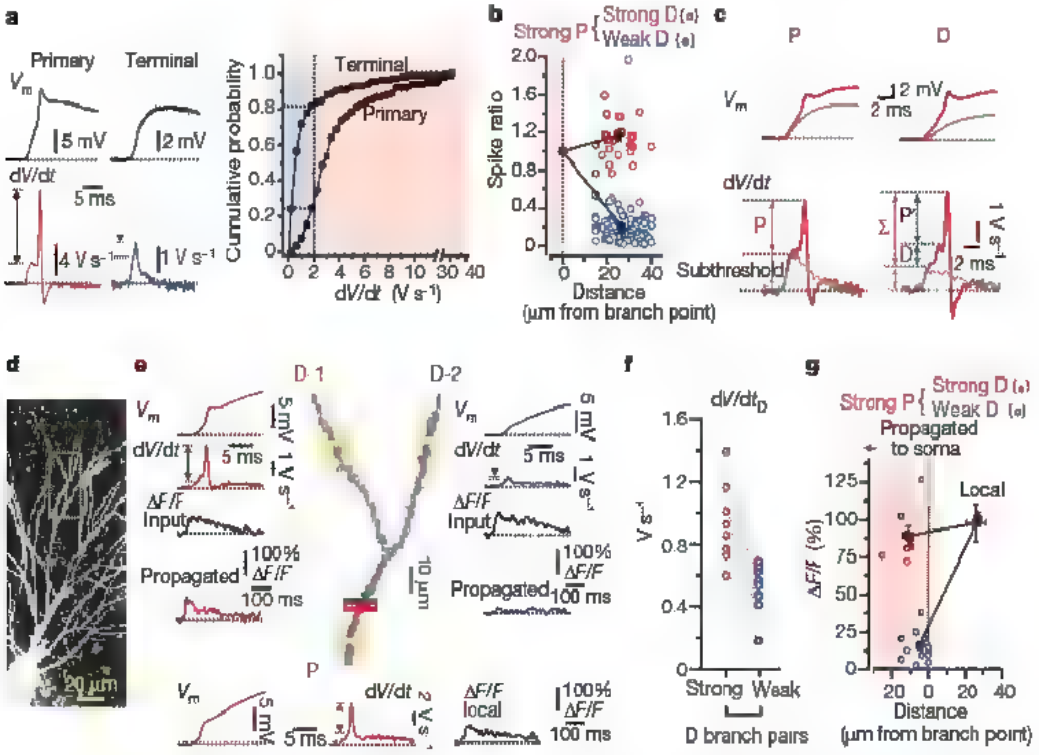

Figure 2 | Relationship of dendritic morphology and branch strength. **a**, Membrane potential (V_m; top) and dV/dt (bottom) traces from a strong primary and a connected weak terminal branch. Right: the cumulative probability of spike dV/dt for all primary and terminal branches is shown. Red, strong; blue, weak. **b**, Spike ratio for daughter (D) branches originating from strong parent (P) versus distance of the input location on the daughter. **c**, V_m and dV/dt from a strong parent (left) and connected strong daughter (right) for suprathreshold (red) and just subthreshold (grey) input. Parent dV/dt has one component (P) whereas the strong daughter (Σ) has two components (D and P). **d**, **e**, Basal arbor with marked region expanded in **e** showing outline of a parent (P) and two connected daughters (D-1 and D-2). Ovals indicate uncaging locations. Blue and red lines, line-scan locations for spike-associated Ca^{2+} signals propagating from daughters into the parent branch. Orange line: input site line scans. Input onto D-1 branch initiated a strong spike (left). Input onto D-2 branch initiated a weak spike (right). Only the spike evoked in D-1 produced a Ca^{2+} signal in P. **f**, dV/dt_D of different sister branches with a common strong parent. **g**, Spike-associated Ca^{2+} signals versus distance relative to branch point.

for potentiation induced by the θ-pairing protocol, as the same repetitive suprathreshold synchronous input alone or back-propagating action potentials paired with only a locally subthreshold (asynchronous) input pattern did not change spike strength (Fig. 4g and Supplementary Fig. 5a–c). This indicates that BSP is an associative form of plasticity. BSP was not, however, dependent on the activation of a specific set of dendritic spines, as the increase in spike strength could still be detected if naive spines close to the initiation site were activated once the potentiation fully developed (Supplementary Fig. 5d). The effect of CCh was prevented by atropine (5 μM), indicating that muscarinic acetylcholine receptors (mAChRs) were involved (dV/dt_D, to 102 ± 16%, $n = 4$, $P = 0.679$; Fig. 4g), and both forms of plasticity were blocked by the NMDAR antagonist D,L-2-amino-5-phoshonovaleric acid (AP5, 50 μM, dV/dt_D for CCh in AP5, to 105 ± 6%, $n = 4$, $P = 0.398$, Fig. 4d, f–g; dV/dt_D for θ-pairing in AP5, to 103 ± 6, $n = 6$, $P = 0.577$, Fig. 4e–g). In summary, repetitive local spiking in weak branches when associated with either mAChR activation or back-propagating action potentials triggers an NMDAR-dependent signalling pathway that leads to a gradual enhancement of local spike propagation that eventually becomes effective enough to activate the more powerful proximal dendrites of the dendritic family.

Voltage-gated ion channel mechanisms

One candidate mechanism for BSP is a long lasting modification of A-type K^+ currents that shape the propagation of both back-propagating action potentials[12,21] and dendritic spikes[4], and that are regulated both by long-term potentiation (LTP)-inducing protocols[12,14] and mAChR activation[22]. A-type K^+ currents can be relatively specifically blocked by low concentrations of Ba^{2+} (ref. 21). We therefore tested the effect of Ba^{2+} (200–250 μM for 10–25 min) on spike propagation in weak daughter branches originating from strong parent dendrites (Fig. 5a). Ba^{2+} caused a clear increase in dV/dt_D of the weak spike (to 156 ± 9%, $n = 6$, $P < 0.001$; Fig. 5a, c), and the strong parent branch spike was activated in all cases (dV/dt_Σ, to 931 ± 102%, $n = 6$; spike ratio: control, 0.13 ± 0.02; Ba^{2+}, 1.16 ± 0.06; Fig. 5a, d). Both effects reversed on Ba^{2+} washout. This result indicates that A-type K^+ currents may have an important role in suppressing the propagation of dendritic spikes in weak branches.

In CA1 pyramidal neurons, A-type K^+ currents are mediated mainly by Kv4.2 K^+ channel subunits[23]. We next performed experiments on transgenic mice in which the *Kv4.2* gene (also called *Kcnd2*) had been silenced (*Kv4.2*$^{-/-}$)[23,24]. Consistent with a role of Kv4.2-mediated currents in limiting spike propagation, dV/dt_D in weak terminal branches was significantly higher in *Kv4.2*$^{-/-}$ mice (0.71 ± 0.66 V s^{-1}, $n = 44$) than in wild-type littermates (0.39 ± 0.26 V s^{-1}, $n = 26$, $P < 0.001$; Supplementary Fig. 6a, c), whereas the strong populations did not differ (Supplementary Fig. 6a, c). Branch strength heterogeneity and the characteristic hierarchical organization of coupling strength in proximal dendritic families were, however, similar between *Kv4.2*$^{-/-}$ and wild-type mice (Supplementary Fig. 6a–d), suggesting that compensatory mechanisms partially counterbalanced the loss of Kv4.2 (refs 23, 24).

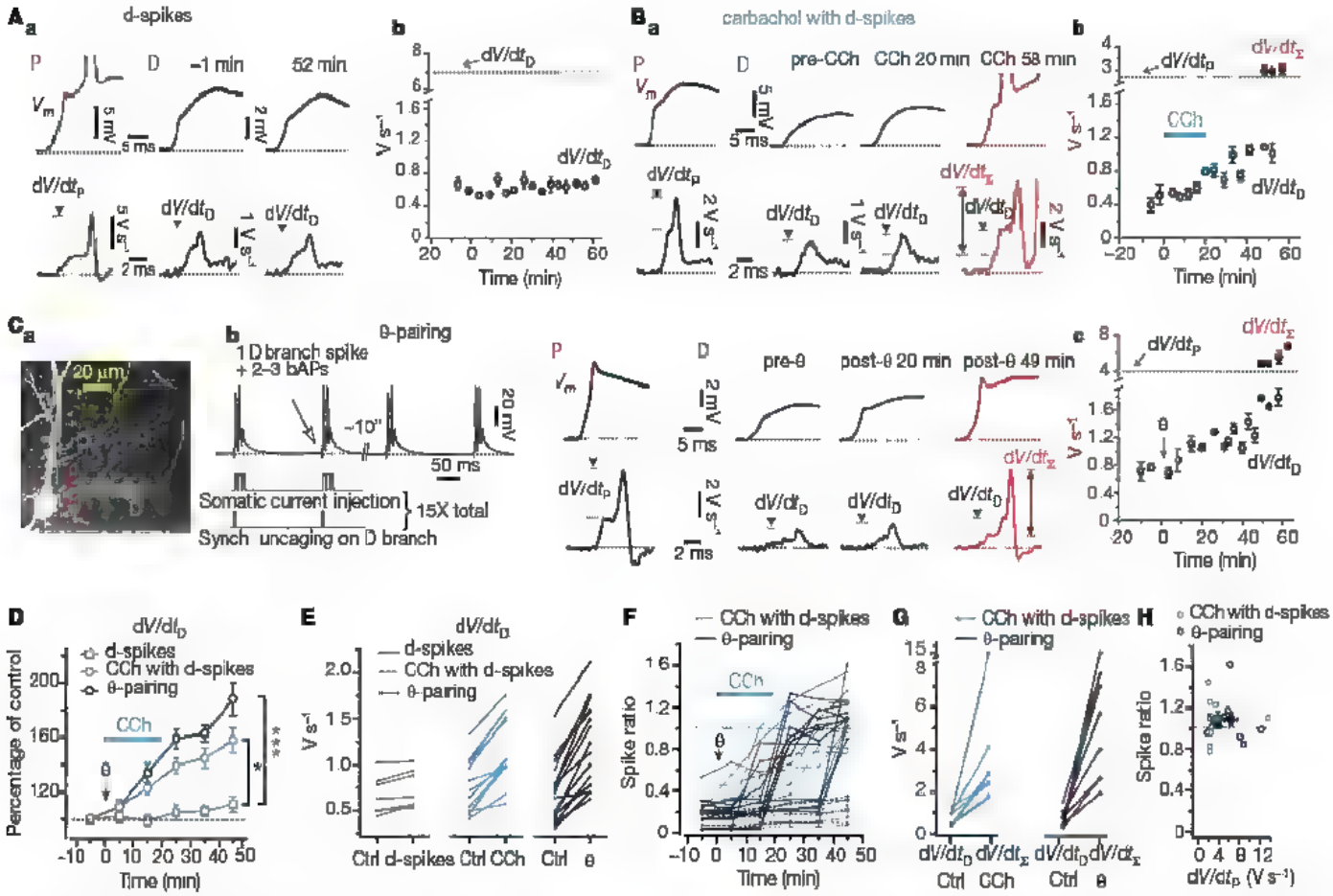

Figure 3 | Branch strength potentiation. **A**, **a**, **b**, V_m and dV/dt from parent (P) and connected daughter (D) at indicated times after the start of local spike initiation protocol (**a**). The entire time course of the experiment (**b**). The dashed line indicates the parent branch dV/dt. **B**, **a**, **b**, V_m and dV/dt from a strong parent (P) and connected daughter before (pre-CCh), 20 min after (CCh 20 min) and 58 min (CCh 58 min, red) after starting carbachol (5 μM) application (**a**). The entire time course of the experiment is shown (**b**). **C**, **a**–**c**, Input locations on parent (red) and daughter (blue) branches in a family (**a**). **b**, Left: V_m (top) and schematic (bottom) showing θ-pairing protocol applied to the daughter branch. bAPs, back-propagating action potentials. Middle V_m and dV/dt of parent. Right V_m and dV/dt of daughter before (pre-θ), 20 min after (post-θ 20 min) and 49 min (post-θ 49 min, red) after θ-pairing. **c**, Entire time course of experiment. **D**, Summary of baseline-normalized dV/dt_D versus time for d-spikes alone, with carbachol and θ-pairing. **E**, dV/dt_D before and after spikes alone, CCh and θ-pairing. **F**, Spike ratio versus time for individual experiments with CCh and θ-pairing. Note that the parent branch spike was recruited at different time points. **G**, Maximal daughter branch spike dV/dt in control (dV/dt_D) and after CCh or θ-pairing (dV/dt_Σ) when parent branch was recruited. **H**, Spike ratio after CCh or θ-pairing versus parent branch dV/dt.

We next determined the effect of Ba^{2+} on weak daughter branches originating from strong parent dendrites in $Kv4.2^{-/-}$ and wild-type mice. Ba^{2+} enhanced branch spike strength in wild-type mice similarly as observed in rats (dV/dt_D, to 205 ± 19%, $n = 4$, $P < 0.05$; dV/dt_Σ, to 2,550 ± 1170%, $n = 3$; Fig. 5c, d and Supplementary Fig. 6e), whereas it had no significant effect on branches from $Kv4.2^{-/-}$ neurons (dV/dt_D, to 111 ± 15%, $n = 8$, $P = 0.839$; Fig. 5b–d), confirming the channel specificity of low Ba^{2+} concentrations. Finally, we tested the ability of the CCh and θ-pairing protocols to induce BSP in $Kv4.2^{-/-}$ and wild-type mice. Notably, in $Kv4.2^{-/-}$ mice, neither induction protocol influenced dV/dt in weak daughter branches (CCh, to 109 ± 8%, $n = 8$, $P = 0.164$, Fig. 5e, g; θ-pairing, to 93 ± 4%, $n = 7$, $P = 0.572$, Fig. 5f, h), whereas BSP was successfully induced in wild-type cells both by CCh (dV/dt_D, to 190 ± 24%, $n = 7$, $P < 0.01$; Fig. 5g and Supplementary Fig. 6f) and θ-pairing (dV/dt_D, to 314 ± 47%, $n = 6$, $P < 0.01$; Fig. 5h and Supplementary Fig. 6g). These results strongly implicate downregulation of A-type K^+ currents, mediated by Kv4.2 subunits, as the underlying mechanism of BSP.

Discussion

In summary, branch coupling strength is not a static feature, as the associative pairing of a highly synchronous input pattern with action potential output or mAChR activation leads to a long-term elevation of coupling strength of only the stimulated branch. Such a selective enhancement could be used to store the occurrence of this uniquely correlated input, as the subsequent arrival of only this specific spatio-temporal input pattern would evoke a precise, invariant form of action

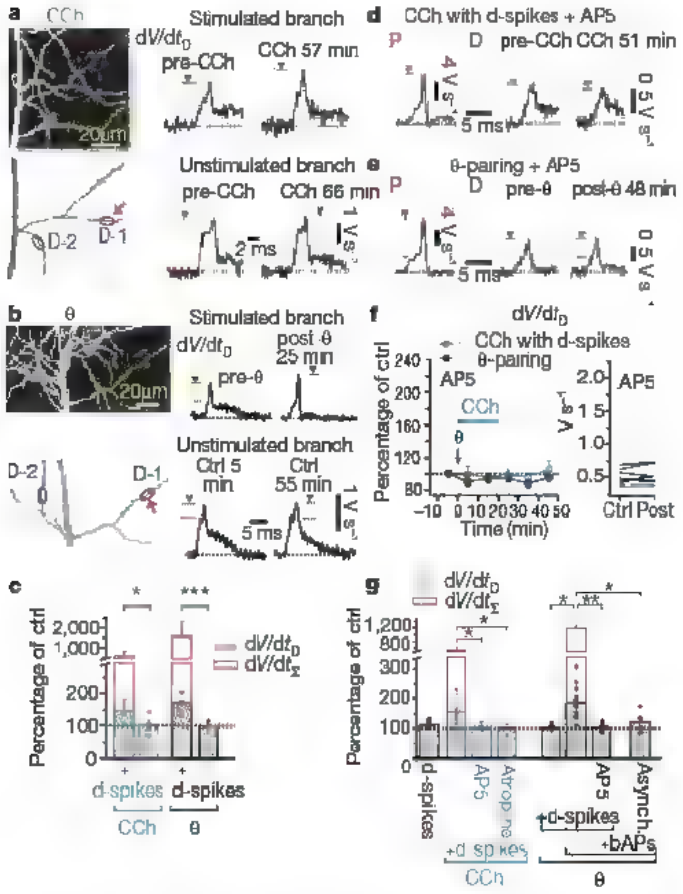

Figure 4 | Specificity and associativity of branch strength potentiation. **a**, Stack image (top left) and outline of two terminal branches (bottom left, D-1 and D-2). Right dV/dt from D-1 that received repeated local spikes in CCh (stimulated branch). D-2 received only CCh application (unstimulated branch). **b**, Similar to **a** but with θ-pairing. **c**, Summary of branch selectivity. **d**, **e**, NMDAR antagonist blocked the effect of both CCh (**d**) and θ-pairing (**e**) on BSP. **f**, Summary of baseline-normalized spike dV/dt versus time for CCh and θ-pairing (left) and summary of dV/dt_D before and after CCh or θ-pairing in AP5 (right). **g**, Summary of the effect of different stimulation forms on daughter branch spike strength.

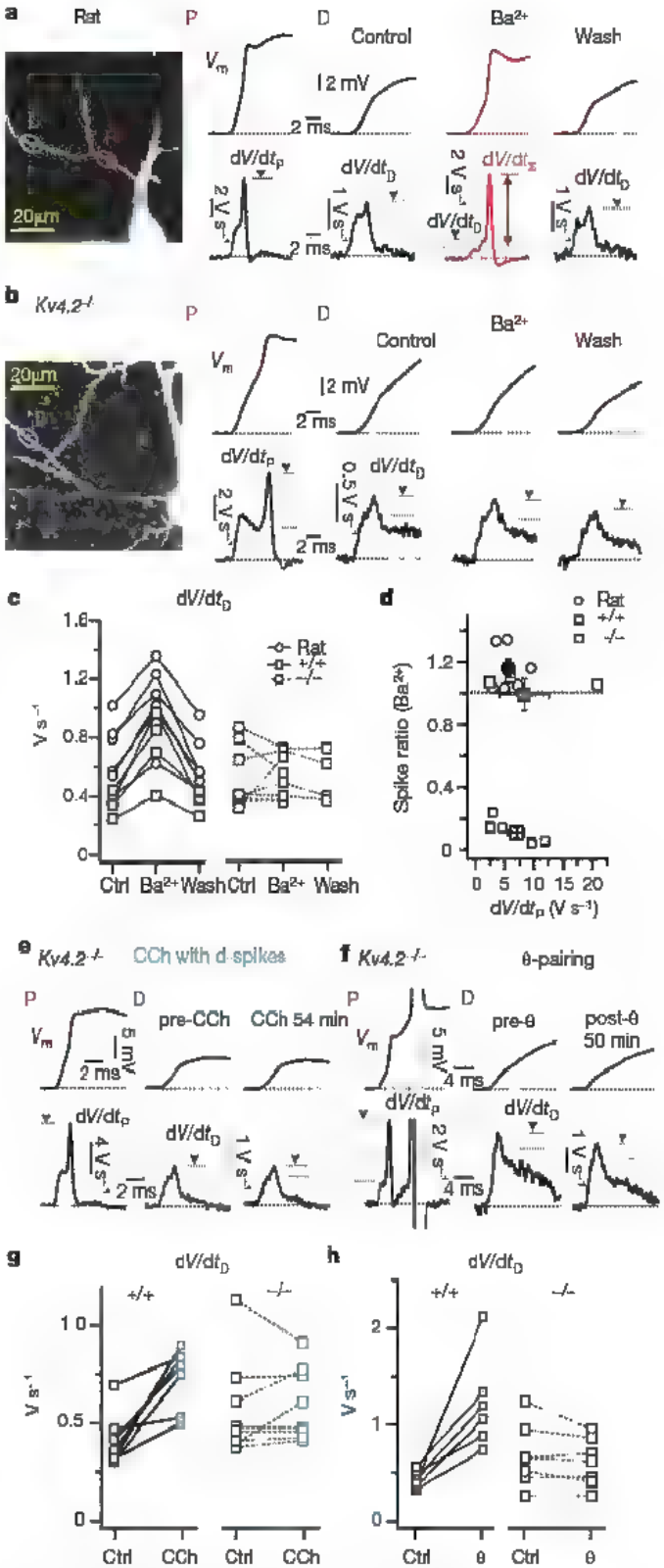

Figure 5 | BSP is mediated by reduced A-type K^+ channel function. **a**, In rat, image showing input locations on strong parent (P) and weak daughter (D). Right V_m (top) and dV/dt (bottom) from parent (P) and daughter (D) before (control), during (Ba^{2+}) and after (wash) Ba^{2+} (200–250 μM) application. **b**, Same as **a** but in $Kv4.2^{-/-}$ mice. **c**, Daughter spike dV/dt_D before, during and after Ba^{2+} application in rat, $Kv4.2^{-/-}$ mice and wild-type littermate mice. **d**, Plot of spike ratio for Ba^{2+} application versus parent dV/dt. **e**, Carbachol has no effect on branch strength in $Kv4.2^{-/-}$ mice. Traces from a strong parent (P) and connecting weak daughter (D) branch before (pre-CCh) and 54 min after (post-CCh 54 min) starting CCh application. **f**, Same as for **e** but for θ-pairing. **g**, **h**, Summary of D branch spike dV/dt_D before and after CCh (**g**) or θ-pairing (**h**) in $Kv4.2^{-/-}$ and wild-type mice.

potential output. BSP might, therefore, be considered input pattern specific, particularly because it will not affect unitary excitatory postsynaptic potential (EPSP) amplitudes[4]. Furthermore, BSP could interact with synaptic plasticity, as LTP of synaptic inputs onto a particular branch[25,26] would increase the probability of future local spike initiation and therefore BSP. The resulting compartmentalized downregulation of Kv4.2 function will also increase action potential back-propagation into that branch, promoting LTP maintenance there[12,23]. Such a positive feedback could elevate the retention time of stored information[27].

Although we focused primarily on the regulation of local Na^+ spike propagation within perisomatic dendrites of CA1 pyramidal neurons, other dendritic nonlinearities (for example, Ca^{2+}/NMDA plateaus) exist both in more distal regions of these cells as well as in dendrites of other neurons[11]. Compartmentalized alterations in ion channel function could also affect the strength of these dendritic spikes. Because of the ubiquity of modifiable active dendritic compartments, BSP is potentially a general feature of neuronal information processing and storage. In the hippocampus, BSP may be particularly applicable for the compressed sequence replay occurring during slow-wave sleep (SWS)[28–30]. Repeated synchronous activation of a CA3 cell ensemble during exploratory SPWs[19] could induce BSP, storing the specific feature represented by these neurons in enhanced branch coupling strength (Supplementary Fig. 1). Subsequent synchronous ensemble activation during SWS would evoke strong dendritic spikes and the associated precise action potential output characteristic of SWS. Consequently, the heterogeneous distribution of branch strengths observed in CA1 neurons may be an imprint of already stored sequence items onto the arborization.

METHODS SUMMARY

Acute hippocampal slices were prepared from 8–12-week-old rats and mice (*Kv4.2*$^{-/-}$ or wild-type littermates). Current-clamp whole-cell recordings were performed at 33–36 °C from soma or proximal apical trunks of hippocampal CA1 pyramidal neurons filled with Oregon green BAPTA-1 or Alexa 488. Two-photon laser-scanning microscopy and two-photon glutamate uncaging were performed using a dual galvanometer-based scanning system with two Ti:sapphire lasers[4]. For glutamate uncaging, MNI glutamate was uncaged at 5–20 visually identified spines (0.2-ms exposure times, with 0.1–0.2-ms interstimulus intervals between exposures at different spines). Repeated local spiking protocols were given as trials of 3–10 local spikes every ~5–30 s with ~5-min inter-trial intervals. In consecutive trials of an experiment, different sets of spines were usually activated, by randomly picking the available spines within a ~10–20 μm region of a dendritic segment in the same focal plane. The θ-pairing protocol consisted of locally suprathreshold uncaging paired with back-propagating action potentials. That is, fifteen trains (five trains at 0.01 Hz repeated three times with a 30-s interval) of two bursts (repeated at 5 Hz), with each burst composed of a local spike (synchronous uncaging on a cluster of 10–15 spines with a 0.1-ms interval) paired with two–three back-propagating action potentials at 100 Hz. The back-propagating action potentials were timed so that the peaks of the action potentials were coincident with the peak of the uncaging evoked EPSP (glu EPSP), as measured at the soma. Different spines were used for the θ-pairing induction and for testing the spikes before and after induction. During θ-pairing induction, different spines were usually used between consecutive sets of trains. Distance measurements and anatomical evaluation were performed on stacked images collected at the end of recordings. All data are given in mean ± s.e.m. In all figures, symbols with error bars indicate mean ± s.e.m., asterisk, $P < 0.05$; double asterisk, $P < 0.01$, triple asterisk, $P < 0.001$.

Full Methods and any associated references are available in the online version of the paper at www.nature.com/nature.

Received 23 October 2007; accepted 24 January 2008.

1. Ariav, G., Polsky, A. & Schiller, J. Submillisecond precision of the input-output transformation function mediated by fast sodium dendritic spikes in basal dendrites of CA1 pyramidal neurons. *J. Neurosci.* **23**, 7750–7758 (2003)
2. Larkum, M. E., Zhu, J. J. & Sakmann, B. Dendritic mechanisms underlying the coupling of the dendritic with the axonal action potential initiation zone of adult rat layer 5 pyramidal neurons. *J. Physiol. (Lond.)* **533**, 447–466 (2001)
3. Polsky, A., Mel, B. W. & Schiller, J. Computational subunits in thin dendrites of pyramidal cells. *Nature Neurosci.* **7**, 621–627 (2004)
4. Losonczy, A. & Magee, J. C. Integrative properties of radial oblique dendrites in hippocampal CA1 pyramidal neurons. *Neuron* **50**, 291–307 (2006).
5. Gasparini, S., Migliore, M. & Magee, J. C. On the initiation and propagation of dendritic spikes in CA1 pyramidal neurons. *J. Neurosci.* **24**, 11046–11056 (2004)
6. Gasparini, S. & Magee, J. C. State-dependent dendritic computation in hippocampal CA1 pyramidal neurons. *J. Neurosci.* **26**, 2088–2100 (2006)
7. Poirazi, P., Brannon, T. & Mel, B. W. Pyramidal neuron as two-layer neural network. *Neuron* **37**, 989–999 (2003).
8. Poirazi, P. & Mel, B. W. Impact of active dendrites and structural plasticity on the memory capacity of neural tissue. *Neuron* **29**, 779–796 (2001)
9. London, M. & Hausser, M. Dendritic computation. *Annu. Rev. Neurosci.* **28**, 503–532 (2005).
10. Zhang, W. & Linden, D. J. The other side of the engram: experience-driven changes in neuronal intrinsic excitability. *Nature Rev. Neurosci.* **4**, 885–900 (2003)
11. Magee, J. C. & Johnston, D. Plasticity of dendritic function. *Curr. Opin. Neurobiol.* **15**, 334–342 (2006).
12. Frick, A., Magee, J. C. & Johnston, D. LTP is accompanied by an enhanced local excitability of pyramidal neuron dendrites. *Nature Neurosci.* **7**, 126–135 (2004).
13. Yasuda, R. *et al.* Supersensitive Ras activation in dendrites and spines revealed by two-photon fluorescent lifetime imaging. *Nature Neurosci.* **9**, 283–291 (2006).
14. Kim, J., Jung, S. C., Clemens, C. M., Petralia, R. S. & Hoffman, D. A. Regulation of dendritic excitability by activity-dependent trafficking of the A-type K^+ channel subunit Kv4.2 in hippocampal neurons. *Neuron* **54**, 933–947 (2007)
15. Golding, N. L. & Spruston, N. Dendritic sodium spikes are variable triggers of axonal action potentials in hippocampal CA1 pyramidal neurons. *Neuron* **21**, 1189–1200 (1998)
16. Bannister, N. J. & Larkmann, A. U. Dendritic morphology of CA1 pyramidal neurones from the rat hippocampus: I. Branching patterns. *J. Comp. Neurol.* **360**, 150–160 (1995)
17. Ishizuka, N., Weber, J. & Amaral, D. Organization of intrahippocampal projections originating from CA3 pyramidal cells of the rat. *J. Comp. Neurol.* **295**, 580–623 (1990).
18. Csicsvari, J., Hirase, H., Czurko, A., Mamiya, A. & Buzsaki, G. Ensemble patterns of hippocampal CA3–CA1 neurons during sharp wave-associated population events. *Neuron* **28**, 585–594 (2000)
19. O'Neill, J., Senior, T. & Csicsvari, J. Place-selective firing of CA1 pyramidal cells during sharp wave/ripple network patterns in exploratory behavior. *Neuron* **49**, 143–156 (2006).
20. Hasselmo, M. E. & Giocomo, L. M. Cholinergic modulation of cortical function. *J. Mol. Neurosci.* **30**, 133–135 (2006)
21. Gasparini, S., Losonczy, A., Chen, X., Johnston, D. & Magee, J. C. Associative pairing enhances action potential back-propagation in radial oblique branches of CA1 pyramidal neurons. *J. Physiol. (Lond.)* **580**, 787–800 (2007).
22. Hoffman, D. A. & Johnston, D. Neuromodulation of dendritic action potentials. *J. Neurophysiol.* **81**, 408–411 (1999).
23. Chen, X. *et al.* Deletion of Kv4.2 gene eliminates dendritic A-type K^+ current and enhances induction of long-term potentiation in hippocampal CA1 pyramidal neurons. *J. Neurosci.* **26**, 12143–12151 (2006).
24. Guo, W. *et al.* Targeted deletion of Kv4.2 eliminates $I_{to,f}$ and results in electrical and molecular remodeling, with no evidence of ventricular hypertrophy or myocardial dysfunction. *Circ. Res.* **97**, 1342–1350 (2005)
25. Govindarajan, A., Kelleher, R. J. & Tonegawa, S. Clustered plasticity model of long-term memory engrams. *Nature Rev. Neurosci.* **7**, 575–583 (2006).
26. Harvey, C. D. & Svoboda, K. Spatially clustered and dynamic synaptic learning rules in pyramidal neuron dendrites. *Nature* **450**, 1195–1200 (2007).
27. Fusi, S., Drew, P. J. & Abbott, L. F. Cascade models of synaptically stored memories. *Neuron* **45**, 599–611 (2005)
28. Wilson, M. A. & McNaughton, B. L. Reactivation of hippocampal ensemble memories during sleep. *Science* **265**, 676–679 (1994)
29. Nadasdy, Z., Hirase, H., Czurko, A., Csicsvari, J. & Buzsaki, G. Replay and time compression of recurring spike sequences in the hippocampus. *J. Neurosci.* **19**, 9497–9507 (1999)
30. Lee, A. K. & Wilson, M. A. Memory of sequential experience in the hippocampus during slow wave sleep. *Neuron* **36**, 1183–1194 (2002).

Supplementary Information is linked to the online version of the paper at www.nature.com/nature.

Acknowledgements We thank G. Buzsaki, D. Johnston, J. Lisman and Z. Nusser for their comments on a previous version of the manuscript. We thank D. Johnston for the Kv4.2 mice and B. K. Andrasfalvy for valuable discussions and help with experiments using Kv4.2 mice.

Author Contributions A.L. and J.K.M. performed and analysed the experiments. A.L., J.K.M. and J.C.M. designed the experiments, and all authors contributed to the manuscript preparation.

Author Information Reprints and permissions information is available at www.nature.com/reprints. Correspondence and requests for materials should be addressed to A.L. (losonczya@janelia.hhmi.org) or J.K.M. (makaraj@janelia.hhmi.org).

ARTICLES

Haematopoietic stem cell release is regulated by circadian oscillations

Simón Méndez-Ferrer[1], Daniel Lucas[1], Michela Battista[1] & Paul S. Frenette[1,2,3]

Haematopoietic stem cells (HSCs) circulate in the bloodstream under steady-state conditions, but the mechanisms controlling their physiological trafficking are unknown. Here we show that circulating HSCs and their progenitors exhibit robust circadian fluctuations, peaking 5 h after the initiation of light and reaching a nadir 5 h after darkness. Circadian oscillations are markedly altered when mice are subjected to continuous light or to a 'jet lag' (defined as a shift of 12 h). Circulating HSCs and their progenitors fluctuate in antiphase with the expression of the chemokine CXCL12 in the bone marrow microenvironment. The cyclical release of HSCs and expression of *Cxcl12* are regulated by core genes of the molecular clock through circadian noradrenaline secretion by the sympathetic nervous system. These adrenergic signals are locally delivered by nerves in the bone marrow, transmitted to stromal cells by the β_3-adrenergic receptor, leading to a decreased nuclear content of Sp1 transcription factor and the rapid downregulation of *Cxcl12*. These data indicate that a circadian, neurally driven release of HSC during the animal's resting period may promote the regeneration of the stem cell niche and possibly other tissues.

Under homeostasis, small numbers of HSCs are detectable in the bloodstream of mammals[1]. The omnipresence of HSCs and their progenitors in the circulation and their rapid clearance after injection suggest a rapid flux between the blood and bone marrow compartments under homeostasis[2]. Studies in humans have previously revealed conflicting patterns in circadian variations of circulating progenitors[3,4]. Mobilization of HSCs and their progenitors into the circulation represents the basis for modern bone marrow transplantation procedures and can be elicited by multiple structurally distinct compounds with various speeds of action[5–8]. The prototypical agent used in the clinic, granulocyte colony-stimulating factor (G-CSF), mobilizes HSCs and their progenitors to the blood through complex mechanisms, involving notably the induction of proteolytic activity that cleaves CXCL12 (or stromal-derived factor-1; SDF-1)[9,10], and the suppression of osteoblast function[11,12], an integral cellular constituent of the HSC niche[13–15]. This leads to decreases in *Cxcl12* expression in the bone marrow microenvironment[10–12] and to HSC/progenitor egress that depends on an intact peripheral sympathetic nervous system (SNS)[11]. Whereas signals from the β_2-adrenergic receptor (encoded by *Adrβ2*)—the sole β-adrenergic receptor expressed in the osteoblast[16]—enhance HSC/progenitor egress, *Adrβ2*-mediated signals are not sufficient to suppress osteoblast function[11], suggesting the contribution of other adrenergic or non-adrenergic mediators. In addition, recent studies suggest that catecholaminergic pathways can promote human $CD34^+$ cell migration and engraftment by acting directly on HSC/progenitor cells, probably through Adrβ2 (ref. 17). Because the mechanisms mediating HSC release in homeostasis are not known, it is not clear whether the pharmacological induction of stem cell egress usurps the endogenous physiological trafficking machinery.

While investigating further the mechanisms mediating enforced mobilization of HSCs and their progenitors by G-CSF, we noted by chance that continuous exposure to light significantly altered the number of colony-forming units in culture (CFU-C) and HSC-enriched lineage-negative (lin^-)$Sca\text{-}1^+c\text{-}Kit^+$ (LSK) cells mobilized by the administration of G-CSF (Supplementary Fig. 1). These results suggested that photic cues, processed in the central nervous system, could influence the trafficking of HSCs in unperturbed steady-state animals. We therefore investigated the circadian patterns and the mechanisms behind HSC release in homeostasis

Circadian HSC release is modulated by photic cues

Under steady-state conditions in which mice are exposed to standard cycles of 12 h light/12 h darkness (LD), the number of circulating progenitors oscillated markedly, peaking 5 h after the initiation of light (Zeitgeber time, ZT5) and reaching a low point at ZT17 (Fig. 1a; analysis of variance (ANOVA): $F_{5,53} = 3.840$, $P = 0.005$, with post hoc test for linear trend $P = 0.002$). To determine whether this circadian oscillation affected stem cells, we analysed LSK cells (Fig. 1b) and conducted competitive repopulation analyses with limiting blood dilutions to quantify long-term (four months) reconstituting HSCs at the peak (ZT5) and the trough (ZT17) (Fig. 1c). These analyses revealed that the number of HSCs in the circulation at ZT5 is about twofold to threefold that at ZT17.

Circadian fluctuations of progenitors were entrained and modulated by photic cues, because the pattern was arrhythmic in mice subjected to continuous light (LL) for two weeks (Fig. 1d; ANOVA: $F_{5,17} = 0.7522$; $P = 0.6$). However, rhythmic oscillations were observed in mice maintained in continuous darkness for two weeks (Fig. 1e; ANOVA: $F_{5,29} = 3.003$, $P = 0.03$, with post hoc test for linear trend $P = 0.002$), which is consistent with free-running circadian rhythms in darkness[18,19]. To assess whether changes in light input were sufficient to alter progenitor trafficking, we subjected mice to a 'jet lag' by advancing the LD cycle by 12 h (Fig. 1f, bottom). Sampling of blood progenitors revealed a markedly flattened, arrhythmic pattern of circulating progenitor counts over the following 24 h in jet-lagged mice in comparison with control LD-maintained animals (Fig. 1f; ANOVA: $F_{5,45} = 1.366$; $P = 0.26$). Thus, a simple change in light cycle is sufficient to bring about a marked alteration in HSC/progenitor behaviour.

[1]Mount Sinai School of Medicine, Department of Medicine and Department of Gene and Cell Medicine, New York, New York 10029, USA. [2]Black Family Stem Cell Institute, New York, New York 10029, USA. [3]Immunology Institute, New York, New York 10029, USA.

Rhythmic *Cxcl12* oscillations in bone marrow

CXCL12 is the only known chemokine capable of directed migration of HSCs[10,21]. The circadian fluctuations in HSCs and their progenitors suggested that CXCL12 might also be subjected to circadian control. To investigate this possibility, we measured the expression of *Cxcl12* in the bone marrow microenvironment by ELISA. Remarkably, CXCL12 protein levels fluctuated in a pattern that mirrored oscillations in circulating HSCs and their progenitors (Fig. 2a; ANOVA: $F_{5,49} = 2.485$, $P = 0.04$, with post hoc test for linear trend $P = 0.006$). Similar rhythmic fluctuations were observed in *Cxcl12* mRNA expression (Fig. 2a), suggesting that CXCL12 is not regulated by proteolytic degradation under homeostasis and that the steady-state circadian oscillations in HSCs and their progenitors are controlled by fluctuations in *Cxcl12* expression. Further, oscillations of *Cxcl12* expression in bone marrow were arrhythmic in mice maintained in constant light (Fig. 2b) or under conditions of jet lag (Fig. 2c), whereas *Cxcl12* expression continued to fluctuate rhythmically in mice maintained in constant darkness (Fig. 2d; ANOVA: $F_{5,18} = 3.664$, $P = 0.02$, with post hoc test for linear trend $P = 0.001$). These results suggest that circadian release of HSCs is triggered by rhythmic expression of *Cxcl12* in the bone marrow.

Neural signals regulate *Cxcl12* through Adrβ3

Because SNS signals affect the G-CSF-induced mobilization of HSCs[11] and modulate osteoblast proliferation through the peripheral expression of core clock genes[22], we next lesioned the SNS of adult mice with 6-hydroxydopamine (6OHDA) to assess the role of SNS signals in the circadian release of HSCs. SNS disruption abolished the normal circadian pattern of circulating progenitors (Fig. 3a). In addition, 6OHDA did not affect the number of CFU-Cs, LSK cells or $CD150^+CD48^-CD41^-$ HSCs[23] in the bone marrow (data not shown), excluding a direct toxicity on HSCs and progenitors. Competitive repopulation assays to evaluate the number of circulating stem cells at ZT5 revealed a marked decrease in long-term repopulating stem cell activity in 6OHDA-lesioned mice compared with control C57BL/6 mice up to 17 weeks after transplantation (Fig. 3b and Supplementary Fig. 2). These results suggested that adrenergic signals are critical for the circadian release of stem cells from the bone marrow.

Because 6OHDA disrupts the SNS systemically, it could be argued that its effect might be mediated either through a loss of soluble catecholamines (for example from the adrenal glands), through other indirect effects to non-haematopoietic organs or through a local delivery of noradrenaline (norepinephrine) from adrenergic nerve terminals in the bone marrow. To distinguish between these possibilities, we surgically sympathectomized the tibiae of mice by unilateral microsection of both the sciatic and femoral nerves. We checked whether the sympathectomy was complete by staining for tyrosine hydroxylase, and found no specific staining for sympathetic fibres in the denervated bone marrow, whereas the contralateral sham-operated side exhibited multiple stained fibres, mostly near blood vessels (Fig. 3c, d). Strikingly, the circadian oscillations of *Cxcl12* expression were severely altered in the denervated tibiae, whereas *Cxcl12* expression showed the characteristic diurnal pattern in the contralateral sham-operated tibiae of the same mice (Fig. 3e, f). These results demonstrate that the rhythmic fluctuations in *Cxcl12* expression and the resulting release of HSCs require adrenergic signals delivered locally in the bone marrow by nerves from the SNS.

To evaluate the exact contribution of adrenergic receptors and the downstream mechanisms, we treated bone marrow stromal cells (MS-5) with selective and non-selective adrenergic agonists and antagonists. Noradrenaline, the natural neurotransmitter of the SNS, and isoprenaline (isoproterenol), a non-selective β-adrenergic agonist, decreased CXCL12 production in a dose-dependent manner (Fig. 4a). A similar decrease in *Cxcl12* mRNA expression was detected with either adrenergic agonist (Supplementary Fig. 3). This effect was mediated by the β_3-adrenergic but not the β_2-adrenergic receptor, because it was induced by a β_3-adrenergic agonist (BRL37344) and inhibited by a selective β_3-adrenergic antagonist (SR59230A), whereas Adrβ2 engagement or blockade had no effect (Fig. 4a, b). Treatment of primary myeloid bone marrow cultures with isoprenaline or BRL37344 markedly suppressed *Cxcl12* expression in stromal

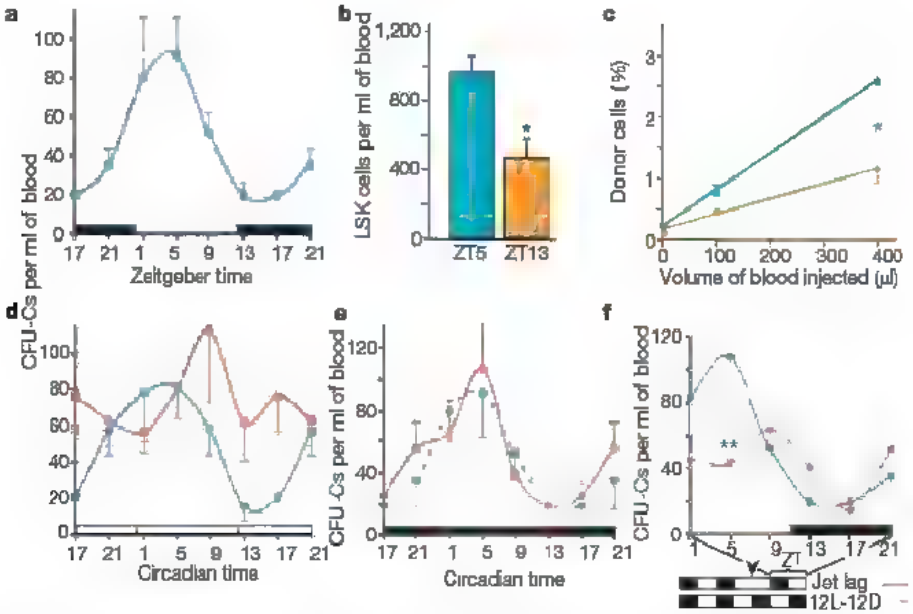

Figure 1 | Circadian traffic of HSCs and their progenitors is entrained by photic input. **a**, **b**, Circadian fluctuations of circulating CFU-Cs (**a**, $n = 10$ mice per time point) and LSK cells (**b**, $n = 6$ or 7) in standard LD conditions. **c**, Stem cell activity using long-term competitive reconstitution assays. Blood harvested at ZT5 (cyan) showed a roughly 2.5-fold increase compared with ZT17 (orange) in competitive repopulation 16 weeks after transplantation ($n = 4$ mice per group). **d**–**f**, Circadian traffic of CFU-Cs was disrupted in mice subjected to altered light cycles and preserved in animals kept in constant darkness: **d**, constant light for 2 weeks (red), control LD (blue) ($n = 4$ mice per time point); **e**, constant darkness for 2 weeks (solid red line), control LD (dashed blue line); $n = 6$ mice per time point; **f** jet lag (red), control LD (blue). The arrowhead in **f** indicates the initiation of light shift. Circulating progenitors were monitored 12 h later and for the next 24 h ($n = 6$–13 mice per time point). Results are shown as means and s.e.m. Asterisk, $P < 0.05$, two asterisks, $P < 0.01$ (unpaired two-tailed *t*-test). In **a** and **d**–**e**, time points 17 and 21 have been duplicated to facilitate viewing of the time curve. All experiments were performed in male C57BL/6 mice six to nine weeks old.

cells and significantly increased the number of released progenitors in the supernatant, whereas the β_2-adrenergic agonist clenbuterol did not affect *Cxcl12* mRNA levels (Fig. 4c). β_3-Adrenergic signalling was sufficient to alter *Cxcl12* expression, because isoprenaline injection sharply decreased the expression of *Cxcl12* in bone marrow *in vivo* 2 h after administration in wild-type animals (Fig. 4d). However, despite the large decrease in bone marrow CXCL12 induced by isoprenaline, no significant elevation of circulating progenitors was observed (data not shown). This suggested the possibility that β-adrenergic signalling might also enhance homing or trapping in tissues. To circumvent this issue, we evaluated the effect of isoprenaline in mice in which HSC/progenitor homing and adhesion in the vasculature are compromised[24–26]. We found a significant increase in circulating progenitors after the administration of isoprenaline when both endothelial selectins and α_4 integrins were absent or blocked (Fig. 4e), suggesting that physiological, locally delivered β_3-adrenergic signals control HSC/progenitor release, whereas the pharmacological administration of non-selective β-adrenergic agonists may also enhance progenitor clearance. Further, a significant decrease in *Cxcl12* expression was observed in the presence of a selective β_2-adrenergic receptor blocker (data not shown) or in stroma derived from *Adrβ2*$^{-/-}$ mice (Supplementary Fig. 4). In sharp contrast, isoprenaline did not affect *Cxcl12* expression in stroma derived from *Adrβ3*$^{-/-}$ mice (Fig. 4f) and induced a significant mobilization of progenitors in control but not *Adrβ3*$^{-/-}$ mice after blockade of endothelial selectins and α_4 integrins (Fig. 4g). Moreover, the effect of isoprenaline was mimicked by a selective β_3-adrenergic agonist (BRL37344; Fig. 4g). Because adrenergic activity in the murine bone marrow follows a circadian variation[27] that closely mirrors fluctuations in *Cxcl12* expression (Fig. 2), we reasoned that the release of noradrenaline in the bone marrow microenvironment might be responsible for the rapid downregulation of *Cxcl12* and the release of progenitors that follow the onset of light (Fig. 2). To test this possibility, we administered a β_3-adrenergic antagonist (SR59230A) at ZT23 (1 h before the onset of light) and harvested circulating progenitors at ZT1. As shown in Fig. 4h, SR59230A prevented the morning increase in circulating progenitors. Furthermore, circadian fluctuations in bone marrow CXCL12 and circulating progenitors were preserved in *Adrβ2*$^{-/-}$ mice and markedly attenuated in *Adrβ3*$^{-/-}$ animals, and additional blockade of Adrβ1 and Adrβ2 in *Adrβ3*$^{-/-}$ mice did not affect the number of circulating progenitors (Supplementary Fig. 5), suggesting a crucial role for *Adrβ3* but not the other β-adrenergic receptors in circadian CXCL12 regulation.

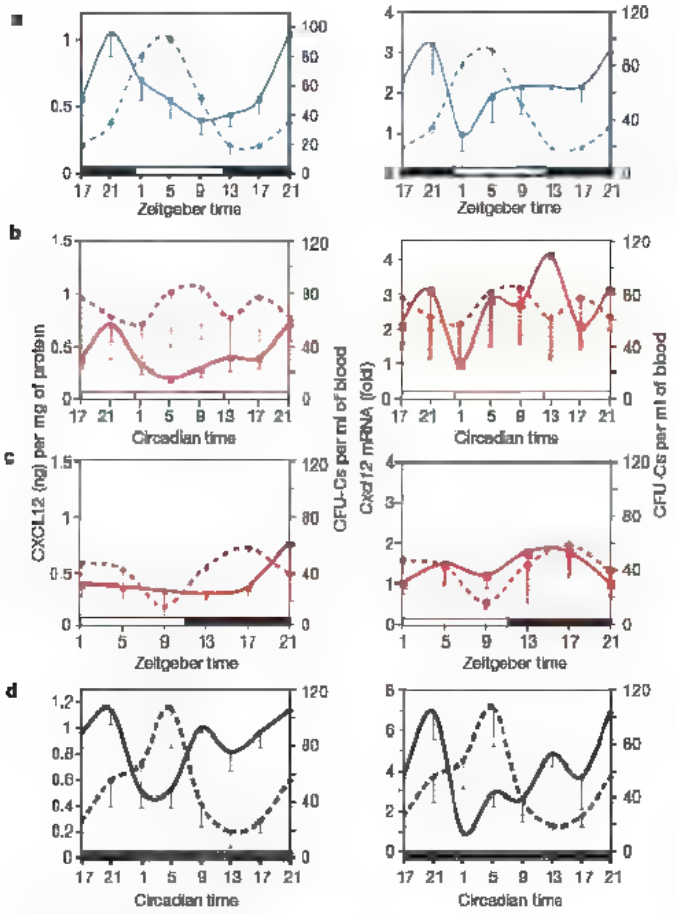

Figure 2 | Bone marrow *Cxcl12* expression oscillates in antiphase with circulating progenitors. CXCL12 content in bone marrow extracellular fluids (solid lines in left panels) and *Cxcl12* mRNA levels in bone marrow (solid lines in right panels) were analysed in mice kept under normal LD cycles (**a**, $n = 10$ mice per time point) or subjected to constant light (**b**), 12 h jet lag (**c**, $n = 4$ mice per time point) or constant darkness (**d**, $n = 6$ mice per time point). CXCL12 levels mirrored fluctuations in circulating progenitors (dashed lines) in all conditions. The decreased amplitude of circulating CFU-C oscillations under constant light and jet lag were also correlated with decreased fluctuations in bone marrow CXCL12 levels. **a**, **b**, **d**, Time points 17 and 21 have been duplicated to facilitate viewing of the time curve. Results are shown as means and s.e.m. Male C57BL/6 mice six to nine weeks old were used.

HSC release is orchestrated by the central clock

The circadian regulation of HSC release suggests a role for the core genes of the molecular clock that orchestrate the expression of numerous target genes centrally from the suprachiasmatic nucleus and/or peripherally in various tissues (reviewed in refs 28, 29). Circulating CFU-C counts and *Cxcl12* expression did not oscillate in a circadian manner in *Bmal-1*$^{-/-}$ mice (Fig. 5a), indicating that clock genes do indeed regulate *Cxcl12*. Because the SNS regulates osteoblast proliferation through the expression of clock genes in osteoblasts[22], we profiled the expression of clock genes in the bone marrow. We observed a trend consistent with the expression patterns

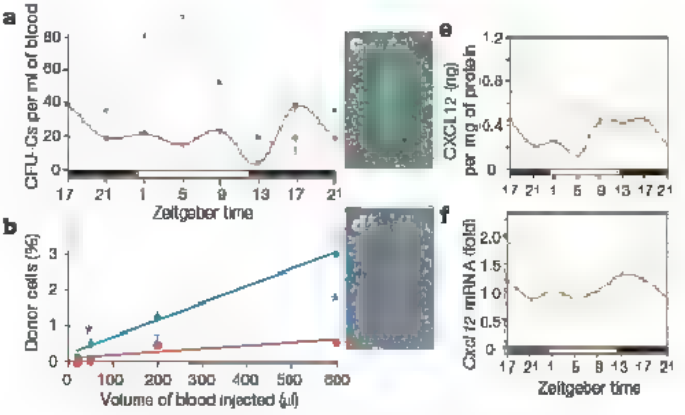

Figure 3 | Adrenergic innervation of the bone marrow regulates oscillations in *Cxcl12* expression and circulating HSCs. **a**, Neurochemical sympathectomy of adult mice with 6OHDA abolished fluctuations in circulating progenitors (solid red lines). The dashed blue line represents control LD ($n = 4$ mice per time point). **b**, Stem cell activity measured with long-term competitive reconstitution assays. Blood harvested at ZT5 from 6OHDA-treated mice (red) showed a marked decrease in competitive repopulation units at 17 weeks. Asterisk, $P < 0.05$ (unpaired two-tailed *t*-test). The estimated number of competitive repopulation units was 1 in 505 μl in 6OHDA-treated mice in comparison with 1 in 42 μl in control mice (Supplementary Fig. 2; 1.5% reconstitution threshold; $n = 4$ mice per dose). **c**–**e**, Surgical denervation of the tibiae of adult mice destroyed catecholaminergic fibres in the bone marrow (**c**, sham-operated bone marrow; **d**, denervated bone marrow; green, immunofluorescence for tyrosine hydroxylase) and abolished fluctuations (red lines) in CXCL12 protein (**e**) and *Cxcl12* mRNA levels (**f**), whereas *Cxcl12* showed the characteristic circadian pattern in the sham-operated contralateral tibiae (**e**, **f**, green lines; $n = 4$ mice per time point). **a**, **e**, **f**, Time points ZT17 and ZT21 have been duplicated to facilitate viewing of the time curve. Results are shown as means and s.e.m. Male C57BL/6 mice six to nine weeks old were used.

reported for *Clock*, *Bmal1*, *Per1*, *Per2*, *Cry1* and *Rev-erbα* in peripheral oscillators under LD[28,29], and apparent alterations under continuous light or conditions of jet lag, but these patterns were not statistically significant (Supplementary Fig. 6). The *Cxcl12* promoter contains several non-canonical E boxes (CGNNAT) that nevertheless suggest the possibility of a direct control of *Cxcl12* by peripheral clock proteins. However, treatment of bone marrow-derived *Bmal-1*$^{-/-}$ or *Per1*$^{-/-}$ *Per2*$^{m/m}$ stromal cells with isoprenaline decreased *Cxcl12* expression to the same extent as that in wild-type control stroma (Fig. 5b). These results therefore suggest that clock genes probably regulate *Cxcl12* and stem cell trafficking indirectly from the central nervous system rather than peripherally in the stromal cells that synthesize CXCL12.

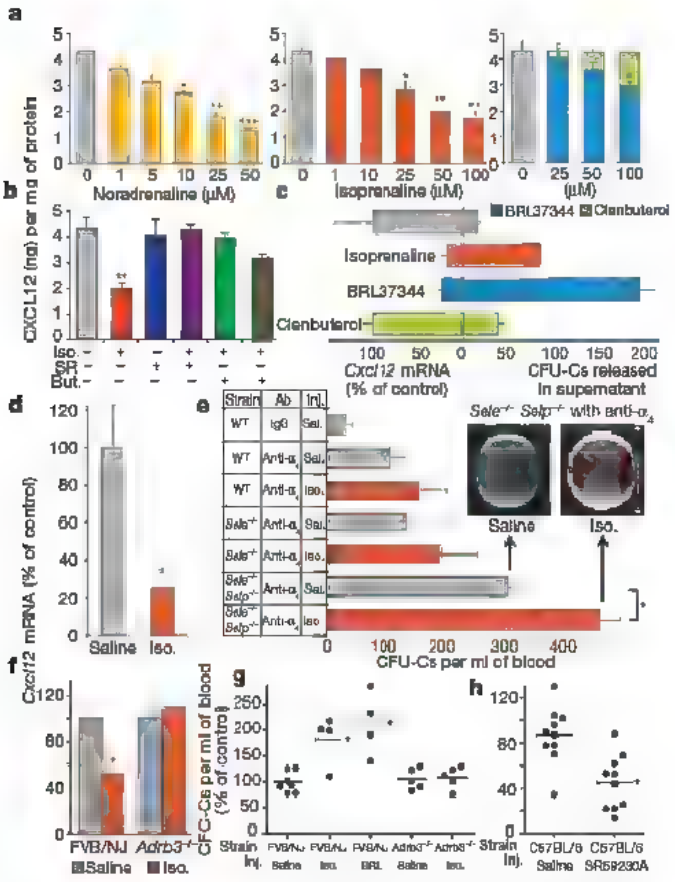

Figure 4 | β_3-Adrenergic receptor activation decreases *Cxcl12* mRNA levels in bone marrow stromal cells and triggers HSC/progenitor mobilization. **a**, Dose-dependent decrease in CXCL12 secretion by MS-5 cells 36 h after treatment with noradrenaline was mimicked by the non-selective β-adrenoceptor agonist isoprenaline and a selective β_3-adrenergic receptor agonist (BRL37344) but not a β_2-adrenergic receptor agonist (clenbuterol), $n = 8$. **b**, The effect of isoprenaline (iso., 50 μM) in MS-5 cells was prevented by a selective β_3-adrenergic receptor antagonist (1 μM SR59230A; SR) but not a β_2-adrenergic receptor antagonist (1 μM butoxamine; but), $n = 8$ **c**, Decrease in *Cxcl12* mRNA levels 2 h after treatment of primary myeloid cultures derived from adult C57BL/6 mice with isoprenaline or BRL37344, but not clenbuterol (50 μM, $n = 4$). This decrease correlated with the number of CFU-Cs that were detached from the stromal layer and released in the supernatant **d**, Isoprenaline (2 mg kg^{-1}, injected intraperitoneally) decreased bone marrow *Cxcl12* mRNA levels by 80% 2 h after its administration to adult C57BL/6 mice ($n = 6$) **e**, Injection of isoprenaline (2 mg kg^{-1}, injected (inj.) intraperitoneally) induced HSC/progenitor mobilization when homing was compromised by injection with anti-α_4 integrin antibodies (Ab) in endothelial selectins-deficient mice (of C57BL/6 genetic background, $n = 6$) Sal., saline. **f**, *Cxcl12* mRNA levels were significantly decreased 2 h after 100 μM isoprenaline treatment of primary myeloid cultures from control FVB/NJ mice but not *Adrb3*$^{-/-}$ mice of the same background ($n = 4$) **g**, Injection of isoprenaline or BRL37344 (2 mg kg^{-1}, injected intraperitoneally) induced, 2 h later, HSC/progenitor mobilization in FVB/NJ but not *Adrb3*$^{-/-}$ mice in which homing was blocked by the injection of antibodies against P-selectin, E-selectin and α_4 integrins ($n = 4$–7) **h**, Morning (ZT1) physiological increase in circulating progenitors was prevented in C57BL/6 mice ($n = 10$) previously injected (ZT23) with a β_3-adrenergic receptor antagonist (SR59230A, 5 mg kg^{-1}, intraperitoneally) Note the smaller numbers of circulating CFU-Cs in C57BL/6 mice than in FVB/NJ mice. Results are shown as means and s.e.m. Asterisk, $P < 0.05$; two asterisks, $P < 0.01$, three asterisks, $P < 0.001$ (unpaired two-tailed *t*-test)

Degradation of Sp1 transcription factor

Previous studies with the human *Cxcl12* promoter have shown the presence of several Sp1 transcription factor-binding sites and significant decreases in promoter activity when only one Sp1-binding motif was mutated[30]. Alignment of the human and mouse *Cxcl12* promoter sequence revealed a remarkable conservation of these Sp1-binding sites. To gain more insight into the mechanisms that regulate the circadian fluctuations of *Cxcl12* expression, we treated MS-5 cells and primary stromal cultures with mithramycin A, an inhibitor of the binding of Sp transcription factors to GC-enriched DNA sequences. Mithramycin A significantly decreased *Cxcl12* expression (Fig. 5c), suggesting a requirement for Sp1 function in efficient *Cxcl12* transcription. Phosphorylation of Sp1 by the cAMP-dependent

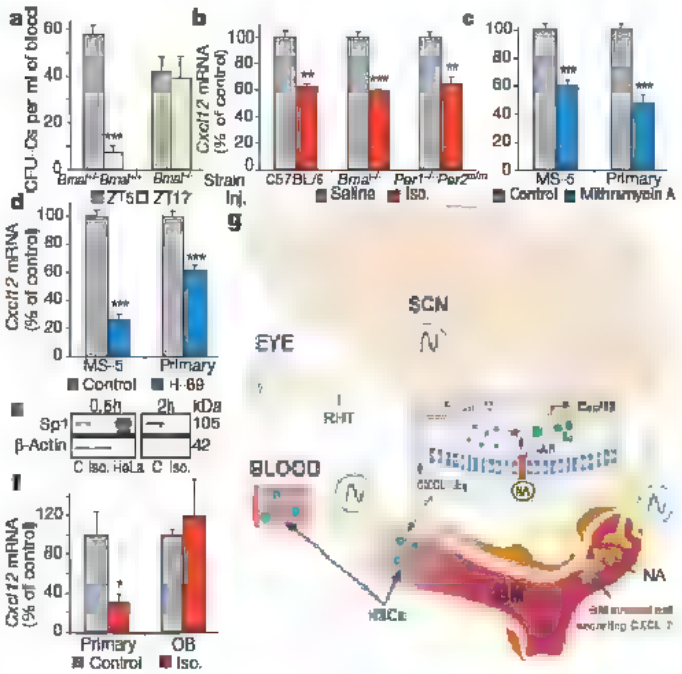

Figure 5 | The central clock regulates *Cxcl12* in bone marrow stromal cells through signals from the sympathetic nervous system. **a**, Circulating progenitors did not oscillate in *Bmal1*$^{-/-}$ mice, compared with *Bmal1*$^{+/+}$ and *Bmal1*$^{+/-}$ controls (C57BL/6 genetic background, $n = 4$). **b**, Decrease in *Cxcl12* mRNA levels 2 h after treatment with 100 μM isoprenaline (iso.) was similar in primary myeloid cultures from C57BL/6, *Bmal1*$^{-/-}$ and *Per1*$^{-/-}$*Per2*$^{m/m}$ mice (of the same genetic background, $n = 4$) **c**, **d**, Treatment of MS-5 cells or myeloid cultures derived from adult C57BL/6 mice for 2 h with either mithramycin A (250 nM), an inhibitor of the binding of Sp transcription factors to DNA (**c**), or the PKA inhibitor H-89 (25 μM) (**d**) significantly decreased *Cxcl12* mRNA levels ($n = 8$) **e**, Sp1 content in nuclear extracts from MS-5 cells after treatment with isoprenaline (100 μM) The left panel shows a marked decrease 30 min after the addition of 100 μM isoprenaline. HeLa, nuclear extracts from HeLa cells Nuclear Sp1 is greatly decreased 2 h after exposure to isoprenaline (100 μM). Two representative experiments of 12 are shown. **f**, Treatment with isoprenaline (100 μM) for 2 h markedly decreased *Cxcl12* mRNA levels in myeloid cultures derived from adult C57BL/6 mice, but not in osteoblasts differentiated from stromal cells for 4 weeks in L-ascorbic acid 2-phosphate (1 mM, $n = 5$) **g**, Model for circadian regulation of trafficking of HSCs and their progenitors. β_3-AR, β_3-adrenergic receptor, BM, bone marrow; NA, noradrenaline; RHT, retinal–hypothalamic tract; SCN, suprachiasmatic nucleus. Results are shown as means and s.e.m. Asterisk, $P < 0.05$, two asterisks, $P < 0.01$, three asterisks, $P < 0.001$ (unpaired two-tailed *t*-test)

protein kinase (PKA) has been shown to enhance its DNA binding activity and subsequently to induce the transcription of target genes[31]. Although β_3-adrenergic receptor stimulation induces PKA through a G_s protein, it can also decrease intracellular cAMP levels after coupling to $G_{i/o}$ proteins[32], eventually leading to decreased Sp1 phosphorylation and *Cxcl12* downregulation. Treatment of MS-5 or primary stromal cells with H-89, a selective inhibitor of PKA, significantly decreased *Cxcl12* expression (Fig. 5d). Lipopolysaccharide, a known HSC mobilizing agent, was recently found to induce noradrenaline release by phagocytes[33], raising the possibility that bone marrow macrophage-derived noradrenaline might participate in lipopolysaccharide-induced HSC mobilization. In addition, lipopolysaccharide can induce Sp1 dephosphorylation and degradation[34], indicating that Sp1 degradation might be relevant to HSC trafficking. Consistent with this possibility was our observation that treatment of MS-5 cells with isoprenaline resulted in a marked and rapid (30 min) decrease in Sp1 content in nuclear extracts (Fig. 5e). Further, Sp1 was almost undetectable 2 h after treatment with isoprenaline (Fig. 5e), indicating that Sp1 degradation after β_3-adrenergic receptor stimulation may be responsible for the downregulation of *Cxcl12* and the subsequent egress of HSCs and progenitors from the bone marrow.

The SNS targets a stromal cell distinct from the osteoblast

The role of *Adrβ3* suggests that the cellular target of the SNS is not a mature osteoblast, because previous studies have reported that *Adrβ2* is the only β-adrenergic receptor expressed in osteoblasts[16]. MS-5 (fibroblastic reticular) and ST-2 (pre-osteoblast) cell lines expressed both *Adrβ2* and *Adrβ3* (Supplementary Fig. 7) and also downregulated *Cxcl12* after treatment with isoprenaline, whereas MC3T3-E1 (differentiated osteoblast) did not express *Adrβ3* and did not respond to isoprenaline (data not shown). We generated osteoblasts from mice carrying the *R26R* allele that also express the Cre recombinase under the control of the *Col1a1* promoter (*Col1a1–LacZ*). Total bone marrow or primary stromal cells expressed both *Adrβ2* and *Adrβ3*, whereas *Adrβ2* was the sole β-adrenergic receptor in osteoblasts derived from stromal cells differentiated in L-ascorbic acid 2-phosphate for four weeks and sorted for *Col1a1* expression (Supplementary Fig. 7). Further, isoprenaline did not decrease *Cxcl12* expression in differentiated primary osteoblasts (Fig. 5f). Thus, these results suggest that an adherent stromal cell producing CXCL12, distinct from the osteoblast, is targeted by the SNS in the bone marrow.

DISCUSSION

Our studies show that HSCs do not steadily or randomly circulate under homeostasis, but rather follow a physiologically regulated rhythmic release. Circadian HSC trafficking is orchestrated in the central nervous system by core genes of the molecular clock that regulate HSC attraction to their bone marrow niches by rhythmic secretion of noradrenaline from nerve terminals, activation of the β_3-adrenergic receptor, degradation of Sp1, and downregulation of *Cxcl12* (Fig. 5g). These studies show that the central nervous system can directly regulate the function of a stem cell niche in peripheral tissues.

Recent studies have suggested that under steady state, HSCs are associated with osteoblasts[13,14,35] and sinusoids[23,36] in the bone marrow. In both cases, HSCs have been localized near CXCL12-abundant reticular cells[36]. Further, $CD146^+$ human stromal cells, recently identified as precursors of both sinusoidal adventitial reticular cells and osteoblasts, may share similarities with mouse CXCL12-abundant reticular cells[37]. The term 'neuro-reticular complex' has been coined[38] to describe the rich association of efferent nerve terminals with sinus adventitial reticular and other stromal cells that are inter-connected by gap junctions around sinusoids of the BM. Taken in this context, our studies suggest that the SNS may regulate a stromal cell associated with the vasculature, possibly an osteoblast precursor, thereby controlling HSC release. Enhanced circulating stem cells in the resting period may constitute an essential component of the regenerative programme of the bone marrow niche itself, or potentially of other tissues by, for instance, the extramedullary restoration of specialized haematopoietic cells[39]. The clinical corollary of rhythmic HSC release implies significantly higher yields if stem cells were harvested at the acrophase.

METHODS SUMMARY

Mouse strains. *Bmal1* $^{-/-}$ (ref. 19) (gift from C. A. Bradfield), *Per1* $^{-/-}$ *Per2*$^{m/m}$ (ref. 40), *Adrb2*^{tm1Bkk}/J (ref. 41) (gift from G. Karsenty), FVB/N-*Adrb3*^{tm1Lowl}/J (ref. 42) and 129S-*Gt(ROSA)26Sor*^{tm1Sor}/J (Jackson Laboratories) mice, FVB-Tg(*Col1a1-cre*)1Kry/Mmcd (ref. 43) (Mutant Mouse Regional Resource Center) and *Sele* $^{-/-}$ *Selp* $^{-/-}$ double knockout mice[44] and the inbred FVB/NJ (Jackson Laboratories) and C57BL/6-CD45.1/2 (Charles River Laboratories) congenic strains were used in this study. Experimental procedures were approved by the Animal Care and Use Committee of Mount Sinai School of Medicine.

Cell culture. MS-5 cells were grown in monolayers in α-MEM medium supplemented with 10% FBS, 2 mM L-glutamine and 2 mM sodium pyruvate. ST-2 cells were grown in RPMI 1640 medium containing 10% FBS. MC3T3-E1 cells were grown in α-MEM medium supplemented with 10% FBS. Cultures were maintained with 1% penicillin–streptomycin (Invitrogen) at 37 °C in a water-jacketed incubator with 5% CO_2 and 1:10 split with 0.05% trypsin-EDTA (Invitrogen) every three or four days, when cells reached about 80% confluence. Cells in passages 3–15 were used in this study.

Flow cytometry. Blood was collected from the retro-orbital sinus and erythrocytes were lysed by incubation in 0.8% NH_4Cl. The number of LSK cells was determined by staining lineage antigens (anti-CD3e, anti-CD11b, anti-CD45R/B220, anti-Ly-6G, anti-Ly-6C and anti-TER119) with the Biotin-Conjugated Mouse Lineage Panel (BD Pharmingen), followed by streptavidin-AMCA (West Grove), Pacific Blue-conjugated anti-Sca1 (Biolegend) and PECy7-conjugated anti-c-Kit (eBioscience). Antibodies against CD45.1 and CD45.2 (eBioscience) were used to determine the percentage of engraftment after competitive bone marrow transplantation. Mobilization of progenitors[31], neurochemical sympathectomy of adult mice[3] and CFU-C assays[24] were performed as described previously. Primary myeloid[45] and osteoclast[46] cultures, CXCL12 ELISA[10], preparation of nuclear extracts[47] and unilateral denervation of the bone marrow[48] were performed as described previously, with some modifications detailed in the full Methods. Conventional western blot analysis was performed with an anti-Sp1 rabbit polyclonal antibody (Upstate) in accordance with the manufacturer's recommendations.

Full Methods and any associated references are available in the online version of the paper at www.nature.com/nature.

Received 26 November 2007; accepted 16 January 2008.
Published online 6 February 2008.

1. Goodman, J. W. & Hodgson, G. S. Evidence for stem cells in the peripheral blood of mice. *Blood* 19, 702–714 (1962).
2. Wright, D. E., Wagers, A. J., Gulati, A. P., Johnson, F. L. & Weissman, I. L. Physiological migration of hematopoietic stem and progenitor cells. *Science* 294, 1933–1936 (2001).
3. Ross, D. D., Pollak, A., Akman, S. A. & Bachur, N. R. Diurnal variation of circulating human myeloid progenitor cells. *Exp. Hematol.* 8, 954–960 (1980).
4. Verma, D. S. *et al.* Diurnal changes in circulating myeloid progenitor cells in man. *Am. J. Hematol.* 9, 185–192 (1980).
5. Lapidot, T. & Petit, I. Current understanding of stem cell mobilization: the roles of chemokines, proteolytic enzymes, adhesion molecules, cytokines, and stromal cells. *Exp. Hematol.* 30, 973–981 (2002).
6. Mendez-Ferrer, S. & Frenette, P. S. Hematopoietic stem cell trafficking: regulated adhesion and attraction to bone marrow microenvironment. *Ann. NY Acad. Sci.* 1116, 392–413 (2007).
7. Thomas, J., Liu, F. & Link, D. C. Mechanisms of mobilization of hematopoietic progenitors with granulocyte colony-stimulating factor. *Curr. Opin. Hematol.* 9, 183–189 (2002).
8. Papayannopoulou, T. Current mechanistic scenarios in hematopoietic stem/progenitor cell mobilization. *Blood* 103, 1580–1585 (2004).
9. Levesque, J. P., Hendy, J., Takamatsu, Y., Simmons, P. J. & Bendall, L. J. Disruption of the CXCR4/CXCL12 chemotactic interaction during hematopoietic stem cell mobilization induced by GCSF or cyclophosphamide. *J. Clin. Invest.* 111, 187–196 (2003).
10. Petit, I. *et al.* G-CSF induces stem cell mobilization by decreasing bone marrow SDF-1 and up-regulating CXCR4. *Nature Immunol.* 3, 687–694 (2002).
11. Katayama, Y. *et al.* Signals from the sympathetic nervous system regulate hematopoietic stem and progenitor cell egress from bone marrow. *Cell* 124, 407–421 (2006).

12. Semerad, C. L. *et al.* G-CSF potently inhibits osteoblast activity and CXCL12 mRNA expression in the bone marrow. *Blood* 106, 3020–3027 (2005)
13. Calvi, L. M. *et al.* Osteoblastic cells regulate the haematopoietic stem cell niche. *Nature* 425, 841–846 (2003)
14. Zhang, J. *et al.* Identification of the haematopoietic stem cell niche and control of the niche size. *Nature* 425, 836–841 (2003)
15. Scadden, D. T. The stem-cell niche as an entity of action. *Nature* 441, 1075–1079 (2006)
16. Elefteriou, F. *et al.* Leptin regulation of bone resorption by the sympathetic nervous system and CART. *Nature* 434, 514–520 (2005)
17. Spiegel, A. *et al.* Catecholaminergic neurotransmitters regulate migration and repopulation of immature human CD34$^+$ cells through Wnt signaling. *Nature Immunol.* 8, 1123–1131 (2007)
18. Arraj, M. & Lemmer, B. Circadian rhythms in heart rate, motility, and body temperature of wild-type C57 and eNOS knock-out mice under light–dark, free-run, and after time zone transition. *Chronobiol. Int.* 23, 795–812 (2006)
19. Bunger, M. K. *et al.* Mop3 is an essential component of the master circadian pacemaker in mammals. *Cell* 103, 1009–1017 (2000).
20. Aiuti, A., Webb, I. J., Bleul, C., Springer, T. & Gutierrez-Ramos, J. C. The chemokine SDF-1 is a chemoattractant for human CD34$^+$ hematopoietic progenitor cells and provides a new mechanism to explain the mobilization of CD34$^+$ progenitors to peripheral blood. *J. Exp. Med.* 185, 111–120 (1997)
21. Wright, D. E., Bowman, E. P., Wagers, A. J., Butcher, E. C. & Weissman, I. L. Hematopoietic stem cells are uniquely selective in their migratory response to chemokines. *J. Exp. Med.* 195, 1145–1154 (2002)
22. Fu, L., Patel, M. S., Bradley, A., Wagner, E. F. & Karsenty, G. The molecular clock mediates leptin-regulated bone formation. *Cell* 122, 803–815 (2005)
23. Kiel, M. J., Yilmaz, O. H., Iwashita, T., Terhorst, C. & Morrison, S. J. SLAM family receptors distinguish hematopoietic stem and progenitor cells and reveal endothelial niches for stem cells. *Cell* 121, 1109–1121 (2005).
24. Frenette, P. S., Subbarao, S., Mazo, I. B., von Andrian, U. H. & Wagner, D. D. Endothelial selectins and vascular cell adhesion molecule-1 promote hematopoietic progenitor homing to bone marrow. *Proc. Natl Acad. Sci. USA* 95, 14423–14428 (1998)
25. Katayama, Y. *et al.* PSGL-1 participates in E-selectin-mediated progenitor homing to bone marrow: evidence for cooperation between E-selectin ligands and α4 integrin. *Blood* 102, 2060–2067 (2003).
26. Katayama, Y., Hidalgo, A., Peired, A. & Frenette, P. S. Integrin α4β7 and its counterreceptor MAdCAM-1 contribute to hematopoietic progenitor recruitment into bone marrow following transplantation. *Blood* 104, 2020–2026 (2004)
27. Maestroni, G. J. *et al.* Neural and endogenous catecholamines in the bone marrow. Circadian association of norepinephrine with hematopoiesis? *Exp. Hematol.* 26, 1172–1177 (1998)
28. Levi, F. & Schibler, U. Circadian rhythms: mechanisms and therapeutic implications. *Annu. Rev. Pharmacol. Toxicol.* 47, 593–628 (2007).
29. Liu, A. C., Lewis, W. G. & Kay, S. A. Mammalian circadian signaling networks and therapeutic targets. *Nature Chem. Biol.* 3, 630–639 (2007)
30. Garcia-Moruja, C. *et al.* Functional characterization of SDF-1 proximal promoter. *J. Mol. Biol.* 348, 43–62 (2005).
31. Rohlff, C., Ahmad, S., Borellini, F., Lei, J. & Glazer, R. I. Modulation of transcription factor Sp1 by cAMP-dependent protein kinase. *J. Biol. Chem.* 272, 21137–21141 (1997)
32. Soeder, K. J. *et al.* The β3-adrenergic receptor activates mitogen-activated protein kinase in adipocytes through a G_i-dependent mechanism. *J. Biol. Chem.* 274, 12017–12022 (1999)
33. Flierl, M. A. *et al.* Phagocyte-derived catecholamines enhance acute inflammatory injury. *Nature* 449, 721–725 (2007).
34. Ye, X. & Liu, S. F. Lipopolysaccharide down-regulates Sp1 binding activity by promoting Sp1 protein dephosphorylation and degradation. *J. Biol. Chem.* 277, 31863–31870 (2002)
35. Arai, F. *et al.* Tie2/angiopoietin-1 signaling regulates hematopoietic stem cell quiescence in the bone marrow niche. *Cell* 118, 149–161 (2004).
36. Sugiyama, T., Kohara, H., Noda, M. & Nagasawa, T. Maintenance of the hematopoietic stem cell pool by CXCL12-CXCR4 chemokine signaling in bone marrow stromal cell niches. *Immunity* 25, 977–988 (2006)
37. Sacchetti, B. *et al.* Self-renewing osteoprogenitors in bone marrow sinusoids can organize a hematopoietic microenvironment. *Cell* 131, 324–336 (2007).
38. Yamazaki, K. & Allen, T. D. Ultrastructural morphometric study of efferent nerve terminals on murine bone marrow stromal cells, and the recognition of a novel anatomical unit, the 'neuro-reticular complex'. *Am. J. Anat.* 187, 261–276 (1990).
39. Massberg, S. *et al.* Immunosurveillance by hematopoietic progenitor cells trafficking through blood, lymph, and peripheral tissues. *Cell* 131, 994–1008 (2007)
40. Zheng, B. *et al.* Nonredundant roles of the *mPer1* and *mPer2* genes in the mammalian circadian clock. *Cell* 105, 683–694 (2001).
41. Chruscinski, A. J. *et al.* Targeted disruption of the β2 adrenergic receptor gene. *J. Biol. Chem.* 274, 16694–16700 (1999).
42. Susulic, V. S. *et al.* Targeted disruption of the β3-adrenergic receptor gene. *J. Biol. Chem.* 270, 29483–29492 (1995)
43. Dacquin, R., Starbuck, M., Schinke, T. & Karsenty, G. Mouse α1-collagen promoter is the best known promoter to drive efficient Cre recombinase expression in osteoblast. *Dev. Dyn.* 224, 245–251 (2002)
44. Frenette, P. S., Mayadas, T. N., Rayburn, H., Hynes, R. O. & Wagner, D. D. Susceptibility to infection and altered hematopoiesis in mice deficient in both P- and E-selectins. *Cell* 84, 563–574 (1996)
45. Katayama, Y. & Frenette, P. S. Galactocerebrosides are required postnatally for stromal-dependent bone marrow lymphopoiesis. *Immunity* 18, 789–800 (2003)
46. Wu, X. B. *et al.* Impaired osteoblastic differentiation, reduced bone formation, and severe osteoporosis in noggin-overexpressing mice. *J. Clin. Invest.* 112, 924–934 (2003)
47. Kavurma, M. M., Santiago, F. S., Bonfoco, E. & Khachigian, L. M. Sp1 phosphorylation regulates apoptosis via extracellular FasL–Fas engagement. *J. Biol. Chem.* 276, 4964–4971 (2001)
48. Benestad, H. B., Strom-Gundersen, I., Iversen, P. O., Haug, E. & Nja, A. No neuronal regulation of murine bone marrow function. *Blood* 91, 1280–1287 (1998)

Supplementary Information is linked to the online version of the paper at www.nature.com/nature.

Acknowledgements We thank M. Garcia-Fernández, J. Jang, Y.-S. Ang, P. Tathineni, A. Peired and members of the Frenette Laboratory for their valuable help, M. Zaldi for advice with osteoblast and osteoclast cultures; and I. Lemischka and K. Moore for comments on the manuscript. This work was supported by the National Institutes of Health and the Department of Defense. S.M.-F. was the recipient of a postdoctoral fellowship from the Spanish Ministry of Education and Science. M.B. is supported by a Research Fellowship from the Cooley's Anemia Foundation. P.S.F. is an Established Investigator of the American Heart Association.

Author Contributions All authors contributed to the design of experiments and analysed data. P.S.F. supervised experiments and wrote the manuscript. S.M.-F. performed circadian measurements of gene expression, circulating progenitors, all Q-PCR, ELISA, *in vitro* experiments, *in vivo* effects of adrenergic agonists, immunostainings, western blots and denervation experiments, and prepared figures and wrote the manuscript. D.L. performed circadian progenitor assessments, long-term competitive reconstitutions and 6OHDA experiments. M.B. performed circadian progenitor assessments and G-CSF mobilization experiments.

Author Information Reprints and permissions information is available at www.nature.com/reprints. Correspondence and requests for materials should be addressed to P.S.F. (paul.frenette@mssm.edu)

LETTERS

Coupling of spin and orbital motion of electrons in carbon nanotubes

F. Kuemmeth[1]*, S. Ilani[1]*, D. C. Ralph[1] & P. L. McEuen[1]

Electrons in atoms possess both spin and orbital degrees of freedom. In non-relativistic quantum mechanics, these are independent, resulting in large degeneracies in atomic spectra. However, relativistic effects couple the spin and orbital motion, leading to the well-known fine structure in their spectra. The electronic states in defect-free carbon nanotubes are widely believed to be four-fold degenerate[1–10], owing to independent spin and orbital symmetries, and also to possess electron–hole symmetry[11]. Here we report measurements demonstrating that in clean nanotubes the spin and orbital motion of electrons are coupled, thereby breaking all of these symmetries. This spin–orbit coupling is directly observed as a splitting of the four-fold degeneracy of a single electron in ultra-clean quantum dots. The coupling favours parallel alignment of the orbital and spin magnetic moments for electrons and antiparallel alignment for holes. Our measurements are consistent with recent theories[12,13] that predict the existence of spin–orbit coupling in curved graphene and describe it as a spin-dependent topological phase in nanotubes. Our findings have important implications for spin-based applications in carbon-based systems, entailing new design principles for the realization of quantum bits (qubits) in nanotubes and providing a mechanism for all-electrical control of spins[14] in nanotubes.

Carbon-based systems are promising candidates for spin-based applications such as spin-qubits[14–19] and spintronics[20–23] as they are believed to have exceptionally long spin coherence times because of weak spin–orbit interactions and the absence of nuclear spin in the ^{12}C atom. Carbon nanotubes may have a particularly interesting role in this context because in addition to spin they offer a unique two-fold orbital degree of freedom that can also be used for quantum manipulation. The latter arises from the two equivalent dispersion cones (K and K') in graphene, which lead to doubly degenerate electronic orbits that encircle the nanotube circumference in a clockwise and anticlockwise fashion[24] (Fig. 1a). Together, the two-fold spin degeneracy and two-fold orbital degeneracy are generally assumed to yield a four-fold-degenerate electronic energy spectrum in clean nanotubes. Understanding the fundamental symmetries of this spectrum is at the heart of successful manipulation of these quantum degrees of freedom.

A powerful way to probe the symmetries is by confining the carriers to a quantum dot and applying a magnetic field $B_{||}$ parallel to the tube axis[4,5,8,10,24,25]. The confinement creates bound states and the field interrogates their nature by coupling independently to their spin and orbital moments. In the absence of spin–orbit coupling, such a measurement should yield for a defect-free nanotube the energy spectrum shown in Fig. 1b. At $B_{||} = 0$ the nanotube spectrum should be four-fold degenerate. With increasing $B_{||}$ the spectrum splits into pairs of anticlockwise and clockwise states (going down and up in energy respectively), each pair having a smaller internal spin splitting. Indications of approximate four-fold degeneracy have been observed in high-field measurements of electron addition spectra[2–10] and inelastic cotunnelling[4,10] in nanotube quantum dots. However, in previous experiments disorder-induced splitting of the orbital degeneracy and electron–electron interactions in multi-electron quantum dots have masked the intrinsic symmetries at low energies.

In this work we directly measure the intrinsic electronic spectrum by studying a single charge carrier, an electron or a hole, in an ultra-clean carbon nanotube quantum dot. Remarkably, we find that the expected four-fold symmetry and electron–hole symmetry are broken by spin–orbit coupling, demonstrating that the spin and orbital motion in nanotubes are not independent degrees of freedom. The observed spin–orbit coupling further determines the filling order in the many-electron ground states, giving states quite different from models based purely on electron–electron interactions.

The geometry of our devices is shown in Fig. 1c. A single small-bandgap nanotube is contacted by source and drain electrodes, and is gated from below by two gates (see Methods). When biased, these gates shift the local Fermi energy in the nanotube, thereby accumulating electrons or holes. In this work we use two independent gates to create a quantum dot that is localized above either the left or the right gate electrode. This is achieved by choosing appropriate combinations of gate voltages that pin the Fermi energy inside the gap on one side of the device while adding carriers to the other side (Fig. 1c). Measurement of the linear conductance, $G = dI/dV_{sd}$, through such a dot (Fig. 1e) shows Coulomb blockade peaks that correspond to the addition of individual carriers to the dot, and allows us to identify the first electron and first hole in the dot (see Supplementary Information for details). Having a single carrier in the dot enables us to study single-particle levels in the absence of electron–electron interactions, and thus to identify unambiguously the presence of spin–orbit coupling. The results reported here were observed in two independent devices and below we present data from one of them.

We probe the quantum states of the nanotube using tunnelling spectroscopy. The differential conductance through the dot, $G = dI/dV_{sd}$, is measured as a function of gate voltage, V_g, and source–drain bias, V_{sd}, as the first electron is added to the dot. Figure 2a shows a typical measurement taken at $B_{||} = 300$ mT. The transition between the Coulomb blockade regions of zero and one electron features distinct resonances that correspond to the ground state (α) as well as the excited states (β, γ, δ) of the first electron. Their energies can be obtained from a line cut at constant V_{sd} (Fig. 2b), by converting the gate voltages into energies (see Methods).

The magnetic field dependence of the one-electron states α, β, γ and δ is measured by taking V_g traces such as in Fig. 2b for different values of $B_{||}$. This is shown in Fig. 2c, where we plot dI/dV_{sd} as a function of V_g and $B_{||}$. The energies of the states α and β decrease with increasing $B_{||}$, so we identify them as anticlockwise orbital states. The

[1]Laboratory of Atomic and Solid State Physics, Department of Physics, Cornell University, Ithaca, New York 14853, USA
*These authors contributed equally to this work

states γ and δ increase in energy with increasing $B_\parallel$ and are thus identified as clockwise orbital states. From the slopes of these resonances with respect to magnetic field we extract an orbital moment of $\mu_{orb} = 1.55\,meV\,T^{-1}$ and estimate the nanotube diameter to be $d \approx 5$ nm (ref. 24).

A striking difference is observed when we compare the measured excitation spectrum with that predicted in Fig. 1b: at zero magnetic field the four states in our measurement are not degenerate but rather split into two pairs. To identify the nature of this splitting we note that with increasing magnetic field the energy difference between the states α and β increases while the difference between states γ and δ decreases, and both differences are consistent with a g-factor of an electron spin (Fig. 2d). This observation allows us to identify unambiguously the spin and orbital composition of each energy level, as shown in the inset of Fig. 2c. At $B_\parallel = 0$ the four-fold degeneracy is split into two Kramer doublets—the lower-energy doublet involves states with parallel alignment of orbital and spin magnetic moments, whereas the higher-energy doublet has states with antiparallel alignment. The zero-field splitting is therefore identified as a spin–orbit splitting, with a value of $\Delta_{SO} = 0.37 \pm 0.02$ meV (extracted from Fig. 2d).

At low fields (Fig. 2e) the intersections of states with opposite spin directions (for example, α and γ) show simple crossing, whereas states with parallel spin (for example, β and γ) show avoided crossing, a signature of disorder-induced mixing between anticlockwise and clockwise orbits ($\Delta_{KK'}$). In previous experiments, the disorder-induced mixing was significantly larger, presumably obscuring the effects of spin–orbit coupling. In our measurements, the mixing is small, $\Delta_{KK'} \approx 65\,\mu eV \ll \Delta_{SO}$, probably owing to smooth electronic confinement, allowing the observation of spin–orbit effects. We further demonstrate the intrinsic nature of the effect by measuring identical excitation spectra for quantum dots formed at different locations along the same nanotube (Supplementary Fig. 1).

Next, we show that spin–orbit coupling significantly affects the many-body ground states of multiple electrons in a quantum dot. Figure 3a shows the magnetic field dependence of the addition energies for the N-electron ground states ($N = -2$ to $+4$), obtained by measuring the linear conductance as a function of V_g and $B_\parallel$. Near zero magnetic field the sign of $dV_g/dB_\parallel$ changes every time an electron is added (or removed), indicating that anticlockwise and clockwise states are filled alternately. Similar addition sequences were explained in the past by repulsive electron–electron interactions driving electrons to occupy different orbits[2-7,9,26] (Fig. 3b). However, in our nanotubes the underlying mechanism is entirely different. Comparing the one-electron excitation spectrum with the two-electron ground state (Fig. 3c), we see that the latter follows exactly the first excited state of the one-electron quantum dot. Specifically, both start with a clockwise slope at low fields and flip to an anticlockwise slope at the field associated with the spin–orbit splitting, $B_\parallel \approx 125$ mT. Thus the two-electron ground state is explained entirely by spin–orbit coupling (Fig. 3d). Note that below $B_\parallel \approx 125$ mT spin–orbit coupling favours each of the two electrons to possess parallel orbital and spin moments, forcing them into two different orbital states. Therefore, the two-electron ground state is neither the spin-triplet state predicted by the electron-interaction-based models nor a spin singlet, but rather a Slater determinant of two single-electron states each of which has parallel orbital and spin magnetic moments.

Spin–orbit effects are commonly assumed to be negligible in carbon-based systems because of the weak atomic spin–orbit splitting in carbon ($\Delta_{at} = E(^2P_{3/2}) - E(^2P_{1/2}) \approx 8$ meV) (ref. 27) and its almost perfect suppression in flat graphene[13]. But recent theories have argued that spin–orbit coupling can nevertheless be significant in carbon nanotubes owing to their curvature and cylindrical topology[12,13]. The predicted effect is illustrated in Fig. 4a. Consider an electron with a spin moment pointing along the nanotube axis and orbiting around the nanotube circumference. The electron occupies the p_z orbitals of the carbon atoms, which are pointing perpendicular to the nanotube surface. In the rest frame of the electron the underlying p_z orbital revolves around the spin exactly once every rotation,

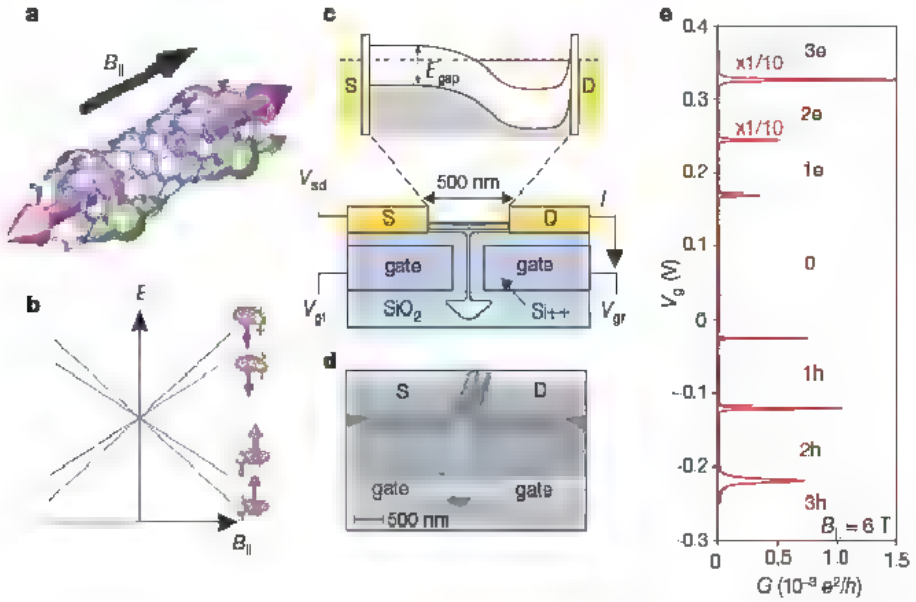

Figure 1 | Few-electron carbon nanotube quantum dot devices. a, Electrons confined in a nanotube segment have quantized energy levels, each four-fold degenerate in the absence of spin–orbit coupling and defect scattering. The purple arrow at the left (right) illustrates the current and magnetic moment arising from clockwise (anticlockwise) orbital motion around the nanotube. The green arrows indicate positive moments due to spin. **b**, Expected energy splitting for a defect-free nanotube in a magnetic field $B_\parallel$ parallel to the nanotube axis in the absence of spin–orbit coupling. At $B_\parallel = 0$ T, all four states are degenerate. With increasing $B_\parallel$ each state shifts according to its orbital and spin magnetic moments, as indicated by purple and green arrows respectively. **c**, Device schematic. A single nanotube makes contact to source and drain electrodes, separated by 500 nm, and is gated from below by two gate electrodes. The two gate voltages (V_{gl}, V_{gr}) are used to create a quantum dot localized above the right or left gate electrodes. The energy band diagram is shown for the first case. **d**, Scanning electron micrograph of the device, taken before nanotube growth to avoid damage to the nanotube. **e**, The measured linear conductance, $G = dI/dV_{sd}$, as function of gate voltage, V_g, for a dot localized above the right gate ($B_\parallel = 6$ T, temperature $T = 30$ mK). The number of electrons or holes in the dot is indicated. The conductance of the top two peaks is scaled by 1/10.

independent of the details of the electron trajectory. In the presence of atomic spin–orbit coupling a constant phase accumulates during each rotation, which can therefore be described by a spin-dependent topological flux, $S_{||}\phi_{SO}$, passing through the nanotube cross-section ($S_{||} = +1/-1$ for spin moment parallel/antiparallel to the nanotube axis). This flux modifies the quantization condition of the wavefunction around the circumference:

$$k_{\perp}\pi d \rightarrow k_{\perp}\pi d - 2\pi S_{||}\,\phi_{SO}/\phi_0 \qquad (1)$$

where $k_{\perp}$ is the electron's wave vector in the circumferential direction as measured from the K and K' points, d is the tube diameter and ϕ_0 is the flux quantum. According to the theory in ref. 12 the flux is given by

$$\phi_{SO} = \frac{\Delta_{\pi\sigma}}{12\varepsilon_{\pi\sigma}}\left(5+3\frac{V_{pp}^{\sigma}}{V_{pp}^{\pi}}\right)\phi_0 \approx 10^{-3}\phi_0 \qquad (2)$$

where $\varepsilon_{\pi\sigma}$ is the energy splitting of the π and σ bands in graphene and V_{pp}^{σ}, V_{pp}^{π} are the hopping elements within these bands. This flux does not depend on the geometrical properties of the nanotube such as its diameter or the shape of its cross-section, signifying its topological origin.

Figure 4b illustrates the consequences of the modified quantization conditions for a small-bandgap tube at $B_{||} = 0$. Near each Dirac cone (K and K') there are two quantization lines for the two spin directions (dashed lines). Combining equation (1) with the linear dispersion, and including the Aharonov–Bohm flux induced by $B_{||}$, $\phi_{AB} = B_{||}\pi d^2/4$, and the Zeeman spin coupling, the energies are

$$E = \pm\hbar v_F\sqrt{k_{||}^2 + k_{\perp}^2} - \frac{g}{2}\mu_B S_{||}B_{||}, \quad k_{\perp} = k_{\perp,0} + \frac{2\phi_{AB}}{d\,\phi_0} + S_{||}\frac{2\phi_{SO}}{d\,\phi_0} \qquad (3)$$

Here v_F is the Fermi velocity, $k_{||}$ is the wave vector parallel to the nanotube axis, and $k_{\perp,0} = \pm E_{gap}/2\hbar v_F$ accounts for the small bandgap, E_{gap}, at zero magnetic field (the opposite signs are for the K' and K points). The resulting energy spectrum is schematically shown in

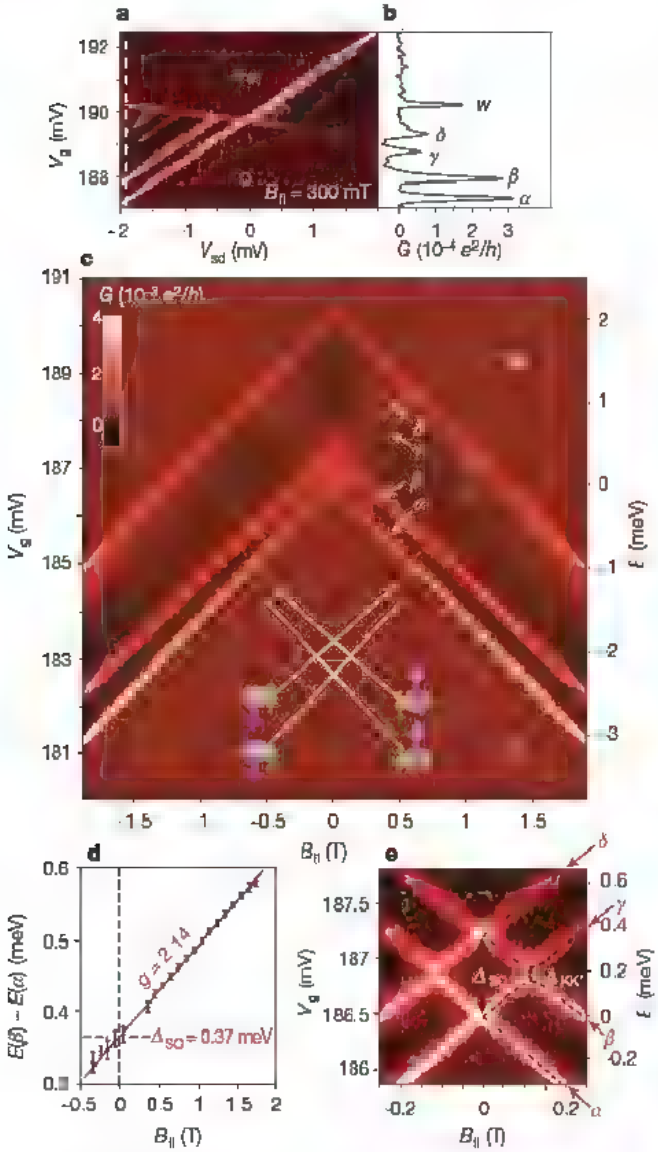

Figure 2 | Excited-state spectroscopy of a single electron in a nanotube dot. a, Differential conductance, $G = dI/dV_{sd}$, measured as function of gate voltage, V_g, and source–drain bias, V_{sd}, at $B_{||} = 300$ mT, displaying transitions from zero to one electron in the dot. **b**, A line cut at $V_{sd} = -1.9$ mV reveals four energy levels α, β, γ and δ as well as another peak w corresponding to the edge of the one-electron Coulomb diamond. **c**, $G = dI/dV_{sd}$ as a function of V_g and $B_{||}$ at a constant bias $V_{sd} = -2$ mV. The resonances α, β, γ, δ and w are indicated. The energy scale on the right is determined by scaling ΔV_g with the conversion factor $\alpha = 0.57$ extracted from the slopes in **a**. Inset: orbital and spin magnetic moments assigned to the observed states. **d**, Extracted energy splitting between the states α and β as a function of $B_{||}$ (dots). The linear fit (red line) gives a Zeeman splitting with $g = 2.14 \pm 0.1$, and a zero-field splitting of $\Delta_{SO} = 0.37 \pm 0.02$ meV (error bars, 1 s.d.). **e**, Magnified view of panel **c** showing the zero-field splitting due to spin–orbit interaction (Δ_{SO}) as well as finite-field anticrossing due to K–K' mixing ($\Delta_{KK'}$). Dashed lines show the calculated spectrum using $\Delta_{KK'} = 65$ μeV.

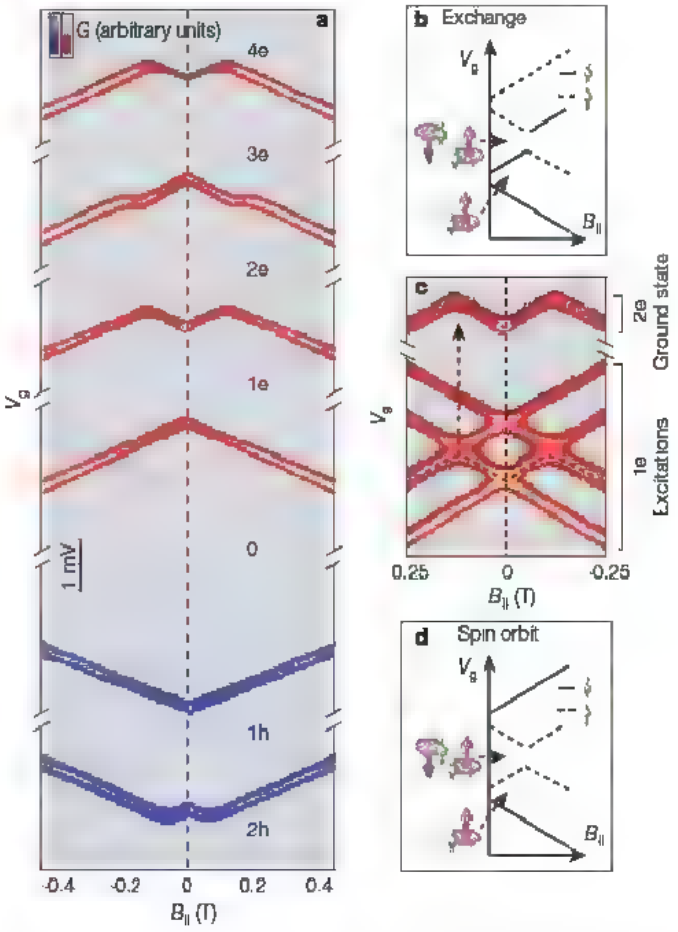

Figure 3 | The many-electron ground states and their explanation by spin-orbit interaction. a, $G = dI/dV_{sd}$, measured as a function of gate voltage, V_g, and magnetic field, $B_{||}$, showing Coulomb blockade peaks (carrier addition spectra) for the first four electrons and the first two holes (data are offset in V_g for clarity). **b**, Incorrect interpretation of the addition spectrum shown in **a** using a model with exchange interactions between electrons. Dashed/solid lines represent addition of down/up spin moments. The two-electron ground state at low fields, indicated at the left, is a spin triplet. **c**, Comparison of the measured two-electron addition energy from **a** with the one-electron excitation spectrum from Fig. 2e. **d**, Schematic explanation of the data in **a** using electronic states with spin–orbit coupling. The two-electron ground state at low fields, indicated on the left, is neither a spin-singlet nor a spin-triplet state.

Fig. 4c, and is in agreement with our measurements. From equation (3) we see that the spin–orbit energy splitting $\Delta_{SO} = \frac{4\hbar v_F}{d}\frac{\phi_{SO}}{\phi_0}$ (assuming $k_\parallel = 0$) is inversely proportional to d. Using the estimated diameter of our nanotube, $d \approx 5$ nm, and the measured splitting (Fig. 2d) we obtain the value $\Delta_{SO} \approx 1.9/d\,\mathrm{meV\,nm^{-1}}$, in agreement with the predicted[13] value of $\Delta_{SO} \approx 1.6/d\,\mathrm{meV\,nm^{-1}}$.

An interesting prediction of the theory[12,13,18] is the breaking of electron–hole symmetry. In the absence of spin–orbit interactions the low-energy spectrum of a nanotube shows electron–hole symmetry such that each allowed state has a matching state with opposite energy; that is, the spectrum is symmetric on reflection about the line $E = 0$. In the presence of spin–orbit interactions and an applied magnetic field, equation (3) predicts that this symmetry is broken, as is evident from the absence of mirror symmetry around $E = 0$ in the spectrum in Fig. 4c. For $\phi_{SO} > 0$, the theory predicts that in the one-electron ground state the orbital and spin magnetic moments are parallel, whereas in the one-hole ground state they are antiparallel. This result allows us to test the breaking of electron–hole symmetry experimentally.

The measured excitation spectra for the first hole in the quantum dot (Fig. 4d) clearly shows a spin–orbit splitting at $B_\parallel = 0$, and a spin g-factor equal to that of the one-electron quantum dot (Fig. 4e). However, in contrast to the one-electron case, here the ground state (α) and the first excited state (β) converge with increasing $B_\parallel$, implying that the orbital and spin moments are aligned antiparallel in the one-hole ground state, opposite to the one-electron case. This observation qualitatively confirms the scheme in Fig. 4c. We note, however, that the spin–orbit splitting observed for the hole ($\Delta_{SO} = 0.21 \pm 0.01$ meV) is somewhat smaller than that of the electron, a difference that is not accounted for by current theory. This might result from different confinement lengths (different $k_\parallel$ in equation (3)) or different electric fields (that is, different V_g) for electrons and holes, but current theories predict an effect that is too small to explain this observation.

The existence of spin–orbit coupling in carbon nanotubes invalidates several common assumptions about the nature of the electronic states in this system, such as four-fold degeneracy and electron–hole symmetry, and further leads to the existence of entangled spin and orbital multi-electron ground states. Currently, carbon-based systems are considered to be excellent candidates for spin-based applications, in part because of the belief that they have weak spin–orbit interactions. Here we have shown that this hypothesis is wrong for nanotubes. Nevertheless, rather than excluding spin-based devices in nanotubes, our findings may actually promote their feasibility, as long as new design principles are adopted for qubits and spintronic

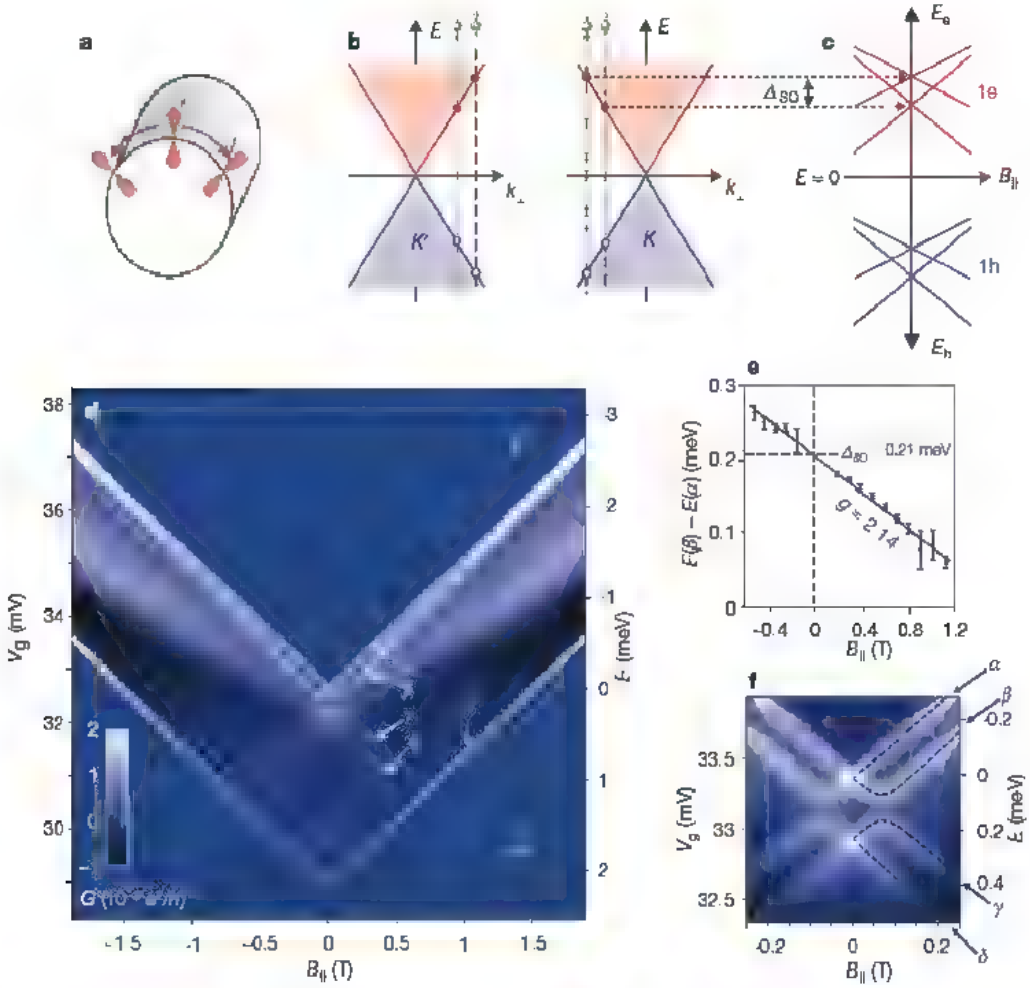

Figure 4 | Theoretical model for spin–orbit interaction in nanotubes and the energy level spectroscopy of a single hole. **a**, Schematic of an electron with spin parallel to the nanotube axis revolving around the nanotube circumference. The carbon p_z orbitals (red) are perpendicular to the surface. In the rest frame of the electron, the p_z orbital rotates around the spin. **b**, Allowed electron and hole energies (red dots and blue circles) at $B_\parallel = 0$ for a small-bandgap nanotube with spin–orbit interaction. The states are derived by cutting the Dirac cones (K and K') with spin-dependent quantization lines (dashed lines). The allowed $k_\perp$-vectors differ for up and down electron spin moments. **c**, Calculated energy levels for an electron (red lines) and a hole (blue lines) as a function of $B_\parallel$. The four distinct slopes arise from the orbital and spin Zeeman shifts. **d**, $G = \mathrm{d}I/\mathrm{d}V_{sd}$ as a function of V_g and $B_\parallel$ at a constant bias $V_{sd} = -2$ mV. The resonances labelled α, β, γ, δ and w arise from tunnelling of holes onto the dot and therefore the energy scale runs in the opposite direction to V_g. The ground state (α) and first excited state (β) cross at $B_\parallel \approx 1.5$ T. **e**, Extracted energy splitting between the states α and β as a function of $B_\parallel$ (dots). The linear fit (blue line) gives a Zeeman splitting with $g = 2.14 \pm 0.1$, and a zero-field splitting of $\Delta_{SO} = 0.21 \pm 0.01$ meV (error bars, 1 s.d.). **f**, Magnified view of the level crossings in **d** and a model calculation using $\Delta_{KK'} = 0.1$ meV (dashed lines).

devices, which make use of the strong spin–orbit coupling. This coupling can provide a valuable capability that has so far been missing from carbon systems: the ability to use electrical gates to manipulate the spin degree of freedom, through its coupling to the orbital electronic wavefunction[14].

METHODS SUMMARY

We fabricated devices from degenerately doped silicon-on-insulator wafers, with a 1.5-μm-thick device layer on top of a 2-μm buried oxide. Two electrically isolated gate electrodes (Fig. 1d) were patterned from the device layer using dry etching and thermal oxidation (thickness 100 nm). Gate contacts (2/50 nm Ti/Pt), source and drain electrodes (5/25 nm Cr/Pt) and catalyst pads were patterned using electron-beam lithography. Nanotubes were grown after completing all patterning to produce clean devices[4]. We made measurements in a ^{3}He/^{4}He dilution refrigerator at base temperature ($T = 30$ mK), using standard lock-in techniques with small excitations (typically 4–10 μV). The electron temperature extracted from Coulomb peak widths was 100–200 mK. The conversion from gate voltage to energy is obtained from the bias dependence of the tunnelling resonances, such as in Fig. 2a, and is $\alpha = 0.57$ for the first electron (Fig. 2) and $\alpha = 0.58$ for the first hole (Fig. 4).

Received 21 November 2007; accepted 5 February 2008.

1. Kane, C. L. & Mele, E. J. Size, shape, and low energy electronic structure of carbon nanotubes. *Phys. Rev. Lett.* 78, 1932–1935 (1997).
2. Cobden, D. H. & Nygard, J. Shell filling in closed single-wall carbon nanotube quantum dots. *Phys. Rev. Lett.* 89, 046803 (2002).
3. Liang, W., J., Bockrath, M. & Park, H. Shell filling and exchange coupling in metallic single-walled carbon nanotubes. *Phys. Rev. Lett.* 88, 126801 (2002).
4. Jarillo-Herrero, P. *et al.* Electronic transport spectroscopy of carbon nanotubes in a magnetic field. *Phys. Rev. Lett.* 94, 156802 (2005).
5. Jarillo-Herrero, P. *et al.* Orbital Kondo effect in carbon nanotubes. *Nature* 434, 484–488 (2005).
6. Moriyama, S. *et al.* Four-electron shell structures and an interacting two-electron system in carbon-nanotube quantum dots. *Phys. Rev. Lett.* 94, 186806 (2005).
7. Sapmaz, S. *et al.* Electronic excitation spectrum of metallic carbon nanotubes. *Phys. Rev. B* 71, 153402 (2005).
8. Cao, J., Wang, Q. & Dai, H. Electron transport in very clean, as-grown suspended carbon nanotubes. *Nature Mater.* 4, 745–749 (2005).
9. Makarovski, A., An, L., Liu, J. & Finkelstein, G. Persistent orbital degeneracy in carbon nanotubes. *Phys. Rev. B* 74, 155431 (2006).
10. Makarovski, A., Zhukov, A., Liu, J. & Finkelstein, G. SU(2) and SU(4) Kondo effects in carbon nanotube quantum dots. *Phys. Rev. B* 75, 241407 (2007).
11. Jarillo-Herrero, P. *et al.* Electron–hole symmetry in a semiconducting carbon nanotube quantum dot. *Nature* 429, 389–392 (2004).
12. Ando, T. Spin-orbit interaction in carbon nanotubes. *J. Phys. Soc. Jpn.* 69, 1757–1763 (2000).
13. Huertas-Hernando, D., Guinea, F. & Brataas, A. Spin–orbit coupling in curved graphene, fullerenes, nanotubes, and nanotube caps. *Phys. Rev. B* 74, 155426 (2006).
14. Nowack, K. C., Koppens, F. H. L., Nazarov, Yu. V. & Vandersypen, L. M. K. Coherent control of a single electron spin with electric fields. *Science* 318, 1430–1433 (2007).
15. Loss, D. & DiVincenzo, D. P. Quantum computation with quantum dots. *Phys. Rev. A* 57, 120–126 (1998).
16. Elzerman, J. M. *et al.* Single-shot read-out of an individual electron spin in a quantum dot. *Nature* 430, 431–435 (2004).
17. Petta, J. R. *et al.* Coherent manipulation of coupled electron spins in semiconductor quantum dots. *Science* 309, 2180–2184 (2005).
18. Bulaev, D. V., Trauzettel, B. & Loss, D. Spin–orbit interaction and anomalous spin relaxation in carbon nanotube quantum dots. Preprint at (http://arXiv.org/abs/0712.3767) (2007).
19. Trauzettel, B., Bulaev, D. V., Loss, D. & Burkard, G. Spin qubits in graphene quantum dots. *Nature Phys.* 3, 192–196 (2007).
20. Awschalom, D. D. & Flatte, M. E. Challenges for semiconductor spintronics. *Nature Phys.* 3, 153–159 (2007).
21. Sahoo, S. *et al.* Electric field control of spin transport. *Nature Phys.* 1, 99–102 (2005).
22. Tombros, N., van der Molen, S. J. & van Wees, B. J. Separating spin and charge transport in single-wall carbon nanotubes. *Phys. Rev. B* 73, 233403 (2006).
23. Tombros, N. *et al.* Electronic spin transport and spin precession in single graphene layers at room temperature. *Nature* 448, 571–574 (2007).
24. Minot, E. D., Yaish, Y., Sazonova, V. & McEuen, P. L. Determination of electron orbital magnetic moments in carbon nanotubes. *Nature* 428, 536–539 (2004).
25. Cobden, D. H. *et al.* Spin splitting and even–odd effects in carbon nanotubes. *Phys. Rev. Lett.* 81, 681–684 (1998).
26. Oreg, Y., Byczuk, K. & Halperin, B. I. Spin configurations of a carbon nanotube in a nonuniform external potential. *Phys. Rev. Lett.* 85, 365–368 (2000).
27. Ralchenko, Yu *et al. Atomic Spectra Database Version 3.1.3* (National Institute of Standards and Technology, Gaithersburg, Maryland) (http://physics.nist.gov/asd3) (accessed, 14 November 2007).

Supplementary Information is linked to the online version of the paper at www.nature.com/nature.

Acknowledgements We thank E. Altman, Y. Gefen, C. L. Henley, Y. Meir, E. Mueller, Y. Oreg, E. I. Rashba, A. Stern and B. Trauzettel for discussions. This work was supported by the NSF through the Center for Nanoscale Systems, and by the MARCO Focused Research Center on Materials, Structures and Devices. Samples were fabricated at the Cornell node of the National Nanofabrication Users Network, funded by NSF.

Author Contributions F.K. and S.I. fabricated the devices and performed the experiments. F.K., S.I., D.C.R. and P.L.M. analysed the data and co-wrote the paper. All authors discussed the results and commented on the manuscript.

Author Information Reprints and permissions information is available at www.nature.com/reprints. Correspondence and requests for materials should be addressed to P.L.M. (mceuen@ccmr.cornell.edu).

LETTERS

Proline-catalysed Mannich reactions of acetaldehyde

Jung Woon Yang[1], Carley Chandler[1], Michael Stadler[1], Daniela Kampen[1] & Benjamin List[1]

Small organic molecules recently emerged as a third class of broadly useful asymmetric catalysts that direct reactions to yield predominantly one chiral product, complementing enzymes and metal complexes[1]. For instance, the amino acid proline and its derivatives are useful for the catalytic activation of carbonyl compounds via nucleophilic enamine intermediates. Several important carbon–carbon bond-forming reactions, including the Mannich reaction, have been developed using this approach[2], all of which are useful for making chiral, biologically relevant compounds. Remarkably, despite attempts[3,4], the simplest of all nucleophiles, acetaldehyde, could not be used in this way. Here we show that acetaldehyde is a powerful nucleophile in asymmetric, proline-catalysed Mannich reactions with *N*-*tert*-butoxycarbonyl (*N*-Boc)-imines, yielding β-amino aldehydes with extremely high enantioselectivities—desirable products as drug intermediates and in the synthesis of other biologically active molecules. Although acetaldehyde has been used as a nucleophile in reactions with biological catalysts such as aldolases[5] and thiamine-dependent enzymes[6], and has also been employed indirectly[7–9], its use as an inexpensive and versatile two-carbon nucleophile in asymmetric, small-molecule catalysis will find many practical applications.

Discovered in 2000 (ref. 10), the proline-catalysed Mannich reaction has evolved into a broadly useful transformation that has been applied to the synthesis of natural products, pharmaceuticals, and several classes of chiral amino acids[2]. Very recently, *N*-Boc-imines have been introduced to the proline-catalysed Mannich reaction[11,12], significantly widening the already large substrate scope and utility of this process. We found that several α-unbranched aldehydes react with aromatic *N*-Boc-imines to furnish crystalline α,β-branched β-amino aldehydes in excellent *syn*-diastereoselectivities and enantioselectivities[12]. However, acetaldehyde, which would be a particularly useful nucleophile in this reaction, could not be used under our original conditions. The resulting amino aldehyde products of such reactions are highly attractive precursors of chiral β^3-amino acids, recently pioneered by Gellman *et al.*[13] and Seebach *et al.*[14] in investigations of β-peptides and pharmaceuticals.

There are several problems associated with the potential use of acetaldehyde in proline-catalysed Mannich reactions (and in enamine catalysis in general). First, acetaldehyde rapidly reacts with itself via aldol condensation, forming coloured oligomers and polymers if treated with proline. Additionally, hypothetical acetaldehyde Mannich products, themselves α-unbranched aldehydes, may undergo further reaction with an additional imine equivalent or eliminate to form the corresponding unsaturated aldehydes.

We have now found that these potential side reactions can be suppressed if a higher excess of acetaldehyde (5–10 equivalents) is used. Treating a variety of *N*-Boc-imines with acetaldehyde in the presence of (*S*)-proline (20 mol%) in acetonitrile at 0 °C gave the desired β-amino aldehydes in extremely high enantioselectivities and reasonable yields (Fig. 1).

The reactions of acetaldehyde with aromatic imines give products 3a to 3e in 40–58% yield and in a minimum of 98:2 enantiomeric ratio. Fural-derived imine 1f provided the Mannich product in moderate yield but maintained excellent enantioselectivity. Most remarkably, we found that even imines derived from aliphatic aldehydes, which so far had not found use in any cross-Mannich reaction of aldehydes, could be utilised. Isovaleraldehyde *N*-Boc-imine 1g reacted with acetaldehyde to give the corresponding product 3g in good yield (55%) and essentially perfect enantioselectivity (>99:1 enantiomeric ratio). Moreover, the highly reactive and unstable imine derived from propionaldehyde 1h could be used. Again, extremely high enantioselectivity was achieved although the yield is only

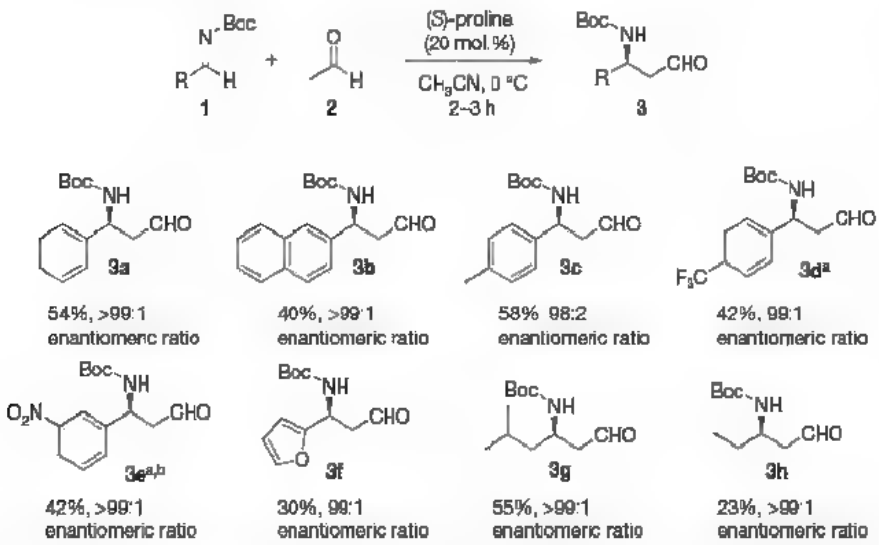

Figure 1 Highly enantioselective proline-catalysed Mannich reactions of acetaldehyde with *N*-Boc-imines. Superscript 'a' refers to the reaction being conducted at room temperature. Superscript 'b' refers to *in situ* reduction ($NaBH_4$, MeOH) to the corresponding alcohol. Yield (in %) and enantiomeric ratio were then determined.

[1]Max-Planck-Institut für Kohlenforschung, Kaiser-Wilhelm-Platz 1, D-45470 Mülheim an der Ruhr, Germany

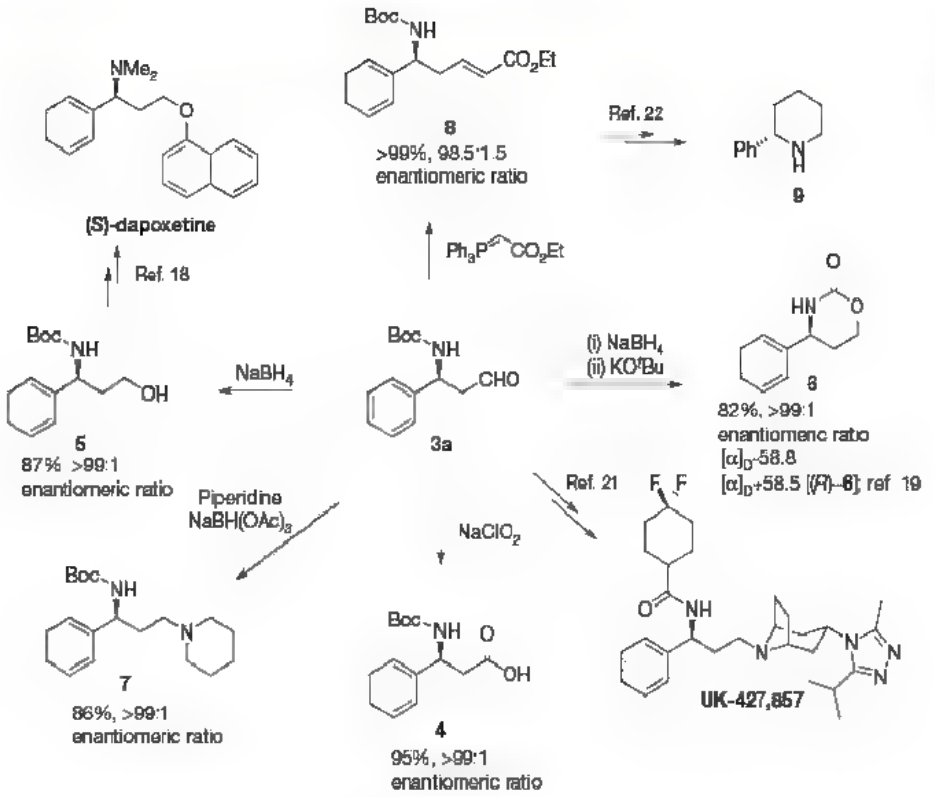

Figure 2 | Utility of Mannich product 3a in the highly enantioselective synthesis of natural products, pharmaceuticals, β^3-amino acids, and other building blocks. KO^t-Bu, potassium *tert*-butoxide

moderate in this challenging case. These are the first examples (to our knowledge) of proline-catalysed cross-Mannich reactions with aliphatic unbranched imine acceptors.

To illustrate the value of our highly enantioselective acetaldehyde Mannich reaction, several useful transformations of product **3a** have been devised (Fig. 2). For example, oxidation of the aminoaldehyde with sodium chlorite provided the corresponding *N*-Boc-amino acid **4** in high yield (95%) without loss of enantiopurity[15]. β^3-Amino acids such as **4** are commonly used in the preparation of β-peptides and our methodology complements Gellman's elegant organocatalytic approach to the isomeric β^2-amino acids[16]. Reduction of aldehyde **3a** to the corresponding alcohol (**5**) was also achieved. Alcohol **5** is a known intermediate in the synthesis of the selective serotonin reuptake inhibitor (*S*)-dapoxetine (created by Ely Lilly)[17,18]. *In situ* cyclisation of alcohol **5** to the corresponding oxazinone **6** was accomplished in high yield and the absolute configuration was determined to be (*S*) by comparison with the optical rotation ($[\alpha]_D$) of the known (*R*)-enantiomer[19]. Reductive amination of aldehyde **3a** to piperidine derivative **7** is also facile. A similar reductive amination of aldehyde **3a** was used in the synthesis of UK-427,857 (developed and marketed as Selzentry by Pfizer), a recently approved CCR5 inhibitor for the treatment of AIDS[20,21]. Wittig reaction of compound **3a** gave δ-amino-α,β-unsaturated ester **8**, an intermediate in the synthesis of 2-phenylpiperidine (**9**) (ref. 22). 2-Substituted piperidine alkaloids are found extensively throughout nature and demonstrate a wide range of biological activities[23].

Thus we have developed a proline-catalysed Mannich reaction of acetaldehyde with *N*-Boc-imines. The reaction is exceptionally enantioselective and the products are of high value for multiple synthetic applications. We are continuing to explore the enormous potential of acetaldehyde as a nucleophile in organic synthesis, including applications in organocatalytic Michael and aldol reactions. The results of these investigations will be reported elsewhere.

METHODS SUMMARY

Mannich reaction of acetaldehyde with aryl *N*-Boc-imines. A 0.74 M stock solution of acetaldehyde (9.5 ml, 7 mmol), prepared by adding 0.63 ml of redistilled acetaldehyde to 14.37 m. of CH_3CN, was transferred via syringe into a vial containing the aryl *N*-Boc-imine (1.4 mmol) at 0 °C. (*S*)-Proline (32.2 mg, 0.28 mmol) was added to the solution and the resulting mixture was stirred for 2–3 h at 0 °C. The reaction was quenched with water and the mixture was extracted with diethylether (50 ml × 3). The organic layer was washed with brine, dried over Na_2SO_4, filtered and the solvent was removed under vacuum. The pure product was isolated by silica gel column chromatography (10–20% ethyl acetate in hexane)

Mannich reaction of acetaldehyde with alkyl *N*-Boc-imines. A solution of the freshly prepared alkyl *N*-Boc-imine (derived from 0.5 mmol of the corresponding phenylsulphonyl alkylamine precursor)[24] was immediately dissolved in CH_3CN (4 ml) and cooled to −10 °C. Redistilled acetaldehyde (300 µl, 5.3 mmol) was added and the mixture was transferred to an addition funnel equipped with a cooling system set at −10 °C. In a separate round-bottomed flask a solution of (*S*)-proline (11.5 mg, 0.1 mmol) in CH_3CN (4 ml) was cooled to 0 °C. The above mixture was added to the catalyst solution over 2 h (the addition funnel was rinsed with 1 ml CH_3CN into the reaction flask) and stirred an additional 30 min at 0 °C after complete addition. The reaction was poured into a separation funnel containing H_2O (30 ml) and extracted with CH_2Cl_2 (25 ml × 3). The combined organic fractions were dried over Na_2SO_4, filtered and the solvent was removed under vacuum. Purification by silica gel column chromatography (10% ethyl acetate in hexane) gave the corresponding product.

Received 9 November 2007; accepted 22 January 2008.
Published online 20 February 2008.

1. List, B. & Yang, J. W. The organic approach to asymmetric catalysis. *Science* 313, 1584–1586 (2006)
2. Mukherjee, S., Yang, J. W., Hoffmann, S. & List, B. Asymmetric enamine catalysis. *Chem. Rev.* 107, 5471–5569 (2007).
3. Córdova, A., Notz, W. & Barbas, C. F. III. Proline-catalyzed one-step asymmetric synthesis of 5-hydroxy (2*E*)-hexenal from acetaldehyde. *J. Org. Chem.* 67, 301–303 (2002)
4. Bøgevig, A., Kumaragurubaran, N. & Jørgensen, K. A. Direct catalytic asymmetric aldol reactions of aldehydes. *Chem. Commun.* 620–621 (2002).
5. Machajewski, T. D. & Wong, C.-H. The catalytic asymmetric aldol reaction. *Angew. Chem. Int. Edn Engl.* 39, 1352–1375 (2000).
6. Goetz, G., Iwan, P., Hauer, B., Breuer, M. & Pohl, M. Continuous production of (*R*)-phenylacetylcarbinol in an enzyme-membrane reactor using a potent mutant of pyruvate decarboxylase from *Zymomonas mobilis*. *Biotechnol. Bioeng.* 74, 317–325 (2001).
7. Enders, D. & Rendenbach, B. E. M. Asymmetric Michael additions via SAMP-/RAMP-hydrazones enantioselective synthesis of β-substituted δ-oxopentanoates and δ-lactones. *Chem. Ber.* 120, 1223–1227 (1987).
8. Denmark, S. E. & Bui, T. Lewis base catalyzed enantioselective aldol addition of acetaldehyde-derived silyl enol ether to aldehydes. *J. Org. Chem.* 70, 10190–10193 (2005)

9 Boxer, M. B. & Yamamoto, H. Tris(trimethylsilyl)silyl-governed aldehyde cross-aldol cascade reaction. *J. Am. Chem. Soc.* **128**, 48–49 (2006)

10. List, B. The direct catalytic asymmetric three-component Mannich reaction. *J. Am. Chem. Soc.* **122**, 9336–9337 (2000)

11 Enders, D. & Vrettou, M. Asymmetric synthesis of (+)-polyoxamic acid via an efficient organocatalytic Mannich reaction as the key step. *Synthesis* 2155–2158 (2006)

12. Yang, J. W., Stadler, M. & List, B. Proline-catalyzed Mannich reaction of aldehydes with *N*-Boc-imines. *Angew. Chem. Int. Edn Engl.* **46**, 609–611 (2007).

13. Porter, E. A., Wang, X., Lee, H.-S., Weisblum, B. & Gellman, S. H. Non-haemolytic β-amino-acid oligomers. *Nature* **404**, 565 (2000)

14. Seebach, D. *et al.* Synthesis of β-hexa- and β-heptapeptides containing novel $\beta^{2,3}$-amino acids with two serine or two cysteine side chains –CD- and NMR-spectroscopic evidence for 3_{14}-helical secondary structures in water. *Helv. Chim. Acta* **83**, 2115–2140 (2000)

15. Ramachandran, P. V. & Burghardt, T. E. Highly diastereoselective and enantioselective preparation of homoallylic amines: application for the synthesis of β-amino acids and γ-lactams. *Chem. Eur. J.* **11**, 4387–4395 (2005).

16. Chi, Y. *et al.* Practical synthesis of enantiomerically pure β^2-amino acids via proline-catalyzed diastereoselective aminomethylation of aldehydes. *J. Am. Chem. Soc.* **129**, 6050–6055 (2007).

17 Sorbera, L. A., Castañer, J. & Castañer R. M. Dapoxetine hydrochloride. *Drugs Fut.* **29**, 1201–1205 (2004).

18. Siddiqui, S. A. & Srinivasan, K. V. Enantioselective synthesis of (*S*)-dapoxetine. *Tetrahedr. Asymm.* **18**, 2099–2103 (2007)

19 Davies, S. G. *et al.* Oxazinanones as chiral auxiliaries: synthesis and evaluation in enolate alkylations and aldol reactions. *Org. Biomol. Chem.* **4**, 2753–2768 (2006)

20 Dorr, P. *et al.* Maraviroc (UK-427,857), a potent, orally bioavailable, and selective small-molecule inhibitor of chemokine receptor CCR5 with broad-spectrum anti-human immunodeficiency virus type 1 activity. *Antimicrob. Agents Chemother.* **49**, 4721–4732 (2005)

21 Price, D. A. *et al.* Initial synthesis of UK-427,857 (Maraviroc). *Tetrahedr. Lett.* **46**, 5005–5007 (2005)

22. Davis, F. A. & Szewczyk, J. M. Synthesis and applications of nonracemic β-amino aldehydes to the asymmetric synthesis of piperidines: (+)-dihydropinidine. *Tetrahedr. Lett.* **39**, 5951–5954 (1998)

23. Fodor, G. B. & Colasanti, B. in *Alkaloids: Chemical and Biological Perspectives* (ed. Pelletier, S. W.) 1–90 (Wiley, New York, 1985)

24. Song, J., Wang, Y. & Deng, L. The Mannich reaction of malonates with simple imines catalyzed by bifunctional cinchona alkaloids: enantioselective synthesis of β-amino acids. *J. Am. Chem. Soc.* **128**, 6048–6049 (2006).

Supplementary Information is linked to the online version of the paper at www.nature.com/nature.

Acknowledgements We acknowledge support by the Max-Planck-Society, the DFG (Priority Program *Organocatalysis*), Novartis (Young Investigator Award to B.L.), Astra Zeneca (Research Award in Organic Chemistry), and by the Fonds der Chemischen Industrie. We also thank J. Rosentreter and S. Ruthe for gas chromatographic measurements, and A. Deege and H. Hinrichs for HPLC measurements.

Author Contributions J.W.Y. and M.S. planned, conducted and analysed experiments for the aromatic Mannich products. C.C. planned, conducted and analysed experiments for the aliphatic Mannich products. J.W.Y., C.C. and D.K. planned and conducted experiments and analysed the data for the compounds to demonstrate the utility of the Mannich products. B.L. designed and directed the project and wrote the manuscript with contributions by J.W.Y., C.C. and D.K. J.W.Y., C.C. and D.K. compiled most of the Supplementary Information. All authors contributed to discussions.

Author Information Reprints and permissions information is available at www.nature.com/reprints. Correspondence and requests for materials should be addressed to B.L. (list@mpi-muelheim.mpg.de).

LETTERS

Tracing the stepwise oxygenation of the Proterozoic ocean

C. Scott[1], T. W. Lyons[1], A. Bekker[2]†, Y. Shen[3], S. W. Poulton[4], X. Chu[5] & A. D. Anbar[6,7]

Biogeochemical signatures preserved in ancient sedimentary rocks provide clues to the nature and timing of the oxygenation of the Earth's atmosphere. Geochemical data[1–6] suggest that oxygenation proceeded in two broad steps near the beginning and end of the Proterozoic eon (2,500 to 542 million years ago). The oxidation state of the Proterozoic ocean between these two steps and the timing of deep-ocean oxygenation have important implications for the evolutionary course of life on Earth but remain poorly known. Here we present a new perspective on ocean oxygenation based on the authigenic accumulation of the redox-sensitive transition element molybdenum in sulphidic black shales. Accumulation of authigenic molybdenum from sea water is already seen in shales by 2,650 Myr ago; however, the small magnitudes of these enrichments reflect weak or transient[7] sources of dissolved molybdenum before about 2,200 Myr ago, consistent with minimal oxidative weathering of the continents. Enrichments indicative of persistent and vigorous oxidative weathering appear in shales deposited at roughly 2,150 Myr ago, more than 200 million years after the initial rise in atmospheric oxygen[1,2]. Subsequent expansion of sulphidic conditions after about 1,800 Myr ago (refs 8, 9) maintained a mid-Proterozoic molybdenum reservoir below 20 per cent of the modern inventory, which in turn may have acted as a nutrient feedback limiting the spatiotemporal distribution of euxinic (sulphidic) bottom waters and perhaps the evolutionary and ecological expansion of eukaryotic organisms[10]. By 551 Myr ago, molybdenum contents reflect a greatly expanded oceanic reservoir due to oxygenation of the deep ocean and corresponding decrease in sulphidic conditions in the sediments and water column.

Numerous geochemical proxies converge on a significant and unidirectional oxygenation of the Earth's atmosphere at about 2,400 Myr ago (refs 1–4), but the response of the ocean to this event is not well constrained. Early workers invoked deep-ocean oxygenation and titration of dissolved iron to explain the disappearance of banded iron formations after about 1,800 Myr ago (ref. 11), but Canfield[8] proposed instead the expansion of sulphidic environments and removal of iron sulphides in response to greater oxidative continental weathering and delivery of sulphur to the ocean. This proposal, which invokes an oxidized surface ocean and a sulphidic deep ocean, finds support in C–S–Fe systematics[9,12,13], molybdenum isotope relationships[14] and biomarker studies[15] from Proterozoic sedimentary rocks. However, the nature and extent of these sulphidic environments is unclear. Canfield[8] envisaged a widely euxinic deep ocean where sulphide accumulated in the water column, but the deep ocean may have been dominated by less reducing conditions[16] where sulphide was confined to pore waters beneath a low-oxygen water column. Regardless, sequestration of trace metals[17] in association with the extension of sulphidic environments has biological implications[10], as many redox-sensitive transition metals are important micronutrients (for example, Fe and Mo).

The strength of molybdenum as a tracer of the Earth's oxygenation results from its uniquely bimodal geochemical characteristics. The primary source of dissolved molybdenum in the modern ocean is riverine delivery of molybdate (MoO_4^{2-}) liberated during oxidative weathering of continental crust containing on average 1 to 2 p.p.m. molybdenum[18,19]. Molybdate, however, is highly conservative with an average present-day seawater concentration of ~100 nM—greater than any other transition element—and an oceanic residence time of ~700,000 yr (see Supplementary Information for a discussion of the modern oceanic Mo budget). The only significant sink for molybdate in well-oxygenated environments is by co-precipitation and burial with Mn-oxyhydroxides[18], a slowly occurring process. Although oxygenated environments cover most of the sea floor today, removal of molybdate in association with Mn-oxyhydroxides accounts for only 35% of the annual riverine flux (see Supplementary Information).

Today, the remainder of the riverine flux is removed in spatially limited sulphidic settings[18] where molybdate is converted to particle-reactive thiomolybdates ($MoO_xS_{4-x}^{2-}$)[20] and Mo removal by organic matter and other reduced substrates outpaces that of oxygenated environments by a factor of 200 to 5,000 (see Supplementary Information). The low end of this range represents non-euxinic sites where hydrogen sulphide is restricted to the sediments, and Mo enrichment is dependent on diffusion of MoO_4^{2-} into pore waters where conversion to thiomolybdates occurs. At the upper end of this range are euxinic basins where sulphide and the highly reactive tetrathiomolybdate ion (MoS_4^{2-}) are present in the water column.

Persistent euxinia is the extreme endmember of sulphidic conditions, and although euxinic shales are common in the rock record, few examples of euxinic basins exist today, with the Black Sea and Cariaco Basin (Venezuela) being the two largest examples[21,22]. Where dissolved Mo is readily available, as in the Cariaco Basin, sediment Mo concentrations (up to 184 p.p.m.; ref. 22) exceed average continental crust by two orders of magnitude, and elevated ratios of Mo to total organic carbon (average Mo/TOC ratio 26 p.p.m. Mo per wt% C) develop[17,21]. Where Mo is exhausted in the water column, as in the highly restricted Black Sea (5 nM Mo below the chemocline)[23], the magnitude of enrichment and Mo/TOC ratios (average 28 p.p.m. and 4.5 p.p.m. per wt%, respectively) drop correspondingly[17]. These characteristics of Black Sea sediments—that is, Mo concentrations and Mo/TOC ratios that are depressed relative to most

[1]Department of Earth Sciences, University of California, Riverside, California 92521, USA. [2]Geophysical Laboratory, Carnegie Institution of Washington, Washington DC 20015, USA. [3]Département des Sciences de la Terre et de l'Atmosphère, Université du Québec à Montréal, H3C 3P8, Canada. [4]School of Civil Engineering and Geosciences, Newcastle University, Newcastle upon Tyne, NE1 7RU, UK. [5]Key Laboratory of Mineral Resources, Institute of Geology and Geophysics, Chinese Academy of Sciences, Beijing 100029, China. [6]School of Earth & Space Exploration, [7]Department of Chemistry and Biochemistry, Arizona State University, Tempe, Arizona 85287, USA. †Present address: Department of Geological Sciences, University of Manitoba, Winnipeg, Manitoba, R3T 2N2, Canada

Phanerozoic euxinic shales and sediments (Figs 1 and 2)—provide an analogue for Mo-deficient ancient oceans[17].

From this perspective, the magnitudes of Mo enrichments and Mo/TOC in euxinic black shales reflect the size of the oceanic Mo reservoir as determined by the weathering flux and the relative influence of the sulphidic and oxic sinks. In the modern ocean, sulphide-rich pore waters and bottom waters represent <2% of the sea floor yet account for 65% of Mo removal (see Supplementary Information). It follows that the expansion of sulphidic environments in the past would have depressed the concentration of dissolved Mo in the ocean until, as in the Black Sea, the magnitude of euxinic enrichment was affected.

To constrain deep-ocean redox state in the early ocean we have measured Mo concentrations ([Mo]) and TOC and generated Mo/TOC ratios (Figs 1 and 2) for a diverse sample set of Precambrian black shales (≤2,700 Myr) and assembled them with published data from Precambrian and Phanerozoic black shales (see Supplementary Information). For interpretation of the size of the oceanic Mo reservoir we focus on units shown independently to reflect the euxinic endmember based on proxies such as the degree of pyritization (DOP) and/or ratios of highly reactive to total Fe (Fe_{HR}/Fe_T) and total iron to aluminium[24]. The motivation for this filter is the exclusion of non-euxinic black shales where the magnitude of Mo enrichment does not necessarily reflect the size of the oceanic reservoir.

From our record of [Mo] and Mo/TOC we delineate three stages of Mo cycling (Figs 1 and 2) based on marked shifts in the magnitudes of enrichment and Mo/TOC. During stage 1, [Mo] and Mo/TOC are typically variable but low, requiring only small amounts of dissolved Mo in the ocean. A prominent enrichment of Mo is recorded in the 2,500-Myr Mount McRae shale[7], but Mo/TOC rises to only ~3 p.p.m. per wt% during this event, relative to a background of ~1.5 p.p.m. per wt%, suggesting that dissolved Mo concentrations remained well below those of the modern deep Black Sea. Such enrichments may reflect mild oxidative weathering of continental materials during the Archaean eon, including transient events of slightly elevated O_2 in the surface ocean and atmosphere, consistent with evidence for the presence of oxygenic photosynthesis by 2,700 Myr ago[25]. Anbar *et al.*[7] proposed recently that continental pyrite and molybdenite could have been oxidized even at the very low partial pressure of oxygen (pO_2) suggested for the atmosphere at this time (less than 10^{-5} of the present level) on the basis of temporal distributions of non-mass-dependent sulphur isotope fractionations[26]. Other possibilities include submarine oxidative weathering in shallow photosynthetic hotspots or ephemeral atmospheric oxygenation[7]. Alternatively, hydrothermal inputs might have supplied small amounts of dissolved Mo to local sulphidic environments. Whether oxidative or hydrothermal, [Mo] and Mo/TOC suggest that the sources of Mo during this first stage were weak or transient and do not reflect vigorous and sustained oxidative weathering of continental crust.

During the second stage of Mo cycling, a persistent oxidative source and strong oceanic sinks resulted in a Proterozoic Mo reservoir intermediate between those of the Archaean and Phanerozoic eons. Enrichments of up to 74 p.p.m. occur in shales deposited between 2,200 and 2,000 Myr ago, coincident with a prominent carbon excursion thought to reflect increases in organic carbon burial and atmospheric O_2 content[1,2]. Coupled burial of Mo and organic carbon would act to pull down the oceanic Mo reservoir and therefore mute the level of enrichment in individual shales. The rise in Mo and Mo/TOC in stage 2 beyond the weaker and possibly transitory enrichments seen earlier (Figs 1 and 2) suggests a larger compensating riverine flux from increased oxidative weathering. Hydrogen sulphide required for Mo uptake in the shales would also increase with the greater delivery of sulphate to the ocean. The gap of ~200 million years between the Great Oxidation Event at ~2,400 Myr and the first persistent enrichment of Mo in shales is intriguing and may track increasing continental sources through repeated cycles of black shale deposition, exhumation and weathering as described by Hannah *et al.*[27]. The 'boundary' between stages 1 and 2 is inherently diffuse (Figs 1 and 2) owing to the complexity of the ocean's initial response to atmospheric oxygenation and poor preservation of the ancient Earth record. However, across this transition, [Mo] and Mo/TOC ratios exceed those observed before and support our arguments for a fundamental shift in ocean–atmosphere redox and associated Mo cycling at that time.

With [Mo] and Mo/TOC from Black Sea sediments[17] as our analogue for Proterozoic black shales, we estimate that the concentration of dissolved Mo remained less than 10–20% of the modern ocean for at least 800 Myr following the initiation of intense Mo cycling at about 2,200 Myr. Considering arguments for an increase in weathering of Mo-bearing sulphides on the continents during the Proterozoic[11,28] and corresponding increase in riverine Mo flux to the ocean, we interpret the suppressed size of the oceanic reservoir as reflecting the persistence or even expansion of sulphidic sinks as opposed to a decrease in the riverine flux. It is important to stress that pervasive euxinia (that is, a sulphidic water column) is not required to exhaust the oceanic Mo reservoir. With a modern riverine flux, expansion of sulphidic pore waters, commonly found below weakly oxygenated bottom waters, to 10% of the sea floor would deplete the oceanic reservoir by 90% in ~200,000 yr (see Supplementary Information). This interpretation of the modern Mo budget does not preclude a more common occurrence of euxinic conditions during the Proterozoic[8,9] but demonstrates that less extreme conditions are required to explain the Mo record. Indeed, global euxinia

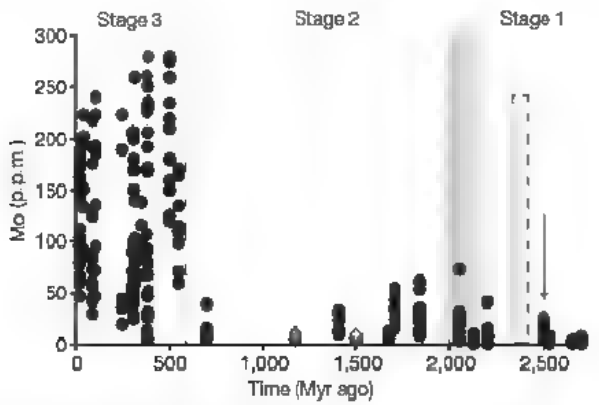

Figure 1 | Temporal trends in Mo enrichment in black shales. Black circles are euxinic examples; grey diamonds refer to non-euxinic, organic-rich shales. The gradient represents the diffuse stage 1–2 boundary as defined in the text. The arrow marks the Mount McRae 'whiff' interval[7]; the dashed area is the Great Oxidation Event as defined by the multiple sulphur isotope record[2]. Stratigraphic and chronological details are provided in the Supplementary Information.

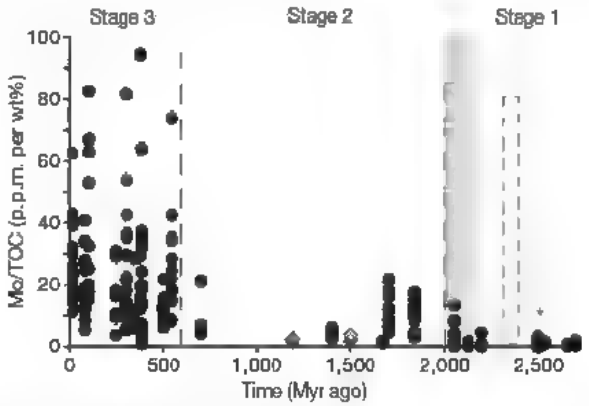

Figure 2 | Temporal trends in Mo/TOC ratios in euxinic black shales. Symbol and boundary descriptions as in Fig. 1.

may have been difficult to achieve and sustain owing to the connection between Mo availability and the nitrogen cycle[10,29].

Recent laboratory results demonstrate that below ~5% of present oceanic concentrations, Mo limitation begins to depress growth rates and rates of nitrogen fixation in cultured cyanobacteria[29]. These results and our estimates for the size of the oceanic reservoir are consistent with the hypothesis[10] that the drawdown of Mo into sulphidic environments may have worked to restrict the occurrence and the evolutionary path of eukaryotes through the bioinorganic bridge linking Mo to N bioavailability. A corollary is that this bioinorganic bridge would also act as a negative feedback limiting the spatial and temporal extent of sulphidic conditions, because organic matter is required for the exhaustion of oxygen and other oxidants as well as subsequent bacterially mediated reduction of sulphate to sulphide. Where productivity is depressed, sulphidic conditions are difficult to maintain.

This feedback mechanism may explain the apparent decline in euxinic deposition after 1,400 Myr ago (Figs 1 and 2). Our sample set includes two well-preserved black shales from the Belt Supergroup in Montana, USA (~1,500 Myr), and the Borden Basin, Canada (~1,200 Myr), which represent restricted marine settings[30] ideally suited for the development of a sulphidic water column. However, these units are characterized instead by degrees of pyritization (0.2–0.4), Mo concentrations (2–12 p.p.m.) and Mo/TOC ratios typical of Phanerozoic non-euxinic shales. Although it is important to stress that artefacts of preservation and sampling complicate our search for euxinic examples, the presence of these well-preserved, non-euxinic black shales may be telling us that similar conditions were common following 1,400 Myr. Molybdenum-sequestering conditions could drive Mo-related nitrogen stress—not only in the absence of euxinic conditions, but also to their exclusion.

In stage 3, extreme Mo enrichments and elevated Mo/TOC typical of Phanerozoic black shales reflect a greatly expanded oceanic Mo reservoir requiring deep-ocean oxygenation with only limited Mo-enriching sulphidic environments. Unlike the more diffuse stage 1–2 boundary, which reflects a complex source–sink interplay, an abrupt step to this final stage of Mo cycling is apparent in the 551-Myr Miaohe member of the Doushantuo Formation, south China (Figs 1 and 2, and Supplementary Information). Samples from the 663-Myr Datangpo Formation, also in south China, reveal [Mo] and Mo/TOC typical of the earlier Proterozoic ocean. Interpretations of the chemistry of the Datangpo Formation are complicated by its temporal proximity to the Sturtian glaciation, yet the possibility remains that it captures a continuation of stage-2 cycling. If so, the Mo record brackets the timing of deep-ocean oxygenation to between 663 and 551 Myr, consistent with recent C–S–Fe studies of Late Neoproterozoic successions arguing for deep ocean oxygenated at 580 Myr ago[5,6] and subsequent radiation of large, structurally complex life forms. Our interpretation of Mo cycling in the Late Neoproterozoic suggests that modern redox and nutrient cycles were well established by 551 Myr, shortly after the initial oxidation of the deep ocean, and that the appearance of the first large animals followed not only the oxidation of the deep ocean but also the establishment of modern biogeochemical cycles.

METHODS SUMMARY

For samples analysed in this study, euxinic deposition is constrained by degree of pyritization, defined as $(Fe_{pyrite}/(Fe_{pyrite} + Fe_{HCl}))$. The term Fe_{HCl} means acid-soluble iron, present primarily as Fe-oxides and Fe-carbonate, which will react readily with free sulphide to form pyrite. We extracted and quantified pyrite sulphur in powdered shale samples by chromium reduction and calculated Fe_{pyrite} stoichiometrically (FeS_2). We extracted Fe_{HCl} with boiling, concentrated HCl. The concentration of HCl-soluble Fe is determined spectrophotometrically. A DOP value of 0.6 is a conservative lower limit for values delineating a sulphidic water column. Total organic carbon was determined on an Eltra CS-500 infrared carbon/sulphur analyser equipped with acidification and furnace modules. Total carbon was determined by combustion, and total inorganic carbon was measured by acidification. TOC was calculated by difference. For trace metal analyses, samples were ashed at 850 °C for 24 h, and the mass lost on ignition was recorded. Ashed splits were dissolved following standard HNO_3–HCl–HF digestion methods and analysed by quadrupole inductively coupled plasma mass spectrometry at approximately 2,000-fold dilution. We used a US Geological Survey standard Devonian reference material (SDO-1) as our external standard.

Full Methods and any associated references are available in the online version of the paper at www.nature.com/nature.

Received 15 June 2007; accepted 31 January 2008.

1. Karhu, J. A. & Holland, H. D. Carbon isotopes and the rise of atmospheric oxygen. *Geology* 24, 867–870 (1996).
2. Bekker, A. *et al.* Dating the rise of atmospheric oxygen. *Nature* 427, 117–120 (2004).
3. Farquhar, J. & Wing, B. A. Multiple sulfur isotopes and the evolution of the atmosphere. *Earth Planet. Sci. Lett.* 213, 1–13 (2003).
4. Rouxel, O. J., Bekker, A. & Edwards, K. J. Iron isotope constraints on the Archean and Paleoproterozoic ocean redox state. *Science* 307, 1088–1091 (2005).
5. Canfield, D. E., Poulton, S. W. & Narbonne, G. M. Late-Neoproterozoic deep-ocean oxygenation and the rise of animal life. *Science* 315, 92–95 (2007).
6. Fike, D. A., Grotzinger, J. P., Pratt, L. M. & Summons, R. E. Oxidation of the Ediacaran ocean. *Nature* 444, 744–747 (2006).
7. Anbar, A. D. *et al.* A whiff of oxygen before the Great Oxidation Event? *Science* 317, 1903–1906 (2007).
8. Canfield, D. E. A new model for Proterozoic ocean chemistry. *Nature* 396, 450–453 (1998).
9. Poulton, S. W., Fralick, P. W. & Canfield, D. E. The transition to a sulphidic ocean ~1.84 billion years ago. *Nature* 431, 173–177 (2004).
10. Anbar, A. D. & Knoll, A. H. Proterozoic ocean chemistry and evolution: A bioinorganic bridge? *Science* 297, 1137–1142 (2002).
11. Holland, H. D. *The Chemical Evolution of the Atmosphere and Oceans* (Princeton Univ. Press, Princeton N., 1984).
12. Shen, Y., Canfield, D. E. & Knoll, A. H. Middle Proterozoic ocean chemistry: Evidence from the McArthur Basin, northern Australia. *Am. J. Sci.* 302, 81–109 (2002).
13. Shen, Y., Knoll, A. H. & Walter, M. R. Evidence for low sulphate and anoxia in a mid-Proterozoic marine basin. *Nature* 423, 632–635 (2003).
14. Arnold, G. L., Anbar, A. D., Barling, J. & Lyons, T. W. Molybdenum isotope evidence for widespread anoxia in Mid-Proterozoic oceans. *Science* 304, 87–90 (2004).
15. Brocks, J. J. *et al.* Biomarker evidence for green and purple sulphur bacteria in a stratified Paleoproterozoic sea. *Nature* 437, 866–870 (2005).
16. Slack, J. F., Grenne, T., Bekker, A., Rouxel, O. J. & Lindberg, P. A. Suboxic deep seawater in the late Paleoproterozoic: Evidence from hematitic chert and iron formation related to seafloor-hydrothermal sulfide deposits, central Arizona, USA. *Earth Planet. Sci. Lett.* 255, 243–256 (2007).
17. Algeo, T. J. & Lyons, T. W. Mo–total organic carbon covariation in modern anoxic marine environments: Implications for analysis of paleoredox and paleohydrographic conditions. *Paleoceanography* 21, doi:10.1029/2004PA001112 (2006).
18. Bertine, K. K. & Turekian, K. K. Molybdenum in marine deposits. *Geochim. Cosmochim. Acta* 37, 1415–1434 (1973).
19. Taylor, S. R. & McLennan, S. M. The geochemical evolution of the continental crust. *Rev. Geophys.* 33, 241–265 (1995).
20. Helz, G. R. *et al.* Mechanism of molybdenum removal from the sea and its concentration in black shales: EXAFS evidence. *Geochim. Cosmochim. Acta* 60, 3631–3642 (1996).
21. Lyons, T. W. & Berner, R. B. Carbon–sulfur–iron systematics of the uppermost deep-water sediments of the Black Sea. *Chem. Geol.* 99, 1–27 (1992).
22. Lyons, T. W., Werne, J. P., Hollander, D. J. & Murray, R. W. Contrasting sulfur geochemistry and Fe/Al and Mo/Al ratios across the last oxic-to-anoxic transition in the Cariaco Basin, Venezuela. *Chem. Geol.* 195, 131–157 (2003).
23. Emerson, S. R. & Huested, S. S. Ocean anoxia and the concentrations of molybdenum and vanadium in seawater. *Mar. Chem.* 34, 177–196 (1991).
24. Lyons, T. W. & Severmann, S. A critical look at iron paleoredox proxies: New insights from modern euxinic marine basins. *Geochim. Cosmochim. Acta* 70, 5698–5722 (2006).
25. Brocks, J. J., Logan, G. A., Buick, R. & Summons, R. E. Archean molecular fossils and the early rise of eukaryotes. *Science* 285, 1033–1036 (1999).
26. Kaufman, A. J. *et al.* Late Archean biospheric oxygenation and atmospheric evolution. *Science* 317, 1900–1903 (2007).
27. Hannah, J. L., Bekker, A., Stein, H. J., Markey, R. J. & Holland, H. D. Primitive Os and 2316 Ma age for marine shale: implications for Paleoproterozoic glacial events and the rise of atmospheric oxygen. *Earth Planet. Sci. Lett.* 225, 43–52 (2004).
28. Kah, L. C., Lyons, T. W. & Frank, T. D. Low marine sulphate and protracted oxygenation of the Proterozoic biosphere. *Nature* 431, 834–838 (2004).
29. Zerkle, A. L., House, C. H., Cox, R. P. & Canfield, D. E. Metal limitation of cyanobacterial N_2 fixation and implications for the Precambrian nitrogen cycle. *Geobiology* 4, 285–297 (2006).

30. Lyons, T. W., Luepke, J. J., Schreiber, M. E. & Zieg, G. A. Sulfur geochemical constraints on Mesoproterozoic restricted marine deposition: lower Belt Supergroup, northwestern United States. *Geochim. Cosmochim. Acta* 64, 427–437 (2000).

Supplementary Information is linked to the online version of the paper at www.nature.com/nature.

Acknowledgements This study was funded by the US NSF-EAR and NASA Astrobiology Institute. A.B. and Y.S. were funded by NSERC. S.W.P. acknowledges financial support from Danmarks Grundforskningsfond and a NERC Research Fellowship. X.C. was funded by NNFSC. The manuscript was improved by comments from J. Hayes and D. Vance. We thank B. Krapež, N. Beukes, F. Gauthier-Lafaye, P. Medvedev, D. Winston and the geological surveys of South Africa and Botswana for field support and access to sample collections. G. Arnold, G. Gordon and S. Severmann provided analytical support. B. Gill compiled Phanerozoic data.

Author Information Reprints and permissions information is available at www.nature.com/reprints. Correspondence and requests for materials should be addressed to C.S. (cscott002@ucr.edu).

LETTERS

Lower-crustal intrusion on the North Atlantic continental margin

R. S. White[1], L. K. Smith[1]†, A. W. Roberts[1], P. A. F. Christie[2], N. J. Kusznir[3] & the rest of the iSIMM Team‡

When continents break apart, the rifting is sometimes accompanied by the production of large volumes of molten rock[1–3]. The total melt volume, however, is uncertain, because only part of it has erupted at the surface. Furthermore, the cause of the magmatism is still disputed—specifically, whether or not it is due to increased mantle temperatures. We recorded deep-penetration normal-incidence and wide-angle seismic profiles across the Faroe and Hatton Bank volcanic margins in the northeast Atlantic. Here we show that near the Faroe Islands, for every 1 km along strike, 360–400 km^3 of basalt is extruded, while 540–600 km^3 is intruded into the continent–ocean transition. We find that lower-crustal intrusions are focused mainly into a narrow zone ~50 km wide on the transition, although extruded basalts flow more than 100 km from the rift. Seismic profiles show that the melt is intruded into the lower crust as sills, which cross-cut the continental fabric, rather than as an 'underplate' of 100 per cent melt, as has often been assumed. Evidence from the measured seismic velocities and from igneous thicknesses are consistent with the dominant control on melt production being increased mantle temperatures, with no requirement for either significant active small-scale mantle convection under the rift or the presence of fertile mantle at the time of continental break-up, as has previously been suggested for the North Atlantic Ocean[4–6].

The Hatton Bank continental margin in the northeast Atlantic was one of the first where high-velocity (>7.2 km s^{-1}) lower crust was identified as being caused by magmatism during continental break-up above a mantle thermal anomaly[7]. High-velocity lower crust is now known to be ubiquitous on volcanic continental margins, including all those in the northern North Atlantic[3–11]. Although the high-velocity section is commonly referred to as 'underplated' igneous material, we show from seismic reflection profiles and tomographic velocity inversions of wide-angle data that on the continent–ocean transition (COT) it actually represents continental crust intruded by sills. Failure to recognize the influence of residual continental crust on the lower-crustal seismic velocity may be responsible for interpretations that infer lower mantle temperatures, active small-scale mantle convection and the presence of fertile mantle during continental break-up[4–6].

We report results from two iSIMM (integrated Seismic Imaging and Modelling of Margins)[12–14] transects that imaged the reflectivity and

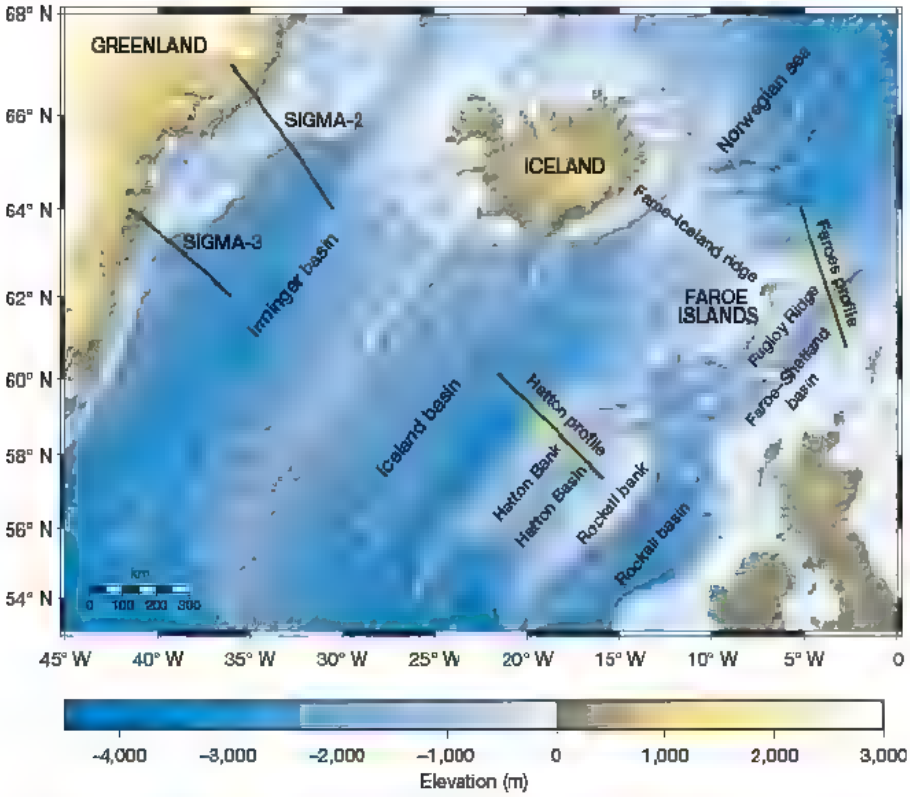

Figure 1 | Location of seismic profiles across the North Atlantic rifted continental margins[4,5,13,14]. The portions of Hatton and Faroes profiles highlighted in yellow are shown in Fig. 2.

[1]Bullard Laboratories, University of Cambridge, Madingley Road, Cambridge CB3 0EZ, UK. [2]Schlumberger Cambridge Research, High Cross, Madingley Road, Cambridge CB3 0EL, UK. [3]Department of Earth Sciences, University of Liverpool, Liverpool L69 3BX, UK. †Present address: BP, Burnside Road, Farburn Industrial Estate, Dyce, Aberdeen AB21 7PB, UK. ‡A list of participants and their affiliations appears at the end of the paper.

velocity structure of the COT. The profiles are 800 km apart (Fig. 1), but exhibit remarkably similar structures. One profile crosses the Hatton margin[7,14], the other crosses the margin near the Faroe Islands, close to the centre of the inferred mantle thermal anomaly[1,8,13]. Both are in similar geological settings, with late Mesozoic failed rifts (the Hatton and Faroe–Shetland basins) separated from the new ocean basins by continental blocks (Hatton Bank and the Fugloy Ridge). We recorded multiple crustal refractions and wide-angle Mohorovičić discontinuity (Moho) reflections, from which two-dimensional velocity models were derived by tomographic inversions (Fig. 2a, b).

A seismic reflection profile along the Faroes line imaged the internal structure of both the extrusive basalt flows and the intruded lower crust (Fig. 2c). Post-rift sediments less than 1 km thick (purple and blue in Fig. 2), lie above basalt flows with seismic velocities that increase downwards from ~4.5 km s^{-1} to ~5.5 km s^{-1}, probably owing to a decrease in weathering and the closure and infilling of cracks and voids with secondary minerals[15]. The basalts reach 7 km thick at the COT and extend ~100 km landward before feathering out in the Faroe–Shetland trough[16]. The base of the basalt flows on the Faroes margin is marked by lower-velocity material (~4.2–4.5 km s^{-1}), presumed to consist of hyaloclastites and early Palaeocene sediments intruded by sills (Fig. 2b, c and Fig. 3b; see also Supplementary Figs 6 and 7, which show examples of the constraints from wide-angle ocean bottom seismometer (OBS) data used to model the low velocity zone). Over the COT, seaward-dipping reflector sequences (SDRS) are imaged well (Fig. 2c, and enlargement in Supplementary Fig. 8). Their arcuate shape results from crustal stretching and subsidence contemporaneous with basalt extrusion, and though the present dip is seaward, the lava was emplaced by landward flow from a subaerial rift[17]. Landward of the COT, flow across the continental hinterland creates layered sub-horizontal basalts.

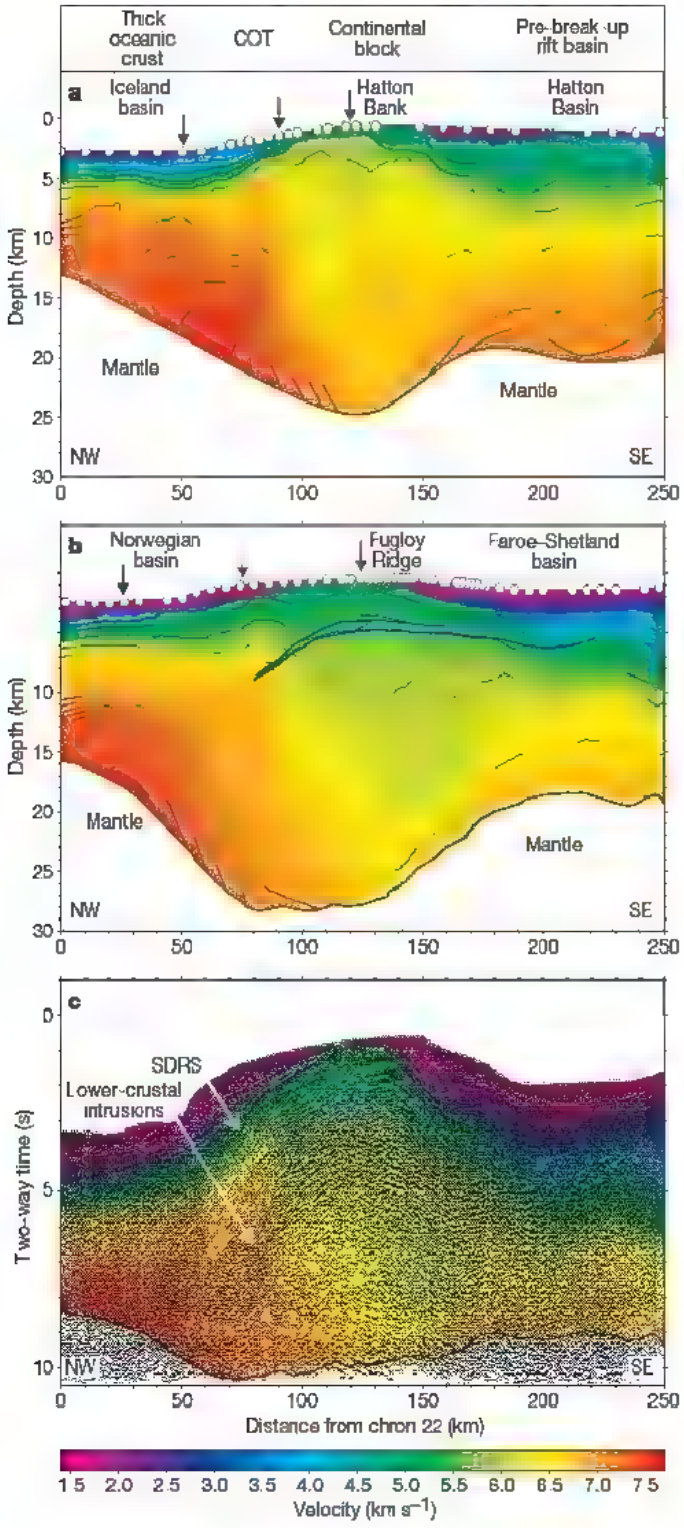

In the lower crust of the COT, strong sub-horizontal reflections interpreted as sills intrude the dipping fabric of the Archaean continental crust (Fig. 2c). On a depth section the continental fabric dips over 10° seaward, while the intersecting sills exhibit variable dips mostly within ±5° of the horizontal, consistent with the variable 'saucer' shapes of sills imaged in sedimentary sections. Synthetic seismogram modelling suggests that the reflections probably represent complex interference patterns from multiple sills, rather than from individual intrusive bodies[18]. They are most prominent at mid-crustal depths, with the reflectivity decreasing downwards as the proportion of intruded material in the crust increases. On the adjacent Faroe–Iceland ridge, with fully igneous crust that is 30–35 km thick[19], little lower-crustal layering is imaged, despite massive melt intrusion[20]. The absence of layering on the Faroe–Iceland ridge and in the deepest part of the COT crust may be explained by low impedance contrasts between sills injected into an igneous section with the same composition[20], in contrast to their injection into the remnant continental crust of the COT at shallower levels.

The COT region with lower-crustal sills coincides with increased seismic velocities compared to the adjacent continental crust of Hatton Bank and the Fugloy Ridge (Fig. 2a, b). The highest lower-crustal velocities are not reached until the onset of mature seafloor spreading, which is marked by linear magnetic anomalies and coincides with the termination of SDRS and submarine rather than subaerial volcanism[21]. We interpret this oceanic crust as comprising 100% igneous rock with restricted lateral flow, in contrast to the large distances over which subaerial basalts flowed from the COT rift.

If the continental velocity–depth profile is taken as an end-member, while the earliest oceanic crust beyond the termination of the SDRS represents the velocity of the fully igneous crust (Fig. 3a, b), then the lower-crustal igneous volume fraction under the COT can be calculated from the average seismic velocity using a linear mixing law. The total melt volume at the COT on the Faroes profile, including the

Figure 2 | Seismic velocity profiles. Seismic velocity structure of crust across the continent–ocean transition near Hatton Bank (**a**) and the Faroe Islands (**b**). **c**, Coincident seismic reflection profile across the Faroes margin with velocity field superimposed. Lava flows are imaged as SDRS between 50–90 km along the Faroes profile and as sub-horizontal layered basalts at >90 km. Lower-crustal layering coincident with high (>7.0 km s^{-1}) velocities, caused by igneous intrusions, lies beneath the basalts on the continent–ocean transition, terminating at ~90 km against continental crust with markedly lower velocities. For line locations see Fig. 1. Profiles are aligned with 0 km distance at seafloor spreading magnetic anomaly chron 22. Arrows mark locations of velocity curves shown in Fig. 3. See Supplementary Information for enlargement of COT portion of reflection profile shown in **c**. Reflection profile processing included source designature, multiple suppression and post-stack time migration. Velocities of post-rift Cenozoic sediments (purple) are constrained by semblance move-out analysis of reflections recorded on the hydrophone streamer and sub-sediment crustal velocities are constrained by tomography using wide-angle reflections and diving waves from OBS data (locations shown by white circles at the sea floor). Colour bands are at 0.1 km s^{-1} intervals, with contours above 7.0 km s^{-1} spaced every 0.1 km s^{-1} to highlight the lower-crustal velocity.

extrusive basalts from the reflection image, is about 900–1,000 km^3 per kilometre along strike. The ratio of intruded to extruded igneous rock is 1.5:1, consistent with suggestions on petrological grounds that the intrusive volume must be 'at least as large as the amount of erupted surface lava'[22] and more precise than previous estimates which range from 0.25:1 to 4:1 (ref. 2).

Good velocity and thickness constraints on the igneous component of the crust allow us to address the controversy over whether the large volumes of melt on volcanic margins were produced by rifting above abnormally hot mantle (a 'mantle plume')[1–3,7–9,19], or by active small-scale convection of lower-temperature mantle under the rift, or by melting enriched, more-fertile mantle[4–6]. Increased mantle temperatures cause increased melt thickness h and increased seismic velocity v_p of the igneous rock generated by mantle decompression beneath rifts[1,4–6,23]. On a h–v_p plot (Fig. 3d), the filled circle shows the average for normal oceanic crust[24,25], with the yellow arrow showing the trend predicted for passive decompression melting of normal mantle as its temperature increases. Active mantle upwelling with no temperature change causes increased igneous thickness with little change in seismic velocity, whereas fertile mantle could generate an increase in igneous thickness and a decrease in seismic velocity (solid black arrows in Fig. 3d). Crustal melt fractionation causes the lower-crustal velocity to increase, while melt fractionated deeper in the mantle causes it to decrease (broken black arrows in Fig. 3d)[6]. These effects work in opposite directions, so they may (to first order) cancel one another. The h–v_p curves in Fig. 3d are calculated for primary melt crystallized at the average pressure (230 MPa) and temperature (150 °C) of the lower oceanic crust on our profiles. We follow ref. 6 in using the average lower-crustal velocity as the best available estimate of the primary igneous composition.

The h–v_p data from the oceanic portions of our profiles and from the SIGMA-3 profile on the Greenland margin conjugate to our Hatton profile[5] (Fig. 1) show a clear trend towards normal oceanic crust (filled symbols in Fig. 3c). This trend can be explained solely by passive decompression melting of normal mantle with a temperature decrease of about 75 °C during seafloor spreading after continental break-up. However, the portions of both the Hatton and Faroes profiles with SDRS show trends of decreasing v_p and increasing thicknesses in a landward direction (open symbols in Fig. 3c). At first, this appears to suggest that the mantle temperature was lower (lower v_p) when the SDRS were formed than when the subsequent oceanic crust was generated, with the observed crustal thickness requiring active local convection under the rift at up to ten times the passive upwelling rate[6]. It is also possible that the mantle was more fertile. This is the interpretation of similar h–v_p patterns found for crust beneath SDRS (termed 'transitional crust' on the SIGMA-2

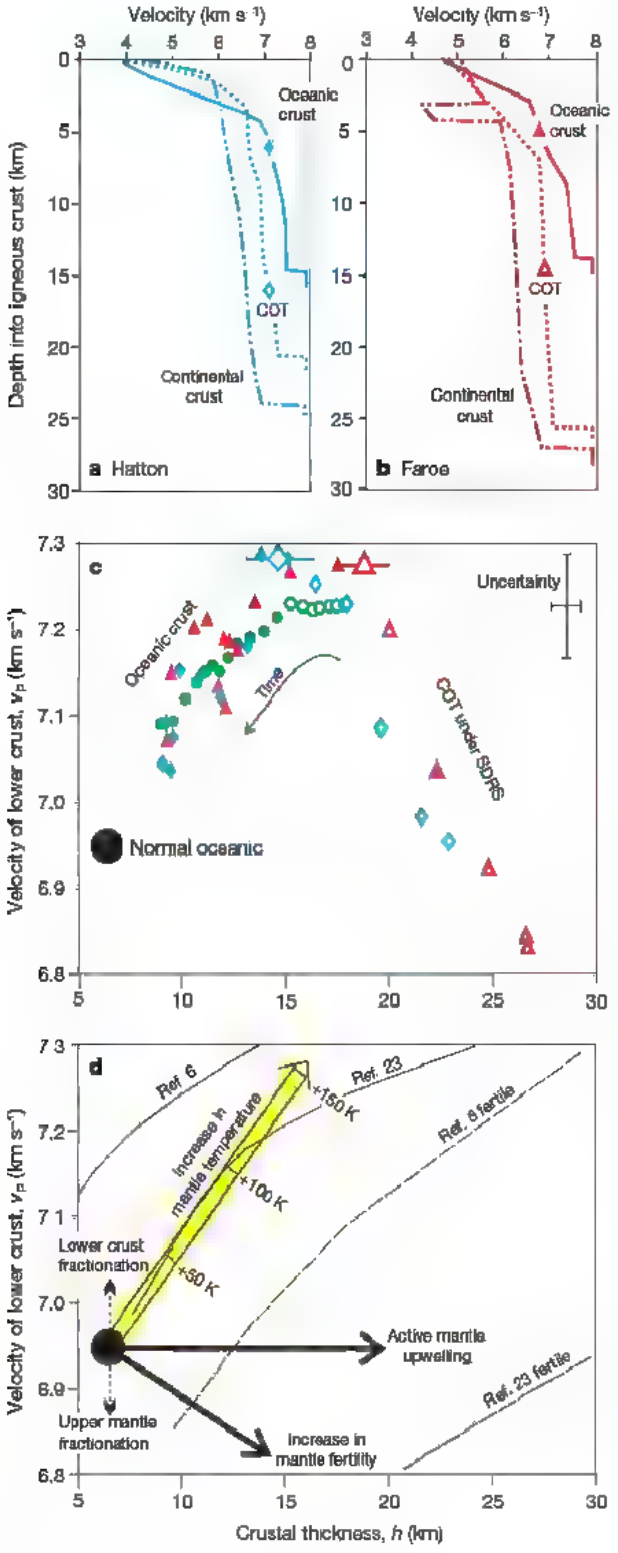

Figure 3 | Crustal velocities and thicknesses. Seismic velocity variation versus depth beneath the base of the sediments at three representative locations on the oceanic crust, on the COT, and on the continental block of the Hatton Bank profile (**a**) and the Faroe profile (**b**). Locations of velocity curves are shown by arrows on Fig. 2. The oceanic crust and lower continental crust are the two end-members, while the COT crust exhibits lower-crustal velocities intermediate between the two owing to intrusion of continental crust by igneous sills. **c**, Average crustal thickness and lower-crustal velocity calculated every 10 km along the Faroes profile (red triangles), the Hatton profile (blue diamonds), including the oceanward end of our profiles beyond those shown in Fig. 2 (ref. 21), and the conjugate east Greenland SIGMA-3 profile[5] after correction to our reference pressure and temperature (green circles). Filled symbols are from oceanic crust; open symbols are from crust lying on the COT beneath arcuate SDRS. The pair of larger triangle and diamond symbols shows the limits of the total (intrusive plus extrusive) igneous thickness across the Faroes and Hatton COTs, respectively. The extrusive volume is calculated from the seismic reflection images and the intrusive volume is calculated from lower-crustal velocity using a linear mixing law between lower continental crust and fully igneous crust. The standard deviations typical of the data points are shown in the top right corner; the theoretical curves have similar uncertainties. The arrow marked 'time' shows the direction in which the basalts become younger. **d**, Theoretical igneous crustal thickness versus seismic velocity of primary melts generated by passive mantle upwelling under an oceanic rift calculated by refs 6 and 23: solid lines are from normal pyrolitic mantle, and broken lines from fertile mantle. Curves are for a reference pressure of 230 MPa and temperature of 150 °C, which are representative of conditions in the lower-crust of the oceanic data in our results. The filled circle shows the average thickness and lower-crustal velocity of normal oceanic crust[24], after correction for along-segment variation in thickness[25]. The yellow arrow shows the representative trend of changes in h and v_p for passive decompression of normal mantle of increasing temperature, with tick marks approximately every 50 K. Solid arrows show the directions of change in h and v_p at fixed mantle temperature for active mantle upwelling under the rift or an increase in the fertility of the parent mantle. Broken arrows show the effect on the lower-crustal velocity of fractionation in the lower crust or in the upper mantle.

profile[4]) on the conjugate Greenland margin[4–6]. If the lower crust beneath the COT (where the SDRS are observed) comprised 100% igneous material, as the term 'underplated' implies, then this interpretation would be correct. We note that this interpretation introduces other significant difficulties, such as requiring a near-vertical boundary between continental and fully igneous crust at a distance of 90 km on Figs 2b and c, and failing to explain how the SDRS remained elevated and subaerial over the inferred lower-temperature mantle but then subsided and became submarine during seafloor spreading when the inferred mantle temperature was higher.

However, the average h–v_P values for only the igneous component of the COT crust (larger open symbols in Fig. 3c), can be alternatively interpreted as representing melt generated by decompression of hot mantle by lithospheric stretching of the COT before the onset of seafloor spreading. There is the possibility of some trade-off between the assumed velocity of the igneous intrusions under the COT and their thicknesses, which would allow the inference of limited small-scale active convection to generate the melt thickness, but even if this were so, modelling shows that increased mantle temperatures are still required[26]. To first order, the observations for both the Hatton and Faroes profiles can be explained by a model in which the mantle temperature was highest at the start of continental break-up, followed by an approximately 75 °C decrease of mantle temperature over about ten million years of seafloor spreading. This also explains the subaerial elevation of the COT with production of SDRS over the hottest mantle, with a change to submarine seafloor spreading as the mantle temperature decreased after continental break-up. It raises the likelihood that the region of crust with SDRS on the Greenland margin, which is twice as wide as that on the conjugate Hatton margin[5,6], is also underlain by highly stretched continental crust, with initial highly asymmetric stretching similar to that frequently found on non-volcanic margins.

METHODS SUMMARY

Acquisition. Wide-angle data were recorded to ranges >140 km by 85 four-component OBSs spaced at 2–10 km along the profiles, with the seismic source provided by a large-volume (6,360 in^3, 104 litres) airgun array towed at 20 m depth[27] (for data examples see Supplementary Information). The deep-penetration seismic reflection profiles across the Faroes margin used a 48-gun source (10,170 in^3, 167 litres), towed at 18 m depth and tuned on the bubble so as to produce a broadband signature centred on 9–10 Hz. This low-frequency seismic signal passed through the layered basalts, which severely attenuate higher frequencies[28]. The 12,000 m streamer was towed at 18 m depth so as to enhance its low-frequency response.

Reflection seismic processing. The processing included source signature deconvolution, model-independent multiple attenuation, cascaded Radon demultiple steps and integrated velocity analysis with OBS wide-angle tomography.

Velocity structure. Velocities within the water column were measured by velocimeter and calculated from the temperature measured by disposable bathy-thermographs. Sediment velocities were calculated from semblance analysis of wide-angle reflections on the streamer data. Travel times of individual traces were picked from the vertical component geophone OBS data, and used to map the crustal velocity structure by first-arrival seismic tomography[29], then refined by ray-tracing inversion[30] and for the Hatton profile by joint reflection and refraction tomographic inversion[4]. On the Faroes profile we fitted 15,531 diving waves and 9,865 Moho reflections to within the picking error uncertainties, on the Hatton profile we fitted 17,639 diving waves and 7,850 Moho reflections. Uncertainties in the velocities were estimated by making multiple inversions with 100 randomized starting velocity models; velocities are generally constrained to better than 0.1 km s^{-1} and Moho depths to 1 km (see Supplementary Information for examples of data and model uncertainty). The top of the oceanic lower crust is marked by the velocity inflection at 6.7 km s^{-1} (Fig. 3a and b).

Full Methods and any associated references are available in the online version of the paper at www.nature.com/nature.

Received 24 October 2007; accepted 8 January 2008.

1. White, R. & McKenzie, D. Magmatism at rift zones: The generation of volcanic continental margins and flood basalts. *J. Geophys. Res.* 94, 7685–7729 (1989).
2. Coffin, M. F. & Eldholm, O. Large igneous provinces: crustal structure, dimensions, and external consequences. *Rev. Geophys.* 32, 1–36 (1994).
3. Eldholm, O. & Grue, K. North Atlantic volcanic margins: dimensions and production rates. *J. Geophys. Res.* 99, 2955–2988 (1994).
4. Korenaga, J. *et al.* Crustal structure of the southeast Greenland margin from joint refraction and reflection seismic tomography. *J. Geophys. Res.* 105, 21591–21614 (2000).
5. Hopper, J. R. *et al.* Structure of the SE Greenland margin from seismic reflection and refraction data: Implications for nascent spreading center subsidence and asymmetric crustal accretion during North Atlantic opening. *J. Geophys. Res.* 108 (B5), 2269–2291 (2003).
6. Korenaga, J., Kelemen, P. B. & Holbrook, W. S. Methods for resolving the origin of large igneous provinces from crustal seismology. *J. Geophys. Res.* 107 (B9), doi:10.1029/2001JB001030 (2002).
7. White, R. S. *et al.* Magmatism at rifted continental margins. *Nature* 330, 439–444 (1987).
8. Barton, A. J. & White, R. S. Crustal structure of the Edoras Bank continental margin and mantle thermal anomalies beneath the North Atlantic. *J. Geophys. Res.* 102, 3109–3129 (1997).
9. Larsen, H. C. & Saunders, A. D. in *Proceedings of the Ocean Drilling Program, Scientific Results* (eds A. D. Saunders, H. C. Larsen & S. W. Wise, Jr) Vol. 152 503–533 (Ocean Drilling Program, College Station, Texas, 1998).
10. Weigel, W. *et al.* Investigations of the east Greenland continental margin between 70° and 72° N by deep seismic sounding and gravity studies. *Mar. Geophys. Res.* 17, 167–199 (1995).
11. Klingelhofer, F., Edwards, R. A., Hobbs, R. W. & England, R. W. Crustal structure of the NE Rockall Trough from wide-angle seismic data modelling. *J. Geophys. Res.* 110, B11105, doi:10.1029/2005JB003763 (2005).
12. White, R. S. *et al.* iSIMM pushes frontiers of marine seismic acquisition. *First Break* 20, 782–786 (2002).
13. Roberts, A. W., White, R. S., Lunnon, Z. C., Christie, P. A. F., Spitzer, R. & iSIMM Team. In *Petroleum Geology: North-West Europe and Global Perspectives—Proc. 6th Petroleum Geology Conf.* (eds A. G. Doré & B. A. Vining) 755–766 (Geol. Soc. London, 2005).
14. Smith, L. K., White, R. S., Kusznir, N. J. & iSIMM Team. In *Petroleum Geology: North-West Europe and Global Perspectives—Proc. 6th Petroleum Geology Conf.* (eds A. G. Doré & B. A. Vining) 947–956 (Geol. Soc. London, 2005).
15. Christeson, G. L., McIntosh, K. D. & Karson, J. A. Inconsistent correlation of seismic layer 2a and lava layer thickness in oceanic crust. *Nature* 445, 418–421 (2007).
16. White, R. S. *et al.* Imaging and regional distribution of basalt flows in the Faroe-Shetland Basin. *Geophysical Prospecting* 51, 215–231 (2003).
17. Mutter, J. C., Talwani, M. & Stoffa, P. L. Origin of seaward-dipping reflectors in oceanic crust off the Norwegian margin by subaerial sea-floor spreading. *Geology* 10, 353–357 (1982).
18. Smallwood, J. R., White, R. S. & Staples, R. K. Deep crustal reflectors under Reydarfjördur, eastern Iceland, Crustal accretion above the Iceland mantle plume. *Geophys. J. Int.* 134, 277–290 (1998).
19. Smallwood, J. R., Staples, R. K., Richardson, K. R., White, R. S. & FIRE Working Group. Crust generated above the Iceland mantle plume: from continental rift to oceanic spreading center. *J. Geophys. Res.* 104, 22885–22902 (1999).
20. McBride, J. H., White, R. S., Smallwood, J. R. & England, R. W. Must magmatic intrusion in the lower crust produce reflectivity? *Tectonophysics* 388, 271–297 (2004).
21. Parkin, C. J., Lunnon, Z. C., White, R. S., Christie, P. A. F. & iSIMM Team. Imaging the pulsing Iceland mantle plume through the Eocene. *Geology* 35, 93–96 (2007).
22. Cox, K. G. A model for flood basalt vulcanism. *J. Petrol.* 21, 629–650 (1980).
23. Sallarès, V., Charvis, P., Flueh, E. R., Bialas, J. & the SALIERI Scientific Party. Seismic structure of the Carnegie ridge and the nature of the Galápagos hotspot. *Geophys. J. Int.* 161, 763–788 (2005).
24. White, R. S., McKenzie, D. & O'Nions, R. K. Oceanic crustal thickness from seismic measurements and rare earth element inversions. *J. Geophys. Res.* 97, 19683–19715 (1992).
25. Bown, J. W. & White, R. S. Variation with spreading rate of oceanic crustal thickness and geochemistry. *Earth Planet. Sci. Lett.* 121, 435–449 (1994).
26. Nielsen, T. K. & Hopper, J. R. Formation of volcanic rifted margins: Are temperature anomalies required? *Geophys. Res. Lett.* 29, 2022, doi:10.129/2002GL015681 (2002).
27. Lunnon, Z. C., Christie, P. A. F. & White, R. S. An evaluation of peak and bubble tuning in sub-basalt seismology: modelling and results. *First Break* 21, 51–56 (2003).
28. Maresh, J. & White, R. S. Seeing through a glass, darkly: strategies for imaging through basalt. *First Break* 23, 27–32 (2005).
29. Zelt, C. A. & Barton, P. J. Three-dimensional seismic refraction tomography: a comparison of two methods applied to data from the Faeroe Basin. *J. Geophys. Res.* 103 (B4), 7187–7210 (1998).
30. Zelt, C. A. & Smith, R. B. Seismic traveltime inversion for 2-D crustal velocity structure. *Geophys. J. Int.* 108, 16–34 (1992).

Supplementary Information is linked to the online version of the paper at www.nature.com/nature.

Acknowledgements iSIMM was supported by Liverpool and Cambridge Universities, Schlumberger Cambridge Research Ltd, Badley Geoscience Ltd, WesternGeco, Amerada Hess, Anadarko, BP, ConocoPhillips, ENI U.K., Statoil, Shell, the Natural Environment Research Council and the Department of Trade and Industry. OBSs were provided by Geopro GmbH and Q-Marine streamer acquisition by WesternGeco.

Author Contributions Wide-angle seismic analysis was undertaken by L.K.S. and A.W.R. as part of their PhD research. Seismic reflection processing for Fig. 2c was by WesternGeco. R.S.W. led the work at sea on RRS *Discovery* on the Faroes profile, N.J.K. on the Hatton profile, and P.A.F.C. oversaw the Faroes seismic profiling on MV *Geco Topaz*. R.S.W. wrote the paper and all authors discussed the results and commented on the manuscript.

Author Information Reprints and permissions information is available at www.nature.com/reprints. Correspondence and requests for materials should be addressed to R.S.W. (rwhite@esc.cam.ac.uk).

The iSIMM team includes, in addition to the other authors A.M. Roberts[4], D. Healy[5], R. Spitzer[6], A. Chappell[6], J. D. Eccles[6], R. Fletcher[5], N. Hurst[5], Z. Lunnon[6], C. J. Parkin[6] & V. J. Tymms[5]

[4]Badley Technology Ltd, North Beck House, North Beck Lane, Hundleby, Spilsby, Lincolnshire PE23 5NB, UK. [5]Department of Earth Sciences, University of Liverpool, Liverpool L69 3BX, UK. [6]Bullard Laboratories, University of Cambridge, Madingley Road, Cambridge CB3 0EZ, UK.

LETTERS

The first hominin of Europe

Eudald Carbonell[1], José M. Bermúdez de Castro[2], Josep M. Pares[2,3], Alfredo Pérez-González[2,4], Gloria Cuenca-Bescós[5], Andreu Ollé[1], Marina Mosquera[1], Rosa Huguet[1], Jan van der Made[6], Antonio Rosas[6], Robert Sala[1], Josep Vallverdú[1], Nuria García[7,8], Darryl E. Granger[9], María Martinón-Torres[2], Xosé P. Rodríguez[1], Greg M. Stock[3,10], Josep M. Vergès[1], Ethel Allué[1], Francesc Burjachs[1,11], Isabel Cáceres[1], Antoni Canals[1], Alfonso Benito[4], Carlos Díez[12], Marina Lozano[1], Ana Mateos[2], Marta Navazo[12], Jesús Rodríguez[2], Jordi Rosell[1] & Juan L. Arsuaga[7,8]

The earliest hominin occupation of Europe is one of the most debated topics in palaeoanthropology. However, the purportedly oldest of the Early Pleistocene sites in Eurasia lack precise age control and contain stone tools rather than human fossil remains[1–5]. Here we report the discovery of a human mandible associated with an assemblage of Mode 1 lithic tools and faunal remains bearing traces of hominin processing, in stratigraphic level TE9 at the site of the Sima del Elefante, Atapuerca, Spain[6–8]. Level TE9 has been dated to the Early Pleistocene (approximately 1.2–1.1 Myr), based on a combination of palaeomagnetism, cosmogenic nuclides and biostratigraphy. The Sima del Elefante site thus emerges as the oldest, most accurately dated record of human occupation in Europe, to our knowledge. The study of the human mandible suggests that the first settlement of Western Europe could be related to an early demographic expansion out of Africa. The new evidence, with previous findings in other Atapuerca sites (level TD6 from Gran Dolina[9–13]), also suggests that a speciation event occurred in this extreme area of the Eurasian continent during the Early Pleistocene, initiating the hominin lineage represented by the TE9 and TD6 hominins.

The Sima del Elefante Site is located in the Sierra de Atapuerca, northern Spain, in the proximity of the well-known sites of Gran Dolina, Galería and Sima de los Huesos (Fig. 1a). All of them have yielded hominin fossils attributed to the species *Homo antecessor* (approximately 0.8 Myr[9–13]) in Gran Dolina and *Homo heidelbergensis* in Galería[14] and Sima de los Huesos[15–17].

The Sima del Elefante site is a cave 18 m deep and up to 15 m wide[6,7], infilled with clastic deposits. The sedimentary sequence is formed by 16 lithostratigraphic units (Fig. 1b) mostly made by debris flow deposits. Entrance clast-supported debris flows correspond to proximal facies, whereas deposits with higher content of brown and reddish-brown clays (HUE 7.5YR or 5YR) correspond to distal facies, derived from terra-rossa slope soils.

We report on the palaeoanthropological, archaeological and palaeontological record of level TE9, including geochronological and biostratigraphic data at Sima del Elefante, which together document the oldest-known site in Europe with hominin fossils and human activity.

A fragment of hominin mandible and an isolated lower LP_4 of the same individual were recovered from square I-31 of the TE9C level. The mandible (ATE9-1) consists of the symphyseal region, a portion of the right corpus from P_3 to the alveolus of M_1 with an irregular broken surface, and the basal part of the left corpus from P_3 to the level of M_1/M_2. Some teeth are preserved *in situ* (Fig. 2 and Supplementary Information).

The mental foramen is single on both sides and lies at the P_3/P_4 interalveolar septum. On the preserved part of the corpus, a well-differentiated torus marginalis is present. Anteriorly, this torus terminates as a well-developed anterior marginal tubercle below the C/P_3 (Fig. 2a). In lateral view (Fig. 2c), there is a slight anterior mandibular incurvatio of the bone between the alveolar border and the base. Thus a modest mentum osseum is expressed. The mental trigone is represented by a faint bone elevation along the midline of the symphysis and a visible mental protuberance. No signs of lateral mental tubercles or mental fossae are present. In anterior view, the lower margin of the symphysis is arched bilaterally, forming a conspicuous incisura submentalis. At the midline of the arch, a strong and pointed interdigastric spine projects downwards between the two digastric impressions, which are shallow but well defined, and placed at the basal part of the symphysis. On the internal surface of the symphysis, the alveolar planum exhibits a minimum inclination, and the superior transverse torus is absent. However, on the right side a modest but clear alveolar prominence below P_3–P_4 is observed. In superior view, the alveolar portion of the corpus tends to diverge to form a parabolic arc, being more open than in early African *Homo* specimens such as OH 13, KNM-ER 1802 and UR 501, or in the Dmanisi mandibles. The thickness of the corpus of ATE9-1 at the M_1 level is similar to that of ATD6-96 from Gran Dolina[12] and falls at the lower limit of the range of the African Early and Middle Pleistocene *Homo* specimens[18]. The height of the corpus of ATE9-1 at the P_3/P_4 level is modest and far from the extreme values seen in many other Pleistocene specimens such as those from Tighenif, Sangiran and D 2600 from Dmanisi (Table 1). The C, P_3 and P_4 exhibit single roots of Tomes' root form (category 1R[19]), with a groove along the mesiolingual root surface. The crown of LP_4 presents an oval outline with a distolingual talonid, and the tip of the lingual cusp is mesial to the tip of the larger buccal cusp

[1]Institut Català de Paleoecologia Humana i Evolució Social, Area de Prehistoria, Universitat Rovira i Virgili, Plaça Imperial Tarraco 1, 43005 Tarragona, Spain. [2]Centro Nacional de Investigacion sobre Evolución Humana, Avenida de la Paz 28, 09004 Burgos, Spain. [3]Department of Geological Sciences, University of Michigan, 2534 CCL Building, Ann Arbor, Michigan 48109 USA. [4]Departamento de Geodinámica, Facultad de Ciencias Geológicas, Universidad Complutense de Madrid, 28040 Madrid, Spain. [5]Área de Paleontología, Facultad de Ciencias, Universidad de Zaragoza, c/ Pedro Cerbuna 12, 50009 Zaragoza, Spain. [6]Departamento de Paleobiología, Museo Nacional de Ciencias Naturales, C.S.I.C., José G. Abascal 2, 28006 Madrid, Spain. [7]Departamento de Paleontología, Facultad de Ciencias Geológicas, Universidad Complutense de Madrid, 28040 Madrid, Spain. [8]Centro de Investigacion (UCM-ISCIII) de Evolución y Comportamiento Humanos, c/ Sinesio Delgado, 4 (Pabellon 14), 28029 Madrid, Spain. [9]Department of Earth and Atmospheric Sciences, Purdue University, West Lafayette, Indiana 47907 USA. [10]Yosemite National Park, 5083 Foresta Road, PO Box 700, El Portal, California 95318, USA. [11]Institució Catalana de Recerca i Estudis Avançats, Plaça Imperial Tarraco 1, 43005 Tarragona, Spain. [12]Laboratorio de Prehistoria, Edificio I + D + i, Universidad de Burgos, Plaza Misael Bañuelos s/n, 09001 Burgos, Spain.

The morphology of the anterior surface of the symphysis and the position of the anterior marginal tubercle suggest similarities between ATE9-1 and early *Homo* specimens like OH 7, OH13, KNM ER 730 and UR 501, and especially with those of Dmanisi. However, the morphology of the posterior surface of the symphysis and the shape of the alveolar part of the corpus are clearly derived in these hominins (see Supplementary Information, Mandible Discussion). Although the symphysis is not represented in the current TD6 hominin hypodigm, so we cannot make the pertinent comparisons, we assign ATE9-1 provisionally to *Homo antecessor*[10].

The lithic assemblage includes 32 artefacts: four simple flakes, five waste flakes (*debris*) and 23 indeterminate items made of Neogene and Cretaceous chert, both raw materials available within 2 km of the archaeological site. There are many indeterminate pieces, owing to the chemical weathering particularly suffered by the Neogene chert.

Hominins probably knapped inside the cave, as deduced from the presence of small waste flakes and two medium-sized Cretaceous chert flakes that seem to belong to the same core. The reduction sequence was devoted to producing simple flakes ranging between 30 mm and 75 mm long. Artefacts were detached by direct hard-hammer percussion on hand-held, medium-sized cores. Knapping strategies were simple, and they tended to remove the irregularities and shape the blank to obtain a single striking platform. Flakes show plane rather than cortical butts, and dorsal scars are parallel to the flake extraction axis, which indicates unidirectional knapping (Fig. 3a–c).

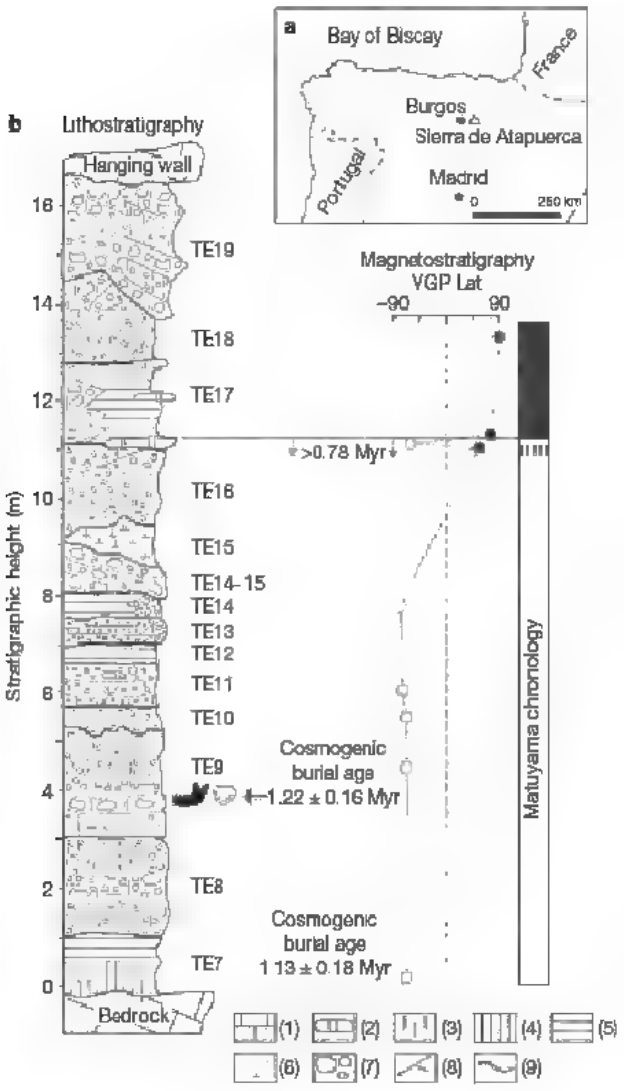

Figure 1 | Geographic setting and geological context. **a**, Geographic setting of the Atapuerca archaeological sites **b**, Summary of the lithostratigraphy and chronology of the Sima del Elefante locality. The synthetic column on the left shows the different stratigraphic units visible at the central–north section, labelled TE. Symbols: 1, Mesozoic limestone; 2, speleothem; 3, lutite/clay; 4, bat guano; 5, clay and laminated sandy silts; 6, marls; 7, gravels and boulders; 8, cross-lamination; 9, main stratigraphic discontinuity. VGP Lat, latitude of the virtual geomagnetic pole. Cosmogenic burial ages are also shown, with the standard error given at the 68% confidence interval

The faunal assemblage[6,7,20,21] (see Supplementary Table 1) provides valuable chronological information. The mustelid *Pannonictis* is a typical Plio-Pleistocene taxon, and the species *P. nestii* is a likely candidate as a last survivor of the genus, which might reach the late Early Pleistocene. In size and in cranial and dental morphology, the specimens from TE level 9 resemble *P. nestii* from the site of Pietrafitta (Italy), dated to around 1.4 Myr[22], suggesting the fossils in TE9 are closer in age to the Italian site than to the last occurrence of this species[23]. The murid *Castillomys*, found in TE levels 8–14[20], has its latest appearance in localities such as Barranco León, with a Matuyama age[1]. The rodents and insectivores of levels TE9–TE13 are primitive compared with those present in Cromerian localities (around 1.0–0.6 Myr); that is, they include advanced forms of *Mimomys savini* as well as *Microtus* species that are absent in levels TE8–TE13[21,24]. Also, the *A/L* index (the relative length of the anteroconid complex in relation to the anteroposterior length of the tooth) of the *Allophaiomys* first lower molar found at Sima del Elefante resembles that of *Allophaiomys* measured at Fuente Nueva 3, Pietrafitta, Pirro Nord and Monte Peglia. The small mammals found at the Sima del Elefante site are notably more primitive than the oldest small mammal assemblages that appear in Gran Dolina[20,21,24], especially the absence of *Microtus* and *Allocricetus bursae*, and the presence of *Asoriculus gibberodon*, *Castillomys* and the *Allophaiomys* species. In addition, the evolution of the insectivore associations at levels TE9–TE13 suggests a general warm and humid palaeoenvironment with warmer–cooler shifts. This could tentatively correlate with the Waalian[20], an Early Pleistocene warm stage also with warmer–cooler shifts, dated to 1.5–1.3 Myr[25].

Large mammals of TE9 are mainly represented by long bones, whereas Leporidae and birds preserve whole anatomical segments, mainly limbs. Some bones of large mammals show clear evidence of hominin processing, such as percussion marks on long bones (Fig. 3d) and on a bovid mandible, pointing to fresh fracture made to access the marrow cavity and other food resources. The mandible and a vertebra of bovid, and some indeterminate macromammal long bones, also show defleshing cut marks[26] (Fig. 3e, f).

Previous work on the chronology of the sedimentary infill at Sima del Elefante has been based on palaeomagnetism[8] and faunal evidence[20]. The initial palaeomagnetic study revealed that stratigraphic layers TE16 and older recorded reverse magnetization directions only, consistent with a Matuyama age of the sediments (1.78–0.78 Myr) and with the mammal assemblage. Layer TE17, on the other hand, showed normal polarity directions. New palaeomagnetic results of a flowstone capping unit TE16 and the overlying poorly consolidated silty sandstones reveal normal polarity directions, constraining the stratigraphic position of the reverse to normal polarity change within the section around a stratigraphic height of 11 m.

The age of level TE9 is further constrained by burial dating based on the radioactive decay of cosmogenic ^{26}Al (half-life, $t_{1/2} = 0.717 \pm 0.017$ Myr) and ^{10}Be ($t_{1/2} = 1.34 \pm 0.07$ Myr) in quartz collected from the sediments. These two radionuclides are produced at a fixed ratio by secondary cosmic rays interacting with quartz near the ground surface. When quartz containing inherited ^{26}Al and ^{10}Be is carried into a cave, the mineral grain is shielded from cosmic rays and the concentrations of these two nuclides decay over time, serving as a chronometer of deposition[27,28]. The burial dating method assumes that quartz was first exposed near the surface in a steadily eroding

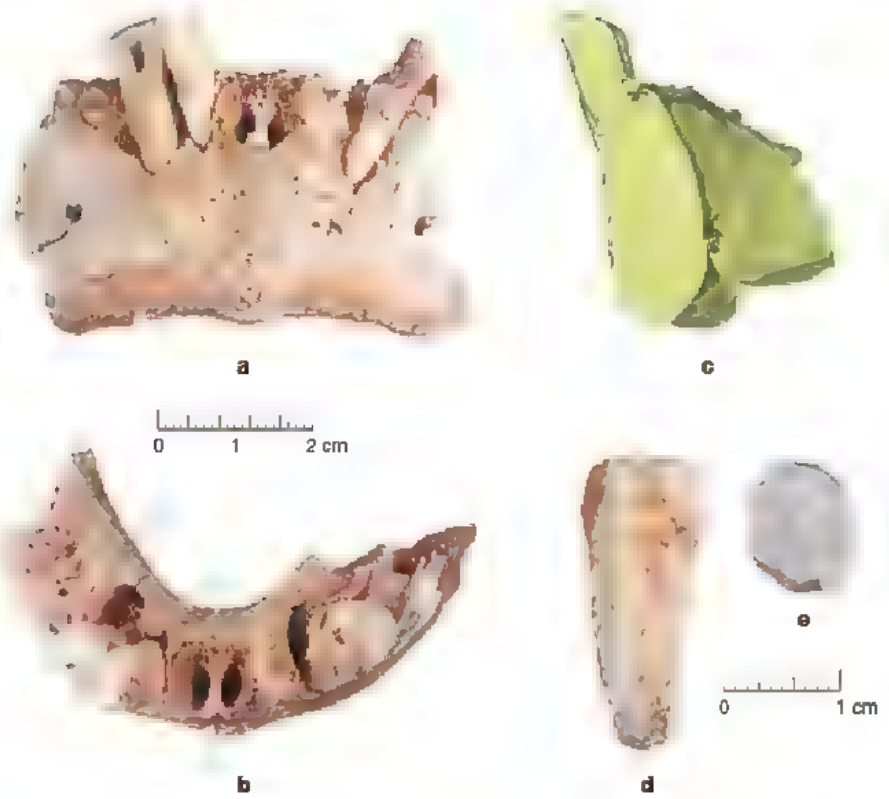

Figure 2 | Mandible ATE9-1. **a**, Frontal view. Arrowheads point to the position of the anterior marginal tubercle, and the arch of the marked incisura submentalis. **b**, Superior view. Arrowheads point to the mental protuberance, the subvertical alveolar planum and the slight alveolar prominence. Note also the parabolic arc formed by the alveolar part of the corpus. **c**, Median sagittal cross-section of the symphysis based on a three-dimensional computed tomography reconstruction. Fossils are housed at the Centro Nacional de Investigacion sobre la Evolución Humana. **d**, Distal view of the LP4 of ATE9-1. **e**, Occlusal view of the LP4; mesiodistal dimension, 8.9 mm; buccolingual dimension, 11.4 mm (estimated).

environment, and was then buried deeply enough in the cave to ensure adequate shielding. We collected two samples from the study area, each shielded by approximately 16 m of bedrock and sediment (see Supplementary Tables 2 and 3).

The first sample was collected from layer 9b, in the central part of unit TE9. This sample was collected about 40 cm above the artefacts and the hominin fossils in layer 9c, and has a burial age of 1.22 ± 0.16 Myr. A second sample was collected from unit TE7, which contains a similar microfaunal assemblage to unit TE9. This second sample has a burial age of 1.13 ± 0.18 Myr, indistinguishable from that of layer TE9b.

Table 1 | Measurements of ATE9-1 compared with some *Homo* specimens

	Thickness (mm)		Height (mm)	
	M_1	Symphysis*	P_3–P_4	Symphysis
ATE9-1	17.0	15.3	30.0	33.5
ATD6-96	16.6		28.5	
D 211	18.1	16.5	26.0	31.0
D 2735	19.3	16.0	24.6	32.0
D 2600	21.6	21.0	42.4	49.0
Sangiran 9†	21.2	18.0	38.2	42.0
Sangiran 22†	17.3	16.1	31.1	36.0
Sangiran 6	27.0		48.0	
Sangiran 1B	16.3		35.7	
KNM-ER 1802‡	23.0	21.3	35.8	36.2
LR 501‡	21.3	16.8	34.1	34.0
OH 13‡	18.0		26.0	
OH 22‡	19.4	18.9	29.0	30.7
KNM ER 730‡	19.0	17.6	31.3	31.0
KNM ER 992‡	20.2		31.0	
Tighenif 1	19.0	18.8	36.2	36.0
Tighenif 2	16.9	18.0	33.4	33.3
Tighenif 3	19.0	19.2	38.4	37.5

The preservation of ATE9-1, D 211 and D 2600 prevents measurement of the height of the corpus at the M1 level. *Taken approximately at a right angle to the axis of the symphyseal inclination. †From Kaifu *et al*[29] ‡From Schrenk *et al*[30]. All other measurements were taken on originals or high-quality casts.

The lithic assemblage found at level TE9 shows similar primary technical features to those from the other Early Pleistocene European sites: a Mode 1 simple technology without handaxes and cleavers, which are the most characteristic tools of Mode 2 or Acheulean. Furthermore, the oldest European assemblages show scarcity or even absence of retouched tools[2–5,9,11], as is the case at TE9. These simple industries usually appear in archaeological contexts related to basic human activities devoted to processing and consuming meat and marrow.

Current archaeological data unequivocally indicate human presence in southern Europe (south of 46° N) quite early in the Early Pleistocene[1–5,13] (see Supplementary Table 4). The recently discovered hominin and lithic industry in level TE9 reported here, and the dating based on palaeomagnetism, biostratigraphy and cosmogenic nuclides, provide the oldest direct evidence, to our knowledge, for a human presence in Europe at 1.2–1.1 Myr. The most parsimonious interpretation of this new finding in the Sierra de Atapuerca is that western Europe was settled during the Early Pleistocene by a hominin population coming from the east. This population may be related to an 'early' expansion of hominins out of Africa. Considering that the TE9 hominin could be also assigned to *H. antecessor*[10], the Sima del Elefante and Gran Dolina TD6 populations would represent a speciation that occurred in this extreme part of Eurasia during the Early Pleistocene.

Overall, the Sima del Elefante site, with other Early Pleistocene, Mediterranean sites (for example Pirro Nord, Barranco León and so on)[1–5,13], strengthens the evidence that peopling of Europe occurred much faster and in a more continuous manner than previously thought.

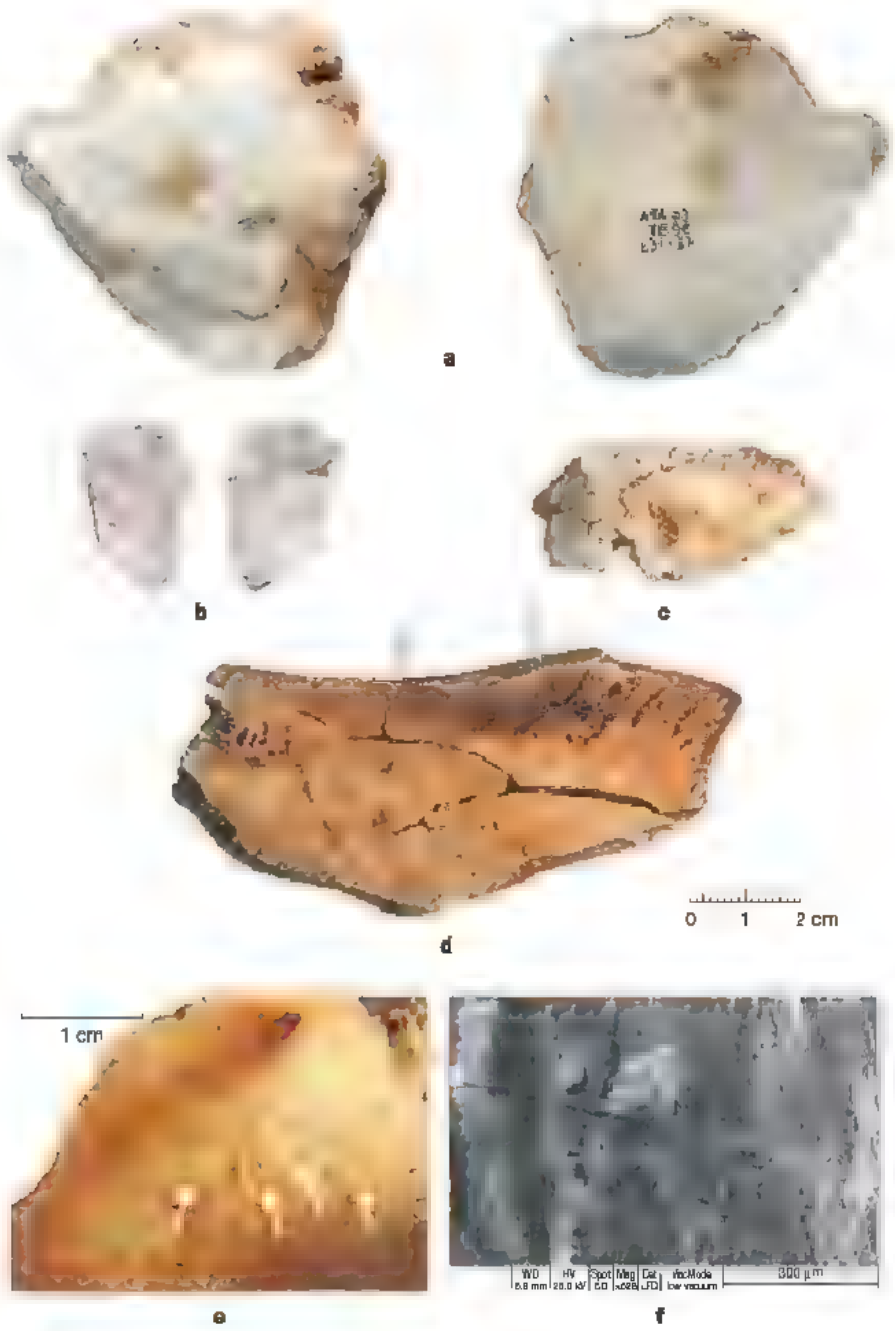

Figure 3 | TE9 lithic tools and faunal remains with cut marks and hominin breakage. **a–c**, Chert artefacts from TE9, 3a and 3b are flakes of Cretaceous chert probably belonging to the same core; 3c is the lower surface of a flake of Neogene chert. **d**, Large mammal bone with fresh fracture to access the marrow; arrows point the percussion marks. **e**, Cut-marked bovid vertebra; arrows point the main group of cut marks. **f**, Detail under environmental scanning electron microscope of one of the recorded cut marks on a bovid mandible.

METHODS SUMMARY

Sierra de Atapuerca (Burgos, Spain) contains several well known Early and Middle Pleistocene sites: Gran Dolina[11], Galería[14], Sima de los Huesos[16] and Sima del Elefante[7], among others. All these sites have been excavated and studied by an interdisciplinary team formed in the late 1970s comprising archaeologists, palaeontologists, taphonomists, zooarchaeologists, geologists, palaeoanthropologists and biologists.

The interdisciplinary approach began with fieldwork, the basis for the archaeological and palaeoanthropological studies. All the Sierra de Atapuerca sites have been studied following systematic excavation, all items recovered were registered in a three-dimensional coordinate system and placed in stratigraphic context. Such thorough background work is required for understanding the context of human evolution, opposite to the interpretations made with isolated discoveries.

Identification, measurement and interpretation of the Sima del Elefante and all the Sierra de Atapuerca specimens follow conventional procedures of comparative anatomy for palaeoanthropology, lithic technology for stone tool production, and zooarchaeology and taphonomy for subsistence strategies. Also, microscopic analyses and archaeological experimentation are common procedures. Results and interpretations were situated in time and in palaeoenvironmental context using geochronological and biochronological analyses.

Full Methods and any associated references are available in the online version of the paper at www.nature.com/nature.

Received 15 October 2007; accepted 4 February 2008.

1. Oms, O. *et al.* Early human occupation of western Europe: paleomagnetic dates for two paleolithic sites in Spain. *Proc. Natl Acad. Sci. USA* 97, 10666–10670 (2000).
2. Arzarello, M. *et al.* Evidence of earliest human occurrence in Europe: the site of Pirro Nord (southern Italy). *Naturwissenschaften* 94, 107–112 (2007).
3. Despriée, J. *et al.* Une occupation humaine au Pléistocène inférieur sur la bordure nord du Massif central. *C.R. Palevol.* 5, 821–828 (2006).
4. Lumley, H., de, Fournier A., Krzepkowska, J. & Echassoux, A. L'industrie du Pleistocène inférieur de la grotte du Vallonnet, Roquebrune-Cap Martin, Alpes Maritimes. *L'Anthropologie* 92, 501–614 (1988).

5 Peretto, C. *et al.* L'industrie lithique de Ca'Belvedere di Monte Poggiolo: stratigraphie, matière première, typologie, remontages et traces d'utilisation. *L'Anthropologie* 102, 343–465 (1998).
6 Rosas, A. *et al.* Le gisement pléistocène de la 'Sima del Elefante' (Sierra de Atapuerca, Espagne). *L'Anthropologie* 105, 301–312 (2001)
7 Rosas, A. *et al.* The 'Sima del Elefante' cave site at Atapuerca (Spain). *Estudios Geológicos* 62, 327–348 (2006)
8 Parés, J. M. *et al.* Matuyama-age lithic tools from the Sima del Elefante site, Atapuerca (northern Spain). *J. Hum. Evol.* 50, 163–169 (2006).
9 Carbonell, E. *et al.* Lower Pleistocene hominids and artifacts from Atapuerca-TD6 (Spain). *Science* 269, 826–830 (1995)
10. Bermúdez de Castro, J. M. *et al.* A hominid from the Lower Pleistocene of Atapuerca, Spain: possible ancestor to neandertals and modern humans. *Science* 276, 1392–1395 (1997).
11 Bermúdez de Castro, J. M., Carbonell, E. & Arsuaga, J. L. (eds) The Gran Dolina site: TD6 Aurora Stratum (Atapuerca, Burgos, Spain). *J. Hum. Evol.* 37 (special issue) 309–700 (1999)
12. Carbonell, E. *et al.* An Early Pleistocene hominin mandible from Atapuerca-TD6, Spain. *Proc. Natl Acad. Sci. USA* 102, 5674–5678 (2005).
13. Parés, J. M. & Pérez-González, A. Paleomagnetic age for hominid fossils at Atapuerca archaeological site, Spain. *Science* 269, 830–832 (1995)
14. Carbonell, E., Rosas, A. & Díez, J. C. (eds) *Atapuerca: Ocupaciones Humanas y Paleoecología del Yacimiento de Galería* 1–390 (Junta de Castilla y Leon, Zamora, 1999)
15. Arsuaga, J. L., Martínez, I., Gracia, A., Carretero, J. M. & Carbonell, E. Three new human skulls from the Sima de los Huesos site in Sierra de Atapuerca, Spain. *Nature* 362, 534–537 (1993).
16. Arsuaga, J. L., Bermúdez de Castro, J. M. & Carbonell, E. (eds) The Sima de los Huesos hominid Site. *J. Hum. Evol.* 33 (special issue), 105–421 (1997)
17 Bischoff, J. L. *et al.* High-resolution U-series dates from the Sima de los Huesos hominids yields 600±66 kyrs: implications for the evolution of the early Neanderthal lineage. *J. Archaeol. Sci.* 34, 763–770 (2007).
18. Rosas, A. & Bermúdez de Castro, J. M. On the taxonomic affinities of the Dmanisi mandible (Georgia). *Am. J. Phys. Anthropol.* 107, 145–162 (1998).
19. Wood, B. A., Abbott, S. A. & Uytterschaut, H. Analysis of the dental morphology of Plio-Pleistocene hominids. IV. Mandibular postcanine root morphology. *J. Anat.* 156, 107–139 (1988)
20 Cuenca-Bescós, G. & Rofes, J. Insectívoros (Mammalia), clima y paisaje de los niveles inferiores de Trinchera Elefante (Pleistoceno Inferior, Atapuerca). *Zona Arqueol.* 4, 150–156 (2004).
21. Rofes, J. & Cuenca-Bescós, G. First evidence of the Soricidae (Mammalia) *Asoriculus gibberodon* (Petényi, 1864) in the Pleistocene of North Iberia. *Riv. Ital Paleontol. Stratigr.* 112, 301–315 (2006)
22 Gliozzi, E. *et al.* Biochronology of selected mammals, molluscs and ostracods from the Middle Pliocene to the Late Pleistocene in Italy. The state of the art. *Riv. Ital. Paleontol. Stratigr.* 103, 369–388 (1997)
23 García, N. & Howell, F. C. New discovery of a large mustelid (Carnivora: Mammalia) from the early Pleistocene locality of Sima del Elefante (Sierra de Atapuerca, Spain). *Palaeontogr. Abt. A* (in the press)
24. Cuenca-Bescós, G., Laplana, C. & Canudo, J. I. Biochronological implications of the Arvicolidae (Rodentia, Mammalia) from the Lower Pleistocene hominid-bearing level of Trinchera Dolina 6 (TD6, Atapuerca, Spain). *J. Hum. Evol.* 37, 353–373 (1999)
25. Zagwijn, W. H. Borders and boundaries: a century of stratigraphical research in the Tegelen-Reuver area of Limburg (The Netherlands). *Med. Ned. Inst. Toegep. Geowetensch. TNO* 60, 19–34 (1998).
26. Huguet, R. *Primeras Ocupaciones Humanas en la Península Ibérica: Paleoeconomía de la Sierra de Atapuerca (Burgos) y la Cuenca de Guádix-Baza (Granada) Durante e. Pleistoceno Inferior*. PhD thesis, Department of History and History of Art, Univ. Rovira i Virgili, Tarragona (2007)
27. Granger, D. E., Fabel, D. & Palmer A. N., Pliocene–Pleistocene incision of the Green River, Kentucky: determined from radioactive decay of cosmogenic ^{26}Al and ^{10}Be in Mammoth Cave sediments. *Geol. Soc. Am. Bull.* 113, 825–836 (2001).
28. Stock, G. M., Anderson, R. S. & Finkel, R. C. Pace of landscape evolution in the Sierra Nevada, California, revealed by cosmogenic dating of cave sediments. *Geology* 32, 193–196 (2004).
29. Kaifu, Y., Aziz, F. & Baba, H. Hominid mandibular remains from Sangiran: 1952–1986 collection. *Am. J. Phys. Anthropol.* 128, 497–519 (2005).
30. Schrenk, F., Bromage, T. G., Betzler, C. G., Ring, U. & Juwayeyi, Y. Oldest *Homo* and Pliocene biogeography of the Malawi Rift. *Nature* 365, 833–836 (1993)

Supplementary Information is linked to the online version of the paper at www.nature.com/nature.

Acknowledgements We acknowledge all the members of the Atapuerca research team involved in the recovery and study of the archaeological and palaeontological record from Sima del Elefante, and C. Lorenzo for the supervision of the fossils. We thank J. Mestre and S. Sarmiento for the hominin pictures and photomontage, and J.M. Carretero, E. Santos and L. Rodríguez for their supervision and scanning of the mandible. We also thank R. Quam for reviewing the English version. S. Antón, F. Spoor and I. Tattersall provided comments on the manuscript. This research was sponsored by Junta de Castilla y León, Ministerio de Educación y Ciencia grant DGI CGL2006-13532-C03, GC ARAGOB 2007, NSF grant EAR 0452936 and a Fundación Atapuerca grant (R.H., M.N.).

Author Contributions E.C., J.M.B. de C. and J.L.A. directed the excavations and the research project. Authors contributed in the following areas: A.P-G., J.V. and A.B., geology, sedimentology and micromorphology; J.M.P., D.E.G. and G.M.S., geochronology; G.C.-B., J. van der M. and N.G., palaeontology of micro- and macromammals; E.C., A.O., M.M., R.S., X.P.R., J.M.V. and M.N., stone tool technology; R.H., I.C., C.D., A.M. and J. Ros., zooarchaeology; J.M.B. de C., A.R., M.M.-T., M.L. and J.L.A., palaeoanthropology; A.C., archaeostratigraphy; E.A., F.B. and J. Rod., palaeoecology. Unless indicated, J.M.B. de C. took the measurements of hominin fossils for Table 1. A.O. and M.M. edited and coordinated the manuscript.

Author Information Reprints and permissions information is available at www.nature.com/reprints. Correspondence and requests for materials should be addressed to E.C. (eudald.carbonell@urv.cat) and J.M.B. de C. (jm.ber@cenieh.es).

LETTERS

Pleiotropic scaling of gene effects and the 'cost of complexity'

Günter P. Wagner[1], Jane P. Kenney-Hunt[2], Mihaela Pavlicev[2], Joel R. Peck[3], David Waxman[3] & James M. Cheverud[2]

As perceived by Darwin, evolutionary adaptation by the processes of mutation and selection is difficult to understand for complex features that are the product of numerous traits acting in concert, for example the eye or the apparatus of flight. Typically, mutations simultaneously affect multiple phenotypic characters. This phenomenon is known as pleiotropy. The impact of pleiotropy on evolution has for decades been the subject of formal analysis[1–6]. Some authors have suggested that pleiotropy can impede evolutionary progress (a so-called 'cost of complexity'[3]). The plausibility of various phenomena attributed to pleiotropy depends on how many traits are affected by each mutation and on our understanding of the correlation between the number of traits affected by each gene substitution and the size of mutational effects on individual traits. Here we show, by studying pleiotropy in mice with the use of quantitative trait loci (QTLs) affecting skeletal characters, that most QTLs affect a relatively small subset of traits and that a substitution at a QTL has an effect on each trait that increases with the total number of traits affected. This suggests that evolution of higher organisms does not suffer a 'cost of complexity' because most mutations affect few traits and the size of the effects does not decrease with pleiotropy.

A set of quantitative traits in strains of inbred mice were chosen to represent a broad cross-section of linear skeletal traits from all major subsystems of the bony skeleton (see Supplementary Table 1). The strains used were initially selected for increased (LG/J) and reduced (SM/J) body size at 60 days *post partum*, respectively, and then inbred for more than 100 generations[7,8]. A QTL mapping analysis of 70 such phenotypic characters was performed on 1,040 mice of the F_2 generation that were derived from a cross between the inbred LG/J and SM/J lines. The number of scored markers used was 471, leading to an average distance between them of 3.98 centimorgans. A total of 102 autosomal QTLs were detected[9]. These QTLs exhibited pleiotropy, as assessed by a specific statistical test[10]. The QTLs identified by this test affected a variable number of characters, up to a maximum of 30, with a mean of 7.8 and a median of 6 (Fig. 1a). This means that in our data, 50% of QTLs affect fewer than 10% of the 70 characters measured. This result suggests that pleiotropic effects tend to be limited to subsets of the total phenotype rather than being widespread, as assumed in models of universal pleiotropy, in which all traits are affected by a mutation (see also Supplementary Fig. 1).

To compare the mutational effects of different QTLs on the affected traits, we calculated a standardized effect for each character by dividing the QTL effect by the trait's phenotypic standard deviation (see Supplementary Note 1). The standardized effect on trait i, denoted by A_i, is half the difference in means between homozygotes. The total effect, T, of a QTL is then defined as the euclidean distance spanned by all the single character effects (Supplementary Note 6):

$$T = \sqrt{\sum_{i=1}^{N} A_i^2}$$

In this equation, N represents the degree of pleiotropy; that is, the number of characters affected by a QTL.

The distribution of the total mutational effect T arising from the QTL data set is illustrated in Supplementary Fig. 2. The distribution is estimated to have a mean of 0.59 and a standard deviation of 0.334. We consider these estimates to be unbiased, because the well-known bias of QTL effects[11] is minimal in sample sizes above 500 as in our study. We use these data to test two well-known models of how the total effect depends on the degree of pleiotropy, the euclidean superposition model and the invariant total effect model.

The euclidean superposition model assumes that the expected squared effect of a mutation on a character $\langle m^2 \rangle$ is the same regardless how many other characters are also affected[4]. Taking the phenotypic standard deviation of a trait to be unity, the expected total effect of a mutation then is $\langle T \rangle = \sqrt{N}\sqrt{\langle m^2 \rangle}$. Thus, the total effect of a mutation is predicted to scale with the square root of the degree of pleiotropy N. This model was used by Rechenberg[2], for evolutionary optimization problems in engineering, and by Turelli[3], Wagner[4,12], Waxman and Peck[13] and others, in a population genetic context. Orr[5] and Wingreen *et al.*[6] proposed alternative models that we term invariant total effect models. These models assume that the probability distribution of total effect, $p(T)$, and hence $\langle T \rangle$ itself, is independent of the degree of pleiotropy. This assumption leads to progressively smaller mutational changes on each trait as the degree of pleiotropy increases and to slower rates of evolutionary adaptation with increased numbers of traits.

We first tested these predictions by considering the dependence of the total effect T on the variable number of traits N affected by a mutation (Fig. 1b). The total effect T is strongly increasing with pleiotropy with a highly significant linear regression coefficient ($t = 24.05$, $P < 0.0001$) and a highly significant regression effect ($F_{1,100} = 578.7$, $P < 0.0001$). This result decisively rules out the invariant total effect models of pleiotropy. However, it is also clear that the data do not support the euclidean superposition model either, because that model predicts a square-root dependence rather than the near-linear dependence that is apparent in Fig. 1b (see Supplementary Note 2). The linear model has a higher R^2, suggesting a linear rather than a square-root dependence (linear regression adjusted $R^2 = 0.8512$, square-root regression adjusted $R^2 = 0.7935$; for more detail see Supplementary Note 2). We compared the fit of the two regression models by calculating their log-likelihood ratio, 3,638. This ratio indicates that the data are about 40-fold less likely under the square-root model than under the linear model. We thus conclude that the data are not only severely inconsistent with the invariant total effect

[1]Department of Ecology and Evolutionary Biology, Yale University, New Haven, Connecticut 06520-8106, USA. [2]Department of Anatomy and Neurobiology, Washington University, St Louis, Missouri 63110, USA. [3]Center for the Study of Evolution, School of Life Sciences, University of Sussex, Brighton BN1 9QG, UK.

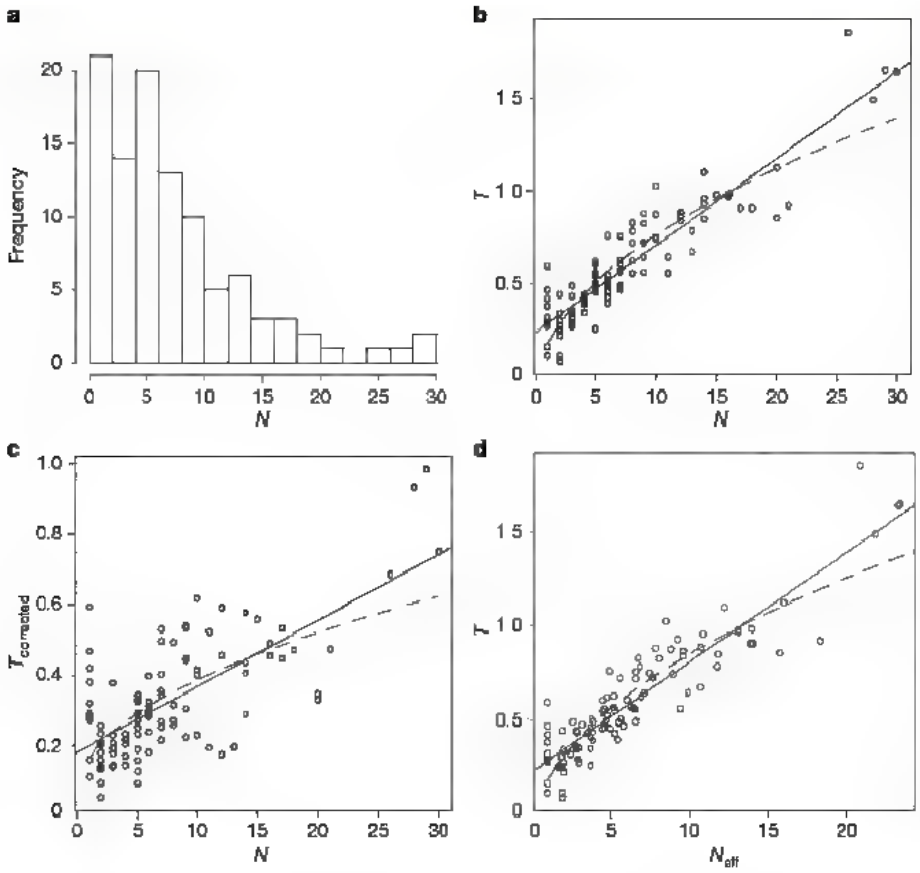

Figure 1 Distribution of QTL effects on 70 skeletal traits in the mouse. **a**, The frequency distribution of the degree of pleiotropy of QTLs. Note that 50% of QTLs affect only up to six traits, but there is a set of QTLs affecting as many as 25–30 traits. **b**, Regression of uncorrected total effect T on the number of traits N affected by a QTL. Note the very tight relationship between T and N. This result does not support the assumption that T is independent of the degree of pleiotropy. It also suggests that T increases more rapidly than predicted by the euclidean superposition model. Solid line, linear dependence; dashed line, square-root dependence. **c**, Regression of weight-corrected T on the number of traits N. The residual effects represent the distribution of mutational effects better than the raw QTL effects, but there is still a strongly positive relationship between corrected T and degree of pleiotropy. Solid line, linear dependence; dashed line, square-root dependence. **d**, To account for the correlations between the traits we calculated the 'effective number of traits' affected by a QTL, as described in the text. This correction reduces the maximal number of pleiotropic effects from 30 (**b**, **c**), to at most 24 effective traits. Even on this scale for pleiotropy the positive regression remains significant, suggesting that pleiotropy strongly influences the total phenotypic effect of a mutation. Solid line, linear dependence; dashed line, square-root dependence.

model but also suggest a stronger increase in the total effect with more traits affected than are predicted by the euclidean superposition model. The total effect of a mutation seems to be increasing more strongly with pleiotropy than predicted if we assume that the effect on each character remains the same.

One concern with this result is that a positive relationship between the number of traits affected by a QTL and the total effect could be caused by an artefact of QTL mapping. For instance, let us assume that all the QTLs have the same degree of pleiotropy and the same total effect on average. Let us further assume that for some QTLs the effects on a few traits are too small to be detected with our experimental design. This would lead to both an underestimate of the number of traits affected and an underestimate in the total effect, because the undetected effects are not added to the estimate of the total effect. In this way QTLs for which fewer effects are detected will also have systematically smaller total effects, leading to a positive regression of the total effect on the estimated pleiotropy (the number of traits affected). To assess whether our result in Fig. 1b can be explained as such an artefact, we calculated the predicted regression slope given the detection limit for QTL effects (see Supplementary Note 3). For our data this slope is predicted to be 0.0033 or less. The observed slope is about tenfold that predicted by this model: 0.047 ± 0.0019. We conclude that the result in Fig. 1b is unlikely to be caused by a detection artefact.

We considered two other ways in which the inferences about a positive relationship between pleiotropy and total effect could be flawed. First, the distribution of QTL effects revealed by this cross might not be an unbiased sample of all mutational effects, because the two lines used in this experiment were created by divergent selection for body weight. Alleles with a larger impact on body weight therefore had a greater chance of being fixed than alleles with smaller effects. The distribution of QTL effects might thus not reflect the true mutational distribution for skeletal traits but might over-represent alleles with large effects on components of overall body size. Second, the degree of pleiotropy might be overestimated because of correlations between traits. We address these two concerns below.

To test whether our conclusions are influenced by the fact that the strains were subject to directional selection on body weight rather than mutation accumulation, we calculated the partial regression of trait value on body weight and re-analysed the weight-corrected trait values. Plausibly, these values are more representative of the distribution of mutational effects. The results are shown in Fig. 1c and Supplementary Fig. 3. There is still a clear positive relationship between the total effect and the number of traits affected. The scatter is greater, but the regression coefficient is clearly positive and significant ($t = 9.887$, $P < 2 \times 10^{-16}$, $F_{1,100} = 97.74$, $P < 0.0001$).

To test whether our inference could be due to an overestimate of the degree of pleiotropy, we considered the hypothesis that the degree of pleiotropy is less than the number of traits as a result of correlations between the traits. To address this, we first tested whether the phenotypic covariance matrix of the traits affected by a QTL has fewer dimensions than the number of traits. As discussed in Supplementary Note 5, error variance has the effect of inflating the dimensionality of a covariance matrix. To correct for this effect, we implemented an adjusted bootstrap procedure that uses an estimated error threshold to test for the dimensionality of the covariance matrix (see Supplementary Methods). All QTLs except one affect sets of characters that have full dimensionality according to this criterion. Another way of assessing the effect of trait correlations on our result is to estimate an 'effective number of traits', N_{eff}. We propose to use the following simple equation (see Supplementary Note 4)

$$N_{\mathrm{eff}} = N - \mathrm{Var}(\lambda)$$

where $\mathrm{Var}(\lambda)$ is the variance of the eigenvalues of the error-corrected correlation matrix. Figure 1d gives the result with QTL effects T and the effective number of traits. Again there is a significant positive relationship (linear regression coefficient $t = 10.99$, $P < 0.0001$; $F_{1,100} = 548.7$, $P < 0.0001$). We therefore conclude that the total effect of a pleiotropic mutation increases with the degree of pleiotropy, even when correlations between traits are taken into account. Regressing weight-corrected mutational effects on effective trait number (Supplementary Fig. 4) still gives a positive relationship between mutation effects and degree of pleiotropy ($t = 8.974$, $P = 1.75 \times 10^{-14}$; $F_{1,100} = 94.96$, $P = 3.59 \times 10^{-15}$; $R^2 = 0.4819$) but does not discriminate between the linear and the square-root regression models.

The observed linear relationship between total effect size and the number of traits implies that the average mutational effect, per trait, is increasing with the square root of the degree of pleiotropy. Mutations with a high degree of pleiotropy have more substantial effects on each trait than mutations with a more limited degree of pleiotropy. This pattern is reminiscent of the decanalizing effects of major mutations[14] except that in this case the alleles are not pathological, as other large effect alleles may be, but are part of the natural variation of the species. In addition, this effect is not due to the release of hidden genetic variation, which is a generic feature of genes with epistasis[15]. We conclude that an increased degree of pleiotropy is accompanied by an increase in the overall phenotypic effects of mutations even among 'minor effect' alleles.

These findings affect predictions about the consequences of complexity on evolvability in two ways. First, the reason that Fisher's geometric model suggests a decrease in evolvability with increasing number of traits (complexity) is that his and all studies following his approach assume that each mutation potentially affects all traits ('universal pleiotropy'). Therefore with increasing complexity it becomes increasingly unlikely that all traits are affected by a mutation in a way that causes fitness to increase. However, the effects we detected in our study are not nearly as widely pleiotropic as assumed by the model of universal pleiotropy. QTL effects are more restricted to parts of the phenotype as suggested by the idea of variational modularity[16,17]. Why this is so is unclear, but there is increasing evidence that natural selection can change pleiotropy such that evolvability increases[18]. If, at any one time, only one or a few characters are maladapted, modularity increases evolvability[19,20]. The second factor that was cited as leading to a lower evolvability of complex organisms is the assumption of constant total effect[5]. This assumption was introduced to accommodate the fact that most mutations have small effects[5,6]. In contrast, the euclidean superposition model with universal pleiotropy predicts that the probability of small-effect mutations becomes very small. This is so because if many characters are affected by each mutation, then it would be unlikely that the total effect is small. The constant-total-effect model, however, has the consequence that the average effect per character decreases and thus the rate of response to directional selection also decreases, leading to another cost of complexity prediction. However, our data show that the total effects of mutation actually increase with pleiotropy. It therefore seems that in real organisms the combination of restricted rather than universal pleiotropy and increasing total effects, could be seen as evolution's answer to the challenges of evolving complex organisms with random variation and selection.

METHODS SUMMARY

The experimental population results from an intercross of inbred mouse strains LG/J and SM/J[21–25]. We measured 70 skeletal traits on 1,040 individuals of the F_2 generation (see Supplementary Table 1). QTLs were calculated by interval mapping[22,24], and correcting for multiple tests[25]. Tests for pleiotropy were performed[10]. The additive effect of an allele is $A - a$/s.d., where a is half the difference between the homozygotes. The total effect of a QTL is $T = \sqrt{\sum A_i^2}$.

To correct for the effects of selection on body size during the generation of inbred lines, we included body weight as a covariate in the course of interval mapping[24]. We determined the true dimensionality by comparing the eigenvalues with the thresholds derived from known trait-specific measurement errors. For each QTL we constructed the phenotypic covariance matrix for the traits affected, and determined its eigenvalues and eigenvectors. The error threshold was estimated as the projection of the error variance onto the respective eigenvector. The significance of the eigenvalue is estimated by a bootstrap procedure.

We further estimated the 'effective number of traits' by accounting for correlations between traits. The measured covariance matrix was corrected for measurement error by subtracting the error variances from the diagonal. From the corrected covariance matrix we calculated the eigenvalues of the correlation matrix. The variance of these eigenvalues was subtracted from the number of traits to obtain the effective dimensionality.

To compare the fit of the data between linear and square-root regression we calculated the respective log likelihood of the model from the regression residuals, assuming a normal distribution of residuals. We used the log-likelihood ratio to estimate the ratio between model fits. We consider a log-likelihood ratio of less than 3.0 to be 'significantly' better support for the particular model.

Full Methods and any associated references are available in the online version of the paper at www.nature.com/nature.

Received 23 August 2007; accepted 28 January 2008.

1. Fisher, R. A. *The Genetical Theory of Natural Selection* (Clarendon, Oxford, 1930).
2. Rechenberg, I. *Evolutionsstrategie: Optimierung technischer Systeme nach Prinzipien der biologischen Evolution* (Fromman-Holzboog, Stuttgart, 1973).
3. Turelli, M. Effects of pleiotropy on predictions concerning mutation-selection balance for polygenic traits. *Genetics* 111, 165–195 (1985).
4. Wagner, G. P. The influence of variation and developmental constraints on the rate of multivariate phenotypic evolution. *J. Evol. Biol.* 1, 45–66 (1988).
5. Orr, H. A. Adaptation and the cost of complexity. *Evolution Int. J. Org. Evolution* 54, 13–20 (2000).
6. Wingreen, N. S., Miller, J. & Cox, E. C. Scaling of mutational effects in models of pleiotropy. *Genetics* 164, 1221–1228 (2003).
7. Chai, C. K. Analysis of quantitative inheritance of body size in mice II. gene action and segregation. *Genetics* 41, 165–178 (1956).
8. Eppig, J. T., Bult, C. J., Kadin, J. A., Richardson, J. E. & Blake, J. A. and the members of the Mouse Genome Database Group. The mouse genome data base (MGD): from genes to mice – a community resource for mouse biology. *Nucleic Acids Res.* 33, D471–D475 (2005).
9. Kenney-Hunt, J. P. *et al.* Pleiotropic patterns of quantitative trait loci for seventy murine skeletal traits. *Genetics* (in the press).
10. Knott, S. A. & Haley, C. S. Multitrait least squares for quantitative trait loci detection. *Genetics* 156, 899–911 (2000).
11. Xu, S. Theoretical basis of the Beavis effect. *Genetics* 165, 2259–2268 (2003).
12. Wagner, G. P. Multivariate mutation-selection balance with constrained pleiotropic effects. *Genetics* 122, 223–234 (1989).
13. Waxman, D. & Peck, J. R. Pleiotropy and preservation of perfection. *Science* 279, 1210–1213 (1998).
14. Waddington, C. H. *The Strategy of Genes* (Macmillan, New York, 1957).
15. Hermisson, J. & Wagner, G. P. The population genetic theory of hidden variation and genetic robustness. *Genetics* 168, 2271–2284 (2004).
16. Wagner, G. P. & Altenberg, L. Complex adaptation and the evolution of evolvability. *Evolution Int. J. Org. Evolution* 50, 967–976 (1996).
17. Hansen, T. F. Is modularity necessary for evolvability? Remarks on the relationship between pleiotropy and evolvability. *Biosystems* 69, 83–94 (2003).
18. Wagner, G. P., Pavlicev, M. & Cheverud, J. M. The road to modularity. *Nature Rev. Genet.* 8, 921–931 (2007).
19. Welch, J. J. & Waxman, D. Modularity and the cost of complexity. *Evolution Int. J. Org. Evolution* 57, 1723–1734 (2003).
20. Martin, G. & Lenormand, T. A general multivariate extension of Fisher's geometrical model and the distribution of mutation fitness effects across species. *Evolution Int. J. Org. Evolution* 60, 893–907 (2006).
21. Cheverud, J. M. *et al.* Quantitative trait loci for murine growth. *Genetics* 142, 1305–1319 (1996).
22. Vaughn, T. T. *et al.* Mapping quantitative trait loci for murine growth: a closer look at genetic architecture. *Genet. Res.* 74, 313–322 (1999).
23. Cheverud, J. M. *et al.* Genetic architecture of adiposity in the cross of LG/J and SM/J inbred mice. *Mamm. Genome* 12, 3–12 (2001).
24. Haley, C. S. & Knott, S. A. A simple regression method for mapping quantitative trait loci in line crosses using flanking markers. *Heredity* 69, 315–324 (1992).
25. Cheverud, J. M. A simple correction for multiple comparisons in interval mapping genome scans. *Heredity* 87, 52–58 (2001).

Supplementary Information is linked to the online version of the paper at www.nature.com/nature.

Acknowledgements We thank A. Pyle, A. Kondrashov and B. Walsh for suggestions that have improved this manuscript. We thank the members of the Wagner and Cheverud laboratories for critical discussion. J.P. and D.W. thank members of the evolution group at Sussex. J.M.C. is funded by the National Institutes of Health and the National Science Foundation (NSF), G.P.W. acknowledges funding from the NSF, the Humboldt Foundation and the John Templeton Foundation. M.P. is funded by the Austrian Science Foundation (FWF) Fellowship, and the work of D.W. was supported by the Leverhulme Trust.

Author Contributions G.P.W. conceived this study, participated in the statistical analysis and wrote the manuscript. J.P.K.-H. collected the morphological data and performed the QTL analysis. M.P. did the statistical analyses. J.M.C. was responsible for generating the mouse populations and the genotype data used in the original mapping and advised on the pleiotropic scaling analysis. J.P. and D.W. performed a theoretical analysis of the scaling of trait effects with pleiotropy. All authors participated in the preparation of the manuscript.

Author Information Reprints and permissions information is available at www.nature.com/reprints. Correspondence and requests for materials should be addressed to G.P.W. (gunter.wagner@yale.edu) or J.M.C. (cheverud@pcg.wustl.edu).

LETTERS

The *Drosophila* pheromone cVA activates a sexually dimorphic neural circuit

Sandeep Robert Datta[1]*, Maria Luisa Vasconcelos[1]*, Vanessa Ruta[1], Sean Luo[1], Allan Wong[1,2], Ebru Demir[3], Jorge Flores[1], Karen Balonze[1], Barry J. Dickson[3] & Richard Axel[1]

Courtship is an innate sexually dimorphic behaviour that can be observed in naive animals without previous learning or experience, suggesting that the neural circuits that mediate this behaviour are developmentally programmed[1]. In *Drosophila*, courtship involves a complex yet stereotyped array of dimorphic behaviours that are regulated by Fru^M, a male-specific isoform of the *fruitless* gene[2–5]. Fru^M is expressed in about 2,000 neurons in the fly brain, including three subpopulations of olfactory sensory neurons and projection neurons (PNs). One set of Fru^+ olfactory neurons expresses the odorant receptor Or67d and responds to the male-specific pheromone *cis*-vaccenyl acetate (cVA)[6–10]. These neurons converge on the DA1 glomerulus in the antennal lobe. In males, activation of $Or67d^+$ neurons by cVA inhibits courtship of other males, whereas in females their activation promotes receptivity to other males[7]. These observations pose the question of how a single pheromone acting through the same set of sensory neurons can elicit different behaviours in male and female flies. Anatomical or functional dimorphisms in this neural circuit might be responsible for the dimorphic behaviour. We therefore developed a neural tracing procedure that employs two-photon laser scanning microscopy to activate the photoactivatable green fluorescent protein[11]. Here we show, using this technique, that the projections from the DA1 glomerulus to the protocerebrum are sexually dimorphic. We observe a male-specific axonal arbor in the lateral horn whose elaboration requires the expression of the transcription factor Fru^M in DA1 projection neurons and other Fru^+ cells. The observation that cVA activates a sexually dimorphic circuit in the protocerebrum suggests a mechanism by which a single pheromone can elicit different behaviours in males and in females.

In initial experiments, we expressed photoactivatable green fluorescent protein (PA-GFP) in flies in which the GAL4 enhancer-trap *GH146* (ref. 12) drives the expression of *UAS-PA-GFP* in 60% of the PNs that innervate most glomeruli in the antennal lobe (Fig. 1a, b). PA-GFP exhibits low-level fluorescence, sufficient to identify

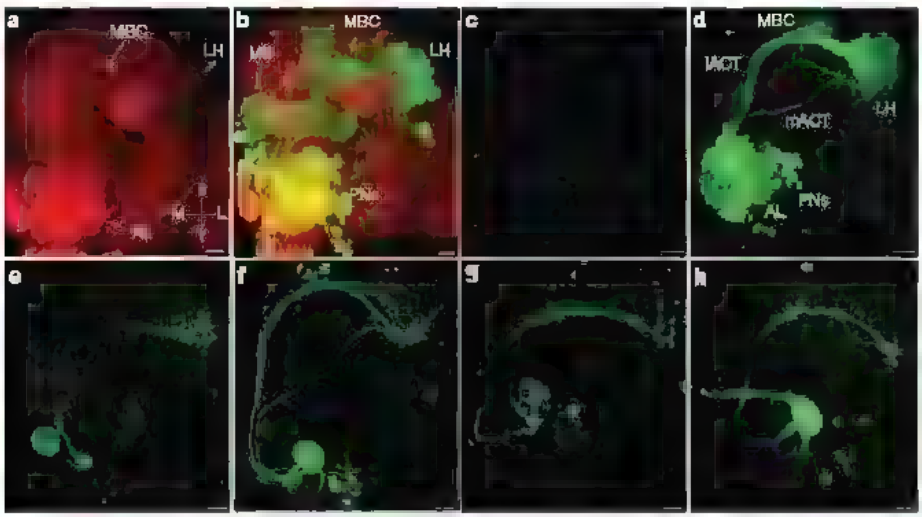

Figure 1 | Tracing populations, subpopulations and single neurons in the *Drosophila* olfactory system. **a**, *Z* projection of a confocal image of a *Drosophila* brain (*GH146; UAS-PA-GFP*) stained with the nc82 antibody (red) reveals neuropil, and highlights structures in the olfactory system including the antennal lobe (AL, note individual glomeruli within the lobe), the lateral horn (LH) and the mushroom body calyx (MBC). D, dorsal, V, ventral, M, medial, L, lateral. **b**, *Z* projection of a confocal image of the same brain in **a** stained with anti-GFP antibodies (green) reveals PA-GFP expression under the control of *GH146* in projection neurons (lateral PN group indicated by PN label) and extrinsic neurons that innervate the mushroom body (MB). **c**, **d**, *Z* projections of two-photon laser scanning microscope imaging of live fly brains expressing PA-GFP under control of the *GH146* driver before (**c**) and after (**d**) photoconversion reveals PN cell bodies and projections from the antennal lobe to the mushroom body and lateral horn. mACT, medial antennocerebral tract; iACT, inner antennocerebral tract. **e**, **f**, Photoconversion of a single glomerulus VM3 (**e**) or DA1 (**f**) in the live fly brain with the *GH146* driver. **g**, Photoconversion of a single *GH146* DA1 PN. **h**, Photoconversion of the DA1 glomerulus in flies expressing PA-GFP under the control of the *Fru* P1 promoter. Note that *GH146* labels six lateral neurons that project through the iACT and one or two ventral PNs that project through the mACT, whereas fru^{GAL4} labels only six lateral neurons that project through the iACT (see Supplementary Fig. 4). All images are oriented similarly to **a**. Scale bars, 10 μm.

[1]Department of Biochemistry and Molecular Biophysics and Howard Hughes Medical Institute, College of Physicians and Surgeons, Columbia University, New York, New York 10032, USA. [2]Division of Biology 216-76 and Howard Hughes Medical Institute, California Institute of Technology, Pasadena, California 91125, USA. [3]Research Institute of Molecular Pathology (IMP), Dr Bohr-gasse 7, A-1030 Vienna, Austria.
*These authors contributed equally to this work.

individual glomeruli, that is enhanced 100-fold after photoconversion with high-energy light. We photoactivated the PA-GFP with a two-photon laser scanning microscope to localize 710-nm light with submicrometre three-dimensional precision. Photoactivation of the antennal lobe neuropil, encompassing all glomeruli, results in intense labelling of the dendritic arbors of *GH146* PNs. Diffusion of PA-GFP from the illuminated dendritic arbors allowed us to also reveal the cell bodies and axonal projections of the multiple *GH146* PNs (Fig. 1c, d). Photoactivation of individual glomeruli (VM3 and DA1) reveals the dendritic arbors, cell bodies and projections of the subpopulation of *GH146* PNs that innervate a single glomerulus (Fig. 1e, f).

We then devised an approach to allow the tracing of individual PNs that innervate identified glomeruli. We exposed the DA1 glomerulus to low levels of photoconverting light and then rapidly imaged the antennal lobe to identify the PN cell bodies that show modest increases in fluorescence intensity. Under these limiting conditions of photoactivation, diffusion of PA-GFP into axonal projections was not observed. We next strongly photoactivated a single weakly labeled PN cell body at higher light intensity to reveal the axonal projections of an individual PN that innervates the DA1 glomerulus (Fig. 1g). Thus, two-photon laser scanning microscope-mediated activation of PA-GFP provides sufficient spatial resolution and photoconversion energy to reveal the neuronal processes of defined neuronal populations as well as individual neurons in the fly brain.

The development of a combined genetic and optical neural tracing method permitted us to compare the topography of projections from Fru^+ PNs that innervate the cVA-responsive DA1 glomerulus in male and female flies. Flies in which GAL4 is expressed under the control of the P1 *fruitless* promoter responsible for generating Fru^M (fru^{GAL4})[2,3] were crossed with flies harbouring the *UAS-PA-GFP* transgene. P1 transcripts from the modified fru^{GAL4} allele do not undergo the sexually dimorphic splicing observed for the wild-type *fru* allele, and they therefore allow us to mark Fru^+ cells in both sexes[2,3]. Unilateral photoactivation of the fly brain reveals many Fru^+ cells, including neurons in the antennal lobe (Supplementary Fig. 1). Specific photoactivation of the DA1 glomerulus reveals six Fru^+ PNs in both male and female flies (Fig. 1h and Supplementary Fig. 4; 6.23 ± 0.13 in females, 6.27 ± 0.14 in males) that innervate this glomerulus. The cell bodies of these neurons reside in the lateral PN cluster, not the dorsal cluster as previously suggested[3].

It is possible that the sex-specific behavioural responses to cVA result from different functional responses of the DA1 glomerulus in the two sexes despite there being no apparent difference in the number or location of Fru^+ DA1 PNs. We therefore expressed the Ca^{2+}-sensitive fluorescent protein GCaMP[13] in Fru^+ neurons and used two-photon imaging to examine increases in Ca^{2+} in the DA1 glomerulus in response to cVA. We detected large increases in Ca^{2+} within the DA1 glomerulus by two-photon imaging after exposure of an intact, behaving fly to cVA (Fig. 2a; see Methods). However, we did not observe any differences between male and female responses over a broad range of cVA concentrations.

These imaging experiments report local changes in the concentration of Ca^{2+} in both the presynaptic and postsynaptic compartments, because both Or67d-expressing neurons and DA1 PNs are Fru^+ (refs 3,4,8,9). We therefore examined whether the electrophysiological properties of Fru^+ DA1 PNs were sexually dimorphic. We photoactivated the DA1 glomerulus to identify Fru^+ DA1 PNs and used the enhanced fluorescence to guide a patch electrode to the cell bodies (Fig. 2b). We recorded from Fru^+ DA1 PNs in the loose patch configuration in an intact fly preparation and noted no significant difference in the spike frequency or response kinetics between males and females when tested at several concentrations of cVA (Fig. 2c, d). These responses are comparable to those previously observed in whole-cell recordings of female DA1 PNs[14]. This result demonstrates that male and female DA1 PNs show similar electrophysiological responses to cVA despite the previously noted dimorphism in the size of the DA1 glomerulus[3,4,13].

We next examined the projection patterns of Fru^+ DA1 PNs in the two sexes. Photoconversion of the DA1 glomerulus allowed us to reveal the projection patterns of the population of DA1 PNs in the lateral horn in living brains. Despite significant similarity in the axonal arbors of DA1 PNs in males and females (Fig. 3a), we observed an increase in the density of ventral axonal branches in the male (Fig. 3a, arrowhead). Quantification of differences in branch patterns in multiple individual male and female flies was hampered by variations in the orientation of the live brain during microscopy. We therefore altered our approach to employ fixed brains stained with the antibody nc82 to label the synaptic neuropil of the lateral horn. We used an image registration algorithm (see Methods) to first 'warp' the nc82 channel of individual brains onto a reference brain[16] and then map the PA-GFP fluorescence onto this reference brain (Fig. 3b). The registration error averaged less than 2 μm in any dimension when measured at the neuropil edge (Supplementary Fig. 2). We observed that the projections from the DA1 glomerulus target the anterior ventromedial region of the LH. The projection pattern is triskelion-shaped, with ventral, lateral and dorsal branches. Fru^+ DA1 projections from males have additional axonal branches that extend ventromedially (Fig. 3c). Superposition of the DA1 projections taken from ten male and ten female flies confirms this observation (Fig. 3d), indicating that information carried by Fru^+ DA1 PNs is differentially segregated in the lateral horn of the two sexes. As a control we performed a similar analysis of the PN projections from the Fru^- glomerulus VM3, which responds to alcohols and acetates[8,9,17]. Superposition of the projections from VM3 reveals no consistent differences in the pattern of axonal projections in the lateral horn between the two sexes (Fig. 3e, f). These observations show that our image alignment procedure does not introduce sex-specific biases in projection patterns and that the dimorphic

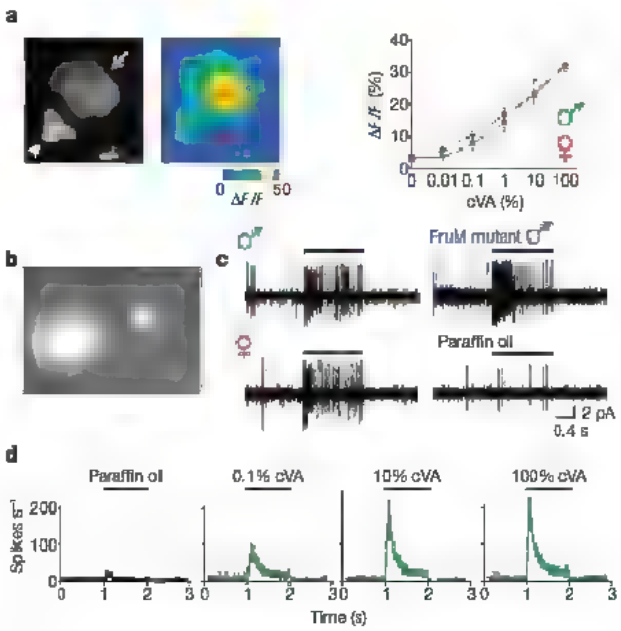

Figure 2 | Functional characterization of the DA1 glomerulus and Fru^+ DA1 PNs. **a**, Two-photon laser scanning microscope imaging of background fluorescence (left) and pseudocoloured maximal response (middle) of the DA1 glomerulus (arrow) and PNs (arrowhead) to cVA in a fly expressing the fluorescent Ca^{2+} reporter GCaMP in Fru^+ cells. Peak average glomerular responses of male (green) and female (red) flies after a 1-s exposure to cVA at the indicated doses (left, $n = 8$ per sex; error bars indicate s.e.m.). **b**, Epifluorescence image of a patch pipette targeting a Fru^+ DA1 PN after photoconversion of the DA1 glomerulus. **c**, **d**, Single traces (**c**) and peristimulus time histograms (**d**) (error bars indicate s.e.m.; $n = 6$ per genotype) of loose patch recordings of male, female and *fru* mutant male flies (colours indicated in **c**) before and after a 1-s exposure to cVA at the doses indicated.

projection patterns we observe for the Fru$^+$ glomerulus DA1 are not a general feature of projections from all glomeruli.

The anatomical dimorphism observed at the level of the population of axons is also shown by the axons of single identified neurons. Tracing individual Fru$^+$ DA1 neurons after warping revealed that the ventral axonal branches of male PNs define a male-specific region of protocerebral space (about 600 μm^3; Figs 4 and 5a, and Supplementary Fig. 3). Each individual male in our data set sends at least one axon branch into this area. This area seems to partly overlap a region of neuropil in the lateral horn that was recently shown to be larger in male flies than in female flies[15]. In addition, the total density of ventrally oriented axonal branches is significantly greater in males than in females (Fig. 5a). In contrast, the total innervation of the dorsal axonal arbor showed no statistically significant differences between sexes (Fig. 5a). We were unable to identify a similar female-specific area, although there are several smaller areas (particularly laterally) that appear to have an increased density of female axons. The data from single-axon tracing, along with our observations from populations of DA1 neurons, indicate that DA1 PN projections are sexually dimorphic.

Fru mutant males court other males with high frequency[2,3]. If the male-specific arbor contributes to the dimorphic behavioural response, we expect that the DA1 PN projection patterns will be regulated by the *fruitless* gene. We therefore made visible the axonal projections of single DA1 PNs in *fru* mutant males, and observed that DA1 PNs lack the characteristic male-specific axonal branches and exhibit a branching pattern more characteristic of wild-type females. However, the feminization is not complete in that the male-specific ventral axonal branches are significantly reduced but not completely eliminated in *fru* mutant males (Figs 4 and 5a). Thus, the male pattern of projections of Fru$^+$ DA1 PNs requires the male-specific isoform of *fru*, Fru^M.

We also show that the ectopic expression of Fru^M in females masculinizes the axonal arbor of their DA1 PNs. Projections of single Fru$^+$ DA1 PNs in female flies that express Fru^M ($fru^{GAL4}/fru^{UAS\text{-}FruM}$; see Methods) exhibit a striking increase in axonal projections to the ventral male-enhanced area (Fig. 4). Quantitative analysis of these

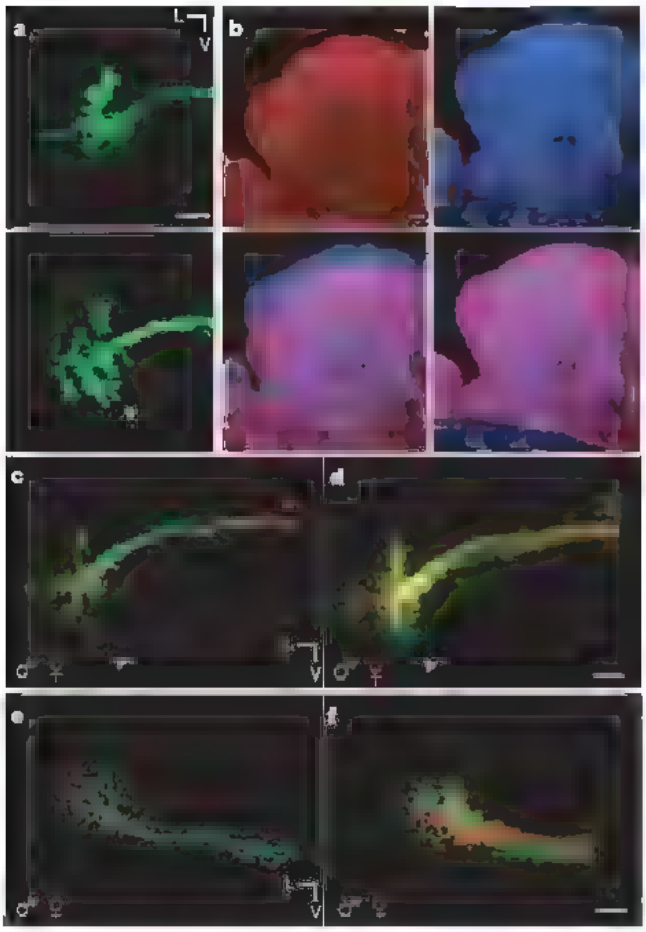

Figure 3 | Tracing and registration of DA1 glomerular projections reveals sexually dimorphic projections in the lateral horn. **a**, *Z* projection of two-photon laser scanning microscope images of the lateral horns of live female (top) and male (bottom) fly brains after photoconversion of the DA1 glomerulus. Apparent increased ventral male density is indicated by an arrowhead. **b**, Top left: two-channel brain image of a single neuron labelled by photoconversion (green) before immunostaining with nc82 antibody (red) to mark neuropil. Top right: reference brain generated by averaging ten male and ten female nc82 channels. Bottom left: superposition of these images before warping. Bottom right: superposition of these images after warping. **c**, Superposition of male (green) and female (red) projections after photoconversion of all Fru$^+$ DA1 PNs in single flies reveals a ventral region of sexual dimorphism (arrowhead). **d**, Superposition of ten male and ten female DA1 projection patterns after photoconversion of all Fru$^+$ DA1 PNs. **e**, Superposition of photoconverted male (green) and female (red) projections from the VM3 glomerulus in single flies, similar to **c**. Note that VM3 typically labels two PNs, which travel in independent pathways through the lACT. **f**, Image similar to **d**, with superposition of seven male and seven female photoconverted VM3 projection patterns. Scale bars, 10 μm.

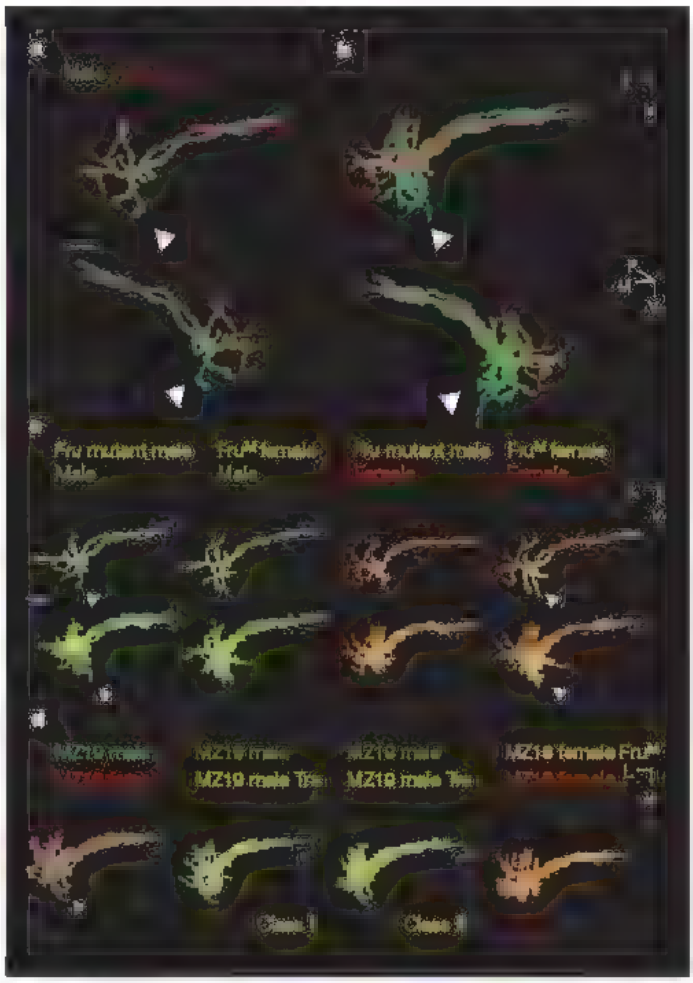

Figure 4 | Fru^M controls sexually dimorphic pheromone response circuitry. **a**, Superposition of traces of single Fru$^+$ DA1 PNs in Z projection (top) and after rotation about 120° about the *Z* axis (lower) projections. Genotypes (male, female) are coloured as indicated. Lateral and ventral correspond to *x* and *y* imaging axes, respectively; posterior corresponds to the *z* axis. **b**, Images as in **a** including three neurons of each genotype. **c**, Single and multiple neurons overlaid as in **a** and **b** in *Z* projection with genotypes (male, female, *fru* mutant male and female expressing Fru^M) in the colours indicated. Arrowheads indicate the ventral region that shows enhanced male innervation. **d**, Superposition of traces of three *MZ19* DA1 PNs in *Z* projection, with genotypes (*MZ19* male, *MZ19* female, *MZ19* male expressing Tra, *MZ19* female expressing Fru^M) in the colours indicated. Enhanced ventral male innervation is indicated by an arrowhead. Class I PNs are male neurons expressing Tra that have masculine arbors, whereas class II PNs have feminine arbors (see Supplementary Fig. 5). Scale bar, 10 μm.

branches reveals that expression of Fru^M in females renders their ventral axon branch pattern statistically indistinguishable from that of males (Fig. 5). The innervation patterns of individual neurons are sufficient for a computational discrimination algorithm to effectively distinguish individual females from Fru^M-expressing females with 100% accuracy, and individual males from *fru* mutant males with more than 91% accuracy (Supplementary Fig. 3). Thus, analysis of the PN projections of both single defined neurons and populations of neurons reveal that Fru^+ DA1 PNs project to different regions of the protocerebrum in male and female flies. Moreover, this anatomical dimorphism in the neural circuit is controlled by the dimorphic transcription factor, Fru^M.

We next examined whether the formation of the male-specific arbor requires the action of Fru^M in DA1 projection neurons. The enhancer-trap *MZ19* (refs 18,19) drives the expression of GAL4 in six DA1 PNs, about ten additional PNs that innervate two Fru^- glomeruli, and 25 extrinsic neurons of the mushroom body (Supplementary Fig. 4a). Flies harbouring fru^{GAL4}, *MZ19* or *MZ19*;fru^{GAL4} all reveal expression of PA-GFP in six DA1 PNs (Supplementary Fig. 4b). This suggests that the six lateral DA1 neurons labelled by the *MZ19* and fru^{GAL4} lines are identical. In accord with this observation, male and female DA1 neurons in *MZ19* flies have a sexually dimorphic pattern of projections that closely resembles the dimorphic branching observed for Fru^+ DA1 PNs (Figs 4d and 5b, and Supplementary Figs 4a and 5). We therefore eliminated Fru^M expression in male *MZ19* neurons by expression of Tra, which directs the female-specific splicing of *fruitless* transcripts[20–22]. Genetic feminization of male DA1 PNs in *MZ19/UAS-tra* flies results in two anatomical classes of DA1 projection neurons. Half of the genetically feminized DA1 PNs show a reduction in the male-specific arbor and closely resemble male DA1 projection neurons defective for Fru^M. The remaining genetically feminized neurons exhibit the wild-type male-specific branching patterns (Fig. 4d and Supplementary Fig. 5). Within a single male *MZ19/UAS-tra* fly, neurons of both anatomical classes were observed. These data suggest that Fru^M is required in DA1 PNs to generate a male-specific projection pattern, but its action in this genetic context is partly penetrant.

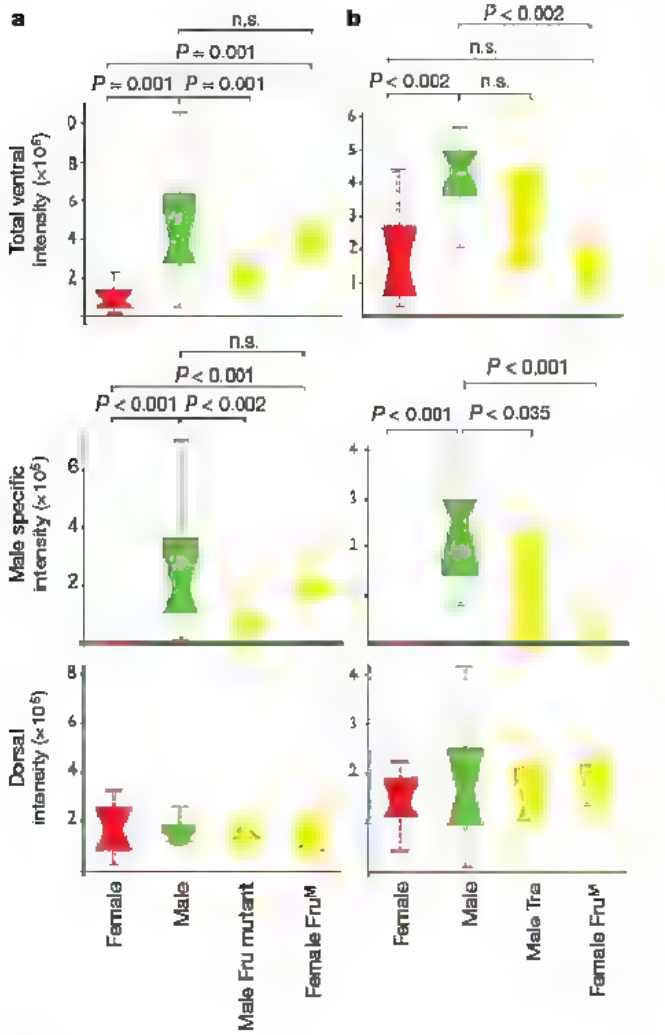

Figure 5 | Quantitative analysis of ventral male-enhanced region. **a**, Box plot of ventrally oriented branch density, male-specific branch density and dorsal branch density of individual traced fru^{GAL4} neurons (see Supplementary Fig. 3 for a graphical illustration of the quantified regions) in arbitrary units, with genotypes as indicated. The median is given by the box-plot waist, the top and bottom of boxes denote the 25th and 75th centiles, and range bars denote the largest and smallest data point within 2 s.d. of the mean, outliers greater than 1.5-fold the interquartile range are not shown ($n = 12$ males, $n = 10$ females, $n = 10$ females expressing Fru^M, $n = 9$ *fru* mutant males) **b**, Analysis similar to that in **a** for *MZ19* males ($n = 10$), *MZ19* females ($n = 10$), *MZ19* males expressing Tra ($n = 10$) and *MZ19* females expressing Fru^M ($n = 9$). *P* values in both panels for relevant comparisons are shown by Wilcoxon pairwise rank sum test.

The anatomical dimorphism we observe in females renders their ventral axon branch pattern statistically indistinguishable from that of males (Fig. 5). The innervation patterns of individual neurons are sufficient for a computational discrimination algorithm to effectively distinguish individual females from Fru^M-expressing females with 100% accuracy, and individual males from *fru* mutant males with more than 91% accuracy (Supplementary Fig. 3). Thus, analysis of the PN projections of both single defined neurons and populations of neurons reveal that Fru^+ DA1 PNs project to different regions of the protocerebrum in male and female flies. Moreover, this anatomical dimorphism in the neural circuit is controlled by the dimorphic transcription factor, Fru^M.

We have also examined whether the expression of Fru^M in female DA1 PNs masculinizes the DA1 axon arbor. DA1 PNs in female *MZ19*; $fru^{UAS\text{-}FruM}$ flies do not significantly innervate the male-specific area, although most send minor branches into the ventral region of the lateral horn (Figs 4d and 5b, and Supplementary Fig. 5). This is in contrast with observations with $fru^{GAL4}/fru^{UAS\text{-}FruM}$ strains that exhibit a transformation of the female DA1 PN branching pattern into a complete male-specific arbor (Figs 4 and 5a). Taken together, these results suggest that Fru^M is required in both DA1 PNs and in other Fru^+ neurons to generate the male-specific pattern of ventral axon arborization in the lateral horn.

In *Drosophila*, courtship behaviour is governed by pheromonal excitation of peripheral olfactory pathways that ultimately activate behavioural circuits in higher brain centres. One pheromone elaborated by the male, cVA, suppresses male–male courtship but in females enhances receptivity to courting males[7]. cVA activates the DA1 glomerulus, which is innervated by PNs[3,4] that have sexually dimorphic projections in the lateral horn. This dimorphic circuit is under control of the transcription factor Fru^M, a male-specific isoform of *fruitless*. Moreover, the dimorphism in this circuit correlates with behaviour. In males mutant for Fru^M, cVA no longer suppresses male–male courtship and males exhibit a feminized pattern of DA1 projections. In females that express Fru^M, DA1 PNs exhibit a male pattern of axonal arbors in the lateral horn, and these females show reduced sexual receptivity (M.L.V. and R.A., unpublished observations). These observations are in accord with a mechanism in which the anatomical differences we observe in Fru^+ DA1 projection neurons contribute to the distinct behaviours elicited by cVA in the two sexes. In *Drosophila*, dimorphism in the Fru^+ SP2 (ref. 3) and mAL neurons[23] has been observed, but the behavioural function of these circuits is unknown.

The anatomical dimorphism we observe may be translated into a behavioural dimorphism if the connections between DA1 PNs and third-order neurons differ between the sexes. Third-order neurons whose dendrites innervate the ventral lateral horn may either receive greater input from male PNs or may restrict their synapses to the male-specific region of the DA1 axon arbor. The relatively small size of the male-specific arbor, about the volume of a glomerulus, implies a precision of connectivity in higher processing centres in the fly brain. The stereotyped and local precision of synaptic connections is an organizing principle in the antennal lobe and may be a common feature of invertebrate nervous systems.

Characterization of specific neural circuits that may mediate behaviour, as we describe here for the pheromone-responsive DA1 pathway requires the development of tracing approaches that label defined populations of neurons. The distinction between genetic approaches—including MARCM[24], Flp-Out[25,26] and PA-GFP-based tracing—and the histological approaches of Golgi and Cajal[27] 100 years ago is the ability to use genetic markers to identify partners

in the neural circuit more precisely. The targeted illumination of PA-GFP permits non-random, optically guided labelling of individual neurons from either anatomically or genetically defined subsets of neurons. Moreover, PA-GFP can be photoactivated in neurons in the living brain and allows electrophysiological recordings of labelled cells. This approach to neural tracing and recording in a defined circuit can be readily adapted to other brain regions in both the fly and mouse.

METHODS SUMMARY

In brief, PA-GFP-based neuronal tracing was performed with *UAS-PA-GFP* flies that were crossed to driver lines expressing Gal4 in specific subsets of neurons. Photoconversion of PA-GFP and tracing of glomerulus-specific projection neurons was achieved after first revealing PA-GFP background fluorescence at the imaging wavelength (925 nm) by two-photon microscopy with relatively high laser powers. These background images allowed the identification of glomeruli (and the specification of regions of interest within these glomeruli to target for photoconversion) on the basis of anatomical position. Because of unavoidable variability in our preparation, each glomerulus was initially subjected to one to three probe pulses of laser light at the photoconversion wavelength (710 nm) to establish empirically the minimum power (range 5–40 mW) required for the effective photoactivation of PA-GFP; this step prevented excessive photodamage or photobleaching of the PA-GFP. We then pulsed the targeted region with 710-nm light using a protocol that incorporated fixed waiting periods to permit the photoconverted PA-GFP to effectively diffuse out of the targeted area and label connected cell bodies and projections. Single neurons were identified for targeted photoconversion by acquiring an initial background *Z*-stack before subjecting the brain to any photoconversion, and then applying one to three probe pulses of photoconverting 710-nm light to the glomerulus of interest as described above. A second *Z*-stack was then acquired, and both *Z*-stacks were compared using the ImarisXT 3D image rendering software (Bitplane). Projection neurons whose fluorescence intensity was increased as a result of photoconversion of a glomerulus were identified, and their cell bodies were targeted for exposure to 710-nm light as described above.

Detailed descriptions of fly stocks, two-photon microscopy, functional imaging, electrophysiology, image registration, image analysis and discriminator construction and analysis are given in the Supplementary Methods section.

Received 20 December 2007; accepted 8 February 2008.
Published online 27 February 2008.

1. Hall, J. C. The mating of a fly. *Science* 264, 1702–1714 (1994)
2. Demir, E. & Dickson, B. J. fruitless splicing specifies male courtship behavior in *Drosophila*. *Cell* 121, 785–794 (2005)
3. Stockinger, P. *et al.* Neural circuitry that governs *Drosophila* male courtship behavior. *Cell* 121, 795–807 (2005)
4. Manoli, D. S. *et al.* Male-specific fruitless specifies the neural substrates of *Drosophila* courtship behaviour. *Nature* 436, 395–400 (2005)
5. Billeter, J. C. *et al.* Isoform-specific control of male neuronal differentiation and behavior in *Drosophila* by the fruitless gene. *Curr. Biol.* 16, 1063–1076 (2006)
6. Clyne, P., Grant, A., O'Connell, R. & Carlson, J. R. Odorant response of individual sensilla on the *Drosophila* antenna. *Invert. Neurosci.* 3, 127–135 (1997)
7. Kurtovic, A., Widmer, A. & Dickson, B. J. A single class of olfactory neurons mediates behavioural responses to a *Drosophila* sex pheromone. *Nature* 446, 542–546 (2007).
8. Couto, A., Alenius, M. & Dickson, B. J. Molecular, anatomical, and functional organization of the *Drosophila* olfactory system. *Curr. Biol.* 15, 1535–1547 (2005)
9. Fishilevich, E. & Vosshall, L. B. Genetic and functional subdivision of the *Drosophila* antennal lobe. *Curr. Biol.* 15, 1548–1553 (2005).
10. Ha, T. S. & Smith, D. P. A pheromone receptor mediates 11-cis-vaccenyl acetate-induced responses in *Drosophila*. *J. Neurosci.* 26, 8727–8733 (2006)
11. Patterson, G. H. & Lippincott-Schwartz, J. A photoactivatable GFP for selective photolabeling of proteins and cells. *Science* 297, 1873–1877 (2002)
12. Stocker, R. F., Heimbeck, G., Gendre, N. & de Belle, J. S. Neuroblast ablation in *Drosophila* P[GAL4] lines reveals origins of olfactory interneurons. *J. Neurobiol.* 32, 443–456 (1997)
13. Nakai, J., Ohkura, M. & Imoto, K. A high signal-to-noise Ca^{2+} probe composed of a single green fluorescent protein. *Nature Biotechnol.* 19, 137–141 (2001)
14. Schlief, M. L. & Wilson, R. I. Olfactory processing and behavior downstream from highly selective receptor neurons. *Nature Neurosci.* 10, 623–630 (2007)
15. Kondoh, Y., Kaneshiro, K. Y., Kimura, K. & Yamamoto, D. Evolution of sexual dimorphism in the olfactory brain of Hawaiian *Drosophila*. *Proc. R. Soc. B* 270, 1005–1013 (2003)
16. Jefferis, G. S. *et al.* Comprehensive maps of *Drosophila* higher olfactory centers: spatially segregated fruit and pheromone representation. *Cell* 128, 1187–1203 (2007)
17. Hallem, E. A. & Carlson, J. R. Coding of odors by a receptor repertoire. *Cell* 125, 143–160 (2006)
18. Ito, K. *et al.* The organization of extrinsic neurons and their implications in the functional roles of the mushroom bodies in *Drosophila melanogaster* Meigen. *Learn. Mem.* 5, 52–77 (1998).
19. Jefferis, G. S. *et al.* Developmental origin of wiring specificity in the olfactory system of *Drosophila*. *Development* 131, 117–130 (2004)
20. Heinrichs, V., Ryner, L. C. & Baker, B. S. Regulation of sex-specific selection of *fruitless* 5′ splice sites by transformer and transformer-2. *Mol. Cell. Biol.* 18, 450–458 (1998)
21. Ito, H. *et al.* Sexual orientation in *Drosophila* is altered by the satori mutation in the sex-determination gene fruitless that encodes a zinc finger protein with a BTB domain. *Proc. Natl Acad. Sci. USA* 93, 9687–9692 (1996).
22. Ryner, L. C. *et al.* Control of male sexual behavior and sexual orientation in *Drosophila* by the *fruitless* gene. *Cell* 87, 1079–1089 (1996)
23. Kimura, K., Ote, M., Tazawa, T. & Yamamoto, D. Fruitless specifies sexually dimorphic neural circuitry in the *Drosophila* brain. *Nature* 438, 229–233 (2005)
24. Lee, T. & Luo, L. Mosaic analysis with a repressible cell marker (MARCM) for *Drosophila* neural development. *Trends Neurosci.* 24, 251–254 (2001)
25. Wong, A. M., Wang, J. W. & Axel, R. Spatial representation of the glomerular map in the *Drosophila* protocerebrum. *Cell* 109, 229–241 (2002)
26. Basler, K. & Struhl, G. Compartment boundaries and the control of *Drosophila* limb pattern by hedgehog protein. *Nature* 368, 208–214 (1994)
27. Cajal, S. R. *Manual de Histologia normal y Tecnica micrografica* (Pascual Aguilar, Valencia, 1889)

Supplementary Information is linked to the online version of the paper at www.nature.com/nature.

Acknowledgements We thank G. Struhl, L. Vosshall, B. Sabatini, B. Bloodgood and members of the Axel laboratory for discussions about the experiments in this manuscript; J. Meier for technical assistance; J. Rafter for assistance in measuring the microscope point-spread function; A. Gerber for assistance with warping techniques; and P. J. Kisloff for assistance in the preparation of this manuscript. Financial support was provided by the Helen Hay Whitney Foundation (S.R.D., V.R.) and the Howard Hughes Medical Institute, the Mathers Foundation and the Gates Foundation (R.A.).

Author Information Reprints and permissions information is available at www.nature.com/reprints. Correspondence and requests for materials should be addressed to R.A. (ra27@columbia.edu)

LETTERS

Molecular identification of a retinal cell type that responds to upward motion

In-Jung Kim[1]*, Yifeng Zhang[1]*, Masahito Yamagata[1], Markus Meister[1] & Joshua R. Sanes[1]

The retina contains complex circuits of neurons that extract salient information from visual inputs. Signals from photoreceptors are processed by retinal interneurons, integrated by retinal ganglion cells (RGCs) and sent to the brain by RGC axons. Distinct types of RGC respond to different visual features, such as increases or decreases in light intensity (ON and OFF cells, respectively), colour or moving objects[1–5]. Thus, RGCs comprise a set of parallel pathways from the eye to the brain. The identification of molecular markers for RGC subsets will facilitate attempts to correlate their structure with their function, assess their synaptic inputs and targets, and study their diversification. Here we show, by means of a transgenic marking method, that junctional adhesion molecule B (JAM-B) marks a previously unrecognized class of OFF RGCs in mice. These cells have asymmetric dendritic arbors aligned in a dorsal-to-ventral direction across the retina. Their receptive fields are also asymmetric and respond selectively to stimuli moving in a soma-to-dendrite direction; because the lens reverses the image of the world on the retina, these cells detect upward motion in the visual field. Thus, JAM-B identifies a unique population of RGCs in which structure corresponds remarkably to function.

Several adhesion molecules of the immunoglobulin superfamily (IgSF) are selectively expressed by RGC subsets in chick[6,7]. On the basis of these results, we surveyed the expression of about 200 IgSF genes in the mouse retina (see Methods). One such gene, *JAM-B*, was expressed by a small fraction of RGCs (Fig. 1a). Analysis of whole mounts showed that the *JAM-B*-positive RGCs were spaced relatively evenly across the retina (Fig. 1b, c), a 'mosaic' arrangement characteristic of many retinal cell types that share specific physiological or molecular properties[1,2,8]. JAM-B has been implicated in tight junction assembly and interactions of haematopoietic cells but expression by neurons has not been reported[9].

To mark these cells for structural and functional study, we generated mice that express a ligand–activated Cre recombinase-oestrogen receptor fusion protein[10] (CreER) under the control of regulatory elements from the *JAM-B* gene (JAM-B–CreER; Fig. 1d). The rationale was as follows: *JAM-B* is expressed at low levels, so that linking *JAM-B* regulatory sequences directly to a reporter might result in inadequate marking. Linking *JAM-B* regulatory elements to Cre recombinase can amplify the signal: such mice can be mated to a line[11] in which Cre-mediated excision of a 'stop' cassette activates the strong expression of yellow fluorescent protein (Thy1-STOP–YFP). However, *JAM-B* is expressed in dynamic patterns in embryos, so in this scheme YFP would mark cells that expressed *JAM-B* transiently during development. The use of CreER circumvents this limitation, because it is only active for a short period after application of its activating ligand, tamoxifen[10]. A few hundred RGCs per retina were marked in JAM-B–CreER;Thy1-STOP–YFP mice after tamoxifen injection (Fig. 1e–h). Among the YFP-positive RGCs, at least 90% of the YFP-positive RGCs expressed *JAM-B* (Supplementary Fig. 1). We refer to the YFP-positive RGCs as J-RGCs.

Analysis of J-RGCs revealed three notable structural features. First, their dendrites were restricted to a narrow band within the outer third of the IPL (Fig. 1e and Supplementary Fig. 2a). The IPL is divided into at least ten sublaminae, and physiological properties of RGCs are related to the sublaminae in which their dendrites arborize[1,2,12]. Dendrites of J-RGCs arborized in a narrow band between processes of dopaminergic and cholinergic amacrines[13], indicating a sublaminar restriction (Fig. 1f) and suggesting that J-RGCs receive few synapses from these two amacrine classes. In contrast, processes of CD15-positive and AII amacrines did overlap with dendrites of J-RGCs (Supplementary Fig. 3) and may therefore provide input to them.

Second, about 85% of J-RGCs had markedly asymmetric dendritic arbors (Fig. 1g). One or two primary dendrites emerged from the soma and branched repeatedly at acute angles to fill a narrow sector; more than 90% of the dendritic field area lay on one side of the soma. In contrast, the vast majority of RGCs have dendrites that radiate far more symmetrically about the soma[14–16].

Third, and most remarkably, dendrites of asymmetric J-RGCs pointed in the same direction, slightly (about 13°) nasal of ventral (Fig. 1h, i). The dendritic orientation was longitudinal, from the dorsal to the ventral pole of the eye, instead of radial relative to the optic nerve head; this was most apparent after the correction of flat mounts for retinal curvature. The roughly 15% of J-RGCs that were not markedly asymmetrical were located near the dorsal and ventral margins of the retina (Fig. 1i). Therefore nearly all J-RGCs in central, nasal and temporal retina were asymmetric. Symmetric and asymmetric J-RGCs alike had dendrites confined to the outer part of the IPL (Supplementary Fig. 2).

The morphology of J-RGCs led to two hypotheses about their function. First, studies combining electrical recording with dye-filling have revealed that RGCs with dendrites in the outer third of the IPL are excited predominantly by dimming of light in the receptive field centre (OFF-RGCs)[1–3,12], suggesting that J-RGCs are OFF cells. Second, the dendritic asymmetry raised the possibility that J-RGCs are sensitive to stimuli with a particular orientation or direction. To test these ideas, we identified J-RGCs in retinal explants with fluorescence optics and recorded their visual responses.

When probed with small flashing spots near the cell soma, almost all J-RGCs fired when the light turned off (Fig. 2a). By contrast, recordings from non-fluorescent RGCs in the same retinae yielded, as expected[3], similar numbers of ON and OFF cells (Fig. 2b). Consistent with these physiological observations, processes of several classes of OFF bipolar cells[17,18] were present in the same sublamina as J-RGC dendrites, whereas processes of ON bipolars overlapped only minimally with J-RGC dendrites (Fig. 1f and Supplementary Fig. 3).

[1]Department of Molecular and Cellular Biology and Center for Brain Science, Harvard University, Cambridge, Massachusetts 02138, USA.
*These authors contributed equally to this work

Thus, J-RGCs are likely to receive inputs from OFF but not ON bipolar cells. Interestingly, J-RGCs failed to fire in response to somewhat larger spots, and responded at light onset when they were larger still (Fig. 2c, d). Thus, the receptive field of J-RGCs is unusual[19] in that the integrated strength of its ON surround exceeds that of the OFF centre.

To probe the sensitivity of J-RGCs to motion, we moved a small spot through the receptive field centre in eight straight trajectories. The firing rate varied strongly with direction of motion (Fig. 2e and Supplementary Fig. 5). The preferred direction corresponded to the direction in which the dendritic tree pointed from the cell soma (Fig. 2f). Thus, in contrast to previously studied direction-selective RGCs, whose shape provides no clue to their physiological selectivity[2,4,5], the direction selectivity of J-RGCs is correlated with structural asymmetry

To gain further insight into mechanisms underlying the direction-selectivity of J-RGCs, we measured their spatio-temporal receptive field by reverse correlation with randomly flickering bars (Fig. 3a, b).

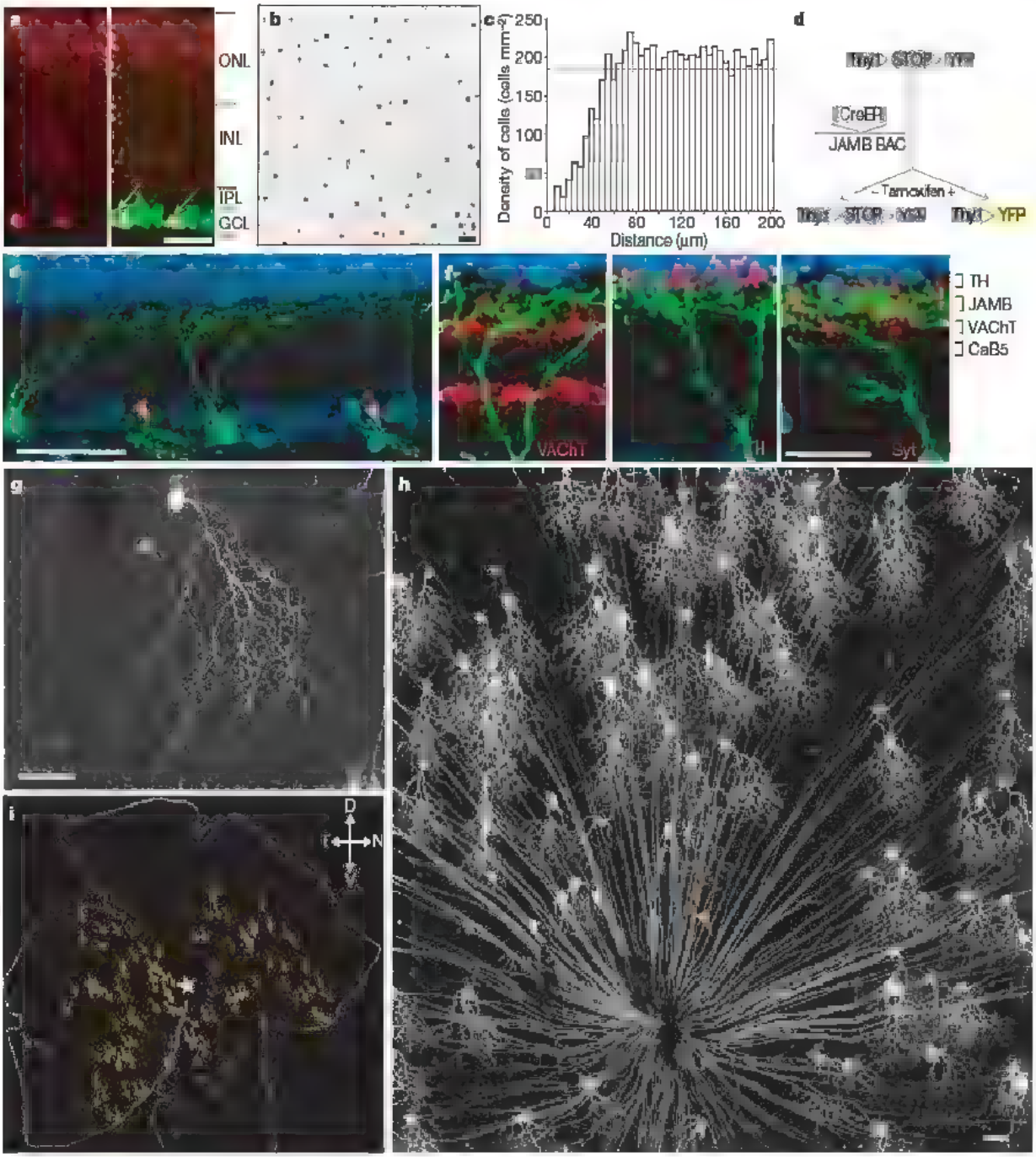

Figure 1 | JAM-B marks a structurally unique subset of RGCs. **a**, *In situ* hybridization of sections from P7 retina with probes to *JAM-B* (red) and *Thy1*, a pan-RGCs marker[29] (green). Left, *JAM-B* alone; right, merge *JAM-B*-positive cells are RGCs (arrows). ONL, outer nuclear layer; INL, inner nuclear layer; IPL, inner plexiform layer; GCL, ganglion cell layer **b**, Regular spacing of *JAM-B*-expressing RGCs revealed by *in situ* hybridization in a whole mount. **c**, Density recovery profile analysis[5] of retinae such as that shown in **b**. The dotted line shows expectation for random distribution at the same overall density. **d**, Transgenic system for marking J-RGCs with YFP. CreER, tamoxifen-activated Cre; open triangles, loxP sites. **e**, J-RGCs labelled with YFP (green) in sections from a JAM-B–CreER;Thy1-STOP–YFP double transgenic mouse. Blue, fluorescent Nissl stain. Dendrites of J-RGCs arborize in the outer part of the IPL. Arrowheads, axon bundles. **f**, Double staining of sections such as that in **e** shows that dendrites of J-RGCs arborize in a sublamina between those occupied by processes of amacrine cells positive for vesicular acetylcholine transporter (VAChT) and tyrosine hydroxylase (TH). Processes of bipolar cells positive for synaptotagmin-2 (Syt2) overlap with J-RGC dendrites. CaB5, calcium-binding protein 5. **g**, Asymmetric J-RGC from a whole mount. **h**, Micrograph of a whole-mounted retina. Arrowhead in **g** and **h** marks RGC axons. **i**, Sketch of another retina, showing orientation of J-RGC dendrites (arrows). Blue stars show cells with symmetric dendrites at the dorsal and ventral margins. White star, optic nerve head. D, dorsal; V, ventral; N, nasal; T, temporal. Scale bar, 50 μm (**a**, **b**, **e**, **g**–**i**) and 20 μm (**f**)

With the help of a 'linear–nonlinear' model[20], this receptive field was used to predict the cell's response to moving spots. The predicted direction selectivity matched the measurements (Supplementary Fig. 4), motivating further analysis of the receptive field for features that shape direction selectivity.

First, the ON-surround is markedly asymmetric, shifted in the preferred direction relative to the centre (Fig. 3d, e). In addition, the receptive field centre has a strongly biphasic time course: a distinct OFF lobe with an ON overshoot at longer latency (Fig. 3c). The ON overshoot of the centre and the ON surround together form a slanted feature in the space-time plane (Fig. 3b). A bright spot travelling in the preferred direction at the appropriate speed passes through both these regions, and the time delay of the centre produces superposition of the two excitations and an enhanced response[21]. This explains why an OFF-type neuron can be highly direction-selective for bright spots (Fig. 2e). Second, the OFF centre itself is also slanted in the space-time plane (Fig. 3b), which similarly renders dark spots more effective when moving in the preferred direction than when moving in the null direction. The space-time slope of the OFF centre, and thus the preferred speed for spot movement, is considerably greater than that of the slanted ON feature. Indeed, dark spots give the most direction-selective response at high speeds, whereas bright spots do so at low speeds (Supplementary Fig. 5).

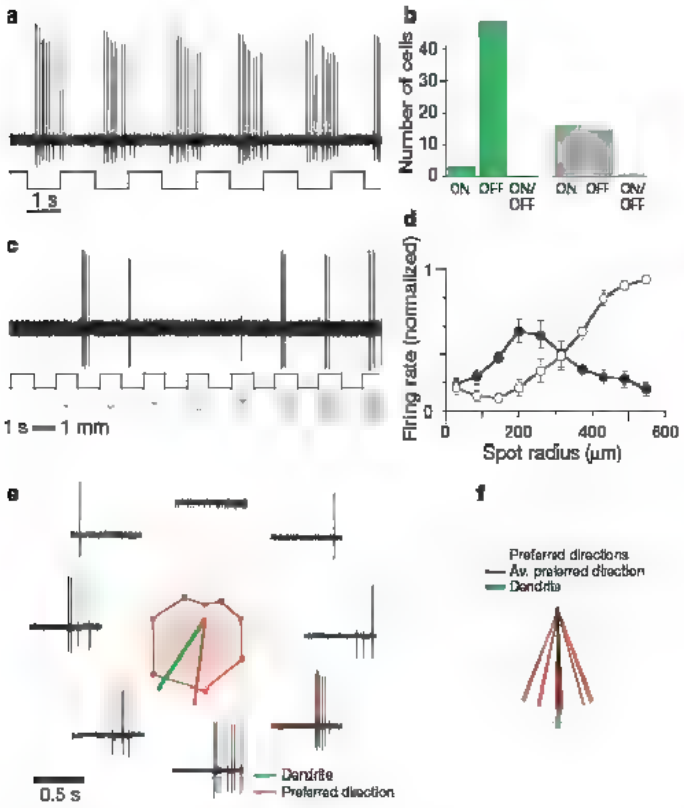

Figure 2 | J-RGCs are direction-selective OFF cells. **a**, Recording from a J-RGC during stimulation with a flashing spot 345 μm in diameter centred on the receptive field. **b**, Summary of response types encountered among 52 J-RGCs (green) and 32 YFP-negative RGCs probed with a flashing spot. **c**, Recording from a J-RGC with a flashing spot of increasing diameter. **d**, Average response of J-RGCs (means ± s.e.m., $n = 10$) to stimulus series in **c**. The graph shows number of spikes at light onset (ON response, open symbols) and offset (OFF response, filled symbols). **e**, Responses of a J-RGC to a small spot moving in directions indicated by dotted lines from the centre (white spot, 115 μm diameter, 575 μm s^{-1}, see Supplementary Fig. 5 for results with black spots). The average responses are displayed in a polar plot. The bold red line indicates the preferred direction, computed as the vector sum of the eight responses; the green line indicates the direction of the dendritic arbor. **f**, Relationship between dendritic asymmetry and direction selectivity of 12 J-RGCs. The preferred direction (computed as in **e**) is plotted relative to the direction of the dendritic arbor, arbitrarily shown as downward. The average preferred direction is indicated with the bold line.

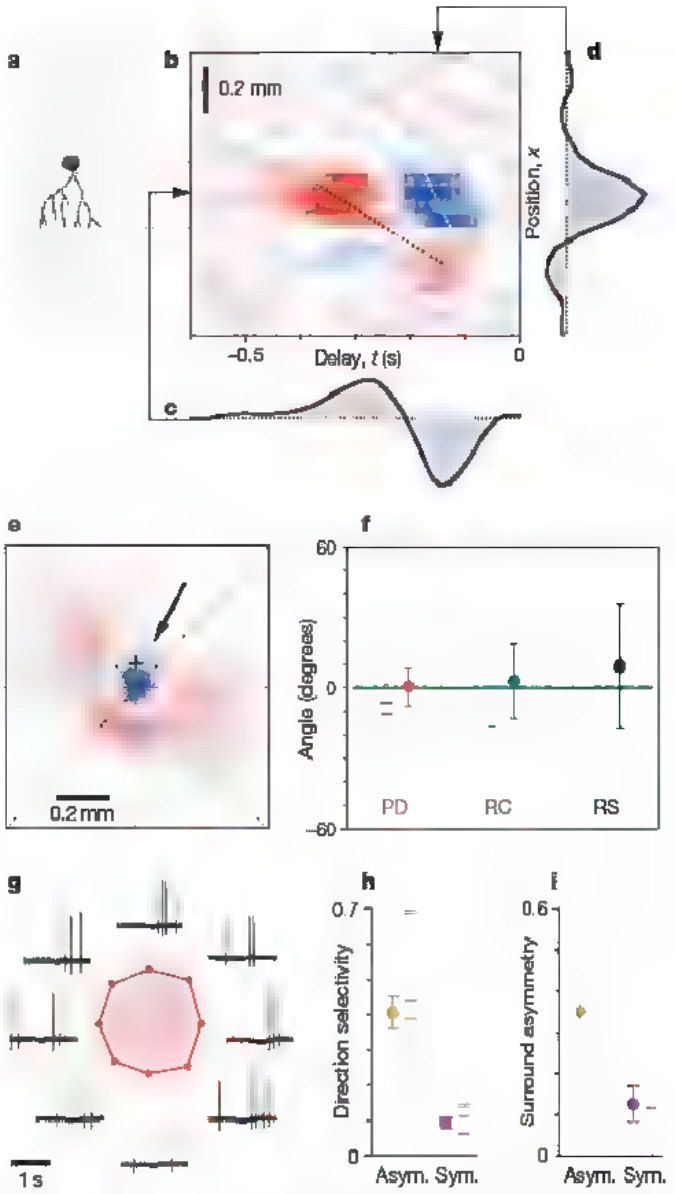

Figure 3 | Asymmetries in J-RGC receptive fields correspond to dendritic asymmetries. **a**, Measurement of receptive fields. The stimulus was a strip of narrow bars centred on the recorded cell. Each bar flickered randomly and independently of the others. **b**, Spatio-temporal receptive field $h(x,t)$ of one J-RGC, computed from responses to the stimulus of **a**. For a bar at position x (vertical axis), a row in this graph reports the average intensity that occurred at time t before a spike (horizontal axis). white, 0; red, positive; blue, negative. $h(x,t)$ approximates the firing rate elicited by a brief flash of light in bar x at time t. Two slanted features are indicated by dotted lines: one links the overshoot of the receptive field centre to the asymmetric surround (left), the other results from space-time slant within the receptive field centre itself (right). A moving bar that follows such a trajectory triggers many contributions from $h(x,t)$ that all have the same sign and thus elicit strong excitation. **c**, **d**, Time course (**c**) and spatial profile (**d**) of the receptive field at locations indicated by arrows. **e**, Two-dimensional spatial profile of the receptive field, obtained by interpolating data from four separate experiments with the grating strips (**a**) rotated at 45° increments. Arrow, preferred direction for spots; cross, location of cell body. **f**, Relation of functional asymmetries of J-RGCs to the direction of their dendrites (at 0°): the preferred direction for moving spots (PD), the direction of movement within the receptive field centre (RC), and the direction of displacement of the receptive field surround (RS). Lines, individual cells; circles, means ± s.d. **g**, Responses from a J-RGC with symmetrical dendrites at the ventral border of the retina, presented as in Fig. 2e. **h**, **i**, Direction selectivity and surround asymmetry of J-RGCs with asymmetrical and symmetrical dendrites. Direction selectivity is an index for asymmetry in the polar plot of moving spot responses (Fig. 2e). Surround asymmetry is an index for displacement of the ON surround relative to the OFF centre (**e**). Lines, individual cells; circles, means ± s.e.m.

In summary, J-RGCs show three functional asymmetries: the direction in which the receptive field surround is displaced (Fig. 3e), the space-time slant within the receptive field centre (Fig. 3b), and the preferred direction for spot movement (Fig. 2e). These three directions matched closely and coincided with the anatomical orientation of the dendritic arbor (Fig. 3f).

Does the direction selectivity of J-RGCs result from their structural asymmetry? To explore this relationship, we took advantage of the structurally symmetrical J-RGCs in ventral retina (Fig. 1i). These cells had no apparent preferred direction of movement and a relatively symmetrical ON surround (Fig. 3g–i). Moreover, across the entire J-RGC population, the degree of direction selectivity was correlated with the degree of asymmetry of the receptive field (Supplementary Fig. 6). Thus, within a single molecularly defined class of OFF-RGCs, dendritic structure and cell function are closely linked, suggesting that the latter arises from the former.

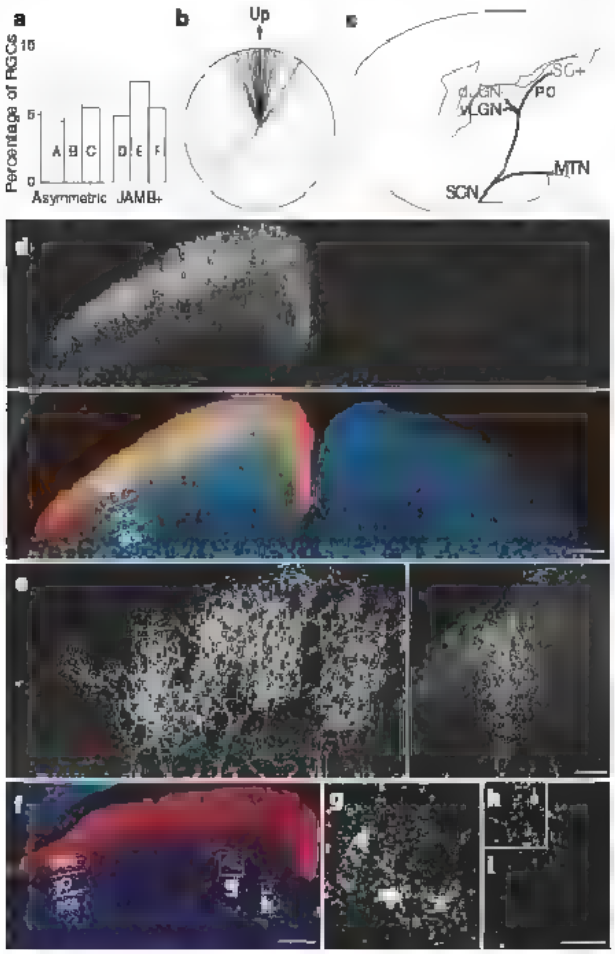

Figure 4 | Numbers and central projections of J-RGCs. a, The number of putative OFF RGCs with asymmetric morphology in mouse retina, reported in previous studies (A, RGC-C6 in ref. 14; B, type 6 in ref. 15; C, M5a in ref. 16) is similar to the number of J-RGCs estimated from JAM-B–CreER;Thy1-STOP–YFP double transgenic mice (D) or *in situ* hybridization (*JAM-B* cells/*Thy1*+ cells in E; *JAM-B* cells/Nissl^{+} cells in F, based on total cell number in ref. 30). **b**, Fig. 6 from ref. 24 (reproduced with permission of the American Physiological Society), showing preference of movement-sensitive cells in mouse superior colliculus for upward motion. **c**, Retinorecipient structures that were (green) or were not (black) innervated by J-RGCs, determined as in **d**. dLGN, dorsal lateral geniculate nucleus; vLGN, ventral LGN; MTN, medial temporal nucleus; PO, preoptic area; SC, superior colliculus; SCN, suprachiasmatic nucleus. **d**, Coronal section through superior colliculus of a JAM-B–CreER;Thy1-STOP–YFP mouse after monocular enucleation and cholera toxin injection. Top: axons of J-RGCs from the intact eye project to the SC. Bottom: overlay of J-RGC axons (green), all RGC axons (marked by cholera toxin, red) and cell bodies (blue). SGS, stratum griseum superficiale; SO, stratum opticum; SGI, stratum griseum intermedium. **e**, High-magnification views of J-RGC axons in superior colliculus. Left, group of arbors; right, single arbor. **f**, Coronal section through superior colliculus of a JAM-B–CreER;CAG-STOP–wheat-germ agglutinin (WGA) double-transgenic mouse. Enucleation and cholera toxin injection were as in **d**. **g–i**, WGA immunoreactivity in areas indicated by boxes in **f** (**g**, **h**) and in the opposite colliculus (**i**). Scale bars, 200 μm (**d**, **f**) and 50 μm (**e**, **g–i**).

Noting that J-RGCs point in a single direction, we considered the possibility that other asymmetric OFF RGCs point in other directions. We therefore compared the number of J-RGCs with the total number of RGCs with asymmetric dendrites in OFF sublaminae. Three previous catalogues of mouse RGCs[4–16] noted and named such cells. They were studied in sparsely labelled retinae, so the uniformity of their asymmetry was not realized, but it seems likely that they included J-RGCs. They comprised 5% of RGCs reconstructed in the three studies (40 out of 782; Fig. 4a). The fraction of RGCs that were *JAM-B*-positive was also about 5%, on the basis of *in situ* hybridization and YFP staining (Fig. 4a). The correspondence of these two numbers suggests that no sizable populations of OFF RGCs exist with asymmetric dendrites pointing in directions other than dorsal-to-ventral.

Where in the brain do J-RGCs send this directional information? We used YFP to trace the axons of J-RGCs. The entire retinal projection was labelled by injecting one eye with an anterograde tracer[22], allowing us to identify all retinorecipient nuclei (Fig. 4c)[22,23]. YFP-positive axons in these nuclei were of retinal origin, as shown by their absence after enucleation (Fig. 4d). J-RGCs projected most heavily to the superior colliculus (Fig. 4c–e), the major retinorecipient structure in mice[22]. Some J-RGCs also projected to the dorsal lateral geniculate nucleus. In contrast, we detected no J-RGCs in the pretectal nucleus, in the ventral nucleus of the lateral geniculate body or in the accessory optic system (Fig. 4c and Supplementary Fig. 7). The accessory optic system is a major site to which other direction-selective RGCs project[23].

The collicular termination of J-RGCs is intriguing in light of a study in which Dräger and Hubel mapped the receptive fields of neurons in the superior colliculus of the mouse[24]. Nearly all of the direction-selective neurons they studied (35 out of 38) preferred upward motion in the visual field (Fig. 4b). This preference corresponds to that of J-RGCs. Dräger and Hubel further noted that the highest densities of direction-selective cells in the colliculus were in two layers, the stratum opticum and intermediate grey layer[24]. To ask whether J-RGCs synapse on cells in these layers, we mated JAM-B–CreER mice to a transgenic line in which Cre-mediated recombination activates expression of the trans-synaptic tracer wheat-germ agglutinin[25]. Wheat-germ agglutinin immunoreactivity was detected in neurons of the stratum opticum and intermediate grey layer (Fig. 4f–i). We therefore propose that the receptive fields of direction-selective collicular cells are built from J-RGCs.

We have used a molecular strategy to identify J-RGCs, which differ in several respects from previously described direction-selective RGCs[4,5]. First, direction-selective OFF RGCs (Fig. 2a, b) have not previously been reported in mammals, although structurally asymmetrical orientation-selective RGCs present in rabbits[26] might be related to J-RGCs. Second, whereas no morphological feature predicted the preferred direction of previously described direction-selective RGCs, the orientation of the dendritic arbor is correlated with the preferred direction in J-RGCs (Figs 1h and 2f). Third, direction-selective ON and ON–OFF RGCs exist in multiple subclasses with distinct preferred directions[27], but direction-selective J-RGCs share a single preferred direction (Fig. 2f). Last, whereas the selectivity of other direction-selective RGCs depends on input from starburst amacrine cells, which themselves show directional responses[4,5], J-RGCs receive little input from these cells (Fig. 1e) and thus must rely on other mechanisms. One possible mechanism is suggested by the finding that inhibitory synapses on some RGCs are concentrated at distal dendrites[28]. Distal inhibition on the asymmetric dendrites of J-RGCs could account for their asymmetrically displaced surround.

One outstanding question is why the mouse has invested so heavily in sensitivity to upward motion. We have been no more successful than Dräger and Hubel[24] in guessing what that significance might be. By mating JAM-B–CreER mice to other transgenics bearing appropriate Cre-activated channels or toxins, we may be able to inactivate this pathway and thereby directly test its function.

METHODS SUMMARY

We obtained sequences of IgSF genes from public databases, and assessed their expression in postnatal retina by *in situ* hybridization[6,7] and RT–PCR. A construct in which regulatory sequences from the mouse *JAM-B* gene drove the expression of CreER was used to generate transgenic mice. These mice were mated to mice in which the expression of reporters[11,25] depended on Cre-mediated excision of STOP sequences. Staining protocols and antibodies used are detailed in Supplementary Methods.

To record visual responses from J-RGCs, we localized the cells by brief excitation (about 100–200 ms) with a blue light-emitting diode (LED) so they could be targeted with a cell-attached patch electrode. Light stimuli of photopic intensity were delivered by a computer-driven video projector.

Full Methods and any associated references are available in the online version of the paper at www.nature.com/nature.

Received 13 September; accepted 24 January 2008.

1. Masland, R. H. The fundamental plan of the retina. *Nature Neurosci.* **4**, 877–886 (2001).
2. Wässle, H. Parallel processing in the mammalian retina. *Nature Rev. Neurosci.* **5**, 747–757 (2004).
3. Nelson, R. & Kolb, H. in *The Visual Neurosciences* (eds Chalupa, L. M. & Werner, J. S.) 260–278 (MIT Press, Cambridge, MA, 2003).
4. Demb, J. B. Cellular mechanisms for direction selectivity in the retina. *Neuron* **55**, 179–186 (2007).
5. Taylor, W. R. & Vaney, D. I. New directions in retinal research. *Trends Neurosci.* **26**, 379–385 (2003).
6. Yamagata, M., Weiner, J. A. & Sanes, J. R. Sidekicks: synaptic adhesion molecules that promote lamina-specific connectivity in the retina. *Cell* **110**, 649–660 (2002).
7. Yamagata, M. & Sanes, J. R. Dscam and Sidekick proteins direct lamina-specific connections in vertebrate retina. *Nature* **451**, 465–469 (2008).
8. Rodieck, R. W. The density recovery profile: a method for the analysis of points in the plane applicable to retinal studies. *Vis. Neurosci.* **6**, 95–111 (1991).
9. Weber, C., Fraemohs, L. & Dejana, E. The role of junctional adhesion molecules in vascular inflammation. *Nature Rev. Immunol.* **7**, 467–477 (2007).
10. Branda, C. S. & Dymecki, S. M. Talking about a revolution: The impact of site-specific recombinases on genetic analyses in mice. *Dev. Cell* **6**, 7–28 (2004).
11. Buffelli, M. *et al.* Genetic evidence that relative synaptic efficacy biases the outcome of synaptic competition. *Nature* **424**, 430–434 (2003).
12. Roska, B. & Werblin, F. Vertical interactions across ten parallel, stacked representations in the mammalian retina. *Nature* **410**, 583–587 (2001).
13. Haverkamp, S. & Wässle, H. Immunocytochemical analysis of the mouse retina. *J. Comp. Neurol.* **14**, 1–23 (2000).
14. Sun, W., Li, N. & He, S. Large-scale morphological survey of mouse retinal ganglion cells. *J. Comp. Neurol.* **451**, 115–126 (2002).
15. Badea, T. C. & Nathans, J. Quantitative analysis of neuronal morphologies in the mouse retina visualized by using a genetically directed reporter. *J. Comp. Neurol.* **480**, 331–351 (2004).
16. Coombs, J., van der List, D., Wang, G. Y. & Chalupa, L. M. Morphological properties of mouse retinal ganglion cells. *Neuroscience* **140**, 123–136 (2006).
17. Fox, M. A. & Sanes, J. R. Synaptotagmin I and II are present in distinct subsets of central synapses. *J. Comp. Neurol.* **503**, 280–296 (2007).
18. Ghosh, K. K., Bujan, S., Haverkamp, S., Feigenspan, A. & Wässle, H. Types of bipolar cells in the mouse retina. *J. Comp. Neurol.* **469**, 70–82 (2004).
19. Croner, L. J. & Kaplan, E. Receptive fields of P and M ganglion cells across the primate retina. *Vision Res.* **35**, 7–24 (1995).
20. Chichilnisky, E. J. A simple white noise analysis of neuronal light responses. *Network* **12**, 199–213 (2001).
21. Barlow, H. B. & Levick, W. R. The mechanism of directionally selective units in rabbit's retina. *J. Physiol. (Lond.)* **178**, 477–504 (1965).
22. Ling, C., Schneider, G. E. & Jhaveri, S. Target-specific morphology of retinal axon arbors in the adult hamster. *Vis. Neurosci.* **15**, 559–579 (1998).
23. Giolli, R. A., Blanks, R. H. & Lui, F. The accessory optic system: basic organization with an update on connectivity, neurochemistry, and function. *Prog. Brain Res.* **151**, 407–440 (2005).
24. Dräger, U. C. & Hubel, D. H. Responses to visual stimulation and relationship between visual, auditory, and somatosensory inputs in mouse superior colliculus. *J. Neurophysiol.* **38**, 690–713 (1975).
25. Braz, J. M., Rico, B. & Basbaum, A. I. Transneuronal tracing of diverse CNS circuits by Cre-mediated induction of wheat germ agglutinin in transgenic mice. *Proc. Natl Acad. Sci. USA* **99**, 15148–15153 (2002).
26. Amthor, F. R., Takahashi, E. S. & Oyster, C. W. Morphologies of rabbit retinal ganglion cells with concentric receptive fields. *J. Comp. Neurol.* **280**, 72–96 (1989).
27. Oyster, C. W. & Barlow, H. B. Direction-selective units in rabbit retina: distribution of preferred directions. *Science* **155**, 841–842 (1967).
28. Lin, B., Martin, P. R., Solomon, S. G. & Grunert, U. Distribution of glycine receptor subunits on primate retinal ganglion cells: a quantitative analysis. *Eur. J. Neurosci.* **12**, 4155–4170 (2000).
29. Barnstable, C. J. & Dräger, U. C. Thy-1 antigen: a ganglion cell specific marker in rodent retina. *Neuroscience* **11**, 847–855 (1984).
30. Jeon, C. J., Strettoi, E. & Masland, R. H. The major cell populations of the mouse retina. *J. Neurosci.* **18**, 8936–8946 (1998).

Supplementary Information is linked to the online version of the paper at www.nature.com/nature.

Acknowledgements We thank S. Dymecki for FlpE mice, A. Basbaum for WGA mice and L. Dräger, S. Haddad, B. Howell, A. Koizumi, T. Kummer, J. Livet, D. Pelusi and E. Soucy for advice and assistance. This work was supported by grants from the National Institutes of Health to M.M. and J.R.S., a Merck Award and a Bushrod H. Campbell and Adah F. Hall Charity Fund Fellowship to J.K., and a Damon Runyon fellowship to Y.Z.

Author Contributions J.K., Y.Z., M.Y., M.M. and J.R.S. conceived the experiments. J.K. and M.Y. performed molecular and histological experiments. Y.Z. performed physiological experiments. Y.Z. and M.M. performed computational analysis. M.M. and J.R.S. wrote the paper.

Author Information Reprints and permissions information is available at www.nature.com/reprints. Correspondence and requests for materials should be addressed to M.M. (meister@fas.harvard.edu) or J.R.S. (sanesj@mcb.harvard.edu).

LETTERS

CO_2 regulator SLAC1 and its homologues are essential for anion homeostasis in plant cells

Juntaro Negi[1], Osamu Matsuda[1], Takashi Nagasawa[1], Yasuhiro Oba[1], Hideyuki Takahashi[2], Maki Kawai-Yamada[3], Hirofumi Uchimiya[2,3], Mimi Hashimoto[1] & Koh Iba[1]

The continuing rise in atmospheric [CO_2] is predicted to have diverse and dramatic effects on the productivity of agriculture, plant ecosystems and gas exchange[1–3]. Stomatal pores in the epidermis provide gates for the exchange of CO_2 and water between plants and the atmosphere, processes vital to plant life[4–6]. Increased [CO_2] has been shown to enhance anion channel activity[7] proposed to mediate efflux of osmoregulatory anions (Cl^- and malate^{2-}) from guard cells during stomatal closure[8,9]. However, the genes encoding anion efflux channels in plant plasma membranes remain unknown. Here we report the isolation of an *Arabidopsis* gene, *SLAC1* (*SLOW ANION CHANNEL-ASSOCIATED 1*, At1g12480), which mediates CO_2 sensitivity in regulation of plant gas exchange. The SLAC1 protein is a distant homologue of bacterial and fungal C4-dicarboxylate transporters, and is localized specifically to the plasma membrane of guard cells. It belongs to a protein family that in *Arabidopsis* consists of four structurally related members that are common in their plasma membrane localization, but show distinct tissue-specific expression patterns. The loss-of-function mutation in *SLAC1* was accompanied by an over-accumulation of the osmoregulatory anions in guard cell protoplasts. Guard-cell-specific expression of SLAC1 or its family members resulted in restoration of the wild-type stomatal responses, including CO_2 sensitivity, and also in the dissipation of the over-accumulated anions. These results suggest that SLAC1-family proteins have an evolutionarily conserved function that is required for the maintenance of organic/inorganic anion homeostasis on the cellular level.

Leaf temperature provides a convenient indicator of transpiration and can be used to detect mutant phenotypes with altered stomatal control[10–12]. We isolated a mutant, *cdi3* (*carbon dioxide insensitive 3*)[13], impaired in CO_2-dependent leaf temperature change, from approximately 30,000 ethyl methanesulfonate (EMS)-mutagenized *Arabidopsis* plants of an M2 population (one generations after mutagenesis). This mutant was allelic to *slac1-1* (ref. 14) and designated as *slac1-2*. In this mutant, high [CO_2]-induced increase in leaf temperature (Fig. 1a) as well as stomatal closure (Fig. 1b) were inhibited. Abscisic acid (ABA) and darkness are signals triggering stomatal closure; *slac1-2* stomata exhibited a strong insensitivity to ABA (Fig. 1c) and a reduced sensitivity to darkness (Fig. 1d). The *slac1-2* mutant was also defective in regulation of transpiration in response to drought stress (Supplementary Fig. 1). Similar results were obtained from the analysis of a transfer DNA (T-DNA) insertion allele *slac1-3* (SALK_099139) (Fig. 1 and Supplementary Fig. 1).

The *SLAC1* locus was mapped to a location between two Cereon single-nucleotide-polymorphism markers, CER474602 and CER474506, on chromosome 1 (Supplementary Fig. 2). Sequencing of this 79-kilobase (kb) region revealed that an open reading frame, At1g12480, harboured a point mutation at nucleotide 656 in the *slac1-2* mutant that resulted in a Gly194-to-Asp substitution (G194D) (Fig. 1e). We transformed *slac1-2* plants with a 4.38-kb genomic fragment, including At1g12480 (*slac1-2/SLAC1*). Four independent homozygous *slac1-2/SLAC1* lines showed *slac1* complementation, as was evident from normal CO_2-dependent leaf-temperature changes (Fig. 1a). A similar result was obtained in *slac1-2/p35S::SLAC1* lines, in which the *SLAC1* complementary DNA was expressed under the control of the cauliflower mosaic virus *35S* promoter. Thus, At1g12480 corresponds to the *SLAC1* gene. Comparison of the cDNA with genomic sequences revealed that *SLAC1* has three exons (Fig. 1e). *SLAC1* was predicted to encode a polypeptide of 557 amino acids containing ten putative transmembrane domains. The mutation found in *slac1-2* was located within the first transmembrane domain (Fig. 1e). The Gly 194-to-Asp substitution seems to disrupt proper conformation of SLAC1; it causes an introduction of a hydrophilic amino acid (Asp) into the highly hydrophobic transmembrane region

To examine the subcellular localization and tissue-specific expression patterns of SLAC1, we used the *SLAC1* promoter (*pSLAC1*) to drive expression of the *GUS* reporter (*pSLAC1::GUS*) and the translational fusion of full-length SLAC1 protein and green fluorescent protein (GFP) (*pSLAC1::SLAC1–GFP*). The latter construct complemented the Slac1 phenotype, indicating that the SLAC1–GFP fusion protein is functional (Supplementary Fig. 3). GUS activity in the *pSLAC1::GUS* transformants was confined to guard cells (Fig. 2b). Using PCR with reverse transcription (RT–PCR) analysis, *SLAC1* messenger RNA also was detected in guard cells (Supplementary Fig. 4b). SLAC1–GFP was localized to the cell surface, whereas GFP alone was localized to the nucleus and cytosol (Fig. 2a). The GFP fusion of the vacuolar marker *Arabidopsis* VAM3 protein, a member of the syntaxin family[15], served to distinguish tonoplast and plasma membranes (Fig. 2a). Together with the presence of transmembrane domains, these results demonstrated that SLAC1 is a plasma-membrane-localized protein of guard cells.

According to database annotations, the SLAC1 protein possesses features of the C4-dicarboxylate transporter family (TDT transporter family)[16]. One member of this family, Mae1 of *Schizosaccharomyces pombe*, has been functionally characterized as a malate uptake transporter[17]. Although the sequence similarity is relatively low between the SLAC1 and Mae1 proteins (approximately 20% amino acid identity)[18], the facts that malate^{2-} is the osmoregulatory organic anion for stomatal opening[19,20] and that the *slac1* mutation causes a constitutive stomatal opening phenotype (Fig. 1b–d) raise a plausible hypothesis: SLAC1 might provide a gate for malate^{2-} transport across the guard-cell plasma membrane. To test the idea, we measured C4-dicarboxylate contents in guard cell protoplasts (GCPs) There was

[1]Department of Biology, Faculty of Sciences, Kyushu University, Fukuoka 812-8581, Japan. [2]Iwate Biotechnology Center, Kitakami, Iwate 024-0003, Japan. [3]Institute of Molecular and Cellular Biosciences, The University of Tokyo, Tokyo 113-0032, Japan

no difference in succinate contents between *slac1-2* and wild-type GCPs. In contrast, in *slac1-2* GCPs, significantly higher contents of malate and fumarate were found compared with wild-type GCPs (Fig. 3a). Although the relative contribution of fumarate accumulation to stomatal movement is uncertain, these results suggest that SLAC1 is involved in the regulation of organic anion homeostasis in guard cells. In addition to organic anions, inorganic ions such as K^+ and Cl^- are important factors in guard cell osmoregulation and stomatal movement[4,5]. We therefore measured inorganic ion contents in GCPs (Fig. 3b); whereas Na^+ levels were similar in wild-type and *slac1-2* GCPs, *slac1-2* exhibited significantly higher contents of K^+ and Cl^-. One possible explanation for this result is that the over-accumulation of Cl^- and organic anions caused a corresponding increase in the levels of K^+ to maintain charge balance[4–6]. Similar results were obtained from the analysis of *slac1-3* GCPs (Supplementary Fig. 5). These results suggested that SLAC1 controls organic and inorganic ion homeostasis in guard cells, which is consistent with the deficiency in stomatal closure in *slac1* mutants (Fig. 1b–d) and with its localization in the plasma membrane (Fig. 2a).

In addition to *SLAC1*, three related genes, here designated as *SLAC1 HOMOLOGUES* (*SLAHs*), are present in the *Arabidopsis* genome (see Methods Summary). The corresponding proteins were 40–50% identical to SLAC1 (Fig. 1e). Like SLAC1, SLAHs were localized to the plasma membrane (Fig. 2c). RT–PCR and histochemical GUS analysis revealed that none of the *SLAHs* was expressed in guard cells (Fig. 2b and Supplementary Fig. 4b). Interestingly, SLAH1 (At1g62280) and SLAH3 (At5g24030) can complement the CO_2-insensitive and organic/inorganic ion accumulation phenotypes of *slac1-2* when expressed under the control of the *SLAC1* guard-cell-specific promoter (Figs 1 and 3). The expression of *pSLAC1::SLAH* transgenes in guard cells was confirmed by RT–PCR analysis (Supplementary Fig. 4b). These findings demonstrated that SLAC1, SLAH1 and SLAH3 have conserved functions but are tissue-specific in *Arabidopsis*, with only SLAC1 having a role in stomatal movement.

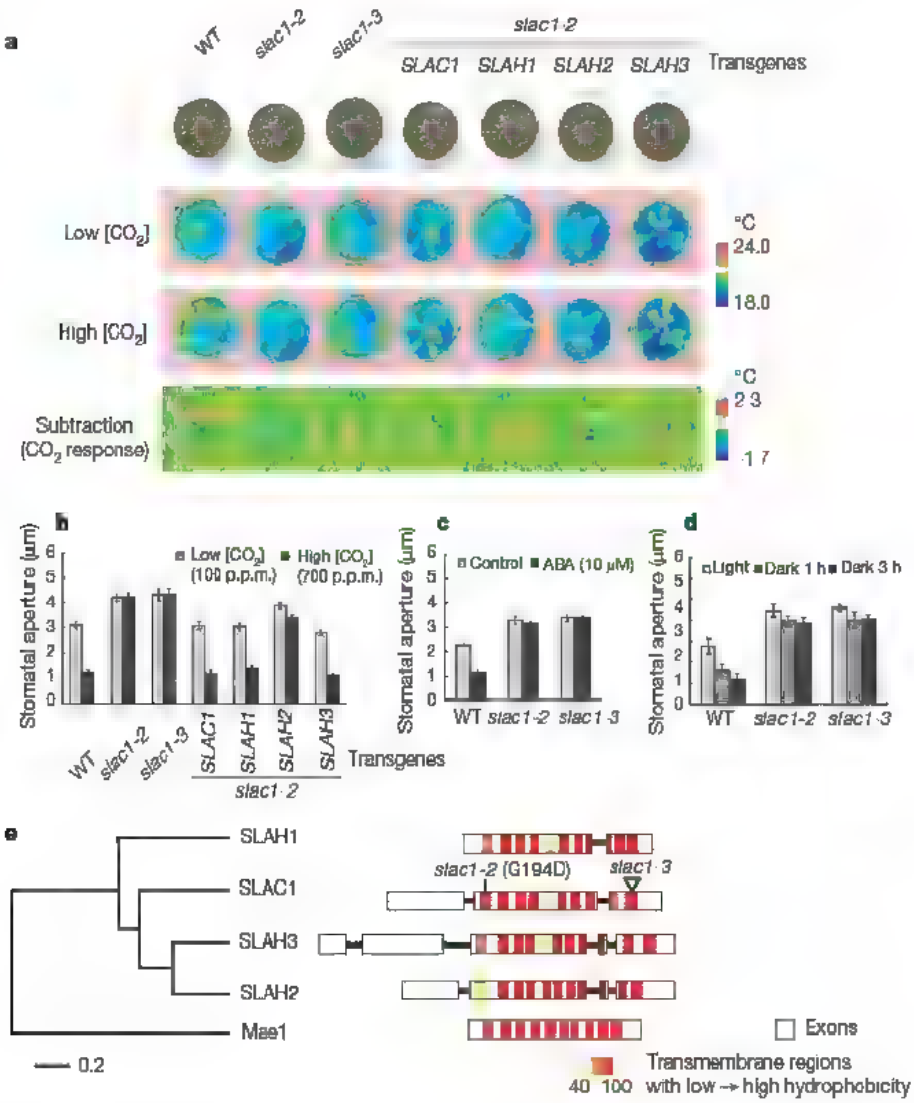

Figure 1 | The *slac1* mutations impair CO_2-, ABA- and dark-induced stomatal closure. a, Thermal images of *Arabidopsis* subjected to low (100 parts per million, p.p.m.) and high (700 p.p.m.) atmospheric [CO_2]. The subtractive images show changes in leaf temperature in response to the transfer from low to high [CO_2] conditions. Two *slac1* mutants (*slac1-2* and *slac1-3*) show CO_2-insensitive, constitutive low-temperature phenotypes. Guard-cell-specific expression of SLAC1 or its family members SLAH1 or SLAH3, but not SLAH2, resulted in restoration of the CO_2-responsive change in leaf temperature. WT, wild type. The transgene structure used for guard-cell-specific expression is illustrated in Supplementary Fig. 4a. **b–d**, Stomatal aperture in the wild-type, *slac1* mutants and the transgenic *slac1-2* plants. Stomata in the wild type close in response to high [CO_2] (**b**), ABA (**c**) and darkness (**d**), whereas those in the *slac1* mutants fail to respond to these signals. The stomatal CO_2 response was restored in transformants expressing *SLAC1*, *SLAH1* or *SLAH3* in the guard cells. Values are shown as mean ± s.e. ($n = 60$) of three independent experiments. **e**, Genomic structures of *SLAC1* and its *Arabidopsis* homologues (*SLAHs*). The *slac1-2* mutation leading to a Gly 194-to-Asp substitution and the T-DNA insertional mutation in *slac1-3* are indicated (right). The phylogenetic relationship of the four SLAC1-family proteins and *S. pombe* Mae1 was predicted on the basis of their primary structures (left). The nucleotide positions encoding potential transmembrane helices were predicted using the TMHMM algorithm[21].

In contrast, SLAH2 (At4g27970) does not seem to substitute for SLAC1 function in guard cells. The SLAC1 protein has more than 70% amino acid similarity with other SLAHs over the transmembrane region[8]. The hydrophobicity of the fifth transmembrane region is high in SLAH2 relative to other SLAC1-family proteins (Fig. 1e), as predicted by the TMHMM algorithm[21], a widely used algorithm for prediction of transmembrane helices base on a hidden Markov model. This might provide an explanation for the functional divergence between SLAH2 and other SLAC1-family proteins.

Malate^{2-} and Cl^- efflux from guard cells by means of anion channels has been proposed to mediate membrane depolarization of guard cells[8], which in turn is essential for driving K^+ efflux from guard cells during stomatal closure[4–6]. However, no genes encoding anion channels involved in stomatal closure or plant-plasma-membrane-localized anion channels in general have been identified so far. A plant homologue of the mammalian CLC anion channels encodes a tonoplast H^+/nitrate exchanger[22]. In this study, we demonstrated that plasma-membrane-localized SLAC1 controls guard-cell anion homeostasis (Fig. 3) as well as stomatal closure (Fig. 1b–d). The SLAC1 protein might participate in the control of anion fluxes across the plasma membrane of guard cells, thus providing a starting point for future studies into the molecular nature of the anion transporters involved.

To analyse *SLAC1* functionally, we attempted heterologous expression and characterization of the gene product. However, introduction of the *SLAC1* cDNA clone into the yeast *mae1* mutant did not rescue the malate-uptake-deficient phenotype of the mutant. When SLAC1 was expressed in *Xenopus* oocytes, no SLAC1-dependent ion current could be observed. However, it has to be stressed that the functionality of a plant channel/transporter protein in heterologous systems might depend on the presence of appropriate regulators. Similar to results described for the plant potassium transporter AKT1 (ref. 23), co-expression of plant regulatory proteins might be a prerequisite for SLAC1 function in heterologous systems. Identification of proteins that interact with SLAC1 will help to address this possibility.

SLAC1-family members exhibit distinctive expression patterns (Fig. 2b). At least two SLAC1 homologues mimicked SLAC1 function when expressed ectopically in guard cells (Figs 1 and 3). In terrestrial angiosperms, anion currents have been reported in the plasma membrane of various cell types[8,24,15]. The expression patterns of *SLAH1* and *SLAH3* (Fig. 2b) are suggestive of an involvement in anion-flux regulation as related to vascular cell anion homeostasis. Thus, the illumination of the modes of action and regulation of the

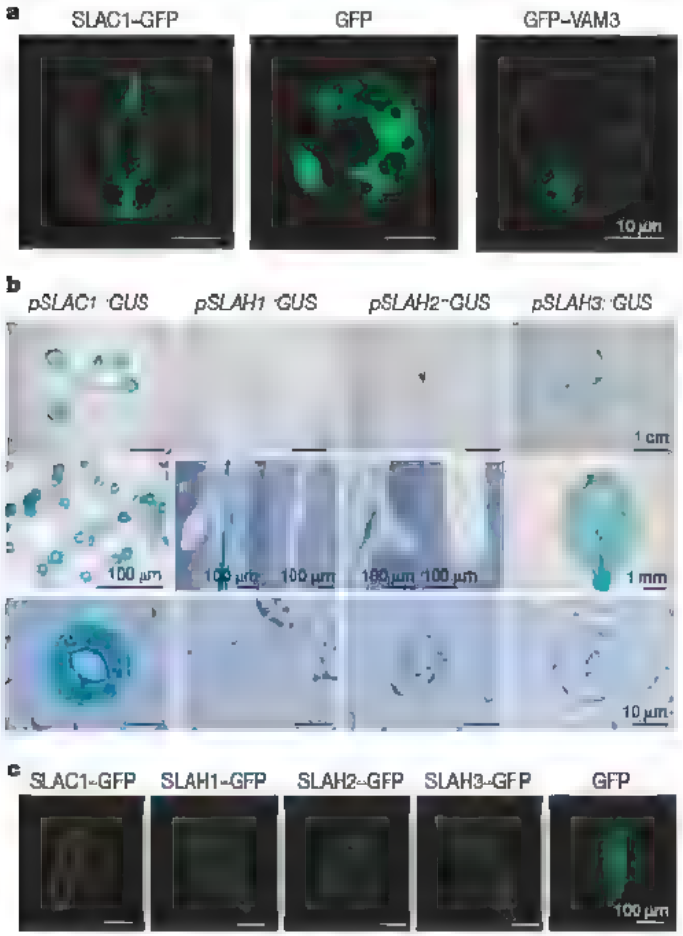

Figure 2 | Tissue-specific expression and subcellular localization of SLAC1-family proteins. **a**, Plasma membrane localization of SLAC1 in guard cells. Expression of SLAC1–GFP fusion protein resulted in functional complementation of the CO_2-insensitive phenotype of the *slac1-2* mutant (Supplementary Fig. 3). The guard-cell-specific distribution of GFP fluorescence was distinct in the SLAC1–GFP plants from that in transgenic plants expressing native GFP or in GFP–VAM3 transformants (tonoplast control). **b**, Expression of *SLAC1* was confined to guard cells, as evidenced by histochemical GUS staining of *pSLAC1::GUS* transformants. Expression of the three *SLAH* genes occurred at lateral root primordia and tap root tips (*SLAH2*) and in the vascular systems of root (*SLAH1*) or whole-plant (*SLAH3*) tissues, but was absent from guard cells. **c**, Transient expression of *SLAC1–GFP* in onion epidermis corroborated the plasma membrane localization of the SLAC1 protein. The GFP fluorescence from SLAH–GFP fusion proteins also was targeted to the periphery of epidermal cells.

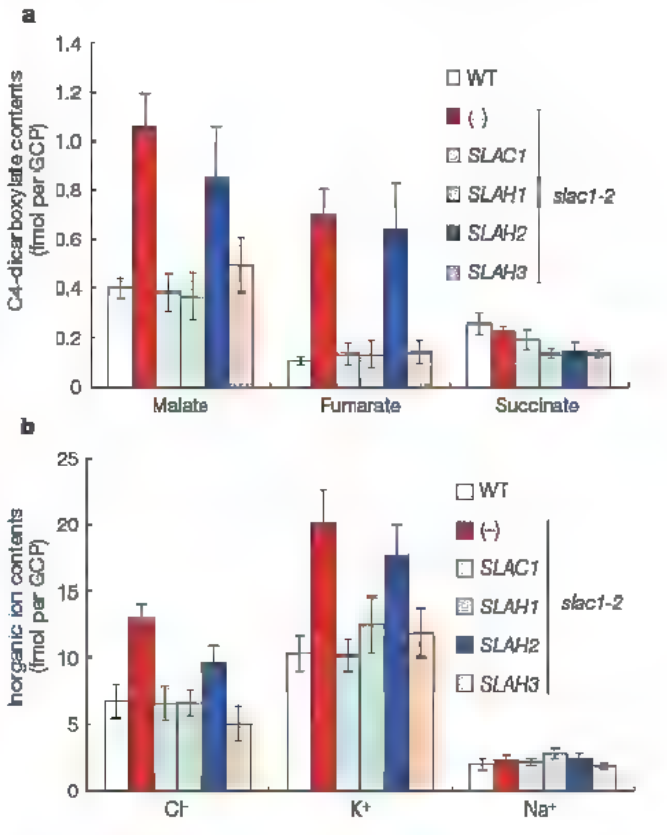

Figure 3 | Implication of SLAC1-family proteins in the maintenance of ion homeostasis across the plant plasma membranes. GCPs were isolated from leaf epidermis of the wild-type (WT), *slac1-2* mutant and the transgenic *slac1-2* plants. Organic/inorganic ion levels were quantified after illuminating the GCPs with white lights (80 μmol m^{-2} s^{-1} for 1 h) sufficient to induce the swelling of GCPs and stomatal opening in intact leaves. **a**, The high level of stomatal aperture in the *slac1-2* mutant (Fig. 1b–d) was correlated with over-accumulation of two major C4-dicarboxylate compounds, malate and fumarate. Guard-cell-specific expression of SLAC1, SLAH1 or SLAH3 in the mutant prevented this over-accumulation. Values are shown as mean ± s.d. ($n = 10$) for the wild type and *slac1-2* mutant, and mean ± s.d. ($n = 4$) for each transgenic line. **b**, The over-accumulation of C4-dicarboxylate compounds was accompanied by a corresponding increase in the levels of Cl^- and K^+, the major osmoregulatory inorganic ions for stomatal movement. Values are shown as mean ± s.d. ($n = 4$).

SLAC1-family proteins promises to further our understanding of essential processes in plant anion transport.

METHODS SUMMARY

All lines of *Arabidopsis* described here were descended from the Columbia wild type. Transgenic plants were generated using *Agrobacterium*-mediated transformation. Transient delivery of *GFP* constructs into onion epidermis was performed using a biolistic device. Plants were routinely grown at 22 °C under continuous white lights (80 μmol m^{-2} s^{-1}) unless otherwise described. The *slac1-2* mutant was isolated through thermal imaging of leaf temperature[10]. Stomatal aperture in response to environmental signals was analysed using epidermal peels prepared from 4- to 5-week-old plants. GCPs were isolated from blended leaf tissues by rounds of enzymatic digestion, nylon mesh filtration, and density gradient centrifugation, with a resulting purity of around 99%. Ionic compounds in the GCPs were extracted by boiling followed by centrifugal membrane filtration. Separation of organic anions was performed by high-performance liquid chromatography. Inorganic ions were separated using an ion chromatography system. For inorganic anion analysis, an electrolytic suppressor device was used. The contents of each ionic compound were estimated based on electroconductivity of eluates. A new SLAC1-family member, At1g62262, was added in TAIR's new genome release, version 7 (23 April 2007). In the present study, we analysed the three SLAC1 homologues (SLAH1, SLAH2 and SLAH3) available in the previous genome release (11 November 2005).

Full Methods and any associated references are available in the online version of the paper at www.nature.com/nature.

Received 22 August 2007; accepted 14 January 2008.
Published online 27 February 2008.

1. Hetherington, A. M. & Woodward, F. I. The role of stomata in sensing and driving environmental change. *Nature* 424, 901–908 (2003)
2. Sellers, P. J. *et al.* Modelling the exchanges of energy, water and carbon between continents and the atmosphere. *Science* 275, 502–509 (1997)
3. Shaw, M. R. *et al.* Grassland responses to global environmental changes suppressed by elevated CO_2. *Science* 298, 1987–1990 (2002)
4. MacRobbie, E. A. C. Signal transduction and ion channels in guard cells. *Phil. Trans. R. Soc. Lond. B* 353, 1475–1488 (1998).
5. Hetherington, A. M. Guard cell signaling. *Cell* 107, 711–714 (2001).
6. Schroeder, J. I. *et al.* Guard cell signal transduction. *Annu. Rev. Plant Physiol. Plant Mol. Biol.* 52, 627–658 (2001)
7. Raschke, K., Shabahang, M. & Wolf, R. The slow and the quick anion conductance in whole guard cells: their voltage-dependent alternation, and the modulation of their activities by abscisic acid and CO_2. *Planta* 217, 639–650 (2003)
8. Schroeder, J. I. & Hagiwara, S. Cytosolic calcium regulates ion channels in the plasma membrane of *Vicia faba* guard cells. *Nature* 338, 427–430 (1989)
9. Willmer, C. M. & Fricker, M. D. *Stomata* 2nd edn (Chapman and Hall, London, 1996)
10. Hashimoto, M. *et al. Arabidopsis* HT1 kinase controls stomatal movements in response to CO_2. *Nature Cell Biol.* 8, 391–397 (2006)
11. Merlot, S. *et al.* Use of infrared thermal imaging to isolate *Arabidopsis* mutants defective in stomatal regulation. *Plant J.* 30, 601–609 (2002)
12. Xie, X. D. *et al.* The identification of genes involved in the stomatal response to reduced atmospheric relative humidity. *Curr. Biol.* 16, 882–887 (2006)
13. Negi, J., Hashimoto, M. & Iba, K. Characterization of CO_2-insensitive *Arabidopsis* mutant *cdi3*. *Plant Cell Physiol.* 46, s176 (2005).
14. Vahisalu, T. *et al.* SLAC1 is required for plant guard cell S-type anion channel function in stomatal signalling. *Nature* (this issue) 10.1038/nature06608
15. Uemura, T., Yoshimura, S., Takeyasu, K. & Sato, M. Vacuolar membrane dynamics revealed by GFP–AtVam3 fusion protein. *Genes Cells* 7, 743–753 (2002)
16. Saier, M. H. *et al.* Phylogenetic characterization of novel transport protein families revealed by genome analyses. *Biochim. Biophys. Acta* 1422, 1–56 (1999)
17. Grobler, J., Bauer, F., Subden, R. E. & van Vuuren, H. J. The *mae1* gene of *Schizosaccharomyces pombe* encodes a permease for malate and other C4 dicarboxylic acids. *Yeast* 11, 1485–1491 (1995).
18. Pfam database. (http://pfam.sanger.ac.uk/family?acc=PF03595) (2007)
19. Vavasseur, A. & Raghavendra, A. Guard cell metabolism and CO_2 sensing. *New Phytol.* 165, 665–682 (2005).
20. Outlaw, D. J. *et al.* Requirements for activation of the signal-transduction network that leads to regulatory phosphorylation of leaf guard-cell phosphoenolpyruvate carboxylase during fusicoccin-stimulated stomatal opening. *Arch. Biochem. Biophys.* 407, 63–71 (2002)
21. TMHMM Server v.2.0 (http://www.cbs.dtu.dk/services/TMHMM/) (2007).
22. De Angeli, A. *et al.* The nitrate/proton antiporter AtCLCa mediates nitrate accumulation in plant vacuoles. *Nature* 442, 939–942 (2006).
23. Xu, J. *et al.* A protein kinase, interacting with two calcineurin B-like proteins, regulates K^+ transporter AKT1 in *Arabidopsis*. *Cell* 125, 1347–1360 (2006)
24. Ryan, P. R., Delhaize, E. & Jones, D. L. Function and mechanism of organic anion exudation from plant roots. *Annu. Rev. Plant Physiol. Plant Mol. Biol.* 52, 527–560 (2001).
25. Köhler, B. & Raschke, K. The delivery of salts to the xylem. Three types of anion conductance in the plasmalemma of the xylem parenchyma of roots of barley. *Plant Physiol.* 122, 243–254 (2000).

Supplementary Information is linked to the online version of the paper at www.nature.com/nature.

Acknowledgements We thank M. H. Sato for providing the tonoplast control plants, I. C. Mori for technical advice, and N. Kawahara for technical assistance. This research was supported by a Core Research for Evolution and Technology (CREST)-type JST grant and a JSPS grant, and by the Ministry of Agriculture, Forestry and Fisheries of Japan (Rice Genome Project IP-5005) grants (K.I.). J.N. is the recipient of scholarships from JSPS and Nara Institute of Science and Technology (NAIST). M.H. is the JST post-doctoral fellow.

Author Information Arabidopsis Genome Initiative (AGI) identifiers for SLAC1-family members are: SLAC1, At1g12480; SLAH1, At1g62280; SLAH2, At4g27970; and SLAH3, At5g24030. Reprints and permissions information is available at www.nature.com/reprints. Correspondence and requests for materials should be addressed to K.I. (koibasch@mbox.nc.kyushu-u.ac.jp).

LETTERS

SLAC1 is required for plant guard cell S-type anion channel function in stomatal signalling

Triin Vahisalu[1,2]*, Hannes Kollist[1,3]*, Yong-Fei Wang[4]*, Noriyuki Nishimura[4], Wai-Yin Chan[4], Gabriel Valerio[4], Airi Lamminmäki[1], Mikael Brosché[1], Heino Moldau[3], Radhika Desikan[5]†, Julian I. Schroeder[4] & Jaakko Kangasjärvi[1]

Stomatal pores, formed by two surrounding guard cells in the epidermis of plant leaves, allow influx of atmospheric carbon dioxide in exchange for transpirational water loss. Stomata also restrict the entry of ozone — an important air pollutant that has an increasingly negative impact on crop yields, and thus global carbon fixation[1] and climate change[2]. The aperture of stomatal pores is regulated by the transport of osmotically active ions and metabolites across guard cell membranes[3,4]. Despite the vital role of guard cells in controlling plant water loss[3,4], ozone sensitivity[1,2] and CO_2 supply[2,5–7], the genes encoding some of the main regulators of stomatal movements remain unknown. It has been proposed that guard cell anion channels function as important regulators of stomatal closure and are essential in mediating stomatal responses to physiological and stress stimuli[3,4,8]. However, the genes encoding membrane proteins that mediate guard cell anion efflux have not yet been identified. Here we report the mapping and characterization of an ozone-sensitive *Arabidopsis thaliana* mutant, *slac1*. We show that *SLAC1* (*SLOW ANION CHANNEL-ASSOCIATED 1*) is preferentially expressed in guard cells and encodes a distant homologue of fungal and bacterial dicarboxylate/malic acid transport proteins. The plasma membrane protein SLAC1 is essential for stomatal closure in response to CO_2, abscisic acid, ozone, light/dark transitions, humidity change, calcium ions, hydrogen peroxide and nitric oxide. Mutations in *SLAC1* impair slow (S-type) anion channel currents that are activated by cytosolic Ca^{2+} and abscisic acid, but do not affect rapid (R-type) anion channel currents or Ca^{2+} channel function. A low homology of SLAC1 to bacterial and fungal organic acid transport proteins, and the permeability of S-type anion channels to malate[9] suggest a vital role for SLAC1 in the function of S-type anion channels.

Stomatal aperture is regulated by light, plant water status, CO_2 concentration, relative air humidity, and among other stresses, drought and ozone (O_3)[3,4]. A number of signalling compounds, including abscisic acid (ABA), reactive oxygen species (ROS), nitric oxide (NO) and Ca^{2+} ions are involved in the regulation of stomatal aperture[3,4]. Adjustment of stomatal apertures is achieved by controlled transport of osmotically active ions and organic metabolites, including potassium (K^+), chloride (Cl^-) and malate across guard cell membranes[3,8–10,11], resulting in changes in osmotic potential. Anion channels have been proposed to function as central regulators of stomatal closure[8,11] by mediating anion efflux and causing membrane depolarization, which controls K^+ efflux through K^+ channels. So far, none of the candidates for plant anion channels — the plant homologues to the animal CLC chloride channels — has been localized to the plasma membrane[10], and the first plant CLC channel that was functionally characterized encodes a central vacuolar proton/nitrate exchanger[12], rather than an anion channel. Thus, despite their proposed importance in several physiological and stress responses in plants[8,10,11], the molecular identity of the guard cell plasma membrane proteins that mediate anion channel activity has remained unknown.

In a mutant screen for O_3 sensitivity, a series of *Arabidopsis* ethyl methanesulphonate (EMS) mutants called *radical-induced cell death* (*rcd*) was identified[13,14]. One of them, a recessive mutant originally referred to as *rcd3* (ref. 14) and here renamed *slac1* (*slow anion channel-associated 1*), showed constitutively higher stomatal conductance than the wild type (Columbia, Col-0) (Fig. 1a). Interestingly, both rapid transient[15] and long-term O_3-induced decreases in stomatal conductance were abolished in *slac1* (Fig. 1a). Water loss from excised *slac1* leaves resulted in 70–80% fresh weight loss after 90 min, whereas in the wild type, fresh weight loss was only 30% after 90 min (Fig. 1b). These differences in fresh weight loss were not a result of variation in stomatal number because *slac1* and wild-type leaves have similar stomatal density (Supplementary Fig. 1). Microarray analyses using messenger RNAs from 3-week-old rosette leaves did not reveal any significant differences in gene expression between *slac1* and the wild type when grown under optimal conditions. Furthermore, no other phenotypic differences have been observed between *slac1* and the wild type. Together these data suggested that the defect in *slac1* lies in defective stomatal regulation and that the O_3 damage of *slac1* leaves (Supplementary Fig. 2) is a result of increased O_3 flux into leaves through more open stomata.

The *slac1-1* mutation was identified in the gene At1g12480 by a combination of mapping, candidate gene expression in guard cell microarrays, and analyses of transfer DNA (T-DNA) insertion mutants (see Supplementary Information). *SLAC1* encodes a predicted membrane protein of 556 amino acids with a calculated molecular weight of 63.2 kDa and a predicted isoelectric point of 9.58. SLAC1 has hydrophilic amino- and carboxy-terminal tails (189 and 60 amino acids, respectively) and 10 predicted transmembrane helices (Fig. 1c, Supplementary Fig. 3), which contain a C4-dicarboxylate transporter/malic acid transport protein domain (InterPro: IPR004695) defined from the *Escherichia coli* TehA and *Schizosaccharomyces pombe* Mae1 proteins. Mae1 is involved in malate uptake[16]. TehA and Mae1 lack the long hydrophilic tail present in the N terminus of SLAC1, but show a weak, 15–20% amino-acid identity over the transmembrane region with SLAC1 (Supplementary Fig. 4a). SLAC1 shows no homology to the aluminium-activated malate transporters that function in plant aluminium resistance[17]. Homozygous

[1]Plant Biology, Department of Biological and Environmental Sciences, University of Helsinki, FI-00014 Helsinki, Finland. [2]Department of Botany, Institute of Ecology and Earth Sciences, University of Tartu, Tartu 51005, Estonia. [3]Institute of Technology, University of Tartu, Tartu 50411, Estonia. [4]Division of Biological Sciences, Cell and Developmental Biology Section, University of California San Diego, La Jolla, California 92093-0116, USA. [5]Centre for Research in Plant Science, University of the West of England, Bristol BS16 1QY, UK. †Present address, Division of Biology, Imperial College London, London SW7 2AZ, UK.
*These authors contributed equally to this work.

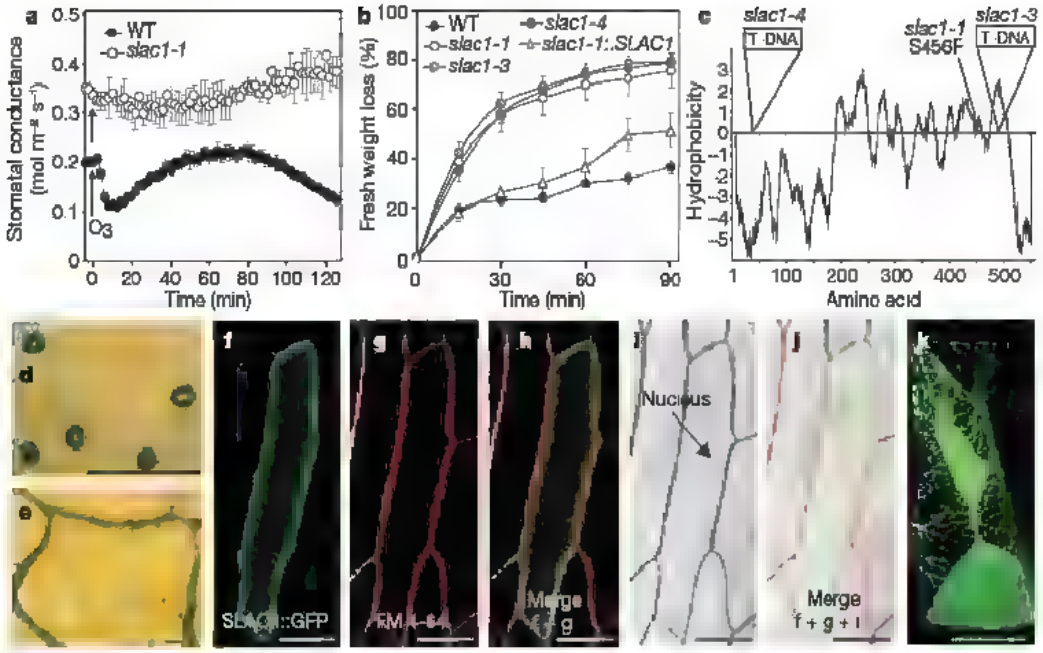

Figure 1 | Membrane protein SLAC1 controls leaf ozone and water-loss responses. **a**, Stomatal conductance ($n = 10$, ± s.e.m.) of *slac1-1* and wild-type plants after onset of 200 p.p.b. ozone, indicated by arrows. **b**, Weight loss from detached leaves of wild type (WT), *slac1* alleles and *slac1-1* complemented with the *SLAC1* gene ($n = 5$, ± s.e.m.) **c**, Membrane spanning hydrophobic regions in SLAC1 protein and the location of mutant alleles. **d**, **e**, GUS activity in *SLAC1* promoter *uidA* reporter lines. **f**, *SLAC1::GFP* translational fusion expressed in onion epidermal cells **g**, Area as in **f**, membranes stained with FM 4-64. **h**, Overlay of **f** and **g**. **i**, Light micrograph of **h**. **j**, Overlay of **h**, and **i**. **k**, *SLAC1–GFP* translational fusion in plasmolysed onion epidermal cells renders the Hechtian strands attaching the plasma membrane to the cell wall visible. Scale bars: **d**–**j**, 100 μm; **k**, 50 μm.

T-DNA insertion lines (SALK_099139 and SALK_137265, referred to as *slac1-3* and *slac1-4*, respectively; Fig. 1c) both showed similar recessive inheritance, and exhibited similar fresh weight loss from excised leaves as *slac1-1* (Fig. 1b). A genomic copy of *SLAC1* complemented the mutant phenotype in stably transformed *slac1-1* (Fig. 1b).

SLAC1 belongs to a small family of five proteins in *Arabidopsis*. Three of the proteins, including SLAC1, have a long hydrophilic N-terminal tail, whereas two have only the transmembrane domains. Rice has nine orthologous proteins. The SLAC1 protein is more similar to its rice orthologue Os04g48530 than to the four other

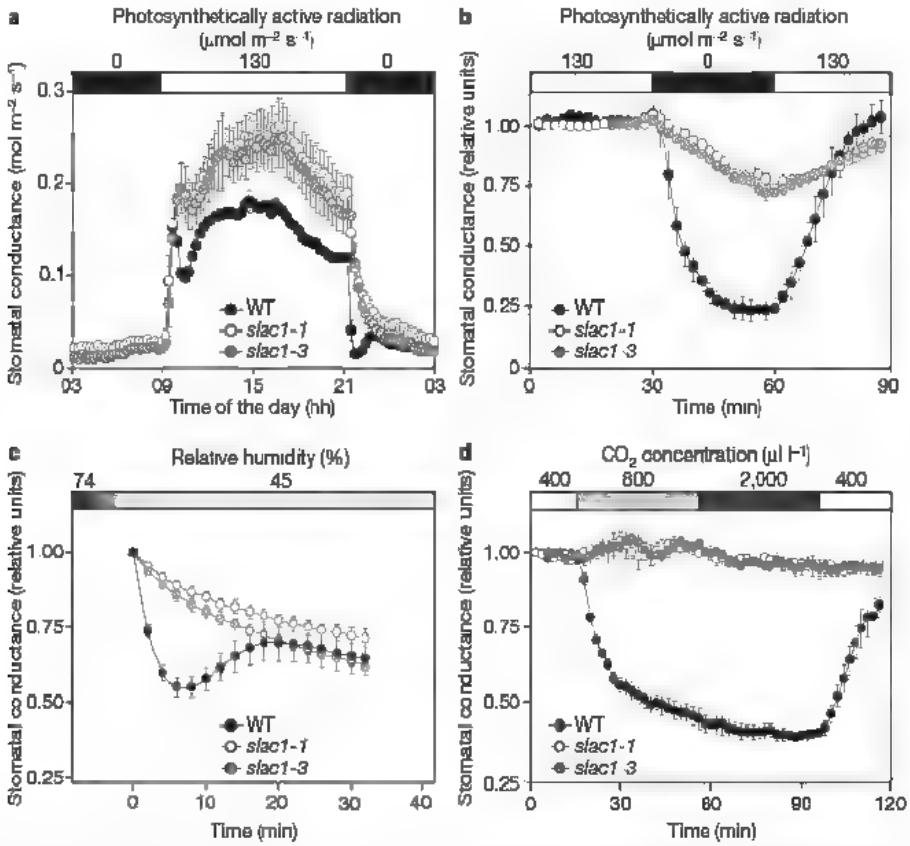

Figure 2 | Mutations in *SLAC1* impair stomatal responses to changes in environment. **a**, Diurnal dark/light stomatal conductance response in *slac1* and wild-type plants with ± s.e.m. ($n = 3$) **b**, Time courses of stomatal responses to changes in light intensity. **c**, Time courses of stomatal response to changes in air humidity. **d**, Time courses of stomatal response to changes in CO_2 concentration. Stomatal responses were monitored with an *Arabidopsis* whole-rosette gas-exchange system[15], and values in **b**–**d** were normalized to conductances at 0 mn and represent averages (±s.e.m.) of four rosettes.

Arabidopsis SLAC1 homologues (Supplementary Fig. 4a, b). The transmembrane domains of *Arabidopsis* and rice SLAC1 homologues and orthologues have several highly conserved amino acids. However, SLAC1 and Os04g48530 also differ from the rest of the proteins in several amino-acid residues (Supplementary Fig. 4a). For example, the amino acid that is mutated in *slac1-1* is a serine in SLAC1 and Os04g48530, whereas other family members have an alanine residue in the same position. The serine mutated in *slac1-1* is surrounded by three conserved threonine residues, suggesting that this region is significant for either the structure, function or regulation of the protein. Additionally, the predicted intracellular loops between the transmembrane domains have several conserved, positively charged amino-acid residues (Supplementary Figs 3, 4a), also suggesting functional significance.

When 1,582 base pairs (bp) of genomic sequence upstream of the *SLAC1* translation start were fused to the reporter gene *uidA*, the resulting β-glucuronidase (GUS) activity in transgenic plants was localized predominantly to guard cells (Fig. 1d), and occasionally to the vascular strands close to the leaf margins (Fig. 1e). No GUS activity was detected in other parts of the plants. Expression data at the Genevestigator database[18] and comparison of gene expression between guard cell and mesophyll cell microarrays also suggest strong preferential guard cell expression of *SLAC1*.

To study the subcellular location of the SLAC1 protein, green fluorescence protein (GFP) fused to the SLAC1 C terminus was transiently expressed in onion epidermal cells (Fig. 1f–k) and in tobacco protoplasts (Supplementary Fig. 5). Fluorescence and confocal imaging showed that in onion epidermal cells, fluorescence from the SLAC1::GFP fusion protein (Fig. 1f) and the membrane-specific stain FM 4-64 (Fig. 1g) colocalized in merged images (Fig. 1h). GFP fluorescence was observed between the cell wall and the nucleus (Fig. 1j; Supplementary Movie), and was connected to the cell wall through Hechtian strands in plasmolysed cells (Fig. 1k), correlating with plasma membrane localization. Expression in tobacco protoplasts showed results that are consistent with plasma membrane localization (Supplementary Fig. 5).

Stomatal aperture is under environmental and hormonal control. We analysed stimulus responses in stomatal conductance by comparing intact[15] *slac1* with wild-type plants. Stomatal conductance in *slac1* was about 1.5-fold higher during the light period (Fig. 2a). Also, the decline in stomatal conductance at the beginning of the dark period took more than 1 h longer in *slac1* compared with the wild type (Fig. 2a). Light/dark transitions during the normal light period caused rapid changes in stomatal conductance in the wild type, whereas *slac1* showed a slow and modest response (Fig. 2b). *slac1* exhibited a much slower response than the wild type to a decrease in the relative air humidity (Fig. 2c), which is known to cause a rapid reduction of stomatal conductance[19]. Doubling of $[CO_2]$ from 400 p.p.m. to 800 p.p.m. reduced stomatal conductance effectively in the wild type, whereas *slac1* showed no responses (Fig. 2d). Thus, *slac1* stomata show only a slow and modest response to changes in light and air humidity, and are completely insensitive to O_3 stress (Fig. 1a) and elevated $[CO_2]$ (Fig. 2d).

The concentration of the plant stress hormone ABA increases under drought and induces stomatal closure through second messengers, including ROS, cytosolic Ca^{2+} and NO[20–22]. We measured stomatal responses to ABA, hydrogen peroxide (H_2O_2), NO and repetitive Ca^{2+} pulses (Fig. 3). Stomata of *slac1* mutants showed a strong insensitivity to ABA (Fig. 3a and Supplementary Fig. 6a). Similarly, they showed significantly reduced responses to H_2O_2 (Fig. 3b) and the NO donor sodium nitroprusside (SNP) (Fig. 3c). Transient addition and removal of Ca^{2+} to the extracellular solution bathing leaf epidermides, while shifting the K^+ equilibrium potential, allows experimental imposition of defined intracellular Ca^{2+} transients in guard cells, resulting in stomatal closure[23–25]. Four repetitive 5-min pulses of 1 mM external Ca^{2+} were applied (Fig. 3d; top inset; Supplementary Fig. 7). The imposed intracellular Ca^{2+} ($[Ca^{2+}]_i$) oscillation pattern of *slac1-1* guard cells was similar to that

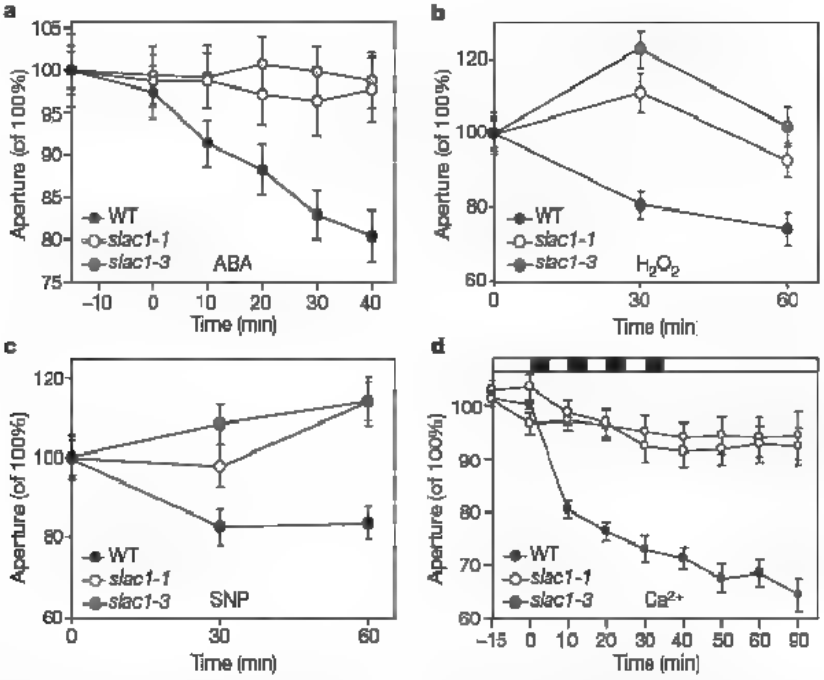

Figure 3 | Impaired stomatal responses to ABA, H_2O_2, NO and Ca^{2+} in *slac1*. **a**, Time-course experiments of ABA-induced stomatal closure. ABA (1 μM) was added at time = 0 (n = 3 experiments, 28, 23 and 57 stomata for *slac1-1*, *slac1-3* and wild type, respectively). Stomatal apertures at time = 0 (100%) corresponded to average stomatal apertures of 2.82 ± 0.16 μm (wild type), 2.88 ± 0.12 μm in *slac1-1* and 3.23 ± 0.08 μm in *slac1-3*. **b**, **c**, Time course of stomatal closure induced by H_2O_2 (100 μM) (**b**) and NO (derived from 50 μM SNP) (**c**). n = 3–5 independent experiments, 20 stomata per experiment. **d**, Impairment in stomatal closure in response to four transient 5-min extracellular applications of 1 mM $CaCl_2$ and 1 mM KCl (black strips at top; n = 3 experiments, 48, 24 and 32 stomata for wild type, *slac1-1* and *slac1-3*, respectively). Imposed intracellular Ca^{2+} transients (see Supplementary Fig. 7) were followed by 5-min exposures to a depolarizing solution containing 0 mM $CaCl_2$ and 50 mM KCl (white strips at top) as previously described[25]. Stomatal apertures at time = 0 (100%) corresponded to average stomatal apertures of 3.56 ± 0.10 μm, 3.93 ± 0.14 μm and 3.56 ± 0.10 μm in wild type, *slac1-1* and *slac1-3*, respectively. Error bars depict means ± s.e.m

of the wild type (Supplementary Fig. 7). The average amplitudes of imposed $[Ca^{2+}]_i$ transients and the integrated total $[Ca^{2+}]_i$ increases per period were statistically similar in wild-type and *slac1-1* guard cells (see Supplementary Information). Imposed $[Ca^{2+}]_i$ transients caused the typical downstream Ca^{2+}-induced reactive and programmed[23,24] stomatal closure in the wild type, whereas the response was greatly impaired in *slac1-1* and *slac1-3* (Fig. 3d). Thus *slac1* mutant guard cells do not abrogate imposed cytosolic Ca^{2+} oscillations, but show a strong impairment in downstream Ca^{2+} oscillation-induced stomatal closing.

The activation of S- and R-type anion efflux channels, both of which can transmit Cl^- and malate efflux from guard cells[8,9,11], is proposed to decrease guard cell osmotic potential, leading to stomatal closure[3,4,8,10,11]. This is consistent with Cl^- and malate efflux occurring in response to ABA[26,27]. We therefore applied whole-cell patch clamp techniques to characterize the functioning of S-type and R-type anion channel activities. In wild-type guard cells, elevated cytosolic Ca^{2+} (2 μM) activated ion currents that were selective for Cl^- over caesium ions (Cs^+) ($n = 16$ guard cells) and showed a relative permeability ratio for malate to chloride anions of 0.125 ($n = 12$ guard cells), consistent with previous anion selectivity analyses of S-type anion channel currents[9] (Supplementary Fig. 8).

S-type anion currents were readily recorded in wild-type guard cells (Fig. 4a, d). However, only very small combined background whole-cell membrane currents and patch-clamp seal currents were observed in *slac1-1* and *slac1-3* guard cells (Fig. 4b–d). R-type anion currents[11] were activated as described[25,28]. Interestingly, no significant differences in R-type anion currents between wild-type and *slac1* guard cells were observed (Fig. 4e, f). Similarly, ABA activation of Ca^{2+}-permeable 'I_{Ca}' channel currents[21] was not disrupted in *slac1* guard cells (Supplementary Fig. 9). However, when ABA activation of S-type anion channels was analysed, *slac1* mutants showed only small whole-cell currents (Fig. 4h–j), whereas S-type anion currents were recorded in wild-type guard cells (Fig. 4g, j).

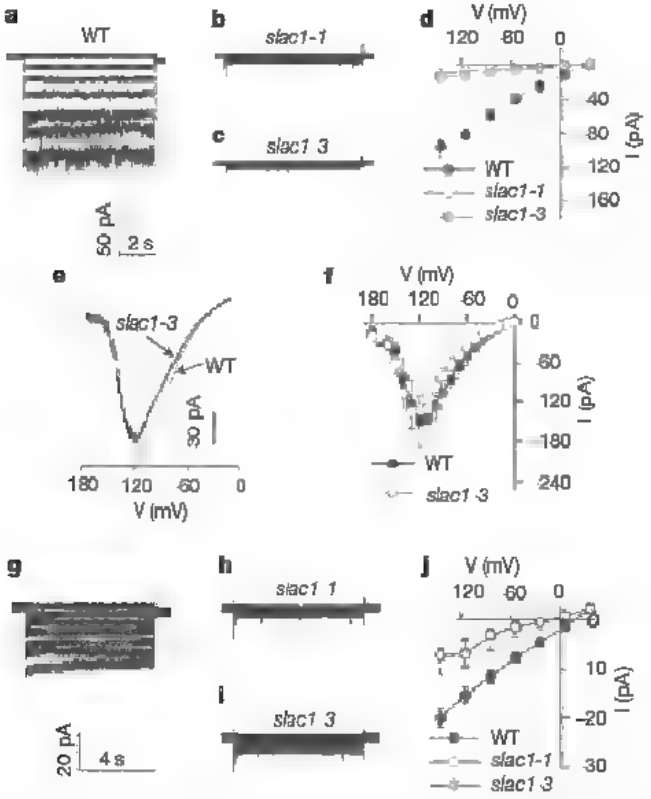

Figure 4 | Ca^{2+} and ABA activations of S-type anion channels are impaired in *slac1* guard cells. **a–d**, Ca^{2+} activation of S-type anion channels. **a–c**, Whole-cell recordings of S-type anion currents in wild type (**a**), *slac1-1* (**b**) and *slac1-3* (**c**). **d**, Average current–voltage curves of S-type anion channel currents recorded in wild type ($n = 7$), *slac1-1* ($n = 12$) and *slac1-3* ($n = 10$). **e, f**, Typical R-type anion channel recordings (**e**), and average current–voltage curves in wild type ($n = 3$) and *slac1-3* ($n = 6$) (**f**). **g–j**, ABA activation of S-type anion channels. **g–i**, Typical recordings in wild type (**g**), *slac1-1* (**h**) and *slac1-3* (**i**). **j**, Average current–voltage curves recorded in wild type ($n = 10$), *slac1-1* ($n = 8$) and *slac1-3* ($n = 8$). Error bars depict means ± s.e.m.

Continuing increases in ozone concentrations in the troposphere owing to human activities are predicted to have a negative affect on crop yields and global carbon sinks in the future[1,2]. The ozone sensitivity of *slac1* leaves (Supplementary Fig. 2), the predominant guard cell expression of *SLAC1* (Fig. 1d, e) and abolishment of O_3-induced stomatal closure in *slac1* mutants (Fig. 1a) together provide direct genetic evidence for the importance of O_3 sensing in guard cells for plant O_3 tolerance. Only a few plant mutants are known that show CO_2 insensitivity[5,6] or a constitutive high CO_2 response[7] in stomatal movements, but no recessive CO_2-insensitive mutant gene has been isolated so far. All *slac1* alleles are recessive and show a complete lack of high CO_2-induced stomatal closure (Fig. 2), illustrating that the SLAC1 protein is a central positive mediator of CO_2-induced stomatal closure.

Experiments with ABA, ROS, NO and Ca^{2+} suggest that SLAC1 is an essential protein functioning downstream of these messengers in mediating stomatal closure (Figs 3, 4 and Supplementary Figs 6, 7, 9). The phenotype of *slac1* differs from the ATP-binding cassette transporter mutant, *atmrp5*, which shows partial repression of ABA-induced stomatal closure, partial S-type anion current activity and impaired Ca^{2+} channel activation[29]. The strong impairment in S-type anion channel and normal Ca^{2+} channel activity in *slac1* guard cells is consistent with SLAC1 being more closely associated with S-type anion channels than is AtMRP5, and provides direct genetic evidence for the model that these anion channels function as a central control mechanism for stomatal closure[8].

R-type anion channel activity was not disrupted in *slac1* guard cells (Fig. 4e, f), providing genetic evidence for a molecular separation of the membrane proteins required for S- and R-type anion channels. It remains possible that these anion channel types share other protein subunits[30]. R-type channels may be responsible for the slow stomatal conductance decrease observed in response to light/dark transitions and decrease in relative humidity (Fig. 2a–c).

The data presented demonstrate that *SLAC1* encodes an essential subunit for S-type anion channel function or regulation. The low homology of SLAC1 to bacterial and fungal organic acid transporters indicates a possible role for SLAC1 in contributing to formation of an anion-transporting pore. Further research on SLAC1 and its homologues should increase the general understanding of plasma-membrane anion channel structure and regulation in plants.

METHODS SUMMARY

Three- to six-week-old *A. thaliana* plants grown in a controlled environment were used. *slac1-1* was isolated from an O_3-sensitivity mutant screen[15]. The mapping population was generated by outcrossing to *Ler*, and an impaired water-loss phenotype was used as a mapping trait. For water-loss analyses, the weight of the detached leaves was followed. Whole-plant stomatal conductance responses to O_3, light/dark transitions, elevated CO_2 and lowered humidity were measured using the *Arabidopsis* whole-rosette gas-exchange system[15]. For GUS activity and complementation analyses, transgenic *SLAC1* promoter-driven *GUS* expression lines and complementation lines with *SLAC1* genomic DNA were analysed. For transient gene-expression studies, a SLAC1::GFP fusion protein under the control of a 35S promoter was delivered into onion epidermides by particle bombardment, and to tobacco protoplasts by electroporation. Images were acquired by confocal microscopy. For stomatal responses to H_2O_2, NO and ABA, stomatal apertures were measured from extracted epidermal fragments after pre-incubation of leaves in opening buffer. Stomatal responses to Ca^{2+} transients and Ca^{2+} imaging experiments were analysed in intact leaf epidermides by imposing extracellular calcium pulses[23,25]. For electrophysiological analyses, *Arabidopsis* guard cell protoplasts were isolated enzymatically, and Ca^{2+} activation of S- and R-type anion currents and ABA activation of S-type anion and I_{Ca} Ca^{2+} currents were recorded as described[25,29].

Full Methods and any associated references are available in the online version of the paper at www.nature.com/nature.

Received 22 August; accepted 31 December 2007.
Published online 27 February 2008.

1. Hopkin, M. Carbon sinks threatened by increasing ozone *Nature* **448,** 396–397 (2007)
2. Sitch, S., Cox, P. M., Collins, W. J. & Huntingford, C. Indirect radiative forcing of climate change through ozone effects on the land-carbon sink *Nature* **448,** 791–794 (2007)
3. MacRobbie, E. A. C. Signal transduction and ion channels in guard cells. *Phil. Trans. R. Soc. Lond. B* **353,** 1475–1488 (1998).
4. Hetherington, A. M. & Woodward, F. I. The role of stomata in sensing and driving environmental change. *Nature* **424,** 901–908 (2003)
5. Webb, A. A. R. & Hetherington, A. Convergence of the abscisic acid, CO_2, and extracellular calcium signal transduction pathways in stomatal guard cells. *Plant Physiol.* **114,** 1557–1560 (1997).
6. Young, J. J. *et al.* CO_2 signaling in guard cells: calcium sensitivity response modulation, a Ca^{2+}-independent phase, and CO_2 insensitivity of the *gca2* mutant *Proc. Natl Acad. Sci. USA* **103,** 7506–7511 (2006).
7. Hashimoto, M. *et al. Arabidopsis* HT1 kinase controls stomatal movements in response to CO_2. *Nature Cell Biol.* **8,** 391–397 (2006)
8. Schroeder, J. I. & Hagiwara, S. Cytosolic calcium regulates ion channels in the plasma membrane of *Vicia faba* guard cells. *Nature* **338,** 427–430 (1989)
9. Schmidt, C. & Schroeder, J. I. Anion-selectivity of slow anion channels in *Vicia faba* guard cells: large nitrate permeability *Plant Physiol.* **106,** 383–391 (1994)
10. Pandey, S., Zhang, W. & Assmann, S. M. Roles of ion channels and transporters in guard cell signal transduction *FEBS Lett.* **581,** 2325–2336 (2007).
11. Keller, B. U., Hedrich, R. & Raschke, K. Voltage-dependent anion channels in the plasma membrane of guard cells. *Nature* **341,** 450–453 (1989).
12. De Angeli, A. *et al.* The nitrate/proton antiporter AtCLCa mediates nitrate accumulation in plant vacuoles. *Nature* **442,** 939–942 (2006).
13. Overmyer, K. *et al.* Ozone-sensitive *Arabidopsis rcd1* mutant reveals opposite roles for ethylene and jasmonate signaling pathways in regulating superoxide-dependent cell death. *Plant Cell* **12,** 1849–1862 (2000)
14. Kangasjärvi, J., Jaspers, P. & Kollist, H. Signalling and cell death in ozone-exposed plants. *Plant Cell Environ.* **28,** 1021–1036 (2005)
15. Kollist, T. *et al.* A novel device detects a rapid ozone-induced transient stomatal closure in intact *Arabidopsis* and its absence in *abi2* mutant. *Physiol. Plant.* **129,** 796–803 (2007)
16. Camarasa, C. *et al.* Characterization of *Schizosaccharomyces pombe* malate permease by expression in *Saccharomyces cerevisiae*. *Appl. Environ. Microbiol.* **67,** 4144–4151 (2001)
17. Sasaki, T. *et al.* A wheat gene encoding an aluminum-activated malate transporter *Plant J.* **37,** 645–653 (2004)
18. Zimmermann, P., Hirsch-Hoffmann, M., Hennig, L. & Gruissem, W. GENEVESTIGATOR. *Arabidopsis* microarray database and analysis toolbox *Plant Physiol.* **136,** 2621–2632 (2004)
19. Xie, X. *et al.* The identification of genes involved in the stomatal response to reduced atmospheric relative humidity *Curr. Biol.* **16,** 882–887 (2006).
20. McAinsh, M. R., Brownlee, C. & Hetherington, A. M. ABA induced elevation of guard cell cytosolic calcium precedes stomatal closure in *Commelina communis*. *Nature* **343,** 186–188 (1990).
21. Pei, Z. M. *et al.* Calcium channels activated by hydrogen peroxide mediate abscisic acid signalling in guard cells. *Nature* **406,** 731–734 (2000)
22. Desikan, R., Griffiths, R., Hancock, J. & Neill, S. A new role for an old enzyme: Nitrate reductase-mediated nitric oxide generation is required for abscisic acid-induced stomatal closure in *Arabidopsis thaliana*. *Proc. Natl Acad. Sci. USA* **99,** 16314–16318 (2002).
23. Allen, G. J. *et al.* A defined range of guard cell calcium oscillation parameters encodes stomatal movements. *Nature* **411,** 1053–1057 (2001)
24. Li, Y. *et al.* The parameters of guard cell calcium oscillation encode stomatal oscillation and closure in *Vicia faba*. *Plant Sci.* **166,** 415–421 (2004)
25. Mori, I. C. *et al.* CDPKs CPK6 and CPK3 function in ABA regulation of guard cell S-type anion- and Ca^{2+}-permeable channels and stomatal closure. *PLoS Biol.* **4,** 1749–1762 (2006)
26. Van Kirk, C. A. & Raschke, K. Release of malate from epidermal strips during stomatal closure. *Plant Physiol.* **61,** 474–475 (1978).
27. MacRobbie, E. A. C. Ion fluxes in 'isolated' guard cells of *Commelina communis* L. *J. Exp. Bot.* **32,** 545–562 (1981)
28. Frachisse, J. M., Thomine, S., Colcombet, J., Guern, J. & Barbier-Brygoo, H. Sulfate is both a substrate and an activator of the voltage-dependent anion channel of *Arabidopsis* hypocotyl cells. *Plant Physiol.* **121,** 253–261 (1999).
29. Suh, S. J. *et al.* The ATP binding cassette transporter AtMRP5 modulates anion and calcium channel activities in *Arabidopsis* guard cells. *J. Biol. Chem.* **282,** 1916–1924 (2007).
30. Linder, B. & Raschke, K. A slow anion channel in guard cells, activating at large hyperpolarization, may be principal for stomatal closing. *FEBS Lett.* **313,** 27–30 (1992)

Supplementary Information is linked to the online version of the paper at www.nature.com/nature.

Acknowledgements We thank M. Luskallio and I. Puzõrjova for technical help. This research was supported by the Academy of Finland Centre of Excellence programme and Helsinki University Environmental Research Centre (to J.K.), by Estonian Science Foundation and University of Tartu start-up grants (to H.K.), by NIH, NSF and, in part, DOE grants (to J.I.S.), and a Leverhulme Trust Early Career Fellowship (to R.D.)

Author Contributions T.V., H.K. and Y.-F.W. contributed equally to this work. J.K. and H.K. designed the experiments in Figs 1 and 2. A.L., H.K. and T.V. identified the *SLAC1* gene. T.V. and M.B. performed the expression, complementation and subcellular localization analyses in Fig. 1 and Supplementary Fig. 5. H.K. and H.M. performed experiments in Fig. 2. H.K. performed experiments in Supplementary Figs 1 and 2. R.D. designed and performed experiments in Fig. 3b, c and Supplementary Fig. 6b. J.I.S. and J.K. designed experiments in Figs 3a and d, and 4, and Supplementary Figs 6a, 7, 8 and 9. W.-Y.C. and G.V. performed experiments in Fig. 3d and Supplementary Fig. 6a. N.N. performed experiments in Fig. 3a and Supplementary Fig. 7. Y.-F.W. performed experiments in Fig. 4 and Supplementary Figs 8 and 9. J.K. and J.I.S. wrote the paper. All the authors discussed the results, and commented on and edited the manuscript.

Author Information The primary microarray data reported has been deposited with the ArrayExpress database under accession number E-MEXP-1388. Reprints and permissions information is available at www.nature.com/reprints. Correspondence and requests for materials should be addressed to J.K. (jaakko.kangasjarvi@helsinki.fi)

LETTERS

SIRT6 is a histone H3 lysine 9 deacetylase that modulates telomeric chromatin

Eriko Michishita[1,5], Ronald A. McCord[1,5], Elisabeth Berber[1,5], Mitomu Kioi[2], Hesed Padilla-Nash[6], Mara Damian[1,5], Peggie Cheung[3], Rika Kusumoto[8], Tiara L. A. Kawahara[4], J. Carl Barrett[7]†, Howard Y. Chang[4], Vilhelm A. Bohr[8], Thomas Ried[6], Or Gozani[3] & Katrin F. Chua[1,5]

The Sir2 deacetylase regulates chromatin silencing and lifespan in *Saccharomyces cerevisiae*[1,2]. In mice, deficiency for the Sir2 family member SIRT6 leads to a shortened lifespan and a premature ageing-like phenotype[3]. However, the molecular mechanisms of SIRT6 function are unclear. SIRT6 is a chromatin-associated protein[3], but no enzymatic activity of SIRT6 at chromatin has yet been detected, and the identity of physiological SIRT6 substrates is unknown. Here we show that the human SIRT6 protein is an NAD^+-dependent, histone H3 lysine 9 (H3K9) deacetylase that modulates telomeric chromatin. SIRT6 associates specifically with telomeres, and SIRT6 depletion leads to telomere dysfunction with end-to-end chromosomal fusions and premature cellular senescence. Moreover, SIRT6-depleted cells exhibit abnormal telomere structures that resemble defects observed in Werner syndrome, a premature ageing disorder[4,5]. At telomeric chromatin, SIRT6 deacetylates H3K9 and is required for the stable association of WRN, the factor that is mutated in Werner syndrome[4,5]. We propose that SIRT6 contributes to the propagation of a specialized chromatin state at mammalian telomeres, which in turn is required for proper telomere metabolism and function. Our findings constitute the first identification of a physiological enzymatic activity of SIRT6, and link chromatin regulation by SIRT6 to telomere maintenance and a human premature ageing syndrome.

Normal human somatic cells have a finite replicative lifespan, and after prolonged replication they undergo cellular senescence as a result of telomere dysfunction[6,7]. Despite the ageing-like phenotype of SIRT6-deficient mice, no effect of SIRT6 deficiency on cellular lifespan has been reported. To determine whether SIRT6 influences cellular senescence, retroviral transduction of short hairpin RNAs (shRNAs) was used to stably knock down *SIRT6* expression in WI-38 human fibroblasts (Fig. 1a). *SIRT6* knockdown (S6KD) cells have a strikingly shortened replicative lifespan, undergoing premature cellular senescence about ten population doublings before control cells, and show increased levels of senescence-associated β-galactosidase (SA-β-gal) staining (Fig. 1b, c, and Supplementary Fig. 2a). These kinetics of premature senescence are similar to those associated with the inactivation of telomere accessory factors (Supplementary Fig. 3a, b)[8]. Premature cellular senescence was also observed with two independent *SIRT6* shRNAs, ruling out off-target shRNA effects, but not with irrelevant shRNAs (Supplementary Figs 2b–d and 3c). We conclude that SIRT6 is crucial in maintaining a normal replicative lifespan and in preventing the premature senescence of human cells.

Replicative cellular senescence can result from dysfunctional telomeres, which are recognized by DNA damage response factors and are detected as telomere dysfunction-induced foci (TIFs)[9,10]. Analysis of TIFs revealed elevated telomere dysfunction in S6KD cells (Fig. 1d, e, and Supplementary Fig. 4a). The telomere signals at TIFs in S6KD cells are weak compared with non-TIF telomere signals, suggesting a subpopulation of telomeres that have undergone significant sequence loss (see below). However, mean telomere length was not significantly reduced in S6KD cells (Supplementary Fig. 5). Together, these observations suggest that S6KD cells undergo accelerated senescence and telomere dysfunction in response to stochastic telomere sequence loss, without increased global telomere erosion.

Loss of proper telomeric protective end structures can lead to dicentric chromosomes as a result of chromosomal end-to-end fusions[11]. We therefore scored chromosomal end fusions in S6KD and control metaphases in several independent cytogenetic analyses. Non-recurrent chromosomal end-to-end fusions were observed in S6KD cells and were more pronounced at later population doublings, but they were rarely observed in control cells (Fig. 1f and Supplementary Fig. 4b, c). These observations indicate that SIRT6 is critical for maintaining functional telomeres to avert chromosomal instability due to aberrant chromosomal end-to-end fusions.

Several experiments provide further evidence that the premature senescence of S6KD cells is due to telomere dysfunction and not to defective base excision repair (BER), which was previously implicated in the phenotypes of *SIRT6* knockout (S6KO) mouse cells[3], or to oxidative stress brought on by supraphysiological oxygen conditions of ambient cell culture conditions[12]. First, telomere stabilization (by the ectopic expression of telomerase (hTERT)) reversed the premature senescence of S6KD, whereas augmenting BER (by the ectopic expression of the DNA polymerase-β dRP lyase domain) did not (Fig. 1g and Supplementary Fig. 6). This DNA polymerase-β domain was previously shown to rescue the hypersensitivity of S6KO mouse cells to alkylating DNA damage agents[3]. Second, S6KD cells underwent premature senescence even when cultured under low (physiological) oxygen conditions (Supplementary Fig. 7). Together, these findings demonstrate that telomere dysfunction, not BER defects or oxidative stress, underlie the premature senescence phenotype of S6KD cells.

The premature cellular senescence, telomere dysfunction and chromosomal fusions observed in S6KD cells are reminiscent of the cellular phenotype of Werner syndrome (WS)[13–16], a hereditary disorder associated with signs of premature ageing[4,5]. The WS-defective protein WRN associates with telomeres (in primary human IMR90 cells and U2OS osteosarcoma cancer cells) and regulates telomere processing during S phase[13,17]. We formed the hypothesis that SIRT6

[1]Department of Medicine, Division of Endocrinology, Gerontology and Metabolism, School of Medicine, [2]Department of Radiation Oncology, School of Medicine, [3]Department of Biological Sciences, and [4]Program in Epithelial Biology, School of Medicine, Stanford University, Stanford, California 94305, USA. [5]Geriatric Research, Education and Clinical Center, VA Palo Alto Health Care System, Palo Alto, California 94304, USA. [6]Genetics Branch, and [7]Laboratory of Biosystems and Cancer, Center for Cancer Research, National Cancer Institute/NIH, Bethesda, Maryland 20892, USA. [8]Laboratory of Molecular Gerontology, National Institute on Aging, NIH, Baltimore, Maryland 21224, USA. †Present address: Novartis Institutes for Biomedical Research, Cambridge, Massachusetts 02139, USA.

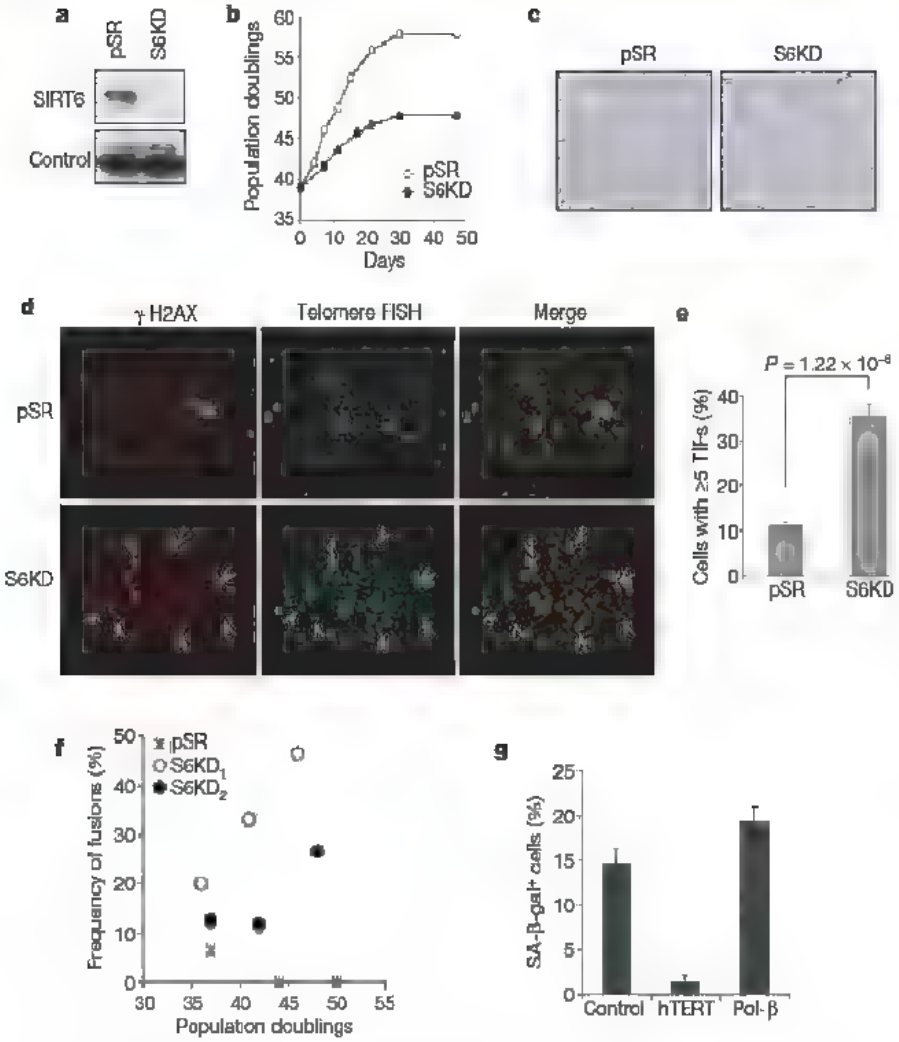

Figure 1 *SIRT6* knockdown leads to premature cellular senescence and telomere dysfunction. **a**, Western analysis of SIRT6 expression in WI-38 *SIRT6* knockdown (S6KD) or control (pSR) cells **b**, Serial passaging experiments revealing premature replicative senescence of S6KD WI-38 cells. Passaging was begun at population doubling 39 and cumulative population doublings were calculated after the indicated days **c**, Increased SA-β-gal$^+$ staining in S6KD cultures at day 11 of serial passaging. **d**, **e**, Increased telomere dysfunction in S6KD WI-38 cells. TIFs were detected (**d**) by co-localization of γ-H2AX and telomeres, and cells with at least five TIFs were scored (**e**). Data represent the average of 20 fields. Error bars indicate s.e.m.; $n = 158$ (pSR), $n = 110$ (S6KD) The P value was calculated with the two-tailed Student's t-test. **f**, Increased chromosome end-to-end fusions in S6KD cells observed by spectral karyotype (SKY) analysis. Values represent the numbers of fused chromosomes as a percentage of total metaphases. $S6KD_1$ and $S6KD_2$ are knockdown cells generated with two independent SIRT6-specific shRNAs. **g**, Stabilizing telomeres by means of hTERT expression reverses the premature senescence of S6KD cells, whereas augmenting BER activity, by expression of the DNA polymerase-β (Pol-β)-dRP lyase domain, does not. hTERT, Pol-β or empty vector were ectopically expressed in S6KD WI-38 cells and passaged in physiological (2%) oxygen conditions. Cells were stained with SA-β-gal at population doubling 36.5. Error bars indicate s.e.m.; $n = 8$ (pSR); $n = 16$ ($S6KD_1$); $n = 20$ ($S6KD_2$)

might function in a similar context. To investigate this possibility, we first examined whether SIRT6 associates with telomeres during S phase by telomere chromatin immunoprecipitation (T-ChIP)[18]. Cell synchronization, release, and analysis by bromodeoxyuridine/propidium iodide staining were performed to enrich for specific cell-cycle phases (Supplementary Fig. 8). T-ChIP analysis at different time points after release from cell synchronization revealed that SIRT6, like WRN, preferentially associates with telomeric chromatin in S-phase-enriched cultures (Supplementary Fig. 9). SIRT6 occupancy at telomeric chromatin was observed for both recombinant Flag-tagged SIRT6 (Fig. 2a, b) and endogenous SIRT6 (Fig. 2c, d), and in both U2OS osteosarcoma cells (Fig. 2b, c) and primary IMR90 cells (Fig. 2d). As controls, the association of Alu repeat sequences with SIRT6 ChIPs was not above background (Fig. 2b–d), and the SIRT6 T-ChIP signal was abolished in S6KD cells, validating the specificity of the signal (Fig. 2d). Together, these data locate SIRT6 at telomeric chromatin in S phase and suggest a potential role for SIRT6 in regulating replication-associated dynamics in telomere structure.

Chromatin at telomeres is enriched for hypoacetylated histone tails[19]. Although no physiological enzymatic activity for SIRT6 on histones or other *trans* substrate has yet been observed, we proposed that SIRT6 might regulate chromatin at telomeres by deacetylating a specific histone tail residue. We therefore used mass spectrometry to screen for NAD-dependent SIRT6 deacetylase activity *in vitro*, on a collection of acetylated histone tail peptides. SIRT6 manifested modest deacetylation activity on peptides containing acetylated H3K9 (H3K9Ac) (Fig. 3a and Supplementary Fig. 10). This activity was highly specific for H3K9Ac, because no deacetylation was detected for 12 other acetylated histone peptides (Fig. 3a and Supplementary Fig. 11). SIRT6 also deacetylated H3K9Ac, but not several other acetylated residues, in the context of purified full-length histone H3, and mutation of a conserved catalytic residue (H133Y) of SIRT6 markedly decreased this activity (Fig. 3b and data not shown). Finally, SIRT6 efficiently and specifically deacetylated H3K9Ac (but not other acetylated histone residues) in 293T cells, whereas the

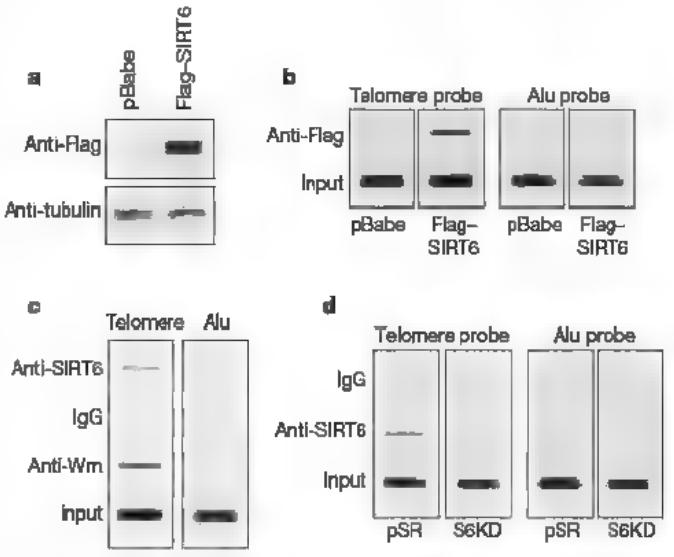

Figure 2 | SIRT6 associates with telomeric chromatin. **a**, Western analysis of U2OS cells transduced with pBabe-Flag-SIRT6 or empty virus (pBabe) control **b**, T-ChIP analysis with anti-Flag antibodies from the cells shown in **a** **c**, T-ChIP assays in U2OS cells with antibodies specific for SIRT6, WRN or IgG negative control. **d**, T-ChIP assays with SIRT6 antibodies in S6KD cells or in control pSR IMR90 cells. In **b**–**d**, slot-blots are shown of telomere or Alu repeat sequences in ChIP and input DNA. Input loaded represents 5% (**b**, **c**) or 2.5% (**d**) of total.

mutant SIRT6 protein did not (Fig. 3c and Supplementary Fig. 12). Together, these observations indicate that SIRT6 is an NAD-dependent deacetylase with specificity for H3K9Ac.

We next sought to identify the physiological context in which SIRT6 deacetylates H3K9Ac. Western analysis of S6KD and control cells did not reveal significant differences in global H3K9Ac levels (data not shown). In contrast, investigation of histone acetylation status at telomeres in S-phase-enriched cultures by T-ChIP revealed H3K9 hyperacetylation in S6KD cells (Fig. 3d–f). SIRT6 is therefore required for the maintenance of the low physiological levels of H3K9 acetylation at telomeric chromatin in S phase, and hyperacetylation of H3K9 in the absence of SIRT6 correlates with telomere dysfunction. H3K9 was also hyperacetylated at telomeric chromatin in S6KO mouse cells, providing *in vivo* evidence for a physiological role for SIRT6 in deacetylating this histone residue (Supplementary Fig. 13a–c).

We next proposed that in SIRT6-deficient cells, hyperacetylation of H3K9 at telomeres in S phase might interfere with the association of WRN. WRN occupancy at telomeres was compared in S-phase-enriched S6KD and control cultures by T-ChIP analysis. In both U2OS and IMR90 cells, *SIRT6* knockdown significantly inhibited the association of WRN with telomeric chromatin (Fig. 4a, b, and data not shown). We conclude that SIRT6 is required for stabilization of WRN at telomeric chromatin. We note that additional functional or physical interactions between SIRT6 and WRN might exist. However, the association of SIRT6 with telomeres was independent of WRN (Supplementary Fig. 13e), and we have not observed a direct interaction between SIRT6 and WRN at chromatin (data not shown). Thus, our data are consistent with the hypothesis that SIRT6 deacetylation of H3K9Ac at telomeric chromatin leads to an altered chromatin state that is required for efficient WRN association in S phase.

WS cells exhibit specific defects that reflect problems with the replication-associated processing and metabolism of telomeres, and analysis of S6KD cells revealed similar abnormalities. First, S6KD metaphases showed elevated levels of missing telomere signals (sister telomere loss) and extra telomere signals (telomere doublets) (Fig. 4d–f), defects observed in WS cells and associated with aberrant telomere processing during replication[8,13,20]. In addition, chromosome fusions in S6KD cells, as in WRN-defective cells[14,15], have weak or no telomere signals at the fusion sites (Fig. 4c). In WS cells this phenotype is proposed to result from stochastic replication-associated telomere loss[5,15], and it contrasts with the strong telomere signals observed at sites of chromosome fusions resulting from deficiency for telomere end-capping factors such as telomeric repeat binding factor 2 (TRF2)[11]. Aberrant replication-associated telomere processing by WRN is proposed to contribute to a delayed completion of S phase observed in WS cells[13,14,21,22]. Similarly, *SIRT6* knockdown in U2OS cells resulted in delayed completion of S phase (Supplementary Fig. 14), which is consistent with a role for SIRT6 in modulating telomeres during replication. Together, these findings suggest that SIRT6 collaborates with WRN at telomeric chromatin to ensure efficient telomere replication and to prevent the accrual of structural abnormalities at telomeres.

Telomeres are specialized structures that function to shield linear chromosome ends from DNA repair, degradation and fusion[7]. Mammalian telomeres are packaged in an unusual chromatin structure with features of heterochromatin[23,24], but relatively little is understood about the role of chromatin modifications on telomere metabolism. In this study we show that human SIRT6 deacetylates H3K9Ac at telomeres to prevent telomere dysfunction. Inactivation of SIRT6 leads to H3K9 hyperacetylation at telomeric chromatin in both human and mouse cells, but the mouse cells do not display the downstream cellular defects observed in human cells, which is consistent with the large functional reserve of mouse telomeres (Supplementary Fig. 13d; data not shown)[14,25]. Our findings regarding SIRT6 provide a direct link between mammalian telomere dysfunction and a histone modifying enzymatic activity. Our results indicate that deacetylation of H3K9Ac by SIRT6 is important during S phase at replicating telomeres. We propose a model (Supplementary Fig. 1) in which the deacetylation of H3K9Ac by SIRT6 promotes the formation of a specialized telomeric chromatin state that is required for the stable association of S-phase-dependent telomere-processing factors such as WRN, to prevent aberrant sequence loss or metabolism of telomeres. The resulting telomere dysfunction then

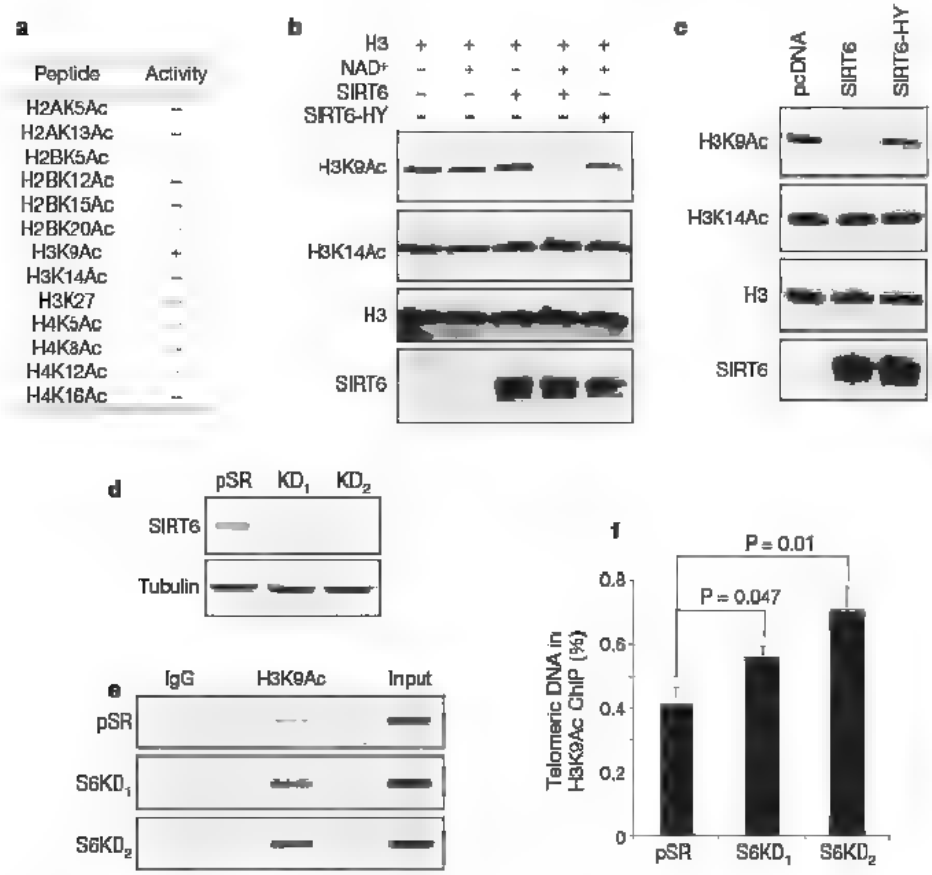

Figure 3 | SIRT6 deacetylates lysine 9 of histone H3 at telomeric chromatin. **a**, Summary of *in vitro* deacetylation assays on acetylated histone tail peptides, analysed by mass spectrometry. **b**, Western analysis showing SIRT6 deacetylation of H3K9 on full-length histone H3 *in vitro*. Reactions with NAD^+, SIRT6 or the catalytic H133Y SIRT6 mutant protein (SIRT6-HY) are indicated. **c**, SIRT6 deacetylates H3K9 in cells. Western analysis of 293T cells overexpressing SIRT6, SIRT6-HY or empty vector. **d**, Western analysis of *SIRT6* knockdown in U2OS cells used for T-ChIP in **e** and **f**. **e**, T-ChIP analysis showing hyperacetylation of H3K9 at telomeric chromatin in S6KD U2OS cells. **f**, Quantification of multiple independent T-ChIP experiments as shown in **e**. Values represent the T-ChIP signal normalized to input signal, and subtracted for background signal in an IgG control. Error bars indicate s.e.m.; $n = 4$. P values were determined by two-tailed Student's t-test.

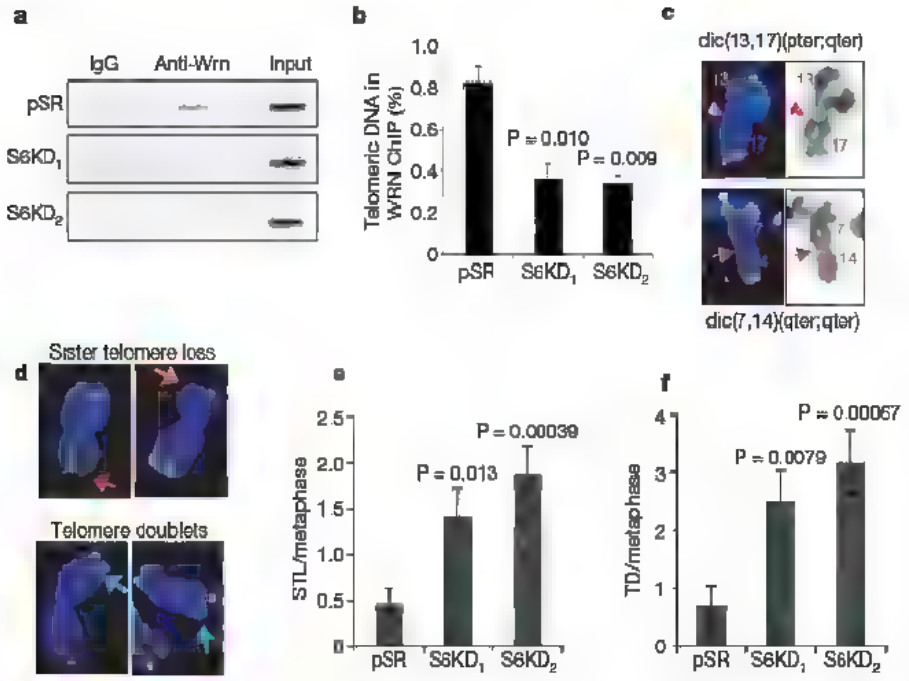

Figure 4 | SIRT6 stabilizes WRN at telomeric chromatin and prevents replication-associated telomere defects. **a**, **b**, T-ChIP experiments showing reduced association of WRN with telomeric chromatin in *SIRT6* knockdown cells. **a**, Representative T-ChIP analysis of WRN occupancy in S6KD and control cells. **b**, Quantification of three independent experiments as shown in **a**. **c**, Representative chromosome end-to-end fusions observed in S6KD cells. Telomere FISH signals are yellow, and DAPI-stained chromosomes are blue. Weak or no telomere signals are detected at the sites of fusion (arrows). dic(13;17)(pter;qter) and dic(7,14)(qter;qter) indicate dicentric chromosomal fusions between the p and q arms of chromosomes 13 and 17, and the q arms of chromosomes 7 and 14, respectively. **d**, Representative S6KD metaphases showing aberrant telomere signals. Red arrows, sister telomere loss; blue arrows, telomere doublets. **e**, **f**, Quantification of sister telomere loss (**e**) and telomere doublets (**f**) in S6KD cells and in pSR control cells. pSR, $n = 15$; $S6KD_1$ and $S6KD_2$, $n = 22$. Error bars in **b**, **e** and **f** indicate the s.e.m., and *P* values were determined by two-tailed Student's *t*-test.

contributes to premature cellular senescence. Our study has identified a crucial function for SIRT6 in chromatin regulation at mammalian telomeres and provides a new mechanism by which the regulation of chromatin is linked to telomere function, cellular senescence and, potentially, organismal ageing.

METHODS SUMMARY

Telomere-ChIP assay. S-phase T-ChIP analysis was performed essentially as described previously[15]. In brief, ChIPs were performed by following the Diagenode protocol (http://www.diagenode.com). DNA eluted from the ChIPs was transferred to slot-blots, and telomeric DNA was detected with the TeloTAGGG telomere length assay kit (Roche Applied Science).

Immunofluorescence *in situ* hybridization TIF assays. Immunofluorescence *in situ* hybridization (immuno-FISH) analysis of TIFs was performed as described previously[26,27]. Cells were fixed with paraformaldehyde, washed, and permeabilized in 100% ethanol or 0.2% Triton X-100. After being blocked and immunostained, cells were treated with 1 mg ml^{-1} dithiobis(succinimidylpropionate), and telomere FISH was performed with the Telomere PNA FISH Kit/fluorescein isothiocyanate (Dako). Laser-scanning confocal microscopy was performed with a Nikon PCM 2000 confocal microscope scanning system.

Cytogenetic chromosome analysis. Metaphase spreads were prepared using standard techniques as previously described[28], and stained with 4,6-diamidino-2-phenylindole (DAPI). Detailed procedures of the spectral karyotype (SKY) analysis, including the preparation of SKY probes, slide denaturation, probe hybridization, detection and image acquisition, are described at http://www.nedlab.nci.nih.gov/protocols and in the Supplementary Information. Detection of telomere sequences by telomere FISH was performed with a Telomere PNA FISH Kit/Cy3 (Dako). Acquisition of metaphase spreads with telomere signals and the companion DAPI images for each sample were analysed with Q-Fluoro software (Leica Imaging Systems).

Full Methods and any associated references are available in the online version of the paper at www.nature.com/nature.

Received 3 December 2007; accepted 23 January 2008.
Published online 12 March 2008.

1. Landry, J. *et al.* The silencing protein SIR2 and its homologs are NAD-dependent protein deacetylases. *Proc. Natl Acad. Sci. USA* 97, 5807–5811 (2000).
2. Imai, S., Armstrong, C. M., Kaeberlein, M. & Guarente, L. Transcriptional silencing and longevity protein Sir2 is an NAD-dependent histone deacetylase. *Nature* 403, 795–800 (2000).
3. Mostoslavsky, R. *et al.* Genomic instability and aging-like phenotype in the absence of mammalian SIRT6. *Cell* 124, 315–329 (2006).
4. Cheng, W. H., Muftuoglu, M. & Bohr, V. A. Werner syndrome protein: Functions in the response to DNA damage and replication stress in S-phase. *Exp. Gerontol.* 42, 871–878 (2007).
5. Multani, A. S. & Chang, S. WRN at telomeres: implications for aging and cancer. *J. Cell Sci.* 120, 713–721 (2007).
6. Campisi, J. Senescent cells, tumor suppression, and organismal aging: good citizens, bad neighbors. *Cell* 120, 513–522 (2005).
7. Verdun, R. E. & Karlseder, J. Replication and protection of telomeres. *Nature* 447, 924–931 (2007).
8. van Overbeek, M. & de Lange, T. Apollo, an Artemis-related nuclease, interacts with TRF2 and protects human telomeres in S phase. *Curr. Biol.* 16, 1295–1302 (2006).
9. Takai, H., Smogorzewska, A. & de Lange, T. DNA damage foci at dysfunctional telomeres. *Curr. Biol.* 13, 1549–1556 (2003).
10. d'Adda di Fagagna, F. *et al.* A DNA damage checkpoint response in telomere-initiated senescence. *Nature* 426, 194–198 (2003).
11. van Steensel, B., Smogorzewska, A. & de Lange, T. TRF2 protects human telomeres from end-to-end fusions. *Cell* 92, 401–413 (1998).
12. Sherr, C. J. & DePinho, R. A. Cellular senescence: mitotic clock or culture shock? *Cell* 102, 407–410 (2000).
13. Crabbe, L., Verdun, R. E., Haggblom, C. I. & Karlseder, J. Defective telomere lagging strand synthesis in cells lacking WRN helicase activity. *Science* 306, 1951–1953 (2004).
14. Laud, P. R. *et al.* Elevated telomere–telomere recombination in WRN-deficient, telomere dysfunctional cells promotes escape from senescence and engagement of the ALT pathway. *Genes Dev.* 19, 2560–2570 (2005).
15. Crabbe, L., Jauch, A., Naeger, C. M., Holtgreve-Grez, H. & Karlseder, J. Telomere dysfunction as a cause of genomic instability in Werner syndrome. *Proc. Natl Acad. Sci. USA* 104, 2205–2210 (2007).
16. Wyllie, F. S. *et al.* Telomerase prevents the accelerated cell ageing of Werner syndrome fibroblasts. *Nature Genet.* 24, 16–17 (2000).
17. Opresko, P. L. *et al.* The Werner syndrome helicase and exonuclease cooperate to resolve telomeric D loops in a manner regulated by TRF1 and TRF2. *Mol. Cell* 14, 763–774 (2004).
18. Loayza, D. & De Lange, T. POT1 as a terminal transducer of TRF1 telomere length control. *Nature* 423, 1013–1018 (2003).
19. Benetti, R., Garcia-Cao, M. & Blasco, M. A. Telomere length regulates the epigenetic status of mammalian telomeres and subtelomeres. *Nature Genet.* 39, 243–250 (2007).
20. Ariyoshi, K., Suzuki, K., Goto, M., Watanabe, M. & Kodama, S. Increased chromosome instability and accumulation of DNA double-strand breaks in Werner syndrome cells. *J. Radiat. Res. (Tokyo)* 48, 219–231 (2007).
21. Takeuchi, F., Hanaoka, F., Goto, M., Yamada, M. & Miyamoto, T. Prolongation of S phase and whole cell cycle in Werner's syndrome fibroblasts. *Exp. Gerontol.* 17, 473–480 (1982).
22. Pool, M., Hoehn, H., Runger, T. M. & Martin, G. M. Impaired S-phase transit of Werner syndrome cells expressed in lymphoblastoid cell lines. *Exp. Cell Res.* 202, 267–273 (1992).
23. Tommerup, H., Dousmanis, A. & de Lange, T. Unusual chromatin in human telomeres. *Mol. Cell. Biol.* 14, 5777–5785 (1994).
24. Blasco, M. A. The epigenetic regulation of mammalian telomeres. *Nature Rev. Genet.* 8, 299–309 (2007).
25. Chang, S. *et al.* Essential role of limiting telomeres in the pathogenesis of Werner syndrome. *Nature Genet.* 36, 877–882 (2004).

26. Herbig, U., Jobling, W. A., Chen, B. P., Chen, D. J. & Sedivy, J. M. Telomere shortening triggers senescence of human cells through a pathway involving ATM, p53, and $p21^{CIP1}$, but not $p16^{INK4a}$. *Mol. Cell* 14, 501–513 (2004).
27. Dimitrova, N. & de Lange, T. MDC1 accelerates nonhomologous end-joining of dysfunctional telomeres. *Genes Dev.* 20, 3238–3243 (2006).
28. Padilla-Nash, H. M. *et al.* Jumping translocations are common in solid tumor cell lines and result in recurrent fusions of whole chromosome arms. *Genes Chromosom. Cancer* 30, 349–363 (2001).

Supplementary Information is linked to the online version of the paper at www.nature.com/nature.

Acknowledgements We thank S. Artandi, J. Karlseder, B. North, E. Verdin, J. Lipsick, H. Wen, L. Christensen and Chua and Gozani laboratory members for reagents, technical assistance and/or advice; and Regeneron Pharmaceuticals for SIRT6 knockout mice. This work was supported by grants from the National Institutes of Health (NIH) (to K.F.C., O.G., H.Y.C., R.A.M. and T.L.A.K.), the American Federation for Aging Research/Paul Beeson Scholar Award and the Department of Veterans Affairs Merit Review (to K.F.C.) and the Burroughs Wellcome Fund and Searle Scholar Award (to O.G.), and by funds from the Intramural Research Program of the NIH, the National Cancer Institute, the Center for Cancer Research and the National Institutes on Aging.

Author Contributions E.M. and R.A.M. contributed independently to this work. E.M. discovered and analysed the cellular senescence, telomere dysfunction, and S-phase defects in S6KD cells, association of SIRT6 with telomeric chromatin, and the effects of SIRT6 on H3K9Ac and WRN levels at telomeres. R.A.M. and O.G. contributed to the identification of H3K9Ac as a SIRT6 substrate. H.P.-N. and T.R. contributed to cytogenetic analysis of chromosomal fusions. F.B., M.D., M.K., P.C., R.K., V.B., J.C.B., T.L.A.K. and H.C. provided experimental assistance and reagents. E.M. and K.F.C. prepared the manuscript.

Author Information Reprints and permissions information is available at www.nature.com/reprints. Correspondence and requests for materials should be addressed to K.F.C. (kfchua@stanford.edu).

naturejobs

By the year 2030, the United States should transform 'health maintenance organizations' into 'healthy living organizations'. Biomedical centres should have a 'school of health' that every aspiring medical and biomedical professional is required to attend. By 2030, a 'national wellness strategy' should be established, backed by congressional mandate and public–private efforts.

This was blue-sky thinking from a group of esteemed health-policy leaders at a forum in Washington DC on 19 March. The first suggestion was from Elias Zerhouni, director of the National Institutes of Health; the second from Julie Gerberding, director of the Centers for Disease Control and Prevention (CDC); and the last from William Novelli, chief executive of the American Association of Retired Persons. Asked to elaborate on how to revamp health care, they and others emphasized the essential role of prevention in combating disease and reducing monumental health-care costs. It is a theme underscored in this week's feature which details the global opportunities in the lively area of vaccine research (see page 498).

Assuming that these US health-policy leaders are prescient, what might this suggest for the budding researcher? Take a hard look at professions related to wellness and prevention — along with vaccines, research into social and biological risk factors biomarkers, as well as professions related to health information technology public health and economic and racial health disparities. They are likely to garner the most attention in coming years.

Unfortunately, there is some reason to believe that others in the US government are not so visionary. A striking disconnect remains between what the experts say and what the policy-makers do. Investments in preventative measures should mean a reduction in health-care costs in the long term. Yet, in the president's budget request for fiscal year 2009, the CDC would see a $433 million, or 7%, budget reduction (see *Nature* **451**, 610–612; 2008). Such an approach seems short-sighted and sends the wrong signal to health professionals looking to bolster efforts to replace a pound of cure with an ounce of prevention.

Gene Russo is editor of *Naturejobs*.

CONTACTS
Editor: Gene Russo

US Head Office
New York
75 Varick Street, 9th Floor
New York, New York 10013-1917
Tel: +1 800 989 7718
Fax: +1 800 989 7103
e-mail: naturejobs@natureny.com

US Sales Manager/Corporations:
Peter Bless
Tel: +1 800 989 7718

San Francisco Office
Classified Sales Representative:
Michaela Bjorkman
West USA/West Corp. Canada
225 Bush Street, Suite 1453
San Francisco,
California 94104
Tel: +1 415 781 3803
Fax: +1 415 781 3805
e-mail: m.bjorkman@nature.com

India
Vikas Chawla
Tel: +91 124 2881057
e-mail: v.chawla@nature.com

European Head Office, London
The Macmillan Building,
4 Crinan Street,
London N1 9XW, UK
Tel: +44 (0) 20 7843 4961
Fax: +44 (0) 20 7843 4996
e-mail: naturejobs@nature.com

European Sales Manager:
Andy Douglas (4975)
Advertising Production Manager:
Stephen Russell
To send materials use London address above.
Tel: +44 (0) 20 7843 4816
Fax: +44 (0) 20 7843 4996
e-mail: naturejobs@nature.com
***Naturejobs* web development:** Tom Hancock
***Naturejobs* online production:** Dennis Chu

Japan Head Office, Tokyo
Chiyoda Building, 2–37
Ichigayatamachi,
Shinjuku-ku, Tokyo 162-0843
Tel: +81 3 3267 8751
Fax: +81 3 3267 8746

Asia-Pacific Sales Manager:
Ayako Watanabe
Tel: +81-3-3267-8765
e-mail: a.watanabe@natureasia.com
Business Development Manager, Greater China/Singapore:
Gloria To
Tel: +852 2811 7191
e-mail: g.to@natureasia.com

JOBS OF THE WEEK

Clinical Immunologist
Joslin Diabetes Center
Boston, MA (USA)
Turn to page 3

Programme Leader Track Appointments
MRC NIMR
London (UK)
Turn to page 2

Full/tenured professorship (W3) in Animal Ecology (Zoology III)
Theodor-Boveri-Institut for Biosciences, University of Würzburg
Würzburg (Germany)
Turn to page 13

Early Career Scientists
HHMI
Chevy Chase, MD (USA)
Turn to page 20

Appointments to the Research Councils
DIUS
Various locations (UK)
Turn to page 8

THE ART OF SELF-DEFENCE

Vaccines are no longer 'worthy but dull'. A heady mix of funding and breakthroughs is bringing this once-quiet area to life, says **Virginia Gewin.**

For a long time, vaccine development was not seen as a terribly exciting or dynamic discipline. The strategy within the field had stayed the same for years: to weaken or inactivate the target microorganism. As such, it seemed to offer little to entice researchers from cutting-edge areas such as stem-cell biology or RNA interference.

Now, all that seems to be changing. A sudden surge in progress during the past decade has created what many people are calling a renaissance in vaccine development. Technological advances have transformed immunology, virology, structural biology and genomics. Global health is high on the world's agenda. And vaccine development has the backing of an extremely wealthy patron, the Bill & Melinda Gates Foundation, which spent US$287 million on AIDS-vaccine research alone in 2006. Researchers in different diseases, once isolated from each other, are increasingly coordinating their efforts and sharing ideas on more strategic vaccine design.

"The vaccine field may be overlooked and under-appreciated, but the opportunities are every bit as exciting as in other areas of science, if not more so," says Gary Nabel, director of the US National Institutes of Health's Vaccine Research Center in Bethesda, Maryland. Perhaps more importantly for scientists early in their careers, there is ample potential for ground-breaking research.

The number of research and training opportunities is growing to meet the demand for scientists who understand the challenges of bringing a vaccine to market — not the least of which is a timeline that is much longer than that for publishing a paper. Vaccines are now poised to have an impact not only on infectious diseases in the developing world, but also on chronic conditions such as addiction or obesity that are plaguing the developed world. Industry, academia and non-profit organizations are recruiting for all facets of basic, translational and clinical work.

This renewed attention is partly due to the economic boost vaccines have given the drug industry. Although it represents only 2% of overall business, the vaccines sector has outperformed most of the rest of the industry in revenue growth (J. W. Almond *Nature Rev. Microbiol.* 5, 478–481; 2007). Vaccines are expected to be among the next blockbuster biotechnology products.

The value of vaccines

Merck and Novartis are leading the pack. "There is a growing recognition of the value of vaccines within the industry," says Keith Gottesdiener, vice-president for vaccine and infectious-disease clinical research at Merck Research Laboratories in Rahway, New Jersey. In the past two years, Merck has registered four new vaccines. Three of those protect against diseases for which there was no vaccine — RotaTeq against the stomach infection rotavirus, Zostavax against shingles and Gardasil against the human papilloma virus. More are in development, requiring more recruits to do research.

Rino Rappuoli, global head of vaccines research at Novartis Vaccines in Sienna, Italy, says he often recruits postdocs from outside the field on the understanding that he will train them. In the past, there have been few academic opportunities to learn about this complex field, which differs markedly from biotechnology or drug development. "Making vaccines is complicated because each one is very different," he says.

Smaller companies and start-ups are also expanding. With three vaccines on the market and dozens in its pipeline, MedImmune, a biotech company (and AstraZeneca subsidiary) in Gaithersburg, Maryland, is recruiting scientists who have a keen interest in both vaccine development and the study of immune-system responses. It needs people with strong molecular-biology skills, experience with infectious diseases and knowledge of immune status and host response.

Rino Rappuoli would like to see more biotech start-ups.

NOVARTIS COMMUNICATIONS, ITALY

A. CABALLERO-REYNOLDS/GETTY

Increased attention on global health, including the grants from the Gates Foundation, has allowed small vaccine companies to finance early-stage projects. It is a welcome change, says Hans Arwidsson, chief executive of Eurocine, a start-up formed at Stockholm's Karolinska Institute in Sweden. Arwidsson says that funding from the Gates Foundation's high-profile efforts raised awareness and made it easier for his company to garner funds from other sources. Eurocine's highest priority, a nasal influenza vaccine, will enter into combined phase I and II trials later this year.

Even the failure to develop the highest profile vaccine of all — one for HIV — has so far not weakened industry's interest. For instance, although Merck's HIV vaccine trial, dubbed STEP, failed in November 2007, Gottesdiener says the company's commitment to HIV remains unchanged. "Merck is still struggling to understand the ramifications of the STEP trial," he says, "but we're not giving up on our plans to continue working in the HIV area. Whether that will be in vaccines or other areas is under consideration."

Still, the immunology expertise gained by working on HIV could yet benefit drug companies. According to Gottesdiener, other vaccine-development skills in demand at Merck include protein chemistry and recombinant protein manufacturing. Merck also seeks epidemiologists, clinical scientists and regulatory scientists. "As the value of vaccines becomes clearer, Merck will invest in long-term projects," he says.

New blood needed

Rappuoli would like to see more start-up biotech firms working on basic vaccine research, as new ideas and technologies are crucial for development. "There is a small group of players in the vaccine arena that all know each other," he says. New ways to characterize immune responses to various pathogens are particularly in demand. Yves Levy, scientific director of ANRS, the Paris-based French national agency for research on AIDS and viral hepatitis, advises interested young scientists to address questions in basic immunology. Focusing on new mechanisms, such as how to put new antigens into vaccines, will provide an understanding of basic immunology and important correlates of vaccine development, he says.

> "The vaccine field may be underappreciated, but the opportunities are every bit as exciting as in other areas of science, if not more so."
> — Gary Nabel

Other hot topics include developing new adjuvants — compounds, molecules or other agents that enhance a vaccine's effectiveness. "Adjuvants today are basically the intersection between immunology and vaccinology," says Rappuoli. They can be designed with chemical and physical properties that enhance a specific action or bind to a known receptor. Traditionally, adjuvants have been identified as a result of trial and error during vaccine development. "We're just at the beginning of a beautiful evolution of what the science of adjuvants of vaccines will be in the future," says Rappuoli. Another active area is the study of how infectious organisms can alter surface proteins to avoid a host immune response, an area dubbed 'antigenic variation'. This often derails efforts to develop vaccines for viruses such as influenza and West Nile virus, which keep an advantage by mutating rapidly.

Hildegund Ertl, director of the Wistar Institute Vaccine Center in Philadelphia, Pennsylvania, notes an influx of people trained in gene therapy into the better-funded vaccine arena, bringing valuable molecular biology skills with them. With such synergies in place, the applications of vaccinology are growing. Ertl hopes to tackle conditions such as obesity and addiction. "Vaccines are going from immediate life savers to long-term quality-of-life insurance," says Rappuoli.

Careers found in translation

Bertus Rima, a virologist at Queen's University in Belfast, Northern Ireland, says that the scientific questions asked by academia and industry are not that different. It is the space between basic academic research and the market — the validation of promising vaccine candidates able to move into clinical trials — that is often overlooked. Increasingly, collaborations of academic and non-profit organizations are funding this translational research, and offering interesting clinical research and training opportunities as a result.

A notorious lack of collaboration in the European vaccine arena stymied development in the past, but the major players are now working together. The ANRS, for example, has collaborations on multiple fronts. Working with the French national biomedical research agency INSERM, the Pasteur Institute in Paris and the Baylor Institute in Dallas, Texas, the ANRS has funding for basic research as well as for clinical-trial postdocs to develop and test new candidate vaccines in France and the United States. As part of EuroVac, the HIV-vaccine project funded by the European Union (EU), the ANRS is conducting a phase II trial of a candidate. It is also working with the Canadian Network for Vaccines and Immunotherapeutics on monitoring facilities to study how to modulate immune responses.

Through the European and Developing Countries Clinical Trials Partnership, the EU is also helping to develop the capacity of African countries to undertake their own research and clinical trials. Britain's Medical Research Council, one of the 18 EU partners, will work on projects involving all of vaccine research — from the development of animal models of disease to the identification of immune biomarkers to verify efficacy. In addition, the council recently launched funding schemes for translational medicine and increased the number of clinical-training research fellowships to help medical doctors gain PhD training.

The translational hubs are often the non-profit

Giuseppe Pantaleo: non-profit opportunities.

research institutes. The newly created Swiss Institute for Vaccine Research will coordinate immunology research and clinical trials to tackle HIV/AIDS, tuberculosis, malaria and cancer immunology with its four academic and hospital partners in Lausanne and Bellinzona, says its chairman, Giuseppe Pantaleo. The institute is recruiting 15–20 people, in two or more groups, whose principal investigators will receive a four-year package to build their own programmes. Although the institute will not have a PhD programme, there will be training opportunities for students at the partner institutions.

Seattle, home of the Gates Foundation, also houses several non-profit organizations. The Infectious Disease Research Institute is breaking new ground with its work on adjuvants for tuberculosis, malaria, leishmaniasis and HIV. "Clinical research on new adjuvants has never been done outside drug or biotech companies," says founder Steven Reed. With Gates funding, the institute is hiring in several areas, including tuberculosis experts, chief of operations and adjuvant specialists. Having worked for a biotech company, Reed says it can be difficult to compete with industry for scientists, but Seattle has a good regional pool of candidates (see *Nature* **447**, 502–503; 2007).

Non-profit research institutes not only have the ability to fill vaccine-development research niches, but have a responsibility to do so, says Larry Corey, head of the infectious-disease programme at the Fred Hutchinson Cancer Research Center, also in Seattle. Vaccines for global health — the most cost-effective strategy for infectious diseases and cancer — will be an important part of biology in the next two decades, he says.

Strength in partnership

Like many research institutes, the Hutchinson centre has an academic partner, in this case the University of Washington, offering cutting-edge training and research at the new Vaccine Center in the Department of Global Health. The new Wistar vaccine centre in Philadelphia offers training opportunities with the University of Pennsylvania. The Wistar Institute has a graduate-training grant geared towards vaccine development and is seeking assistant professors and postdocs. It uses its relationship with nearby GlaxoSmithKline and Merck to offer training in applied vaccinology, focusing on industrial-scale manufacturing concerns such as technology licensing.

Although vaccine centres are popping up at universities throughout the United States, not all will make an impact.

Ronald Montelaro: qualified candidates are hard to find.

UNIVERSITY OF PITTSBURG

"It's survival of the fittest, so to speak," says Ronald Montelaro, associate director of the University of Pittsburgh's Center for Vaccine Research. Programmes with the most comprehensive research approach will stand the test of time, he says. His centre is putting together a programme strong in what Montelaro calls 'horizontal expertise' (specializing in vaccinology across different pathogens), with vertical expertise (focusing on a specific pathogen). With positions still available in both arenas, Montelaro admits it's difficult to find the qualified candidates, given the tight funding from the National Institutes of Health. "Postdocs are opting for government or industry where they don't have to fight the grant situation," he says.

Innovation and tradition

Other initiatives rely on their interdisciplinary collaborations. For example, the Oregon Health and Sciences University, which has a vaccine and gene-therapy institute in Portland, is to build another one in St Lucie, Florida, bringing together immunologists, virologists, cell biologists, computational mathematicians and immunogeneticists to work on problems associated with the host–pathogen response. The Portland centre has done a lot of work in primates; the St Lucie branch will focus on applying primate work to humans.

Although the growing number of university-based vaccine centres offers new and tempting training options, traditional immunology programmes continue to offer the strong core background necessary for vaccine research. Matthew Fenton, chief of the asthma, allergy and inflammation branch of the US National Institute of Allergy and Infectious Diseases, says existing immunology programmes can train a larger percentage of vaccine researchers. "Immunologists can plug two holes — they understand innate immunity as well as how to use immune responses to design better adjuvants," he says.

But even immunology programmes are reinventing themselves. Queen's University in Belfast has a new one focused primarily on cell signalling and virology, in which vaccinology plays a major part. It has about 10 postdoctoral positions open. Bertus Rima says the programme reflects the current UK interest in translational aspects of medicine in general — where virology is focused more on questions of vaccinology and pathogenesis instead of basic virology.

Even as the number of vaccine-related research opportunities and collaborations grows, global programmes are increasingly interconnected, says Yves Levy. "Young scientists should know that at the international level, we are all speaking together to develop new paradigms, concepts and vaccines," he says. Vaccine-research collaborations offer instant connections to high level scientists in different laboratories and across borders.

For Gary Nabel, the real career achievement is the satisfaction of having an impact on global health. Not many fields, he says, offer the potential to affect millions, if not billions, of people's lives. ■

Virginia Gewin is a freelance science writer based in Portland, Oregon.

OHSU

Many hands: collaborations are the way forward in a growing number of vaccine centres.

The Swedish University of Agricultural Sciences (SLU)

Faculty of Veterinary Medicine and Animal Science

PROFESSOR IN VETERINARY IMMUNOLOGY

at the Department of Biomedical Sciences and Veterinary Public Health

The Faculty of Veterinary Medicine and Animal Science at SLU conducts research and education to promote the health and well-being of animals as well as humans, and to develop biologically and economically sustainable animal management. The faculty's research comprises basic biomedical sciences, animal management, -health and -welfare, veterinary medicine, veterinary public health and the influence of animals for the health and well-being of humans. We are now seeking a dynamic, creative leader and outstanding investigator to play a central role in the development of our Faculty. The successfu candidate with established network will be expected to build an extramurally funded research program and to have a genuine interest in teaching issues.

Subject description: The subject comprises veterinary immunology with special reference to infection diseases in domestic animals.

Duties: Overall responsibility for research and teaching within the subject. Main duties include research, education at doctorate level and teaching within the department's comprehensive teaching task at bachelor and master levels. Collaboration with other disciplines within the SLU regarding immune system functions. Furthermore the remit includes administrative tasks and assignments within the department and the faculty.

Application should be submitted to the Registrar of SLU no later than **12 May 2008.**

Complete notice of the position can be found on

http://personal.slu.se/jobb

W128384R

DIVISIONS OF IMMUNE CELL BIOLOGY AND MOLECULAR IMMUNOLOGY AND IMMUNOREGULATION

MRC National Institute for Medical Research

PROGRAMME LEADER TRACK APPOINTMENTS

Applications are invited for three Programme Leader Track positions on the Institute's Scientific Staff to lead three new independent research groups.

- **Division of Immune Cell Biology: Reference NIMR08/137**
  Candidates who wish to study signaling in immune cells, especially using imaging, biophysical, or biochemical approaches
- **Division of Molecular Immunology: Reference NIMR08/138**
  Candidates who have experience in cellular and molecular immunology and wish to investigate the consequences of exposure to infectious organisms on the immune system
- **Division of Immunoregulation: Reference NIMR08/172**
  Candidates who have experience in cellular and molecular immunology and a strong interest in researching the immune response to respiratory viral infections

Candidates should have an internationally strong track record of independent research, and an ability to lead a research team, pursuing original approaches to long term research goals in immunology. The research programme will be supported by the Medical Research Council.

NIMR is the largest MRC institute, supporting some 70 research groups and 500 bench scientists and offers an outstanding range of facilities and expertise in molecular, cellular and physiological sciences, (http://www.nimr.mrc.ac.uk/) providing multiple opportunities for collaborative studies.

Appointment will be made at either Programme Leader or Programme Leader Track depending on experience and achievements. Further information about NIMR08/137 is available from **Victor Tybulewicz** (vtybule@nimr.mrc.ac.uk), NIMR08/138 from **Dimitris Kioussis** (dkiouss@nimr.mrc.ac.uk) and about NIMR08/172 from **Anne O'Garra** (aogarra@nimr.mrc.ac.uk)

Successful Programme Leader Track candidates will be considered for appointment to full Programme Leader status, normally after six years. Salary will be commensurate with the seniority and experience of the successful candidate and will be at the appropriate level on the Council's pay structure. MRC final salary Pension Scheme is available. Assistance with relocation expenses is also available.

Applications for this role should now be made online at http://jobs.mrc.ac.uk. Please upload a full CV, a brief statement of research accomplishments and of proposed future research and the names and addresses of three referees.

If you do not have internet access or you experience technical difficulties please call + 44 (0)1793 301157 **quoting the appropriate reference.**

Closing date: 30 May 2008

The MRC is an Equal Opportunities Employer

U127718R

University Hospital Essen

Medical Faculty of the University Duisburg-Essen

Institute of Virology, Essen University Hospital has an immediate opening for a

Post-doc position.

The successful candidate will be responsible for a project dealing with the development of a new HCV immunogen on the basis of virus-like particles and characterization of HCV-specific B- and T-cell immune responses. This project will be run in the frame of the clinical working group "Optimization of living liver transplantation" formed in the Essen University Hospital.

Position is open for three years with a possibility of extention.

Requirements: Ph.D. or equivalent in Biology Biochemistry or Chemistry, advanced experience in immunology and molecular biology

Applications including the detailed CV and the names of three references should be submitted to: **Prof. Dr. med. M. Roggendorf, Institut für Virologie, Universitätsklinikum Essen, 45122 Essen**
eMail: michael.roggendorf@uni-due.de

UNIVERSITÄT DUISBURG ESSEN

Heart/Circulation Oncology Transplantation

W128844R

The Ruggero Ceppellini Advanced School of Immunology

in collaboration with
The Istituto Italiano per gli Studi Filosofici
The Federico II University of Naples

The European Federation of Immunological Societies-European Journal of Immunology, offers the following Advanced Course on

Tumor Immune Escape Mechanisms

Directors: Soldano Ferrone and Barbara Seliger
Hillman Cancer Center, University of Pittsburgh Cancer Institute, Pittsburgh, USA
Martin-Luther University, Institute of Medical Immunology, Halle-Wittenberg, Germany

Sorrento, Italy — October 16-19, 2008

Further information will soon be available at: www.ceppellini.it • contact sfontana@unina.it

W128323F

dkfz.

German Cancer Research Center
(DKFZ, Deutsches Krebsforschungszentrum) Member of the Helmholtz-Gemeinschaft, HGF

Faculty of Biosciences University of Heidelberg

The mission of the German Cancer Research Center (DKFZ) is to unravel mechanisms of cancer development and to establish novel approaches for the diagnosis, treatment, and prevention of cancer. As a leading biomedical research center in Germany, our programs focus on basic and translational cancer research. The German Cancer Research Center is a foundation under public law and a member of the Helmholtz Association of National Research Centers (Helmholtz-Gemeinschaft Deutscher Forschungszentren)

The following position is available at the German Cancer Research Center (DKFZ) in cooperation with the Faculty of Biosciences at the University of Heidelberg

Professorship (W3) and Division Head for Cellular Immunology

We are seeking a candidate with an outstanding research record and international reputation, who studies fundamental questions in immunology, continuing a tradition of excellence in this discipline at DKFZ. The research program of the successful candidate is expected to strengthen the existing research program "Tumor Immunology" of the DKFZ. Candidates should hold a PhD or MD degree. The successful candidate will have the possibility to participate in graduate and postgraduate programs of the Faculty of Biosciences at the University of Heidelberg

The professorship is tenured. First professorial appointments are limited in time before tenure can be granted. DKFZ is committed to increase the percentage of female scientists and encourages in particular female applicants. Among candidates of equal aptitude and qualifications, a person with disabilities will be given preference.

Applications, including curriculum vitae, list of publications, and a research program, should be sent to Prof. Dr. Otmar D. Wiestler, Chairman, Deutsches Krebsforschungszentrum, Im Neuenheimer Feld 280, 69120 Heidelberg, Germany (e-mail: o.wiestler@dkfz.de) not later than May 2, 2008.

W128378R

Chairperson of Department of Tropical Medicine

Tulane University School of Public Health and Tropical Medicine seeks candidates for the combined position of Chair of the Department of Tropical Medicine and the William G. Vincent Professor of Tropical Diseases.

The Department has strong research programs in infectious diseases, including vector-borne diseases. AIDS and several other areas with extensive global research and teaching activities in Latin America, Africa, and elsewhere. There are also strong ties and excellent growth opportunities with the Schools of Medicine, and Science and Engineering as well as the Tulane National Primate Research Center. More information about the School and the Department is available at http://www.sph.tulane.edu/

The candidate is expected to have a nationally and internationally recognized research program, including a strong track record in obtaining extramural research funding, publications in quality peer reviewed journals, and the ability to mentor junior faculty as they establish a research program. The candidate should have a documented record of leadership, administrative ability, and communication and teaching skills. Areas of specialization are not limited, although candidates with expertise in vector-borne infectious diseases, parasitology and/or virology are strongly encouraged to apply. Candidates must have a doctoral degree in a related discipline (MD, PhD, ScD or equivalent).

Interested candidates should submit a Curriculum Vitae and a statement of research interests to: Paula Furr, Dean's Office TW 13, Tulane University School of Public Health & Tropical Medicine, 1440 Canal Street, Suite 2430, New Orleans, LA 70112.

NW128703R

The chance to prove your talent.

AMC Fellowship 2008

The Executive Board of the Academic Medical Center, University of Amsterdam, has launched a new dynamic AMC Fellowship scheme in 2005. With this scheme the AMC intends to attract talented young scientists, as well as foster translational and clinical research. With the AMC Fellowsh p scheme the AMC supports young, talented (bio)medical scientists who have shown extraordinary originality and dedication, have a marked capacity for self-direction, and who are seeking an opportun'ty to establish their own independent research group One AMC Fellowship s granted each year. In 2008 the fourth AMC Fellowship will be awarded.

Applicants should have four to six years of postdoctoral work experience, although consideration can be given to exceptional candidates with less experience after their PhD An AMC Fellowship is awarded for 3 years, with a possible extension of another 2 years. Subject to normal probationary procedures, the AMC Fellowship will lead to a permanent position at the Academic Medical Center. The Fellowship provides an appropriate salary for the applicant as well as budget for technical assistance, equipment and general infrastructure. In total a budget of € 600.000,- for five years is available for each Fellowship.

We are now accepting applications for the AMC Fellowship 2008. Applications should include an outline of the applicant's current and future research interests, a curriculum vitae including a list of publications, and at least two letters of support written by internationally acknowledged, senior scientists. n these letters motivated support should be given for the candidate as well as for the proposed research program. Applications can be sent by e-mail to the attention of Prof. C.J.F. van Noorden to AMCFellowship@amc.nl, the deadline is monday 19 May 2008. W'thin three weeks of receipt the applicant will be notified whether his/her application is taken into consideration, and if so will be informed of further details of the procedure.

amc It's your world, too

UNIVERSITY OF AMSTERDAM

W128690R

Be at the sharp end.

MHRA

The MHRA (The Medicines and Healthcare products Regulatory Agency) is the government agency that plays a key role in safeguarding the nation's health. We do this by ensuring that all medicines and medical devices are effective, of high quality and acceptably safe.

Pharmaceutical Assessor

£35,687 - £51,344 Biological and Biotechnology Unit, Vauxhall, London

The Licensing Division is responsible for the quality, safety and efficacy evaluation of all new medicinal products approved for use in the UK, and incorporates a dedicated Biological and Biotechnology Unit which specialises in cell and gene therapy products, recombinant proteins, vaccines and blood products.

Working at the cutting edge of both science and healthcare regulations, it's a challenging role that will involve analysing and assessing data, compiling reports and making recommendations as to whether specific products should receive a licence.

All new biotechnology medic nal products are approved through a centralised European procedure, and you will have the opportunity to work with the relevant European expert committees in evaluating these products

You will also use your expertise and understanding to provide guidance to pharmaceutical companies at all stages of the drug development process. You will work with all types of biological and biotech products, as well as specialising in areas such as cell therapy or recombinant proteins. We would particularly welcome candidates with experience in regenerative medicine, tissue engineering, cell therapy, immunotherapy or related disciplines.

Coming from an industry or academic research background, you'll bring a well-developed understanding of development, manufacture and evaluation of biotech products e.g. recombinant proteins, blood products, cell therapies and/or vaccines. You will have strong analytical and decision-making skills. This will be matched with a relevant life sciences degree and relevant post graduate qualifications to PhD level or equivalent. Knowledge of specific therapeutic areas will also be highly valued.

To apply, please visit www.mhra.gov.uk/jobs or email jobs@mhra.gsi.gov.uk

Closing date: 15th April 2008.

As an Equal Opportunities employer the Department welcomes applications regardless of gender, race, disability or sexuality

Safeguarding public health

POSITIVE ABOUT DISABLED PEOPLE

INVESTOR IN PEOPLE

U128211B

Programm zur Förderung der Rückkehr des wissenschaftlichen Spitzennachwuchses aus dem Ausland

Der Forschungsstandort Nordrhein-Westfalen steigert seine Attraktivität für die Rückkehr des Spitzennachwuchses aus dem Ausland. Hier werden gut ausgestattete Positionen für den Aufbau und die Leitung **selbstständiger Nachwuchsgruppen im Bereich der Nanotechnologien** ausgeschrieben.

Je Nachwuchsgruppe stellt die Landesregierung für einen Zeitraum von fünf Jahren bis zu 1,25 Mio EUR zur Verfügung. Die Leitungsposition ist mit Entgeltgruppe 15 TVL – vergleichbar W2 – dotiert. Sie erhalten eine personengebundene Finanzierungszusage und etablieren Ihr Labor an einer Hochschule Ihrer Wahl in Nordrhein-Westfalen, welche Ihnen die beste Zukunftsperspektive und eventuell auch tenure (track) bietet.

Sie forschen derzeit außerhalb Deutschlands im Bereich der Nanotechnologien, verfügen über eine qualifizierte Promotion, die in der Regel nicht länger als 6 Jahre zurückliegt, Ihr Lebensmittelpunkt lag vor dem Auslandsaufenthalt in Deutschland und Sie können insgesamt mindestens 24 Monate erfolgreicher wissenschaftlicher Forschung außerhalb Deutschlands vorweisen. Wenn dies alles auf Sie zutrifft, freuen wir uns auf Ihre Bewerbung unter

www.rueckkehrerprogramm.nrw.de

Ihre Bewerbungsunterlagen in englischer Sprache enthalten Lebenslauf, Publikationsliste, einen Arbeitsplan für die nächsten fünf Jahre, eine Zusammenfassung Ihrer bisherigen wissenschaftlichen Leistungen, bis zu drei Ihrer wichtigsten Veröffentlichungen und Referenzen. Weitere Informationen sowie eine detaillierte Beschreibung des Programms finden Sie auf der angegebenen Internetseite.

Bitte reichen Sie Ihre Bewerbungsunterlagen bis zum **1. Mai 2008 (Deadline)** online ein.

Das Land Nordrhein-Westfalen fördert die berufliche Entwicklung von Frauen. Bewerbungen von Frauen werden daher besonders begrüßt. Bewerbungen geeigneter schwerbehinderter Menschen sind erwünscht.

Ministerium für Innovation, Wissenschaft, Forschung und Technologie des Landes Nordrhein Westfalen

NRW.

W127517B

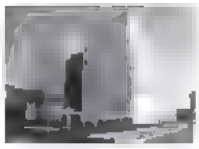

National Institute for Materials Science (NIMS), Japan

Postdoctoral Scientists for Organic & Polymeric Materials

The Organic Nanomaterials Center at NIMS, Tsukuba, Japan, is seeking postdoctoral scientists having a strong background in organic synthesis, macromolecular science, surface & colloid chemistry, and/or nano-materials. The NIMS/Max Planck Institute International Joint Lab, Potsdam, Germany, also can offer positions. ***Applicants should select one of the groups listed below and submit a full CV/publication list to:***

Reiko Miyajima, Secretary
Organic Nanomaterials Center, 1-1, Namiki, Tsukuba,
Ibaraki 305-0044, Japan.
FAX: +81-29-852-7449; E-mail: MIYAJIMA.Reiko@nims.go.jp

Organic Nanomaterials Center, Tsukuba, Japan

Functional Thin Films G.	**(Dr. Izumi ICHINOSE)**
Functional Modules G.	**(Dr. Dirk G. KURTH)**
Macromolecules G.	**(Dr. Masayuki TAKEUCHI)**
Reticular Materials G.*	**(Dr Omar M. YAGHI)**
Supermolecules G.	**(Dr. Katsuhiko ARIGA)**

Max Planck Institute of Colloids and Interfaces, Potsdam, Germany
Supramolecular Nanomaterials G. (Dr. Takashi NAKANISHI)

Annual salary ranges from JPY 5,800,000 to 4,500,000, including taxes and other charges. For the salary at the Joint Lab, please contact Dr. NAKANISHI. *Group to be started from April 1, 2008. For details, please see http://www.nims.go.jp/onc/index_e.html

JP127381R

nature

Nature needs an

Associate News & Views Editor, Physical Sciences

News & Views is a highly popular section of *Nature* and covers all of the sciences. Its reputation depends on publishing timely, readable and authoritative articles about the latest developments in science. Deadlines are often tight.

This post involves working as part of a multidisciplinary team of editors, and the following qualifications are essential:

- Education to postgraduate level in one of the physical sciences, preferably physics, astronomy or Earth science.
- A highly developed sense of literacy
- A critical and lively interest in science in general.

Research experience would be advantageous, and preference will be given to applicants with a demonstrably strong interest in the communication of science. The main responsibility will be commissioning and editing News & Views articles, which requires an awareness of news values and of the demands of non-specialist readers, sub-editing skills and tact in dealing with authors.

This position will be based in our modern London offices. To enquire informally about this post, e-mail Tim Lincoln at t.lincoln@nature.com, providing a phone number.

To apply, please send your CV, a covering letter describing your suitability for the job, and details of current salary and notice period to Geetika Juneja at londonpersonnel@macmillan.co.uk quoting reference number NPG/LON/851.

All candidates must demonstrate the right to live and work in the UK to be considered for the vacancy.

nature publishing group npg

Closing date: 14th April 2008

IN128521R

University of Oxford SGC

The SGC
A World Leader in the Structural Biology of Human Proteins

The SGC (Structural Genomics Consortium) solves the structures of medically-relevant human proteins with a commitment to providing fundamental scientific information for biomedical research and drug development through depositions into the public domain. The SGC is organised at three sites, the Universities of Oxford and Toronto and at the Karolinska Institute in Stockholm. Each site focuses upon separate protein target areas.

An international team of 60 scientists at the SGC in Oxford offers a stimulating environment for individual and collaborative research in the areas of **protein kinases, protein phosphatases and cancer, epigenetic regulation, oxidoreductases and metabolic enzymes and DNA repair.** A special focus is placed on **integral membrane proteins,** a challenging area with tremendous medical importance.

The SGC currently collaborates with > 80 research groups worldwide. We are part of the Nuffield Department of Clinical Medicine and are located in the new Institute for Cancer Medicine. The centre's institutions, which include Clinical Pharmacology, Radiation Oncology and the Ludwig Institute of Cancer Research, offer many opportunities for collaborations to extend the impact of biochemical and structural studies into drug development and clinical applications.

We are seeking skilled and motivated scientists with experience or interest in protein expression and biochemistry, X-ray crystallography, membrane proteins, chemical biology or any of the target areas we study.

If you wish to join us as a postdoctoral fellow or research assistant, or to conduct a short-term project as a visiting scientist/student, we'd like to hear from you. Please visit our website, www.sgc.ox.ac.uk for listed positions or send your CV and research interests to contact@sgc.ox.ac.uk for other opportunities.

U128686R4

The University are Equal Opportunity Employers.
We positively encourage applications from people of all backgrounds

www.sgc.ox.ac.uk/jobs

School of Computing Sciences

UEA NORWICH

Two Post-doctoral Research Associates

Post 1 - Ref: RA474 - 5 years fixed-term
Post 2 - Ref: RA476 - 5 years fixed-term

£28,290 to £33,780 per annum (w.e.f. 01/05/2008)

These BBSRC funded Postdoctoral Research Associates are based at the University of East Anglia in the group of J. Andrew Bangham, working together with Prof. Enrico Coen from the nearby John Innes Centre. The Associates will be involved in developing computational tools for analysing and modelling the growth of plants. Why? Plants are important. Think, for example, about feeding the world and maintaining the ecological environment. These posts are available from 1 May 2008.

You need not have a background in biology, but must have:

- a PhD (or equivalent) and experience of programming at least one of
  - o Computer vision
  - o Image processing
  - o Graphics
- skills in programming in Matlab, C++ or equivalent.

More information about the School of Computing Sciences can be found at http://www.cmp.uea.ac.uk/

Closing date: 1 May 2008.
Interview date: Mid May 2008.

Further particulars and an application form can be obtained from the University's web page at: http://www.uea.ac.uk/hr/jobs/ or by e-mail at: hr@uea.ac.uk or by calling the answerphone on 01603 593493 or by mail to the Human Resources Division, University of East Anglia, Norwich NR4 7TJ.

U128647R

University of Oxford

Nuffield Department of Clinical Medicine

PhD Studentship - Hypoxia Signaling Pathways in Cancer

An MRC PhD studentship is available from October 2008 to work in the hypoxia biology group of Professor Peter Ratcliffe FRS at the Henry Wellcome Building for Molecular Physiology, Old Road Campus, University of Oxford.

Hypoxia is a critical feature of the tumour microenvironment and activation of the hypoxia inducible factor (HIF) transcriptional cascade is central to many features of aggressive cancer including excessive angiogenesis and altered metabolism. The project capitalises on recent genetic insights into the mode of activation of these pathways and seeks to better understand the driving pathways underlying tumour development in the renal epithelium.

The project will be co-supervised by Professor Ratcliffe and Dr Patrick Pollard and involves a broad range of molecular and cell biology including transgenic and 'knock-out' technology. Oxford University's Old Road Campus is one of the UK's fastest growing biomedical research centres, employing in excess of 500 biomedical scientists and offering a vibrant multidisciplinary environment for postgraduate training. The studentship will be suitable for graduates in biological sciences with interests in molecular oncology, cell biology, genetics and disease models.

This 3 year studentship is available to candidates who are either UK nationals or those who have been resident in the UK for at least the previous three years and who have no restrictions on the period for which they may stay in the UK (further details on eligibility can be found on the MRC website, http://www.mrc.ac.uk). The studentship will provide an annual stipend and financial support for fees. Interested applicants should visit http://www.well.ox.ac.uk for further particulars, or alternatively e-mail Dr Patrick Pollard (paddy@well.ox.ac.uk) with any informal enquiries.

Applications must be made through the University Graduate Admissions application process - please do not send CVs, as these will not be considered. For details of how to apply, please visit http://www.admin.ox.ac.uk/postgraduate/apply/ Please note that candidates need to submit TWO copies of their full application and that a cheque for £25 (made out to the University of Oxford) should be included to cover processing costs. The Graduate Admissions deadline for applications is the 14 April 2008 - any applications received after this date will not be considered. Once your application has been submitted, please e-mail sarah.noujaim@ndm.ox.ac.uk quoting reference NDM/mrcdta08/Nature so that your application can be safely tracked.

As an Equal Opportunity employer, we positively encourage applications from people of all backgrounds

U126606FM

www.ox.ac.uk/jobs

MDC

MAX DELBRUECK CENTER FOR MOLECULAR MEDICINE BERLIN-BUCH

in the HELMHOLTZ-GEMEINSCHAFT e.V.

The MAX DELBRÜCK CENTER FOR MOLECULAR MEDICINE (MDC) BERLIN-BUCH is inviting applications for

Independent Junior Group Leader Positions
Function and Dysfunction of the Nervous System
(5 years, Tenure track)

The MDC Berlin Buch is a member of the Helmholtz Association of National Research Centers, supported by the Federal Government of Germany and the Land Berlin. It is a biomedical research institute dedicated to interdisciplinary research in the areas of (i) Cardiovascular and Metabolic diseases, (ii) Cancer, and (iii) Function and Dysfunction of Nervous System.

The MDC is committed to expanding its impact in the field of Neuroscience and is seeking applications from outstanding individuals. Applications are encourage from individuals working in all areas of neuroscience. Applicants using molecular approaches to study synaptic function and disfunction or state of the art in vivo methods to analyze neuronal activity in behaving animals are especially encouraged.

Successful candidates will conduct visionary independent research, obtain extramural funding and engage in collaborative projects with groups at the MDC and the MDC-associated clinics of the Charité Universitätsmedizin Berlin.

Successful candidates may be invited to apply for a Helmholtz-University Young Investigator Group or a Helmholtz Young Investigator Group, sponsored by the President's Initiative and Networking Fund (see: **http://www.helmholtz.de/de/Aktuelles/Helmholtz-Ausschreibungen/Helmholtz-Nachwuchsgruppen.html**). The applications of women are explicitly encouraged.

For further information about the MDC Berlin-Buch please visit our web site (**http://www.mdc-berlin.de**). For enquiries about the position please contact Christina Quensel (cquensel@mdc-berlin.de).

Applications should be sent by May 5, 2008, including a curriculum vitae, list of publications, an outline of present and planned research and other relevant material to:

Max Delbrück Center for Molecular Medicine (MDC) Berlin-Buch
Scientific Director, Prof. Dr. Walter Birchmeier
POB 740238, 13092 Berlin, Germany

W126391FM

Department of Innovation, Universities and Skills

APPOINTMENTS TO THE RESEARCH COUNCILS 2008

Department for Innovation, Universities & Skills

The Appointments Panels for AHRC, ESRC and NERC are seeking applications from suitably qualified academics and experienced individuals from the industrial/commercial sector to fill a number of vacancies for part-time membership on the following Councils, which are expected to arise during 2008.

The Arts and Humanities Research Council (AHRC)

The Economic and Social Research Council (ESRC)

The Natural Environment Research Council (NERC)

THE CLOSING DATE FOR THE RECEIPT OF APPLICATIONS IS 24th April 2008

The Secretary of State for Innovation, Universities and Skills appoints members to the Councils on merit after considering advice from the Appointments Panel. The Secretary of State is committed to the principle of public appointment on merit with independent assessment, openness and transparency of process and to providing equal opportunities for all, irrespective of race, age, disability, gender, marital status, religion, sexual orientation, transgender and working patterns.

An honorarium of £6,570 is paid annually.

Interviews for AHRC will be held on 6 and 10 June 2008 in London
Interviews for ESRC will be held on 6 June 2008 in London
Interviews for NERC will be held on 9 June 2008 in London

Further information about the vacancies and application forms are available to download via our web site at

http://www.berr.gov.uk/dius/science/research-councils/public-appointments/council-members/page15706.html

If you do not have internet access please contact:

Cecilia Sparke telephone number **0117 987 6822** for **AHRC's vacancies**.
Joanne Goddard telephone number **01793 444527** for **ESRC's vacancies**.
Samantha Way telephone number **01793 442570** for **NERC's vacancies**.

U126493B

Online Editor, Protein Structure Initiative Knowledgebase

Nature Publishing Group is looking for a dynamic, organized and creative science graduate with a background in structural biology to launch and maintain the forthcoming Protein Structure Initiative (PSI) Knowledgebase. The successful applicant will also have a keen interest in and ideas for making the site accessible to a broad audience of molecular and cellular biologists as well as geneticists.

Launching in 2008, the Knowledgebase will be an accessible online publication widely read by the research community. The site will encompass editorial content updated monthly on recent research, news and events, as well as databases and other information resources from the PSI. The Knowledgebase is an innovative publication of a type that is becoming increasingly important in academic publishing, and we are looking for someone who is eager to establish the Knowledgebase as a major information resource for researchers.

The Editor will take responsibility for the site's content and high scientific quality, including writing summaries of key research developments. The editor will work as part of the existing teams in NPG's Web Publishing department and at *Nature Structural and Molecular Biology*, and will liaise with the PSI. They will have, or will be shortly expecting to receive, a PhD in a structural biology-related discipline, and will have a broad interest and understanding of the structural biology field, including technologies and their applications. A sound knowledge of good web practice and a passion for the exploitation of the medium as a means of scientific communication are crucial.

Key personal qualities for this position include:

- Excellent writing skills
- A strong ability to communicate with leading scientists
- An acute eye for detail, and the ability to work to firm deadlines

The successful candidate will ideally be based in our offices in New York, although other localities may be possible.

To Apply: Send cover letter stating salary requirements and resume via email to admin@natureny.com (Nature Publishing Group, Human Resources Department) no later than **April 14, 2008**. Note "Online Editor" in the subject header.

NPG is an Equal Opportunity Employer

nature publishing group

IN128171R

Assistant Editor

Nature Biotechnology

Nature Biotechnology seeks an Assistant Editor for its editorial team based in New York. Expertise in systems biology and/or computational biology would be desirable, but not required.

Members of the editorial team evaluate manuscripts, oversee the peer review process, commission and edit secondary materials such as Reviews, and write short pieces and editorials for the journal. The successful applicant will attend scientific meetings and visit laboratories to maintain contact with the international scientific community. The position will play a key role in consolidating *Nature Biotechnology*'s presence in the fields of systems biology and computational biology.

Excellent communication skills and a willingness and ability to learn new fields are a must. Applicants should have completed a Ph.D. in the biological sciences.

To apply, an interested candidate should submit a curriculum vitae, a short (500-1000 words) News and Views-style article on an exciting and newsworthy recent development in biotechnology, and a cover letter explaining their interest in the position to Human Resources Department, Nature Publishing Group.

All applications should be sent via email to: admin@natureny.com.

Please place "Assistant Editor Nature Biotechnology" in the subject line.

All applicants will be reviewed upon receipt with a close date of March 31 2008.

Nature Publishing Group
75 Varick Street
New York, New York 10013, USA

nature publishing group

Zebrafish Neurobiology Tenure-Track Faculty Position

Université de Montréal

An Assistant Researcher position leading to tenured professorship is available in the Department of Pathology and Cell Biology at the Université de Montreal (http://www.patho.umontreal.ca/), one of the top research institutions in Canada with an excellent neuroscience graduate training program. We are seeking a neurobiologist with a Ph.D. or equivalent with postdoctoral experience and with expertise in transgenesis, genetics or gene regulation to expand our new group of neurobiologists (Pierre Drapeau, Louis Saint-Amant and Julien Ghislain) using the zebrafish as a model. This person will also collaborate with the new Université de Montréal Centre of Excellence in Neuromics on a large-scale genomic screen of mutations in human synaptic genes linked to brain diseases and their validation in genetic model organisms. The recruit will have access to a large zebrafish facility and other common resources and will be provided with an attractive start-up package. The candidate has to eventually develop a capacity for limited teaching in French. Please send a CV, short description of your research plan and three letters of reference by **May 1st, 2008**, to:

Dr Pierre Drapeau, Chair
Department of Pathology and Cell Biology
Université de Montréal
PO Box 6128, Downtown Station
Montreal, Quebec H3C 3J7
Fax, 514-343-5755, E-mail: p.drapeau@umontreal.ca

In accordance with Canadian immigration requirements, priority will be given to Canadian citizens and permanent residents of Canada. The Université de Montréal is involved in a program that promotes equal work opportunities for women as well as for ethnic and visible minorities, aboriginals and the handicapped.

www.med.umontreal.ca

Université de Montréal

NW128837R

Advancing science. Serving patients.

Amgen, a biotechnology pioneer, discovers, develops and delivers innovative human therapeutics. Our medicines have helped millions of patients in the fight against cancer, kidney disease, asthma and other serious illnesses. With a deep and broad pipeline of potential new medicines, we continue to advance science to serve patients

We have two positions available in Thousand Oaks, CA in support of our Inflammation Research Therapeutic Area:

Senior Scientists

You will discover and develop therapeutics for chronic autoimmune and inflammatory diseases such as asthma, IBD, RA, MS and OA. These positions require a PhD and/or MD with at least four years of postdoctoral experience in an area relevant to immunology/ inflammation research. Small molecule and/or protein drug development experience would also be beneficial.

For one of the positions, preferred candidates will have expertise with in vivo models of autoimmune disease and knowledge of B cell biology. For the other position, you should have experience working with ex vivo cartilage explants and conducting animal models of osteoarthritis (OA), including evaluation of candidate therapeutics in these models.

In addition to supporting ongoing programs within the department, you must be able to lead research programs that seek to identify new targets. You must also be able to work well in a cross-functional multi-location team environment. Strong communication skills are essential.

Please apply online at www.amgen.com/careers and reference the appropriate code

Senior Scientist Inflammation, Thousand Oaks: * 50187161*

Senior Scientist Inflammation, Thousand Oaks: * 50184030*

AMGEN

Pioneering science delivers vital medicines™

www.amgen.com/careers

As an EEO/AA employer, Amgen values a diverse combination of perspectives and cultures. M/F/D/V.

NW128630R

STAFF SCIENTIST
Full-Time

Blood Systems Research Institute (BSRI), a dynamic blood research institute in San Francisco and an affiliate of the University of California, San Francisco is seeking a motivated Staff Scientist. This position will participate in human translational research on transfusion safety. The successful applicant would need to work well on a team and oversee staff performing a wide variety of immunology assays supporting several transfusion safety research projects. Excellent communication and writing skills are essential. Experience with assay validation and good laboratory practices (GLP) preferred. MS or MPH degree in related field required, MD or PhD preferred

Two years of post-graduate experience required and at least two English language first author publications in PubMed database or career development award required. Previous supervisory experience is preferred

To express your interest please submit your Resume by April 4, 2008 to: Human Resources, Blood Systems Research Institute 270 Masonic Ave., San Francisco, CA 94118; E-Mail: BSRIcareers @bloodsystems.org

Pre-employment drug screen required.
EOE M/F/D/V

NW128484R

MOTOR NEURON CENTER

COLUMBIA UNIVERSITY
IN THE CITY OF NEW YORK

Motor Neuron Center/ ALS Center Faculty Recruitment

The Columbia University Center for Motor Neuron Biology and Disease (MNC) and the Eleanor and Lou Gehrig MDA/ALS Research Center are recruiting faculty with interests in motor neuron biology, SMA, ALS or related motor neuron diseases to join a translational program involving basic and clinical research. Individuals in any of these areas may apply but we are particularly interested in hiring a clinician-scientist to see ALS patients at the ALS Center and in parallel carry out their own research program in any of the basic or clinical areas covered by the Motor Neuron Center (www.ColumbiaMNC.org). We are also seeking clinical and/or basic scientists with an active research program focused on therapeutic strategies and disease mechanisms in animal models of SMA or ALS

We encourage applications for positions at the Assistant or Associate Professor level, but will also consider applications from more senior investigators for positions at the level of full Professor

Columbia University has a world-renowned program in neurobiology and behavior and in medical and surgical neurology. Faculty will be affiliated with the Departments of Neurology and/or Pathology and Cell Biology, but will interact with other programs at the Medical Center and Morningside Heights campus. As members of the MNC, faculty will have access to core facilities including high-throughput screening and internal grant programs

Applications should be submitted by June 1st, 2008. A curriculum vitae, a cover letter including statement of interests, and three letters of reference under separate cover should be e-mailed care of Mr. Michael Shelley at ms3561@columbia.edu. In addition, please mail a hard copy of these documents to

Chair, Motor Neuron Center Search Committee
c/o Mr. Michael Shelley
BB 302
630 West 168th Street
New York, NY 10032, USA

Columbia University takes affirmative action to ensure equal opportunity

NW128483R

W128317R

Westfalian Wilhelms-University Muenster, Germany

The Medical Faculty of the Westfalian Wilhelms-University Muenster offers the position of a

University Professor (W3, life time position) for Cardiology and Angiology

in the Department of the Medical Clinic C with the main focus on cardiology starting March 1, 2009. The future holder of the position (male/female) must fully represent the subject with regard to research, teaching and patient care.

The occupation of the position aims at the enhancement of the established research field in cardiovascular medicine. The successful candidate (male/female) must have an internationally recognized research profile in the field of cardiology. Documented excellent experiences in the complete field of cardiology including all common interventional techniques and intensive care are requested.

Candidates are expected to participate in joint research programs of the Medical Faculty, such as "Interdisciplinary Clinical Research Centre" (IZKF), the "Centre of Clinical Studies" (ZKS), the Collaborative Research Programs (Sonderforschungsbereiche) the Max-Planck- Institute of Molecular Biomedicine and the Leibniz Institute for Arteriosclerosis Research.

Prerequisite for the application are scientific achievements as a junior professor; alternatively, scientific achievements can result from a postdoctoral lecture qualification (habilitation), work as a research scientist at a school of higher education/university, non-university institute, industry, administration, or other fields of society within or outside Germany.

Applications of women are specifically invited. In the case of similar qualification, competence, and specific achievements, women will be considered on preferential terms within the framework of the legal possibilities. Handicapped candidates with equivalent qualification will be given preference.

According to a resolution by the Conference of the German Ministers for Science and Education of November 19, 1999, professors with clinical tasks will principally be employed on the basis of individually negotiable contracts (exceptions are possible, if applicants are already employed as life time professor of the salary group C3-4/W2-3). The clinical duties affiliated with this professorship will be laid down in a separate contract with the Universitätsklinikum.

Documents in support of an application, enclosing CV, scientific career, structured catalogue of publications, acquired third party funds and reprints of the ten most important publications should be submitted to the **Dean of the Faculty of Medicine, University of Münster, Domagkstr. 3, 48129 Münster, Germany,** by **April 25th 2008.**

References: http://campus.uni-muenster.de/service/Merkblatt_Berufungen.pdf

Max Planck Institute for Neurological Research

MAX PLANCK GESELLSCHAFT

At the Max Planck Institute for Neurological Research Cologne

a full-time postdoctoral position
on cancer cell biology and cancer genomics

is available starting June 1 2008 for a period of 3 years in the Functional Cancer Genomics lab led by Roman Thomas

Our group is a highly dynamic and competitive research lab with active collaborations with global leaders in the area at Harvard, M.I.T., other Max Planck Institutes and the Pharmaceutical Industry.

Our research is focused on understanding functional cell biology aspects of cancer genomics. We apply high-density SNP arrays for analysis of gene copy number changes, as well as expression arrays and gene mutation analyses to generate genetic lesion profiles of large cancer cell line collections. We apply computational biology and molecular cell biology methods to understand the biological impact of these genetic alterations. In particular, we use high-throughput cell based compound screening as well as systematic reverse RNA interference to define signaling pathway dependencies and novel potential drug targets in human cancers. In-vivo experiments can be performed in collaboration with the molecular imaging groups at the Institute. Overall, our approaches are systematic in nature with in-depth molecular follow up of single leads in order to identify fundamental molecular principles governing oncogenic transformation and growth.

The position requires a PhD or MD degree in a relevant field, such as cancer research, molecular cell biology, computational biology, biostatistics or oncology. Experience in molecular biology, cancer genomics, as well as mathematical and scripting skills (preferably R or MATLAB) are highly desirable. For further information please contact Roman Thomas (e-mail: rthi@nf.mpg.de) or see our website at www.nf.mpg.de/index.php?id=197&L=1

The Max Planck Society is an equal opportunity employer and particularly welcomes applications from individuals with disabilities.

Please submit your application including a detailed CV, list of publications, two references, and a brief statement of research interests as a single .pdf file by email only by April 30, 2008 to Roman Thomas: rthi@nf.mpg.de.

W128668R

University of Oxford

Head of Clinical BioManufacturing Facility
Grade 10: Salary £45,397 - £52,628 with a discretionary range to £57,508 p.a.

An exciting opportunity has arisen to head up this unique and innovative facility embedded within the Nuffield Department of Clinical Medicine, University of Oxford. The CBF has a Manufacturer's Authorisation for Investigational Medicinal Products (IMP's) from the Medicines and Healthcare products Regulatory Agency (MHRA). Currently the CBF is manufacturing adenoviral vectors for use as novel vaccines and cancer therapies and is entering a phase of continued growth.

We are seeking an experienced scientist/engineer to manage the day-to-day operation of the CBF and be actively involved in the production and development of IMP. Working with a team of 8 other staff and supported by a senior management committee, you will ensure the cGMP compliance of the facility, co-ordinate the activities of production, development, quality assurance, regulatory compliance and H&S.

Interested applicants should have a post graduate qualification in a related field and relevant experience in a regulated environment along with cGMP manufacturing experience of biological IMP's and excellent managerial skills.

Prior commercial experience would be an advantage as the postholder will be involved in the strategic development of the facility, business plans, financial management, project planning and drawing up technical agreements between CBF and its customers.

Position is offered for two years in the first instance.
Closing date of applications 11th April 2008. Initial enquiries should be made to Shirley Varney on 01865 617604 quoting reference HC-03-101-GS, or email orcrb.personnel@ndm.ox.ac.uk

As an Equal Opportunity employer, we positively encourage applications from people of all backgrounds

U128645RM

www.ox.ac.uk/jobs

www.naturejobs.com

Newcastle University

U128687R

Northern Institute for Cancer Research

Lecturer (Molecular Genetics/ Cytogenetics)

£29,139 - £40,335 p.a.

Based in the Leukaemia Research Cytogenetics Group (LRCG), part of the Northern Institute for Cancer Research, you will work with Professor Christine Harrison (Professor of Childhood Cancer Cytogenetics) and Dr Anthony Moorman (Reader in Genetic Epidemiology) and will conduct molecular genetics and other related technologies as part of the ongoing research programme funded by the Leukaemia Research Fund. You will have expertise in most of the following areas of molecular genetics, cytogenetics, fluorescence in situ hybridisation (FISH), genomic arrays, gene expression, functional analysis and preferably experience in techniques of genetic modification.

Working in a multidisciplinary team, your research will focus on the discovery and characterisation of genetic abnormalities in acute leukaemia. As well as further developing your own area of research, you will play a leading role in maintaining the international reputation of the LRCG. You will be involved in some teaching and supervision of PhD students and other junior staff. The post is available from 1 May 2008 as a temporary position for an initial period of three years, further programme grant funding will be sought at that time.

For further details or an informal discussion relating to academic activities please contact Professor Christine Harrison, e-mail: c.j.harrison@soton.ac.uk or tel: (023) 8079 8783 or Dr Anthony Moorman, e-mail: anthonymoorman@ncl.ac.uk or tel: (0191) 246 4460). Additional information about the Northern Institute for Cancer Research can be found at: http://www.ncl.ac.uk/nicr/

Closing date: 18/04/08.

Job reference: A048A.

Research Associate (Molecular Genetics/ Molecular Biology)

Starting salary up to £29,139

Based in the Northern Institute for Cancer Research (NICR) and working closely with other groups involved in leukaemia research, you will join Professor Christine Harrison's Leukaemia Research Cytogenetics Group (LRCG): a world leader in leukaemia genetics, molecular cytogenetics and related state-of-the-art technologies. You will be involved in projects aimed at the identification and detailed investigation of novel genes in acute leukaemia in relation to their clinical associations within the UK acute leukaemia treatment trials. You will have a good publication record, as well as experience of conducting research on specific projects within the Leukaemia Research programme. You will train, supervise, advise and aid other researchers within the team, as appropriate. This is an excellent opportunity for a scientist with interests in translational research related to leukaemia genetics.

Informal approaches can be made to Professor Christine Harrison, e-mail: c.j.harrison@soton.ac.uk or Dr. Anthony Moorman, e-mail: anthony.moorman@ncl.ac.uk. The post is tenable for until 31/03/11

Closing date: 18/04/08.

Job reference: A049R.

Please apply on line at http://www.ncl.ac.uk/vacancies/

Committed to Equal Opportunities www.ncl.ac.uk/vacancies

Julius Maximilians-
UNIVERSITÄT
WÜRZBURG

The Biocenter at the University of Würzburg (Germany) invites applications for a **full/tenured professorship (W3)** in the field of

Animal Ecology (Zoology III)

The Chair of Zoology III (Animal Ecology) is part of the Theodor-Boveri-Institut for Biosciences at the University of Würzburg, Germany.

Successful applicants will be expected to represent the subject of Animal Ecology in teaching and research. They should have a distinguished international research record in current and active areas of Animal Ecology. Applicants with a strong background in Tropical Biology will be preferred. Their research should complement existing fields of research in the Biocenter, particularly the collaborative research centers "Mechanisms of Inter-Specific Interaction of Organisms (SFB 567)" and "Mechanisms and Evolution of Arthropod Behavior (554)". We expect enthusiasm for cooperation in interdisciplinary research, the willingness to participate in the graduate school of life sciences, and involvement in the academic administration.

Qualified applicants should hold a Ph.D., have experience in lecturing and teaching at the university level, and have completed the German "Habilitation" or have an equivalent qualification, e.g. by having been a junior group leader.

Applicants should not be older than 52 years at the moment of the actual acceptance of the professorship (apart from exceptional cases allowed by Bavarian Law (Art. 10 Abs. 3 Satz 2 BayHSchPG).

The University of Würzburg wants to increase the proportion of women in the academic staff and thus explicitly encourages women to apply for this position. At other qualification being similar, handicapped persons will be preferentially hired. Detailed instructions for applications and electronic submission can be found on our website (http://www.dekanat.biozentrum.uni-wuerzburg.de). Please submit applications as hardcopy and electronically **by May 9, 2008** to:

Dekan der Fakultät für Biologie
Biozentrum, Am Hubland, 97074 Würzburg

W128490A

徳島大学大学院ヘルスバイオサイエンス研究部
代謝栄養学分野　研究員募集

下記のテーマに沿って研究および教育を行っていただける人を若干名募集します。

（A）腸管病原性細菌の病原性発揮機構について
（B）微生物の殺菌システムの開発

毎年更新、2年まで、状況によりさらに継続の可能性あり。決定次第できるだけ早くの着任希望。応募者には個別に連絡します。

書類提出先・問い合わせ先
〒770-8503 徳島県徳島市蔵本町3−18−15
徳島大学大学院ヘルスバイオサイエンス研究部
生体システム栄養科学部門医療栄養科学講座、代謝栄養学分野　高橋 章
Tel. +81-88-633-9249　Fax. +81-88-633-7113
E-mail. akiratak@nutr.med.tokushima-u.ac.jp

JP128315A

POSTDOCTORAL RESEARCH SCIENTIST

(Ref 01/04/08)

Applications are invited for a Postdoctoral Research Scientist position in the area of bacterial genomics, proteomics and molecular pathogenesis. The appointee is expected to apply innovative "omics" approaches to the analyses of significant bacterial pathogens, preferably but not exclusively in the area of foodborne pathogens, principally *Campylobacter*. Applications from candidates with expertise in relevant zoonotic, human or animal pathogens are welcome. The appointee will progress an innovative research topic and will be expected to collaborate with colleagues within and out with the Institute.

Salary – circa £25,400

For application details and further information please visit www.moredun.org.uk or telephone +44 (0) 131 445 5111

Closing date for applications: 18 April 2008.

Moredun

U128651A

NETHERLANDS INSTITUTE FOR NEUROSCIENCE

The Netherlands Institute for Neuroscience (NIN) is an institute of the Royal Netherlands Academy of Arts and Sciences (KNAW). Its main activity is fundamental and strategic scientific research in the field of the neurosciences, with an emphasis on brain research and research of the visual system.

Within the Dept. Retinal Signal Processing, headed by Prof. Dr. M. Kamermans, positions are available for

Postdocs in visual neuroscience

The projects include: 1) Mechanism and function of lateral inhibition in the outer retina; 2) Contribution of outer retinal lateral inhibition to the surround responses of ganglion cells and the visual performance of the whole animal; 3) Information coding in the outer retina and its consequences for color vision; and 4) The role of connexins and pannexins in retinal processing.

The lab is strongly multidisciplinary and has a background in electrophysiology, morphology, molecular biology, computational modeling and behavioral essays. The group makes extensive use of the wild-type and transgenic zebrafish.

Candidates with expertise in patch clamping, two-photon imaging or zebrafish genetics are strongly encouraged to apply. Knowledge of the visual system is highly appreciated.

The postdoc positions involve a temporary appointment for 4 years.

To apply, please send application letter, CV and two letters of recommendation, before

1 May 2008, to:

Prof. Dr. M. Kamermans
The Netherlands Institute for Neuroscience
Dept. Retinal Signal Processing
Meibergdreef 47
1105 BA AMSTERDAM
The Netherlands
Phone. +31 20 5665180
Email: m.kamermans@nin.knaw.nl
Webpage: www.nin.knaw.nl/~kamermans

W128331A

MANCHESTER
1824

The University of Manchester

www.manchester.ac.uk/jobs

Faculty of Medical and Human Sciences

School of Clinical and Laboratory Sciences

Research Associate

(Ref MHS/80227)

Salary £26,666 p.a.

We seek an enthusiastic individual to study the roles of Rac kinases in cardiac electrical and contractile functions using a model in which this enzyme is specifically deleted in cardiomyocytes.

You will be highly motivated with a PhD or equivalent in molecular biology, biochemistry, physiology or pharmacology. A research background in cell signalling and/or cardiovascular biology is desired as is competence in the use of transgenic models and in vivo techniques.

You will join a large, dynamic community of cardiovascular scientists with modern well-equipped facilities for the measurement of the physiology and molecular biology of cardiac function.

The post is tenable from 1 June 2008 for 3 years.

Informal enquiries may be addressed to: Dr. Ming Lei, Tel: 0161 275 1194 E-mail: ming.lei@manchester.ac.uk or Dr. Xin Wang, Tel: 0161 275 5516, Email: xin.wang@manchester.ac.uk or Dr. Elizabeth Cartwright, Tel: 0161 275 1629, Email: elizabeth.j.cartwright@manchester.ac.uk

Application forms and further particulars can be obtained at www.manchester.ac.uk/news/vacancies. If you are unable to go online you can request a hard copy of the details from Barbara Milnes, Tel: +44-161-275-1190. E-mail: barbara.milnes@manchester.ac.uk.

Closing date: 11 April 2008. Please quote reference MHS/80227.

The University will actively foster a culture of inclusion and diversity and will seek to achieve true equality of opportunity for all members of its community.

U128671A

TOXICOLOGY UNIT

Three Career Development Fellowships - Mechanisms of Neuronal Apoptosis and Neurodegeneration

MRC Medical Research Council

The Medical Research Council Toxicology Unit, a leading research centre for mechanisms of cell injury and death directed by Pierluigi Nicotera, invites applications from highly motivated scientists to work on the following project areas:

Ref: TOX08/150 Molecular mechanism of mitochondrial dysfunction in neurodegeneration using *Drosophila* models and mammalian neuronal culture systems.

Ref: TOX08/151 The implications of mitochondrial DNA damage and autophagy on synaptic plasticity and survival of central neurons.

Ref: TOX08/152 The role and functions of p73 and p63 in neuronal degeneration, with emphasis on the control of cell death and mitochondrial function.

These are three-year training and development positions for recently graduated postdoctoral scientists or those wishing to move into a new research discipline. Experience of molecular and cell biology techniques is essential. The Toxicology Unit, located at the University of Leicester, has multidisciplinary programmes in apoptosis, cancer and neurodegeneration with state-of-the-art facilities for cell imaging, genomics and proteomics. The minimum starting salary will be from £25,368 per annum.

For further information about these vacancies and research programmes please visit http://www.le.ac.uk/mrctox/

Applications must be made online at http://jobs.mrc.ac.uk inputting the relevant reference. If you do not have internet access or experience technical difficulties please call 01793 301257.

Closing date for applications: 24th April 2008

U128653R

Universität Karlsruhe (TH)
Forschungsuniversität · gegründet 1825

KIT Karlsruhe Institute of Technology

The University of Karlsruhe (TH) and the Research Centre Karlsruhe have recently merged to the **Karlsruhe Institute of Technology (KIT)** and are jointly planning their future research strategies. The Faculty of Chemistry and Life Sciences at the University of Karlsruhe (TH) has an immediate opening for a

W3-Professorship for Organic Chemistry

(successor for Prof. Dr. Dr. Richert)

We are in search of a highly reputed scientist who is able to represent the entire field of Organic Chemistry in research and teaching. The future colleague should be engaged in a modern topic of Organic Chemistry to complement the existing research areas at the institute and KIT. She/He is invited to actively participate in local graduate schools and research networks such as the Centre for Functional Nanostructures (CFN).

The teaching responsibilities of the professor encompass her/his comprehensive participation in ongoing and new study courses, including English and interdisciplinary syllabuses (e. g. in "Chemical Biology").

Applicants are expected to have gained a "Habilitation" or equivalent scientific qualifications.

The university is an equal opportunity employer and encourages applications from qualified females.
Handycapped persons will be preferentially considered when equally qualified.

Conditions of employment are regulated by § 47 of the Federal State law for universities in Baden-Württemberg.

Applications including the usual documents, a resumé of previous and planned research and teaching activities, as well as reprints of the 5 most relevant publications, should be submitted **by May 15th 2008** to the **University of Karlsruhe (TH), Dean of the Faculty of Chemistry and Life Science, 76131 Karlsruhe, Germany.**

W128679R

Post Doctoral Fellow

MRC National Institute for Medical Research

Situated in Mill Hill, North West London, NIMR is the largest MRC institute, supporting some 70 research groups and 500 bench scientists. The institute provides excellent training for researchers in a multi-disciplinary environment and is equipped with state of the art facilities. http://www.nimr.mrc.ac.uk/employment/

Division of Mathematical Biology- 3 year fixed term position

We are offering a 3 year MRC funded Career Development Fellowship. The project will focus on computational approaches for the analysis and prediction of protein structure. It will involve applying these methods to proteins of biomedical interest and also to protein design.

You should have a PhD, preferably in a bioinformatics related subject with knowledge of protein structure and ideally experience in protein structure prediction or design. Good programming skills are expected preferably with a knowledge of C and perl.

For informal enquires please contact Dr Willie Taylor Tel: 0208 816 2298 or email wtaylor@nimr.mrc.ac.uk

Starting salary range is from £26,808 - £32,488 per annum inclusive of Location Allowance. MRC final salary Pension Scheme is available.

Applications for this role should be made online at http://jobs.mrc.ac.uk. If you do not have internet access or you experience technical difficulties please call 01793 301157 quoting reference **NIMR08/165.**

The closing date is **24 April 2008.**

The MRC is an Equal Opportunities Employer

U128652R

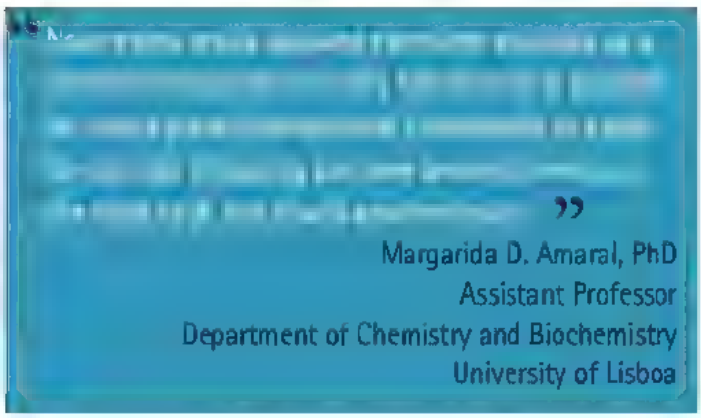

Technische Universität München

The Faculty of Life and Food Sciences at Freising-Weihenstephan invites applications for a

Full Professor (W3) of Animal Nutrition

The person filling this position should represent the field of Animal Nutrition in teaching and research at an internationally approved standard. In research, the candidate is expected to place an emphasis on molecular nutrition physiology and performance physiology of animals used for food production. Based on this knowledge, modern concepts of Animal Nutrition should be developed which allow for the production of healthy food of animal origin. In teaching, the whole spectrum of the nutrition of farm animals must be presented. The successful candidate will primarily teach in the Bachelor study program "Land Use (Agricultural and Horticultural Science)" and in the Master study program "Agricultural Science". Participation in other biological courses of the Technische Universität München is required.
Preconditions for employment as a professor are: successful completion of academic studies at an institute of higher education, pedagogical aptitude, Ph.D./doctorate and postdoctoral lecturing qualification or certification of an equivalent academic achievement, which may also have been obtained outside an university environment. At the time of appointment, applicants should not be older than 52 years. Under certain circumstances the age limit may be lifted (see Art. 12 (3) sentence 2 BayHSchlG). In case of equal eligibility, preferential consideration will be given to disabled candidates.
The TUM is striving to increase the proportion of women in research and education and thus expressly invites qualified female scientists to apply for this position.
Applications with the usual supporting information (CV, list of publications, copies of the most important papers, testimonials, certificates, etc.) should be submitted by **April 30, 2008** to:

Dekan der Fakultät Wissenschaftszentrum für Ernährung, Landnutzung und Umwelt,
Alte Akademie 8, 85354 Freising-Weihenstephan, Germany

W128511R

The University of Edinburgh is an exciting vibrant, research-led academic community offering opportunities to work with leading international academics whose visions are shaping tomorrow's world.

MRC and University of Edinburgh Centre for Regenerative Medicine

The MRC Centre for Regenerative Medicine at the University of Edinburgh (www.scrm.ed.ac.uk) is a new initiative supported by major investment from Scottish Enterprise, Scottish Funding Council, and MRC. Our focus is the fundamental biology of stem cells and tissue regeneration and related translational/clinical research.

We are actively recruiting internationally competitive groups investigating the properties and potentials of vertebrate stem and progenitor cells, to complement our existing strengths. We are interested in applications from researchers active in both basic biology and translational areas, including technology development.

We currently have openings, supported by the University and other funding bodies, available at all career stages from Career Development Fellow to Chair.

For informal enquiries, please contact Professor Sir Ian Wilmut (ian.wilmut@ed.ac.uk), Professor Charles ffrench-Constant (cffc@ed.ac.uk) or Professor Claus Nerlov (Nerlov@embl.it), c/o MRC Centre for Regenerative Medicine, University of Edinburgh, Chancellor's Building, 49 Little France Crescent, Edinburgh EH16 4SB. Tel. +44 131 242 6630. Fax: +44 131 242 6629. E-mail: scrm@ed.ac.uk

Closing date: 31 May 2008

Committed to Equality and Diversity

J128666R

MANCHESTER 1824

The University of Manchester

www.manchester.ac.uk/jobs

Faculty of Life Sciences

Post Doctoral Research Associate in Breast Cancer Research

(Ref LS/80203)

£26,666 - £32,796 per annum

You will join the Welcome Trust Centre for Cell-Matrix Research and the Manchester Breast Centre. The project is part of ongoing programme of research that aims to determine how Focal Adhesion Kinase regulates mammary gland biology and breast cancer.

You should hold (or expect to obtain shortly) a PhD in a relevant subject. The position would suit a molecular or cell biologist with relevant experience, preferably in the area of cell signalling and cancer.

The position is funded by the Breast Cancer Campaign for up to three years.

Informal enquiries may be addressed to: Dr Andrew Gilmore +44 (0)161 275 3892 Email: agilmore@manchester.ac.uk, or to Professor Charles Streuli, Tel: +44 (0)161 275 5626 Email: charles.streuli@manchester.ac.uk

Application forms and further particulars can be obtained at www.man.ac.uk/news/vacancies or from The Directorate of Human Resources. Tel: ++44 (0) 161 275 8836 Email: Lifesciences-hr@manchester.ac.uk

The closing date for applications is 11 April 2008. Please quote reference LS/80203.

The University will actively foster a culture of inclusion and diversity and will seek to achieve true equality of opportunity for all members of its community

J128648R

INTERNATIONAL PhD PROGRAM

MOLECULAR BIOLOGY OF CANCER AND INFECTION / ISREC – GHI

FALL SESSION 2008

LAUSANNE – SWITZERLAND

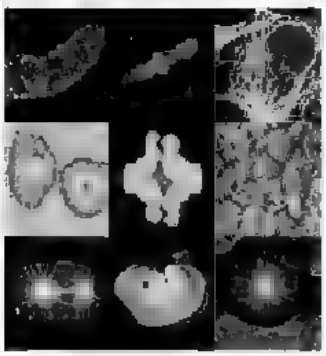

APPLICATION DEADLINE JUNE 1ST, 2008

WWW.INTERNATIONAL-PHD.CH / OFFICIAL LANGUAGE IS ENGLISH

ÉCOLE POLYTECHNIQUE FÉDÉRALE DE LAUSANNE

EPFL (ECOLE POLYTECHNIQUE FÉDÉRALE DE LAUSANNE)
SCHOOL OF LIFE SCIENCES
ISREC (SWISS INSTITUTE FOR EXPERIMENTAL CANCER RESEARCH)
GHI (GLOBAL HEALTH INSTITUTE)

W128113R

UNIVERSITY OF DELHI

Advt. No.: Estab-IV/201/2008 **Dated: 12th March, 2008**

Applications are invited in the prescribed form for the teaching positions in the following Departments of the Faculties of Science and Mathematical Sciences The last date for submission of application is 21-4-2008.

Faculties/Departments	No. of Vacancies							
	P	R	L					RA
			TOTAL	SC	ST	OBC	UR	
Faculty of Science								
Anthropology	1	1	5	2	1	1	1	-
Dr B.R. Ambedkar Centre for Biomedical Research	1	-	2	-	1	-	1	-
Botany	6 P/R		-	-	-	-	-	-
Centre for Hill Environment	-	1	3	1	-	1	1	-
Chemistry	6	5	3	-	2	1	-	2
Centre for Professional Development and Higher Education	-	1	-	-	-	-	-	-
Environmental Biology	-	-	2	1	-	-	1	-
Geology	1 P/R		2	-	-	-	2	1
Physics & Astrophysics	2	6	4	1	1	2	-	-
Zoology	7	3	1	-	1	-	-	-
Faculty of Mathematical Sciences								
Computer Science	1	-	1	1	-	-	-	-
Mathematics	1	1	2	-	1	-	1	-
Operational Research	-	3	2	1	-	-	1	-
Statistics	2	1	1	-	-	-	1	-

P – Professor, R – Reader, L – Lecturer, RA – Research Associate
SC – Scheduled Caste, ST – Scheduled Tribe, OBC – Other Backward Class, UR–Unreserved.

For further details regarding scale of pay, Essential Qualifications (Annexure-I), Special/ Desirable Qualifications (Annexure-II), and application form, please see Delhi University website www.du.ac.in OR contact Estab-IV, Room No.205, New Administrative Block, University of Delhi, Delhi – 110007, INDIA, Ph.– +91 11 2766 2021, e-mail : estabiv@yahoo.co.in

REGISTRAR

RW128775R

University of Reading

www.reading.ac.uk/jobs

Reader/Senior Lecturer in Palaeoecology

School of Human & Environmental Sciences

This appointment is full-time, permanent and starts on 1 September 2008
Grade 8 – £42,791 to £48,161 per annum

A Reader/Senior Lecturer in Palaeoecology is required to expand the range of teaching and research excellence within Environmental Archaeology, Quaternary Science and Physical Geography.

We are especially interested in candidates with an expertise in palynology, but are willing to consider those with other palaeoecological specialisms. We are seeking a candidate with an excellent track record of research, an ability to convene the NERC funded MSc Geoarchaeology and who can contribute to the School's enterprise agenda.

You will have:

- an excellent track record of securing research funding and project completion
- extensive experience of teaching palaeoecology at undergraduate and postgraduate level
- a track record of PhD student recruitment and supervision
- ideally, experience of academic management and leadership or the potential to provide these
- ideally, experience of enterprise activity or the potential to contribute to such activity within the School
- ideally, experience of inter-disciplinary research, or the potential to engage in such activity within the School

The University provides excellent opportunities for further training within its Centre for Staff Development

Informal enquiries: contact the Head of School, Professor Steven Mithen on +44 (0)118 378 6102 or email s.j.mithen@reading.ac.uk alternatively, contact the Director of Laboratories, Professor Martin Bell or +44 (0)118 378 7724 or email m.g.bell@reading.ac.uk

Closing date: 25 April 2008
Interview date: 3 June 2008

Further information and application forms are available at www.reading.ac.uk/jobs, or from:
Human Resources, University of Reading, Whiteknights, PO Box 217, Reading RG6 6AH,
Telephone +44 (0)118 378 6771 (voicemail)

Please quote reference number RD08001

We value a diverse workforce and welcome applications from all sections of the community

The Queen's Anniversary Prizes 2005

U128776R

UNIVERSITY OF BIRMINGHAM

The University of Nottingham

Midlands Ultracold Atom Research Centre

midlands physics alliance

Lecturers (Four posts)

Experimental cold atom physics

£30,012 - £40,335 pa

Salary can progress to £46,759 per annum, subject to performance

For more details and/or to apply on-line please access:

The University of Nottingham
http://jobs.nottingham.ac.uk/CJ254115
Please quote ref. CJ/254115
Tel: 0115 951 3262/Fax: 0115 951 5205

University of Birmingham
http://www.punit.bham.ac.uk/vacancies/
Please quote ref. S43262
Tel. 0121 414 2931/Fax: 0121 414 4802

Closing date: 30 April 2008.

U128774R

http://jobs.nottingham.ac.uk

Friedrich-Alexander-University of Erlangen-Nuremberg, Germany

The Faculty of Natural Sciences invites applications for a tenured

W3-Professorship for Bioinorganic Chemistry (chair)

in the Department of Chemistry and Pharmacy.

The newly established chair of bioinorganic chemistry is expected to adequately represent both research and teaching functions. The main research focus should lie on bioinorganic chemistry. A matter of particular interest are mechanistical studies on the activation of small molecules by biomimetic catalysts as well as model systems. A collaboration with the SFB 583 "Redoxaktive Metallkomplexe – Redox Active Metal Complexes" will be required.

Qualifications include university undergraduate and doctoral degrees, good teaching skills, and a habilitation or equivalent other qualification, which may have been gained outside the University or within a "Junior Professorship".

At the time of appointment the candidate must not be older than 52 years of age. The Ministry for Science, Research and Art may allow an exception in special cases, which has to be approved by the Ministry of Finance.

The University of Erlangen-Nuremberg actively encourages applications from female candidates in an effort to increase female representation in research and teaching.

Applications from the severly disabled having the same suitability for appointment as other candidates will be given priority.

The position is to be filled as soon as possible.

Application documents (curriculum vitae, photograph, list of publications and teaching activities, certified copies of degree certificates but no publications) and a brief statement of research interests must be sent by the latest **April 24, 2008** to Dekan der Naturwissenschaftlichen Fakultät der Universität Erlangen-Nürnberg, Universitätsstr 40, 91054 Erlangen, Germany

Friedrich-Alexander-Universität Erlangen-Nürnberg

www.uni-erlangen.de

W128780R

MAX-PLANCK-GESELLSCHAFT

The **Max Planck Institute for Immunobiology** in Freiburg, Germany, offers a

Postdoctoral Position

which is for an initial two-years appointment with the possibility of extension. The position is available in the Department of Molecular Embryology (Head: R. Kemler).

The research activities of the department focus on **E-cadherin**-mediated cell adhesion and on **Wnt/β-catenin** signaling in mouse embryonic development (http://www.immunbio.mpg.de)

Candidates with experience in these research areas will be at an advantage. Profound knowledge in protein biochemistry, cell and molecular biology, as well as in mouse developmental biology is required.

Payment will be a postdoctoral fellowship of the Max-Planck Society.

Women are especially encouraged to apply and handicapped applicants with equal qualification will be given preferential treatment. A childcare facility is attached to the Institute. Scientific business at the Institute is carried out in English.

Applications (by e-mail) should include a curriculum vitae with names of three references and a list of publications

Max Planck Institute for Immunobiology, Personnel Department
Stübeweg 51, 79108 Freiburg, Germany
or weigold@immunbio.mpg.de

W128726R

Applications will be accepted until **June 30, 2008.**

For further information please contact Prof. Dr. Rolf Kemler (Phone: +49-761-5108-471; Fax: +49-761-5108-474, e-mail: kemler@immunbio.mpg.de).

The Source Event

London 26/09/2008

[redacted]

www.source-event.com

UNIVERSITY OF KONSTANZ

The University of Konstanz is one of nine top-level universities identified by the Excellence Initiative in Germany. The Zukunftskolleg is a central scientific institution of the University of Konstanz for the promotion of young scientists in the natural sciences, humanities, and social sciences and is an integral component of the institutional strategy »Modell Konstanz – towards a culture of creativity«. The Zukunftskolleg forms a platform for interdisciplinary discourse between excellent researchers in Germany and abroad and provides young scientists with resources for obtaining third party funding.

The Zukunftskolleg of the University of Konstanz offers

5 research positions
(salary bracket 14 or 15 TV-L)

for the development and implementation of individual research projects/research groups. The initial appointments will commence on October 1, 2008 and end on March 31, 2010. An extension for an additional 3.5 years is foreseen, provided that external third party funding has been granted.

The Zukunftskolleg provides a professional infrastructure and an appropriate workplace for conducting research. A pool for funding cooperative projects, research assistants, research trips and the acquisition of equipment is available. Additionally, fellows may nominate recognized experts in their field of research as senior fellows, who will be invited to Konstanz for a period of 3–12 months and who, in addition to their research work and involvement in cooperative projects, will advise young scientists belonging to the Zukunftskolleg.

The prerequisites for acceptance are a doctoral degree and outstanding scientific qualification as documented by research activities and publications. International experience in teaching or research and a strong interest in interdisciplinary topics are desirable. Each fellow is a member of both a department of the university and the Zukunftskolleg. Involvement in teaching is possible. The foreseen topical connection of the project to the research profile of the University of Konstanz should be demonstrated in the project outline. Active participation in the regular weekly meetings of the Zukunftskolleg as well as residence in Konstanz is expected.

The selection of the fellows will be made on the basis of the project outlines and a two day workshop to be held on September 1-2, 2008 at the University of Konstanz.

Information about the fellowships and additional opportunities for participation in the Zukunftskolleg can be found on our website:
http://www.uni-konstanz.de/zukunftskolleg

The full version of this announcement is available at:
http://www.uni-konstanz.de/stellen

Applicants should send their application form (see www.uni-konstanz.de/zukunftskolleg), their project outline (maximum length 6 pages), a letter of motivation (one page), application documents (curriculum vitae, publication list, and degree certificates) and a reading excerpt (maximum length 20 pages) as PDF file to: zukunftskolleg@uni-konstanz.de

Application deadline: May 31, 2008

W128680A

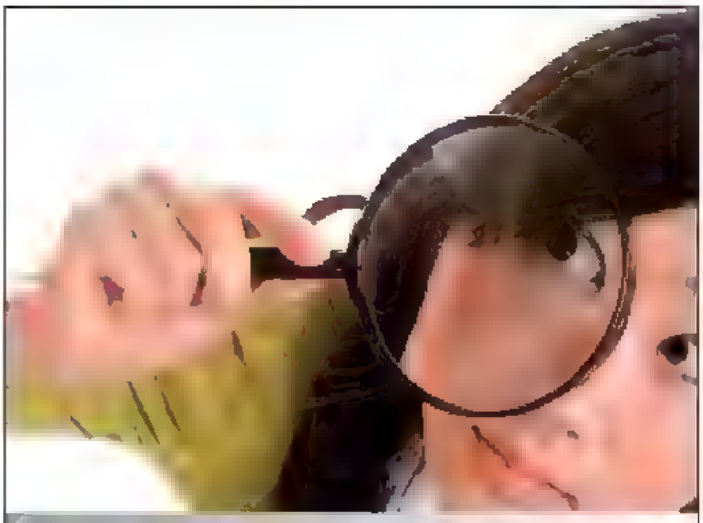

The Remedios Caro Almela Prize for Research in Developmental Neurobiology

YEAR 2008

AN UNRESTRICTED AWARD OF 18.000€ FOR A EUROPEAN INVESTIGATOR WORKING IN DEVELOPMENTAL NEUROBIOLOGY, WHO IS PRESENTLY IN A HIGHLY PRODUCTIVE PERIOD OF HIS/HER SCIENTIFIC CAREER

Application: prizerca@umh.es
Deadline: June 30th, 2008
Information: www.ina.umh.es

CSIC

W125296A

Brain Bank Tender

As part of our continuing commitment to build research capacity related to Parkinson's and multiple sclerosis, the Parkinson's Disease Society (PDS) and Multiple Sclerosis (MS) Society are inviting Expressions of Interest to host a brain bank. Researchers may apply to host a joint PDS/MS Society brain bank, a PDS brain bank only or a MS Society brain bank only. Multiple applications are permitted. The grant is for five years and tenable at a UK institution only.

The Specification Sheet and Expression of Interest form may be obtained from www.parkinsons.org.uk or www.mssociety.org.uk or by emailing research@parkinsons.org.uk

Closing date: Friday 25 April 2008

Parkinson's Disease Society of the United Kingdom. Charity registered in England and Wales No. 258197 and in Scotland No. SCO37554

The MS Society is charity registered No. 207495.

Multiple Sclerosis Society

Parkinson's Disease Society

U128728A

HOWARD HUGHES MEDICAL INSTITUTE

HHMI Seeks Early Career Scientists

The Howard Hughes Medical Institute invites applications from highly promising scientists from the full range of disciplines relevant to biological and medical inquiry who have led independent laboratories for two to six years. HHMI will provide flexible research support to as many as 70 individuals.

Eligibility

- Tenure-track or equivalent position at an eligible U.S. institution with a rank of assistant professor or higher
- Two to six years of experience since first appointment as an assistant professor or equivalent

Candidates must indicate their intent to apply before submitting an application.

Deadline for intent to apply:
April 30, 2008, at 2:00 p.m. ET

Application deadline:
June 10, 2008, at 2:00 p.m. ET

Intent to apply and application:
www.hhmi.org/earlycareer2009/nat

The HHMI Early Career Scientist Program comes at a critical time for the nation and the long-term health of its research infrastructure. The initiative reflects HHMI's view that the constrained funding environment has inhibited the ability of highly creative academic scientists to establish and develop their research programs.

HHMI will select up to 70 early career scientists who have led laboratories for two to six years at one of the approximately 200 U.S. medical schools, universities, and research institutes that are eligible for this competition. Early career scientists will receive nonrenewable six-year appointments to HHMI and substantial research support while remaining affiliated with their home institutions. Candidates must apply directly to HHMI.

HHMI, a nonprofit medical research organization, plays a powerful role in advancing biomedical research and education in the United States. HHMI's flagship program in biomedical research rests on the conviction that scientists of exceptional talent, commitment, and imagination will make fundamental biological discoveries for the betterment of human health if they receive the resources, time, and freedom to pursue challenging questions.

The Howard Hughes Medical Institute is an equal opportunity employer.

HHMI
HOWARD HUGHES MEDICAL INSTITUTE

NW125713R

COURSES AND CONFERENCES

wellcome trust

COURSES AND CONFERENCE PROGRAMMES

Genetics...illuminated.

2008 Courses, Workshops, and Meetings (subject to change)

Jan. 26-Jan. 27	13th Annual Maine State Symposium on Osteoporosis, Sugarloaf USA*
Feb. 12, 13, 14, 15	Advanced Surgical Techniques in Mice: Jugular Vein & Carotid Artery Cannulations, Scripps Research Institute, La Jolla, California
Feb. 17-Feb. 19	Colony Management: Principles and Practices, Scripps Research Institute, La Jolla, California
April 20-April 25	Workshop on Surgical Techniques in the Laboratory Mouse
April 25-April 26	34th Maine Biological and Medical Sciences Symposium, Mount Desert Island Biological Laboratory
April 30-May 2	Workshop on Shipping and Reconstitution of Cryopreserved Embryos
May 4-May 9	Workshop on Cryopreservation of Mouse Germplasm
May 16-May 18	Colony Management: Principles and Practices, University of North Carolina, Chapel Hill
May 27-May 29	Discovery Strategies Conference: Modeling Human Autoimmune Diseases in the Laboratory Rodent, Mission Bay Conference Center, UCSF, San Francisco*
June 22-26	Comprehensive Approaches to the *in vivo* Assessment of Cardiovascular Function*
June 30-July 3	Frontiers in Microscopy: Whole Animal Imaging
July 20-Aug. 1	49th Annual Short Course in Medical and Experimental Mammalian Genetics*
Aug. 22-Aug. 31	17th Annual Short Course on Experimental Models of Human Cancer*
Sept. 2-Sept. 4	Genetic Basis of Work-Related Disease: Science, Ethics, and Policy*
Sept. 4-Sept. 12	Genomic and Proteomic Approaches to Complex Heart, Lung, Blood, & Sleep Disorders*
Sept. 15-Sept. 19	Phenotyping Mouse Models of Human Lung Disease*
Sept. 19-Sept. 21	The Mouse as an Instrument for Ear Research III*
Sept. 21-Sept. 27	7th Annual Workshop on the Pathology of Mouse Models for Human Disease, Cornell University College of Veterinary Medicine, Ithaca, New York*
Sept. 23-Sept. 29	Short Course on Systems Genetics
Oct. 15-Oct. 18	Methods in Human Embryonic Stem Cell Research
Oct. 26-Oct. 30	Workshop on Surgical Techniques in the Laboratory Mouse
Nov. 16-Nov. 20	Colony Management: Principles and Practice

All events are held at The Jackson Laboratory in Bar Harbor, Maine unless otherwise specified. Details and updates available online www.jax.org/courses. Dates subject to change. *CME information pending.

The Jackson Laboratory

Leading the search for tomorrow's cures

600 Main Street
Bar Harbor, Maine 04609-1500
www.jax.org/courses
coursesandconferences@jax.org

MW124033E

An Emergence & Convergence mini-symposium
Multiple Sclerosis: From Pathogenesis to Therapy

Multiple sclerosis is an inflammatory autoimmune disease targeting the central nervous system, leading to demyelination and axon degeneration and to severe disability as the disease progresses. Multiple sclerosis presents as a clinically heterogeneous disease, which has been problematic for efforts to develop appropriate animal models. Many environmental and genet c factors have been identified that may initiate disease. Various immune and neural cells have been found to play key roles in disease pathogenesis and progression. This Emergence & Convergence mini-symposium will address open questions in multiple sclerosis research, with the goal of identifying future directions that may lead to therapy.

June 6, 2008
Espace Charles-Louis-Havas, Paris, France

CHAIR
Jean-François Bach
(Hôpital Necker, France)

SPEAKERS
Burkhard Becher
(Univeristy of Zurich, Switzerland)
Christian Confavreux
(Hôpital Neurologique Pierre Wertheimer, France)
Britta Engelhardt
(University of Bern, Switzerland)
Vijay Kuchroo
(Harvard Medical School, USA)
Roland Martin
[redacted]
Stephen Sawcer
(University of Cambridge, UK)
Kenneth J. Smith
(University College London, UK)
Larry Steinman
(Stanford University, USA)

ORGANIZERS
Eva Chmielnicki
(*Nature Medicine*, USA)
Laurie Dempsey
(*Nature Immunology*, USA)
Yves Christen
(Fondation IPSEN, France)

Application and Abstract Submission deadline: March 31, 2008

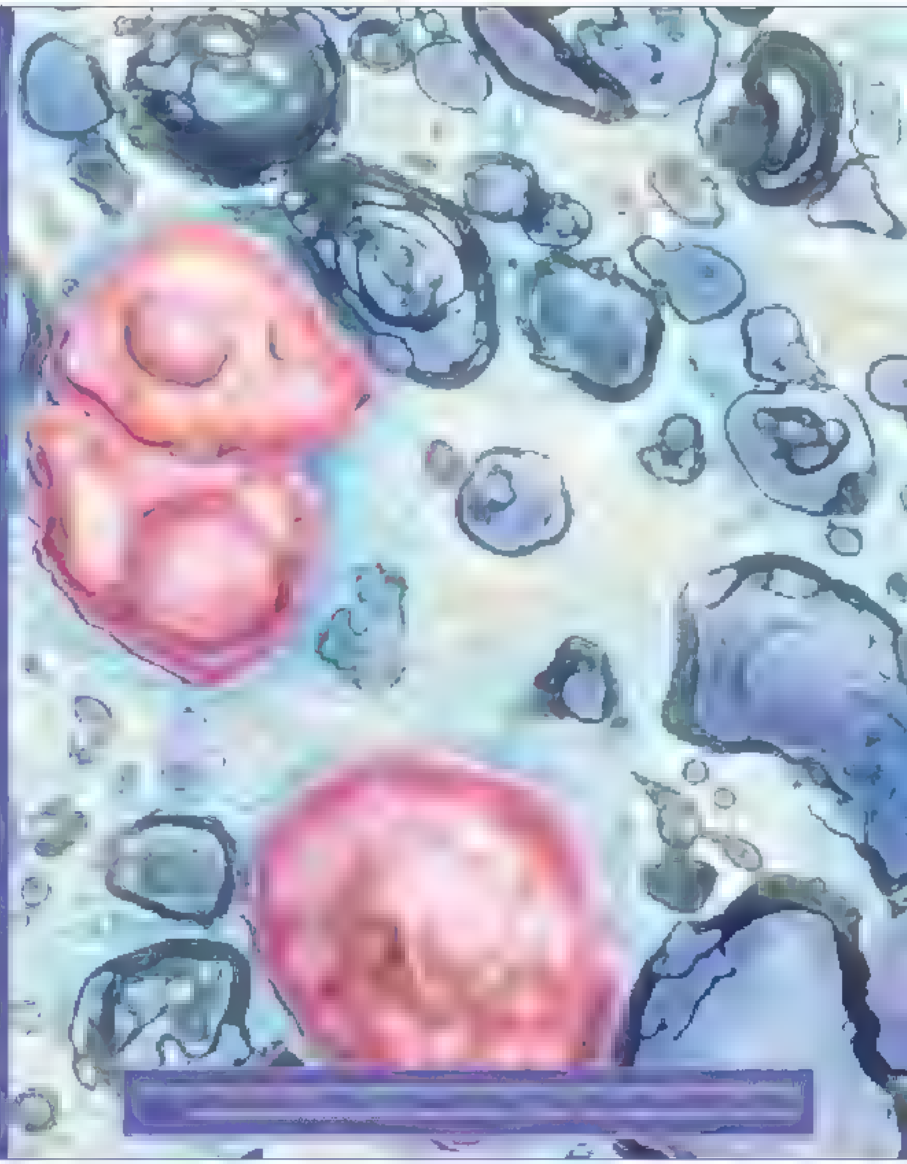

Attendance at this meeting is free on acceptance of application.
To apply and for more information visit **www.nature.com/natureconferences/eandc/MS**

nature conferences

FONDATION IPSEN

nature medicine

nature immunology

IN122209E

nature events

Directory 2008
get your free digital edition!

Events are essential for every scientist. From delegates discussing hot issues and opinion, through to networking and collaboration. Events provide a platform for learning and advancement.

With a burgeoning number of events across the globe, where can you find a complete resource to ensure you attend the right events in 2008?

The *Natureevents* Directory is published once a year and covers a complete range of scientific events, conferences and courses around the world.

Plan your year ahead, go to **www.natureevents.com** and download the digital edition of the 2008 *Natureevents* Directory for free.

If you are interested in advertising an event please call +44 (0)20 7014 4015
for US please call +1 800 989 7718 or email natureevents@nature com

www.natureevents.com

---

nature events

nature publishing group npg

Images courtesy of "SOHO (ESA & NASA)"

EUROPEAN SCIENCE FOUNDATION
SETTING SCIENCE AGENDAS FOR EUROPE

ESF RESEARCH CONFERENCES
2008 Programme now available!

The 2008 ESF Research Conference Programme is open for consultation at www.esf.org/conferences/2008

The ESF Research Conference Scheme (www.esf.org/conferences) provides European and international scientists, including young researchers, with an informal discussion framework in interactive, remote venues for exploring the latest developments in their areas of research. They promote synergy and the creation of new scientific communities on topics that range over all disciplines, from Physics to Humanities. Interdisciplinary approaches are encouraged as appropriate. ■ It develops principally through the establishment of long-term partnerships between the ESF and national and international organisations, including universities. ■ ESF Research Conferences are open to scientists world-wide, whether from academia or industry. Conferences generally last for four or five days and up to 150 participants and invited speakers may attend. ■ Closing date for applications: 3-4 months prior to a conference.

CALENDAR OF EVENTS

■ Quantum Optics: From Photons and Atoms to Molecules and Solid State Systems, Austria, 24 February - 1 March ■ Rare Diseases: Channels and Transporters, Spain, 8-12 March ■ Robotics: Experimental Cognitive Robotics, Japan, 9-15 March ■ Molecular Bioenergetics of Cyanobacteria: Towards Systems Biology Level of Understanding, Spain, 29 March - 3 April ■ Antiviral Applications of RNA Interference, Spain, 5-10 April ■ Systems Biology, Spain, 12-17 April ■ B Cells 2008: Complexity, Integration & Translation, Spain, 16-21 May ■ Natural Products Chemistry, Biology and Medicine, Italy, 18-23 May ■ High-Pressure Physics*, UK, 26 May - 6 June ■ The Transfer of Resources across Generations: Family, Income, Human Capital and Children's Wellbeing, Sweden, 9-13 June ■ Nanotechnology for Sustainable Energy, Austria, 14-19 June ■ Theory and Particle Physics: The LHC Perspective and Beyond*, France, 14-26 June ■ Operator Theory, Analysis and Mathematical Physics, Bedlewo, Poland, 15-22 June ■ Pharmacogenetics and Pharmacogenomics: Adverse Drug Reactions, Spain, 27 June - 2 July ■ Non-Commutative Harmonic Analysis with Applications to Probability, Bedlewo, Poland, 17-23 August ■ Imaging War: Intergenerational Perspectives, Sweden, 3-7 September ■ Reforming the European State System in the Long Eighteenth Century, Sweden, 10-14 September ■ Bacterial Networks, Spain, 13-18 September ■ Nanomedicine, Spain, 19-24 September ■ Systems Chemistry, Italy, 3-8 October ■ The Right of the City: Challenges to the State, Sweden, 11-15 October ■ New Challenges in Earthquake Dynamics: Observing and Modelling a Multi-Scale System, Austria, 18-23 October ■ Protein Design and Evolution for Biocatalysis, Spain, 25-30 October ■ Biobanks, Spain, 1-6 November ■ Chemical Control with Electrons and Photons, Austria, 22-27 November ■ 26th Jerusalem Winter School in Theoretical Physics: String Theory and LHC*, Israel, 29 December - 8 January

* ESF Summer/Winter Schools in Physics

For further information, please visit **www.esf.org/conferences** or send an email to **conferences@esf.org**
European Science Foundation | ESF Research Conferences
149 avenue Louise | Box 14 | 1050 Brussels | Belgium
Tel. +32 (0)2533 2020 | Fax: +32 (0)2538 8486
www.esf.org/conferences

W125439E

ISMB Institute of Structural Molecular Biology

'At the interface of Structural Biology, Chemical Biology, Bioinformatics and Biophysical Chemistry'

Institute of Structural Molecular Biology
3rd Symposium | 19 – 20 June 2008

The Institute of Structural Molecular Biology (ISMB) at UCL and Birkbeck is pleased to announce its 3rd international symposium.
It will be held on 19-20 June 2008 at University College London. We are delighted to announce the following programme:

Chemical Biology

Peter Seeberger	ETH Zürich, Switzerland
Stefan Howorka	University College London, UK
Tom Muir	The Rockefeller University, USA

Structural Biology

Stephen Harrison	Harvard University, USA
Neil McDonald	Birkbeck College London, UK
Marc Baldus	Max Planck Institute for Biophysical Chemistry, Germany

Biophysics/Proteomics

Ruedi Aebersold	ETH Zürich, Switzerland
Carlos Bustamante	University of California, Berkeley, USA
Peter Rich	University College London, UK

Bioinformatics

Peer Bork	EMBL, Germany
Irilenia Nobeli	Birkbeck College London, UK
Michael Sternberg	Imperial College, UK

Places for the Symposium are limited. If you would like to attend please send an email to Anne-Cécile Maffat by 16 May (ismb-admin@ismb.lon.ac.uk) to register and to receive further details. www.umb.lon.ac.uk/symposium2008.html

U128143E

The Annual Harvard/Paul F. Glenn
Symposium on Aging
June 23rd, 2008

Speakers:
Tom Rando (Stem Cells and Aging)
Gary Ruvkun (Energy Metabolism and Lifespan)
Scott Lowe (Senescence, heterochromatin and Aging)
Jan Vijg (DNA Damage as a Driver of Aging)
Heidi Tissenbaum (Fat & Lifespan regulation in *C elegans*)
Toren Finkel (Linking β-catenin and Aging)
Keith Blackwell (Skn-1 in Longevity and Stress Resistance)
and
Lenny Guarente (Chair of Discussion Panel)
with Richard Miller & David Sinclair on
"Is aging simply a collection of predictable diseases?"

Pre-Register online
www.hms.harvard.edu/agingresearch

The Joseph B. Martin Conference Center
New Research Building,
Harvard Medical School
Boston, Massachusetts, U.S.A.*

Further information contact: Susan_DeSisto@hms.harvard.edu, 1-(617)-432-3991. Harvard Medical School, All Rights Reserved
* 77 Avenue Louis Pasteur Ave, Boston, MA, USA, 02115

NW126724E

REPROGRAPHICS: CTT, London E17 6BU UK and Alden Multimedia, Northampton UK.
PRINTED BY: St. Ives Plymouth Ltd. UK; Publishers Press, Lebanon Junction, Ky, USA and Obun Printing Co Inc, Tokyo, Japan

Acting up

Never work with children or animals.

Elizabeth Counihan

To: lukas@dreamlightfilms.org
From: william@londonthesps.co.uk
4/1/2015 — 21:15 GMT

Hi Luke,
How's it going down there in sunny LA? Now you know me, Luke, I never moan, but I have some problems up here that I hope you can fix.

I'm not complaining about the shuttle sickness. My fault — should have taken a pill, but it was my first trip and we're not all old hands at weightless travel like you! And I wasn't the only one either.

Don't get me wrong. I love animals. I own two beautiful cats back in London. But that poor dog did throw up all over me just as I was getting used to the eating arrangements on the spacecraft. I noticed that Donita had two whole passenger bays to herself. I realize she's the star of the movie but Toto is her pet, so why did I have to share a back seat with him? I don't think he meant to bite me, not enough to draw blood anyway. Donita told me not to worry about rabies and blood poisoning as "Darling Toto has had all his shots as he travels everywhere with me". Then she asked me if I had had all mine, as she didn't want Toto to catch a cold from me! Like I said, I'm absolutely great with kids and animals. And Donita is so talented. I did admire her in *Space Orphans* — those big blue eyes! Wonderful how the camera just loves some people who look quite ordinary when you see them for real.

I was amazed to find so many tourists on the Moon, even with the new cheap shuttle flights. (I couldn't believe it — bungee jumping at 1/6th gee!) Donita was surrounded by fans. Well, I suppose she is still a 'child star', although she must be at least 15. But no time to sign autographs. Merle had us all packed into our trailers and out to the location before you could say "Cut"! Merle is a wonderful director, so enthusiastic, almost like someone directing their first feature film. I watched out of the trailer window, very happy to pick up tips on low-gravity acting from such an old hand as Donita. Toto looked so cute bouncing around in his pooch-suit!

By the time I was needed I was ready for a coffee break. But the show must go on! They put me in this crazy rubber outfit with an incorporated oxygen pack. I had quite a shock, Luke. I didn't realize I was expected to play a Moon tree! I told Merle the concept was ridiculous. Everyone knows there are no trees on the Moon. Merle was very short — told me to shut up and act! I told her I was a highly trained professional with years of experience and she said I was a pompous Brit! This is not what I'm used to. But I did as she said — bouncing about like a rubber ball with a lot of other 'trees'. I felt a complete idiot!

Donita sang one of the main numbers from the show, asking Toto to protect her, but we had to have several takes because Toto quite lost control and kept jumping around us like he was on springs. We all heard his yapping over the sound system. I think he took us for real trees.

In the evening I felt one of my migraines coming on, but they told me the studio doctor was attending Toto for 'a nervous breakdown', so I had to retire to bed without the benefit of medical help! It was disappointing to find I was room sharing with another tree — an absolute nobody on his first professional job. I had to complain. I do have my reputation to live up to. But apparently nothing could be done. Time pressure. The bottom line.

At least we were inside the complex for today's schedule, so no need for pressure suits. A dresser appeared and glued me into another rubber costume. This time I was supposed to be a Moon zombie, whatever that is.

I asked Merle why we couldn't stay on Earth and use CGI like in the good old days, and save the real actors for real acting. She looked at me like I was a cockroach and told me a) CGI technicians were a lot more expensive than rookie actors and old has-beens and b) there were great tax breaks for movie makers filming at the Moon colony and we had one week to complete the shoot, so would I kindly not waste any more of her time! I was most insulted and felt another headache coming on.

This evening I felt happier. We were, at last, able to meet our fans. Donita was surrounded by autograph hunters of course. Then a delightful elderly couple came up to me waving an autograph book. They had seen my Hamlet on tour with the Shakespeare Players years ago out in Canada. I had just found a pen when Toto came rushing up, barking furiously. He suddenly recognized me as a 'tree' and treated my leg like one. This time he wasn't wearing his pooch-suit. I was mortified! Hearing the fuss, Donita ran up and gave me a furious look as if it was my fault. So I was left there holding my pen while everyone had a good laugh!

Luke, this gig isn't quite what I thought I'd signed up to.

My tuxedo is ruined.

Best,
William

To: william@londonthesps.co.uk
From: lukas@dreaml.ghtfilms.org
4/1/2015 — 22:00 GMT

Hi William,
You're fired. Merle e-mailed me. She has found a dog-owning Greenpeace activist who's very happy to play a tree. I'll buy you a new tuxedo.

Best,
Luke ■

Elizabeth Counihan has had stories published in *Asimov's*, *Realms of Fantasy*, *Interzone* and several anthologies. She edits the British fantasy magazine *Scheherazade*. She used to be an NHS family doctor.

Image supplied by Genevac

Aiming high

The frontier of high-throughput screening technology

High-throughput screening (HTS) has been made feasible through advances in robotics and high-speed computer technology. While automation is an important element in HTS, the smaller elements such as plates and pipettes are also key to carrying out a successful assay. Today, drug development companies have the technology available to routinely screen hundreds of thousands of compounds per day, but researchers still face some challenges. These challenges lead to continued innovation and improvement in the products available.

Genomics and proteomics

Takara Bio's *e*2TAK DNA Polymerase is a novel, economical PCR enzyme which provides excellent product yield, sensitivity, and length (up to 8KB of human genomic DNA) for routine and high throughput PCR applications. *e*2TAK also possesses superior priming efficiency, resulting in reduced annealing times and lowered total reaction times. *e*2TAK can be substituted for standard Taq Polymerase in a variety of general PCR experiments, providing improved efficiency, speed and performance at reduced cost. *e*2TAK is supplied with buffer and high-purity dNTPs.

OriGene Technologies' Genome wide Full length cDNA (GFC) Transfection Array is an innovative tool for high-throughput gene screening of functional activity. GFC-Transfection arrays are a much quicker, easier and more comprehensive alternative to the traditional method of testing individual genes one by one. The arrays are multiwell plates with a standardised amount of a unique, expression-ready, full length cDNA clone in each well. Researchers can screen hundreds to thousand of genes by simply adding a transfection reagent and cultured cells before performing any number of functional, cell based assays. With over 30,000 full-length expression-ready cDNA clones available, OriGene offers a wide and customisable selection of GFC-Transfection arrays for nearly any application.

In collaboration with **BioTrove, Applied Biosystems** will develop and market custom built arrays of **TaqMan® SNP Genotyping Assays** pre-loaded on BioTrove's **OpenArrayT platform**. This platform will integrate the ease-of-use, accuracy, and reproducibility of Applied Biosystems' TaqMan SNP Genotyping Assays with BioTrove's flexible high-density assay format, enabling researchers to rapidly perform high-throughput genotyping studies at a lower total cost compared to alternative commercially available methods. The genotyping platform provides an extremely fast, high throughput screening and validation tool for researchers in agricultural, pharmaceutical, and other commercial industries, as well as academic institutions. "By streamlining researchers' genotyping workflows, we are accelerating the discovery and utilisation of science, impacting public health in many ways; from healthier foods to better healthcare." said Al Luderer, Ph.D., president and CEO of BioTrove, Inc.

Pronostics' disease screening platform **UltraPlex™ IMMUNOMICS** can be used to diagnose many different complex diseases in a single blood test. The platform comprises the Ultraplex™ assay, which is able to accurately screen many tens of assays simultaneously using a digitalised 'barcode' system, and the molecular profiling or 'biological fingerprinting' platform, Fingerprint™ IMMUNOMICS, which can

Pipet-Lite Adjustable Spacer Pipette from RAININ

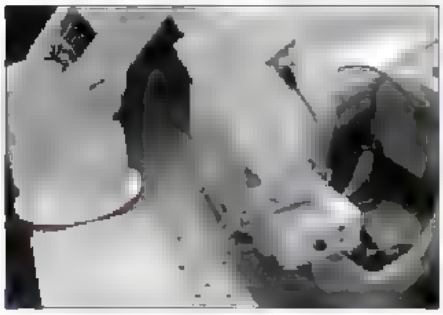

Beckman Coulter's Cell Lab Quanta SC MPL

cost-efficiently and rapidly generate biological profiles for any disease that causes a response from the immune system. Using its library of protein biomarkers, Pronostics is able to test for a number of diseases from a single drop of blood, providing a real-time immunological profile allowing rapid and inexpensive diagnosis. In addition, the Immunomics approach can be used to monitor the effects of therapeutic interventions, allowing treatment to be tailored depending upon the patient's immune response.

Cellular analysis

Beckman Coulter has integrated its **Cell Lab Quanta SC MPL** into a fully automated 'seed and feed' cell culture system. The integrated system provides data and cellular growth parameters for the evaluation of clone selection, cell expansion and protein expression results. The Quanta SC MPL is integrated online with other peripheral devices and a robotic arm that moves cell culture plates to the flow cytometer for analysis. Data from the analysis is automatically captured by the Quanta SC MPL's software for real-time and subsequent analysis and interpretation. The ability to integrate this advanced flow cytometer provides an expanded range of measurements for high throughput walkaway cell analyses, including measures such as cell count and viability, apoptosis, cell cycle and cell surface markers. These applications produce data which are valuable in monitoring and process optimisation during the drug discovery and development process.

Promega Corporation, recently launched its **CytoTox Glo Assay**. Whether monitoring chemical toxicity, anti-cancer drug efficacy or cytokine response, the CytoTox-Glo Assay provides a highly sensitive, simple, luminescent method that allows the user to detect small changes in cell viability. The assay measures a distinct 'dead-cell' protease biomarker released from cells that have lost membrane integrity, a key indicator of cytotoxicity. The assay uses a peptide substrate, that after cleavage by the 'dead-cell' protease, releases luciferin. This is a substrate for a proprietary thermostable luciferase (**Ultra-Glo™ Recombinant Luciferase**). The luciferase/luciferin reaction produces light in the form of a stable 'glow-type' luminescent signal. The intensity of the signal correlates with dead cell number. The CytoTox-Glo Assay has a large dynamic range with excellent linearity, providing unprecedented sensitivity in 96-well plates or high density formats. The high sensitivity and scalability minimises both the number of cells required and the amount of compound used. This results in reduced cell culture and compound costs.

Accessories

Genevac's HT-12 Series II systems are designed to provide the ideal solution for evaporation bottlenecks in high throughput and production laboratories. The versatile system offers options for integration into automated environments, for handling potentially explosive solvents and a version for use with strong acids. The HT-12's high performance and high sample capacity make it ideal for applications including fast lyophilisation, combinatorial chemistry, parallel synthesis, compound purification, plate re-formatting, and plate replication that require high throughput evaporation. The unique design of the HT 12 multi layer rotor ensures efficient use of valuable laboratory bench space as well as providing high performance and efficient evaporation. Incorporating the latest scroll pump technology, the HT-12 Series II does not require any pumping fluid or lubricant in order to operate which increases operational uptime and makes the system ideal for use in harsh chemistry environments.

Glen Spectra has introduced a new range of high throughput **QuantaMAX** filter sets, the latest in a long line of microscopy filter set innovations. QuantaMAX sets enable very weak fluorescence signals to be easily imaged and visualised. The QuantaMAX filters give the highest transmission and deepest blocking currently available in the marketplace resulting in the brightest image with the darkest contrast. Filter set performance and high throughput are a function, not just of peak transmission, but also of deep blocking. QuantaMAX provides extremely high signal-to-noise ratio, allowing very weak signals to be detected, a critical factor for confocal, multiphoton, live cell and in vivo applications where photons are scarce and exposure times critical. The use of state-of the-art Energetic Process coatings which are stable, mechanically robust and hygrophobic gives an extremely long life filter even in the harshest environments. Zero pixel shift is standard in these high performance sets. The multi-substrate construction provides protection from mechanical abrasion while maintaining the high wavefront integrity required in imaging applications.

RAININ's new Pipet-Lite® Adjustable Spacer Pipette allows fast format change for multi well plates.

Pipet-Lite Adjustable Spacer, the newest addition to RAININ's line of manual multichannel pipettes, lets the user easily and rapidly change nozzle spacing between 9-14 mm (8-channel) or 9-19mm (6-channel) to accommodate work processes involving different plate and tubing formats, e.g., microcentrifuge tubes, 24, 48, and 96-well plates. Precise cam-actuated spacing adjustment allows reproducible spacing at any point between maximum and minimum positions. The LTS® Tip Ejection System ensures correct tip sealing for consistent sample pick-up.

"By streamlining researchers' genotyping workflows, we are accelerating the discovery and utilisation of science, impacting public health in many ways; from healthier foods to better healthcare."

Al Lederer, Ph.D., president and CEO of BioTrove, Inc.

Companies listed in editorial:

Applied Biosystems - www.appliedbiosystems.com
Beckman Coulter - www.beckmancoulter.com
BioTrove - www.biotrove.com
Genevac - www.genevac.com
Glen Spectra - www.glenspectra.co.uk
OriGene Technologies - www.origene.com
Promega - www.promega.com
Pronostics - www.pro-nostics.com
Rainin - www.rainin.com
Takara Bio - www.takara-bio.com

NATURE|Vol 452|27 March 2008

THE CAREERS MAGAZINE FOR SCIENTISTS

- FOCUS
- SPOTLIGHT
- RECRUITMENT
- ANNOUNCEMENTS
- EVENTS

nature jobs

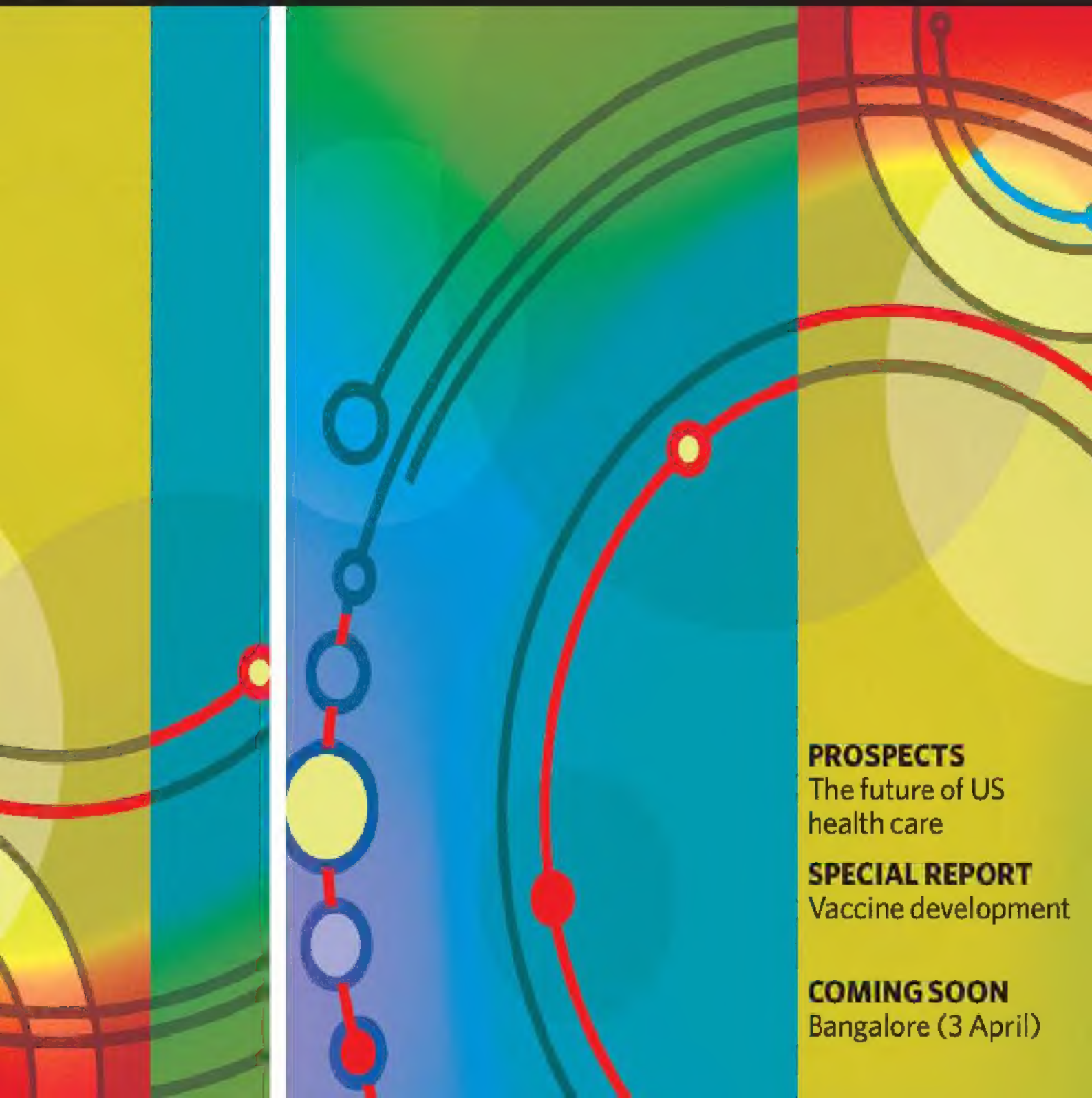

PROSPECTS
The future of US health care

SPECIAL REPORT
Vaccine development

COMING SOON
Bangalore (3 April)

ONE GREAT IDEA.
TWO PAGES TO FILL OUT.
$100,000 TO PROVE IT.

Grants available now to help solve some of the grand challenges in global health.

The Bill & Melinda Gates Foundation seeks novel ideas from every scientific discipline as part of its new grantmaking initiative.

Grand Challenges Explorations is an accelerated approach to grantmaking. We require only a short, two-page application, and no preliminary data.

We'll award grants multiple times per year at approximately $100,000 each, and provide additional funding of $1 million or more for projects that show promise.

The first round of proposals will be accepted through May 30, 2008.

Please visit www.gcgh.org/explorations for topics and complete application details.

Grand Challenges | EXPLORATIONS

NW127170R

25,000 Tagged ORF Clones

including the ones you want

TrueORF™

for tagged protein expression

TrueORF enables the expression of the encoded transcript as a C-terminally tagged protein with Myc and FLAG® epitopes, facilitating multiple applications that utilize an anti-tag antibody, such as protein detection, protein purification, subcellular localization, etc.

- Genome-wide coverage
- Sequence verified and guaranteed
- The C-terminal dual tag of Myc and FLAG®
- Transfection-ready: Provided as 10 ug of purified plasmid
- Easy shuttling into 20 tagged vectors using PrecisionShuttle™ system

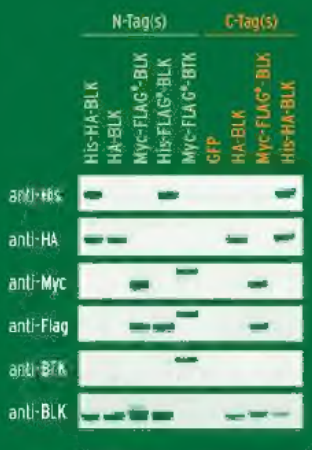

The Western blot analysis of HEK293 cell lysate over-expressing BLK or BTK tagged with indicated epitopes.

FLAG® is a registered trade mark of Sigma-Aldrich

ORIGENE
Your Gene Company

1-888-267-4436 • origene.com

Did you know

that one in ten people lives on an island?

And that Sigma-Aldrich is everywhere there's science.

Research projects today are often cooperative efforts of labs in several countries on different continents. Even if you're poles apart from your colleagues, our worldwide reach offers your entire team the same quality products and service 24/7. All our products share Sigma-Aldrich's core strengths of responsive technical service, content-rich Web site, customized Internet-based procurement solutions for your business staff – and our ability to deliver your products on time anywhere in the world.

SIGMA Life Science ALDRICH Chemistry SUPELCO Analytical Fluka Analytical

sigma-aldrich.com SIGMA-ALDRICH™